

**SYNTHESIS AND CHARACTERIZATION OF
NOVEL LOW-VALENT COMPOUNDS OF MAIN
GROUP ELEMENTS: APPLICATION IN
ORGANIC TRANSFORMATIONS**

**A THESIS
SUBMITTED TO PARTIAL FULFILMENT OF THE DEGREE
OF
DOCTOR OF PHILOSOPHY
IN CHEMISTRY**

**BY
RAVINDRA KRUSHNAJI RAUT**

ID: 20153361

**UNDER THE GUIDANCE OF
DR. MOUMITA MAJUMDAR**



**INDIAN INSTITUTE OF SCIENCE EDUCATION AND RESEARCH,
PUNE**

2020

CERTIFICATE

Certified that the work incorporated in the thesis entitled, “*Synthesis and Characterization of Novel Low-valent Compounds of Main Group Elements: Application in Organic Transformations*” Submitted by **Mr. Ravindra Krushnaji Raut** was carried out by the candidate, under my supervision. The work presented here or any part of it has not been included in any other thesis submitted previously for the award of any degree or diploma from any other University or Institution.



(Supervisor)

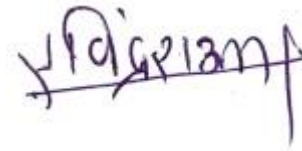
Dr. Moumita Majumdar
(Associate Professor)

Date: 04-NOV-2020

DECLARATION

I hereby declare that, this written submission represents my ideas in my own words and where other's ideas have been included; I have adequately cited and referenced the original sources. I also declare that I have adhered to all principles of academic honesty and integrity and have not misrepresented or fabricated or falsified any idea/data/fact/source in my submission. I understand that violation of the above will be cause for disciplinary action by the institute. It can also evoke penal action from the sources which have thus not been appropriately cited or from whom proper permission has not been taken when needed.

Date: 19/10/2020



Ravindra Krushnaji Raut
Registration No. 20153361
IISER Pune

ACKNOWLEDGMENTS

Foremost, I would like to express my sincere gratitude to my advisor **Dr. Moumita Majumdar** for the continuous support throughout my Ph.D. study and research for her patience, motivation, enthusiasm, and immense knowledge. Her guidance helped me in all the time of research and writing of this thesis. I could not have imagined having a better advisor and mentor for my Ph.D. study.

Besides my advisors, I enormously thankful to the Research Advisory Committee (RAC) members, Prof. Sujit K. Ghosh and Prof. Avinash Kumbhar for their encouragement, insightful comments, fruitful discussion, and appropriate questions during the RAC meetings. I am also extremely thankful to former director Prof. K.N. Ganesh and current director Prof. Jayant B. Udgaonkar of IISER-Pune, for the academic support and the facilities provided to carry out the research work at the institute. I am thankful to the IISER Pune and CSIR for financial support during the Ph.D. degree.

At this stage of life without funding PhD would have been impossible for me, many thanks to funding agencies IISER Pune and CSIR India.

I am incredibly thankful to Dr. Sayam Sen Gupta, IISER Kolkata, and Dr. Gautam K. Lahiri, IIT Bombay, for allowing me to carry out EPR experiments in their labs, which is part of chapter 2B. I am also grateful to Dr. Rajesh Gonnade (NCL, Pune) and Dr. Shyampada Nandi for teaching me SC-XRD techniques and clarifying my doubts without any hesitation. I also thank all administrative staff of IISER Pune especially Mr. Mahesh, Mr. Yathish, Mr. Ganesh, Mr. Mayuresh, Mrs. Megha, Mr. Sanjay, Mr. Tushar, Mrs. Sayalee and instrument operators (particularly NMR, HRMS, SC-XRD) Mr. Chinmay, Mr. Sandeep, Mr. Nitin, Mr. Ravindar, Mrs. Archana, Mrs. Deepali.

I am worthy of having wonderful and helpful lab members so special thanks to them; Naveen Kumar, Padmini, Joy, Vikas Kumar, Farhan Amin, Akash, Purva, and Saddam for devoting their precious time and made many valuable suggestions, which indeed helped me during this research work. A special thanks to Naveen Kumar for accompanying me since the start of PhD to till finishing my PhD, which includes many beautiful moments. I am grateful to Padmini for partly helping me in thesis work. I want to extend my special thanks to Dr. Moreshwar Chaudhary and Dr. Sohan Patil, for their excellent suggestions regarding research. These thanks also continue to Dr. Prabhakar Pawar, Dr. Shahaji More, Iranna, Pramod.

No words are sufficient to acknowledge my prized friends in and out of IISER Pune, who have helped me at various stages of my work in IISER. I wish to thank Dr. Debanjan, Dr. Madan, Dr. Soumendu, Yogeshwar, Anish, Gulab, Sachin, Gayathri, Pavan, Mohan, Jagan, Pooja, and all other IISER Pune's friends also grateful to non-IISER friends: Shibin, Sagar, Hrishikesh, Dr. Sumit. It's my pleasure to thank all my school and college friends Sumit, Yogesh, Amol, Vijay, Dr. Sachin, Sai, and Dinesh.

And finally, a Tons of thanks to my beloved father, **Mr. Krushnaji Raut**, and my brother **Mr. Devendra Raut** for their dedication, motivation, patient, and caring throughout my life. I wish to express my extreme indebtedness to loving sisters Mrs. Manisha, Mrs. Rohini, and my Sister-in-Law Mrs. Mayuri for their contribution to my achievements. Last but most important person who always guided me in the proper direction and without her support (mental, motivational, and emotional) I may never have completed this thesis, is my wife **Sanhita**.

With sincere thanks,
Ravindra Krushnaji Raut



*Dedicated to
My Beloved
Mother Late
Alka Raut*

TABLE OF CONTENTS

Abbreviation	I	
Synopsis	III-VI	
<hr/>		
Chapter 1		
<hr/>		
Chapter 1: Introduction		
<hr/>		
1.1	Chemistry of Main Group Elements	2
1.2	Carbene and its Heavier Analogues	3
1.2.1	Germylenes	5
1.2.2	Stannylenes	6
1.2.3	Cationic Germylenes and Stannylenes	8
1.3	Applications of Low Valent Main Group Elements	10
1.3.1	Small Molecule Activation and Catalysis	10
1.4	Organocatalysis	17
1.4.1	Transition-metal-free C-C Bond Formation Reactions	18
1.4.2	Transition-metal-free C-B Bond Formation Reactions	19
1.5	References	22
<hr/>		
Chapter 2		
<hr/>		
Section 2A: Synthesis and Characterization of Stannylenes and Their Transition Metal Complexes		
<hr/>		
2A.1	Introduction	31
2A.2	Results and Discussion	33
2A.2.1	Stannylene Synthesis by Transamination	33
2A.2.2	Bisstannylene Synthesis	37
2A.2.3	Tetracoordinate Monostannylene with C-C Coupling in Ligand Backbone	40
2A.2.4	Tetracoordinate Monostannylene Synthesis	43
2A.2.5	Reactivity Study of Stannylenes	44
2A.3	Conclusion	49
2A.4	Experimental Details	50
2A.4.1	General Remarks	50
2A.4.2	Synthetic Procedures	50

2A.4.3	Plots of NMR Spectra	58
2.4.4.4	UV/Vis Spectra	70
2A.4.5	X-ray Crystallographic Data	71
2A.5	References	74

Section 2B: Synthesis, Characterization and Reactivity of Novel Tin(II) Cationic Compound

2B.1	Introduction	78
2B.2	Results and Discussion	80
2B.2.1	Sn(II) Synthesis from Stannylenes	80
2B.2.2	Neutral N-Donor Stabilized Sn(II) Cations and Dications	83
2B.2.3	Reactivity Study of Sn(II) Dication	87
2B.3	Conclusion	89
2B.4	Experimental Details	90
2B.4.1	General Remarks	90
2B.4.2	Synthetic Procedures	90
2B.4.3	Plots of NMR Spectra	95
2B.4.4	X-ray Crystallographic Data	105
2B.5	References	109

Chapter 3

Section 3A: Direct Coordination of Germanium (II) Dicationic Center to Transition Metals

3A.1	Introduction	113
3A.2	Results and Discussion	115
3A.2.1	Chlorogermylumylidene and Germanium (II) Dication	115
3A.2.2	Crystal Structure Analysis	116
3A.2.3	DFT Study	117
3A.2.4	Electrophilic Nature	118
3A.2.5	Nucleophilic Nature	119
3A.2.6	Crystal Structure Analysis	120
3A.2.7	DFT study	122

3A.3	Conclusion	123
3A.4	Experimental Details	123
3A.4.1	General Remarks	123
3A.4.2	Synthetic Procedures	123
3A.4.3	Plots of NMR Spectra	127
3A.4.4	UV/Vis Spectra	136
3A.4.5	X-ray Crystallographic Data	140
3A.4.6	X-Ray Crystal Structure	145
3A.5	References	146

Section 3B: Bis(chlorogermylumylidene) and its Significant Role in an Elusive Reductive Cyclization

3B.1	Introduction	149
3B.2	Results and Discussion	151
3B.2.1	Bis(chlorogermylumylidene)	151
3B.2.2	Solid State Structure of 2	152
3B.2.3	Computational Details	153
3B.2.4	Reduction of Bis(chlorogermylumylidene)	154
3B.2.5	Mechanistic Investigation of Reductive Coupling	155
3B.2.6	Reduction of Germanium (II) Dication and Chlorogermylumylidene	159
3B.3	Conclusion	161
3B.4	Experimental Details	161
3B.4.1	General Remarks	161
3B.4.2	Synthetic Procedures	162
3B.4.3	Plots of NMR Spectra	168
3B.4.4	HRMS of Piperazine 3	173
3B.4.5	UV/Vis Spectra	174
3B.4.6	Cyclic Voltammetry	175
3B.4.7	EPR Spectra	176
3B.4.8	X-ray Crystallographic Data	177
3B.4.9	X-Ray Crystal Structure	182

Chapter 4

Chapter 4: Organo-main-group Compound Promoted C-C and C-B Bond Forming Reactions

4.1	Introduction	187
4.1.1	Transition Metal Catalyzed Coupling Reactions	187
4.1.2	Transition-metal-free Cross Coupling Reactions	187
4.2	Result and Discussion	194
4.2.1	Organosilicon Additive Promoted C-B and C-C Bond Forming Reactions	194
4.2.2	Organoboron Additive Promoted C-B and C-C Bond Forming Reactions	199
4.3	Conclusion	211
4.4	Experimental Details	212
4.4.1	General Remarks	212
4.4.2	EPR Measurement	212
4.4.3	Synthetic Procedures	212
4.4.4	Spectroscopic Data	219
4.4.5	Plots of NMR Spectra	223
4.4.6	X-ray Crystallographic Data	245
4.5	References	247

Abbreviations

Chemical Abbreviation

ACN	Acetonitrile	CAAC	Cyclic Alkyl Amino Carbene
Ad	Adamantyl	FLP	Frustrated Lewis Pair
Ar	Aryl	TFT	Trifluorotoluene
C ₆ D ₆	Deuterated benzene	Triflic	Trifluoromethanesulphonic
CD ₃ CN	Deuterated Acetonitrile	MsOH	Methanesulphonic acid
CDCl ₃	Deuterated chloroform	Nu	Nucleophile
Cp	Cyclopentadienyl	AIBN	Azoisobutyronitrile
DCM	Dichloromethane	B ₂ Pin ₂	Bispinolatodiboron
Dipp	2,6-Diisopropylphenyl	KO- <i>t</i> -Bu	Potassium tert-butoxide
DMSO	Dimethyl sulfoxide	Ph	Phenyl
EtOH	Ethanol	MTBE	Methyl tert-butyl ether
EtOAc	Ethyl Acetate	Pz	Pyrazine
MsOH	Methanesulphonic acid	BiPy	Bipyridine
<i>i</i> Pr	Isopropyl	THF	Tetrahydrofuran
MeOH	Methanol	TMSCl	Trimethylsilylchloride
Me	Methyl	TMSOTf	Trimethylsilyl trifluoromethanesulphonate
Mes	2, 4, 6 –trimethylbenzene	NaH	Sodium hydride
Mes*	2,4,6-tri- <i>t</i> butylphenyl	DMSO	Dimethylsulphoxide
<i>n</i> -BuLi	<i>n</i> -butyllithium	THF	Tetrahydrofuran
NHC	<i>N</i> -Heterocyclic Carbene	TFT	Trifluorotoluene
NHSi	<i>N</i> -Heterocyclic Silylene	Triflic	Trifluoromethanesulphonic
NHGe	<i>N</i> -Heterocyclic Germylene	<i>t</i> Bu	Tertiary butyl
Np	Neopentyl	<i>t</i> BuNC	Tertiarybutyl Isocyanide
OTf	Trifluoromethanesulphonate	py	Pyridine
PMe ₃	Trimethyl Phosphine	Trip	2,4,6-Triisopropylphenyl
PhLi	Phenyllithium		

Abbreviations

Units, Standard terms and general notations

<i>J</i>	Coupling constant in NMR	Anal.	Analysis
Equiv.	Equivalents	Calcd.	Calculated
HRMS	High Resolution Mass Spectrometry	λ	Wavelength
NMR	Nuclear Magnetic Resonance	CCDC	Cambridge Crystallographic Data Centre
g	gram(s)	CIF	Crystallographic Information file
mmol	milimol	°C	Degree Centigrade
VT	Variable temperature	DFT	Density Functional Theory
Cat.	catalyst	mg	Milligram
mL	Mili Litre	h	Hour
DFT	Density Functional Theory	Hz	Hertz
UV	Ultra-Violate	min.	Minute
Vis	Visible	M.P.	Melting Point
NMR	Nuclear Magnetic Resonance	NBO	Natural Bond Order
SC-XRD	Single Crystal X-Ray Diffraction	WBI	Wiberg Bond Indices
Decomp	Decomposition	NPA	Natural Population Analysis
EPR	Electron Paramagnetic Resonance	%	Percentage
δ	Chemical shift	MHz	Mega Hertz

Synopsis

Title: Synthesis and Characterization of Novel Low-valent Compounds of Main Group

Elements: Application in Organic Transformations

Though the intriguing properties of main group compounds are harvested in every aspect of chemistry, there is a lot of scope for developing main group chemistry. In low valent state main group elements can mimic the transition metal owing to match in frontier orbitals with d-orbitals of transition metals. Low valent main group elements are already used in dihydrogen activation, activation of small molecules like carbon dioxide, carbon monoxide, dinitrogen, ammonia, oxygen, alkene, and alkynes. The low valent and the usual oxidation state main group elements also found plentiful catalytic application in organic synthesis. Still, the stability, viable synthetic routes, and a limited library of known compounds hamper this field's development. This thesis focuses on developing accessible synthetic ways of stable and novel main group compounds with their proper characterization. We have also utilized them in C-C and C-B bond formation reactions with enough mechanistic evidence, which claims the importance of main group center.

Chapter 2 deals with the stannylenes and stannylum cations stabilization using multidentate redox non-innocent Schiff base ligands followed by their reactivity study. This chapter is divided into two sections, **a** and **b**.

Section a deals with the synthesis of donor stabilized stannylene by transamination reaction of pyridyl functionalized or phosphine functionalized Schiff based ligands. *N,N,N',N'*-Tetrakis(trimethylsilyl)- λ^2 -Stannanediamine ($\text{Sn}[\text{N}(\text{SiMe}_3)_2]_2$) is basic in nature which removes the acidic proton from iminopyridine ligand, generate the respective stannylenes by ene-amide formation. In case transamination of *N',N'*-bis(1-(pyridin-2-yl)ethyl)ethane-1,2-diamine as reactant, deprotonation leads to the formation of imine from secondary amine. The reaction mechanism is tried to rationalize by variable temperature ^{119}Sn NMR. The phosphine functionalized diamines gave the dimeric stannylene as the only product. Single crystal X-Ray diffraction revealed the dimeric nature of stannylene, which was further confirmed by variable temperature ^1H and ^{31}P NMR spectroscopy. The ene-amid reaction of bis(α -iminopyridines) with $\text{Sn}[\text{N}(\text{SiMe}_3)_2]_2$, gave different products depending on the stoichiometry of reactant. In the case of 1:2 reaction of bis(α -iminopyridines) with $\text{Sn}[\text{N}(\text{SiMe}_3)_2]_2$ lead to the formation of

bisstannylene. In contrast, 1:1 reaction gave stannylene as a product with very unusual C-C coupling in the ligand backbone occurred via dehydrocoupling. The mechanism was elucidated with the help of time dependant NMR spectroscopy and H₂ detection by gas chromatography. The α -iminopyridine ligand was also allowed to react with Sn[N(SiMe₃)₂]₂, leading to the formation of tri- and tetra-coordinated stannylenes. The donor stabilized stannylenes have high donating ability, which was utilized in stabilizing the Au(I) and Ag(I) cations for the first time. The complexes are characterized by X-Ray crystallography and NMR spectroscopy.

Section b deals with the syntheses and stabilization of stannylum {Sn(II)} cations with N-donor ligands. The stabilization of cations is achieved either from donor stabilized stannylenes. It is also synthesized directly from SnCl₂ by autoionization or by using any halide abstracting agent. The stannylenes are allowed to react with tris(pentafluorophenyl)borane giving zwitterionic stannylum cation. When stannylene was attempted for one-electron oxidation by NOSbF₆ gave Stannylum {Sn(II)} monocation. Tin(II) cations with stereochemically active lone pair are synthesized from SnCl₂ and multidentate ligands which was missing in the earlier reports. The synthesized Sn(II) dication aimed to utilize as ligands, but the attempts were unsuccessful with transition metal because of tin's redox nature. The reaction of Sn(II) dication with GeCl₂.Dioxane gave the transmetallation product. All the compounds are characterized by SC-XRD and NMR spectroscopy.

The prominent s-character of the Tin(II) lone pair in stannylene dication hamper its use as the ligand. Later we turned out attention on germanium {Ge(II)} cations. **Chapter 3** is again divided into two sections, **a** and **b**.

Section a deals with the stabilization of Ge(II) cations with stereochemically active lone pair. The tetradentate bis(α -iminopyridine) ligand has opted for stabilization. The Ge(II) cations were synthesized by the reaction of GeCl₂.Dioxane with tetradentate ligand along with halide abstracting agent TMSOTf. The cations are obtained in good yield and characterized by SC-XRD, NMR, and UV-VIS study. DFT study revealed the HOMO is composed of germanium lone pair having directionality (s- p- mixed). Further, the dipositive germylene was reacted with Ag(I) and Au(I) cations overall giving Ge-M-Ge complex. The DFT study revealed that there is σ -donation from germanium to transition metal simultaneously π - a back donation from metal to germanium.

In the previous section, the reactivity of Ge(II) dication was tested with a transition metal. Next, we were interested in reactivity with main group metal salts. **Section b** includes the reactivity of Ge(II) dication with GeCl₂.Dioxane leading to the formation of bis(chlorogermylumylidene). Two chlorogermylumylidene units are stabilized in one ligand and don't show any interaction between two germanium. By having a glance at atomic orbitals, the LUMO is residing on the ligand imino functionality, and HOMO is the lone pair on germanium. The reduction of bis(chlorogermylumylidene) by a harsh reducing agent like potassium, sodium did not give any anticipated reductive cyclized product. The selective use of mild organosilicon reducing agent 1,4-bis(trimethylsilyl)-1,4-dihydropyrazine (^{Si}Pz) gave the pyridyl substituted piperazine by reductive cyclization. The reaction was going via transient radical cation of germanium (II), which was further confirmed by EPR spectroscopy. The possible mechanism was elucidated by performing a control experiment and stabilizing intermediate.

The organosilicon reducing agents can act as one electron donor generating the radical cation. We anticipated the use of these organo-main-group compounds in organocatalysis via radical pathway reactions. **Chapter 4** deals with organo-main-group compound promoted C-C and C-B bond formation reactions.

The aryl diazonium salts are highly electron-deficient species and can generate the aryl radical quickly by getting a single electron. The organosilicon reducing agents used catalytically for the C-C and C-B bond-forming reactions, but unfortunately, the catalyst was diminishing in the reaction progress, giving very low yields. Using the selective nucleophile/base, the electron donor species are generated from organosilicon compounds, and this concept is used in the C-B coupling reactions via a radical pathway. The reaction is good for the generation of aryl boronate esters from aryl Iodide. However, the reaction was not efficient for aryl bromides and also for C-C coupling reactions. The C-B and C-C couplings are achieved with aryl bromides by using organoborane compounds as additive/catalyst. The attack of the base on organoborane compounds generates the electron donor species, which are suitable for converting the aryl halides into aryl radicals. The aryl radical then added to give the C-C and C-B coupled products depending on the reagent used. The reaction mechanism is elucidated with experimental proofs in this chapter.

Noteworthy Finding

1. Chapter 2
 - a) Dipolar stannylenes are synthesized, and their reactivity with Lewis acid is explained.
 - b) Developed new synthetic routes for Sn(II) cations.
2. Chapter 3
 - a) Synthesized Ge(II) dication with stereochemically active lone pair used this dipositive compound as a ligand in the stabilization of Au(I) and Ag(I) cations for the first time.
 - b) Stereo-selective synthesis of novel pyridyl substituted piperazine achieved via reductive cyclization, the role of germanium in reductive cyclization is also elucidated.
3. Chapter 4
 - a) Organosilicon additive promoted radical borylation of aryl halides was achieved.
 - b) Organoborane compound used as catalyst/additive in C-C and C-B bond formation reaction with mechanistic details.

List of Publications

1. **Ravindra K. Raut**, Padmini Sahoo, Dipti Chimnapure, and Moumita Majumdar* Versatile coordinating abilities of acyclic N₄ and N₂P₂ ligand frameworks in conjunction with Sn[N(SiMe₃)₂]₂. *Dalton Trans.* **2019**, 48, 10953-10961.
2. **Ravindra K. Raut** and Moumita Majumdar* A pyramidal Tin(II) dications and its reactivity studies. *J. Organomet. Chem.* **2019**, 887, 18-23.
3. Padmini Sahoo, **Ravindra K. Raut**, Devesh Maurya, Vikas Kumar, Pooja Rani, Rajesh G. Gonnade and Moumita Majumdar* Stabilization of bis(chlorogermylumylidene)s within bifunctional PNNP ligand frameworks and their reactivity studies. *Dalton Trans.* **2019**, 48, 7344-7351.
4. Moumita Majumdar*, **Ravindra K. Raut**, Padmini Sahoo and Vikas Kumar Bis(chlorogermylumylidene) and its significant role in elusive reductive cyclization. *Chem. Commun.* **2018**, 54, 10839.
5. **Ravindra K. Raut**, Sheikh Farhan Amin, Padmini Sahoo, Vikas Kumar and Moumita Majumdar*. One-Pot Synthesis of Heavier Group 14 N-Heterocyclic Carbene Using Organosilicon Reductant. *Inorganics* **2018**, 6, 69.
6. **Ravindra K. Raut** and Moumita Majumdar* Direct Coordination of Germanium(II) Dicationic Center to Transition Metals. *Chem. Comm.* **2017**, 53, 1467-1469.

Chapter 1

Introduction

Abstract

This chapter gives a brief introduction of challenges in understanding the bonding situations in main group elements and stabilization of low valent main group elements. Recent examples of main group elements, where it shows the close mimicking with transition metals, and can replace these expensive, toxic, rare transition metals with earth-abundant main group elements in every aspect of chemistry. The key highlights of the stabilization of low valent main group elements along with their application ranges from catalysis to small molecule activation are described here. In a greener approach, the transition metal-free C-C and C-B bond formation reactions have gain attention over the years, and certainly, the main-group catalyst/organocatalyst can replace them. Several organocatalysts are reported to date for C-H arylation of unactivated arenes, out of which the major contributions are highlighted here.

1.1 Chemistry of Main Group Elements and its History

The s- and p-block elements include the collection of earth abundant elements, which are solid, liquid and gases with metallic, non-metal and metalloid properties with the electron deficient, electron rich and electronically satisfied elements in the periodic table collectively called as main group elements.¹ Fundamental study of main group chemistry has provided many different bonding terms and novel unique structures.

		Main Group Elements									
		1	2	13	14	15	16	17	18		
1		1 H							2 He	K	
2		3 Li	4 Be	5 B	6 C	7 N	8 O	9 F	10 Ne	L	
3		11 Na	12 Mg	13 Al	14 Si	15 P	16 S	17 Cl	18 Ar	M	
4		19 K	20 Ca	31 Ga	32 Ge	33 As	34 Se	35 Br	36 Kr	N	
5		37 Rb	38 Sr	49 In	50 Sn	51 Sb	52 Te	53 I	54 Xe	O	
6		55 Cs	56 Ba	81 Th	82 Pb	83 Bi	84 Po	85 At	86 Rd	P	
7		87 Fr	88 Ra	113 Nh	114 Fl	115 Mc	116 Lv	117 Ts	118 Og	Q	

Main Shell
Non-metals
Alkali metals
Alkaline earth metals
Metals
Metalloids
Halogens
Noble Gases

Figure 1.1 Recent periodic table classified as per the properties.

The study by Lipscomb (Noble Prize 1976)² on boron hydride provided a classical example of three center-two electron bonding in boron hydrides. Linus Pauling mostly dealt with main group elements and marked his contribution by writing the book “The Nature of the Chemical Bond” (Noble Prize 1954), which mainly dealt with main group compounds.³ The main group elements containing compounds like Grignard reagent (Noble Prize 1912)⁴, boron, and phosphorous compounds (Brown and Wittig, noble prize 1979)⁵ have tremendous contribution in the development of organic chemistry. The several industrial syntheses of inorganic compounds like ammonia (an important ingredient of chemicals, fertilizers) by Haber (Noble prize 1918) developed in the early 19th century and still have no synthetic alternative.⁶ The Ziegler-Natta (Noble Prize 1963) catalyst is commercially being used for the production of polymers like polyethylenes and polypropylenes.⁷ These landmarks in history are not the only contributions made in the development of main group chemistry; several other discoveries also created a path.

Due to lack of facilities in the first half of the twentieth century, the growth of main group elements was limited only to their higher oxidation states, which were stable at ambient

conditions. In the second half, the development of sterically encumbered ligands for kinetic stabilization of low coordinated transition metals by Bradley and co-workers motivated the chemist to use in stabilization of reactive, unsaturated main group compounds.⁸ First, it has been used by Lappert in the 1970's for the synthesis of tin(II) alkyl dimer $\{\text{Sn}[\text{CH}(\text{SiMe}_3)_2]_2\}_2$. It was the first example of multiple bonding in heavier main group elements under ambient conditions.⁹ After this, chemists started developing sterically hindered bulky aryl ligands for the synthesis of multiply bonded heavier main group elements. The landmark disilene $\text{Mes}_2\text{Si}=\text{SiMes}_2$ ($\text{Mes} = 2,4,6\text{-trimethylphenyl}$) **1.1** was prepared and characterized by West in 1981.¹⁰ In the same year Yoshifuji reported the stable diphosphene ($\text{Mes}^*\text{P}=\text{PMes}^*$) **1.2** molecule using bulky supermesityl ($\text{Mes}^* = \text{C}_6\text{H}_2\text{-}2,4,6\text{-}^t\text{Bu}$) group.¹¹ These compounds broke the pre-existing famous “double bond rule”, which was stating that only second row p-block elements are allowed to form double bond not it's heavier congeners due large size and more diffused *p*-orbitals have ineffective overlap and thus a lower π -bond energy.¹²

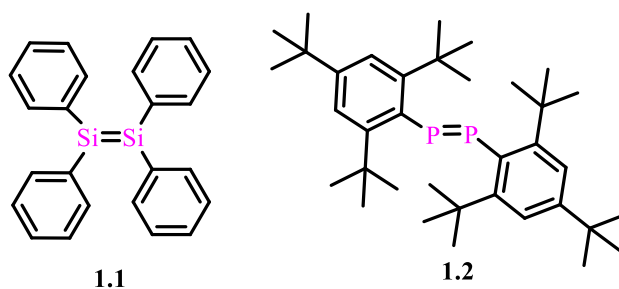
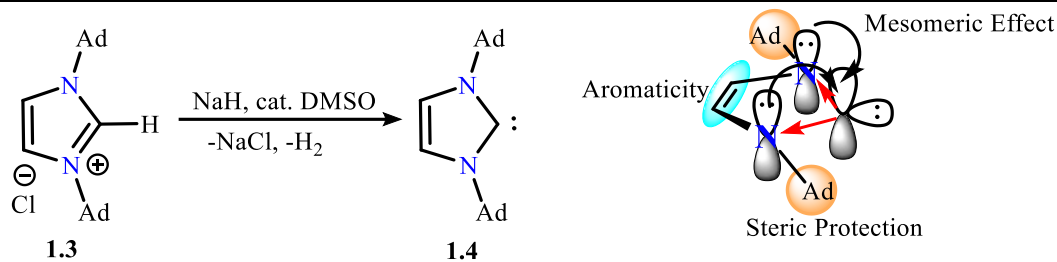


Chart 1.1 Initial discoveries of p-block elements with multiple bond.

1.2 Carbene and its Heavier Hnalog

In 1991, Arduengo and co-workers developed the synthetic method for isolable, bottleable N-Heterocyclic carbene by taking the benefit of steric and electronic stabilization. The synthetic procedure for carbene **1.4** involves the deprotonation of 1,3-di-1-adamantylimidazoliumchloride **1.3** by sodium hydride.¹³ The adamantyl group provides kinetic stabilization by the steric bulk and also has electronic influence. The asymmetry in the carbene can be introduced by having a different substituent on nitrogen. The adjacent nitrogen atoms are σ -electron-withdrawing and π -electron-donating stabilize the carbene centre by inductive as well as mesomeric effect. The number of heteroatoms in carbene changes the electronic properties drastically. The double bond in the cyclic backbone provides electronic stabilization due to aromaticity in the pentacyclic ring. Substituents on the backbone carbon also change the carbene electronic properties.



Scheme 1.1 Synthesis of isolable N-Heterocyclic Carbene and its electronic properties.

The property of carbene can be tuned by changing one of the adjacent nitrogen atom with another atom or by introducing the functional group in the backbone. The electrophilicity or nucleophilicity of carbene is much dependant on the functional group in the backbone of the ring. After its first appearance, the NHC's have dominated as a ligand in the organometallic chemistry.¹⁴ The toxic phosphines are replaced by NHC ligand in transition metal chemistry, and this replacement also shown the positive effect on the catalytic performance of many TM complexes. In an example, the stability and catalytic performance of the Grubbs-Hoveyda second-generation catalyst in olefin metathesis remarkably increased after the incorporation of NHCs.¹⁵ In another application, NHCs itself was used as organocatalyst in some of the organic transformations.¹⁶ Later Bertrand and co-workers developed the synthetic route for cyclic alkyl amino carbenes (CAACs) by replacing one of the adjacent nitrogen atom by carbon atom.¹⁷ The NHCs and CAACc have been utilized immensely by the main group chemist as a neutral, strong two electron donor ligand in stabilization and isolation of reactive low valent main group elements, which was not possible by using traditional ligands.¹⁸ Almost every issue of the variety of journals include the reports on the utility of carbenes. They are commercially available, and also synthetic routes are not that laborious.

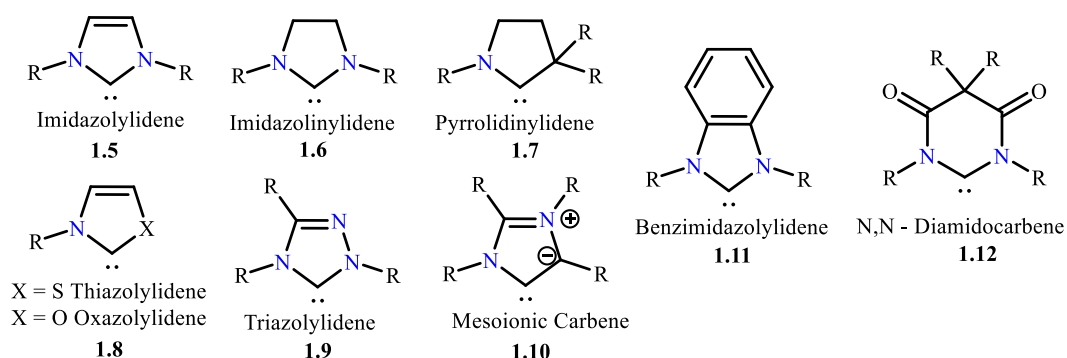


Chart 1.2 Structure of different classes of carbenes.

The structural mimics of carbene are one of the important classes of compounds for chemists due to its unique properties. Some of the heavier analogs of NHCs are known before

the Arduengos carbene owing to their higher stability. In the initial phase they were synthesized only for fundamental study, however recent study revealed their applications. For example, boryl anion **1.13** are hard anionic substituents and strong σ donor ligand,¹⁹ whereas cationic phosphonium **1.15** found as very good ligand in transition metals due to their inverse property to NHC's as they are poor σ donor and good π acceptor.²⁰ Several group-13 and 14 carbene analogs also utilized as a ligand in catalysis or small molecule activations.²¹ The N-heterocyclic sulfur dication **1.16** is used for insertion in carbodiimide and cycloalkenes owing to its Lewis acidic properties.²²

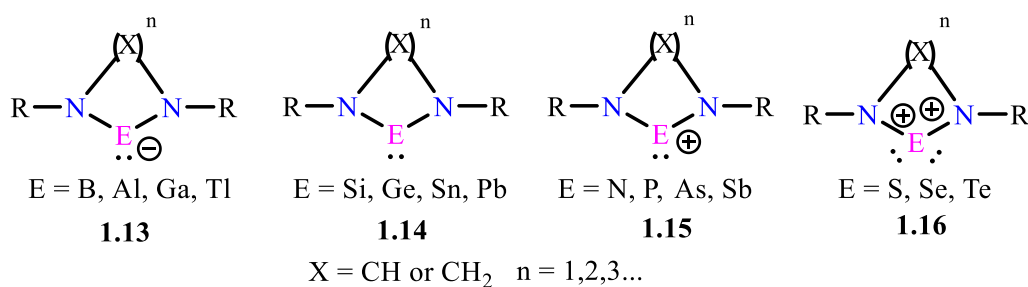


Chart 1.3 Carbene analogs of p-block elements.

The properties of a heavier p-block elements in their stable +2 oxidation state enables their relatively easy isolation. However, on this basis one can anticipate that the lead (II) compounds are the most easy targets for separation, but in fact, some of the dialkyl Pb (II) compounds which are without steric and electronic protection known to dissociate into Pb(0) and Pb (IV) species. It is challenging to isolate heavier carbenes under ambient conditions due to their highly electrophilic nature.²³ The chemistry of carbenes and silylenes is extensively studied, whereas germylenes and stannylenes are remained unexplored relatively. The Moderate and tunable properties of germylenes and stannylenes over other carbenes make them potential candidates in catalysis to small molecule activations. A few of the main group elements in their low valent state pertaining to this thesis work are explained below in brief.

1.2.1 Germylene

Germylenes are the divalent compounds of germanium featuring a lone pair of orbital and empty *p*-orbital. They are comparatively less reactive than their lighter congener due to large size and wide separation between the *sp*-orbitals.²⁴ Lappert synthesized the first unusually stable dicoordinated, acyclic dialkylamido organogermylene **1.17** in the year of 1974 by the reaction of GeCl_2 .dioxane with lithium hexamethyldisilazane.²⁵ Immediately after that, he synthesized the di-coordinated alkyl-substituted germylene **1.18** analog in 1976.²⁶ These

compounds are monomer in the solution and gas-phase however, they are dimetallene in the solid state.

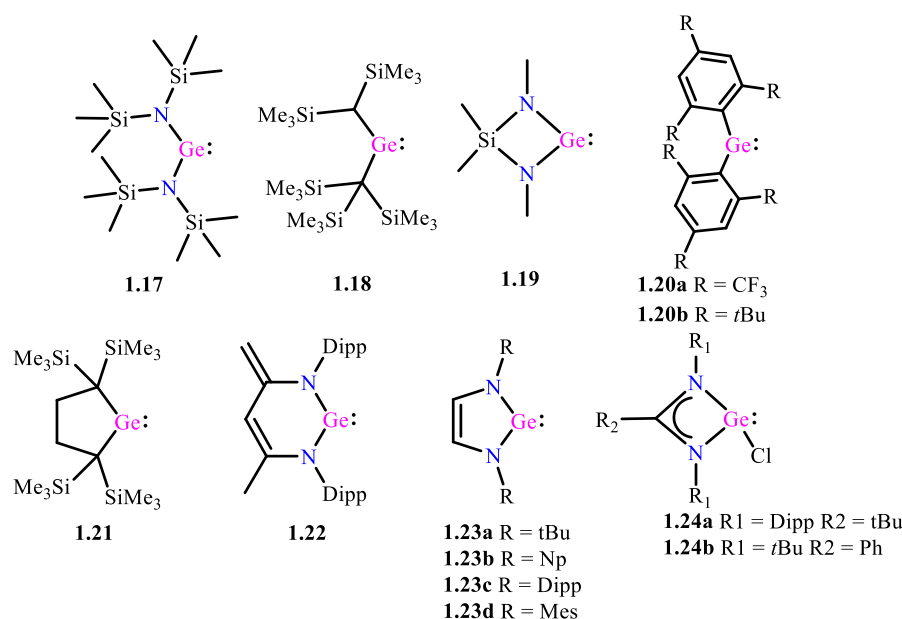


Chart 1.4 Selected examples of Germynes.

The cyclic analog of germylene **1.19** is synthesized by Veith and co-workers in 1987, where the thermodynamic stabilization was achieved by incorporating the hetero (N) atoms.²⁷ After that, several groups stabilized the germynes either by taking the benefit of kinetic stabilization or thermodynamic stabilization. The notable examples are diaryl germylene **1.20a-b**²⁸, Kira's cyclic dialkyl substituted germylene **1.21** analogous to Lappert's acyclic dialkyl substituted germylene²⁹, β -ketinate stabilized germylene **1.22** with exocyclic double bond³⁰, N-heterocyclic germylene where germylene center is thermodynamically stabilized by two nitrogen atom directly bonded at α position to germylene center **1.23a-d**³¹ and chlorogermylene in amidinate ligand where one nitrogen-germanium bond is coordinate, whereas another one is covalent bond **1.24a-b**.³²

1.2.2 Stannylene

The divalent species of stannylene are easily accessible as they are highly stable. Actually, they are stable in their divalent halo salts (SnCl₂) however, these halo salts exist in polymeric form or ion-pair in solid or solution state. In order to investigate properties of monomeric metallylenes, the introduction of various kinds of substituents is attempted. The chemical properties of stannylenes are highly depended on the substituents. Due to their intrinsic electrophilicity, they are stable either two coordinated or more than two coordinated species.

The diamido/dialkyl substituted stannylenes (**1.25** & **1.26**) reported long back by Lappert in the 1970s, but the metallylene in solution state was found metallene in solid state.

³³ Other alkyl-substituted examples are Kira's pentacyclic stannylene **1.27** was the first monomeric dialkyl substituted tin(II) compound.³⁴ The diaryl stannylene (aryl=Mes*= 2,4,6-tri-tertbutylphenyl) Mes_2^*Sn : **1.28** are the monomeric stannylene in solid state was reported by Weidenbruch in 1994 however, they undergo intramolecular cyclization to afford alkyl aryl stannylene **1.29** as stable metallylene.³⁵ Some of the stable diarylstannylenes which are structurally characterized stabilized using extremely bulky ligand showing as monomers in solid state **1.30**.³⁶

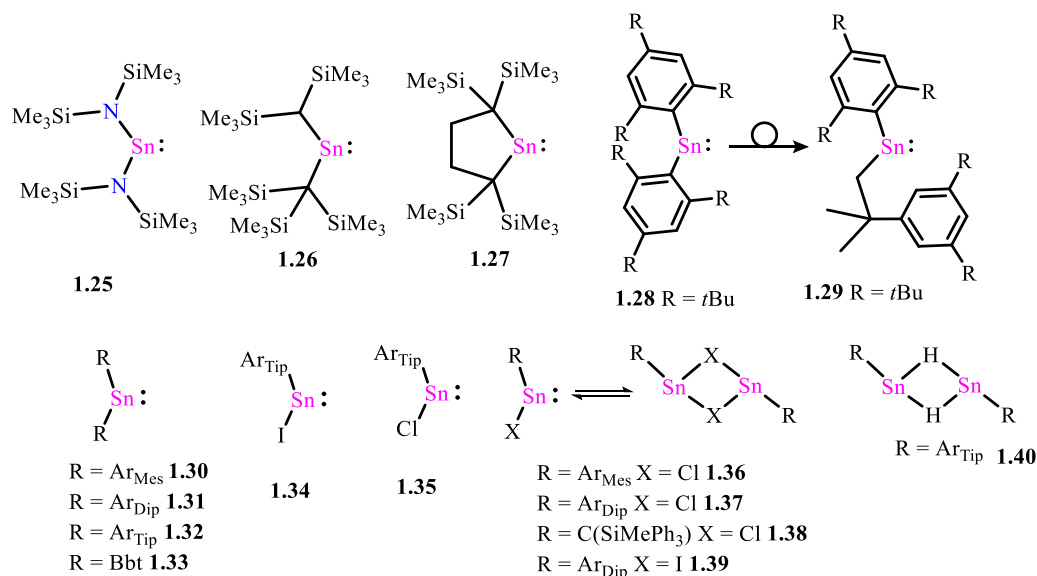


Chart 1.5 Selected examples of Stannylenes.

All the aryl group substituted halostannylenes are monomers in the solution state, while in the solid state, most of them are halo- bridged dimer, and very few are reported as monomers. The ArTip substituted Iodo- **1.34**³⁷ and chlorostannylenes **1.35**³⁸ are monomer in solid state due to the bulk of the aryl group is sterically encumbered. Still, by decreasing down the bulkiness of ligand they turned dimer in solid state **1.36-1.39**. The terphenyl ligand substituted hydrostannylene **1.40** are also dimeric in nature in the solid state.³⁹ Tin center in stannylenes is highly electrophilic in nature and seeks electron density either from a solvent molecule or from extra donor groups in the ligand. There are several examples of donor stabilized stannylene with more than two coordination.⁴⁰

1.2.3 Cationic Germylene and Stannylene

The cationic counterparts of tetrylenes are known as tetrylium-ylidenes, which possess a lone pair orbital and two vacant *p*- orbitals for monocations, and in case of dications, a lone pair of orbital and three vacant *p*- orbitals. Due to the cationic charge and empty *p*- orbitals, they are

highly electrophilic in nature. In order to synthesize this species, kinetic and thermodynamic stabilization strategies implemented. The neutral donor ligands can provide electron density in the vacant orbitals turn them to less electrophilic. In another approach, using the bulky ligand which provides steric protection from the attack of the nucleophile, it is possible to stabilize these cationic tetrylenes. The cationic charge is also stabilized by surrounding weakly coordinating anions.⁴¹

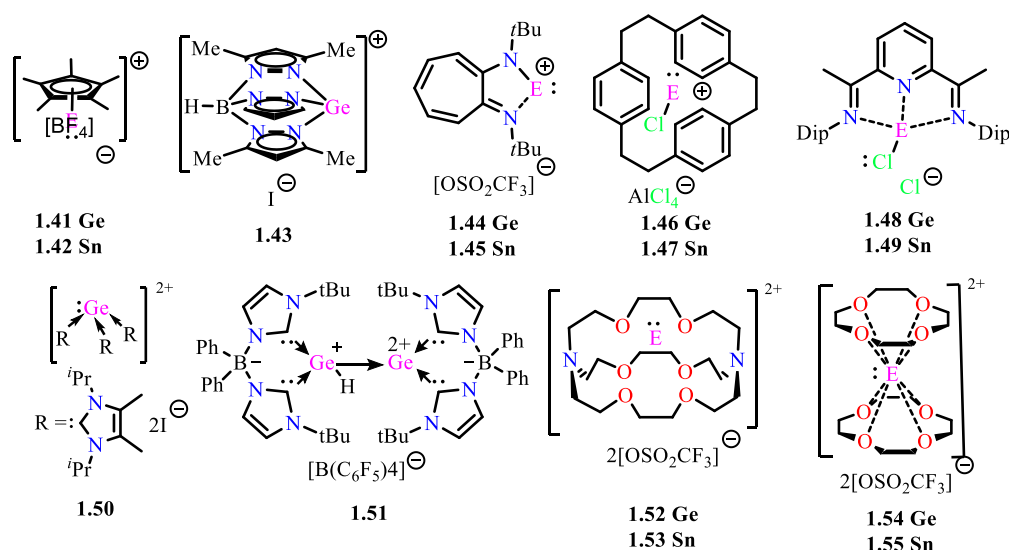


Chart 1.6 Selected examples of cationic Germylenes and Stannylenes.

Cationic analogs of germylene and stannylenes are reported long back in literature. In the year of 1980, Jutzi and co-workers synthesized cyclopentadienyl(CP*) germylumylidene **1.41** and stannylumylidene **1.42** molecule with BF_4^- , AlCl_4^- and CF_3SO_3^- as counter anions. They are either synthesized by the reaction of dicyclopentadienyl germylene(II)/stannylene(II) with electrophiles, proceeds by attack at CP* rings. In alternate way, pentamethylcyclopentadienyl germanium(II)/tin(II) chloride on reaction with AlCl_3 as halide abstracting agent lead to formation of cyclopentadienyl germanium(II)/tin(II) cations.⁴² Later several sandwich complexes of germanium(II) cations are reported by Jutzi in $[\eta^2\text{-Me}_4\text{C}_5\text{H}]\text{Me}_2\text{Si}[\eta^5\text{-Me}_4\text{C}_5]$ ligand.⁴³ Poly(pyrazolyl) borate, which are nitrogen donor ligands also used for isolation of $[\text{HB}(3,5\text{-Me}_2\text{pz})_3\text{Ge}]^+$ **1.43** by Reger and Coan resulted in the kick start of nitrogen donor ligands for isolation.⁴⁴ In 1996, Dias and co-workers used 10 π electron aminotropominate (ATI) ligands in isolation for Ge (II)/Sn(II) cations **1.44-1.45** [45]. In this ligand, the extra imine donor group stabilizes the cationic centre. The Schmidbauer and co-worker isolated germanium (II) cations **1.46** and tin(II) cation **1.47** in [2.2.2]cyclophane ligand, where three aryl rings show η^6 coordination [46]. The reaction of dihalides with Schiff base

ligand 2,6-diacetylpyridinebis-(2,6-diisopropylanil) led to the isolation of cation **1.48** and **1.49** by autoionization of metal halide salts.⁴⁷

In 2007, Baines and co-workers stabilized the germanium (II) dication **1.50** by N-heterocyclic carbene as donor ligands.⁴⁸ The NHCs coordinate with vacant sites of the germanium and knock out the iodide anion. The two positive charges are delocalized over the three NHC's. This compound can be explained by two types of bonding models, 1) dative model 2) Lewis model as depicted in the figure. **4**. In another example bis-NHC's with borate spacer used for isolation of zwitterionically stabilized cationic germanium compound **1.51**, where the monocationic germanium is bonded to dication germanium atom.⁴⁹

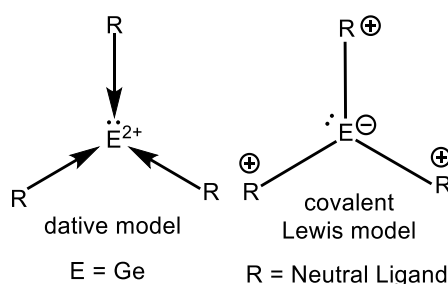


Figure 1.4 Lewis models for E^{2+} centers.

Later in 2008, Baines group used an electron-rich [2, 2, 2]-cryptand and crown ethers for isolation of Ge(II)/Sn(II) cation **1.52-1.55**.⁵⁰ It was the first report of isolation of main group cations in macrocycles other than *s*- and *d*-block element, where the cationic germanium centre is encapsulated within the ligand. After that, several groups isolated the germanium and tin cations using neutral donor ligands, and these examples are covered in a perspective article by Sen.⁵¹

1.3 Application of Low Valent Main Group Elements.

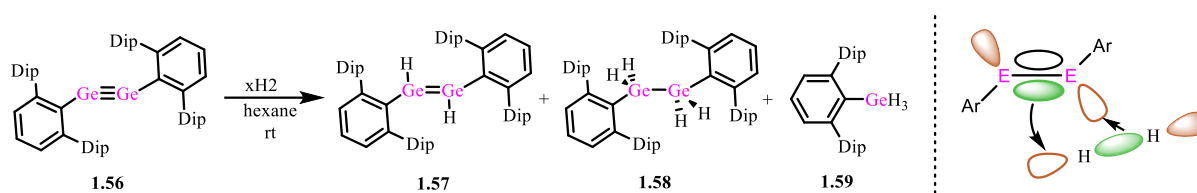
Due to the unique properties of low valent main group elements, they have found applications ranging from small molecule activation to catalysis to materials chemistry. The major landmark applications of main group elements and the applications of germylene and stannylene are highlighted here.

1.3.1 Small Molecule Activation and Catalysis

1.3.1.1 Historical Achievements

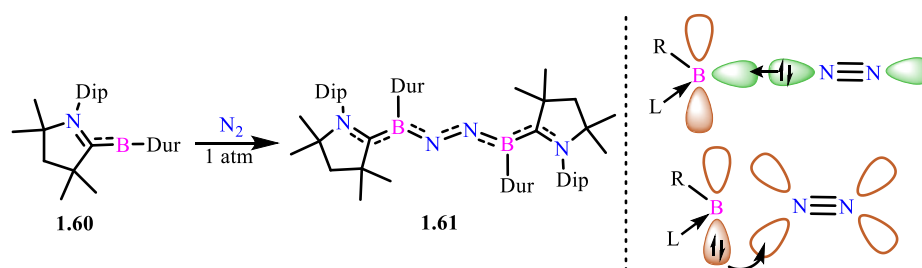
Transition metals are well known for the activation of non-polar, stable molecules like H_2 and N_2 due to the availability of unoccupied and occupied molecular orbitals. Similarly, the low

valent/unsaturated main group compounds revealed the reactivity with H₂ and N₂, which is a preliminary step in the process of utilizing the main group catalytically.



Scheme 1.2 Hydrogen activation by alkyne analog of germanium and interaction of orbitals.

Until 2005, the oxidative addition of H₂ was only limited to transition metals (due to availability of occupied and unoccupied d orbitals), but the Power and co-workers first time reported the oxidative addition of H₂ over alkyne analog of germanium [ArGeGeAr; Ar = 2,6-Trip₂C₆H₃ (Trip = 2, 4, 6-*i*Pr₃C₆H₂)] **1.56** giving the hydrogenated products ArHGe=GeHAr (**1.57**), Ar(H)₂Ge-Ge(H)₂Ar (**1.58**) and ArGeH₃ (**1.59**) at ambient condition. The theoretical calculation showed the initial step involves the interaction of frontier orbitals of digermine with H₂.⁵² Very next year, Stephan and co-workers introduced the frustrated Lewis pair concept and used the phosphine borane FLP for reversible binding of H₂ under near-ambient condition. These reactions prevent the formation of Lewis acid-base adduct due to the steric bulk over phosphine, which allows the interaction of empty 2p orbital of borane and lone pair of phosphine with bonding and antibonding orbitals of H₂.⁵³ In 2007, Bertrand group showed the addition of H₂ over acyclic carbene :C(*t*-Bu)Ni-Pr₂, which gave the addition product H₂C(*t*-Bu)Ni-Pr₂, however typical Arduengo type carbene (NHC) are unable to activate the H₂. High nucleophilicity and electrophilicity of this carbene are responsible for the cleavage of H₂.⁵⁴



Scheme 1.3 N₂ activation at Borylene and orbital interaction.

Another milestone in small molecule activation at the main group centre is the recent study of N₂ activation at the boron centre concluded by the Braunschweig group in 2018. N₂ is one of the most challenging molecules to activate even at transition metal center, but CAAC stabilized borylenes [(CAAC)BDur] **1.61** activate N₂ at boron centre generating compound

1.62 as diborylene coordinated N_2 . The borylene centred lone pair donated to the antibonding orbital of N_2 , whereas empty p orbital of boron accept a lone pair from nitrogen.⁵⁵

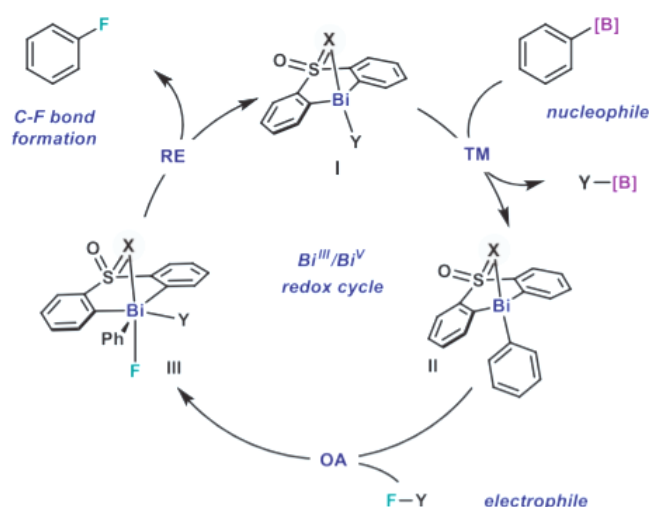
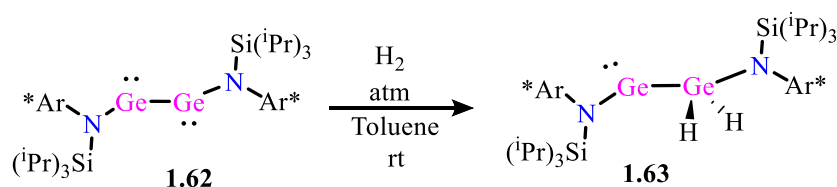


Figure 1.5 catalysis at Bismuth(III)/(V) redox cycle.

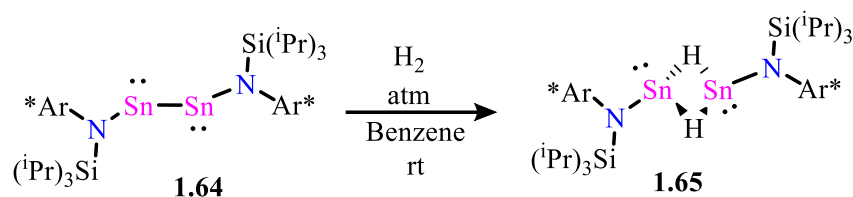
In a very recent example Bi(III)/Bi(V) redox cycle used in catalysis, where bismuth complex undergoes the oxidative addition, reductive elimination, and transmetalation similar to transition metal complexes. The Bi(III)/Bi(V) catalyst was employed for the fluorination of aryl boronic ester, which is a benchmark reaction.⁵⁶

1.3.1.2 H_2 Activation by Germynes and Stannylenes



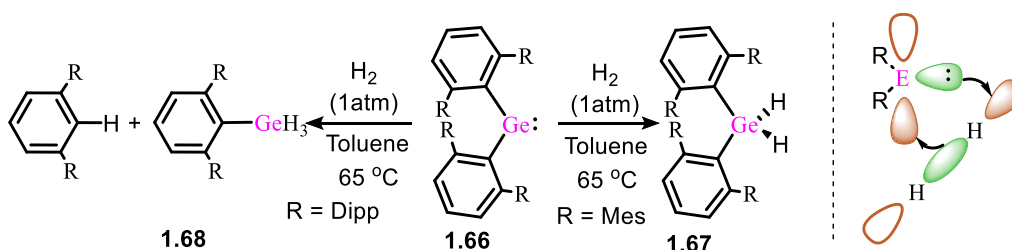
Scheme 1.4 H_2 activation at digermine.

In 2011, Cameron Jones reported the activation of dihydrogen by amido-digermine $[L^1Ge-GeL^1]$ [$L^1 = N(2,6-(C(H)Ph)_2-4MeC_6H_2)(SiMe_3)$] where two germanium possess a single bond (it is basically two gerymylene units connected by the single bond). On the addition of H_2 in the solid compound at room temperature, instantly, it reacts to give germanium hydride **1.63** $L^1Ge-eH_2L^1$, whereas in solution state reaction requires $-20\text{ }^\circ\text{C}$ temperature. Interestingly by the addition of more equivalent H_2 , it did not lead to a digermane compound.⁵⁷



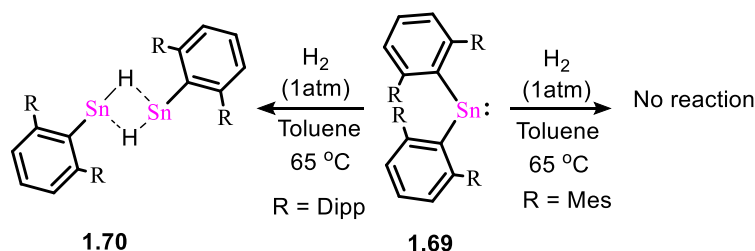
Scheme 1.5 H₂ activation at distannyne.

Similarly distannyne **1.64** [$L^2Sn-SnL^2$ ($L^2 = N(2,6-(C(H)Ph_2)-4MeC_6H_2)(Si^iPr_3)$)] the tin analog of **1.62** in solution state at room temperature activate the H₂, the reaction is sluggish for Sn compare to Ge analog giving 70% yield of $L^2Sn(\mu-H)_2SnL^2$ hydride bridged distannyne **1.65** after 24 hours.⁵⁸



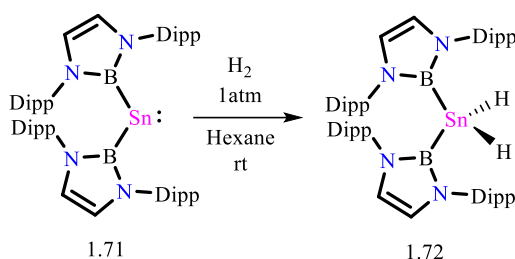
Scheme 1.6 H₂ activation at aryl substituted germylene.

In 2009, Power and co-workers achieved the dihydrogen activation with bulky divalent di-coordinated germylene **1.66**. The bulk of the ligand play a crucial role in product formation during dihydrogen activation. The germylene $:GeAr^{Mes}_2$ ($Ar^{Mes} = 2,6-(2,4,6-Me_3C_6H_2)_2C_6H_3$), when allowed to react with H₂, afforded the respective germane product **1.67**, however the sterically encumbered $:GeAr^{Dipp}_2$ afforded the trihydro germane **1.68** as product with one free HAr^{Dipp} . To elucidate the formation of respective germane products, the theoretical calculation suggests the interaction of σ orbital with the empty orbital of germylene with a simultaneous back donation from lone pair of germylene to σ* orbital of H₂. In the case of bulky Ar^{Dipp} ligand, the strain causes the elimination of HAr^{Dipp} with the formation of tri-hydro germane **1.68**.⁵⁹



Scheme 1.7 H₂ activation at diaryl substituted stannylene.

Analogous to germylene, the divalent, di-coordinated stannylenes **1.69** react with H₂ however, the reaction does not work for :SnAr^{Mes}₂ even after heating up to 70 °C. In the case of :SnAr^{Dipp}₂, more sterically crowded stannylene, it readily reacts with H₂. Unlike analogous germylene, the product observed was divalent hydride bridged stannylene **1.70**, along with the formation of free arene. The reactivity difference is ascribed to the lower energy separation between frontier orbitals of substituted stannylenes.⁶⁰

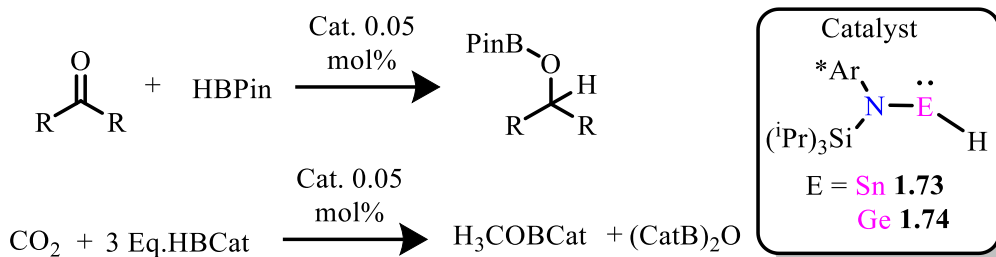


Scheme 1.8 H₂ activation at diboryl substituted Stannylene.

In the case of tetrylenes, ligand attached to central atom play crucial role in deciding the reactivity. The electron-withdrawing ligands has more contribution of *p* orbital from the central atom, results in more *s*-electron character of lone pair orbital. Whereas in the case of electron-rich ligands, a smaller gap in frontier orbitals.⁶¹ It is exemplified by the example where the reaction of bis(boryl)stannylene **1.71** [:Sn(B(N(Dipp)CH₂=))₂]₁ with 1atm H₂ at room temperature, yielded the product **1.72** H₂Sn(B(N(Dipp)CH₂=))₂ after oxidative addition. Here the boryl ligand is highly electron-donating/ σ -donating ligand, which ease the cleavage of H₂.⁶²

1.3.1.3 Tetrylenes in Catalysis (Neutral and Cationic)

In recent years, the transition metal-free catalysis have made vast progress. At the same time the main group elements are also getting attention due to cheap and wide availability in the earth crust. However, very few examples are reported till date, where a low valent main group center is used as a single site catalyst. Only the catalysis using FLP has got much attention and studied carefully as a catalyst in organic transformations.⁶³ The review by Philip Power brings forth the ability of low valent main group elements to mimic the transition metals in the activation of small molecules. Heavier carbene analogs of group 14 are ambiphilic in nature and consist of a lone pair of orbital and empty *p*-orbital. These properties allow them to choose them as a potential catalyst which can mimic the transition metal complexes.⁶⁴



Scheme 1.9 catalysis by hydrosstannylene **1.73** and hydrogermylene **1.74**.

In 2014, Jones and co-workers for the first time used the bulky amidostannylene hydride **1.73** [L^1SnH] and amidogermylene hydride **1.74** (L^1GeH) [$\text{L}^1 = \text{N}(2,6\text{-}(\text{C}(\text{H})\text{Ph}_2)\text{-}4\text{MeC}_6\text{H}_2)(\text{SiMe}_3)$] as a catalyst for hydroboration of unactivated and bulky carbonyl compounds.⁶⁵ This catalyst was as efficient as other transition metal catalysts reported for hydroboration reaction. Later they also used this coordinated, divalent L^1GeH **1.74** and L^1SnH **1.73** as a single-site catalyst system for efficient reduction of carbon dioxide to methanol using secondary borane as hydrogen source.⁶⁶

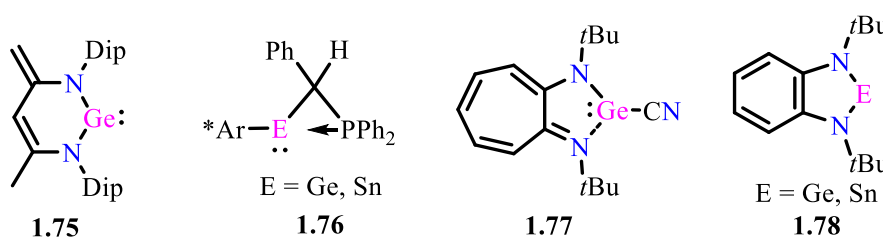
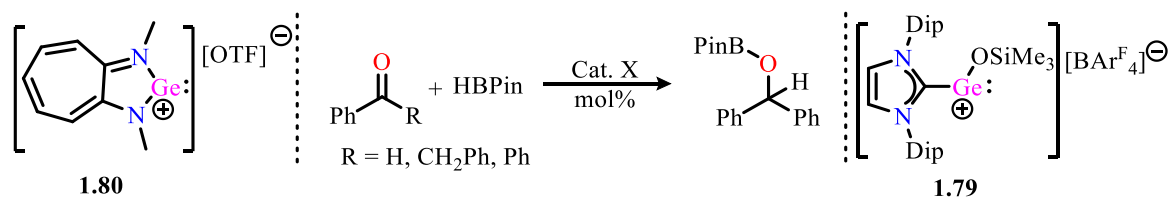


Chart 1.7 Reported germylene and stannylene catalyst.

1.75 to **1.78** are the examples of germylene and stannylene used as catalysts for hydroboration and cyanosilylation reactions of carbonyl compounds reported in the literature in recent years.⁶⁷ Considering the higher Lewis acidity of cationic counterpart, the germylene cations are employed as catalysts for the hydroboration of aldehydes and ketones. In 2018, Rivard and co-workers used NHC stabilized germanium monocation **1.79** [$\text{IPr}.\text{Ge}(\text{OSiMe}_3)_3$]⁺ as a catalyst for hydroboration of sterically hindered ketone. The enhanced Lewis acidity at germanium center due to cationic nature efficiently catalyzes the reaction at the ambient condition with 10 mol% of the catalyst.⁶⁸

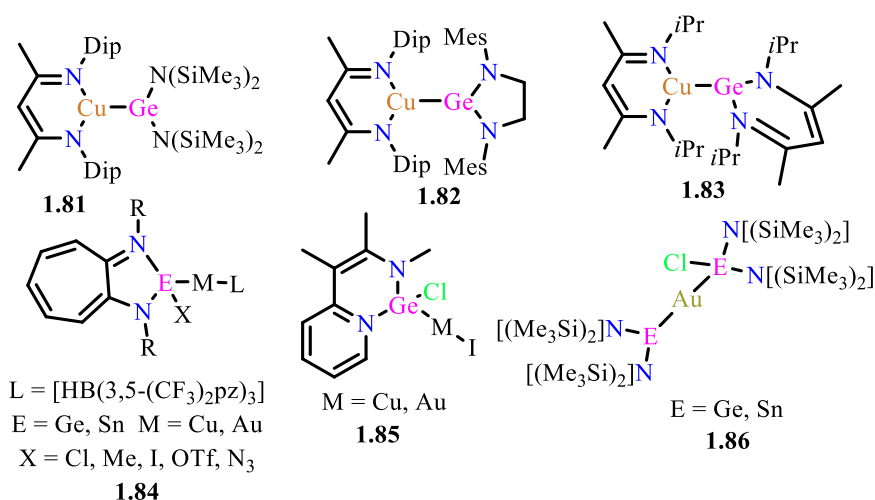


Scheme 1.10 Catalysis by cationic germylenes **1.79** & **1.80**.

Similarly, the Nagendran and co-workers reported the Ge(II) cation [(ATP)Ge]⁺ and Sn(II) cation [(ATP)Sn]⁺ **1.80** catalyzed hydroboration of ketones and aldehydes. Mechanism involves the coordination of carbonyl compound to Lewis acidic germanium cation, followed by the addition of H-BPin bond to carbonyl compound.⁶⁹

1.3.1.4 Coinage Metal Complexes of Germylene and Stannylene

N-heterocyclic carbenes are widely used as ligands in the main group and transition metal chemistry owing to their strong donor properties.⁷⁰ The donor-acceptor properties of NHCs are also easily tuneable according to requirement, and a wide library of NHCs are reported to date with different features.⁷¹ The Metal-complexes of NHCs have numerous applications in chemistry. Mostly they are used in catalysis. In contrast, the heavier carbene analogs (HCAs) of group 14 elements are rarely used despite their unique donor-acceptor properties. Although, the heavier analogs of carbenes are used as a ligand in transition metal complexes for last 45 years, the instability of these complexes has hampered the development of this field. In particular, the heavier carbene-coinage metal complexes are rarely reported due to their high instability and difficulty in synthesis. When these carbene analogs are allowed to react with coinage metal halides, they have the propensity to go insertion in TM-Cl bond.⁷² The HCAs are also known to undergo ligand exchange reaction with metal halides and or in some cases, the redox reaction occurs, which generate oxidized product.⁷³

**Chart 1.8** Selective examples of germylene/stannylene-group 11 metal complexes.

The first germanium-group 11 metal complex was synthesized in the way back to 1962 by Glockeling and Hooten by metathesis reaction of triphenylgermyl lithium and group 11 halo

salt.⁷⁴ In contrast, the stannyl complex was obtained by reaction of SnCl₂ with group 11 halo salt, which gave the insertion of stannylene into M-Cl bond.⁷⁵ In the recent examples, the Lappert's diamino-germylene **1.81** and saturated N-heterocyclic germylene **1.82** was shown to coordinate to Cu(I) complex stabilized in β-diketiminato ligand.⁷⁶ Mochida and co-worker reported the Cu-Ge complex **1.83**, where both metals stabilized in separate β-diketiminato ligand.⁷⁷ Dias and co-workers used aminotropionate ligand stabilized germylene, which shown coordination with copper (I) and silver (I) salts **1.84** [78]. Pyridyl-1-azaallyl stabilized germanium (I) chloride was coordinate with copper and gold **1.85**.⁷⁹ The base stabilized divalent gold complex was obtained very recently, where amidinatogermylene coordinate to gold (I) atom **1.86**.⁸⁰

There is only fingerpicked cationic digermylene-group 11 complex reported in the literature, and only one distannylene-Ag cationic complex reported so far. The cationic tetrylene group 11 complex can be synthesized by two ways, i) using neutral tetrylene stabilizing cationic group 11 metal center and ii) using cationic tetrylene stabilizing cationic/neutral group 11 metal center. In 2015, Cabeza and co-workers synthesized the cationic complex of silver by two neutral amidinatogermylene units [L(*t*Bu)Ge-Ag-Ge(*t*Bu)L]⁺ (L = PhC(N*t*Bu)₂). This complex was characterized structurally by SC-XRD whereas the Cu-digermylene cationic complex [L(*t*Bu)Ge-Cu-Ge(*t*Bu)L]⁺ (L = PhC(N*t*Bu)₂) was characterized by NMR only.⁸¹ The stannylene analog of these complex was reported very recently by Khan and co-workers where two stannylenes donated electron density to silver cation.⁸² The Sn-Ag-Sn bond is deviating from linearity and shows the coordination of counteranion SbF₆⁻ with Ag.

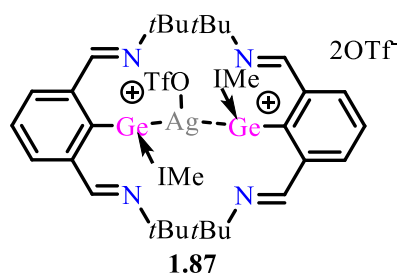


Chart 1.10 Bis(germyliumlylidene)silver(I) complex **1.87**.

Recently, So and co-workers isolated dicationic Bis(germyliumlylidene)silver(I) complex **1.87**, where the silver is coordinated by two cationic germylenes (Germyliumlylidene). The reaction of 2,6-bis(imino)pyridinephénylgermylene chloride with 3 Eq. of silver triflate followed by the addition of 2 equivalents of IMe carbene [:CN₂C₂(Me₄)] resulted in the complex **1.93** as a sole product.⁸³

1.4 Organocatalysis

Organocatalyst is the small organic molecule that accelerates the chemical reaction by the addition of substoichiometric quantity. They have certain advantages, like less toxic or non-toxic, less pollution causing, economically readily available, and more benign. This field has seen tremendous interest over the past few years, resulting due to conceptual novelty and efficiency, and selectivity of organocatalytic reaction meets the standards of organic reaction.⁸⁴ Organocatalysis is known long back in organic chemistry, but in the past few years, its use in enantioselective catalysis has emerged. There are several reviews that gave detailed information about the reported organocatalyst.⁸⁵

Several organic molecules are used as organocatalysts, depending on their properties. The carbenes were found to be exceptional ligands for transition metals; they were also excellent organocatalysts in organic chemistry. The divalent carbon center in neutral carbene possesses six valence electrons. The most well-known application of NHC as organocatalyst is found in benzoin condensation, where NHCs change the polarity of aldehyde molecule. Which generate the acyl anion equivalent and adds to another equivalent of aldehyde⁸⁶ or alkene (Stetter reaction)⁸⁷ to yield the product. There are several other catalytic transformations⁸⁸ achieved using NHC catalyst which are mentioned in figure 1.6.

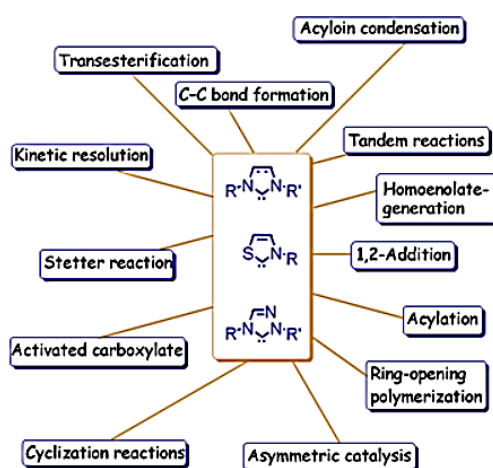
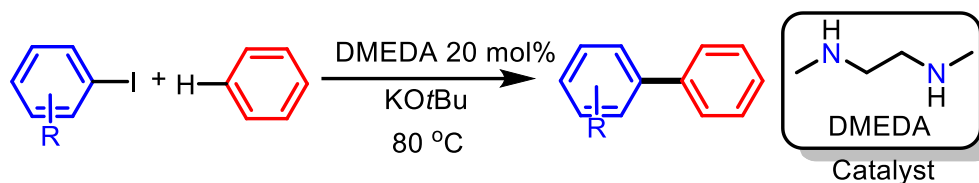


Figure 1.6 NHC catalyzed reported organic transformations.

1.4.1 Transition-metal-free C-C Bond Formation Reaction

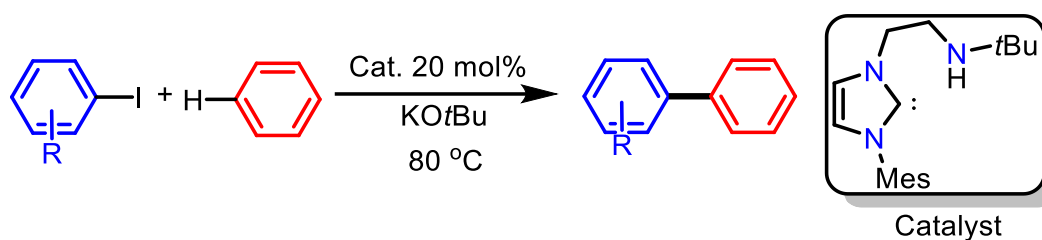
Transition metal-free C-C bond formation reactions can be performed catalytically (Organocatalytic), or they may require a stoichiometric amount of organic/inorganic additive. Until 2010, there was no organocatalytic protocol of synthesizing biaryls via direct C-H arylation of unactivated benzene. Lei and co-workers used catalytic amount of N,N-

Dimethylethylenediamine for direct C-H arylation of unactivated Benzene with potassium tert-butoxide as a base.⁸⁹ The DMEDA coordinates to potassium ion and helps in electron transfer.



Scheme 1.11 DMEDA catalysed C-H arylation reactions.

In 2016, amino linked N-Heterocyclic carbene was used as a catalyst for similar coupling reactions reported by Cheng and Ong. Carbenes with tethered amino groups only serve as a good catalysts.⁹⁰ Several other organic molecules which have binding sites were used catalytically in the intramolecular and intermolecular coupling reactions of unactivated arenes.⁹¹

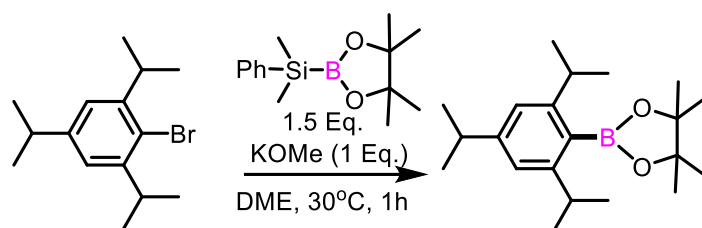


Scheme 1.12 NHC catalyzed C-H arylation reaction.

1.4.2 Transition-metal-free C-B Bond Formation Reaction

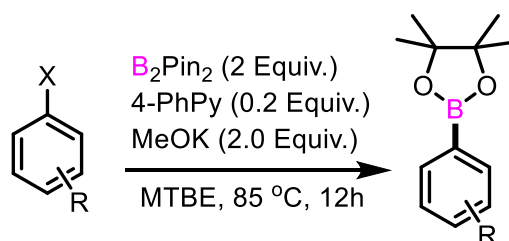
Aryl boronate esters are highly demanding substrate in chemical synthesis, owing to their utility in Suzuki-Miyaura coupling⁹² or Chan-Lam reactions.⁹³ They also have biological applications in medicinal chemistry, and nowadays, they are being utilized in drug discovery.⁹⁴ Non-toxic nature, good functional group tolerance are some of the characteristics of these aryl boronates, which are uncommon in other organometallic reagents, made them special reagent in organic chemistry. Due to these properties, their efficient synthetic routes are highly sought after in chemistry. The synthetic routes involve the nucleophilic attack of an organometallic reagent to boron electrophiles, which gives highly undesired side-products and not followed.⁹⁵ Ishiyama and co-workers in 1995, developed Pd catalyzed synthetic method of aryl boronates from aryl halides.⁹⁶ Since these early reports, developments occurred in the synthetic methods and which were not limited to expensive Pd catalyst.⁹⁷ Although the development of efficient protocols for metal-catalyzed aryl borylation, the strong desire of metal-free synthesis, particularly in the area of pharmaceutical compounds where transition metal contaminants are

highly undesirable, metal-free methods are developed. Yamamoto and co-workers developed transition-metal-free strategy by exploiting unusual reactivity of silylboranes. The reaction found to work at ambient conditions and also has good functional group tolerance.⁹⁸



Scheme 1.13 Borylation of aryl bromide using silylborane reagent.

In the seminal work by König and co-workers, the photocatalytic pathways for deaminative borylation was developed.⁹⁹ Later in 2017, radical borylation was achieved using a catalytic amount of pyridine with potassium methanoate at high temperatures.¹⁰⁰



Scheme 1.14 Metal-free radical borylation of aryl halides.

Scope of the Work

The low valent main group chemistry is catching the attention of chemists due to unique bonding features and extraordinary properties. This dissertation focuses on the fundamental synthesis of main group compounds in low oxidation states and a subsequent investigation into their onwards reactivity. As per the previous discussion, the continuing advancement in this area is, in large part, to the development and exploitation of sophisticated bulky ligands, primarily those that are anionic, however neutral donors such as NHCs have emerged. For stabilization of main group elements, we have chosen neutral N-donor ligands, whose synthesis just involves the condensation reaction. The rigidity of two iminopyridine framework and flexibility due to -CH₂-CH₂- linker allows the bidentate as well as the tetradentate mode of the ligand. This ligand mostly used with transition metals however, it is hardly used in main group chemistry

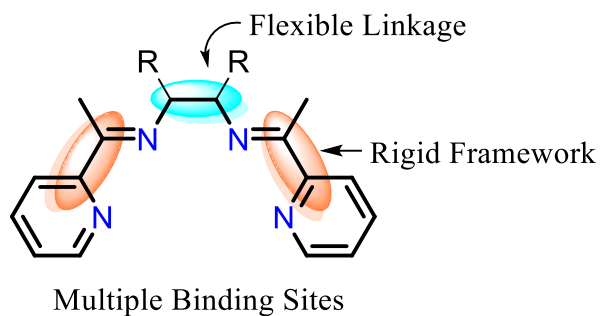


Figure 1.6 Neutral N-Donor bis(α -iminopyridine) ligand.

The Organo-main-group compounds have much polar bonds which can be cleaved easily by weaker nucleophile to generate the electron donor species, such strategies are lacking. We have focused on strategies that involve the use of such organo-main-group compounds in organic synthesis.

Objectives and scope of Projects

➤ **Stabilization and Application of Stannylenes and Stannylium Cations**

Generally, the stannylenes are synthesized by salt metathesis reaction of SnCl_2 and organometallic reagent, which encounter a problem of over reduction at the tin center. Another way is the transamination reaction or ene-enamine stannylene formation from amines or imine ligand, but this reaction gives unusual products depending on the stoichiometry or the reaction condition. We have used a similar route to obtain unusual and electron-rich stannylenes, which were further utilized in complex formation. This adds new ligands to the library of group 14 metallylenes. Also, the observed homo-coupled alkene fragment of the ligand in stannylene synthesis was tried to explain by appropriate mechanism, and this will be undoubtedly helpful in understanding the importance of main group element in such kind of unusual coupling reaction.

➤ **Isolation and Application of Dicationic Ge(II) Compounds**

There are very few examples reported where cationic germanium (II) stabilized in neutral donor ligands. Even though having a lone pair of an electron with these cationic germylenes, their reactivity study was not performed except a few examples. In this study, we have focused on the isolation of Ge(II) dication, which will have stereochemically active lone pair. We have further utilized these nucleophiles for complex formation with transition metals. Metal-free reduction of germanium bismonocation was also performed to get hitherto unknown substituted stereoselective Piperazine molecule with appropriate mechanistic details. This study certainly brings

forth the new group 14 cationic compounds as ligands, which will enhance the Lewis acidity of the metal center. More to this, the study also helps in understanding the role of main group elements in decreasing the reduction potential of imines and their subsequent reductive coupling to stereoselective products.

➤ **Organo-main-group Compound Promoted C-B and C-C Bond Formation**

The C-C and C-B bond formation reaction are mostly catalyzed by transition metals. In recent time transition metal-free approaches are discovered, but these reactions require a higher temperature and lack the mechanistic details which hamper the development of this field. In this study, we have tried to utilize organo-main-group compound as an additive for C-C and C-B bond formation reactions. The wide substrate scope and relatively mild reaction conditions increase the applicability of reaction. The proper mechanistic study is important to understand the role of an additive compound, which was controversial. These studies can also stem the interest of chemists in search of new organo-main-group compounds for organic transformation.

1.5 References

1. (a) Henderson, W. *Main Group Chemistry*; Abel, E. W. Ed.; Royal Society of Chemistry: Cambridge, 2000; Vol. 3; (b) Massey, A. G. *Main Group Chemistry*; 2nd ed.; WILEY-VCH, 2000; (c) *Modern Aspects of Main Group Chemistry*; Lattman, M.; Kemp, R. A., Eds.; ACS Symposium Series; American Chemical Society: Washington, DC, 2005; Vol. 917, p. 484.
2. (a) Laszlo, P. *Angew. Chem. Int. Ed.* **2000**, *39*, 2071; (b) Sträter, N. *Angew. Chem. Int. Ed.* **2011**, *50*, 7730.
3. Pauling, L. *The Nature of the Chemical Bond and the Structure of Molecules and Crystals*; Cornell University Press: New York, 1939; p. 644.
4. Kagan, H. B. *Angew. Chem. Int. Ed.* **2012**, *51*, 7376.
5. (a) Wittig, G. *Angew. Chem.* **1980**, *92*, 671; (b) Brown, H. C. *Angew. Chem.* **1980**, *92*, 675.
6. (a) Appl, M. Ammonia. *Ullmann's Encyclopedia of Industrial Chemistry*; Wiley-VCH Verlag GmbH & Co. KGaA: Weinheim, Germany, 2006; (b) Smil, V. *Nature* **1999**, *400*, 415.
7. *Handbook of Transition Metal Polymerization Catalysts*; Hoff, R.; Mathers, R. T., Eds.; John Wiley & Sons, Inc., 2010; p. 575
8. For a representative compounds list, see: (a) Bradley, D. C.; Chisholm, M. H. *Acc. Chem. Res.* **1976**, *9*, 273; (b) Fisher, K. J.; Bradley, D. C. *J. Am. Chem. Soc.* **1971**, *93*, 2058; (c) Lappert, M. F.; Pedley, J. B.; Sharp, G. J.; Bradley, D. C. *J. Chem. Soc. Dalton Trans.* **1976**, 1737; (d) Bradley, D. C.; Hursthouse, M. B.; Rodesiler, P. F. *J. Chem. Soc. D Chem. Commun.* **1969**, 14; (e) Bradley, D. C.; Hursthouse, M. B.; Smallwood, R. J.; Welch, A. J. *J. Chem. Soc. Chem. Commun.* **1972**, 872; (f) Alyea, E. C.; Bradley, D. C.; Copperthwaite, R. G. *J. Chem. Soc. Dalton Trans.* **1972**, 1580; (g) Alyea, E. C.; Bradley, D. C.; Lappert, M. F.; Sanger, A. R. *J. Chem. Soc. D Chem. Commun.* **1969**, 1064; (h) Alyea, E. C.; Basi, J. S.; Bradley, D. C.; Chisholm, M. H. *Chem. Commun.* **1968**, 495.
9. Cotton, J. D.; Davidson, P. J.; Leppert, M. F. *J. Chem. Soc. Dalton Trans.* **1976**, 2275.
10. West, R.; Fink, M. J.; Michl, J. *Science* **1981**, *214*, 1343.
11. Yoshifuji, M.; Shima, I.; Inamoto, N.; Hirotsu, K.; Higuchi, T. *J. Am. Chem. Soc.* **1981**, *103*, 4587.
12. (a) Power, P. P. *Chem. Rev.* **1999**, *99*, 3463; (b) Fischer, R. C.; Power, P. P. *Chem. Rev.* **2010**, *110*, 3877; (c) Rivard, E.; Power, P. P. *Inorg. Chem.* **2007**, *46*, 10047.
13. Arduengo, A. J.; Harlow, R. L.; Kline, M. *J. Am. Chem. Soc.*, **1991**, *113*, 361.

-
14. (a) *N-Heterocyclic Carbenes in Synthesis*; Nolan, S. P., Ed.; John Wiley and Sons, Inc.: New York and Oxford, 2006; p. 319; (b) *N-Heterocyclic Carbenes in Transition Metal Catalysis and Organocatalysis*; Cazin, C. S. J., Ed.; Catalysis by Metal Complexes; Springer, 2011; p. 340; (c) *N-Heterocyclic Carbenes*; Diez-Gonzalez, S., Ed.; Royal Society of Chemistry: Cambridge, 2011; p. 422
 15. Grubbs, R. H. *Angew. Chem. Int. Ed.* **2006**, *45*, 3760.
 16. Enders, D.; Niemeier, O.; Henseler, A. *Chem. Rev.* **2007**, *107*, 5606.
 17. Lavallo, V.; Canac, Y.; Präsang, C.; Donnadiou, B.; Bertrand, G. *Angew. Chem. Int. Ed.* **2005**, *44*, 5705; (b) Lavallo, V.; Canac, Y.; DeHope, A.; Donnadiou, B.; Bertrand, G. *Angew. Chem. Int. Ed.* **2005**, *44*, 7236.
 18. (a) Nestorov, V.; Reiter, D.; Bag, P.; Frisch, P.; Holzner, R.; Porzelt, A.; Inoue, S. *Chem. Rev.* **2018**, *118*, 9678. (b) Melaimi, M.; Jazzar, R.; Soleilhavoup, M.; Bertrand, G. *Angew. Chem. Int. Ed.* **2017**, *56*, 10046.
 19. (a) Protchenko, A. V.; Birjkumar, K. H.; Dange, D.; Schwarz, A. D.; Vidovic, D.; Jones, C.; Kaltsoyannis, N.; Mountford, P.; Aldridge, S. *J. Am. Chem. Soc.* **2012**, *134*, 6500; (b) Protchenko, A. V.; Dange, D.; Harmer, J. R.; Tang, C. Y.; Schwarz, A. D.; Kelly, M. J.; Phillips, N.; Tirfoin, R.; Birjkumar, K. H.; Jones, C.; Kaltsoyannis, N.; Mountford, P.; Aldridge, S. *Nat. Chem.* **2014**, *6*, 315; (c) Saleh, L. M. A.; Birjkumar, K. H.; Protchenko, A. V.; Schwarz, A. D.; Aldridge, S.; Jones, C.; Kaltsoyannis, N.; Mountford, P. *J. Am. Chem. Soc.* **2011**, *133*, 3836.
 20. (a) Caputo, C. A.; Brazeau, A. L.; Hynes, Z.; Price, J. T.; Tuononen, H. M.; Jones, N. D. *Organometallics* **2009**, *28*, 5261; (b) Abrams, M. B.; Scott, B. L.; Baker, R. T. *Organometallics* **2000**, *19*, 4944; (c) Dube, J. W.; Farrar, G. J.; Norton, E. L.; Szekely, K. L. S.; Cooper, B. F. T.; Macdonald, C. L. B. *Organometallics* **2009**, *28*, 4377.
 21. Assay, M.; Jones, C.; Driess, M. *Chem. Rev.* **2011**, *111*, 354.
 22. Dube, J.; Ragogna, P. *Inorg. Chem.* **2010**, *49*, 8164.
 23. Hadlington, T. J.; Driess, M.; Jones, C. *Chem. Soc. Rev.* **2018**, *47*, 4176.
 24. (a) Jutzi, P.; Hoffmann, H. J.; Brauer, D. J.; Krueger, C. *Angew. Chem.* **1973**, *85*, 1116; (b) Stobart, S. R. *J. Chem. Soc., Chem. Commun.* **1979**, 911.
 25. (a) Harris, D. H.; Lappert, M. F. *J. Chem. Soc., Chem. Commun.* **1974**, 895.
 26. Davidson, P. J.; Harris, D. H.; Lappert, M. F. *J. Chem. Soc. Dalton Trans.* **1977**, 2268.
 27. Veith, M. *Angew. Chem. Int. Ed. Eng.* **1987**, *26*, 1.
-

-
28. (a) Tokitoh, N.; Manmaru, K.; Okazaki, R. *Organometallics* **1994**, *13*, 167; (b) Tokitoh, N.; Matsumoto, T.; Manmaru, K.; Okazaki, R.; *J. Am. Chem. Soc.* **1993**, *115*, 8855; (c) Tokitoh, N.; Kishikawa, K.; Matsumoto, T.; Okazaki, R. *Chem. Lett.*, **1995**, 827.
 29. Kira, M. I.; S.; Iwamoto, T.; Ichinohe, M.; Kabuto, C.; Ignatovich, L.; Sakurai, H. *Chem. Lett.* **1999**, 263.
 30. Driess, M.; Yao, S.; Brym, M.; van Wuelen, C. *Angew. Chem., Int. Ed.* **2006**, *45*, 4349.
 31. (a) Herrmann, W. A.; Denk, M.; Behm, J.; Scherer, W.; Klingan, F.-R.; Bock, H.; Solouki, B.; Wagner, M. *Angew. Chem., Int. Ed. Engl.* **1992**, *31*, 1485; (b) Kuehl, O.; Loennecke, P.; Heinicke, J. *Polyhedron* **2001**, *20*, 2215; (c) Baker, R. J.; Jones, C.; Mills, D. P.; Pierce, G. A.; Waugh, M. *Inorg. Chim. Acta* **2008**, *361*, 427; (d) Raut, R.K.; Amin, S, F.; Sahoo, P.; Kumar, V.; Majumdar, M. *Inorganics* **2018**, *6*, 69.
 32. Jones, C.; Rose, R. P.; Stasch, A. *Dalton Trans.* **2008**, 2871; (g) Foley, S. R.; Bensimon, C.; Richeson, D. S. *J. Am. Chem. Soc.* **1997**, *119*, 10359; (h) Nagendran, S.; Sen, S. S.; Roesky, H. W.; Koley, D.; Grubmüller, H.; Pal, A.; Herbst-Irmer, R. *Organometallics* **2008**, *27*, 5459.
 33. (a) Harris, D. H.; Lappert, M. F. *J. Chem. Soc., Chem. Commun.* **1974**, 895; (b) Davidson, P. J.; Lappert, M. F. *J. Chem. Soc. Chem. Commun.* **1973**, 317.
 34. Kira, M.; Yauchibara, R.; Hirano, R.; Kabuto, C.; Sakurai, H. *J. Am. Chem. Soc.* **1991**, *113*, 7785.
 35. Weidenbruch, M.; Schlaefke, J.; Schafer, A.; Peters, K.; Vonschnering, H. G.; Marsmann, H. *Angew. Chem., Int. Ed. Engl.* **1994**, *33*, 1846.
 36. (a) Yang, X. J.; Wang, Y. Z.; Wei, P. R.; Quillian, B.; Robinson, G. H. *Chem. Commun.* **2006**, 403. (b) Tajima, T.; Takeda, N.; Sasamori, T.; Tokitoh, N. *Organometallics* **2006**, *25*, 3552. (c) Simons, R. S.; Pu, L. H.; Olmstead, M. M.; Power, P. P. *Organometallics* **1997**, *16*, 1920. (d) Spikes, G. H.; Peng, Y.; Fettingner, J. C.; Power, P. P. *Z. Anorg. Allg. Chem.* **2006**, *632*, 1005. (e) Kano, N.; Shibata, K.; Tokitoh, N.; Okazaki, R. *Organometallics* **1999**, *18*, 2999.
 37. Eichler, B. E.; Pu, L. H.; Stender, M.; Power, P. P. *Polyhedron* **2001**, *20*, 551.
 38. Pu, L. H.; Olmstead, M. M.; Power, P. P.; Schiemenz, B. *Organometallics* **1998**, *17*, 5602.
 39. Eichler, B. E.; Power, P. P. *J. Am. Chem. Soc.* **2000**, *122*, 8785.
 40. Mizuhata, Y.; Sasamori, T.; Tokitoh, N. *Chem. Rev.* **2009**, *109*, 3479.
 41. Engesser, T. A.; Lichtenthaler, M. R.; Schleep, M.; Krossing, I. *Chem. Soc. Rev.* **2016**, *45*, 789
-

-
42. Jutzi, P.; Kohl, F.; Hofmann, P.; Krüger, C.; Tsay, Y.-H. *Chem. Ber.* **1980**, *113*, 757.
 43. (a) Kohl, F. X.; Dickbreder, R.; Jutzi, P.; Müller, G.; Huber, B. *J. Organomet. Chem.* **1986**, *309*, C43; (b) Kohl, F. X.; Dickbreder, R.; Jutzi, P.; Müller, G.; Huber, B. *Chem. Ber.* **1989**, *122*, 871.
 44. Reger, D. L.; Coan, P. S. *Inorg. Chem.* **1996**, *35*, 258.
 45. (a) Dias, H. V. R.; Wang, Z. *J. Am. Chem. Soc.* **1997**, *119*, 4650; (b) Dias, H. V. R.; Jin, W. *J. Am. Chem. Soc.* **1996**, *118*, 9123.
 46. Probst, T.; Steigelmann, O.; Riede, J.; Schmidbaur, H. *Angew. Chem., Int. Ed. Engl.* **1990**, *29*, 1397.
 47. Singh, A. P.; Roesky, H. W.; Carl, E.; Stalke, D.; Demers, J.-P. Lange, A. *J. Am. Chem. Soc.* **2012**, *134*, 4998.
 48. Rupar, P. A.; Staroverov, V. N.; Ragogna, P. J.; Baines, K. M. *J. Am. Chem. Soc.* **2007**, *129*, 15138.
 49. Xiong, Y.; Szilvási, T.; Yao, S.; Tan, G.; Driess, M. *J. Am. Chem. Soc.* **2014**, *136*, 11300.
 50. (a) Rupar, P. A.; Staroverov, V. N.; Baines, K. M. *Science*, **2008**, *322*, 1360; (b) Macdonald, C. L. B.; Bandyopadhyay, R.; Cooper, B. F. T.; Friedl, W. W.; Rossini, A. J.; Schurko, R. W.; Eichhorn, S. H.; Herber, R. H. *J. Am. Chem. Soc.* **2012**, *134*, 4332; (c) Avery, J. C.; Hanson, M. A.; Herber, R. H.; Bladec, K. J.; Rupar, P. A.; Nowik, I.; Huang, Y.; Baines, K. M. *Inorg. Chem.*, **2012**, *51*, 7306.
 51. (a) Swamy V.S.V.S.N.; Pal, S.; Khan, S.; Sen, S. S. *Dalton. Trans.* 2015, *44*, 12903; (b) Engesser, T. A.; Lichtenthaler, M. R.; Schleep, M.; Krossing, I. *Chem. Soc. Rev.* **2016**, *45*, 789.
 52. Spikes, G. H.; Fettingner, J. C.; Power, P. P.; *J. Am. Chem. Soc.* **2005**, *127*, 12231.
 53. Welch, G. C.; San Juan, R. R.; Masuda, J. S.; Stephan, D. W. *Science* **2006**, *314*, 1124.
 54. Frey, G. D.; Lavallo, V.; Donnadiou, B.; Schoeller, W. W.; Bertrand, G. *Science* **2007**, *316*, 439.
 55. Lagare, M.-A.; Belanger-Chabot, G.; Dewhurst, R. D.; Welz, Li.; Krummenacher, I.; Engels, B.; Braunschweig, H. *Science*, **2018**, *359*, 896.
 56. Planas, O.; Wang, F.; Leutzsch, M.; Cornella, J. *Science* **2020**, *367*, 313.
 57. Li, J.; Schenk, C.; Goedecke, C.; Frenking, G.; Jones, C. *J. Am. Chem. Soc.* **2011**, *133*, 18622.
 58. (a) Hadlington, T. J.; Hermann, M.; Li, J.; Frenking, G.; Jones, C. *Angew. Chem. Int. Ed.* **2013**, *52*, 10199; (b) Hadlington, T. J.; Jones, C. *Chem. Comm.* **2014**, *50*, 2321.
-

-
59. Peng, Y.; Guo, J.-D.; Ellis, B. D.; Zhu, Z.; Fettinger, J. C.; Nagase, S.; Power, P. P. *J. Am. Chem. Soc.* **2009**, *131*, 16272.
 60. Peng, Y.; Ellis, B. D.; Wang, X.; Power, P. P. *J. Am. Chem. Soc.* **2008**, *130*, 12268.
 61. Wilfing, P.; Schittelkopf, K.; Flock, M.; Herber, R. H.; Power, P.P.; Ficher, R.C. *Organometallics* **2015**, *34*, 2222.
 62. Protchenko, A.V.; Bates, J.I.; Saleh, L. M. A.; Blake, M. P.; Schwarz, A.D.; Kolychev, E.L.; Thompson, A.L.; Jones, C.; Mountford, P.; Aldridge, S. *J. Am. Chem. Soc.* **2016**, *138*, 4555.
 63. (a) Stephan, D. W. *Acc. Chem. Soc.* **2015**, *48*, 306; (b) Stephan, D. W.; Erker, G. *Angew. Chem. Int. Ed.* **2010**, *49*, 46; (c) Berkefeld, A.; Peirs, W. E.; Parvez, M. *J. Am. Chem. Soc.* **2010**, *132*, 10660.
 64. Power, P. P. *Nature* **2010**, *463*, 171.
 65. Hadlington, T. J.; Hermann, M.; Frenking, G.; Jones, C. *J. Am. Chem. Soc.* **2014**, *136*, 3028.
 66. Hadlington, T. J.; Kefalidis, C. E.; Maron, L.; Jones, C. *ACS Catal.* **2017**, *7*, 1853.
 67. (a) Wu, Y.; Shan, C.; Sun, Y.; Chen, P.; Ying, J.; Zhu, J.; Liu, L. L.; Zhao, Y. *Chem. Comm.* **2016**, *52*, 13799; (b) Schneider, J.; Sindlinger, C.-P.; Freitag, S.-M.; Schubert, H.; Wesemann, L. *Angew. Chem. Int. Ed.* **2017**, *56*, 333; (c) Siwatch, R. K.; Nagendran, S. *Chem. -Eur. J.* **2014**, *20*, 13551; (c) Dasgupta, R.; Das, S.; Hiwase, S.; Pati, S. K.; Khan, S. *Organometallics*, **2019**, *38*, 1429.
 68. Roy, M. M. D.; Fujimori, S.; Ferguson M. J.; McDonald, R.; Tokitoh, N.; Rivard, E. *Chem. -Eur. J.* **2018**, *24*, 14392.
 69. (a) Sinhababu, S.; Singh, D.; Sharma, M. K.; Siwatch, R. K., Mahawar, P.; Nagendran, S. *Dalton. Trans.* **2015**, *48*, 4094; (b) Sharma, M. K.; Ansari, M.; Mahawar, P.; Rajaram, G.; Nagendran, S. *Dalton. Trans.* **2019**, *48*, 664.
 70. (a) Nesterov, V.; Reiter, D.; Bad, P.; Frisch, P.; Holzner, R.; Porzelt, A.; Inoue, S. *Chem. Rev.* **2018**, *118*, 9678; (b) *N-heterocyclic Carbene in Transition metal Catalysis*; Springer: Berlin Heidelberg, New York, 2007, Vol.2.
 71. (a) *N-heterocyclic Carbene in Transition Metal Catalysis and organocatalysis*; Springer: Berlin Heidelberg, New York, 2011, Vol. 32; (b) Peris, E. *Chem. Rev.* **2018**, *118*, 9988.
 72. (a) Veith, M.; Stahl, L.; Huch, V. *Inorg. Chem.* **1989**, *28*, 3280; (b) Hawkins, S. M.; Hitchcock, P. B.; Lappert, M. F. *J. Chem. Soc., Chem. Commun.* **1985**, 1592.
-

-
73. (a) Wrackmeyer, B.; Weidinger, J.; Milius, W. *Z. Anorg. Allg. Chem.*, **1998**, 624, 98; (b) Hitchcock, P. B.; Lappert, M. F.; Pierssens, L. J.-M. *Chem. Commun.* **1996**, 1189; (c) Veith, M.; Grosser, M.; Huch, V. *Z. Anorg. Allg. Chem.*, **1984**, 513, 89.
74. Glockling, F.; Hooton, K. A. *J. Chem. Soc.* **1962**, 2658.
75. Dilts, J. A.; Johnson, M. P. *Inorg. Chem.* **1966**, 5, 2079.
76. York, J. T.; Young, V. G.; Tolman, W. B. *Inorg. Chem.* **2006**, 45, 4191.
77. Arai, H.; Nakadate, F.; Mochida, K. *Organometallics* **2009**, 28, 4909.
78. (a) Dias, H. V. R.; Wang, X.; Diyabalange, H. *Inorg. Chem.* **2005**, 44, 7322. (b) Dias, H. V. R.; Ayers, A. E. *Polyhedron* **2002**, 21, 611. (c) Ayers, A. E.; Dias, H. V. R. *Inorg. Chem.* **2002**, 3259. (d) Dias, H. V. R.; Wang, Z. *Inorg. Chem.* **2000**, 39, 3890.
79. Leung, W.-P.; So, C.-W.; Chong, K.-H.; Kan, K.-W.; Chan, H.-S.; Mak, T. *Organometallics* **2006**, 25, 2851.
80. Cabeza, J. A.; Fernandez-Colinas, J. M.; Garcia-Alvarez, P.; Polo, D. *Inorg. Chem.* **2012**, 51, 3896.
81. Alvarez-Rodriguez, L.; Cabeza, J. A.; Garcia-Alvarez, P.; Polo, D. *Organometallics* **2015**, 34, 5479.
82. Parvin, N.; Dasgupta, R.; Pal, S.; Sen, S. S.; Khan, S. *Dalton. Trans.* **2017**, 46, 6528.
83. Seow, C.; Ismail, B. L. B.; Xi, H.-W.; Lim, K.-H.; So, C.-W. *Organometallics* **2017**, 37, 1368.
84. (a) Dalko, P. I.; Moisan, L. *Angew. Chem. Int. Ed.* **2004**, 43, 5138; (b) Oliviera, V. G.; Cardoso, M. F. C.; Forezi, L. S. M. *Catalysts* **2018**, 8, 605.
85. (a) Chen, D.-F.; Han, Z.-Y.; Zhou, X.-L.; Gong, L.-Z. *Acc. Chem. Res.* **2014**, 7, 2365; (b) Volla, C. M. R.; Atodiresei, I.; Rueping, M. *Chem. Rev.* **2014**, 114, 2390; (c) Kiesewetter, M. K.; Shin, E. J.; Hedrik, J. L.; Waymouth, R. M. *Macromolecules* **2010**, 43, 2093; (d) Special issue of *Chem. Rev.* **2007**, 107, Nr. 12.
86. Menon, R. S.; Biju, A. T.; Nair, V. *Beilstein J. Org. Chem.* **2016**, 12, 444.
87. Stetter, H. *Angew. Chem. Int. Ed.* **1976**, 15, 639.
88. (a) Marion, N.; Diez-Gonzalez, S.; Nolan, S. P. *Angew. Chem. Int. Ed.* **2007**, 46, 2988; (b) Enders, D.; Niemeter, O.; Henseler, A. *Chem. Rev.* **2007**, 107, 5606; (c) Izquierdo, J.; Hutson, G.; Cohen, D. T.; Scheidt, K. A. *Angew. Chem. Int. Ed.* **2012**, 51, 11686; (d) Flanigen, D. M.; Romanov-Michailidis, F.; White, N. A.; Rovis, T. *Chem. Rev.* **2015**, 115, 9307.
89. Liu, W.; Cao, H.; Chang, H.; Ching, K. H.; He, C.; Kwong, F. Y.; Lei, A. *J. Am. Chem. Soc.* **2010**, 132, 16737.
-

-
90. Chen, W.-C.; Hsu, Y. -C.; Shih, W.-C.; Lee, C. -Y.; Chaung, W. H.; Tsai, Y. F.; Chen, P. -Y.; Ong, T. -G. *Chem. Commun.* **2012**, *48*, 6702.
 91. Sun, C-L.; Shi, Z-J. *Chem. Rev.* **2014**, *114*, 9219.
 92. Miyaura, N.; Suzuli, A. *Chem. Rev.* **1995**, *95*, 2457.
 93. Chan, D.; Monaco, K.; Li, R.; Bonne, D.; Clark, C.; Lam, P. *Tetrahedron Lett.* **2003**, *44*, 3863.
 94. (a) Ban, S. H.; Nakamura, H. *Chem. Rec.* **2015**, *15*, 616; (b) Diaz, D. B.; Yudin, A. K. *Nat. Chem.* **2017**, *9*, 731.
 95. Neeve, E. C.; Geier, S. J.; Mkhaliid, I. A. I.; Westcott, S. A.; Marder, T. B. *Chem. Rev.* **2016**, *116*, 9091.
 96. Ishiyama, T., Murata, M., and Miyaura, M. *J. Org. Chem.* **1995**, *60*, 7508.
 97. Murata, M. *Heterocycles* **2012**, *85*, 1795.
 98. Yamamoto, E.; Izumi, K.; Horita, Y.; Ito, H. *J. Am. Chem. Soc.* **2012**, *134*, 19997.
 99. Hari, D. P.; Schroll, P.; König, B. *J. Am. Chem. Soc.* **2012**, *134*, 2958.
 100. Zhang, L.; Jiao, L. *J. Am. Chem. Soc.* **2017**, *139*, 607.

Chapter 2

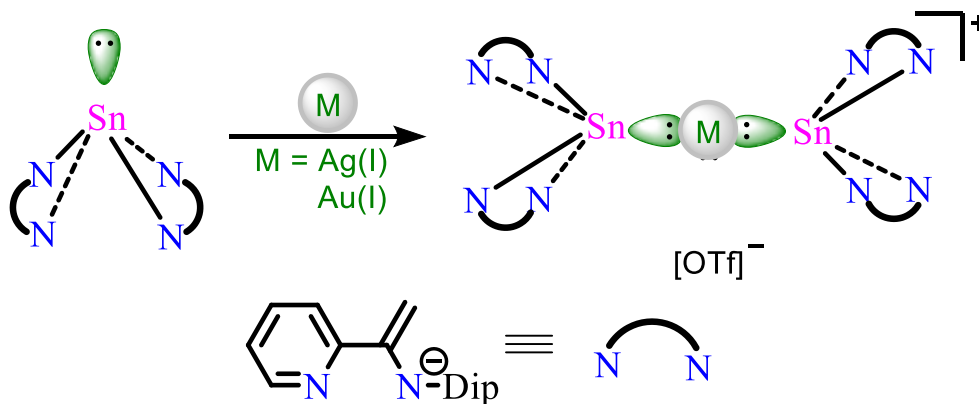
Section 2A: Synthesis and Characterization of Stannylenes and Their Transition Metals Complexes

Section 2B: Synthesis, Characterization and Reactivity of Novel Tin(II) Cationic Compounds

Synthesis and Characterization of Stannylenes and Their Transition Metals Complexes

Abstract

The bidentate and tetradentate iminopyridine (IP) based ligands (**L**, **L1**, **L4**), their reduced form aminopyridine (**L2**), and phosphine functionalized bisamine (**L3**) ligands were used to synthesize mono- and bis(stannylenes). The reaction of aminopyridine **L2** with $\text{Sn}[\text{N}(\text{SiMe}_3)_2]_2$ underwent an electron transfer reaction, ultimately leading to bis(α -iminopyridine) isolation. A 1:1 stoichiometric reaction between **L3** and $\text{Sn}[\text{N}(\text{SiMe}_3)_2]_2$ led to the isolation of a dimeric monostannylene **5** having a step-like structure with a Sn_2N_2 central ring. The reaction of **L**, **L1**, and **L4** with $\text{Sn}[\text{N}(\text{SiMe}_3)_2]_2$ resulted in the mono- and bis(stannylenes). 1:1 reaction of tetradentate iminopyridine ligand with $\text{Sn}[\text{N}(\text{SiMe}_3)_2]_2$ resulted into intermolecular C-C coupled product in stannylene ligands. The reaction of bis(stannylene) **3** with silver trifluoromethane sulfonate led to the formation of ligand stabilized Sn(II) dication **7**, while monostannylene **6** gave the Sn-Ag-Sn coordination complex **10**.



2A.1 Introduction

The coordination chemistry of stannylenes towards coinage metals is scarcely investigated when compared with lighter congeners since the complex instability is a measure problem that hampers the investigation of stannylene coinage metal complexes. The lower stability of resultant complexes towards oxidation, substitution process as the stannylene-TM bond strength depleted while going down the group.¹ Generally, the stannylene ligand can play the role of lone electron pair donor or acceptor (*Z*-type ligand) with transition metals.² The metal complexes of stannylene generally require extra donor substituents on the ligand as a consequence of strong Lewis acidity of Sn, and the donating ability of heavier carbenes decreases down the group. Thus the choice of ligand to form stannylene plays a very important role during the synthesis of stannylene metal complexes.

Acyclic tetradentate ligands wherein the two bidentate coordinating fragments are tethered by $-\text{CH}_2\text{-CH}_2-$ bridges have been widely used in stabilizing a variety of transition metals and lanthanide complexes. The flexibility at the alkyl backbone empowers the ligand denticity to vary from stabilizing mononuclear complexes to bimetallic complexes. Recent examples are the bis(Schiff-base) type ligand bis(α -iminopyridine) crafting bimetallic Cu(I) complexes,³ Polynuclear Fe(III) clusters,⁴ dinuclear Ln(III) complexes with single-molecule magnet behaviour,⁵ luminescent Zn(II)/Hg(II) complexes,⁶ Co(II) coordination polymer⁷ etc. The bidentate iminopyridine ligand, a smaller version of tetradentate bis(α -iminopyridine) ligand, has also been employed in transition metal complexes.⁸ Although there are plentiful examples of the utilization of these ligand types in transition metal chemistry, they have been less frequently known in low-valent main group chemistry.⁹ With the increasing success of main-group ligand systems in transition metal catalysts and homogeneous catalytic transformations,¹⁰ the stabilization of main-group elements within newer ligand frameworks stands appropriate. Therefore, the versatile binding possibilities make these much-coveted ligands (**L**, **L1**, and **L4**) further to explore the stabilization of various low-valent main-group compounds.

The tetradentate ligands with a variety of different donor groups N_2X_2 ($\text{X} = \text{P}, \text{O}, \text{S}$) are intriguing as they potentially impose on the metals to discriminate between binding sites.¹¹ In recent times, a variety of PNNP tetradentate ligand frameworks have gained popularity in stabilizing pincer-type *N*-Heterocyclic tetrylene (PNNP)E ($\text{E} = \text{Ge}, \text{Sn}$).¹² Such phosphine functionalized germylene and stannylene pincer-type ligands with a rigid or flexible backbone

have emerged as versatile frameworks appropriate for metal coordination and catalytic applications.¹³ Such flexible PNNP ligands have been previously reported to stabilize both dinuclear and mononuclear transition metal complexes as efficient catalysts.¹⁴ Thus, appropriate utilization of this multi-faceted N2P2 ligand in main-group chemistry is certainly a worthwhile study.

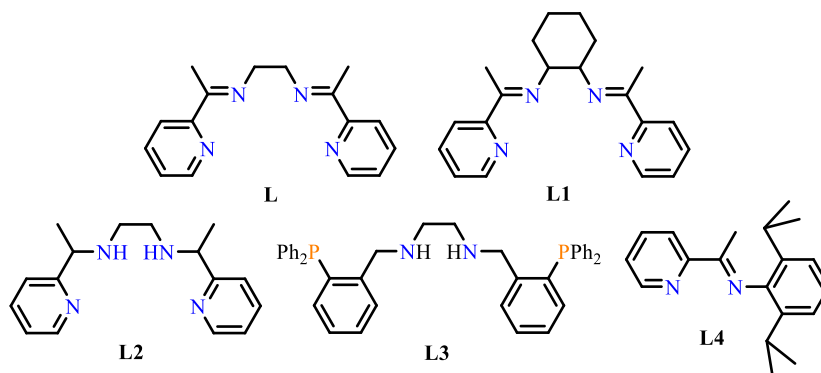


Chart 2A.1. Iminopyridine based ligands **L**, **L1**, **L4**, and reduced form aminopyridine **L2** phosphine functionalized amino ligand **L3**.

In this work, we have chosen **L-L4** (Chart 2A.1) as the five competent ligand frameworks with bidentate *N2*, tetradentate *N4*, and *N2P2* donor sites and studied their coordinating abilities in combination with $\text{Sn}[\text{N}(\text{SiMe}_3)_2]_2$. The facile cleavage of Sn-N bond makes $\text{Sn}[\text{N}(\text{SiMe}_3)_2]_2$ as the appropriate precursor for a variety of stannylene compounds. The formation of a stannylene by methylimine deprotonation of **L**, **L1** and **L4**, the conversion of **L2** to **L** in the presence of $\text{Sn}[\text{N}(\text{SiMe}_3)_2]_2$, and the formation of dimeric PSnP pincer-type ligand with free P pockets through transamination reaction from **L3** is achieved. The reactivity study of stannylenes with coinage metals salt was also performed. Notably, the hitherto unknown conversion of the bis(stannylene) to a **L1** stabilized Sn(II) dication in the presence of Lewis acids has been reported herewith along with the first example of cationic Sn(II)-Au(I)-Sn(II) complex.

Scope of the work

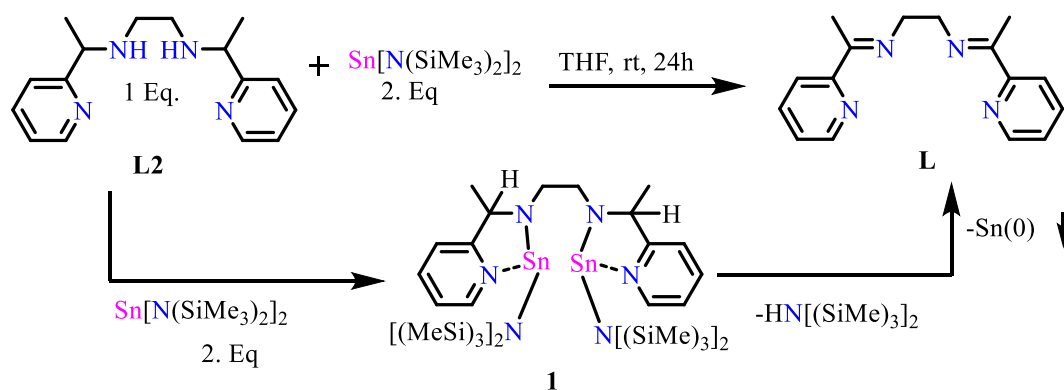
The ability of stannylene-metal (Sn-M) bond to activate small molecules can be desirable. Still, due to the instability of the complexes, less number of stannylene coinage metal complexes are reported in the literature. The stannylenes are reactive molecules so require kinetic or thermodynamic stabilization. The substituents or ligand on the stannylene plays a crucial role in determining the nature of resultant stannylenes. The only example of cationic Sn(II)-Ag(I)-Sn(II) complex and no examples of similar

cationic stannylene gold complex, the reactivity study of Sn(II)-M bond was not studied properly. Herein we have chosen iminopyridine based ligand for stannylene synthesis by transamination reaction or by ene-amide stannylene formation reaction. The stoichiometric ratio between stannylene reagent and ligand dictates product formation. The synthesized stannylenes with different coordination react differently with coinage metal salts. This study gives new observations on the coupling in ligands of stannylene, anticipated as mediated by tin. The exciting new cationic stannylene-metal complexes are also reported, which may be further utilized for photophysical study or as heterometallic complexes in small molecule activation.

2A.2 Results and Discussion

2A.2.1 Stannylene Formation by Transamination

A handful of bis(stannylenes) have been reported by Hahn and co-workers by a transamination reaction between a tetraamine and $\text{Sn}[\text{N}(\text{SiMe}_3)_2]_2$.¹⁵ The transamination reaction was revisited in this contribution. In an effort to prepare bis(stannylene) by transamination, we reacted **L2** with two equivalents of $\text{Sn}[\text{N}(\text{SiMe}_3)_2]_2$ in tetrahydrofuran at room temperature (Scheme 2A.1). Immediate, intense red colouration along with precipitation, was observed. Single crystals grown from ethereal solvent post-filtration showed the generation of bis(α -iminopyridine) **L** in good amounts (crystallization yield = 70%) after 4 days.



Scheme 2A.1 Transamination reaction between $\text{Sn}[\text{N}(\text{SiMe}_3)_2]_2$ and **L2**.

Essentially, ligand **L2** being redox non-innocent triggers the conversion of the *in situ* generated stannylene to **L** and $\text{Sn}(0)$ along with the generation of $\text{HN}(\text{SiMe}_3)_2$. Low temperature ^{119}Sn NMR study in $\text{THF-}d_8$ of the reaction between **L2** and $\text{Sn}[\text{N}(\text{SiMe}_3)_2]_2$ reveals the initial formation of stannylene **1** via transamination.

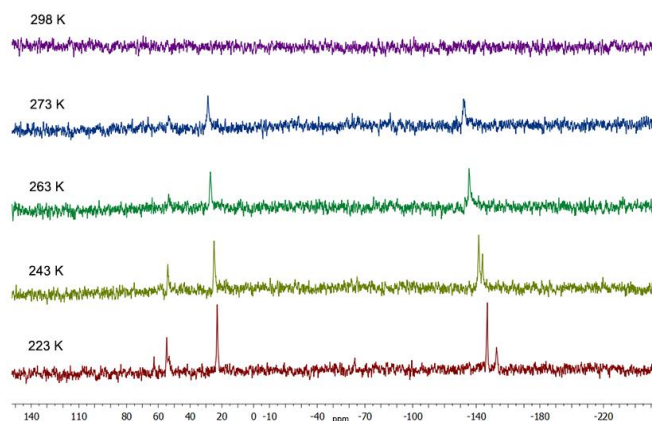
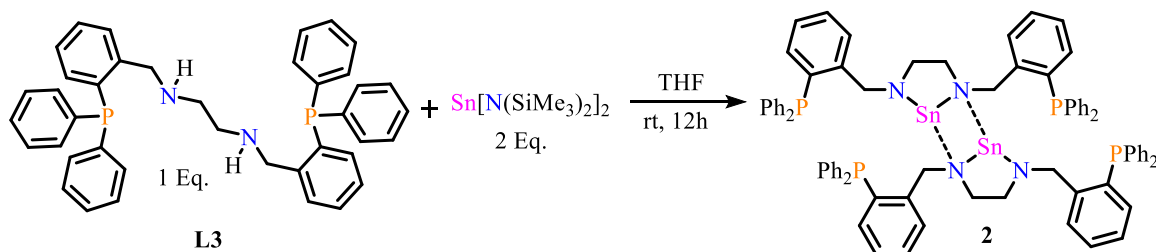


Figure 2A.1 Variable temperature ^{119}Sn NMR of reaction mixture between $\text{Sn}[\text{N}(\text{SiMe}_3)_2]_2$ and **L2**

Subsequently, raising the reaction mixture from 223 K to 298 K (room temperature) led to the disappearance of the peaks in the ^{119}Sn NMR spectra due to the formation of metallic tin precipitate (Figure 2A.1). ^1H NMR spectrum of the reaction mixture post-workup recorded at room temperature after 4 days shows the formation of **L** along with small amounts of **L2** and stannylene majorly. Analogous observation has been reported in the case of a heteroleptic bis(stannylene), which eventually led to the isolation of 2,6-diiminopyridine stabilized stannylene.¹⁶



Scheme 2A.2 Transamination reaction between $\text{Sn}[\text{N}(\text{SiMe}_3)_2]_2$ and **L3**.

Compound **2** was synthesized by a transamination reaction between **L3** and $\text{Sn}[\text{N}(\text{SiMe}_3)_2]_2$ taken in 1:1 ratio in toluene solvent at room temperature (Scheme 2A.2). Small amounts of metallic tin was removed by filtration. Colourless single crystals of the dimeric monostannylene **2** appropriate for X-ray diffraction were obtained from the filtrate in a good yield of 80%. Compound **2** was characterized in its solution state by NMR spectroscopy in $\text{Tol-}d_8$.

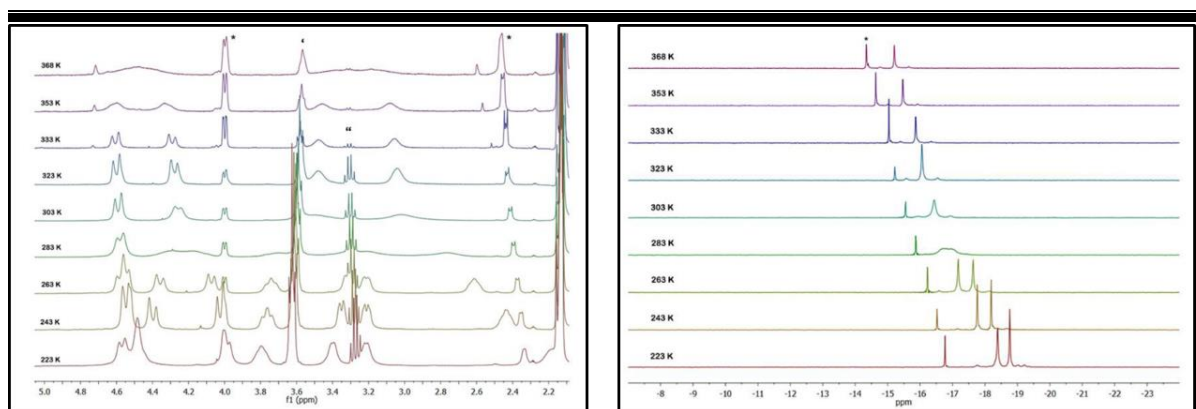


Figure 2A.2 Variable Temperature ^1H (Zoom Aliphatic region) and ^{31}P NMR spectrum.

Room temperature ^1H NMR spectrum in Toluene- d_8 shows two broad doublets for the two $-\text{CH}_2\text{Ar}$ at 4.61 ppm and 4.25 ppm and two peaks for the $-\text{CH}_2-\text{CH}_2-$ protons at 3.49 ppm and 2.99 ppm corresponding to the dimer **2**. Upon lowering the temperature, these characteristic peaks split further, due to the restricted rotation of the phosphine appendages in the dimer under low-temperature conditions (Figure 2A.2 & 2A.38). The possible free rotations of the phosphine appendages upon rising the temperature causes the peaks to merge, as observed in the NMR spectra. The further merging of the two peaks each assigned for $-\text{CH}_2\text{Ar}$ and $-\text{CH}_2-\text{CH}_2-$ protons provides the diagnostic feature identifying the possible formation of the monomer under high temperature conditions. Notably, the NMR peak intensity for the free ligand **L3** increases under higher temperature conditions, hinting the instability of the monomer formed. The $^{31}\text{P}\{^1\text{H}\}$ NMR spectrum shows resonances of only one singlet resonance at -15.14 ppm with ^{119}Sn satellites having a weak coupling constant of 175.6 Hz. Correspondingly a triplet has been observed in the $^{119}\text{Sn}\{^1\text{H}\}$ NMR at 46.12 ppm with a weak $\text{Sn}\cdots\text{P}$ coupling constant of 174.8 Hz.¹² Variable temperature $^{31}\text{P}\{^1\text{H}\}$ NMR spectra also echoes the phenomenon observed in the proton NMR of **5**.

The dimer **2** has been obtained as the only product even when an excess of $\text{Sn}[\text{N}(\text{SiMe}_3)_2]_2$ has been taken in the reaction mixture. Worth mentioning, the Sn(II) center in the half unit of **2** has been electronically saturated by the N donor from the other half resulting in a dimeric structure at room temperature. This is unlike the case of phosphine functionalized pincer-type stannylene, where the two P appendages coordinate to the Sn(II) center to stabilize the monomer.¹⁷ Presumably, in our case, the presence of the methylene bridge along with the

phosphine bulk deters the P \rightarrow Sn coordination and favors stabilization through dimer 5 formation.

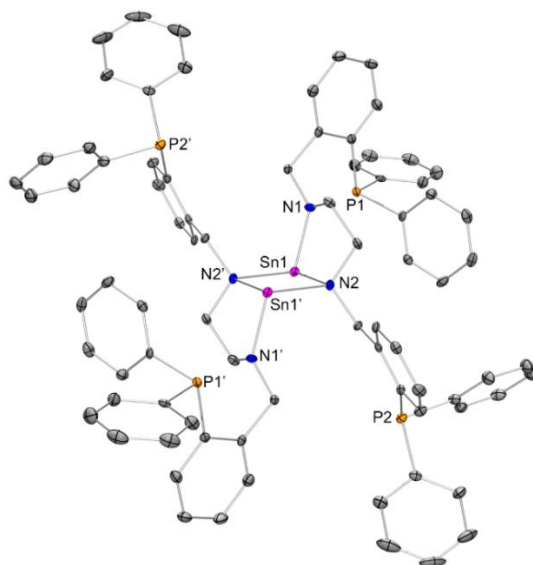


Figure 2A.3. Molecular structure of **2** in the solid state (thermal ellipsoids at 30%, H atoms are omitted for clarity). Selected bond lengths [\AA], and angles [$^\circ$]: Sn1-N1 2.088(3), Sn1-N2 2.235(3), Sn1-N2 2.299(4), N1-Sn1-N2 80.30(13).

Compound **2** crystallized in the centrosymmetric P-1 space group, as observed in the X-ray analysis. The solid-state structure shows a dimer of the monostannylene unit (Figure 2A.3). The molecular unit involves three edge-bridged rings giving rise to a step-like structure.¹⁸ The two puckered five-membered diamido-stannylenes dimerize through N \rightarrow Sn donor-acceptor interaction to form a central Sn₂N₂ four-membered planar ring. The covalent and coordinate Sn1-N2 and Sn1-N2' bond distances in the central rhomboid are 2.235(3) \AA and 2.299(4) \AA , respectively. The Sn1-N1 covalent bond distance is 2.088(3) \AA . Notably, in contrast to N1, N2 acts as a μ_2 bridging donor to the two stannylene centers from the two monomers. Within the four-membered ring, the internal N2-Sn1-N2 and Sn1-N2-Sn1 angles are 81.61(14) $^\circ$ and 98.39(14) $^\circ$ respectively. The four pendant phosphine groups in the dimeric structure **2** are away from the stannylene sites, the closest Sn1 \cdots P1 distance is 3.785(12) \AA . Nonetheless, the presence of flexible methylene in the appendages allows for structural rearrangement and phosphine coordinating sites available for further metalation.¹²⁻¹³

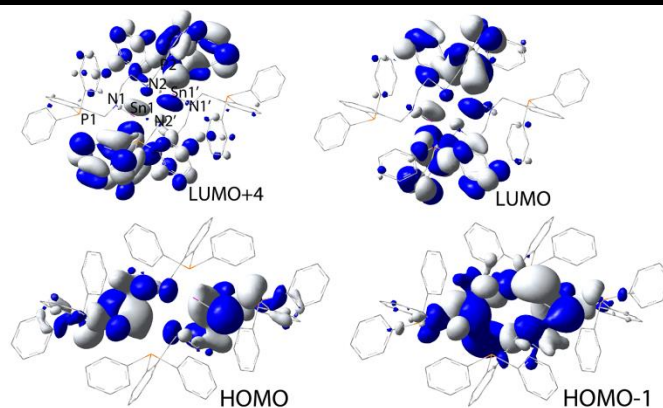
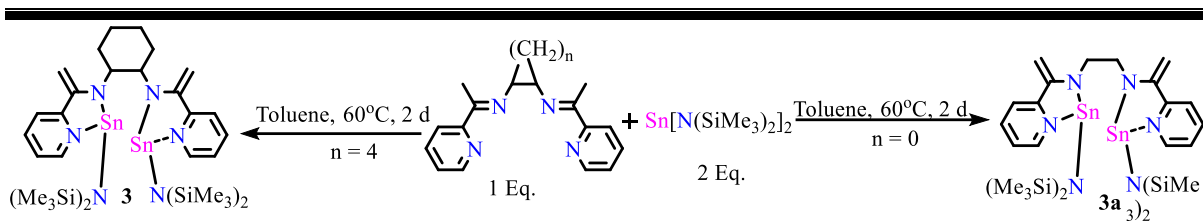


Figure 2A.4. Relevant contour plots of **2'** at an isovalue of 0.02 au.

In order to elucidate the electronic features, DFT calculations were carried out for compounds **2** at the B3LYP level, using 6-31G(d,p) as the basis set for C, H, N, Si, P and LANL2DZ for Sn.¹⁸ Compounds **2** have been optimized, and the optimized geometry of **2'** satisfactorily replicate the key metrical parameters. The HOMO-1 to HOMO-3 orbitals of **2'** reveal the major contributions from the Sn lone pairs. The vacant p-orbital on the Sn centers are depicted in LUMO along with P-C σ^* - π^* conjugation and majorly in LUMO+4 (Figure 2A.4). The WBI value for the single bonds N1-Sn1 is 0.48, and N2-Sn1 is 0.32. The difference obviously arises from the bridging donor nature of N2 in contrast to N1 and correlates well with the experimental findings. The Sn1-N2' bond between the two monomeric units in **2'** has a WBI value of 0.29. The dissociation energy of the dimer has been calculated to be 17.3 kcal/mol, thereby favouring dimer formation at room temperature. Furthermore, the dissociation energies have been calculated in toluene, tetrahydrofuran, and acetonitrile solvent medium using the polarization continuum model. Although apparently, the dissociation energy of the dimer increases with the decrease in the dielectric constant of the medium, the change is small (within 0.5 kcal/mol), which indicates that electrostatic interactions do not predominate. Therefore, the formation of the dimer **2** may involve partial covalent interaction.

2A.2.2 Bis(stannylene) Synthesis

The bis(stannylene) compounds **3** and **3a** (Scheme 2A.3) was obtained from a reaction between **L/L1** and Sn[N(SiMe₃)₂]₂ taken in a 1:2 ratio in toluene for 2 days at room temperature. Deprotonation of the two methylimines occurs to generate the ene-amide stabilized bis(stannylene) **3/3a** with concomitant elimination of NH(SiMe₃)₂, which was removed under reduced pressure.



Scheme 2A.3 Syntheses of compound **3** and **3a**.

Compound **3** was obtained in 82% yield as an orange precipitate by the addition of small amounts of pentane. Orange colored single crystals of **3** suitable for X-ray analysis were grown at -40°C from the hexane solution. Alternately, compound **1** has also been synthesized in a good yield of 85% under solvent-free conditions by heating the two precursors **L1** and $\text{Sn}[\text{N}(\text{SiMe}_3)_2]_2$ taken in a 1:2 ratio at 60°C . Notably, minimal amounts of metallic tin formation were observed under both the reaction conditions, which was removed by filtration from the toluene solution. Compound **3** has been characterized using hetero-nuclear NMR techniques. The ^1H NMR spectrum shows the clear disappearance of the $-\text{CH}_3$ proton in **L1** and the presence of the terminal $\text{H}_2\text{C}=\text{C}$ protons at 4.87 and 4.43 ppm. The corresponding ^{13}C NMR spectrum shows peak at 82.13 ppm for the terminal alkenyl carbon. A singlet resonance at -47.05 ppm appears in the $^{119}\text{Sn}\{^1\text{H}\}$ NMR spectrum of compound **1** in Benzene- d_6 , which falls within the range of reported stannylene chemical shift values [12, 16]. UV/Vis spectra of compound **3** in tetrahydrofuran solvent exhibits the longest wavelength absorption $\lambda_{\text{max}} = 401$ nm ($\epsilon = 2797 \text{ M}^{-1}\text{cm}^{-1}$). There are two literature precedences in main-group chemistry where the redox-active iminopyridine based ligands form ene-amide complexes with Al(III) [9a] and Sn(II).¹²

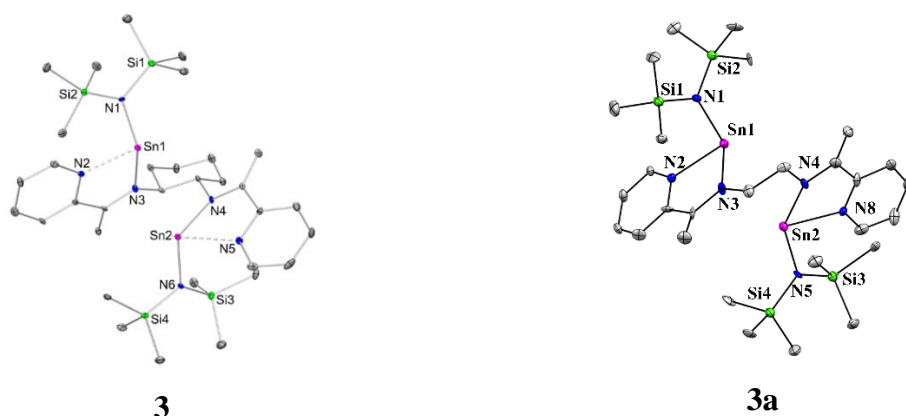


Figure 2A.5. Molecular structure of **3** and **3a** in the solid state (thermal ellipsoids at 30%, H atoms are omitted for clarity). Selected bond lengths [\AA] and angles for **3** [$^\circ$]: Sn1-N1 2.126(5), Sn1-N3 2.191(5), Sn2-N4 2.178(6), Sn2-N6 2.140(5), N2-Sn1-N3 73.1(2). N5-Sn2-N4

71.7(2). Selected bond lengths [\AA] and angles for **3a** [$^\circ$]: Sn1-N1 2.131(13), Sn1-N2 2.294(13), Sn2-N4 2.131(13), Sn2-N008 2.308(13), N2-Sn1-N3 72.6(5). N5-Sn2-N4 100.2(5).

In the case of Sn(II), the 2,6-diiminopyridine ligand (2,6-[ArN=C(Me)]₂(NC₅H₃) (Ar = C₆H₃-2,6-*i*Pr₂)) undergo ene-amide formation only on one side leading to the stabilization of the heteroleptic monostannylene.¹² Compound **3** crystallizes in the monoclinic crystal system with P2₁/n space group (Figure 2A.5). The ligand **L1** backbone represents the transformed features with bis(ene-amide) functionality. Each of the two stannylene centers has been stabilized, involving two Sn-N covalent bonds of parameters (\AA): Sn1-N1 = 2.126(5), Sn1-N3 = 2.191(5), Sn2-N4 = 2.178(6), Sn2-N6 = 2.140(5). The two strong pyridyl N \rightarrow Sn donor-acceptor bonds of lengths Sn1-N2 = 2.254(6) \AA and Sn2-N5 = 2.336(6) \AA further stabilize the respective stannylene centers. Both the covalent and coordinate bond parameters in compound **3** agree well with those reported in the literature.¹² While the five-membered ring stabilizing Sn1 is almost planar, Sn2 is raised by 0.72 \AA above the N5-C16-C14-N4 coordinating plane. The exocyclic C=C bonds of the five-membered rings stabilizing the two stannylene centers exhibit bond lengths: C6-C7 = 1.352(10) \AA and C14-C15 = 1.372(10) \AA . Concurrently, the C-N bonds show bond lengths: C6-N3 = 1.386(9) \AA and C14-N4 = 1.365(8) \AA . The N2-Sn1-N3 and the N4-Sn2-N5 bond angles within the five-membered rings are 73.1(2) $^\circ$ and 71.7(2) $^\circ$ respectively. The two Sn centers are separated by 3.540(8) \AA and are canted by a Sn1-N3-N4-Sn2 torsional angle of 90.77(18) $^\circ$ due to the flexible cyclohexyl linker between the two coordinating fragments. Such bis(stannylene) geometries serve as appropriate chelating ligands in transition metal chemistry.¹⁴

In order to elucidate the electronic features, DFT calculations were carried out for compounds **3** at the B3LYP level, using 6-31G(d,p) as the basis set for C, H, N, Si, P and LANL2DZ for Sn. Compounds **3** have been optimized, and the optimized geometries **3'** satisfactorily replicates the key metrical parameters. The filled frontier orbitals HOMO to HOMO-2 of **3'** show the maximum contributions from the lone pairs on the two stannylene centers (Figure 2A.6). The LUMO is ligand-centred and reveals the anti-bonding interaction of the terminal C=C (Figure 2A.6). The vacant p-orbital on Sn(II) centers are the energetically high-lying LUMO+4 and LUMO+5 orbitals (Figure 2A.6). The Wiberg bond indices from NBO analysis clearly help to differentiate between the covalent and dative bonds in this molecule. The average WBI values of Sn-N_{ene-amide} and Sn-N_{amide} covalent bonds are 0.35 and 0.45, respectively, while the value for donor-acceptor Sn-N_{py} is comparatively low being 0.23.

The average WBI for the C-C bond in the ene-amide is 1.62, reflecting their double bond character. There exists no covalent bonding between the two Sn centers, as confirmed from the very low WBI value of 0.18. The Mulliken charges on the stannylene centers are +0.91. The simulated UV/Vis spectrum of **3'** by TD-DFT calculations shows the λ_{max} at 454 nm (HOMO \rightarrow LUMO+1, $f = 0.0477$), corresponding to the $n(\text{Sn}) \rightarrow \pi^*(\text{L1})$ transition (see ESI†), which is close by the experimentally obtained value.

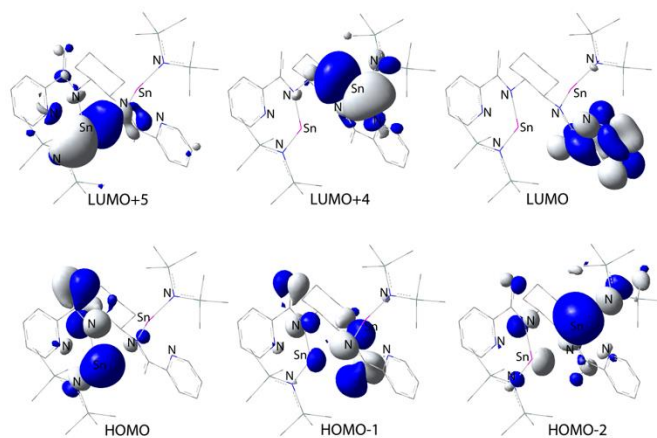
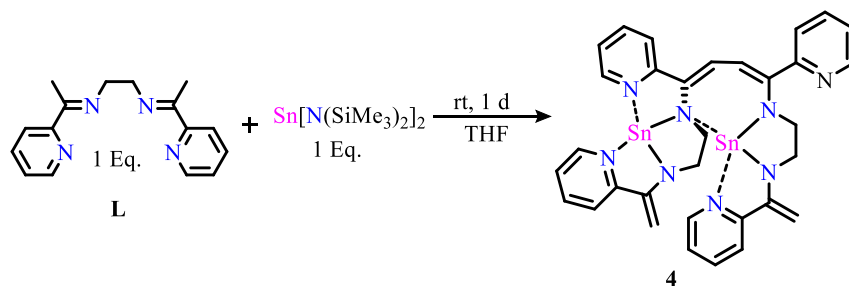


Figure 2A.6 Relevant contour plots of **3'** at an isovalue of 0.04 au.

2A.2.3 Tetra-coordinate Monostannylene synthesis with C-C Coupling in Ligand Backbone

The reaction between **L** and $\text{Sn}[\text{N}(\text{SiMe}_3)_2]_2$ taken in a 1:1 ratio in tetrahydrofuran solvent for 24 hours at room temperature led to formation of tetra-coordinated stannylene **4** with surprisingly intermolecular coupling in the ligand backbone (Scheme 2A.4). Primarily the deprotonation of two methylamines occurs to yield the ene-amide stabilized stannylene **4** with simultaneous elimination of $\text{NH}(\text{SiMe}_3)_2$. Compound **4** obtained in the yield of 40% yield as intense dark purple crystals from the concentrated THF solution.



Scheme 2A.4 Synthesis of **4** from **L**.

The compound **4** was characterized by ^1H and ^{119}Sn NMR techniques. In the ^1H NMR spectra due to differences in the coordination environment of two stannylene centre or

asymmetry in the structure, several peaks appeared. The $^{119}\text{Sn}\{^1\text{H}\}$ NMR spectrum of compound **4** in Benzene- d_6 shows two peaks for two different stannylene centres at a chemical shift value of -298.86 ppm and -335.91 ppm, match well with the literature reported chemical shift for tetra-coordinated stannylene.¹⁹

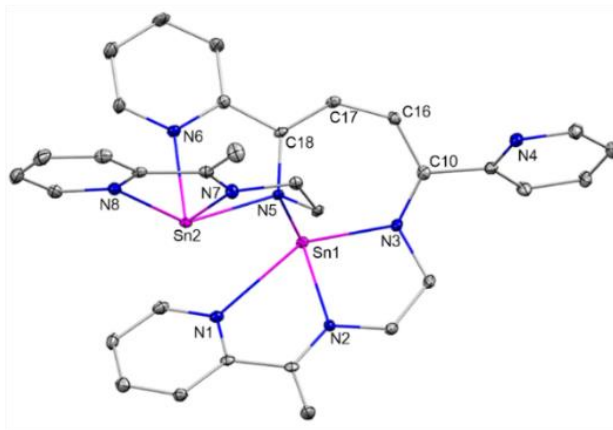


Figure 2A.7 Molecular structure of **4** in the solid state (thermal ellipsoids at 30%, H atoms are omitted for clarity). Selected bond lengths [\AA]: Sn1-N1 2.541(4), Sn1-N2 2.153(3), Sn1-N3 2.234(4), Sn1-N5 2.272(3), Sn2-N5 2.319(3), Sn2-N6 2.255 (3), Sn2-N7 2.127(3), Sn2-N8 2.443(4), C18-C17 1.384 (5), C17-C16 1.414 (5), C16-C10 1.402(10), Sn1...Sn2 3.836.

Compound **4** was crystallized in the monoclinic crystal system with P21/c space group. In the solid state structure, two THF solvent molecules crystallized. The C-C homo-coupling of the alkene framework of the two ene-amide stabilized stannylene generates the cyclobutadiene kind of systems. The C18-C17, C17-C16, and C16-C10 bond lengths are 1.384 (5), 1.414 (5), and 1.402 (10) \AA , respectively, falls in the range of conjugated single and double bond distances. The torsional angle for C18-C17-C16-C10 is 26.02° , which compares well with the literature reported value for the coordinated 1,3-cyclobutadiene (torsional angle range $22 - 30^\circ$) system.²⁰ One stannylene center has two coordinate pyridyls $\text{N} \rightarrow \text{Sn}$ bond with a bond distance of $\text{Sn2-N6} = 2.256 (3)$ and $\text{Sn2-N8} = 2.443 (3)$ \AA whereas two covalent $\text{Sn2-N5} = 2.318 (3)$ and $\text{Sn2-N7} = 2.126 (3)$ \AA . The second stannylene center has one pyridyl $\text{N1} \rightarrow \text{Sn1}$ [2.539 (3) \AA] and another amide $\text{N} \rightarrow \text{Sn}$ [2.272 (3) \AA] coordinate bond, whereas two covalent $\text{N} \rightarrow \text{Sn}$ have bond distances of 2.154 (3) and 2.233 (3) \AA . Both the stannylene center are pyramidal and have Sn-Sn distance of 3.838 \AA , which are much larger than Sn-Sn single bond distance.²¹

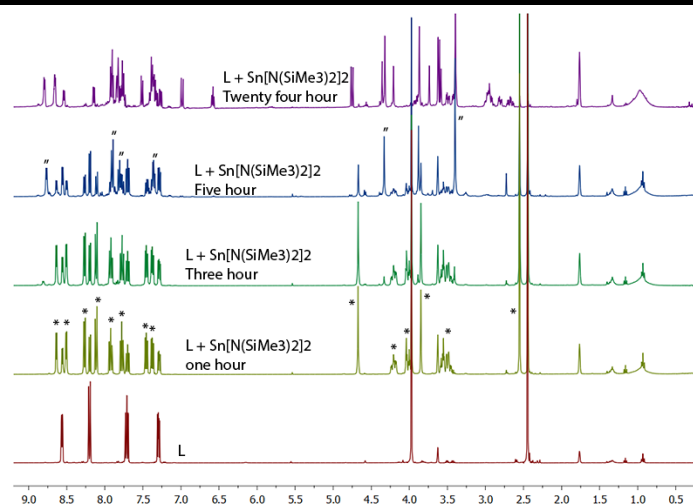
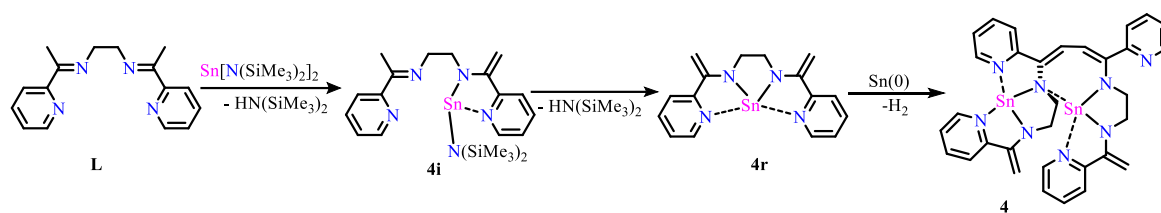


Figure 2A.8 Time dependant ^1H NMR of reaction mixture.



Scheme 2A.5 Stepwise formation of compound **4**.

In order to elucidate the mechanism of the intermolecular conjugated C-C coupling in the ligand backbone, a time-dependent ^1H NMR study was performed for the reaction of 1 equivalent of the ligand with 1 equivalent of tin amide $[\text{Sn}\{\text{N}(\text{SiMe}_3)_2\}_2]$. The reaction is very spontaneous with the intermediate formation of tri-coordinated monostannylene **4i** with one exocyclic double bond (peaks marked with * are for stannylene **4i**) similar to the observation of Flock and co-workers.¹⁶ The asymmetry in the structure cause's different chemical shift in the two pyridyl protons of iminopyridine ligand. Over the course of the reaction, the tri-coordinated monostannylene turned into tetra-coordinated symmetrical monostannylene **4r** with the elimination of $\text{HN}(\text{SiMe}_3)_2$ revealed in the ^1H NMR (peaks marked with # are for stannylene **4r**). Two units of monostannylene **4r** coupled to each other at exocyclic double bond by intermolecular dehydrogenative coupling giving compound **4**.

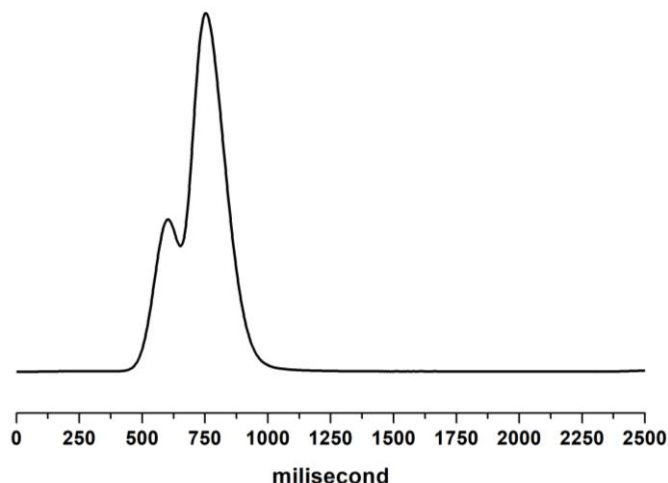
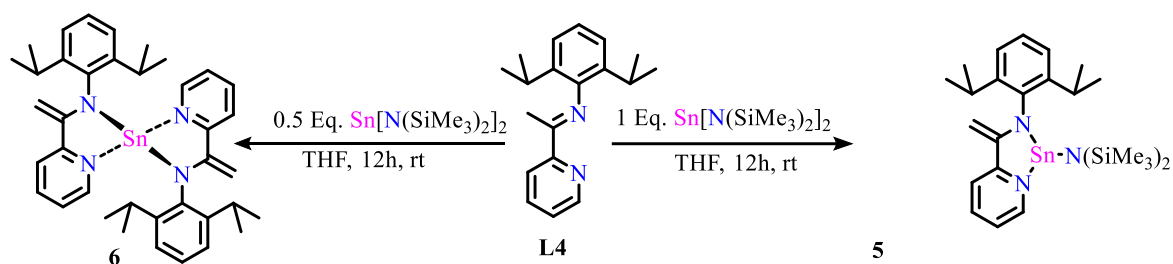


Figure 2A.9 H₂ detection by GC.

The dehydrogenative coupling was confirmed by H₂ elimination in the reaction mixture, which was examined by injecting the gaseous reaction mixture to GC with a thermal conductivity detector (TCD), which shows the peak for Hydrogen gas confirms the dehydrogenative coupling.

2A.2.4 Tetra-coordinated Stannylene



Scheme 2A.6 Synthesis of **5** and **6**.

With the mesmerizing results obtained in the above reaction, motivated us to try similar reaction for iminopyridine (IP) ligand **L4** which is the half of ligand **L**. Mono-stannylene compound **6** was obtained by reaction of 1 equivalent of ligand **L4** when reacted with 0.5 equivalent of Sn[N(SiMe₃)₂]₂ in diethyl ether solvent at room temperature. Deprotonation of terminal methyl protons of iminopyridine ligand led to stabilization of ene-amide stabilized tetra-coordinated stannylene as a yellow color powder with the yield of 70%. The suitable single crystal of compound **6** was grown from the saturated diethyl ether solution. The stoichiometric reaction of **L4** with Sn[N(SiMe₃)₂]₂ led to the formation of tri-coordinated mono-stannylene **5** with the elimination of HN(SiMe₃)₂ and the formation of one exocyclic double bond. Both compounds are characterized by heteronuclear NMR techniques. In the ¹H

NMR of **6**, new methylene proton of exocyclic double bond appeared at 4.58 ppm and 3.63 ppm due to the deprotonation of methyl protons. In the ^{119}Sn NMR single peak appeared at a chemical shift of 303.57 ppm for tetra-coordinated **6** and at 0.23 ppm for tri-coordinated **5** matches well with reported values.¹⁹

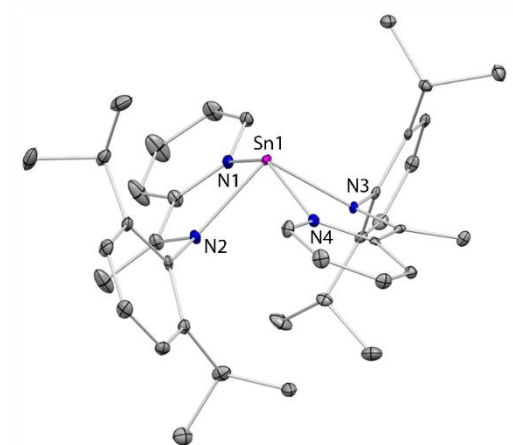
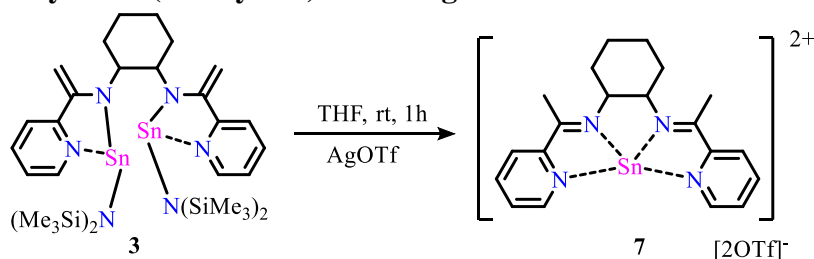


Figure 2A.10. Molecular structure of **6** in the solid state (thermal ellipsoids at 30%, H atoms are omitted for clarity). Selected bond lengths [\AA] and bond angles [$^\circ$]: Sn1-N1 2.4244(19), Sn1-N2 2.1751(19), Sn1-N3 2.4109(19), Sn1-N4 2.1544(18), N1-Sn1-N2 70.26(7), N3-Sn1-N4 70.89(7).

The compound **6** crystallized in monoclinic crystal system with $C/2c$ space group. Four nitrogen of the two iminopyridine ligands are coordinated to stannylene centre, overall forming a pyramidal structure. Two pyridines N – Sn coordinate bond distances are 2.4244 (19) and 2.4109 (19) \AA , whereas two N – Sn covalent bond distances are 2.1751 (19) and 2.1544 (19) \AA . The sum of the bond angle around the Sn1 centre is 297.46° reveal the pyramidal structure where Sn is displaced apically from the distorted plane of four basal nitrogen (N1-N2-N3-N4) 1.035° .

2A.2.5 Reactivity Study of Stannylene

2A.2.5.1 Reactivity of Bis(stannylene) **3** with AgOTf



Scheme 2A.7 Synthesis of Sn(II) dication **7**.

The reaction of bis(stannylene) **3** with silver trifluoromethane sulfonate in tetrahydrofuran at room temperature led to the isolation of crystals of **L1** stabilized Sn(II) dication **7** in 40% yield. Presumably, the solvent acts as the proton source. Compound **7** has been characterized using hetero-nuclear NMR techniques in acetone-*d*₃. The ¹H NMR spectrum of **7** appears considerably downfield shifted compared to the free ligand **L1**, indicating the coordination of the Sn(II) dication to **L1** binding sites. The ¹⁹F NMR peak at -79.29 ppm reflects the presence of the triflate anion. The ¹¹⁹Sn NMR spectrum displays a peak at -595.80 ppm, which is considerably downfield shifted compared to the literature reported chemical shifts of [Sn(C₇H₈)₃][B(C₆F₅)₄]₂ (-1468 ppm)²² and [Sn(CH₃CN)₆][Al(ORF)₄]₂ (RF = C(CF₃)₃) (-1490 ppm)²³ in CD₃CN. This suggests that compound **7** has a lower net coordination number in CD₃CN. The formation of stannylene-silver coordination complex²⁴ has not been observed in this reaction.

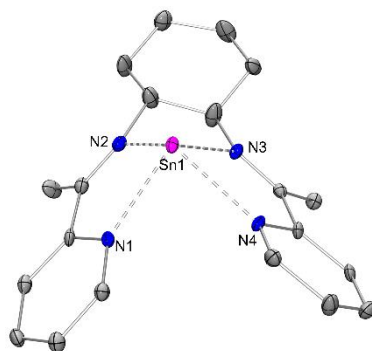
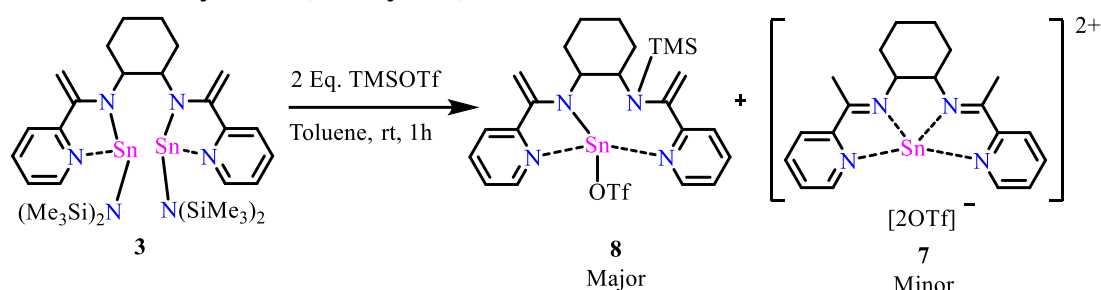


Figure 2A.11. Molecular structure of **7** in the solid state (thermal ellipsoids at 30%, H atoms, and triflate counter anions are omitted for clarity). Selected bond lengths [Å]: Sn1-N1 2.350(7), Sn1-N2 2.344(8), Sn1-N3 2.301(7), Sn1-N4 2.345(7).

The structural formulation of **7** was unequivocally confirmed from single crystal X-ray diffraction studies. Compound **7** crystallizes in the triclinic crystal system with P-1 space group (Figure 2A.11). The structural parameters of **7** are similar to our earlier reported Sn(II) dication [25]. Amongst the four coordinating nitrogen donor sites to the Sn(II) dication center, the two Sn-N_{im} (imino-N atoms) bonds are shorter with bond distances Sn1-N2 2.343(8) Å and Sn1-N3 2.301 (7) Å, while the Sn-N_{py} (pyridyl-N atoms) are slightly longer with Sn1-N1 2.350 (7) Å and Sn1-N4 2.345 (7) Å bond lengths. As in the case of compound **7** and our earlier report [25], the four nitrogen atoms form a slightly distorted basal coordinating plane (fold angle N2-N3-N4-N1 is approximately 13.04°) with the Sn(II) center being displaced perpendicularly by 1.33 Å. The resultant overall dome-shaped or pyramidal structure has a sum of bond angle 285.14° at Sn center. Despite the known weakly coordinating nature of triflate anion, it is

excluded from the coordination sphere of Sn(II) dicationic center, the closest approach Sn1-O2 distance being 3.014(8) Å. It is apparent from the crystal structures of **2** and **3** that the presence of bulky boryl substituents makes **2** with a comparatively flattened pyramid.

2A.2.5.2 Reactivity of Bis(stannylene) with TMSOTf



Scheme 2A.8 Synthesis of compound **8**.

On the other hand, the reaction of **3** with two equivalents of trimethylsilyl trifluoromethane sulfonate in toluene at room temperature led to a mixture of products. Layering dichloromethane solution of the reaction mixture with pentane led to co-crystallization of compounds **8** and an Sn(II) monocation **7** in a minor amount. The electrophilic attack of the trimethylsilyl cation on the ene-amido nitrogen led to the formation of heteroleptic Sn(II) monocation **8**.

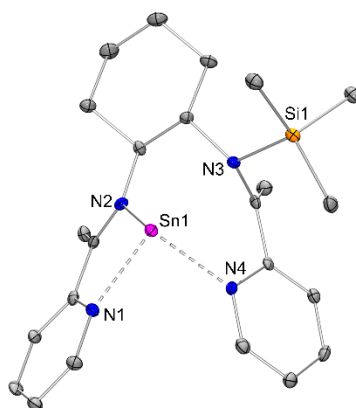
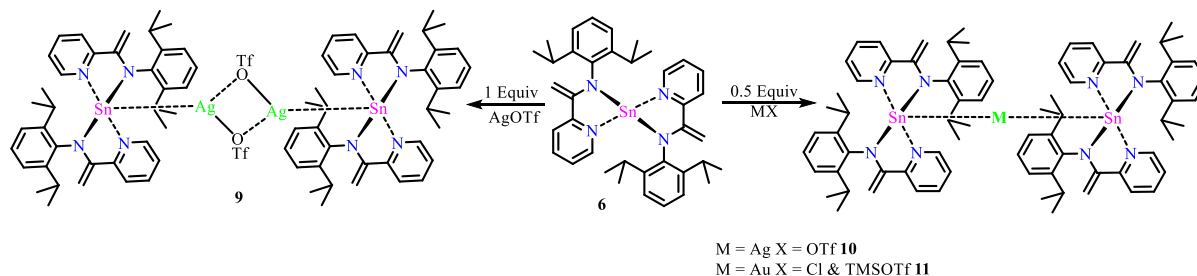


Figure 2A.12. Molecular structure of **8** in the solid state (thermal ellipsoids at 30%, H atoms and triflate counter anions are omitted for clarity). Selected bond lengths [Å]: Sn1-N1 2.323(5), Sn1-N2 2.095(6), Sn1-N4 2.323(5), Si1-N3 1.791(6).

Compound **8** crystallized in the monoclinic crystal system with P21/c space group (Figure 2A.12). The molecular structure reveals the stabilization of an Sn(II) monocation covalently bonded to the ene-amido nitrogen and electronically saturated by the two pyridyl nitrogen within the unsymmetrical N4 ligand framework. The Sn-N_{amido} bond length is 2.095(6) Å, and the Sn-N_{py} bond lengths are 2.323(5) Å in Sn1-N1 and 2.311(5) Å in Sn1-N4 bonds. The Sn(II)

center is pyramidalised in **4** with the closest approach Sn1-O1 distance of the triflate anion being 3.080(5) Å.

2A.2.5.3 Reactivity of Stannylene with Coinage Metal Cations



Scheme 2A.9 Synthesis of Stannylene-Coinage metal complexes **9**, **10** and **11**.

Limited examples of cationic stannylene-Coinage metal complexes in literature²⁶ aroused our interest to synthesize stannylene coinage metal cations. In order to understand the donor ability of stannylene, initially, **6** was treated with the equimolar amount of silver triflate in tetrahydrofuran solvent at room temperature. To our surprise, we found a stoichiometric complex of stannylene-silver triflate **9** in the dimeric form in moderate yield. The yellow block single crystal was obtained by layering the THF solution of the complex with pentane. The complex was confirmed by single crystal XRD in solid state.

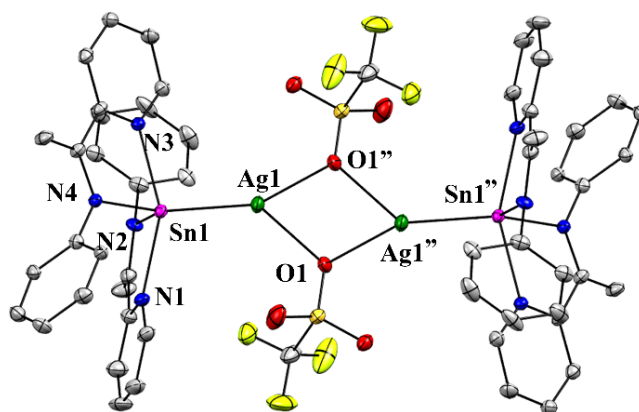


Figure 2A.13. Molecular structure of **9** in the solid state (thermal ellipsoids at 30%, H atoms and isopropyl groups are omitted for clarity). Selected bond lengths [Å] and bond angles [°]: Sn1-N1 2.320(4), Sn1-N2 2.098(4), Sn1-N3 2.319(5), Sn1-N4 2.096(5), Sn1-Ag1 2.5593(9), Ag1-O1 2.290(4) Sn1-Ag1-O1 156.09(11).

In the molecular structure, **9** was crystallized in triclinic crystal system with P -1 space group. Two stannylene units are coordinated to Ag₂O₂ core, where the O atoms are from triflate group bridged between two silver atoms. The Sn-Ag bond distance is 2.559 Å, which is comparable with the Sn-AgX type of complexes.²⁶ The lone pair donations to silvers made

stannylene electron-deficient, grabbing electron density from nitrogen and which is evident from the shortening of Sn–N bond lengths. The covalently bonded Sn – N bond distances are 2.094 (5) and 2.105 (4), whereas Pyridyl N – Sn coordinate bond distances are 2.319 (5) and 2.321 (4) Å much shorter than the free stannylene **6**. The Sn atom held perpendicular at a distance of 0.890 Å to the distorted basal plane of four nitrogen atoms, which show flattened pyramid after coordination silver cation.

The reaction of **6** with 0.5 equivalent of AgOTf or 0.5 equivalent of AuCl and TMSOTf in THF solvent at room temperature leads to the formation of complexes **10** and **11**, respectively. Both the compounds were characterized well by NMR spectroscopy and confirmed by single-crystal XRD. Single crystal of **10** and **11** was grown by layering the THF solution of the respective complex with pentane.

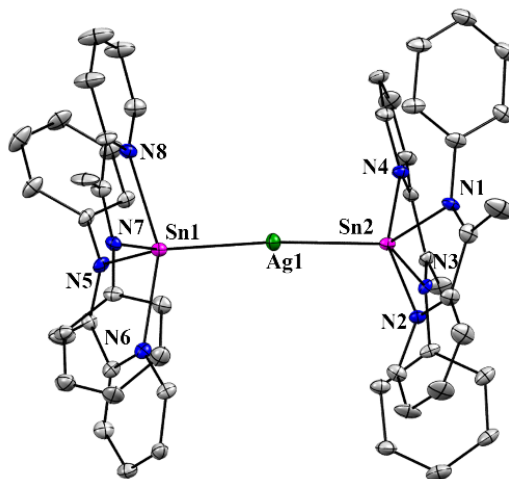


Figure 2A.14. Molecular structure of **10** in the solid state (thermal ellipsoids at 30%, H atoms, THF solvent molecules and isopropyl groups are omitted for clarity). Selected bond lengths [Å] and bond angles [°]: Sn2–N1 2.100(5), Sn2–N2 2.301(5), Sn2–N3 2.095(5), Sn2–N4 2.305(5), Sn1–N5 2.097(5), Sn1–N6 2.307(5), Sn1–N7 2.084(5), Sn1–N8 2.337(5), Sn1–Ag1 2.598(7), Sn2–Ag1 2.5997(7), Sn1–Ag1–Sn2 174.90(2).

Complex **10** was crystallized in P 21/n space group. The triflate counter anion is far away from the coordination sphere of silver with closest distance of 5.986 Å. The Sn–N bond lengths are almost similar of complex **10**. The Ag1–Sn1 and Ag1–Sn2 bond lengths are 2.5980 (7) and 2.5997 (7) Å, respectively, which are comparable with the reported Sn–Ag cationic complex.²⁷ Surprisingly, the Sn1–Ag1–Sn2 bond angle is almost close to linearity 174.90° (2), in earlier reported amidinatostannylene silver complex Sn–Ag–Sn bond angle is 147.57° bent due to the coordination of SbF₆[−] counter anion with silver.^{27d} To the best of our knowledge, it is the first

cationic compound where Sn–Ag–Sn bond angle is almost linear and free from the coordination of counter anion.

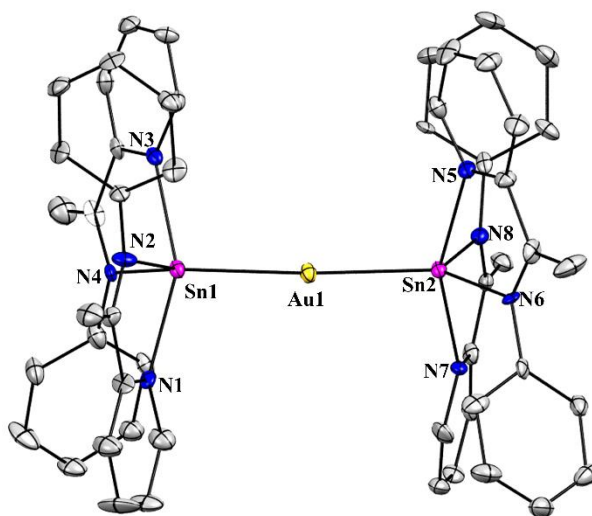


Figure 2A.15. Molecular structure of **11** in the solid state (thermal ellipsoids at 30%, H atoms, THF solvent molecules and isopropyl groups are omitted for clarity). Selected bond lengths [Å] and bond angles [°]: Sn1–N1 2.307(8), Sn1–N2 2.083(9), Sn1–N3 2.285(8), Sn1–N4 2.084(8), Sn2–N5 2.299(8), Sn2–N6 2.057(8), Sn2–N7 2.297(7), Sn2–N8 2.066(8), Sn1–Au1 2.5518(8), Sn2–Au1 2.5528(8), Sn1–Au1–Sn2 176.20(3).

Compound **11** was crystallized in P 21/n space group with two THF molecules in the asymmetric unit cell. The Sn–N bond lengths are slightly shortened when compared to silver complex **10**. The covalently bonded N – Sn bond distances are 2.083 (9) and 2.084 (8) Å, whereas the coordinate pyridyl N–Sn distances are 2.307 (8) and 2.285 (8) Å. The Sn1–Au1 and Sn2–Au1 bond distances are 2.5518 (8) and 2.5528 (8) Å, respectively, which are slightly shorter than the reported Sn–Au coordinate bonds.^{26e} The Sn1–Au1–Sn2 bond angle is 176.20 (3), which almost linear. The two stannylenes are staggered to each other. This is the first example where Au(I) cation is stabilized with two stannylenes.

2A.3 Conclusions

To summarize, the adaptability of the iminopyridin ligands **L-L4** along with the readily cleavable Sn–N bond in Sn[N(SiMe₃)₂]₂ have been utilized to stabilize stannylenes. Ligand **L** and **L1** stabilize a bis(stannylene) involving the ene-amide transformation of the ligand by maintaining 1:2 ratio of ligand to Sn source whereas the 1:1 ratio led to the formation of monostannylene with unusual dehydrogenative C–C coupling in the ligand backbone. Ligand **L3** stabilizes a monostannylene through a straightforward transamination reaction. However, the monostannylene stabilizes in a dimeric form, with four P coordinating sites available for

further metallation. The ligand **L4** was able to stabilize three and four coordinated monostannylenes. The bis(stannylyene) has been observed to undergo the unprecedented conversion to ligand stabilized tin(II) dication by reaction with silver triflates by redox reaction. Whereas the reaction of monostannylyene **6** stabilized by **L4** with Silver and gold triflate gave the hitherto unknown cationic coordination Sn(II)-M(I)-Sn(II) complexes.

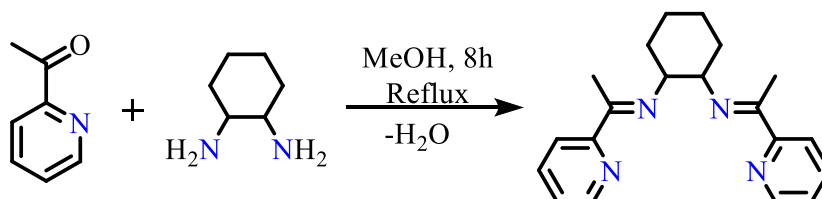
2A.4 Experimental

2A.4.1 General Remarks.

All manipulations were carried out under a protective atmosphere of argon, applying standard Schlenk techniques or in a dry box. Tetrahydrofuran and Toluene were refluxed over sodium/benzophenone. Methanol was dried with magnesium cake and stored over 3Å molecular sieves. All the solvents were distilled and stored under argon and degassed before use. Benzene-*d*₈ and Toluene-*d*₈ were purchased from Sigma Aldrich (Sigma Aldrich Co., St. Louis, MO, USA) and dried over potassium. Acetonitrile-*d*₃ was purchased from Sigma Aldrich and used as it is. All chemicals were used as purchased. ¹H, ¹³C{¹H}, and ²⁹Si{¹H} NMR spectra were referenced to external SiMe₄ using the residual signals of the deuterated solvent (¹H) or the solvent itself (¹³C). ³¹P{¹H} NMR was referenced to external 85% H₃PO₄. ¹¹⁹Sn NMR was referenced to SnMe₄ as the external standard. ¹¹B NMR was referenced to BF₃.OEt₂ as the external standard. ¹⁹F NMR was referenced to C₆H₅CF₃ as the external standard. NMR spectra were recorded on Bruker AVANCE III HD ASCEND 9.4 Tesla/400 MHz and Jeol 9.4 Tesla/400 MHz spectrometer. Solution phase UV/Vis spectra were acquired using a Thermo-Scientific Evolution 300 spectrometer using quartz cells with a path length of 1 cm. Melting points were determined under argon in closed NMR tubes and are uncorrected. Elemental analyses were performed on the Elementar Vario EL analyzer. Single crystal data were collected on Bruker SMART APEX four-circle diffractometer equipped with a CMOS photon 100 detectors (Bruker Systems Inc.) with a Cu Kα radiation (1.5418 Å).

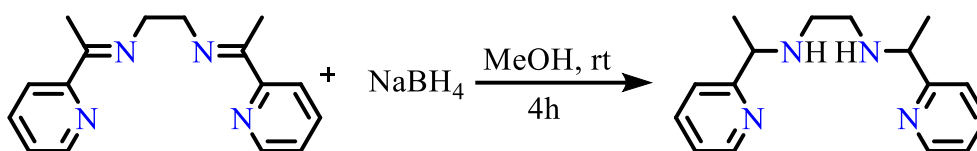
2A.4.2 Synthetic Procedures

Synthesis of Ligand L1:



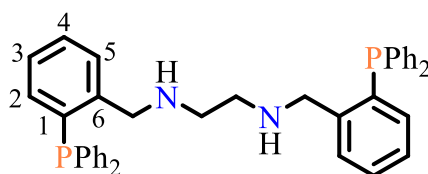
6.48 mL (57.7 mmol) of 2-acetyl pyridine was added to solution of 3.47 mL (28.8 mmol) of 1,2-cyclohexyldiamine in 50 mL of dry methanol and reaction mixture was set to reflux for 8 h. MeOH was evaporated from reaction mixture under reduced vacuum. The residue was dissolved in minimum amount of diethyl ether, and flask kept aside to get colourless crystals of ligand **L1** with the yield of 71% (6.56 g). ^1H NMR (400 MHz, Chloroform- d_3 , TMS) δ 8.48 (m, 2H, Pyr-*H*); 7.91 (m, 2H, Pyr-*H*); 7.58 (m, 2H, Pyr-*H*); 7.18 (m, 2H, Pyr-*H*); 3.89 (m, , 2H, -*CH*-Cyclohexyl); 2.35 (s, 6H, -*CH*₃); 1.94-1.45 (m, 8H, -*CH*₂-*CH*₂-cyclohexyl) ppm. $^{13}\text{C}\{^1\text{H}\}$ NMR (101 MHz, Chloroform- d_3 , TMS) δ 164.66 (C-*CH*₃); 158.39(C-Pyr); 148.14(C-Pyr); 136.31(C-Pyr); 123.83(C-Pyr); 120.99(C-Pyr); 65.70 (-*CH*-Cyclohexyl); 31.58 (-*CH*₂-*CH*₂-cyclohexyl); 24.64(-*CH*₂-*CH*₂-cyclohexyl); 14.44 (-*CH*₃) ppm. Elemental Analysis: Calcd. for C₂₀H₂₄N₄: C, 74.97; H, 7.55; N, 17.48. Found: C, 75.09; H, 7.63; N, 17.61.

Synthesis of Ligand **L2**:



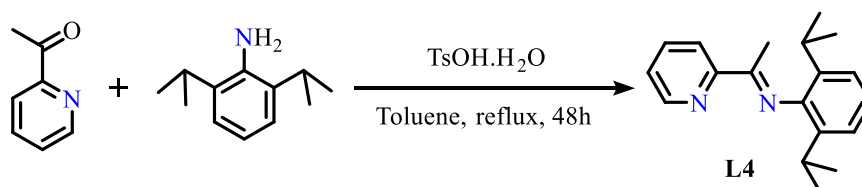
NaBH₄ (0.511 g, 13.51 mmol) was added portionwise in ligand **L** (0.9 g, 3.38mmol) in 20 mL of dry MeOH at room temperature under inert atmosphere. The reaction mixture was stirred for 4h at room temperature. Solvent was evaporated and residue was quenched with water. Product was extracted in dichloromethane, dried over sodium sulphate. Solvent was removed under vacuum yielding 0.81g (90%) pale yellow viscous liquid **L2**. ^1H NMR (400 MHz, Benzene- d_6 , TMS) δ 8.42 (td, $J = 1.6, 4.8$ Hz, 2H, Pyr-*H*); 7.07-7.03 (m, 4H, Pyr-*H*); 6.55 (m, 2H, Pyr-*H*); 3.85-3.77 (m, 2H, -*CH*-*CH*₃); 2.50-2.43 (m, 4H, -*CH*₂-*CH*₂); 1.86 (bs, 2H, -*NH*-); 1.31 (d, $J = 8$, 6H, -*CH*₃) ppm. $^{13}\text{C}\{^1\text{H}\}$ NMR (101 MHz, Benzene- d_6 , TMS) δ 165.65 (C-Pyr); 149.24(C-Pyr); 135.69(C-Pyr); 121.30(C-Pyr); 120.58(C-Pyr); 59.68(-*HC*-*CH*₃); 47.85 (-*CH*₂-*CH*₂-); 23.09 (-*HC*-*CH*₃) ppm. Elemental Analysis: Calcd. for C₁₆H₂₂N₄: C, 71.08; H, 8.20; N, 20.72. Found: C, 71.25; H, 8.35; N, 20.81.

ynthesis of Ligand **L3**:



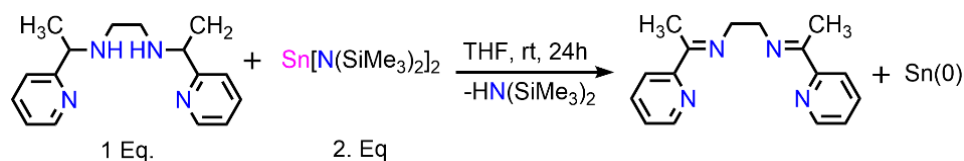
Corresponding diiminodiphosphine ligand (1 g, 1.65 mmol) and LiAlH_4 (0.282 g, 7.44 mmol) were taken in 30 mL of diethyl ether and stirred at room temperature for 24 hours. The mixture was quenched with water and extracted with DCM. The organic layer was separated and dried over anhydrous Na_2SO_4 . The solvent was evaporated under vacuum to obtain a pale yellow sticky solid yielding 0.58 g (57.62%) of **L3**. ^1H NMR (400 MHz, Chloroform- d_3 , TMS) δ 7.45 (ddd, $J=7$ Hz, 4.8Hz, 0.8 Hz, 2H, HC-2); 7.34-7.24 (m, 22 H, Ar-H); 7.16 (dt, $J = 7.6$ Hz, 0.8 Hz, 2H, HC-4); 6.90 (ddd, $J = 7.6$ Hz, 4.4Hz, 1.2 Hz, 2H, HC-5); 3.92 (s, 4H, Ar- CH_2 -NH); 2.50 (s, 4H, - CH_2 - CH_2 -); 1.55 (br s, 2H, NH) ppm. ^{13}C NMR (101 MHz, Chloroform- d_3 , TMS) δ 144.84(d, C-1, $J_{\text{P-C}} = 23.8$ Hz); 136.94 (d, C-6, $J_{\text{P-C}}=10.1$ Hz), 135.81(d, Ar-Cipso, $J_{\text{P-C}} = 13.7$ Hz); 134.06 (d, ArCo, $J_{\text{P-C}} = 19.8$ Hz); 133.66 (C-5); 129.17 (d, Ar-Cm, $J_{\text{P-C}} = 5.4$ Hz); 129.02 (Ar-Cp); 128.79 (C-3); 128.67 (d, C-2, $J_{\text{P-C}} = 6.9$ Hz); 127.23 (C-4); 52.41 (d, N- CH_2 , $J_{\text{P-C}} = 21.16$ Hz); 48.68 (- CH_2 - CH_2 -) ppm. ^{31}P NMR (162 MHz, Chloroform- d_3 , H_3PO_4) $\delta = -15.42$ ppm. Elemental Analysis: Calcd. for $\text{C}_{40}\text{H}_{38}\text{N}_2\text{P}_2$: C, 78.93; H, 6.29; N, 4.60. Found: C, 78.91; H, 6.43; N, 4.55.

Synthesis of Ligand L4:



2,6-diisopropylaniline (4.83 g, 27.25 mmol), 2-acetylpyridine (3.30 g, 27.25 mmol), catalytic amount of $\text{TsOH}\cdot\text{H}_2\text{O}$ (130 mg, 0.78 mmol), and 36 mL toluene charged in a 50 mL round bottom flask adapted with Dean-Stark apparatus. The pale yellow solution was refluxed for 48h. The volatiles were removed under vacuum to afford a dark orange oil, to which Diethylether (40 mL) and sat. NaHCO_3 (aq, 20 mL) were added. The layers were separated, and the aqueous layer was extracted again with diethylether (20 mL). The combined organic extracts were dried over Na_2SO_4 , filtered, and concentrated under vacuum. The concentrated solution was kept overnight to produce 5 g of light yellow crystals (70% yield) of **L4**. ^1H NMR (400 MHz, Chloroform- d_3 , TMS) δ 1.15(d, 12H, 7 Hz), 2.22 (s, 3H), 2.75 (sept, 2H, 7 Hz), 7.10 (m, 1H), 7.19 (m, 2H), 7.39 (ddd, 1H, 7 Hz, 5 Hz, 1 Hz), 7.82 (td, 1H, 8 Hz, 2 Hz), 8.36 (dt, 1H, 8 Hz, 1 Hz), 8.69 (ddd, 1H, 5 Hz, 2 Hz, 1 Hz). ^{13}C NMR (101 MHz, Chloroform- d_3 , TMS) δ 17.46, 23.04, 23.37, 28.39, 121.45, 123.11, 123.70, 124.91, 135.91, 136.60, 146.55, 148.72, 156.61, 167.08

Deprotonation of L2 by Sn[N(SiMe₃)₂]₂ leading to L:



Tetrahydrofuran was added to mixture of ligand **L2** (0.2 g, 0.74 mmol) and Sn[N(SiMe₃)₂]₂ (0.65 g, 1.48 mmol). Immediate colour change with instant precipitate is occurred in the reaction mixture. The reaction mixture was stirred for 24h at room temperature. Reaction mixture was filtered and filtrate was evaporated under vacuum to get red coloured solid. Solid was dissolved in diethyl ether and kept for crystallization to get 70% (0.14 g) of **L**. ¹H NMR (400 MHz, Chloroform-*d*₃, TMS) δ 8.60 (ddd, *J* = 1.2, 2.0, 4.8 Hz, 2H, Pyr-*H*); 8.09 (td, *J* = 0.8, 8 Hz, 2H, Pyr-*H*); 7.71 (td, *J* = 1.6, 7.6 Hz, 2H, Pyr-*H*); 7.29 (ddd, *J* = 1.2, 5.2, 7.2 Hz, 2H, Pyr-*H*); 4.00 (s, 4H, -CH₂-CH₂-); 2.45 (s, 6H, -CH₃) ppm. ¹³C{¹H} NMR (101 MHz, Chloroform-*d*₃, TMS) δ 167.60 (C-CH₃); 157.82 (Pyr-C); 148.33 (Pyr-C); 136.37 (Pyr-C); 124.11 (Pyr-C); 120.98 (Pyr-C); 53.62 (-CH₂-CH₂-); 14.48 (-CH₃)ppm. Elemental Analysis: Calcd. for C₁₆H₁₈N₄: C, 72.15; H, 6.81; N, 21.04. Found: C, 72.30; H, 6.95; N, 21.22

NMR scale reaction: In a NMR tube, THF-*d*₈ was added to mixture of ligand **L2** (20 mg, 0.07 mmol) and Sn[N(SiMe₃)₂]₂ (65 mg, 0.14 mmol) at -50 °C and shaken well. NMR spectra were recorded at different temperatures.

Synthesis of 2: Toluene (20 mL) was added to mixture of ligand **L3** (0.3g, 0.49 mmol) and Sn[N(SiMe₃)₂]₂ (0.22g, 0.49 mmol). The orange reaction mixture was stirred for 12h at room temperature. The pale yellow reaction mixture was filtered and filtrate was concentrated and kept for crystallization to get colourless crystals of compound **5** (Decomp. 128-130 °C) with the yield of 0.28g (80%).

Characterization of **2**: ¹H NMR (400 MHz, Toluene-*d*₈, TMS) δ 7.31-7.39 (m, 8H, Ar-*H*); 7.02-7.13 (m, 18H, Ar-*H*); 6.89 (t, *J* = 8 Hz, 2H, Ar-*H*); 4.61 (d, *J* = 16 Hz, 2H, -CH₂-); 4.25 (bs, 2H, -CH₂-); 3.49 (bs, 2H, -CH₂-); 2.99 (bs, 2H, -CH₂-) ppm. ³¹P{¹H} NMR (162 MHz, Tol-*d*₈) δ -16.54 (*J*_{P-Sn} = 175.5 Hz) ppm ¹¹⁹Sn{¹H} NMR (149.27 MHz, Toluene-*d*₈) δ 46.12 (t, *J*_{Sn-P} = 173.2 Hz) ppm. Elemental Analysis: Calcd. for C₈₀H₇₂N₄P₄Sn₂: C, 66.23; H, 5.00; N, 3.86. Found: C, 66.19; H, 5.20; N, 3.95.

VT NMR for 2: Compound 2 was dissolved in Tol-*d*₈ and NMR (¹H and ³¹P) were recorded at temperature ranges from 223 K to 368 K with difference of 20 K

Synthesis of 3 and 3a:

Method A Toluene (10 mL) was added to a mixture of ligand **L/L1** (1.25 mmol) and Sn[N(SiMe₃)₂]₂ (2.5 mmol) and stirred it for 48 h at room temperature. All the volatiles were evaporated under vacuum to get green solid. The green solid was washed with 4-5 mL of pentane to get yellow coloured residue. The yellow residue was further dissolved into diethyl ether and filtered to remove small amount of metallic tin. Solvent was removed under vacuum to get yellow coloured powder of **3** in 82% (0.87 g) (Decomp. 165 – 167 °C).

Method B Ligand **L/L1** (1.25 mmol) and Sn[N(SiMe₃)₂]₂ (2.5 mmol) was heated in a schlenk tube at 60°C for 1 h. The residue was washed with small amount of pentane to get orange solid. The solid was dissolved in toluene and filtered to remove small amount of metallic tin. Solvent was removed under vacuum to get orange yellow solid in 85% (0.93 g) of **3**.

Characterization of **3**: ¹H NMR (400 MHz, Benzene-*d*₆, TMS) δ 7.66 (ddd, *J* = 5.36, 1.6, 0.84 Hz, 2H, Pyr-*H*); 7.43 (d, *J* = 8.48 Hz, 2H, Pyr-*H*); 6.72 (td, *J* = 7.4, 1.68 Hz, 2H, Pyr-*H*); 6.22 (td, *J* = 0.96, 7.2 Hz, 2H, Pyr-*H*); 4.87 (d, *J* = 1.52 Hz, 2H, C=CH₂); 4.43 (d, *J* = 1.52 Hz, 2H, C=CH₂); 4.15 (d, *J* = 8 Hz, 2H, -CH-CH- cyclohexyl); 2.97 (d, 2H, *J* = 12 Hz, -CH-CH- cyclohexyl); 1.83-1.51 (m, 6H, -CH₂-CH₂- cyclohexyl); 0.34 (s, 36H, SiMe₃-*H*) ppm. ¹³C{¹H} NMR (101 MHz, Benzene-*d*₆, TMS) δ 158.79 (C=CH₂); 151.91 (Pyr-C); 142.88 (Pyr-C); 137.96 (Pyr-C); 122.36 (Pyr-C); 121.69 (Pyr-C); 82.13 (C=CH₂); 63.24(-CH-CH- cyclohexyl); 31.07 (-CH₂-CH₂- cyclohexyl); 25.71 (-CH₂-CH₂- cyclohexyl); 6.76 (-Si(CH₃)₃)ppm. ²⁹Si{¹H} NMR (79.53 MHz, Benzene-*d*₆) δ -1.30 ppm. ¹¹⁹Sn{¹H} NMR (149.7 MHz, Benzene-*d*₆) δ -47.05 ppm. Elemental Analysis: Calcd. for C₃₂H₅₈N₆Si₄Sn₂: C, 43.84; H, 6.67; N, 9.59. Found: C, 43.89; H, 6.61; N, 9.45.

Synthesis of Compound 4: Tetrahydrofuran (10 mL) was added to a mixture of ligand **L** (0.4 g, 1.25 mmol) and Sn[N(SiMe₃)₂]₂ (0.545 g, 1.25 mmol) and stirred it for 24 h at room temperature. The intense purple solution was filtered through a plug of celit. The resultant purple filtrate was concentrated and kept aside for crystallization. The intense purple crystal appeared after 24 h which was separated to get **4** as purple solid with 40% (0.230 g)

Characterization of **4** ^1H NMR (400 MHz, Toluene- d_8) δ 8.62 (d, $J = 4.8$ Hz, 1H), 8.32 (d, $J = 5.8$ Hz, 1H), 7.81 (d, $J = 4.4$ Hz, 1H), 7.71 (d, $J = 4.9$ Hz, 1H), 7.68 (d, $J = 8.3$ Hz, 1H), 7.39 (d, $J = 7.7$ Hz, 1H), 7.34 (d, $J = 8.3$ Hz, 1H), 7.24 (td, $J = 7.6, 1.8$ Hz, 1H), 7.06 (s, 1H), 6.91 – 6.70 (m, 5H), 6.52 (dd, $J = 22.2, 6.9$ Hz, 2H), 5.92 (t, $J = 6.7$ Hz, 1H), 5.19 (d, $J = 10.1$ Hz, 1H), 4.64 (s, 1H), 4.29 (s, 1H), 4.17 (s, 1H), 3.91 (s, $J = 10.9$ Hz, 1H), 3.74 (t, $J = 12.5$ Hz, 2H), 3.32 (d, $J = 27.0$ Hz, 1H), 3.23 (s, 2H), 2.99 (t, $J = 16.5$ Hz, 2H) ppm. ^{13}C NMR (101 MHz, Toluene- d_8) δ 162.93, 161.93, 159.37, 157.54, 157.03, 154.60, 152.11, 148.71, 144.79, 143.43, 142.28, 123.93, 123.37, 122.10, 121.65, 121.50, 120.92, 120.44, 114.26, 96.78, 78.16, 76.76, 53.66, 53.10, 50.28, 47.63, 46.72 ppm. ^{119}Sn NMR (149 MHz, Toluene- d_8) δ -298.86, -375.91 ppm. Elemental Analysis: Calcd. for $\text{C}_{16}\text{H}_{22}\text{N}_4$: C, 50.30; H, 3.96; N, 14.67. Found: C, 51.02; H, 3.75; N, 15.10

Time dependant NMR for 4: In NMR tube, 0.04 g of **L** and 0.052 g of $\text{Sn}[\text{N}(\text{SiMe}_3)_2]_2$ was added in 0.6 mL of THF- d_8 . The NMR tube shaken well and submitted for NMR, NMR were recorded at a different time interval.

Synthesis of Compound 5: Tetrahydrofuran (10 mL) was added to a mixture of ligand **L4** (0.35 g, 1.25 mmol) and $\text{Sn}[\text{N}(\text{SiMe}_3)_2]_2$ (0.545 g, 1.25 mmol) and stirred it for 24 h at room temperature. The solvent was removed under vacuum from reaction mixture to get yellow solid powder which was dissolved in diethyl ether, and then filtered. Solvent was evaporated from the filtrate to obtained compound **5** as a yellow coloured solid powder with the yield of 80% (0.56 g)

Characterization of **5** ^1H NMR (400 MHz, C_6D_6) δ 7.74 (d, $J = 5.4$ Hz, 1H), 7.34 (dd, $J = 6.5, 2.7$ Hz, 1H), 7.26 (dd, $J = 9.1, 5.2$ Hz, 3H), 7.15 (s, 1H), 6.74 (t, $J = 7.8$ Hz, 1H), 6.38 – 6.31 (m, 1H), 4.57 (s, 1H), 4.00 (dt, $J = 13.7, 6.9$ Hz, 1H), 3.79 (d, $J = 0.9$ Hz, 1H), 3.05 (dd, $J = 13.7, 6.9$ Hz, 1H), 1.49 (d, $J = 6.9$ Hz, 3H), 1.40 (d, $J = 6.8$ Hz, 3H), 1.30 (dd, $J = 8.8, 7.0$ Hz, 6H), 0.19 (s, 18H). ^{13}C NMR (101 MHz, C_6D_6) δ 157.95, 153.00, 148.16, 145.71, 143.62, 141.80, 138.33, 125.77, 124.63, 123.65, 122.84, 122.23, 86.08, 28.31, 28.15, 26.09, 25.96, 24.56, 24.33, 6.36. ^{29}Si NMR (80 MHz, C_6D_6) δ 0.523. ^{119}Sn NMR (149 MHz, C_6D_6) δ 0.23.

Synthesis of Compound 6: Tetrahydrofuran (10 mL) was added to a mixture of ligand **L4** (0.70 g, 2.5 mmol) and $\text{Sn}[\text{N}(\text{SiMe}_3)_2]_2$ (0.545 g, 1.25 mmol) and stirred it for 24 h at room temperature. The solvent was removed under vacuum from the reaction mixture to get yellow solid powder which was dissolved in diethyl ether, and then filtered. Solvent was evaporated

from the filtrate to obtained compound **4** as yellow coloured solid powder with the yield of 76% (0.82 g)

Characterization of **6**: ^1H NMR (400 MHz, C_6D_6) δ 7.42 (d, $J = 8.4$ Hz, H), 7.34 (dd, $J = 7.7$, 1.6 Hz, 2H), 7.19 (t, $J = 7.7$ Hz, 2H), 6.91 (dd, $J = 7.7$, 1.5 Hz, 2H), 6.87 (ddd, $J = 5.4$, 1.7, 0.9 Hz, 2H), 6.72 (ddd, $J = 8.4$, 7.4, 1.7 Hz, 2H), 6.22 (ddd, $J = 7.3$, 5.4, 1.0 Hz, 2H), 3.68 (dt, $J = 14.0$, 7.0 Hz, 2H), 3.56 – 3.44 (m, 2H), 1.53 (d, $J = 6.9$ Hz, 6H), 1.39 (d, $J = 6.8$ Hz, 6H), 1.35 (d, $J = 6.8$ Hz, 6H), 0.51 (d, $J = 6.9$ Hz, 6H). ^{13}C NMR (101 MHz, Benzene- d_6) δ 155.84, 151.66, 148.65, 145.97, 145.45, 144.16, 136.36, 124.87, 124.25, 123.36, 121.46, 120.80, 83.85, 28.46, 28.00, 26.46, 26.41, 25.27, 21.95. ^{119}Sn NMR (149 MHz, C_6D_6) δ -303.57.

Synthesis of compound 7: AgOTf (0.14g, 0.54 mmol) was added to a tetrahydrofuran (20 mL) solution of comp. **3** (0.2g, 0.27 mmol) at room temperature. Colour of the reaction mixture instantly changed from yellow to orange. The reaction mixture was stirred for 1 h at room temperature and then it was concentrated, followed by layering with pentane to get colorless crystals of compound **7** with crystallization yield of 40% (0.067g).

Characterization of **7**: ^1H NMR (400 MHz, Acetonitrile- d_3 , TMS) δ 9.16 (s, 2H, Pyr-*H*); 8.41 (dt, $J = 8$, 1.6 Hz, 2H, Pyr-*H*); 8.31 (td, $J = 8$, 1Hz, 2H, Pyr-*H*); 8.02 (s, Pyr-*H*); 4.56 (s, 2H, Cy-*H*); 2.69 (s, 6H, - CH_3); 2.47 (s, 2H, Cy-*H*); 2.04 (m, 4H, Cy-*H*); 1.66 (t, 2H, Cy-*H*) ppm. $^{13}\text{C}\{^1\text{H}\}$ NMR (101 MHz, Acetonitrile- d_3 , TMS) 150.57 (CH_3 -C); 148.33 (Pyr-Co); 143.29 (Pyr- Co); 129.41 (Pyr-Cp); 126.93 (Pyr-Cm); 125.74 (Pyr-Cm); 122.55, 119.37 (CF_3SO_3); 66.64 (Cy- CH -); 31.06 (Cy- CH_2); 24.61 (Cy- CH_2); 17.64 (CCH_3) ppm. $^{19}\text{F}\{^1\text{H}\}$ NMR (377 MHz, Acetonitrile- d_3 , TMS) δ -79.34 (TMSOTf- *F*) ppm $^{119}\text{Sn}\{^1\text{H}\}$ NMR (149.74 MHz, C_6D_6) δ -595.80 ppm Elemental Analysis: Calcd. for $\text{C}_{22}\text{H}_{24}\text{F}_6\text{N}_4\text{O}_6\text{S}_2\text{Sn}$: C, 35.84; H, 3.28; N, 7.60. Found: C, 35.98; H, 3.50; N, 7.91.

Reaction of 3 with TMSOTf: Trimethylsilyl trifluoromethane sulphonate (41 μL , 0.228 mmol) was added to toluene solution of compound **1** (0.1 g, 0.114 mmol) and reaction mixture was stirred for 1 h at room temperature. Solvent was removed by evaporation and the residue was dissolved in DCM. The reaction mixture was filtered and the filtrate was concentrated. Concentrated DCM solution was layered with pentane to get colourless crystals of compound **7** and **8**.

Synthesis of compound 9: AgOTf (0.05 g, 0.194mmol) was added to 10 mL of THF solution of **6** (0.131 g, 0.194mmol) at room temperature and reaction mixture was stirred for 2h. The

reaction mixture was concentrated and layered with diethyl ether to get yellow coloured of crystal of compound **9** in 30% (0.054 g) yield (Crystallization Yield). Due to high instability of the complex, we were unable to record NMR spectra.

Synthesis of compound 10: AgOTf (0.05 g, 0.194mmol) was added to 10 mL of THF solution of **6** (0.262g, 0.388mmol) at room temperature and the reaction mixture was stirred for 2h. The reaction mixture was concentrated and layered with diethyl ether to get yellow-colored of crystal of compound **10** in 45% yield (0.14 g, Crystallization Yield). Due to high instability of the complex, we were unable to record NMR spectra..

Synthesis of compound 11: TMSOTf (30 μ L, 0.167 mmol) was added to 10 mL THF solution of AuCl.SMe₂ (0.05 g, 0.167 mmol), to that of **6** (0.226g, 0.334mmol) was added at room temperature and the reaction mixture was stirred for 2h. The reaction mixture was concentrated and layered with diethyl ether to get yellow colored of crystal of compound **11** in 32% yield (0.090 g, Crystallization Yield). Due to high instability of the complex, we were unable to record NMR spectra..

2A.4.3 Plots of NMR Spectra

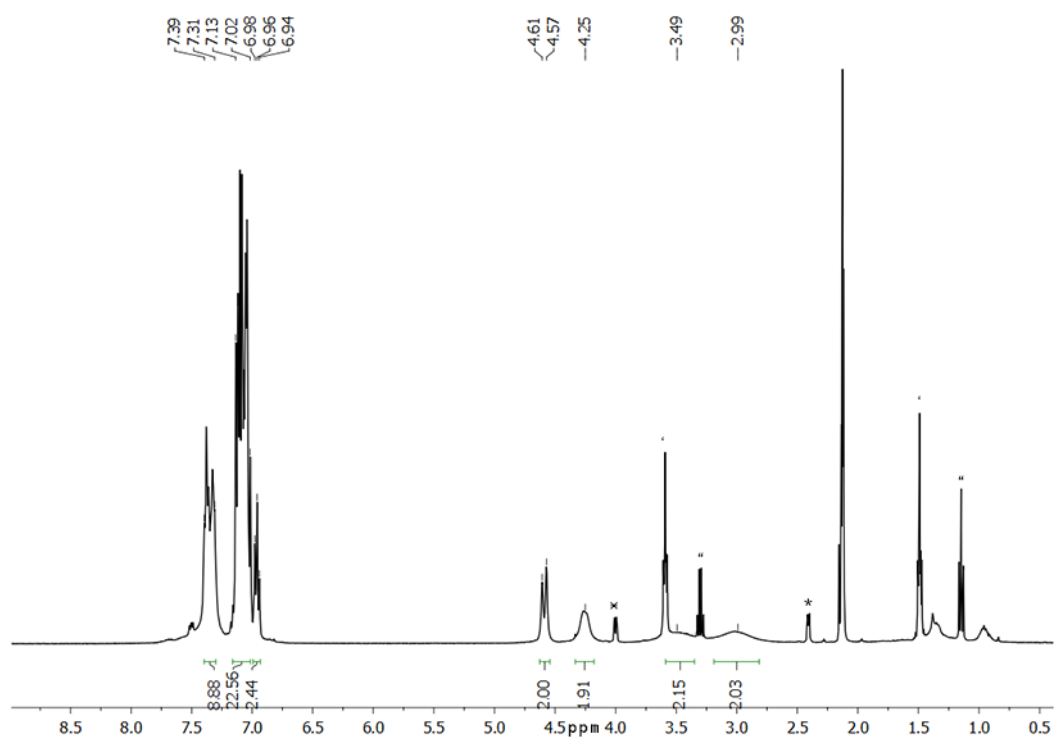


Figure 2A.16. ^1H NMR of 2 (* = starting Material, ' = Tetrahydrofuran, " = Diethyl Ether).

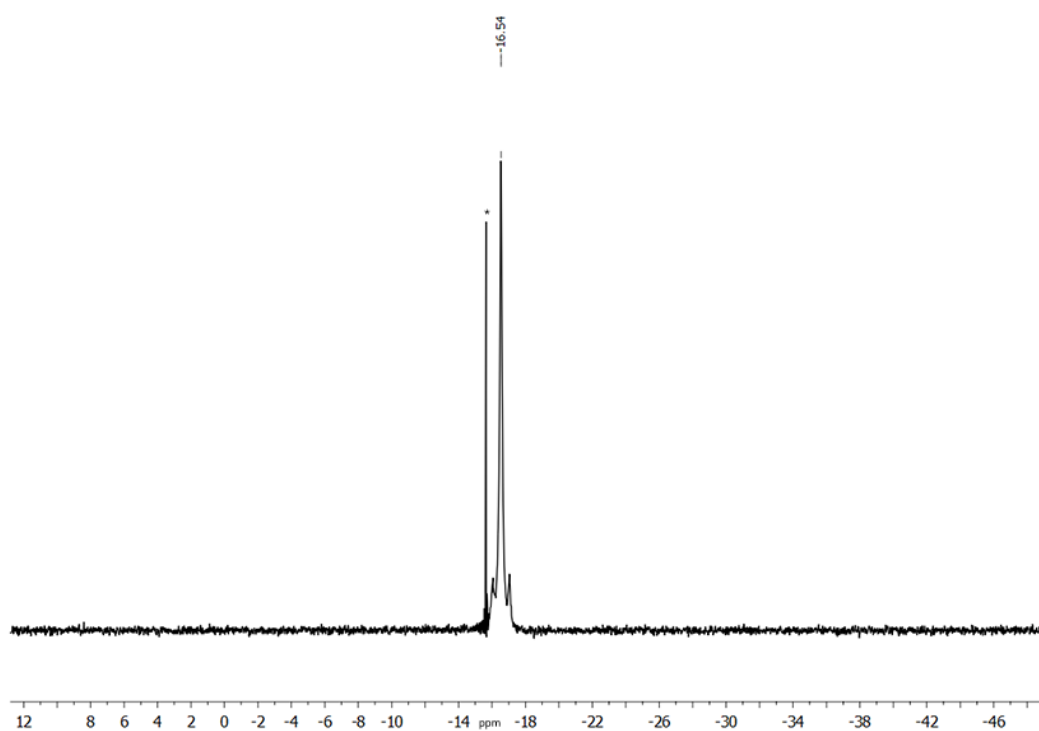


Figure 2A.17. ^{31}P NMR of 2 (* = Starting Material).

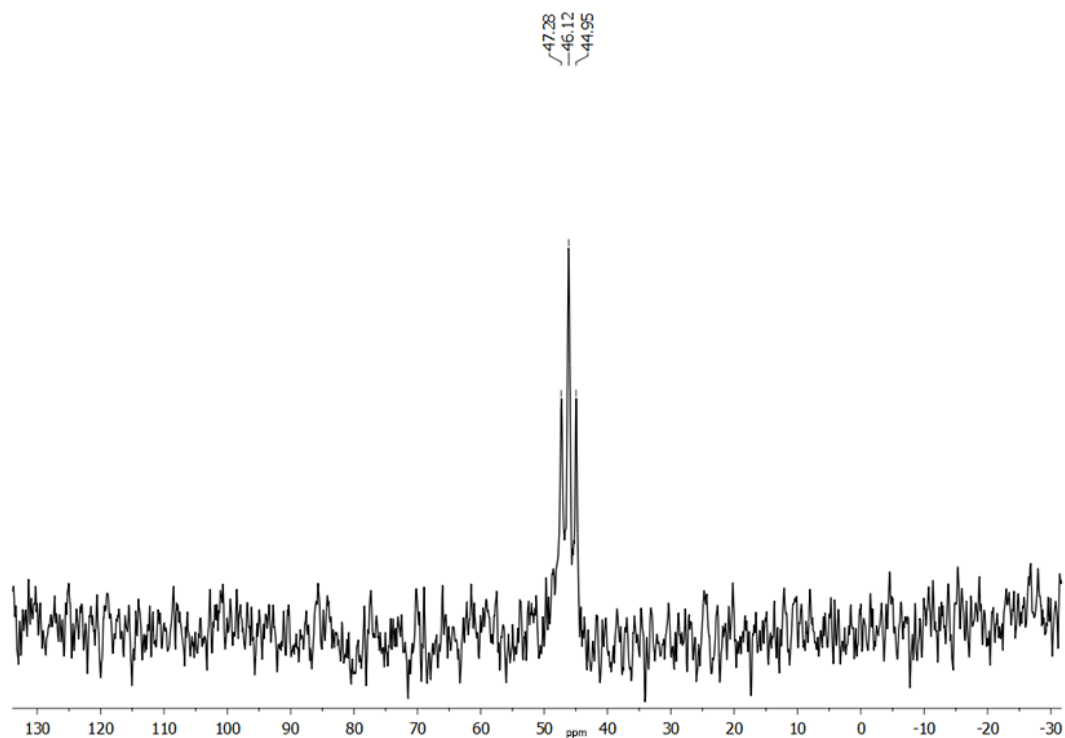


Figure 2A.18. ^{119}Sn NMR of **2**.

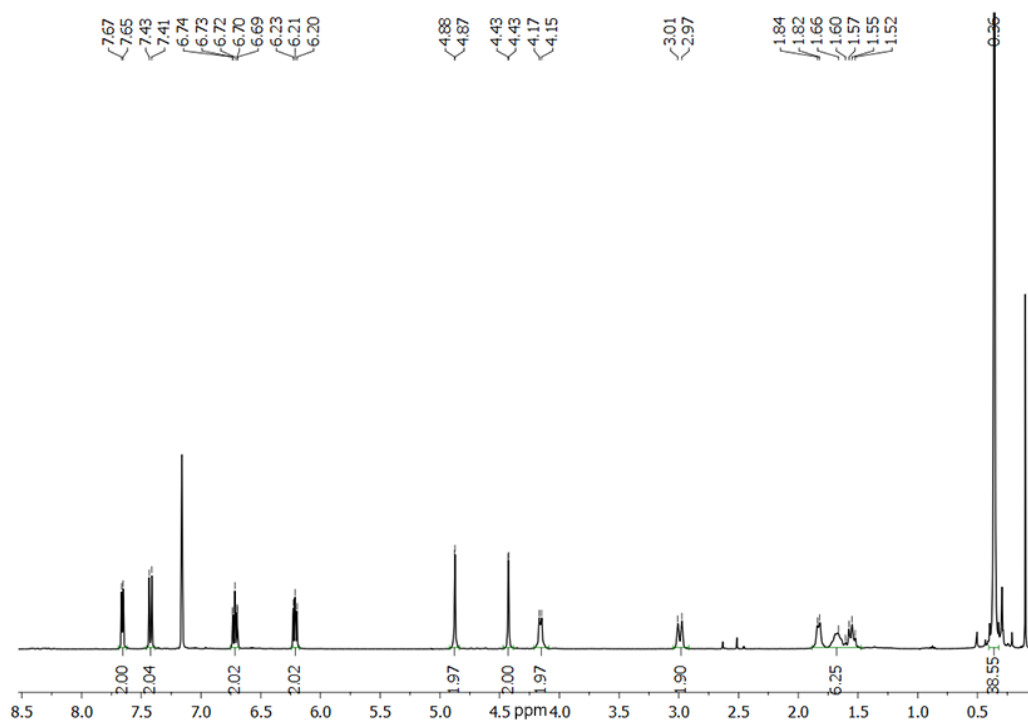


Figure 2A.19. ^1H NMR of **3**.

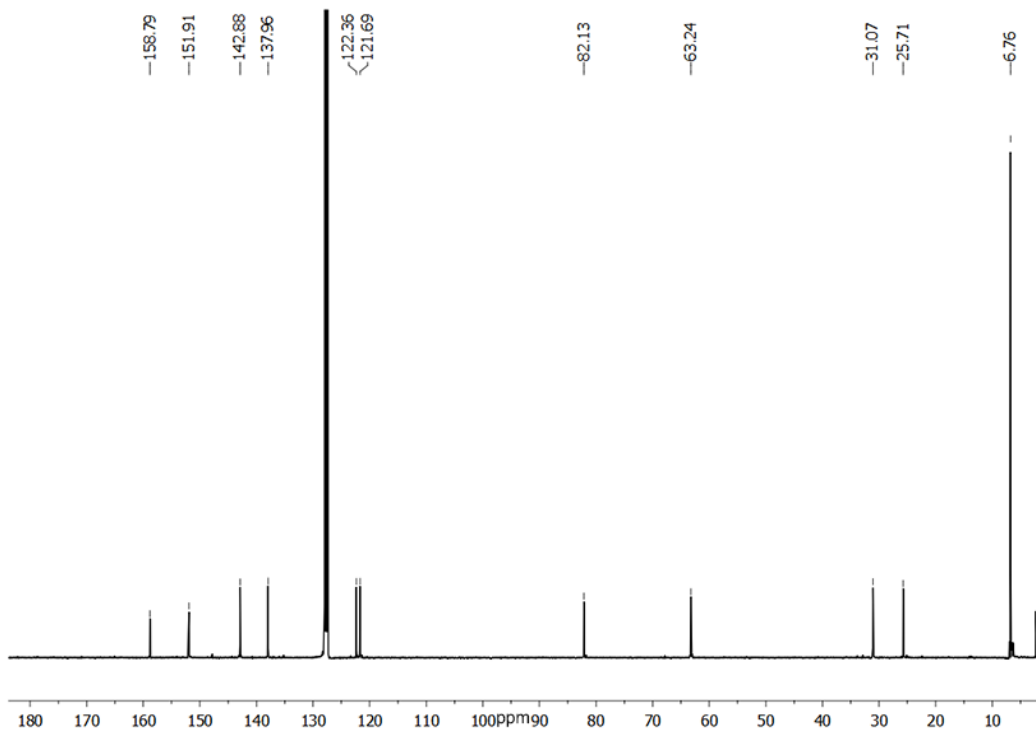


Figure 2A.20. ^{13}C NMR of 3.

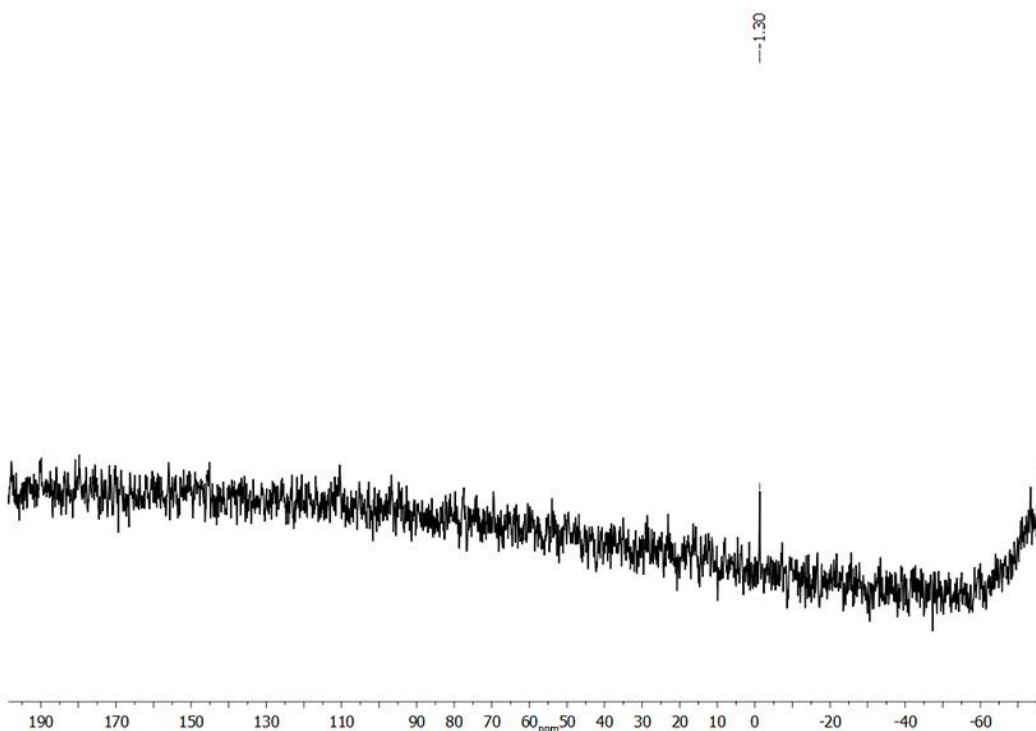


Figure 2A.21. ^{29}Si NMR of 3.

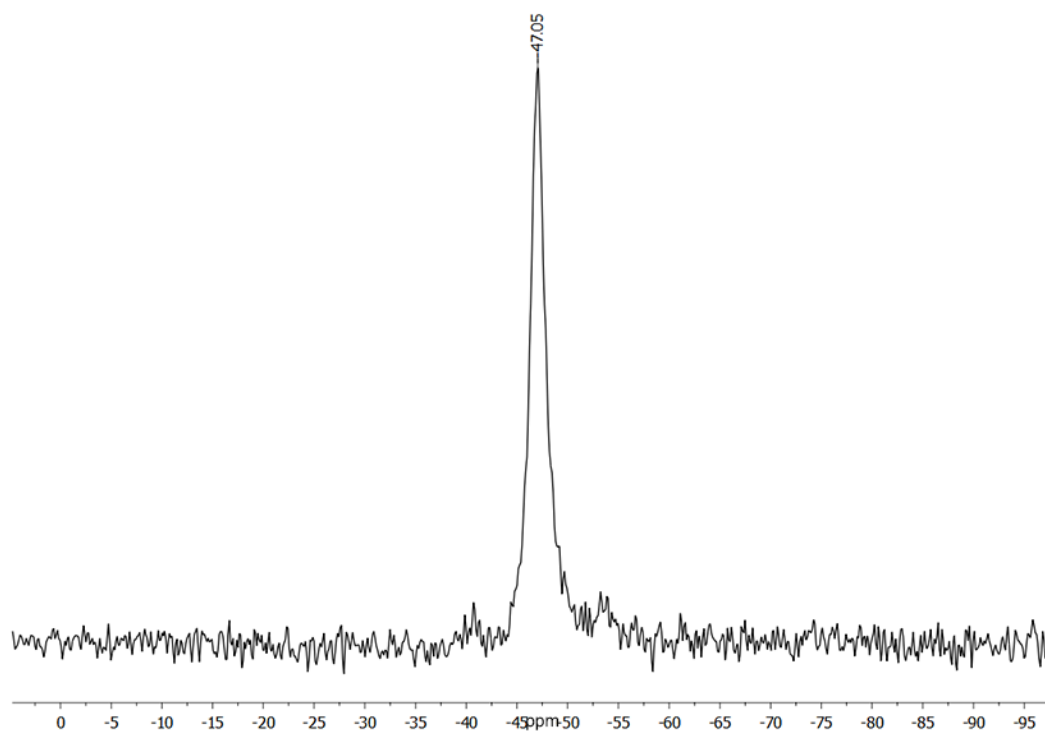


Figure 2A.22. ^{119}Sn NMR of 3.

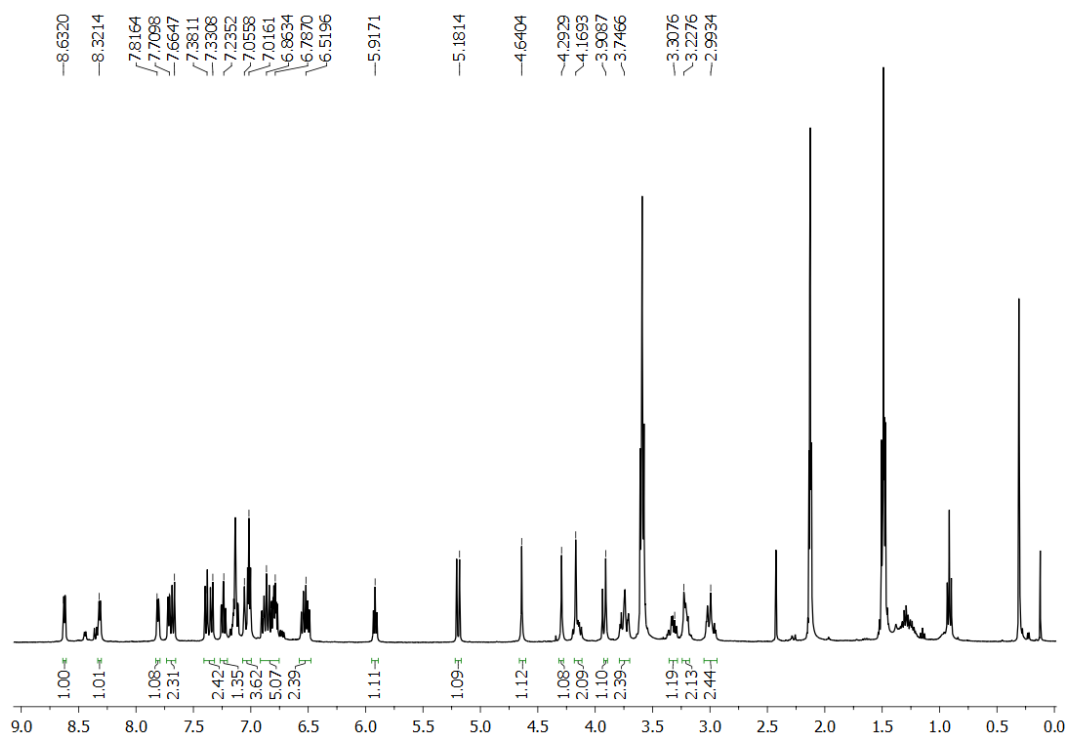


Figure 2A.23. ^1H NMR of 4.

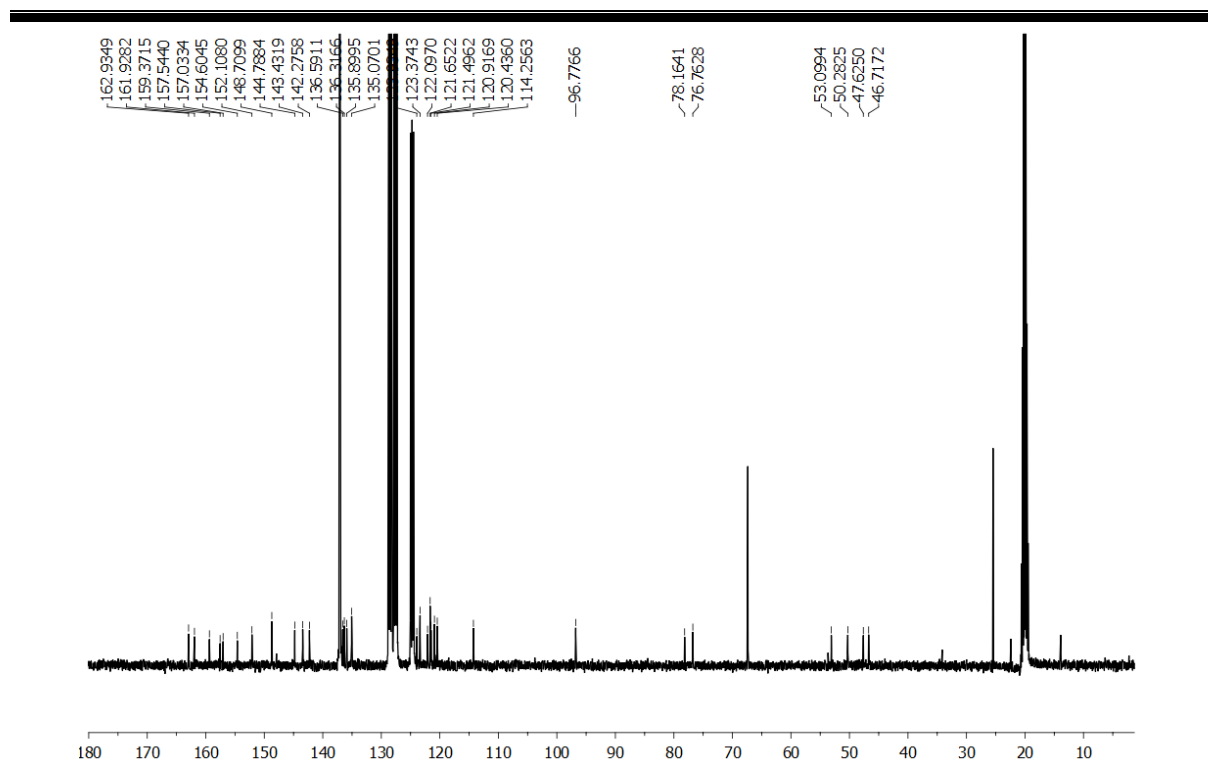


Figure 2A.24. ^{13}C NMR of 4.

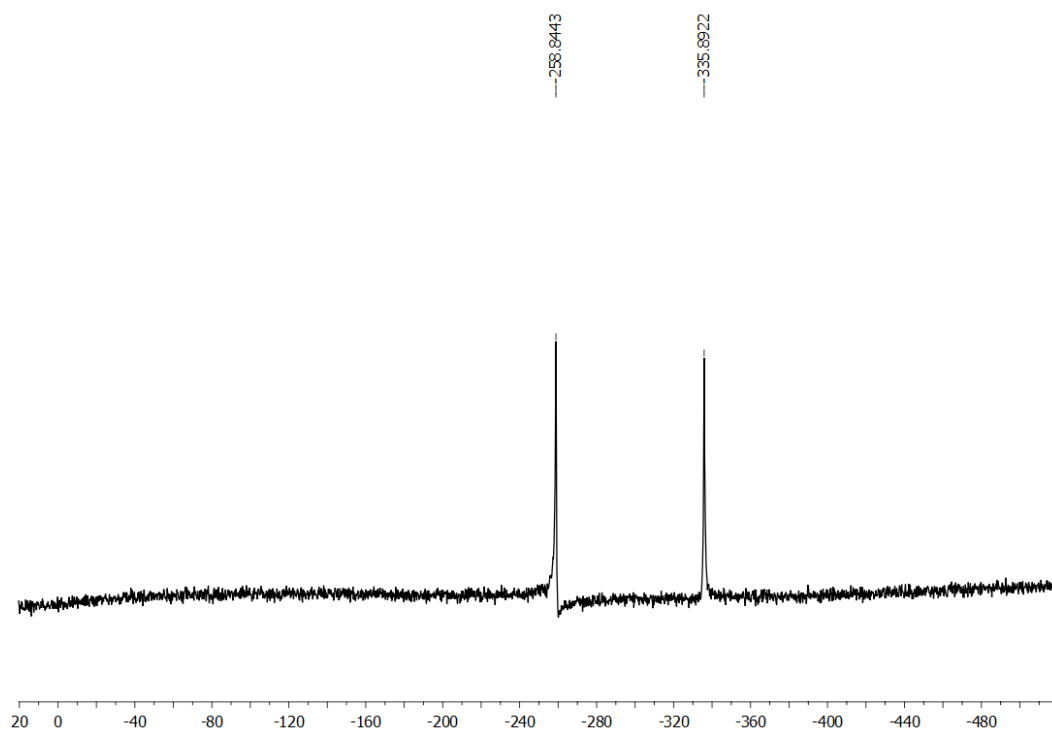


Figure 2A.25. ^{119}Sn NMR of 4.

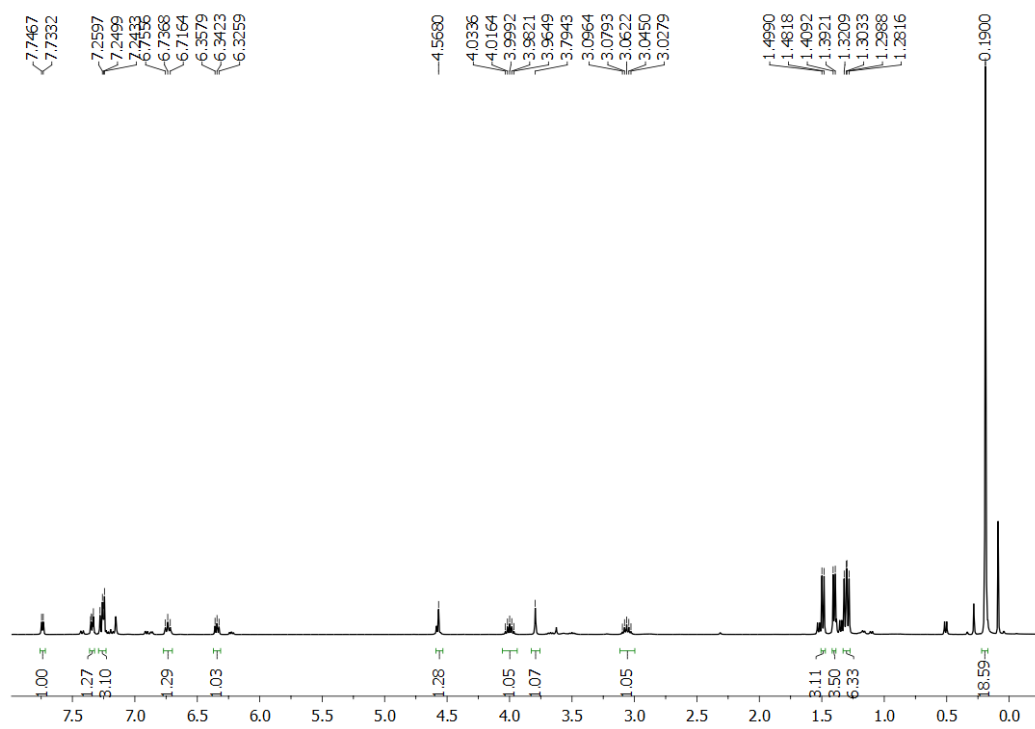


Figure 2A.26. ^1H NMR of 5.

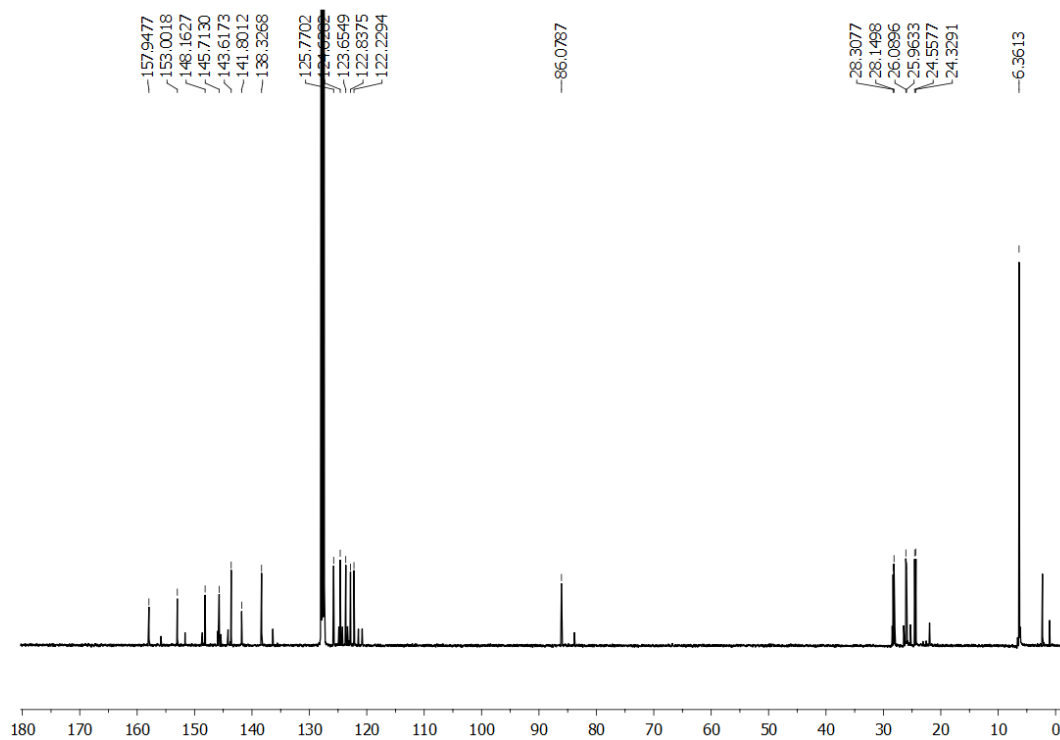


Figure 2A.27. ^{13}C NMR of 5.

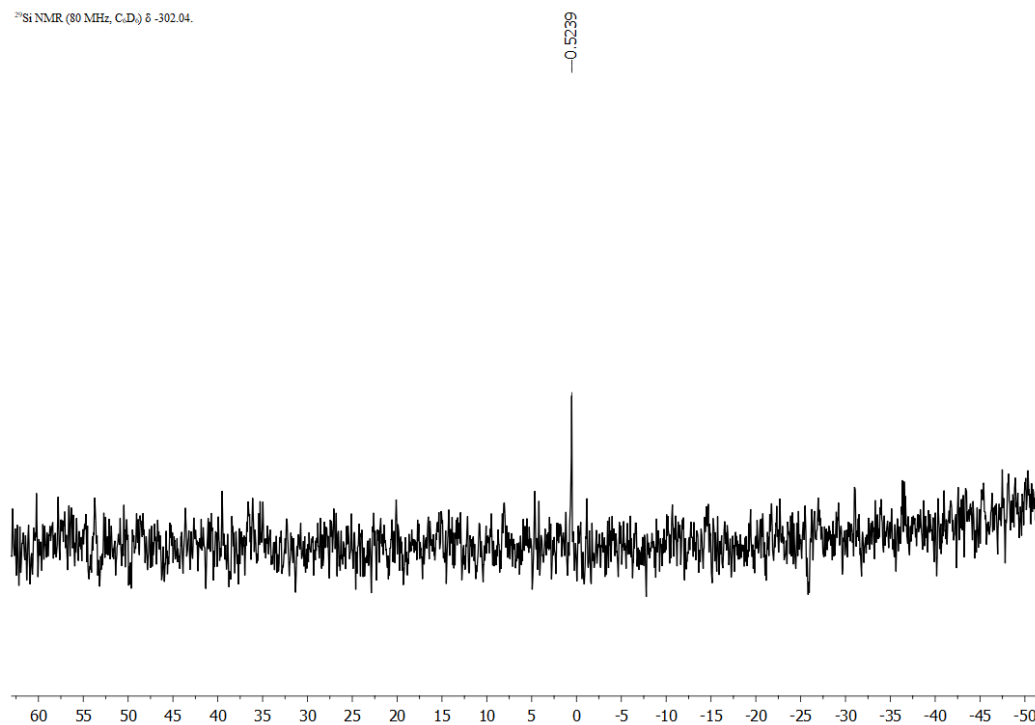


Figure 2A.28. ^{29}Si NMR of **5**.

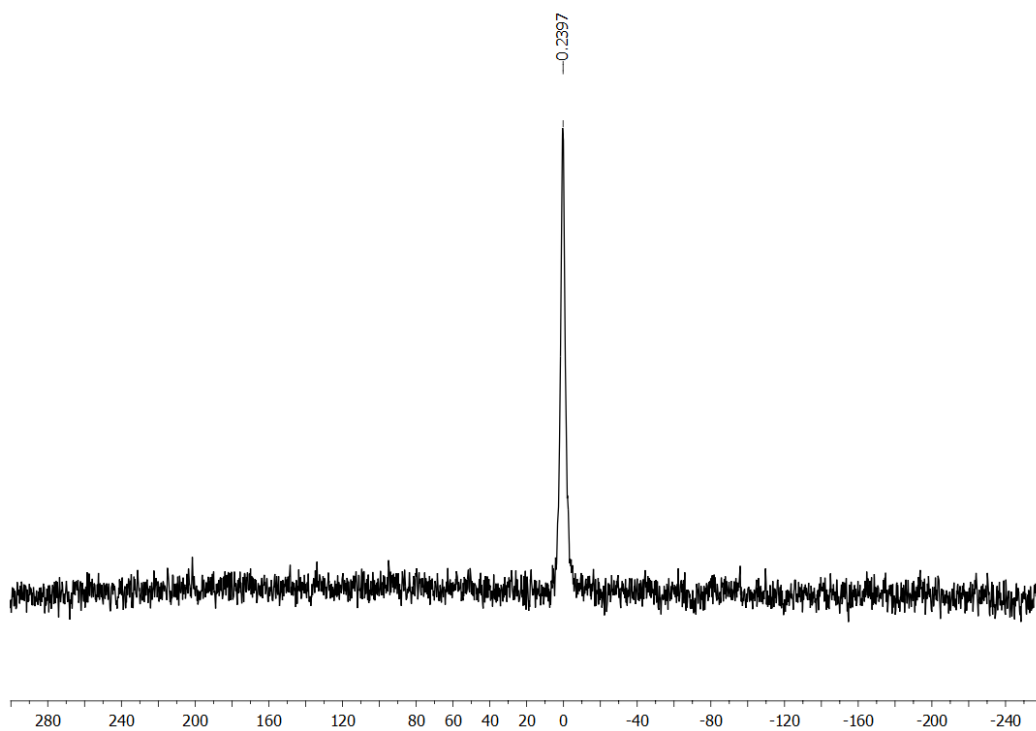


Figure 2A.29. ^{119}Sn NMR of **5**.

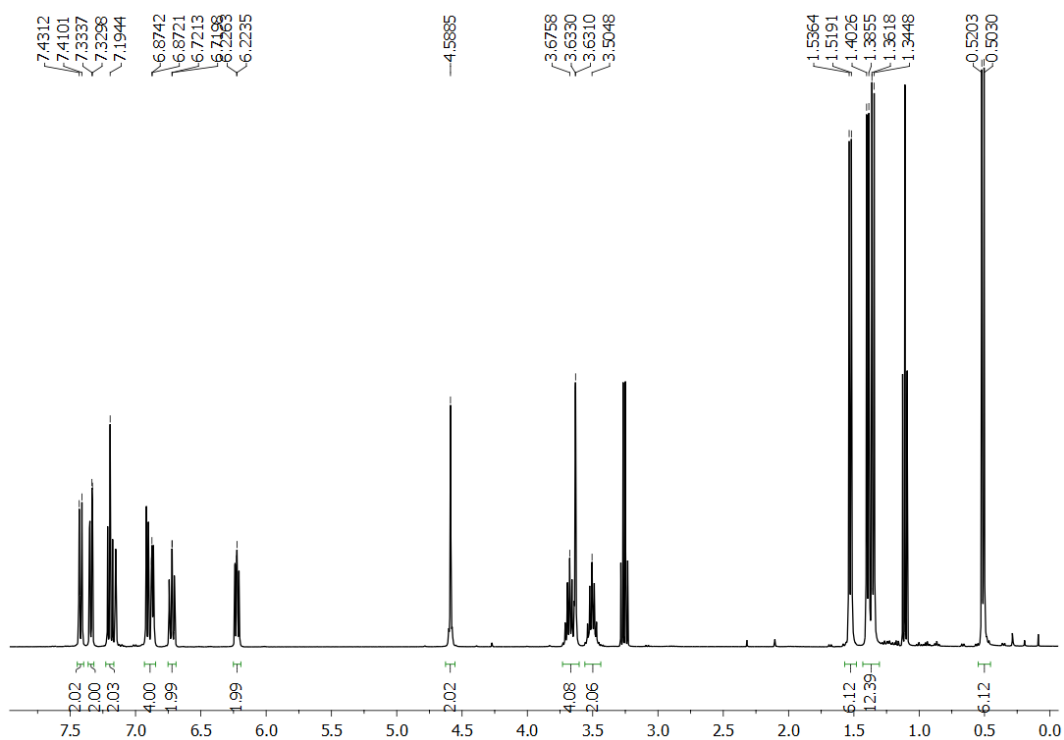


Figure 2A.30. ^1H NMR of 6..

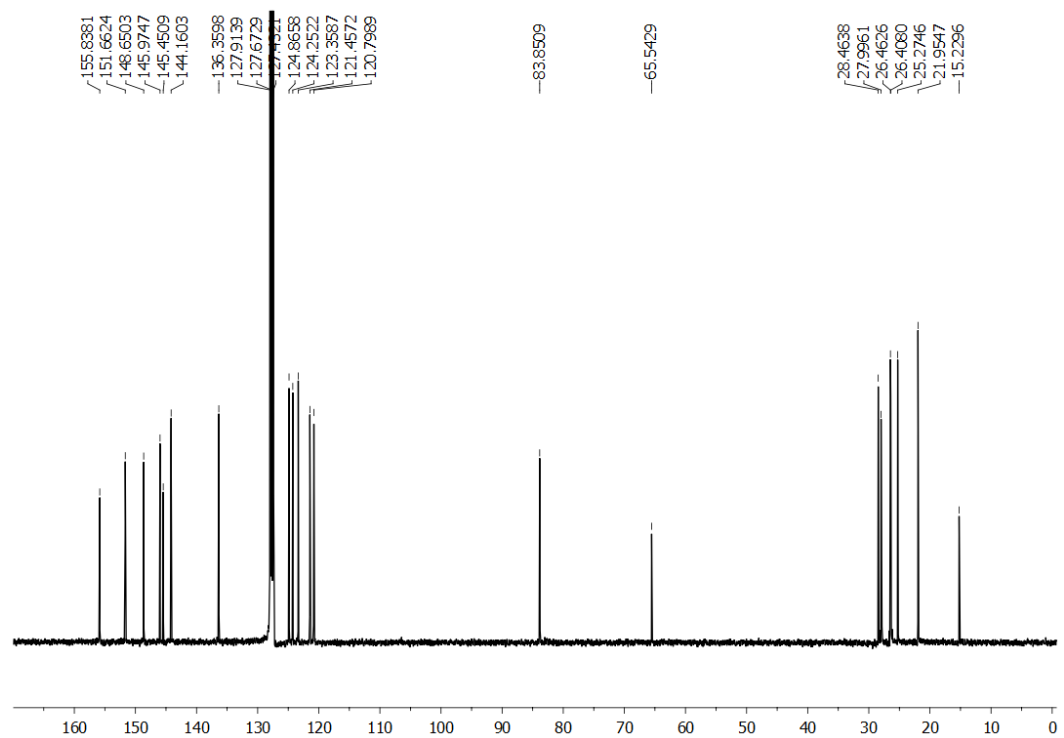


Figure 2A.31. ^{13}C NMR of 6.

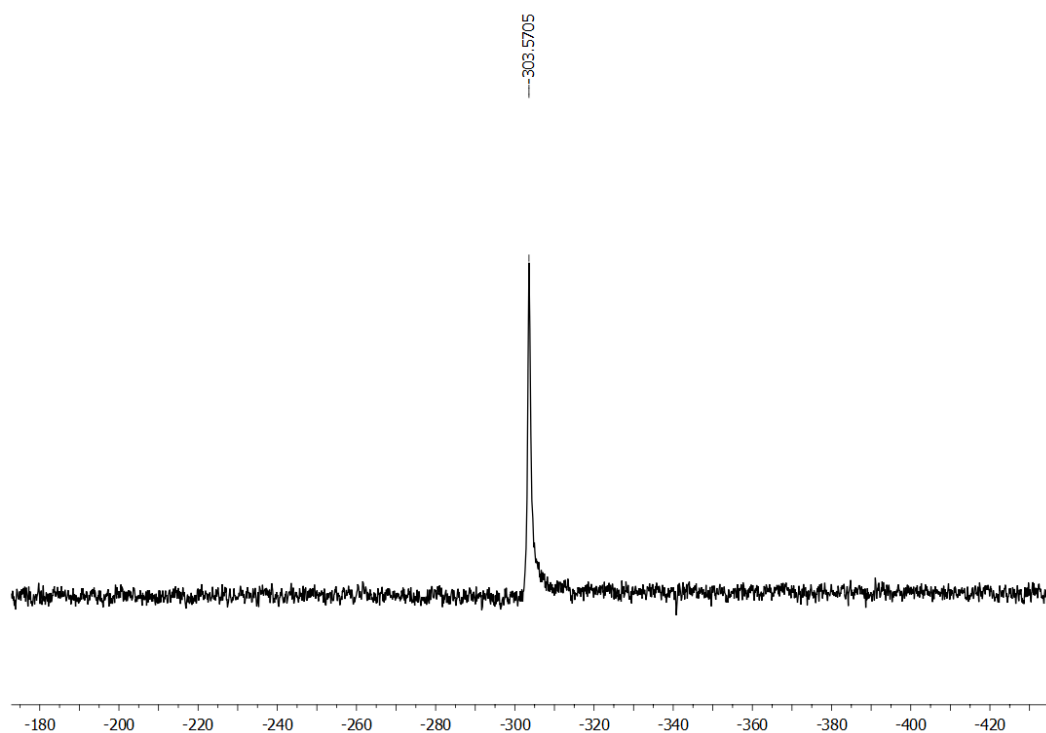


Figure 2A.32. ^{119}Sn NMR of **6**.

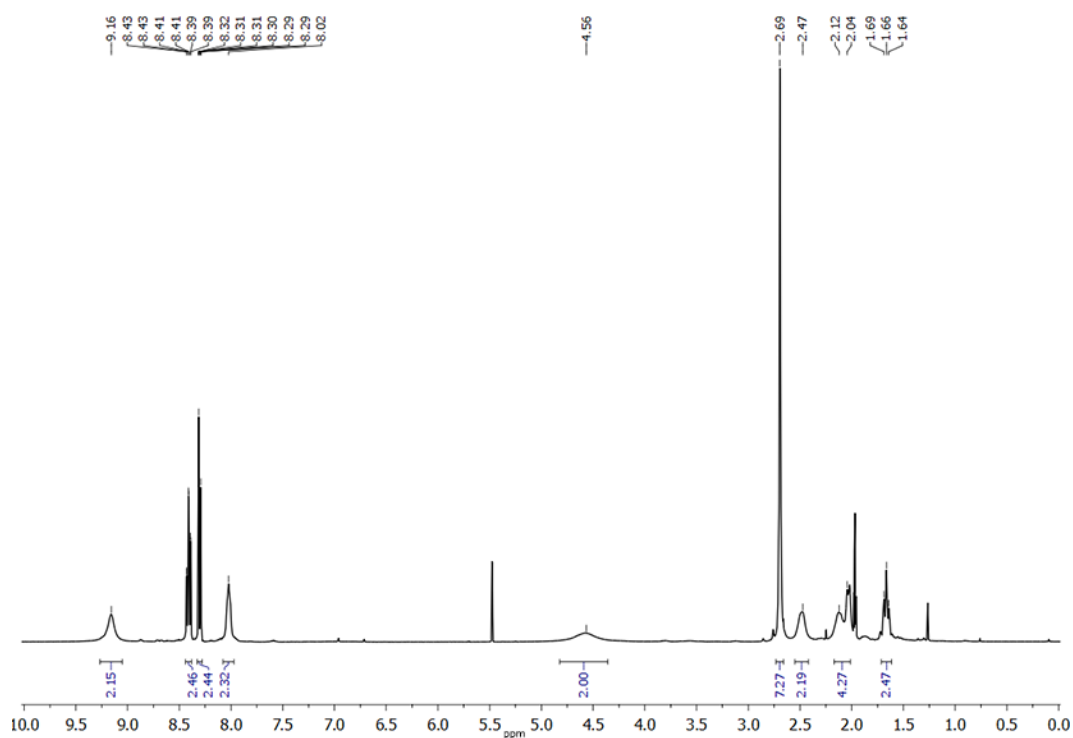


Figure 2A.33. ^1H NMR of **7**.

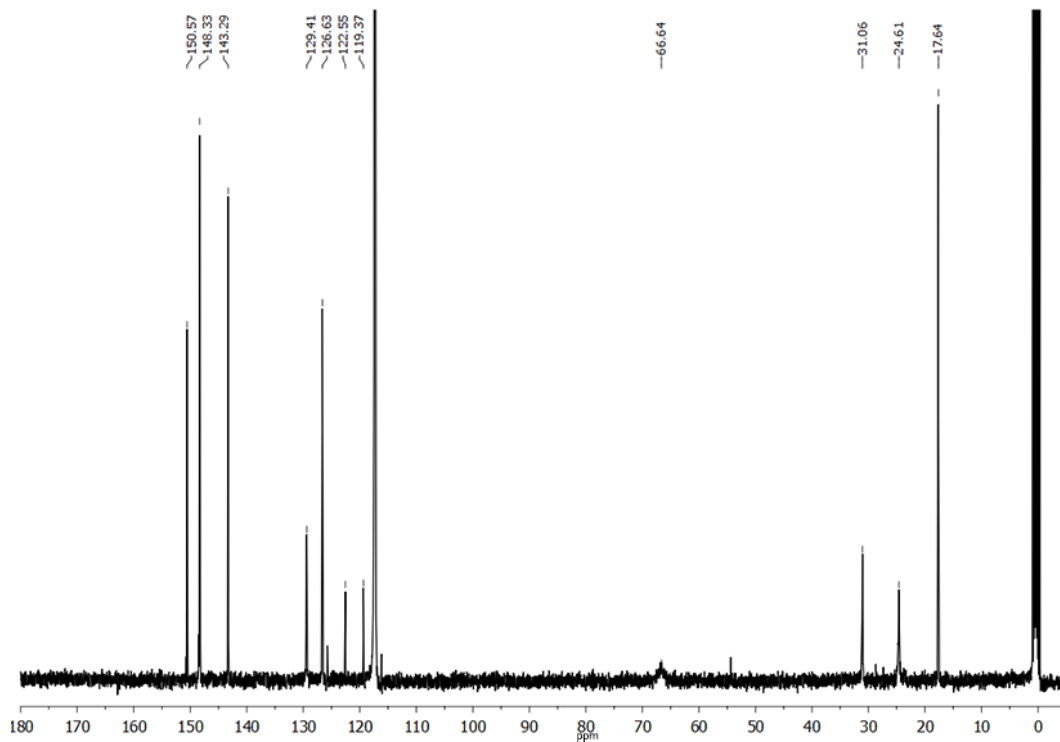


Figure 2A.34. ^{13}C NMR of 7.

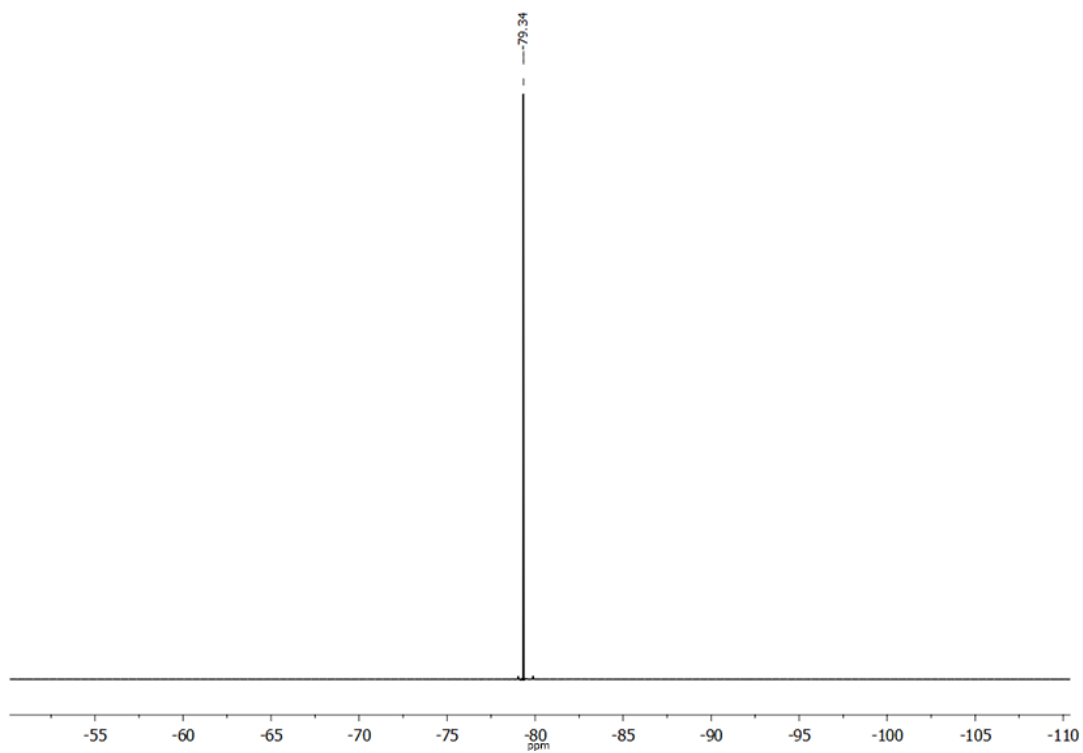


Figure 2A.35. ^{19}F NMR of 7.

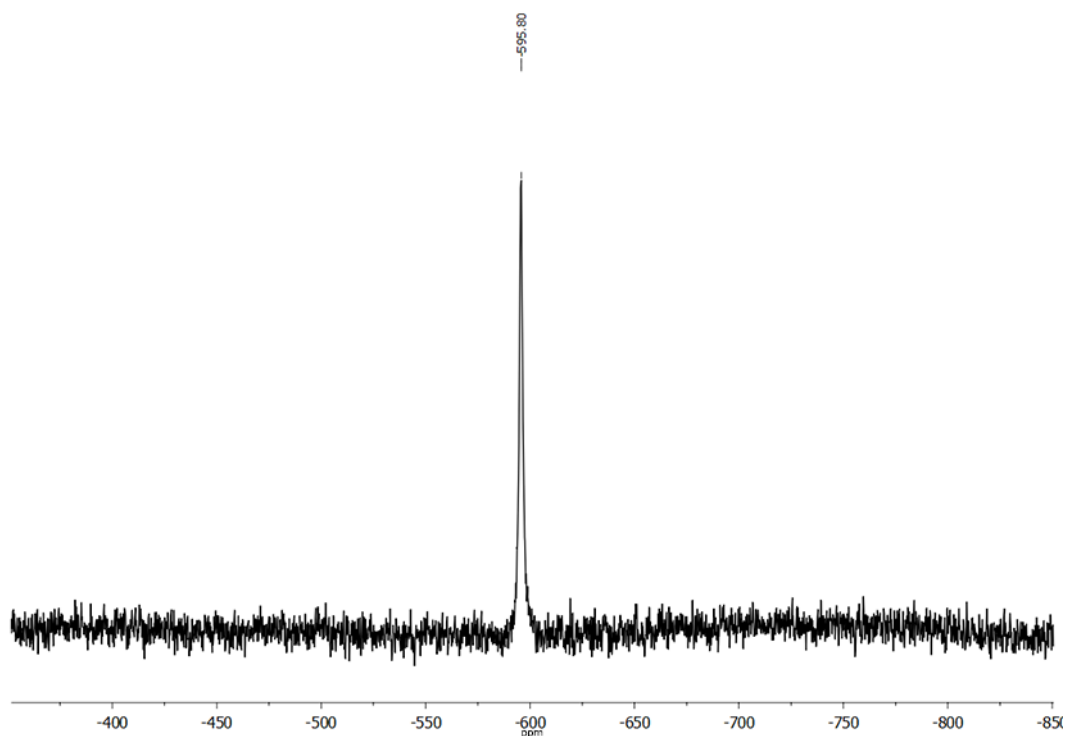


Figure 2A.36. ^{119}Sn NMR of **7**.

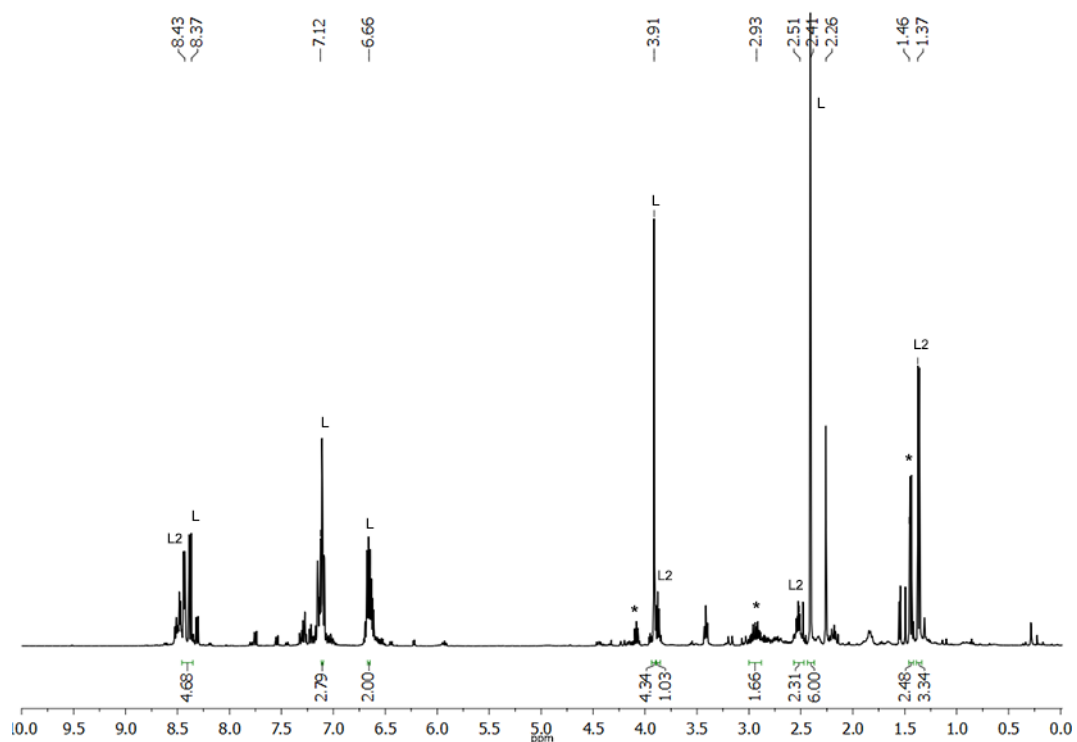


Figure 2A.37. ^1H NMR in C_6D_6 of reaction mixture obtained after 4 days from the reaction between **L2** and $\text{Sn}[\text{N}(\text{SiMe}_3)_2]_2$ (* = stannylene).

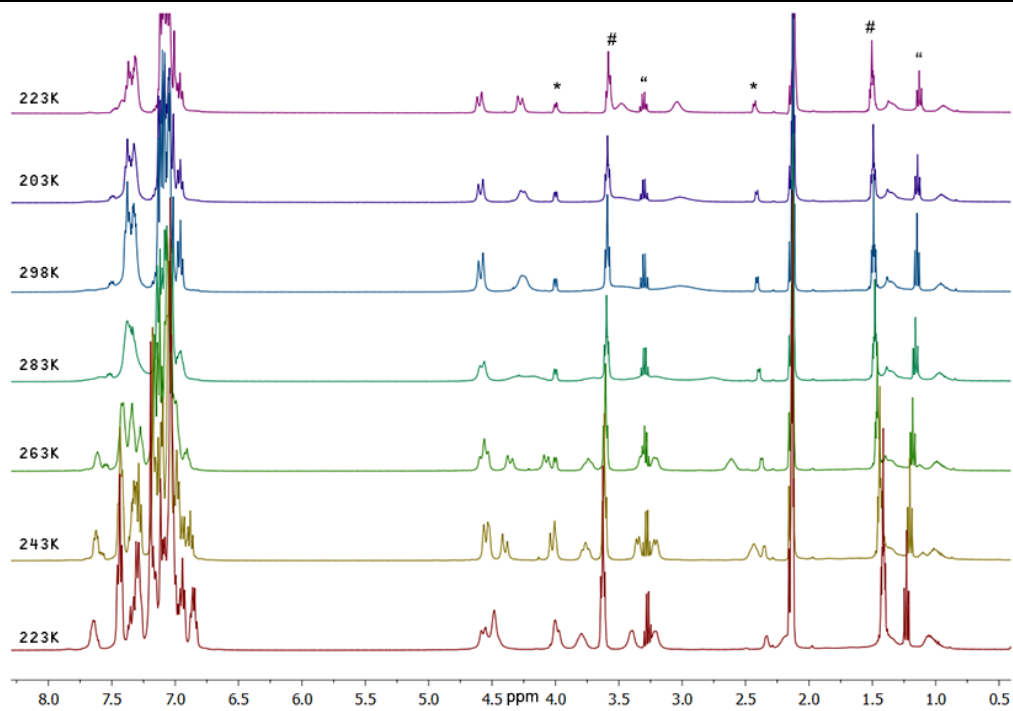


Figure 2A.38. ^1H variable temperature NMR for the **2**.

2A.4.4 UV-Vis Spectra

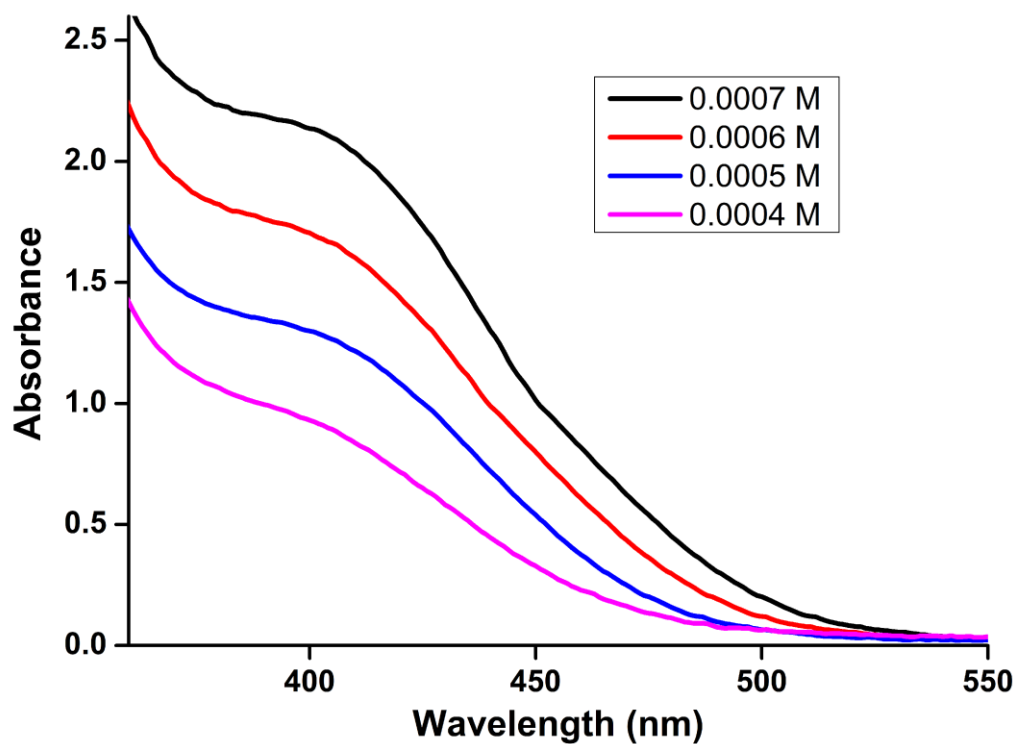


Figure 2A.39. UV-Vis Spectra of **3** in Tetrahydrofuran.

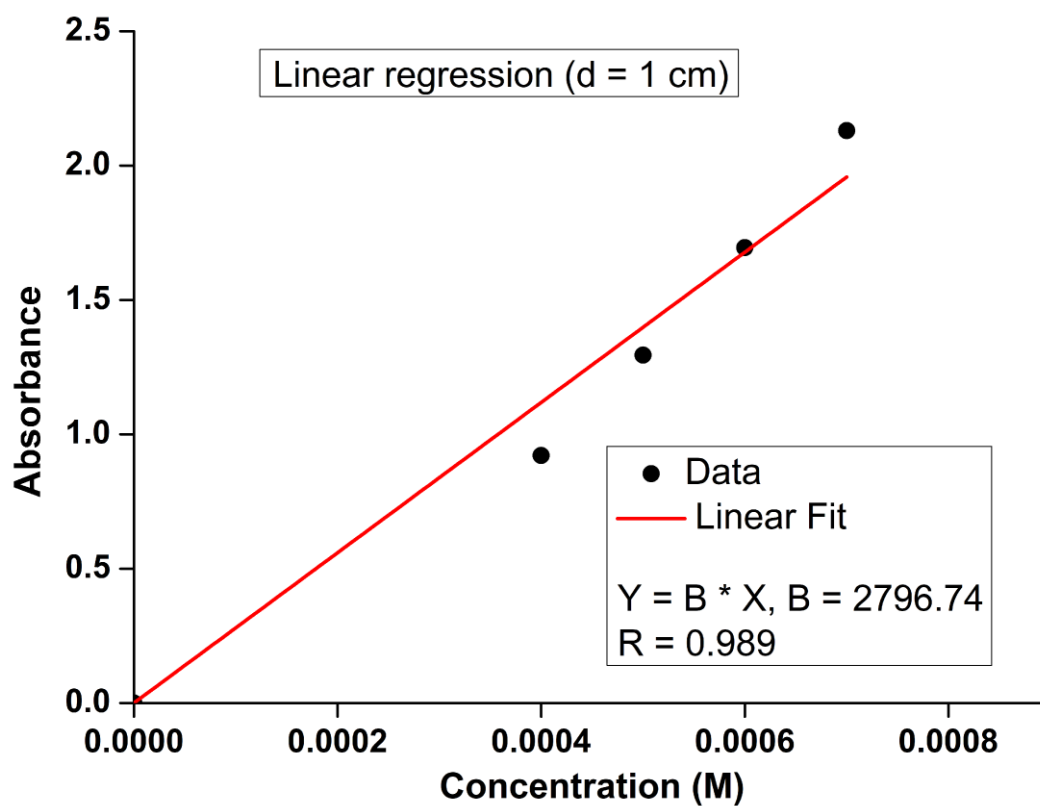


Figure 2A.40. Linear Fit for UV-Vis data of **3**.

2A.4.5 X-Ray Crystallography Data

Table 2A.1

Compound	2	3	4
Empirical Formula	C ₈₀ H ₇₂ N ₄ P ₄ Sn ₂	C ₃₂ H ₅₈ N ₆ Si ₄ Sn ₂	C ₄₀ H ₄₆ N ₈ O ₂ Sn ₂
Formula Weight [g mol⁻¹]	1450.67	876.58	908.23
Crystal colour, shape	Colourless. Block	Orange. Plates	Purple, Block
Crystal Size (mm)	0.05 x 0.04 x 0.03	0.09 x 0.08 x 0.07	0.16x0.14x0.13
Crystal System	Triclinic	Monoclinic	Monoclinic
Space Group	P -1	P 21/n	P 21/c
Formula units	1	4	4
Temperature [K]	100 (2)	100 (2)	100 (2)
Unit cell dimensions [Å] and [°]	a = 10.4508(7) b = 11.1315(7) c = 15.4211(10) α = 81.375 (4) β = 75.530 (4) γ = 81.525 (4)	a = 11.7813(13) b = 25.808(3) c = 14.0899(15) α = 90 β = 109.687(6) γ = 90	a = 17.7879(10) b = 14.2924(8) c = 16.0566(9) α = 90 β = 111.019(2) γ = 90
Cell volume [Å³]	1706.1 (2)	4033.7 (8)	3810.5(4)
ρ_{calc.} [g cm⁻³]	1.412	1.443	1.583
μ (Cu Kα) [mm⁻¹]	7.072	11.209	10.793
θ_{min} / θ_{max} [°]	2.980 – 67.134	3.425 – 66.676	2.661–66.768
Reflections measured	19241	36575	50370
Independent Reflections	6039 [R (int) = 0.0780]	7100 [R(int) = 0.1359]	5917 [R(int) = 0.0416]
R₁ (I > 2σ(I))	0.0439	0.0543	0.0345
wR₂ (all data)	0.0985	0.1567	0.0876
Goof	1.045	0.982	0.889
Largest diff. peak and hole [e Å⁻³]	1.941 /-0.648	1.333/ -0.957	1.679/-1.651

Table 2A.2

Compound	6	7	8
Empirical Formula	C ₄₀ H ₅₁ N ₄ OSn	C ₂₂ H ₂₃ F ₆ N ₄ O ₆ S ₂ Sn	C ₂₄ H ₃₁ F ₃ N ₄ O ₃ SSiSn
Formula Weight [g mol⁻¹]	722.53	736.25	659.37
Crystal colour, shape	Yellow. Block	Yellow, Plates	Yellow, Plates
Crystal Size (mm)	0.09 x 0.08 x 0.07	0.09x 0.07 x 0.03	0.09 x 0.08 x 0.04
Crystal System	Monoclinic	Triclinic	Monoclinic
Space Group	C 2/c	P -1	P 21/c
Formula units	8	2	4
Temperature [K]	100 (2)	100 (2)	100 (2)
Unit cell dimensions [Å] and [°]	a = 37.547(3) b = 11.654(8) c = 17.7286(12) α = 90 β = 113.634(2) γ = 90	a = 8.182 (15) b = 11.154(14) c = 16.25(2) α = 72.46(13) β = 79.32(13) γ = 73.70(12)	a = 16.533 (4) b = 10.968(4) c = 17.061(7) α = 90 β = 75.530 (4) γ = 90
Cell volume [Å³]	7106.8 (8)	1349 (4)	2746.1 (17)
ρ_{calc.} [g cm⁻³]	1.351	1.812	1.595
μ (Cu Kα) [mm⁻¹]	5.991	9.789	9.004
θ_{min} / θ_{max} [°]	4.005 – 66.701	2.869 – 66.826	3.011 – 66.956
Reflections measured	40632	12140	28820
Independent Reflections	6278 [R(int) = 0.0290]	4728 [R(int) = 0.0613]	4857 [R (int) = 0.0572]
R₁ (I > 2σ(I))	0.0296	0.0873	0.0900
wR₂ (all data)	0.0721	0.1384	0.1012
Goof	1.033	0.995	1.045
Largest diff. peak and hole [e Å⁻³]	2.418/ -0.958	1.320 / -0.845	0.718 /-0.868

Table 2A.3

Compound	9	10	11
Empirical Formula	C ₄₃ H ₅₄ AgF ₃ N ₄ O ₄ SS	C ₈₅ H ₁₀₃ AgF ₃ N ₈ O ₅ S	C ₈₅ H ₁₀₇ AuF ₃ N ₈ O ₃ SSi
Formula Weight [g mol⁻¹]	1006.52	1751.06	1844.19
Crystal colour, shape	Yellow. Block	Yellow, Plates	Yellow, Plates
Crystal Size (mm)	0.9 x 0.13 x 0.11	0.15x 0.12 x 0.10	0.09 x 0.07 x 0.06
Crystal System	Triclinic	Monoclinic	Monoclinic
Space Group	P -1	P 21/n	P 21/n
Formula units	2	4	4
Temperature [K]	100 (2)	100 (2)	100 (2)
Unit cell dimensions [Å] and [°]	a = 11.820(4) b = 12.9037(18) c = 16.130(3) α = 70.14(2) β = 79.21(2) γ = 87.831(19)	a = 15.9852(17) b = 19.694(2) c = 26.316(3) α = 90 β = 96.778(6) γ = 90	a = 15.9166 (12) b = 19.707 (2) c = 26.334 (2) α = 90 β = 96.161 (5) γ = 90
Cell volume [Å³]	2272.1 (9)	8226.7(15)	8212.7 (12)
ρ_{calc.} [g cm⁻³]	1.471	1.414	1.492
μ (Cu Kα) [mm⁻¹]	8.721	7.414	8.824
θ_{min} / θ_{max} [°]	3.643 – 73.407	2.809 – 67.388	2.806 – 56.812
Reflections measured	24314	99966	62980
Independent Reflections	8806 [R(int) = 0.0612]	14630 [R(int) = 0.0597]	10876 [R (int) = 0.0566]
R₁ (I > 2σ(I))	0.1157	0.0838	0.1005
wR₂ (all data)	0.1687	0.1434	0.1394
Goof	0.964	1.041	0.974
Largest diff. peak and hole [e Å⁻³]	1.432/ -1.253	1.016 / -1.943	1.092 /-1.186

2A.5 Notes and references

1. Nguyen, T. A. N.; Frenking, G. *Chem. Eur. J.* **2012**, *18*, 12748.
2. (a) Krebs, K. M.; Freitag, S.; Schubert, H.; Gerke, B.; Pöttgen, R.; Wesemann, L. *Chem. Eur. J.* **2015**, *21*, 4628. (b) Wagner, M.; Dorogov, K.; Schürmann, M.; Jurkschat, K. *Dalton Trans.* **2011**, *40*, 8839; (c) Martinčová, J.; Jambor, R.; Schürmann, M.; Jurkschat, K.; Honzíček, J.; Almeida Paz, F. A. *Organometallics* **2009**, *28*, 4778. (d) Martinčová, J.; Dostálová, R.; Dostál, L.; Růžička, A.; Jambor, R. *Organometallics* **2009**, *28*, 4823; (e) Kilian, M.; Wadepohl, H.; Gade, L. H. *Organometallics* **2008**, *27*, 524; (f) Zabula, A. V.; Pape, T.; Hepp, A.; Hahn, F. E. *Organometallics* **2008**, *27*, 2756; (g) Zabula, A. V.; Pape, T.; Hepp, A.; Hahn, F. E. *Dalton Trans.* **2008**, 5886; (h) Kilian, M.; Wadepohl, H.; Gade, L. H. *Eur. J. Inorg. Chem.* **2008**, 1892; (i) Zdeňka Padělková, I. C.; Fejfarová, K.; Holubová, J.; Růžička, A.; Holeček, J.; Collect. Czech. *Chem. Commun.*, **2007**, 629; (j) Veith, M.; Müller, A.; Stahl, L.; Nötzel, M.; Jarczyk, M.; Huch, V. *Inorg. Chem.* **1996**, *35*, 3848; (k) Veith, M.; Stahl, L.; Huch, V. *Inorg. Chem.* **1989**, *28*, 3278.
3. (a) Díaz, D. E.; Llanos, L.; Arce, P.; Lorca, R.; Guerrero, J.; Costamagna, J.; Aravena, D.; Ferraudi, G.; Oliver, A.; Lappin, A. G.; Lemus, L. *Chem. Eur. J.* **2018**, *24*, 13839.
4. Abhervé, A.; Clemente-Juan, J. M.; Clemente-León, M.; Coronado, E.; Boonmark, J.; Youngme, S. *New J. Chem.*, **2014**, *38*, 2105.
5. (a) Li, M.; Wu, H.; Yang, Q.; Ke, H.; Yin, B.; Shi, Q.; Wang, W.; Wei, Q.; Xei, G.; Chen, S. *Chem. Eur. J.* **2017**, *23*, 17775; (b) Sun, Q.; Chen, P.; Li, H-F.; Gao, T.; Sun, W-B.; Li, G-M.; Yan, P-F. *CrystEngComm* **2016**, *18*, 4627.
6. Wang, X-M.; Chen, S.; Fan, R-Q.; Zhang, F-Q.; Yang, Y-L. *Dalton Trans.* **2015**, *44*, 8107.
7. Bhar, K.; Khan, S.; Costa, J. S.; Ribas, J.; Roubeau, O.; Mitra, P.; Ghosh, B. K. *Angew. Chem. Int. Ed.* **2012**, *51*, 2142.
8. (a) Lu, C. C.; Bill, E.; Weyhermüller, T.; Bothe, E.; Wieghardt, K. *J. Am. Chem. Soc.* **2008**, *130*, 3181; (b) Van Gastel, M.; Lu, C. C.; Wieghardt, K.; Lubitz, W. *Inorg. Chem.* **2009**, *48*, 2626; (c) Lu, C. C.; Weyhermüller, T.; Bill, E.; Wieghardt, K. *Inorg. Chem.* **2009**, *48*, 6055; (d) Shejwalkar, P.; Rath, N. P.; Bauer, E. B. *Dalton Trans.* **2011**, *40*, 7617; (e) Bheemaraju, A.; Lord, R. L.; Müller, P.; Groysman, S. *Organometallics* **2012**, *31*, 2120. (f) Volpe, E. C.; Wolczanski, P. T.; Darmon, J. M.; Lobkovsky, E. B. *Polyhedron* **2013**, *52*, 406; (g) Williams, V. A.; Hulley, E. B.; Wolczanski, P. T.; Lancaster, K. M.; Lobkovsky, E. B. *Chem. Sci.* **2013**, *4*, 3636.

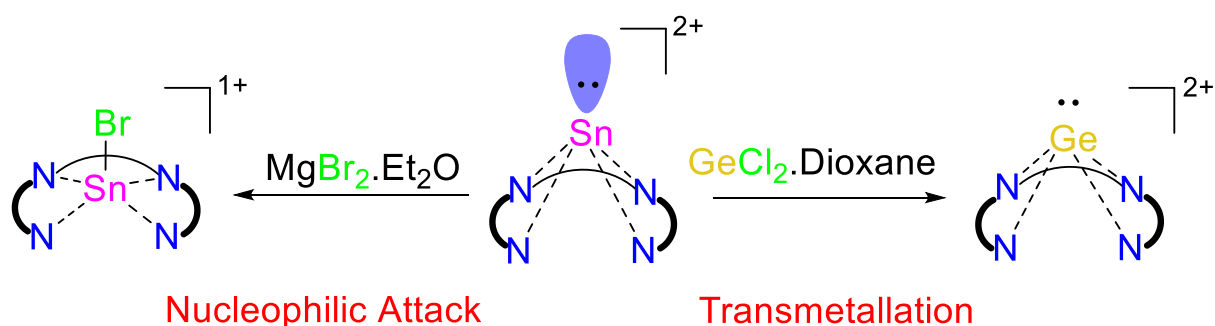
-
9. (a) Myers, T. W.; Berben, L.A. *Inorg. Chem.* **2012**, *51*, 1480. (b) Myers, T. W.; Kazem, N.; Stoll, S.; Britt, R. D.; Shanmugam, M.; Berben, L. A. *J. Am. Chem. Soc.* **2011**, *133*, 8662. (c) Myers, T. W.; Berben, L. A. *J. Am. Chem. Soc.* **2011**, *133*, 11865.
10. (a) Wang, W.; Inoue, S.; Irran, E.; Driess, M. *Angew. Chem. Int. Ed.* **2012**, *51*, 3691; (b) Brück, A.; Gallego, D.; Wang, W.; Irran, E.; Driess, M.; Hartwig, J. F. *Angew. Chem. Int. Ed.* **2012**, *51*, 11478; (c) Gallego, D.; Brück, A.; Irran, E.; Meier, F.; Kaupp, F.; Driess, M. *J. Am. Chem. Soc.* **2013**, *135*, 15617; (d) Ren, H.; Zhou, Y.-P.; Bai, Y.; Cui, C.; Driess, M. *Chem. Eur. J.* **2017**, *23*, 5663; (e) Zhou, Y.-P.; Karni, M.; Yao, S.; Apeloig, Y.; Driess, M. *Angew. Chem. Int. Ed.* **2016**, *55*, 15096; (f) Metsänen, T. T.; Gallego, D.; Szilvási, T.; Driess, M.; Oestreich, M. *Chem. Sci.* **2015**, *6*, 7143.
11. Nartop, D.; Clegg, W.; Harrington, R. W.; Henderson, R. A.; Wills, C. Y. *Dalton Trans.* **2014**, *43*, 3372.
12. (a) Bestgen, S.; Rees, N. H.; Goicoechea, J. M. *Organometallics* **2018**, *37*, 4147; (b) Alvarez-Rodriguez, L.; Brugos, J.; Cabeza, J. A.; Garcia-Alvarez, P.; Perez-Carreno, E. Polo, D. *Chem. Commun.* **2017**, *53*, 893; (c) Brugos, J.; Cabeza, J. A.; Garcia-Álvarez, P.; Pérez-Carreño, E.; Polo, D. *Dalton Trans.* **2018**, *47*, 4534.
13. (a) Álvarez-Rodríguez, L.; Brugos, J.; Cabeza, J. A.; GarcíaÁlvarez, P.; Pérez-Carreno, E. *Chem. Eur. J.* **2017**, *23*, 15107; (b) Krebs, K. M.; Freitag, S.; Maudrich, J. J.; Schubert, H.; Sirsch, P.; Wesemann, L. *Dalton Trans.* **2018**, *47*, 83; (c) Takaya, J.; Miyama, K.; Zhu, C.; Iwasawa, N. *Chem. Commun.* **2017**, *53*, 3982.
14. (a) Meyer, N.; Lough, A. J.; Morris, R. H. *Chem. Eur. J.* **2009**, *15*, 5605; (b) Sui-Seng, C.; Freutel, F.; Lough, A. J.; Morris, R. H. *Angew. Chem. Int. Ed.* **2008**, *47*, 940; (c) Sonnenberg, J. F.; Morris, R. H. *ACS Catal.* **2013**, *3*, 1092.
15. (a) Hahn, F. E.; Zabula, A. V.; Pape, T.; Hepp, A.; Tonner, R.; Haunschild, R.; Frenking, G. *Chem. Eur. J.* **2008**, *14*, 10716; (b) Zabula, A. V.; Pape, T.; Hepp, A.; Hahn, F. E. *Dalton Trans.* **2008**, 5886; (c) Zabula, A. V.; Pape, T.; Hepp, A.; Hahn, F. E. *Organometallics* **2008**, *27*, 2756.
16. Flock, J.; Suljanovic, A.; Torvisco, A.; Schoefberger, W.; Gerke, B.; Pöttgen, R.; Fischer, R. C.; Flock, M. *Chem. Eur. J.* **2013**, *19*, 15504.
17. Kim, S.-J.; Lee, Y.-J.; Kim, S. H.; Ko, J.; Cho, S.; Kang, S. O. *Organometallics* **2002**, *21*, 5358.
18. Gaussian 09, Revision E.01, Gaussian, Inc., Wallingford CT, 2009

-
19. Hansen, M. N.; Niedenzu, K.; Serwatowska, J.; Serwatoski, J.; Woodrum, K. R. *Inorg. Chem.* **1991**, *30*, 866.
20. Petrov, V. A.; Marshall W. *J. Fluorine Chem.* **2015**, *179*, 56.
21. (a) Hadlington, T. J.; Hermann, M.; Li, J.; Frenking, G.; Jones, C. *Angew. Chem. Int. Ed.* **2013**, *52*, 10199; (b) Hadlington, T. J.; Jones, C. *Chem. Comm.* **2014**, *50*, 2321.
22. Schäfer, A.; Winter, F.; Saak, W.; Haase, D.; Pöttgen, R.; Müller, T. *Chem. Eur. J.* **2011**, *17*, 10979.
23. Schleep, M.; Hettich, C.; Kratzert, D.; Scherer, H.; Krossing, I. *Chem. Commun.* **2017**, *53*, 10914.
24. Ayers, A. E.; Rasika Dias, H. V. *Inorg. Chem.* **2002**, *41*, 3259.
25. Raut, R. K.; Majumdar, M. *J. Organomet. Chem.* **2019**, *887*, 18.
26. (a) Dias, H. V. R.; Wang, X.; Diyabalange, H. *Inorg. Chem.* **2005**, *44*, 7322; (b) Dias, H. V. R.; Ayers, A. E. *Polyhedron* **2002**, *21*, 611; (c) Ayers, A. E.; Dias, H. V. R. *Inorg. Chem.* **2002**, 3259; (d) Dias, H. V. R.; Wang, Z. *Inorg. Chem.* **2000**, *39*, 3890; (e) Cabeza, J. A.; Fernandez-Colinas, J. M.; Garcia-Alvarez, P.; Polo, D. *Inorg. Chem.* **2012**, *51*, 3896.
27. (a) Findeis, B.; Gade, L. H.; Scowen, I. J.; McPartlin, M. *Inorg. Chem.* **1997**, *36*, 960; (b) Hitchcock, P. B.; Lappert, M. F.; Pierssens, L. J.-M. *Organometallics* **1998**, *17*, 2686; (c) Ayers, A. E.; Dias, H. V. R. *Polyhedron*, **2002**, *21*, 611 (d) Parvin, N.; Dasgupta, R.; Pal, S.; Sen, S. S.; Khan, S. *Dalton Trans.* **2017**, *46*, 6528.

Synthesis, Characterization and Reactivity of Novel Tin(II) Cationic Compounds

Abstract

Zwitterionically stabilized tin(II) cations **12** and **13** are synthesized from dipolar stannylene by reacting them with an excess of tris(pentafluorophenyl)borane. One electron oxidation of stannylene stabilized in redox-active ligand by NO.SbF₆ led to the formation of tin(II) monocation **14**. The donor stabilized tin(II) cations **15**, and **16** were also synthesized with acyclic flexible bis (α -iminopyridine) ligand by the autoionization method. The syntheses involve the abstraction of chloride from the tin dichloride precursor using trimethylsilyl trifluoromethane sulfonate. The apically disposed tin(II) dication exhibits electrophilic behavior and undergoes a transmetallation reaction with GeCl₂.dioxane, resulting in stabilizing the Ge(II) dication. All the compounds have been characterized by NMR techniques and single crystal X-ray crystallography.



2B.1 Introduction

Research on low-valent Group 14 (poly) cations has increased in the last couple of decades.¹ Kinetic or electronic stabilization approaches have been used to isolate Group 14 E(II) (E = Si-Pb) monocations and dications.² Much advances have been possible in the stabilization of Ge(II) and Sn(II) cations owing to the operational inert pair effect³ descending the group.

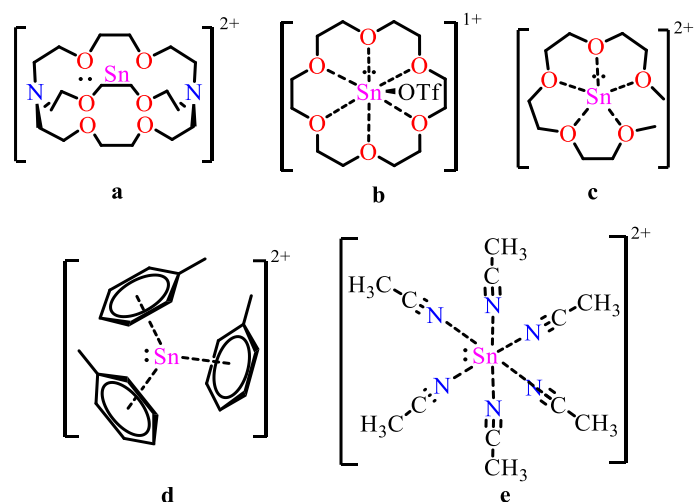


Chart 2B.1 Reported Sn(II) cations and dications.

A handful of Ge(II) and Sn(II) dications have been stabilized within cryptand and crown ether cavities.⁴ In the case of Sn(II), cryptand^{4e} and only crown ether^{4h} with larger cavity size can encapsulate the dication forming 1:1 complexes. Whereas, with the smaller crown ethers 2:1 sandwich complexes are formed.^{4h} The constraint-free acyclic glyme ligands have proved efficient in stabilizing Sn(II) dications.^{4f} Worth mentioning, many of these cases have the weakly coordinating trifluoromethanesulfonate (OTf) counter anion bound to the cationic site. Even the seminal work on [2.2.2] paracyclophane stabilized Sn(II) dication has one coordinated $[\text{AlCl}_4]^-$ to the tin centre.⁵ Till date, there are only two reports where only solvent molecules (Toluene, acetonitrile) coordinate to the Sn(II) dication and are devoid of any close contact anions.^{4d,4g} Nonetheless, in all these cases, the highly electrophilic Sn(II) dicationic centre is completely sequestered (chart 1), leaving the lone pair on tin(II) with high *s*-character. To the best of our knowledge, there are no examples where an Sn(II) dicationic site is barely allowing room for lone pair reactivity.

Notably, the lone pair on Sn(II) monocation is known to coordinate to transition metal fragment in $[\{2,6-(\text{MeOCH}_2)_2\text{C}_6\text{H}_3\}\text{SnCr}(\text{CO})_5]^+\text{X}^-$ (X = OTf or $\text{CB}_{11}\text{H}_{12}$).⁶ The Sn(II) monocations have been majorly stabilized using bi- or poly-dentate *N*-donor ligands, anionic

or neutral aromatic rings⁷ or using sterically bulky ligands in the case of low-coordinate Sn(II) monocation.⁸

Interestingly in these cationic tetrylenes, the main group center bears a positive or dipositive charge and empty orbital/s, which makes them attractive in the field of catalysis. The isolation of the above-said compound would have been difficult without the choice of appropriate ligands, which provide thermodynamic stabilization through the donor groups and kinetic stabilization by bulky substituents. Thus the search for the ligand is very crucial for the stabilization and isolation of these subvalent compounds. The versatile library, tuneability, and viable synthetic routes of Schiff base ligand made them better choice ligands. The redox properties of iminopyridine based ligands proven beneficial in stabilizing transition metals in various oxidation states. However, the less explored chemistry of redox noninnocent ligands with main group elements could open new aspects of redox chemistry, which is generally done with transition metals. The fewer possible oxidation states of group 14 elements can be studied well with tunable redox properties of ligand.

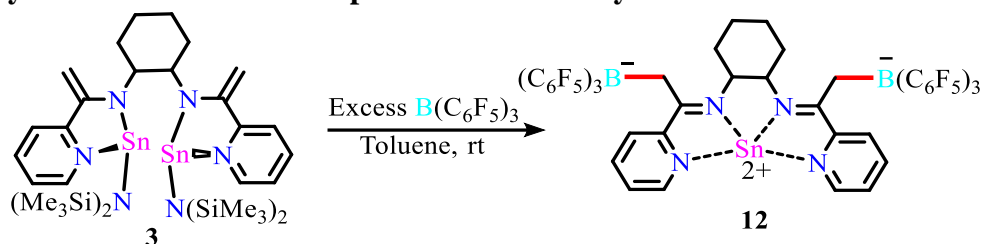
Scope of the work

The reactivity study of Sn(II) cation and dications are far from being complete due to inappropriate synthetic routes or instability and sensitivity of such cations. Recent advances in stabilization on low valent stannylumylenes or Sn(II) dications using neutral donor ligands does not allow to check the reactivity due to encapsulation of reactive cationic centres in ligand frameworks. In order to headway this field, the prime challenge is to develop simple, elegant synthetic routes and to synthesize the bare cationic centre which will have open reactive sites.

In this study, we have developed synthetic routes for Sn(II) cations from neutral dipolar stannylenes **3** and **6** synthesized in first section of this chapter by reaction with boranes or by simple one-electron oxidation aided by redox non-innocent ligand. We have also synthesized donor stabilized pyramidal Sn(II) dication **15**, taking advantage of the flexible acyclic bis(α -iminopyridine) ligand framework. The metathetical reactivity and the electrophilic behavior of **15** have been reported herewith. In this work, we also report the stabilization of chlorostannylumyldene $[:\text{SnCl}]^+$ within the same ligand framework. The role of the flexible acyclic bis(α -iminopyridine) ligand framework in the stabilization of Sn(II) dication and monocation has been discussed.

2B.2 Results and Discussion

2B.2.1 Synthesis of Cationic Compounds from Stannylenes



Scheme 2B.1 Synthesis of zwitterionic Sn(II) dication.

The reactivity of bis(stannylene) **3** with Lewis acids have been studied with two equivalents of $B(C_6F_5)_3$ at room temperature in toluene to afford the zwitterionic adduct **12** (Scheme 2B.1) with the elimination of one equivalent of $Sn[N(SiMe_3)_2]_2$. The colorless crystals of the zwitterionic **12** were obtained in a yield of 48% by layering with pentane. Compound **12** has been characterized by 1H , ^{19}F and ^{11}B NMR spectroscopy in Chloroform- d_3 . Two peaks at -12.30 and -13.29 ppm appear in the ^{11}B spectrum, revealing the two different environments around the B centers within the molecule even in solution state in the NMR time scale. The ^{19}F NMR spectrum shows peaks that corroborates with the borate group. The characteristic $-CH_2B(C_6F_5)_3$ proton peak appears at 3.85 and 3.24 ppm in the 1H NMR spectrum of **12**. ^{119}Sn and ^{13}C NMR were not obtained owing to the poor solubility of the zwitterionic compound **12**. Precedence to zwitterionic adduct formation with $B(C_6F_5)_3$ have been reported in the case of β -ketiiminato stabilized silylene and germylene.⁹ To the best of our knowledge, this is the first example of a stannylene exhibiting such a dipolar behavior ultimately leading to the conversion to an Sn(II) dication.

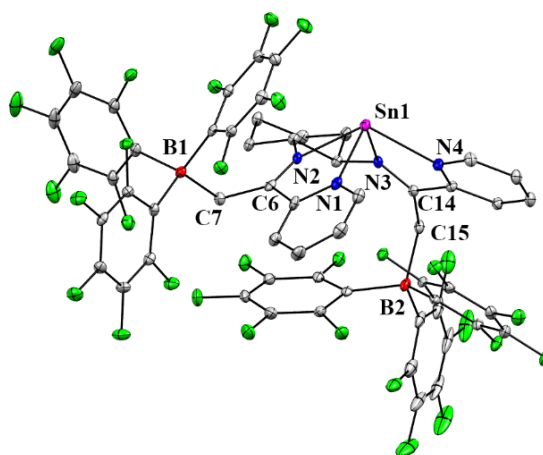
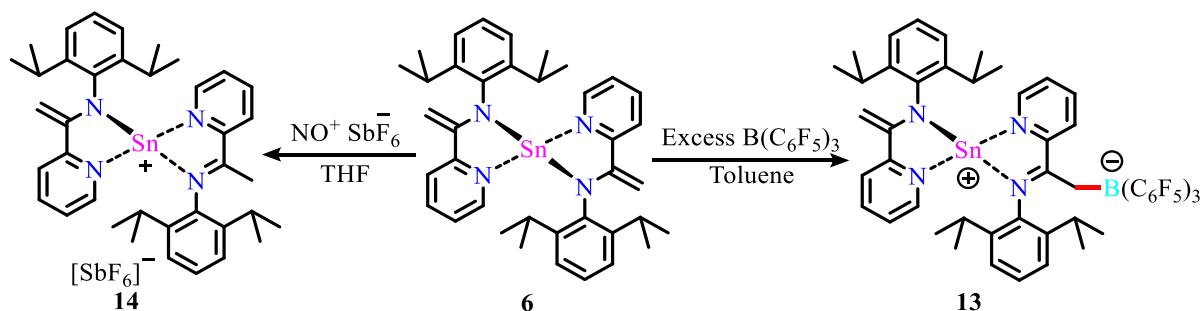


Figure 2B.1. Molecular structure of **12** in the solid state (thermal ellipsoids at 30%, H atoms are omitted for clarity). Selected bond lengths [\AA]: Sn1-N1 2.329(3), Sn1-N2 2.274(3), Sn1-N3 2.273(3), Sn1-N4 2.328(3), B1-C7 1.718(5), B2-C14 1.702(5).

Compound **12** crystallized in the monoclinic crystal system with $P2_1/n$ space group as observed in the single crystal X-ray analysis (Figure 2B.1 and Table 2B.1). The unit cell shows the presence of three toluene solvent molecules in the crystal lattice. At the core of the molecular structure, the four N donor sites coordinate to the Sn(II) dicationic center with average Sn-N_{im} (im = imino) distance of 2.27 Å and average Sn-N_{py} (py = pyridyl) distance of 2.33 Å. Similar to our earlier reports, the four N atoms form a mildly distorted basal coordinating plane (fold angle N3-N2-N1-N4 is approximately 11.65°) with the Sn(II) center being perpendicularly disposed by 1.21 Å. The overall structure appears pyramidal with the sum of bond angle around Sn being 295.7°. In the periphery of the molecular structure **2**, the two flanking bulky B(C₆F₅)₃ substituents on the methylene carbon are placed at a dihedral angle B1-C7...C14-B2 of approximately 135°, with B1...B2 separated by a distance of 7.93 Å. The average B-C_{methylene} bond distance is 1.71 Å, indicating that they are single bonds



Scheme 2B.2 Synthesis of Sn(II) monocations.

Similarly, the dipolar monostannylene **6**, which is synthesized from iminopyridine ligand when reacted with an excess of B(C₆F₅)₃ in toluene solvent at room temperature, led to the formation of zwitterionic adduct **13** as highly air and moisture sensitive compound. Interestingly in the case of bis(stannylene), reaction with an excess of borane leads to the formation of zwitterionically stabilized tin(II) dication. Although having two exocyclic double bonds, two dipolar sites are available for borane coordination, but the steric bulk of 2,6-diisopropylphenyl groups in the case of **6** prevent the further reaction with borane and gave only tin(II) monocation **13**. Compound **13** has been characterized by heteronuclear NMR in solution state and SC-XRD in the solid state. In the ¹H NMR spectrum, the terminal =CH₂ protons appeared at 3.37 and 4.43 ppm, whereas the characteristic -CH₂-B(C₆F₅)₃ peak appeared at 2.63 ppm. The single peak at -12.71 ppm in ¹¹B NMR compared well with the reported tetra-coordinated borates.⁹ The only peak at -352.99 ppm in ¹¹⁹Sn NMR match well with the literature reported values.⁴

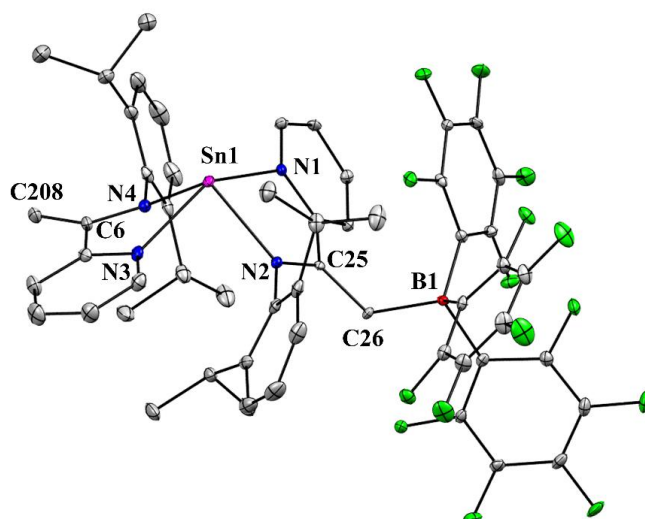


Figure 2B.2. Molecular structure of **13** in the solid state (thermal ellipsoids at 30%, H atoms are omitted for clarity). Selected bond lengths [\AA] and angle [$^\circ$]: Sn1-N1 2.438(3), Sn1-N2 2.326(3), Sn1-N3 2.415(3), Sn1-N4 2.138(3), C6-C208 1.349(5) C25-C26 1.494(5) B1-C26 .694(5), N2-Sn1-N1 68.12(10), N4-Sn1-N3 71.48(11).

Compound **13** crystallized in triclinic space group with P-1 space group. Two disordered toluene molecules are crystallized in the asymmetric unit cell. Compound **13** consists of a pyramidal N₄Sn core with exocyclic B(C₆F₅)₃ group attached to C26. Out of the four Sn-N distances, the Sn1-N4 is a covalent bond and which is shortest [2.138 (3) \AA], whereas the other three Sn-N bond distances are in between 2.326-3.438 \AA comparable with the coordinate N-Sn bonds. The characteristic C6-C208 bond distance is 1.349(5) \AA exocyclic double bond, and another C25-C26 bond distance is 1.494(4) increased compared to parent stannylene due to C-B bond formation. The cationic charge sharpened the pyramid compared with parent stannylene with the summation of the bond angle at Sn1 is 311.24 $^\circ$.

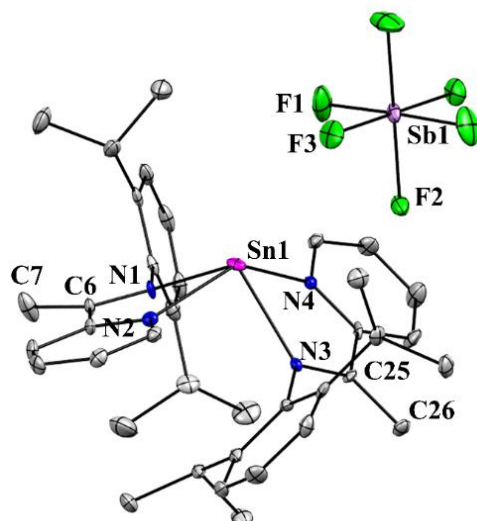
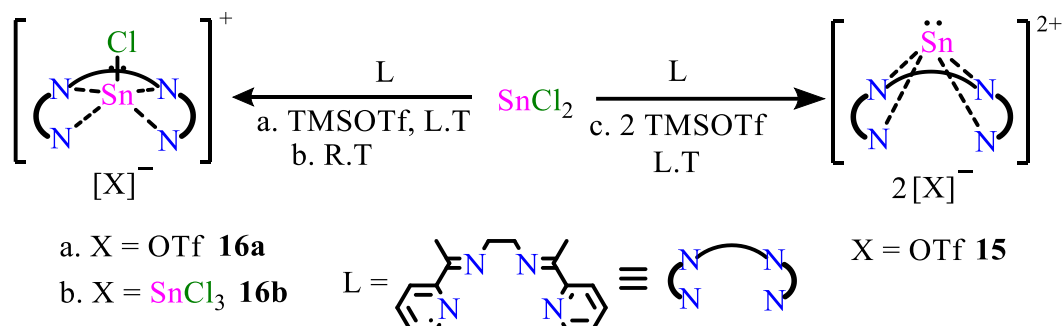


Figure 2B.3. Molecular structure of **14** in the solid state (thermal ellipsoids at 30%, H atoms are omitted for clarity). Selected bond lengths [\AA]: Sn1-N1 2.183(4), Sn1-N2 2.389(5), Sn1-N3 2.311(4), Sn1-N4 2.427(4), N2-Sn1-N1 70.50(16), N4-Sn1-N3 68.37(15).

The one-electron oxidation of monostannylene by nitrosonium hexafluoroanionate resulted in the formation of **14** as few crystals from the reaction mixture. The reaction is expected to have gone through the Sn(II) radical cation, an elusive species, which must have grabbed the proton from solvent molecule. The compound was characterized by SC-XRD techniques, but unable to characterize by NMR techniques due to insufficient quantity of product. Colorless crystals of compound **14** were crystallized in monoclinic crystal system with P 21/n space group. The structural features of **14** are similar to **13**. The counteranion SbF_6^- is away from the coordination sphere, the closest Sn...F distance is 3.42 \AA .

2B.2.2 Neutral N-donor Stabilized Sn(II) Cations and Dication



Scheme 2B.3 Synthesis of **15**, **16a** and **16b**.

The $[\text{LSn}][\text{OTf}]_2$ **15** (L = bis(α -iminopyridine)) was synthesized in good yields from the addition of two equivalents of trimethylsilyl trifluoromethanesulfonate (TMSOTf) to a 1:1

mixture of SnCl₂ and ligand **L** taken in dichloromethane solvent (Scheme 2B.3). Compound **15** was characterized using NMR techniques and single crystal X-ray crystallography. As anticipated, ¹H NMR spectrum of compound **15** undergoes a downfield shift in comparison to the free ligand (**L**), indicating the coordination of [Sn:]²⁺ with the binding sites of the ligand. Chemical shift value at -79.35 ppm in ¹⁹F NMR reflects the presence of the triflate anion. The ¹¹⁹Sn NMR of **1** in Acetonitrile-*d*₃ displays a significantly upfield shifted singlet resonance at -636.96 ppm. This value downfield shifted compared to the literature reported chemical shifts of [Sn(C₇H₈)₃][B(C₆F₅)₄]₂ (-1468 ppm)^{4g} and the more recently reported [Sn(CH₃CN)₆][Al(OR^F)₄]₂ (R^F = C(CF₃)₃) (-1490 ppm) in CD₃CN.^{4d} This suggests that compound **15** has a less net coordination number in the NMR solvent.^{4g}

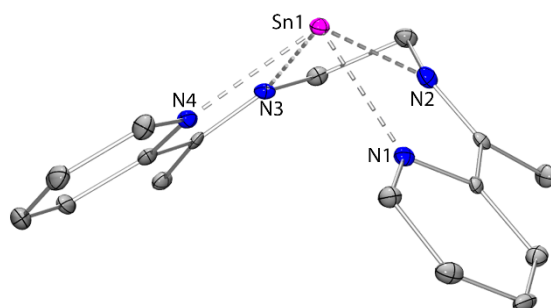


Figure 2B.4. Molecular structure of **15** (thermal ellipsoid at 30%, H atoms and triflate counterions are omitted for clarity). Selected bond lengths [Å] and angles [°]: Sn1-N1 2.375 (4), Sn1-N2 2.282 (4), Sn1-N3 2.318 (4), Sn1-N4 2.355 (4), N1-Sn1-N2 68.01 (14), N2-Sn1-N3 65.85 (13), N3-Sn1-N4 68.58 (13).

Colorless single crystals of compound **15** suitable for X-ray measurement were grown by layering acetonitrile solution of the compound with diethyl ether at room temperature and were unequivocally confirmed by single crystal X-ray diffraction (Figure 2B.4). Compound **15** crystallizes in P2₁/n space group. Herein, the four nitrogen donor sites coordinate to the Sn(II) dication center. The two Sn-N_{im} (imino-N atoms) bonds are shorter with bond distances Sn1-N2 2.282(4) Å and Sn1-N3 2.318 (4) Å, while the Sn-N_{py} (pyridyl-N atoms) are slightly longer with Sn1-N1 2.375 (4) Å and Sn1-N4 2.355 (4) Å bond lengths. The four nitrogen atoms form a somewhat distorted basal coordinating plane (fold angle N2-N3-N4-N1 is approximately 15.12°) with the Sn(II) center being displaced perpendicularly by 1.32 Å, resulting in an overall dome-shaped structure (sum of the bond angle at Sn center = 286.4°). The ligand **L** has less restrictive binding modes both because it is acyclic in nature and the torsional magnitude

provided by the $-(\text{CH}_2)_2-$ linker. Therefore, basal N_4 with weakened coplanarity coordinates to the $\text{Sn}(\text{II})$ dication center disposed at the apex resulting in a dome-shaped or pyramidal geometry. The triflate anion despite its known coordinating nature, is excluded from the coordination sphere of $\text{Sn}(\text{II})$ dicationic center in compound **15**, the closest approach Sn1-O2 distance being 2.953 Å.^{4e} This manifests the stabilizing effect of the ligand **L** and hence the apical $\text{Sn}(\text{II})$ dication is completely bare allowing further reactivity. Apparently, the apical $\text{Sn}(\text{II})$ center in compound **15** exhibits an inverted tetrahedral geometry with an unprotected lone pair of electrons. This structure is on contrary to the reported tin(II) dications, where the dicationic site is rather encapsulated.^{4d-h} Notably, the only other acyclic glyme ligand binds the $\text{Sn}(\text{II})$ dicationic center in a belt-like manner and has triflate anions as contact ion pairs.^{4f}

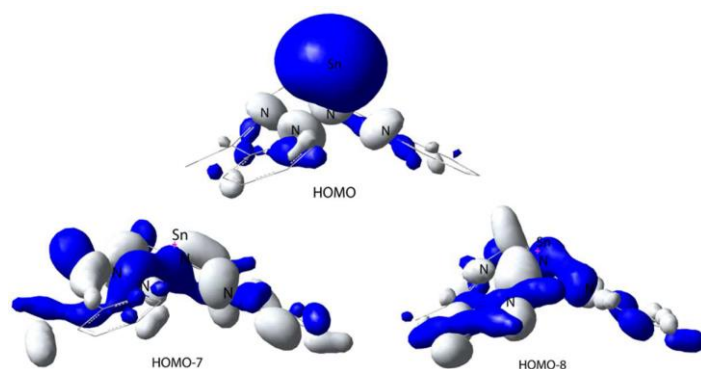


Figure 2B.5. Relevant contour plots of **15** (isovalue 0.04 au).

We have performed DFT calculations in search of the unusual bonding situations in the pyramidal $\text{Sn}(\text{II})$ dication **15**. We have employed B3LYP as the level of theory and 6-31G(d,p) as the basis sets for C, H, N, O, F, S, and LANL2DZ for Sn in this study.¹⁰ The optimized dicationic species **15'** (triflate anion omitted in the input geometry), is in close agreement with the X-ray geometry of **15**. The HOMO of **15'** clearly shows the presence of a lone pair at the apex $\text{Sn}(\text{II})$ center with a significant s-character (Figure 2B.5). On the contrary to our earlier report on nucleophilic **L** stabilized $\text{Ge}(\text{II})$ dication, the p-mixing in the lone pair orbital on $\text{Sn}(\text{II})$ is significantly lessened. The empty p_x and p_y atomic orbitals of apical $\text{Sn}(\text{II})$ overlap with the four nitrogen based orbitals, giving rise to 5-centre 4-electron bonding situations (HOMO-8 and HOMO-9), depicted in Figure 2B.5. The calculated Wiberg Bond Indices for the Sn-N bonds in **15'** lies in the range between 0.25 – 0.27, which is less than found in $[\text{LGe:}]^{2+}$ due to weakened orbital overlap. The Mulliken charge distribution analysis shows a +1.09 positive charge on $\text{Sn}(\text{II})$ center reflecting cumulative electron donation from the nitrogen centers of **L**.

Treatment of SnCl₂ with ligand **L** taken in an equimolar ratio in dichloromethane solvent, followed by drop-wise addition of one equivalent of trimethylsilyl triflate (TMSOTf), led to the complete precipitation of the Sn(II) monocation compound **16a** (Scheme 2B.3) within 12 hours. The orange precipitate was separated (yield = 90%), and single crystals were grown by layering diethyl ether over acetonitrile solution of compound **16a**. Compound **16a** was characterized by NMR techniques and X-ray crystallography (Figure 2B.6). As anticipated, ¹H NMR spectrum of compound **16a** undergoes a downfield shift in comparison to the free ligand (**L**), indicating the coordination of [SnCl]⁺ with the binding sites of the ligand. Chemical shift value at -79.29 ppm in ¹⁹F NMR reflects the presence of the triflate anion. The ¹¹⁹Sn NMR chemical shift of **16a** in Acetonitrile-*d*₃ appears at -572.38 ppm, which is again upfield shifted compared to the *N*-donor stabilized tin(II) monocation.⁷ This high upfield shift is possibly attributed to the acetonitrile coordination to the Sn(II) center in the solution state. The chlorostannylium ylidene has been synthesized in an alternate route by auto-ionization of SnCl₂ in the presence of ligand **L**, leading to the formation of [LSnCl][SnCl₃] (**2b**) (Scheme 2B.3). Analogous to compound **16a**, the formation of **16b** has been confirmed using NMR techniques and X-ray crystallography.

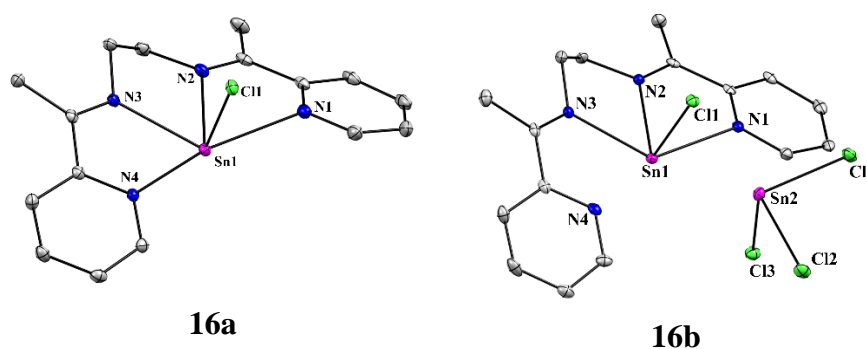


Figure 2B.6. Molecular structure of **16a** (thermal ellipsoid at 30%, H atoms and triflate counter anions are omitted for clarity). Selected bond lengths [Å]: Sn1-N1 2.578 (2), Sn1-N2 2.404 (2), Sn1-N3 2.388 (2), Sn1-N4 2.579 (2), Sn1-Cl1 2.464 (7). Structural features of **16b** are almost similar to **16a**.

Compound **16a** crystallizes in the monoclinic crystal system with P2₁/c space group with one dichloromethane molecule in the unit cell. The Sn(II) center is coordinated by two shorter imino-N atoms (*N_{im}*), Sn1-N2 2.404 (2) Å, Sn1-N3 2.388 (2) Å, and has two pyridyl-N atoms (*N_{py}*) N3 and N4 at larger distances, with average Sn-*N_{py}* distance being > 2.58 Å (Figure 2B.6). The four nitrogen atoms are approximately coplanar, with the Sn(II) displaced only 0.32 Å from the plane average. The chlorine atom is perpendicular (average N-Sn-Cl angle 85.1°) to

the SnN_4 basal plane having Sn1-Cl1 bond distance 2.465 (7) Å. The triflate anion is not coordinated to the Sn(II) cationic center (closest approach Sn1-O1 = 3.244 Å). All the S-O bond length in triflate counter anion remains unperturbed, revealing the ionic nature of triflate and away from the coordination sphere of tin(II). Compound **16b** also shows analogous metric parameters with the pyramidal SnCl_3 counter anion found at a significant distance from the Sn(II) cation center (closest approach Sn1-Cl3 = 3.656 Å).

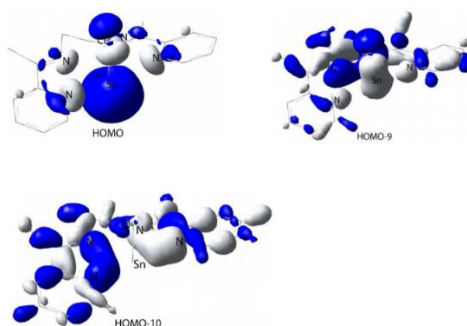


Figure 2B.7 Contour plots of **16a** at isovalue of 0.04.

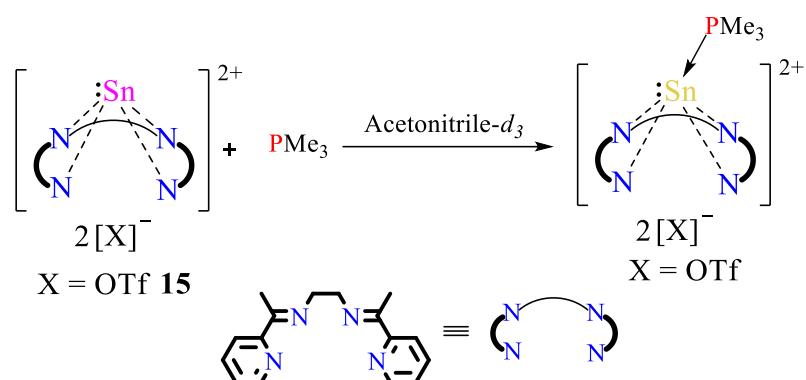
In order to ascertain the electronic nature of compound **16a**, we have carried out DFT calculations using the same level of theory and basis sets chosen as in the case of compound **15**. The optimized geometry **16a'** of the mono cation (without triflate anion) matches closely with the X-ray geometry. The HOMO has the maximum contribution from Sn(II) lone pair orbital, which is positioned opposite to Sn-Cl bond, on a predominant s-character. The two vacant p-orbitals are stabilized by the *N*-donor sites as reflected in HOMO-9 and HOMO-11 (Figure 2B.7). The average Wiberg bond indices for the two N_{im} -Sn are 0.22 and N_{py} -Sn are 0.14, whereas, Sn-Cl single bond is 0.60. These low range values indicate the weak coordinate bonds between nitrogens and Sn(II) center. Nonetheless, their cumulative effect in stabilization is significant. The charge on Sn(II) center is +0.91 from Mulliken charge distribution analysis.

The tetradentate ligand **L** electronically stabilizes the electrophilic $[\text{SnCl}]^+$ unit. Similar stabilizations have been reported using mostly bi/tridentate *N*-donor ligands, though surprisingly, there has been no earlier reports on *N*-donor ligands stabilizing a Sn(II) dication. As a matter of fact, this is the first example, where a Sn(II) monocation and dication can be step-wise synthesized by chloride abstractions and stabilized within a multiple *N*-donor ligand framework.

2B.2.3 Reactivity Study of Sn(II) Dication

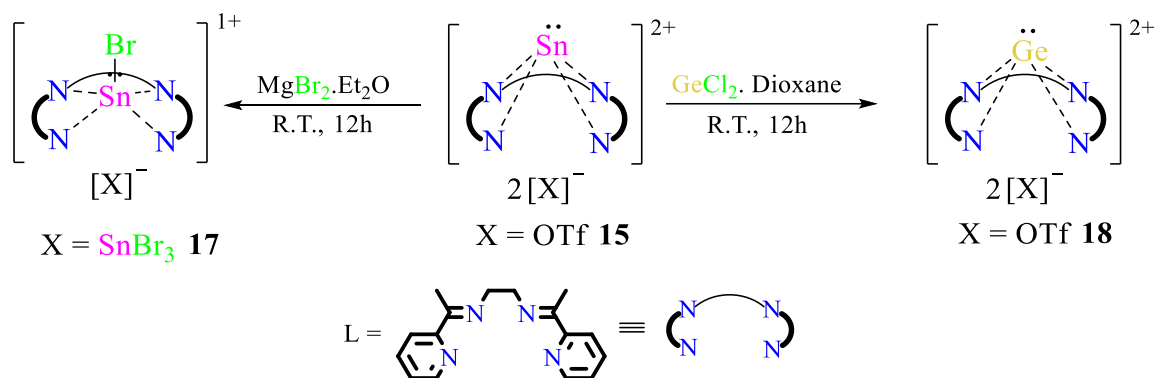
Sn(II) dication **12** & **15** both have the bare lone pair available for nucleophilic reactivity. Still, the simple, straightforward synthetic route and high yield of **15**, further reactivity study was

only performed with **15**. The existence of lone pair electron on the Sn(II) center in **15**, prompted us to investigate its nucleophilic properties towards transition metals. In this vein, initially, compound **15** was reacted with the AuCl.SMe₂ at room temperature, which gave a black precipitate of metallic Sn(0) due to the involved redox steps. Despite numerous trials with transition metals, we have not been successful in establishing nucleophilic behavior of the lone pair in **15**, presumably because of its significant s-character.¹¹



Scheme 2B.4 Coordination of PMe₃ to Sn(II) dication.

In order to check the electrophilic nature of **15**, we have carried out NMR scale reaction with PMe₃ at room temperature. The ¹H NMR spectra show a slight upfield shift while the ³¹P NMR clearly shows a downfield shift, attributing to base coordination to the cationic tin(II).



Scheme 2B.5 Reactivity of Compound **15**.

The electrophilic Sn(II) dication **15** reacted readily with MgBr₂.Et₂O acting as a bromide source,¹² thereby leading to the formation of [L₂SnBr][SnBr₃] **17** (Scheme 2B.5). The crystal structure of compound **17** (Figure 2B.8) has similar features to that of compound **16a**. As expected, the Sn-N_{im} bond distances are shorter, and the Sn-N_{py} bond distances are longer. The Sn1-Br1 distance in the cationic part is 2.6063 (8) Å and the average N-Sn-Br angle is 85.09, which is consistent with the earlier reported structures.^{4e} In the SnBr₃ counter anion, the three

Br atoms are at 2.6950 (9), 2.6259 (9), 2.7043 (9) Å distances respectively from the tin, exhibiting comparable literature values.^{4c} The closest distance between the cationic Sn1 and Br2 of the SnBr₃ counter anion is 3.877 Å, revealing the absence of any contact ion pairs.

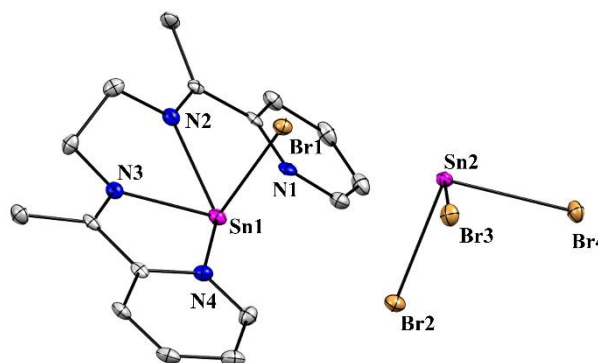


Figure 2B.8. Molecular structure of **16a** (thermal ellipsoid at 30%, H atoms and triflate counter anions are omitted for clarity). Selected bond lengths [Å] and angles [°] Sn1- N2 2.391 (5), Sn1-N3 2.342 (4), Sn1-N4 2.532 (25), Sn1-Br1 2.606 (8), N3-Sn1-N2 71.86(15), N3-Sn1-N4 65.86(15), N3-Sn1-Br1 91.16(11).

Compound **15** undergoes transmetallation reaction with GeCl₂.dioxane, resulting in the isolation of the L-stabilized Ge(II) dication [LGe:]²⁺ **18** (Scheme 2B.5). Transmetallation reactions of the tin precursors are well-established by the groups of Veith et al.¹³ and Schulz et al.¹⁴ Worth mentioning, are the transmetallation reaction between the planar N₂Sn₂ core distannadiazane with ECl₃ (E = Sb, Bi).¹⁵

2B.3 Conclusion

Zwitterionic Sn(II) monocationic and dicationic compounds are synthesized from dipolar stannylene **6** and bis(stannylene) **3** by reaction with Lewis acidic boranes. The reaction proceeds with C-B bond formation instead of forming Lewis acid-base adduct. In another approach, Sn(II) cation was isolated by oxidation of stannylene stabilized in redox-active ligand. We have also synthesized chlorostannylumylidene and an apically disposed tin(II) dication, and both stabilized within bis(α -iminopyridine) L ligand framework. This is the first example where the dicationic tin(II) center is bare, thereby being potentially reactive in nature. We have reported the electrophilic behavior of the Sn(II) dication, and its transmetallation reaction with GeCl₂.dioxane. Nonetheless, the L stabilized Sn(II) dication did not show any nucleophilic behavior due to its high *s*-character.

2B.4 Experimental Details

2B.4.1 General Remarks

All manipulations were carried out under a protective atmosphere of argon, applying standard Schlenk techniques or in a dry box. Toluene and Tetrahydrofuran (THF) were refluxed over sodium/benzophenone. Dichloromethane (DCM) and acetonitrile (ACN) were stirred and refluxed over calcium hydride and kept over 3 Å molecular sieves. All solvents were distilled and stored under argon and degassed before use. Acetonitrile- d_3 ampoules and Chloroform- d_3 were purchased from Sigma Aldrich and used as it is. All chemicals were used as purchased. The tetradentate ligand **L** was prepared according to literature procedure.¹⁶ ^1H and $^{13}\text{C}\{^1\text{H}\}$ NMR spectra were referenced to external SiMe_4 using the residual signals of the deuterated solvent (^1H) or the solvent itself (^{13}C). ^{11}B NMR was referenced to $\text{BF}_3\cdot\text{OEt}_2$ as the external standard. ^{19}F and $^{31}\text{P}\{^1\text{H}\}$ NMR were referenced to external $\text{C}_6\text{H}_5\text{CF}_3$ (TFT) and 85% H_3PO_4 , respectively. ^{119}Sn NMR was referenced to external SnMe_4 . Melting points were determined under argon in closed NMR tubes and are uncorrected. Elemental analyses were performed on the Elementar vario EL analyzer. Single crystal data were collected on both Bruker SMART APEX four-circle diffractometer equipped with a CMOS photon 100 detectors (Bruker Systems Inc.) with a Cu $K\alpha$ radiation (1.5418 Å), and Bruker SMART APEX Duo diffractometer using Mo $K\alpha$ radiation (0.71073 Å).

2B.4.2 Synthetic Procedures

Compound 12

$\text{B}(\text{C}_6\text{F}_5)_3$ (0.07 g, 0.136 mmol) was added to toluene solution of compound **3** (0.05 g, 0.068 mmol) and the pale yellow reaction mixture was stirred for 1 h at room temperature. The reaction mixture was concentrated and layered with pentane to get colorless crystals of compound **12** with a yield of 48% (0.040 g).

Characterization of **12**: ^1H NMR (400 MHz, Chloroform- d_3 , TMS) δ 8.87 (d, $J = 4.1$ Hz, 1H, Pyr- H); 8.59 (d, $J = 5.2$ Hz, 1H, Pyr- H); 8.27 (d, $J = 8.1$ Hz, 1H, Pyr- H); 8.19 (t, $J = 7.9$ Hz, 1H, Pyr- H); 7.98 (t, $J = 8.0$ Hz, 1H, Pyr- H); 7.89 (t, $J = 5.2$ Hz, 1H, Pyr- H); 7.80 (t, $J = 6$ Hz, 1H, Pyr- H); 7.64 (d, $J = 5.2$ Hz, 1H, Pyr- H); 3.84 (m, 3H, Cy- H & CH_2); 3.57 (t, $J = 8.0$ Hz, 1H, Cy- H); 3.27 (s, 2H, CH_2); 2.57 (d, 2H, Cy- H); 1.29 (m, 1H, Cy- H); 2.05 (s, 1H, Cy- H); 1.95 (d, 1H, Cy- H); 1.28 (m, 2H, Cy- H); 0.91 (t, $J = 8$ Hz, 2H, Cy- H) ppm. $^{19}\text{F}\{^1\text{H}\}$ NMR (377 MHz, Chloroform- d_3 , TFT) δ -164.21 (t, $J = 19.4$ Hz, m -F); -163.99 (t, $J = 19.3$ Hz, m -F); -159.31 (t, $J = 20.6$ Hz, p -F); -159.06 (t, $J = 20.4$ Hz, p -F); -129.88 (bs, o -F); -130.77 (bs, o -F) ppm. $^{11}\text{B}\{^1\text{H}\}$ NMR (128.43 MHz, Chloroform- d_3 , $\text{BF}_3\cdot\text{OEt}_2$) δ -13.29 & -12.30 ppm.

Elemental Analysis: Calcd. for C₅₆H₂₂B₂F₃₀N₄Sn: C, 46.03; H, 1.52; N, 3.83. Found: C, 46.50; H, 1.32; N, 3.95

Compound 13

B(C₆F₅)₃ (0.075 g, 0.147 mmol) was added to toluene solution of compound **3** (0.1 g, 0.147 mmol) and the pale yellow reaction mixture was stirred for 1 h at room temperature. The reaction mixture was concentrated and layered with pentane to get colorless crystals of compound **13** with a yield of 60% (0.105 g).

Characterization of **13**: ¹H NMR (400 MHz, Benzene-*d*₆, TMS) δ 7.38 (d, *J* = 8.0 Hz, 1H), 7.19 (s, 2H), 7.07 (s, 2H), 6.98 (s, 1H), 6.88 (s, 2H), 6.60 (t, *J* = 7.8 Hz, 1H), 6.45 (d, *J* = 7.6 Hz, 1H), 6.42 – 6.35 (m, 2H), 6.06 – 6.01 (m, 1H), 5.81 (dd, *J* = 7.3, 5.4 Hz, 1H), 4.43 (s, 1H), 3.93 (s, 1H), 3.49 (s, 1H), 3.37 (s, 1H), 3.19 (dt, *J* = 13.3, 6.5 Hz, 1H), 3.01 (dt, *J* = 13.6, 6.8 Hz, 1H), 2.63 (dt, *J* = 13.5, 6.7 Hz, 2H), 1.44 (d, *J* = 6.7 Hz, 3H), 1.31 – 1.17 (m, 9H), 0.95 (d, *J* = 6.7 Hz, 3H), 0.71 (d, *J* = 6.5 Hz, 3H), 0.40 (d, *J* = 6.9 Hz, 3H), -0.03 (d, *J* = 6.7 Hz, 3H) ppm. ¹³C NMR (101 MHz, Benzene-*d*₆, TMS) δ 186.10, 154.73, 150.04, 149.54, 146.52, 145.61, 144.57, 144.44, 142.80, 141.52, 141.00, 139.94, 137.72, 137.51, 136.48, 128.95, 128.18, 125.79, 125.72, 125.31, 124.83, 123.98, 123.62, 122.45, 121.23, 89.19, 28.57, 28.38, 28.09, 27.82, 26.76, 26.00, 25.81, 23.49, 23.31, 22.68, 22.35, 22.06, 21.05 ppm. ¹¹B NMR (128 MHz, Benzene-*d*₆, BF₃.OEt₂) δ -12.71. ¹⁹F NMR (377 MHz, Benzene-*d*₆, TFT) δ -131.31, -161.13, -165.46 ppm. ¹¹⁹Sn NMR (149 MHz, Benzene-*d*₆, SnMe₄) δ -352.99 ppm.

Compound 14

NOSbF₆ (0.039 g, 0.147 mmol) was added to the thf solution of compound **6** (0.1 g, 0.147 mmol), instant liberation of NO gas in the form of gas bubbles through reaction mixture appeared. The colorless reaction mixture was concentrated and layered with pentane to obtain colorless few crystals of **14**. Compound 14 was characterized only with SC-XRD.

Synthesis of 15

Ligand **L** (0.3 g, 1.13 mmol) was dissolved in dichloromethane and was added to a suspension of SnCl₂ (0.21 g, 1.13 mmol) in dichloromethane, followed by drop-wise addition of TMSOTf (0.41 mL, 2.25 mmol) at 0°C. The solution was stirred overnight when white precipitation occurred. The precipitate was isolated via filtration and washed thrice with THF. The product was dried under vacuum yielding 0.65g (85%) of **2** (decomp. 209-205°C) as white solid.

Crystals of compound **1** suitable for X-ray measurement were grown by layering acetonitrile solution of the compound with diethyl ether at room temperature.

Characterization of **15**: ^1H NMR (400 MHz, Acetonitrile- d_3 , TMS) δ 9.20 (d, $J=5.4$, 2H, *o*-Pyr-*H*); 8.42 - 8.32 (m, 4H, *p*-Pyr-*H* & *m*-Pyr-*H*); 8.02 (m, 2H, *m*-Pyr-*H*); 4.41 (s, 4H, $-\text{CH}_2-\text{CH}_2-$); 2.65 (s, 6H, $-\text{CH}_3$) ppm. $^{13}\text{C}\{^1\text{H}\}$ NMR (101 MHz, Acetonitrile- d_3 , TMS) δ 173.06(*C*- CH_3); 149.29 (Pyr- Co); 148.65 (Pyr-Co); 142.85 (Pyr-Cp); 129.29 (Pyr-Cm); 126.89 (Pyr-Cm); 122.46, 119.34 (CF_3SO_3); 48.29 ($-\text{CH}_2-\text{CH}_2-$); 16.53 (CCH_3) ppm. $^{19}\text{F}\{^1\text{H}\}$ NMR (377 MHz, Acetonitrile- d_3 , TFT) δ -79.35 (TMSOTf- *F*) ppm. $^{119}\text{Sn}\{^1\text{H}\}$ NMR (149.74 MHz, Acetonitrile- d_3 , SnMe $_4$) -636.94 ppm. Elemental Analysis: Calcd. for $\text{C}_{18}\text{H}_{18}\text{F}_6\text{N}_4\text{O}_6\text{S}_2\text{Sn}$: C, 31.65; H, 2.66; N, 8.20. Found: C, 31.70; H, 2.75; N, 8.11.

Synthesis of **16a**

Ligand **L** (0.28 g, 1.05 mmol) was dissolved in DCM and was added to SnCl $_2$ (0.2 g, 1.05 mmol) in DCM, followed by drop-wise addition of trimethylsilyl trifluoromethanesulphonate (0.19 mL, 1.05 mmol) at 0°C. The reaction mixture was stirred overnight, orange color product precipitated throughout the reaction. The product was isolated via filtration and washed thrice with THF. The product was dried under vacuum yielding 0.538 g (90%) of [LSnCl][OTf] (decomp. 197-193°C) as an orange solid. Crystals of **16a** suitable for X-ray measurement were grown by layering acetonitrile solution of the compound with diethyl ether at room temperature.

Characterization of **16a**: ^1H NMR (400 MHz, Acetonitrile- d_3 , TMS) δ 8.96 (d, $J = 4.7$ Hz, 2H, *o*-Pyr-*H*); 8.22 (m, 4H, *p*-Pyr-*H* & *m*-Pyr-*H*); 7.80 (m, 2H, *m*-Pyr-*H*); 4.18 (s, 4H, $-\text{CH}_2-\text{CH}_2-$); 2.70 (s, 6H, $-\text{CH}_3$) ppm. $^{13}\text{C}\{^1\text{H}\}$ NMR (101 MHz, Acetonitrile- d_3 , TMS) δ 171.71(*C*- CH_3); 149.81 (Pyr- Co); 147.14 (Pyr-Co); 139.81 (Pyr-Cp); 127.71 (Pyr-Cm); 125.65 (Pyr-Cm); 122.75, 119.56 (CF_3SO_3); 50.02 ($-\text{CH}_2-\text{CH}_2-$); 17.27 (CCH_3) ppm. $^{19}\text{F}\{^1\text{H}\}$ NMR (377 MHz, Acetonitrile- d_3 , TFT) δ -79.29 (TMSOTf- *F*) ppm. $^{119}\text{Sn}\{^1\text{H}\}$ NMR (149.74 MHz, Acetonitrile- d_3) -572.38 ppm. Elemental Analysis: Calcd. for $\text{C}_{17}\text{H}_{18}\text{ClF}_3\text{N}_4\text{O}_3\text{SSn}$: C, 35.85; H, 3.19; N, 9.84. Found: C, 33.72; H, 3.14; N, 9.89.

Synthesis of **16b**

Ligand **L** (0.28 g, 1.05 mmol) was dissolved in DCM and was added to a DCM solution of SnCl $_2$ (0.4 g, 2.10 mmol). Orange colored precipitation occurred upon overnight stirring. The precipitate was isolated via filtration and washed thrice with THF. Product was dried under vacuum yielding 0.63 g (93%) of [LSnCl][SnCl $_3$] (decomp. 185-183°C) as an orange/ yellow solid. Crystals suitable for X-ray measurement were grown by layering DCM solution of reaction mixture by pentane solution.

Characterization of **16b**: ^1H NMR (400 MHz, Acetonitrile- d_3 , TMS) δ 8.96 (d, $J=4.4$ Hz, 2H, *o*-Pyr-*H*); 8.18-8.24 (m, 4H, *p*-Pyr-*H* & *m*-Pyr-*H*); 7.78-7.81 (m, 2H, *m*-Pyr-*H*); 4.18 (s, 4H, -CH₂-CH₂-); 2.70 (s, 6H, -CH₃) ppm. Elemental Analysis: Calcd. for C₁₆H₁₈Cl₄N₄Sn₂: C, 29.77; H, 2.81; N, 8.68. Found: C, 29.81; H, 2.90; N, 8.85.

Synthesis of 17

Compound **15** (0.2 g, 0.29 mmol) was dissolved in acetonitrile and was added to a solution of MgBr₂.Et₂O (0.075 g, 0.29 mmol) in acetonitrile at room temperature. The solution turned yellow and stirred overnight. The solvent was evaporated and residue was washed with THF to remove MgBr₂. The yellow coloured residue as product was dried under vacuum yielding 0.14g (60%) of compound **4** as orange powder ((decomp. 192-190°C). Crystals of **15** suitable for X-ray measurement were grown by layering acetonitrile solution of the compound with diethyl ether at room temperature.

Characterization of **17**: ^1H NMR (400 MHz, Acetonitrile- d_3 , TMS) δ 9.20 (d, $J=5.4$, 2H, *o*-Pyr-*H*); 8.42 - 8.32 (m, 4H, *p*-Pyr-*H* & *m*-Pyr-*H*); 8.02 (m, 2H, *m*-Pyr-*H*); 4.41 (s, 4H, -CH₂-CH₂-); 2.65 (s, 6H, -CH₃) ppm. Elemental Analysis: Calcd. for C₁₆H₁₈Cl₄N₄Sn₂: C, 23.34; H, 2.20; N, 6.80. Found: C, 23.40; H, 2.30; N, 6.70.

Synthesis of 18

Compound **1** (0.2 g, 0.7 mmol) was dissolved in acetonitrile and was added to a suspension of GeCl₂.Dioxane (0.067 g, 30.7 mmol) in acetonitrile at room temperature. The solution turned yellow and stirred overnight. The solvent was evaporated and residue was washed with THF to remove SnCl₂. The yellow coloured residue was dried under vacuum yielding 0.14 g (73%) as compound **18**.

Characterization of **18**: ^1H NMR (400 MHz, Acetonitrile- d_3 , TMS) δ 9.30 (d, $J=5.4$, 2H, *o*-Pyr-*H*); 8.52 (td, $J=7.8, 1.4$, 2H, *p*-Pyr-*H*); 8.45 (d, $J=7.6$, 2H, *m*-Pyr-*H*); 8.14 – 8.09 (m, 2H, *m*-Pyr-*H*); 4.52 (s, 4H, -CH₂-CH₂-); 2.75 (s, 6H, -CH₃) ppm. $^{13}\text{C}\{^1\text{H}\}$ NMR (101 MHz, Acetonitrile- d_3 , TMS) δ 172.34 (C-CH₃); 148.20 (Pyr- Co); 146.95 (Pyr-Co); 143.98 (Pyr-Cp); 129.95 (Pyr-Cm); 126.90 (Pyr-Cm); 122.51, 119.35 (CF₃SO₃); 46.95 (-CH₂-CH₂-); 16.21 (CCH₃) ppm. $^{19}\text{F}\{^1\text{H}\}$ NMR (377 MHz, Acetonitrile- d_3 , TMS) δ -79.29 (TMSOTf- *F*) ppm. Elemental Analysis: Calcd. for C₁₈H₁₈F₆GeN₄O₆S₂: C, 33.93; H, 2.85; N, 8.79. Found: C, 33.97; H, 2.95; N, 8.85.

Reaction of **15** with PMe_3

In a NMR tube, PMe_3 (8.9 μL , 0.088 mmol) was added to compound **1** (0.060 g, 0.088 mmol) dissolved in 0.6 mL of Acetonitrile- d_3 , and shaken well. The NMR spectra were monitored at room temperature at different time intervals.

2B.4.3 Plots of NMR spectra

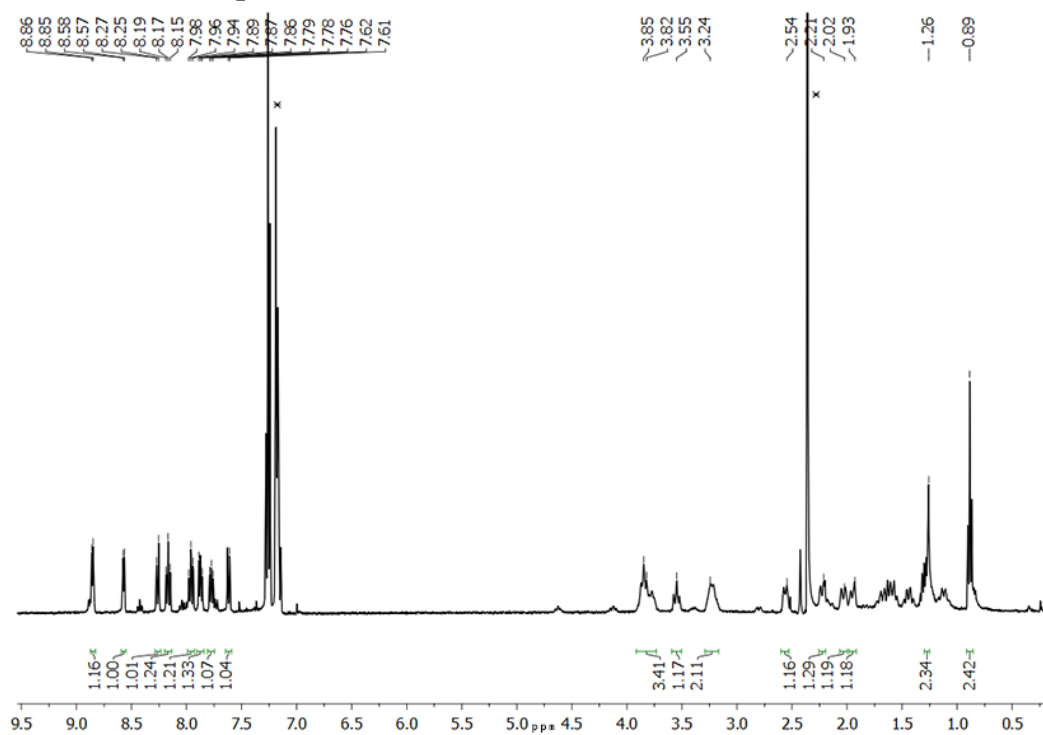


Figure 2B.9. ¹H NMR of comp. 12 in CDCl₃ (* Toluene)

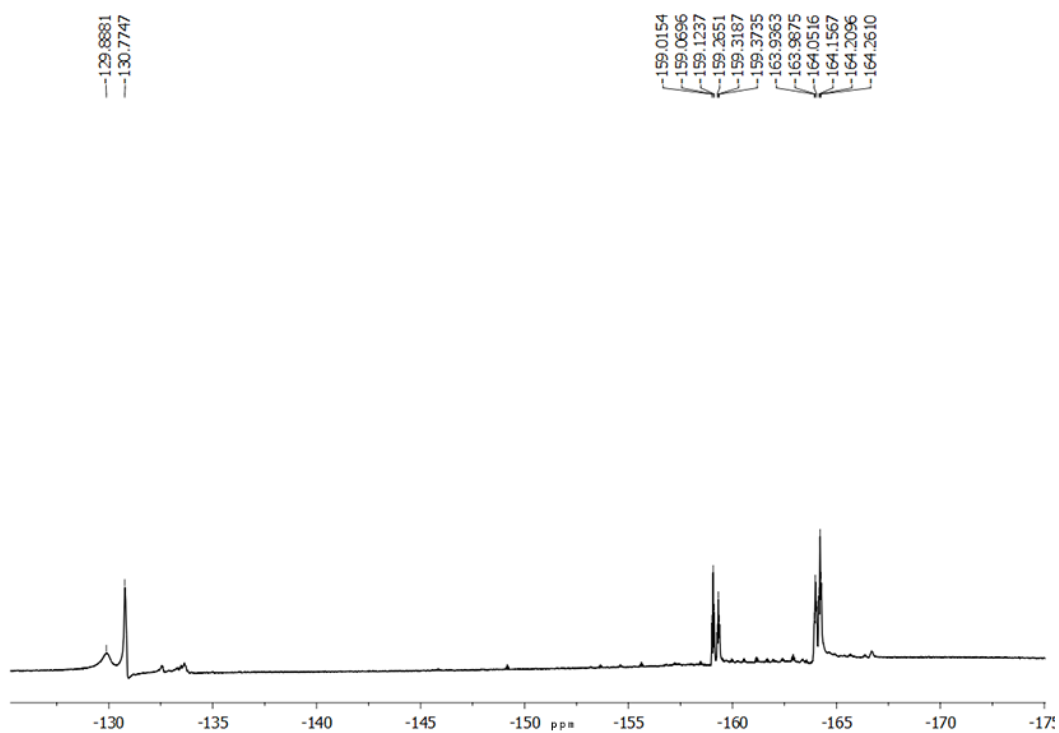


Figure 2B.10. ¹⁹F NMR of comp. 12 in CDCl₃

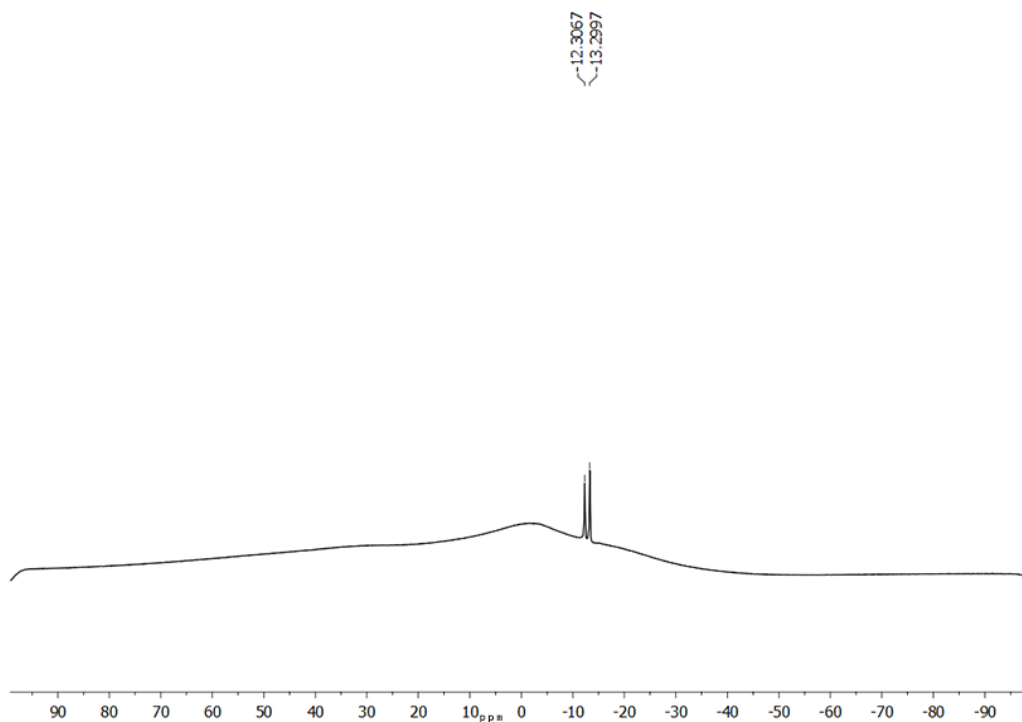


Figure 2B.11. ^{11}B NMR of comp. **12** in CDCl_3

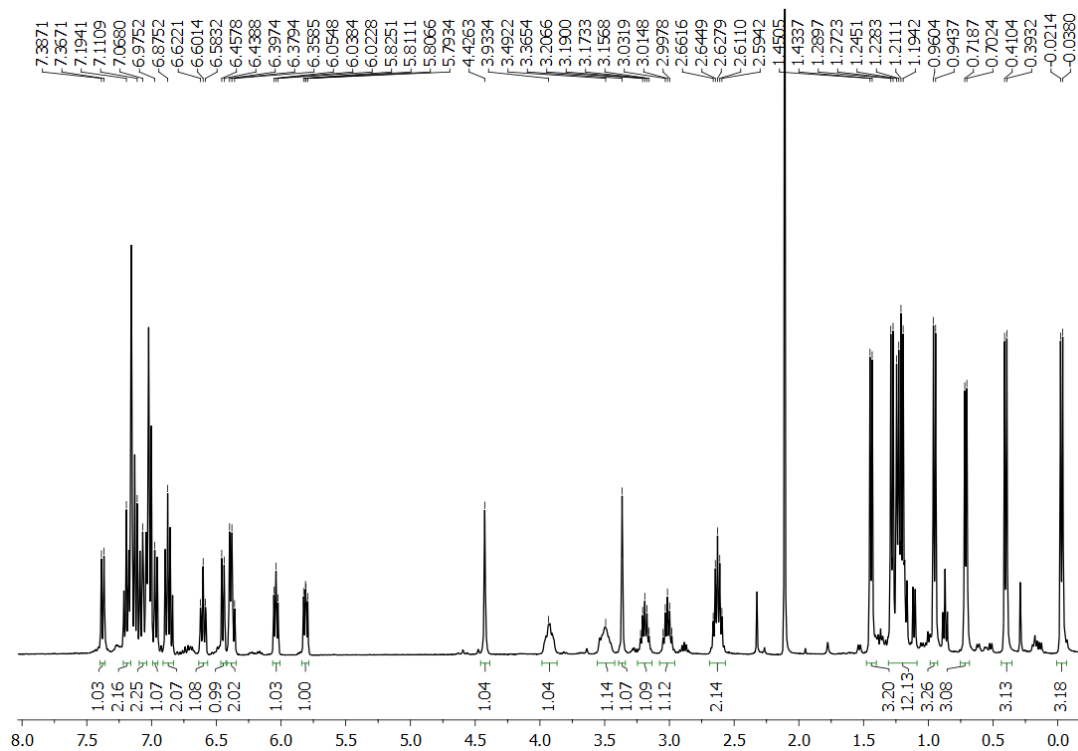


Figure 2B.12. ^1H NMR of comp. **13** in CDCl_3

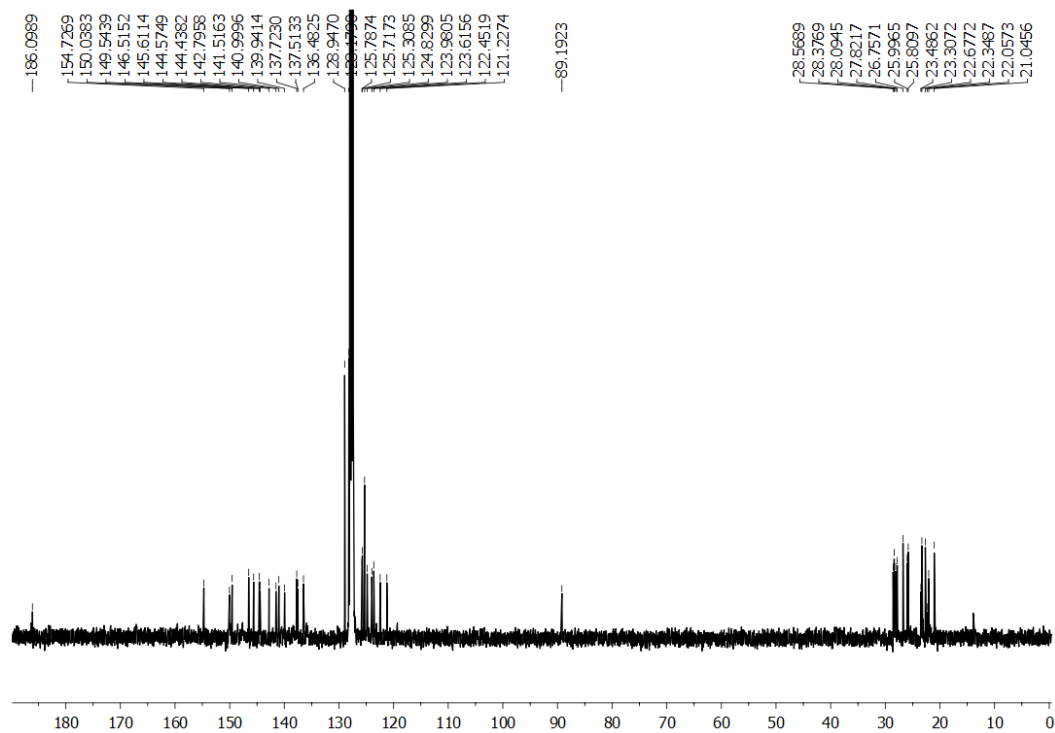


Figure 2B.13. ^{13}C NMR of Compound 13 in CDCl_3

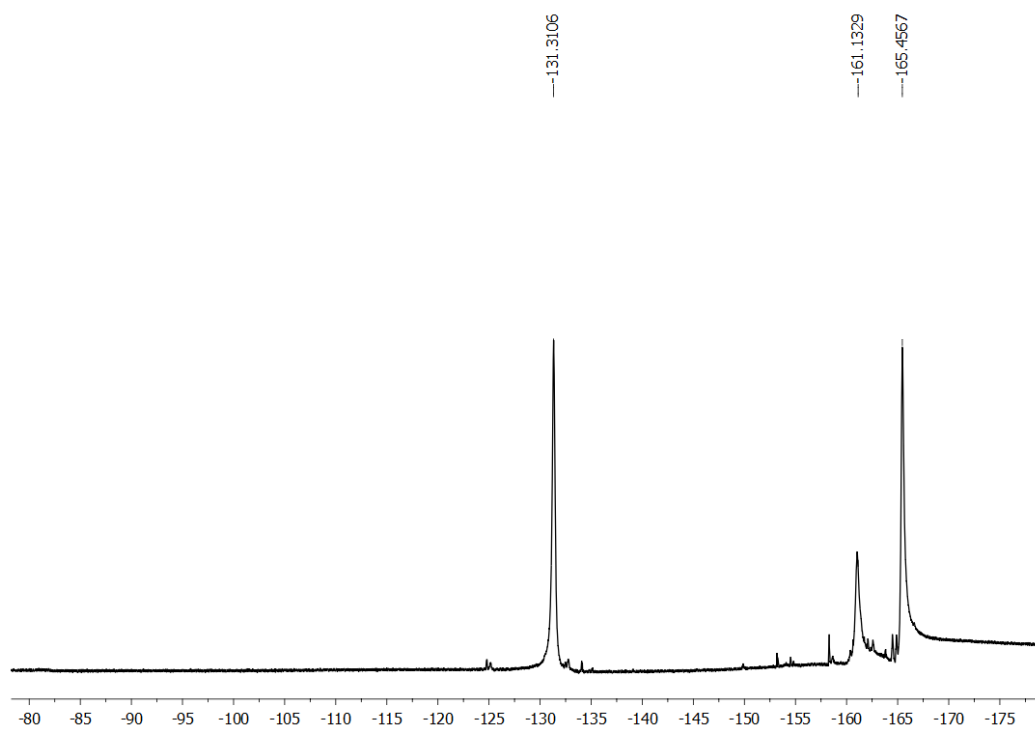


Figure 2B.14. ^{19}F NMR of comp. 13 in CDCl_3

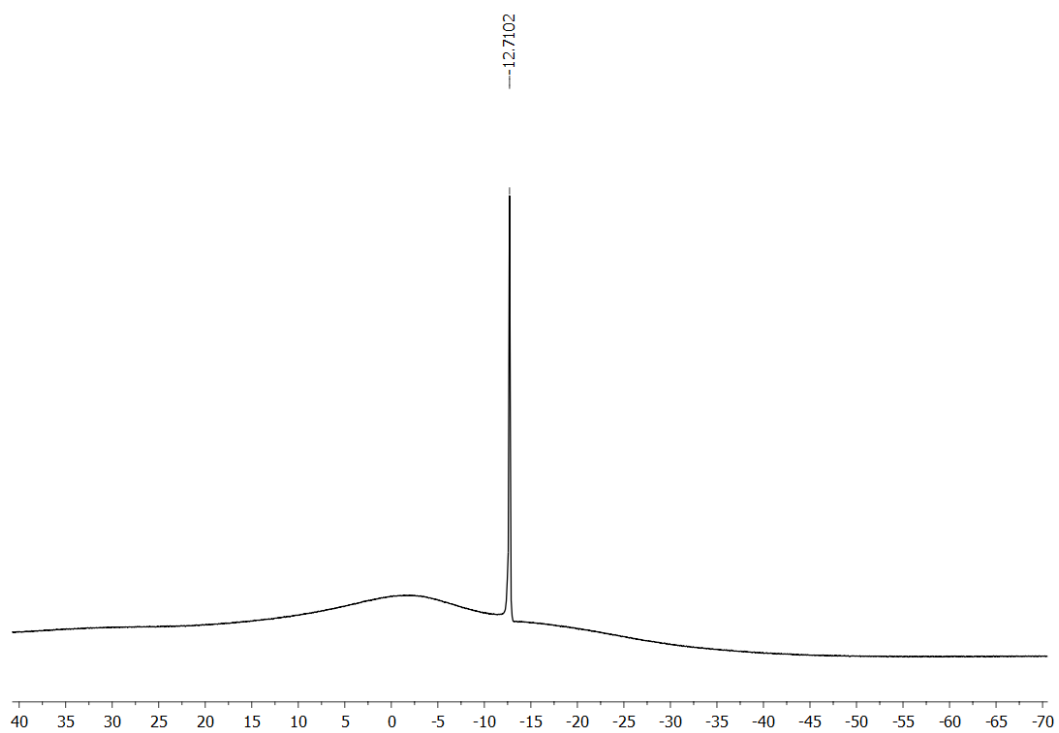


Figure 2B.15. ^{11}B NMR of comp. **13** in CDCl_3

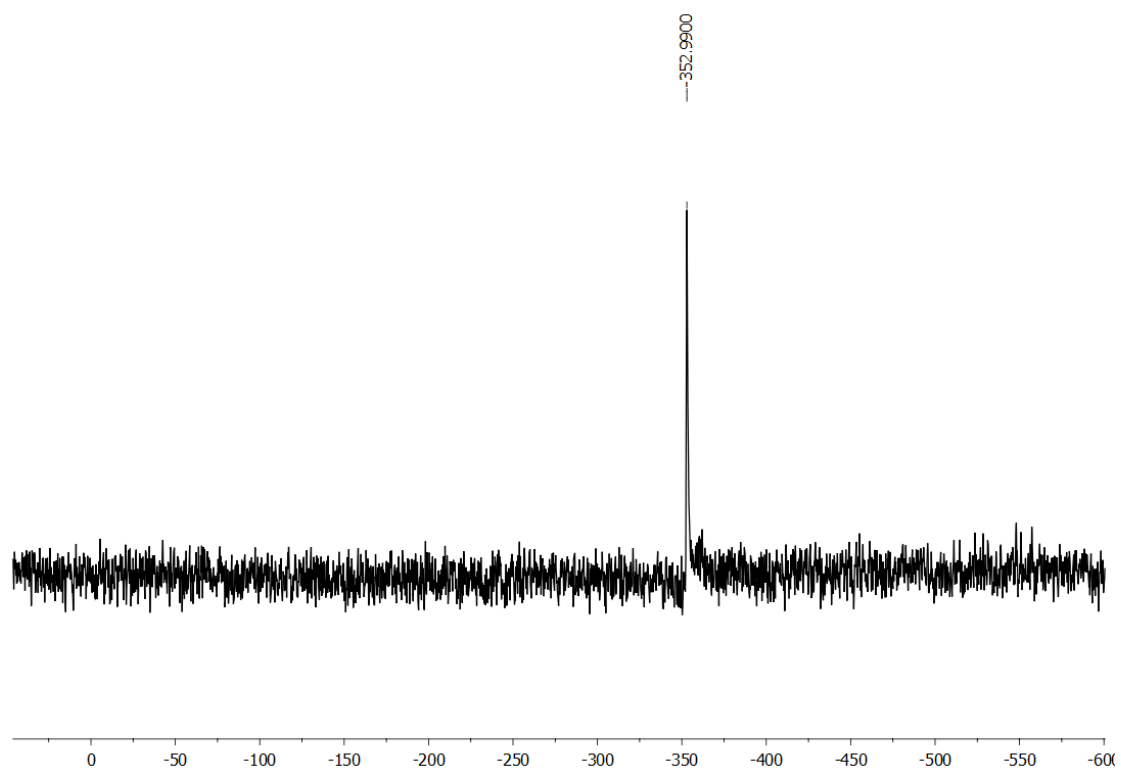


Figure 2B.16. ^{119}Sn NMR of Compound **13** in CDCl_3

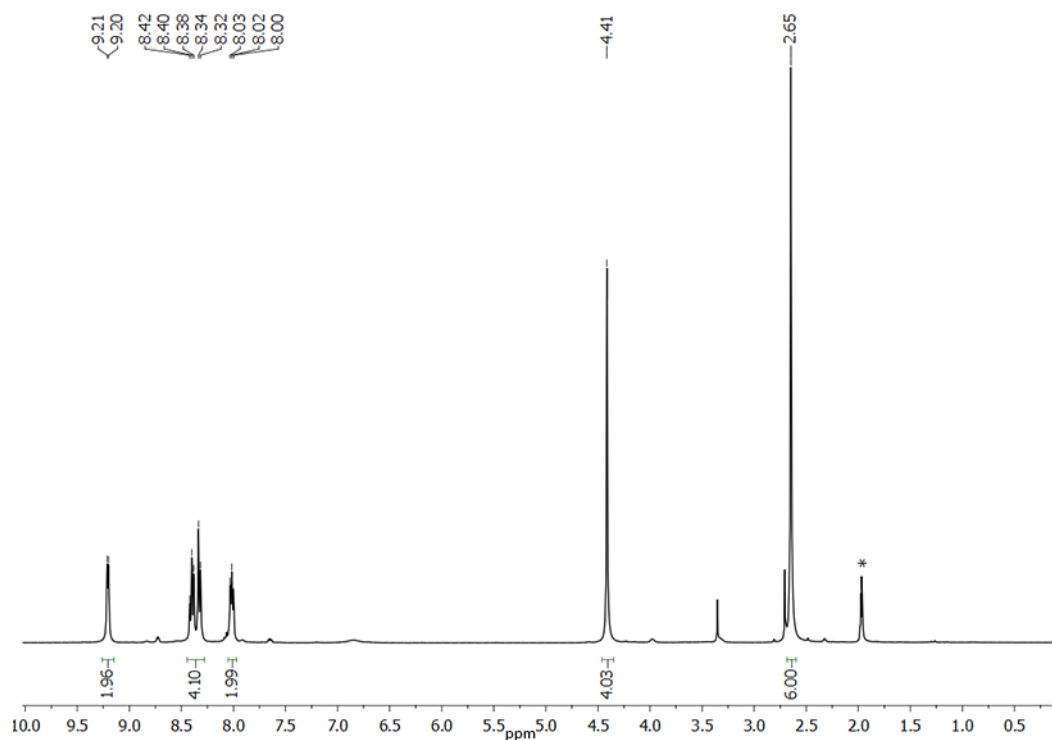


Figure 2B.17. ^1H NMR of Compound **15** (* residual solvent peak)

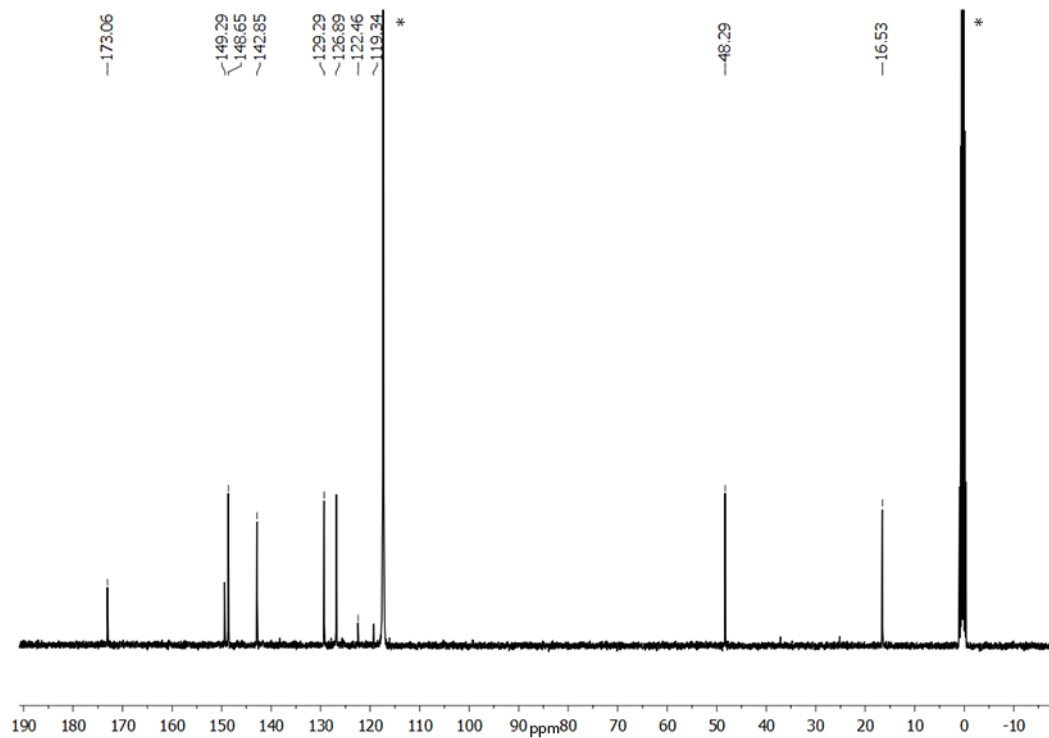


Figure 2B.18. ^{13}C NMR of Compound **15** (* residual solvent peak)

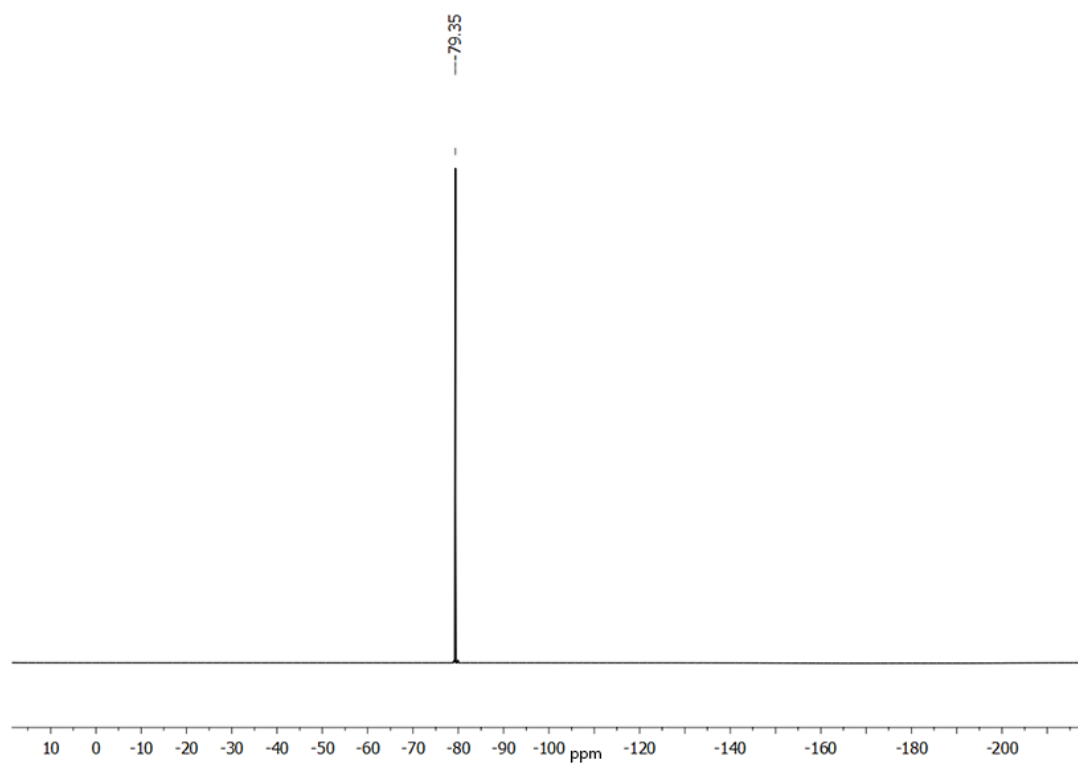


Figure 2B.19. ^{19}F NMR of Compound **15**

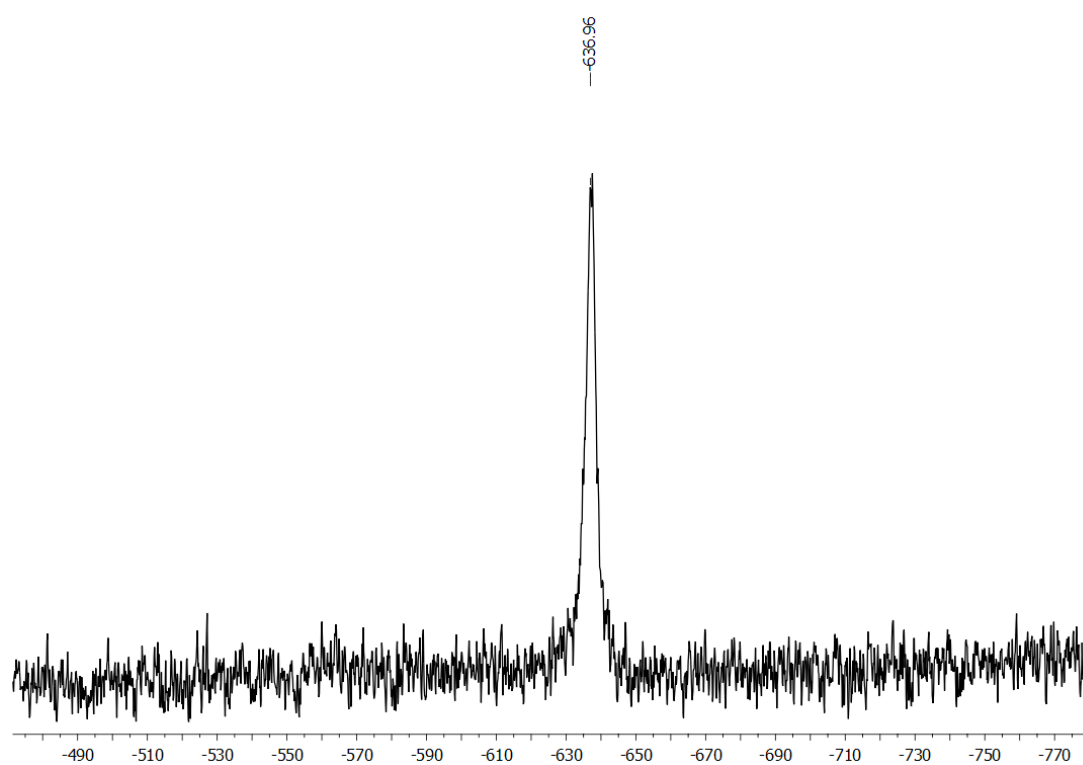


Figure 2B.20. ^{119}Sn NMR of Compound **15**

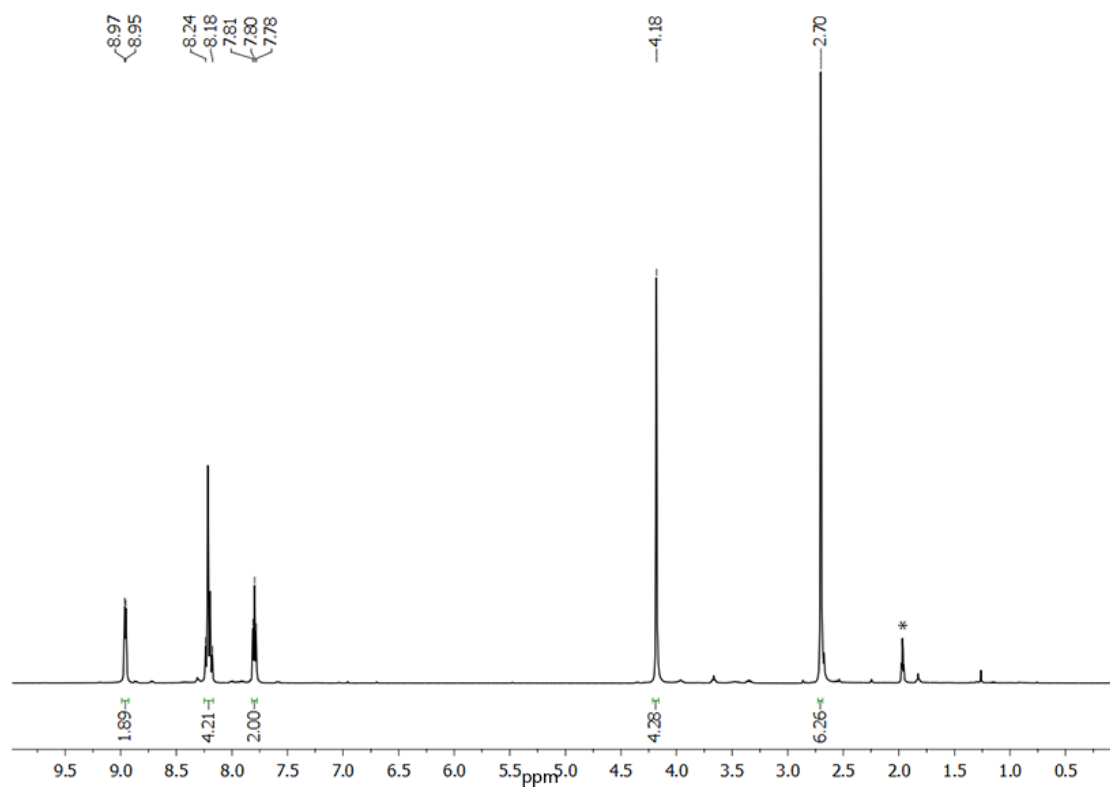


Figure 2B.21. ^1H NMR of Compound 16a (* residual solvent peak)

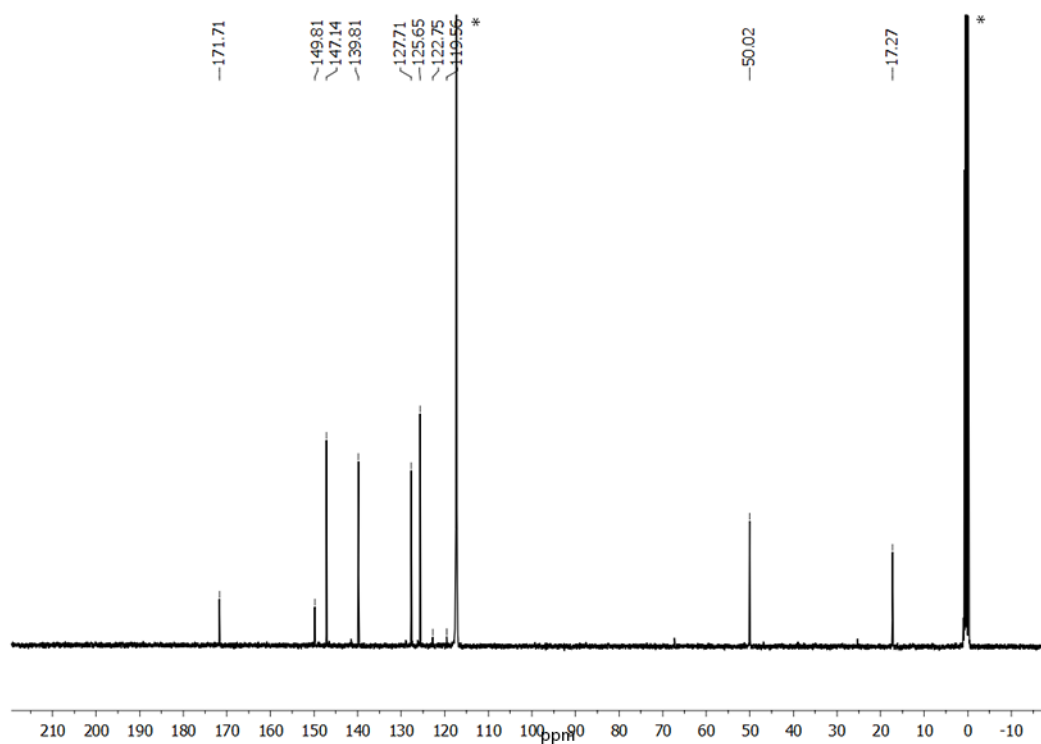


Figure 2B.22. ^{13}C NMR of Compound 16a (* residual solvent peak)

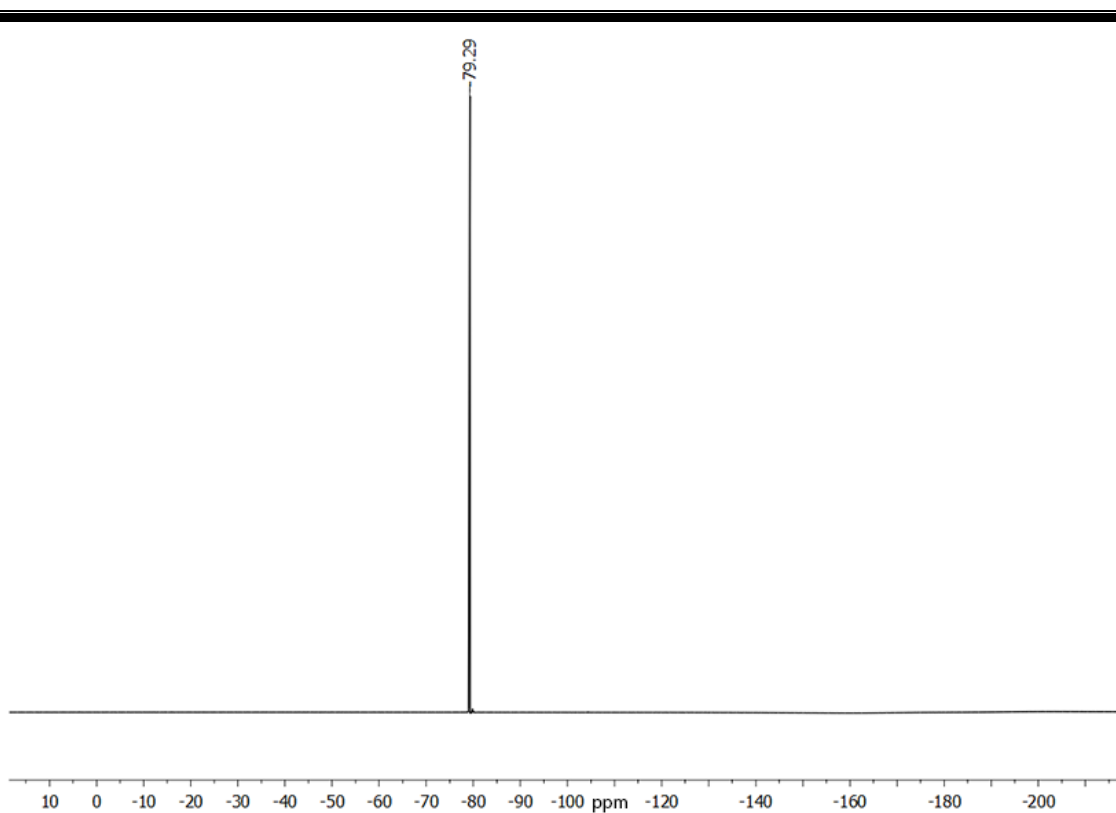


Figure 2B.23. ^{19}F NMR of Compound **16a**

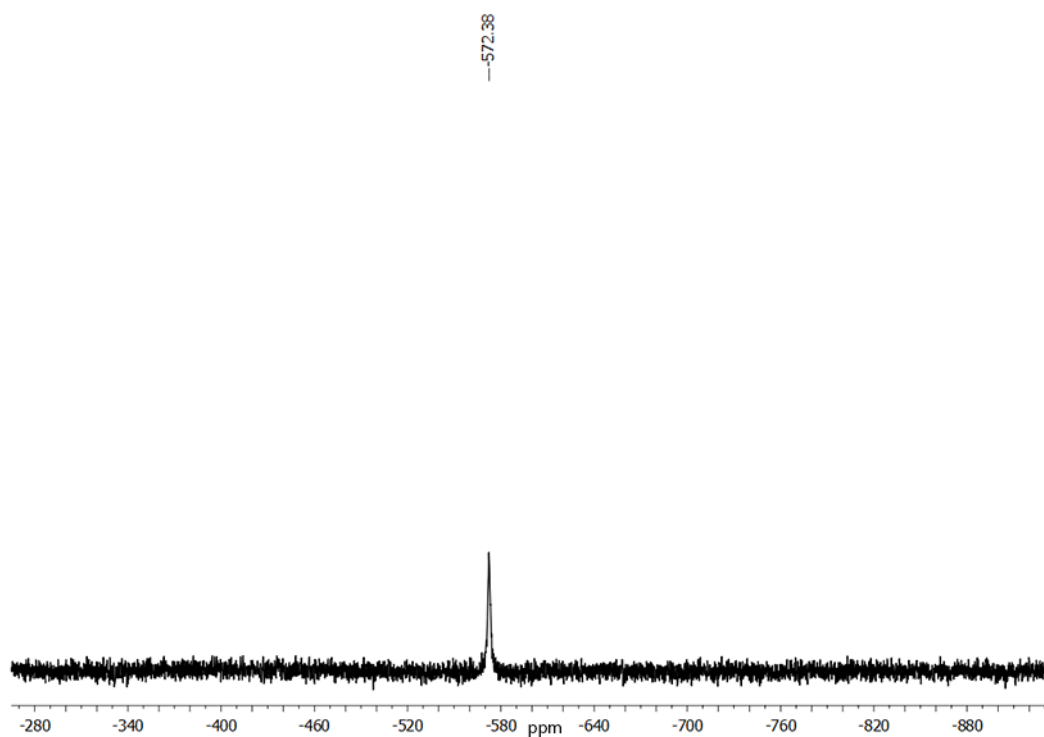


Figure 2B.24. ^{119}Sn NMR of Compound **16a**

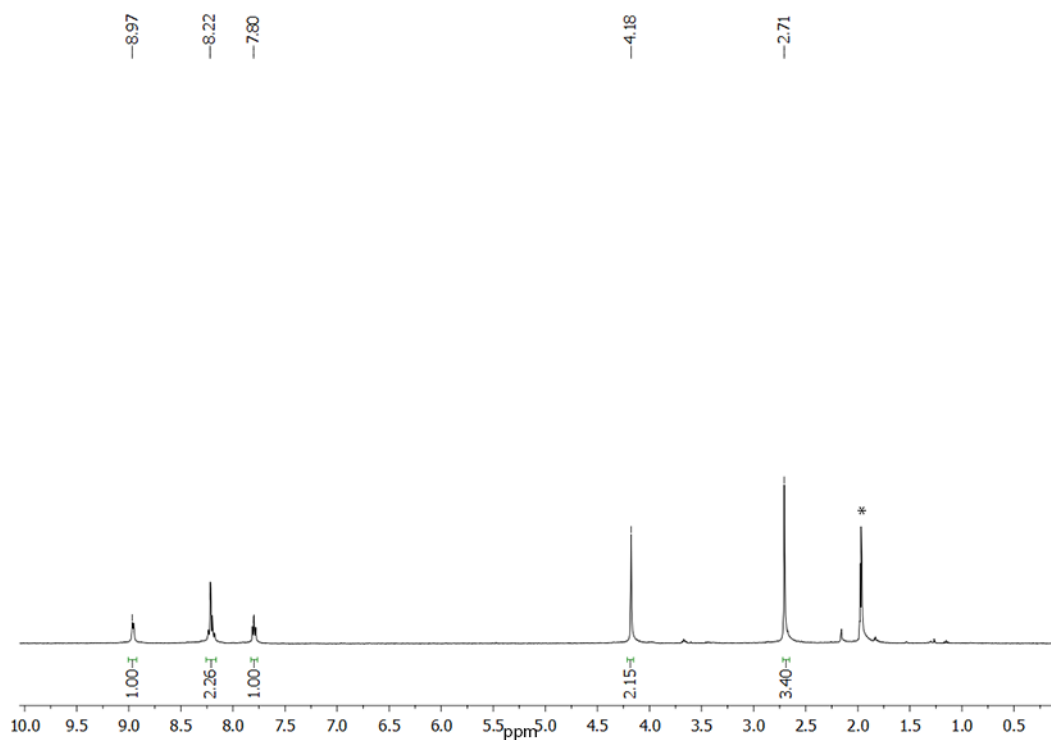


Figure 2B.25. ^1H NMR of Compound **17b** (* residual solvent peak)

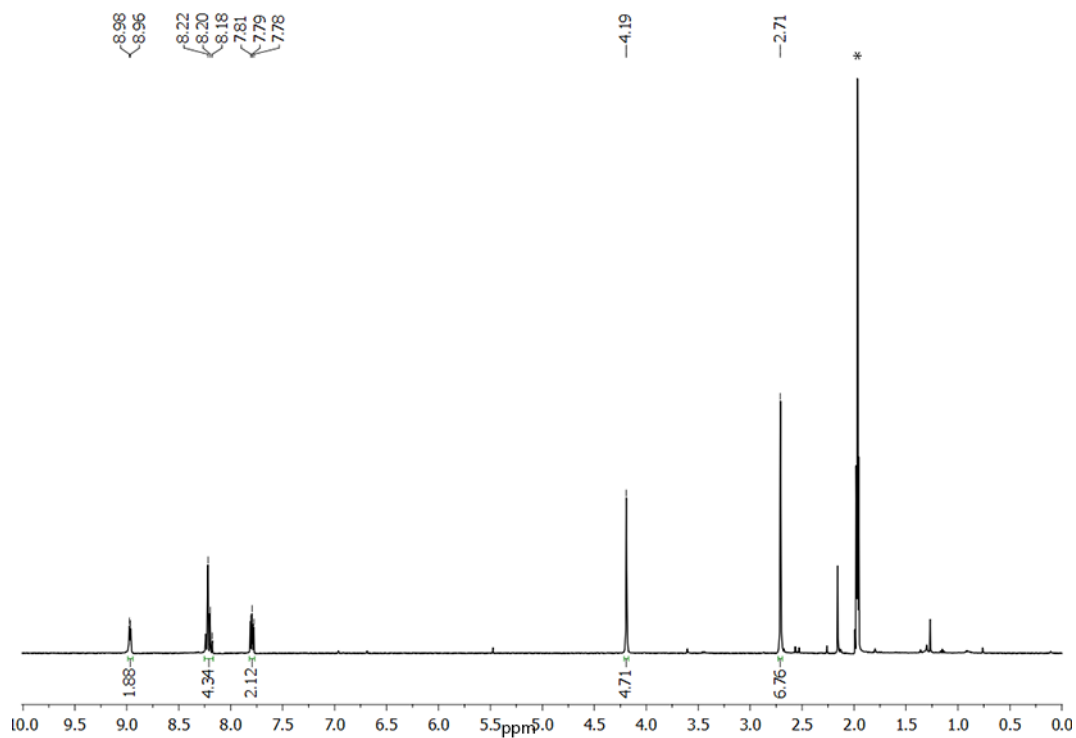


Figure 2B.26. ^1H NMR of Compound **18** (* residual solvent peak)

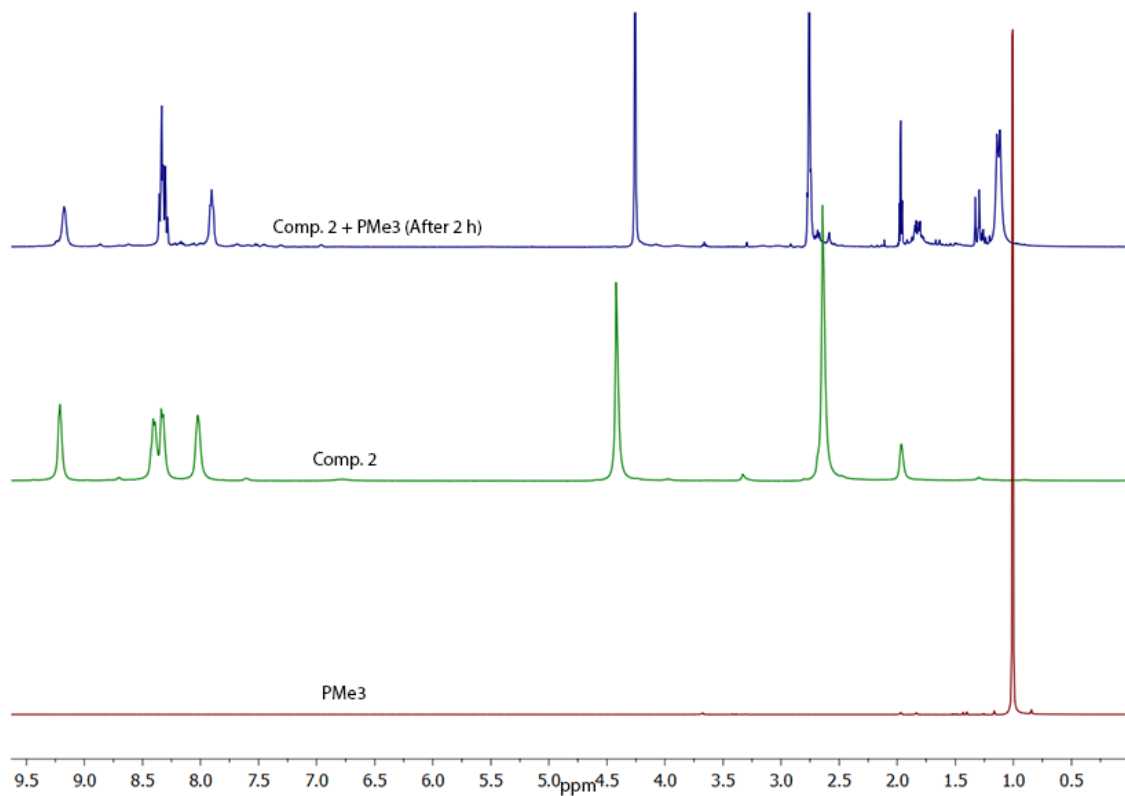


Figure 2B.27. ^1H NMR of PMe_3 Experiment

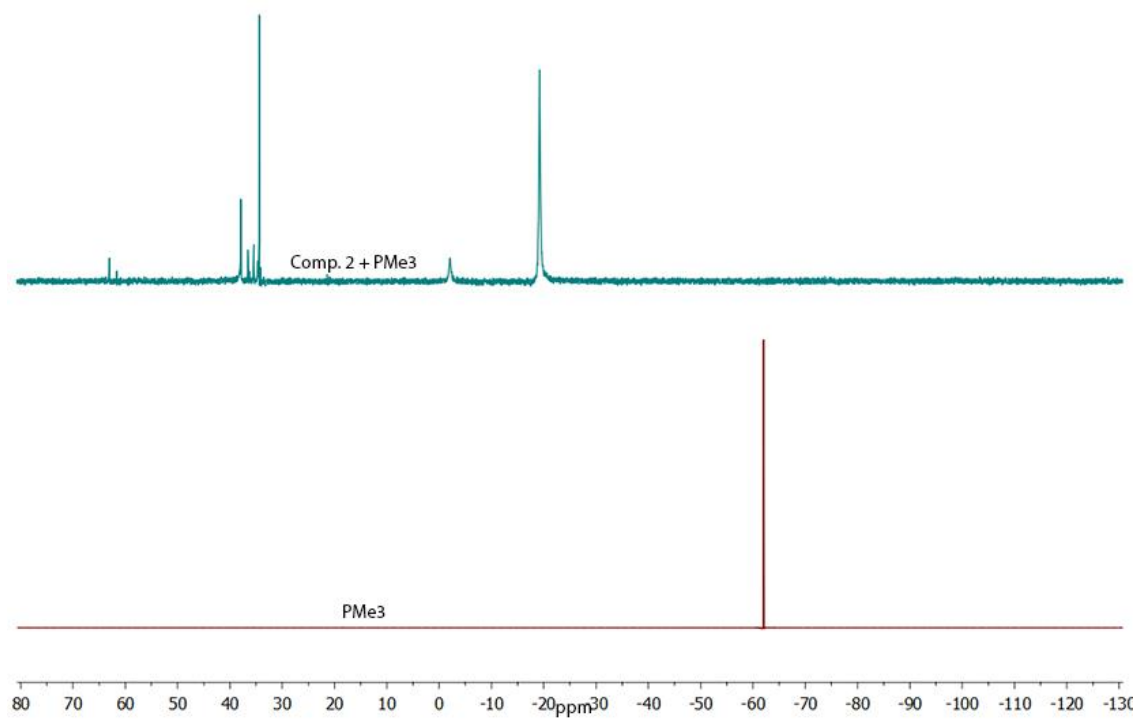


Figure 2B.28. ^{31}P NMR of PMe_3 Experiment

2B.4.4 X-Ray Crystallographic Data

Table 2B.1. Crystal data and structure refinement for Compound **12** and **13**.

Empirical formula	C74 H43 B2 F30 N4 Sn	C71 H46 B F15 N4 Sn
Formula weight	1692.43	1369.2
Temperature	100 K	100 K
Wavelength	1.54178 Å	1.54178 Å
Crystal system	Monoclinic	Triclinic
Space group	P 21/n	P -1
Unit cell dimensions	a = 10.2239(8) Å α = 90 b = 15.6566(12) Å β = 95.994(4) c = 41.352(3) Å γ = 90	a = 12.3697 (18) Å α = 94.182(5) b = 12.5359 (18) Å β = 100.161 (5) c = 19.278 (3) Å γ = 92.184(5)
Volume	6583.1 (2) Å ³	2930.7 (7) Å ³
Z	4	2
Density (calculated)	1.708g/cm ³	1.552 g/cm ³
Absorption coefficient	4.311 mm ⁻¹	4.314 mm ⁻¹
F(000)	3368	1380
Crystal size	0.09 x 0.08 x 0.06 cm ³	0.15 x 0.12 x 0.012 cm ³
Theta range for data collection	3.020 to 66.889°.	2.336 to 67.127°.
Index ranges	-12<=h<=11, -18<=k<=18, - 49<=l<=49	-14<=h<=14, -14<=k<=14, - 22<=l<=22
Reflections collected	84616	26513
Independent reflections	9280 [R(int) = 0.0392]	10223 [R(int) = 0.0533]
Completeness to theta = 28.38°	99.3 %	97.6 %
Absorption correction	Multi-scan	Multi-scan
Max. and min. transmission	0.5944 and 0.7440	0.5719 and 0.7528
Refinement method	Full-matrix least-squares on F ²	Full-matrix least-squares on F ²
Data / restraints / parameters	11636 / 0 / 1003	9656 / 0 / 828
Goodness-of-fit on F ²	1.018	1.053
Final R indices [I>2sigma(I)]	R1 = 0.0392, wR2 = 0.0886	R1 = 0.0510, wR2 = 0.1395
R indices (all data)	R1 = 0.0595, wR2 = 0.0946	R1 = 0.0533, wR2 = 0.1418
Largest diff. peak and hole	0.620 and -0.581 e.Å ⁻³	0.883 and -1.072 e.Å ⁻³

Table 2B.2. Crystal data and structure refinement for Compound **14** and **15**.

Empirical formula	C ₄₂ H ₅₅ F ₆ N ₄ O Sb Sn	C ₁₆ H ₁₈ N ₄ Sn, C F ₃ O ₃ S, C F ₃ O ₃ S
Formula weight	986.34	683.17
Temperature	100 K	100 K
Wavelength	1.54178 Å	1.54178 Å
Crystal system	Monoclinic	Monoclinic
Space group	P 21/n	P 21/n
Unit cell dimensions	a = 11.459(3) Å α = 90 b = 12.267(4) Å β = 90.59310) c = 30.353(8) Å γ = 90	a = 16.6860 (8) Å α = 90 b = 8.0446 (4) Å β = 98.160 (3) c = 18.2587 (10) Å γ = 90
Volume	4266 (2) Å ³	2426.1 (2) Å ³
Z	4	4
Density (calculated)	1.536 g/cm ³	1.870 g/cm ³
Absorption coefficient	10.210 mm ⁻¹	10.828 mm ⁻¹
F(000)	1992	1352
Crystal size	0.18 x 0.18 x 0.15 cm ³	0.06 x 0.05 x 0.04 cm ³
Theta range for data collection	2.912 to 72.558°.	3.359 to 66.623°.
Index ranges	-14 ≤ h ≤ 13, -12 ≤ k ≤ 14, -36 ≤ l ≤ 379	-19 ≤ h ≤ 19, -9 ≤ k ≤ 9, -21 ≤ l ≤ 21
Reflections collected	29779	9856
Independent reflections	7579 [R(int) = 0.0638]	3575 [R(int) = 0.0404]
Completeness to theta = 28.38°	99.3 %	100 %
Absorption correction	Multi-scan	Multi-scan
Max. and min. transmission	0.3216 and 0.7536	0.548 and 0.648
Refinement method	Full-matrix least-squares on F ²	Full-matrix least-squares on F ²
Data / restraints / parameters	8153 / 0 / 505	4286 / 0 / 336
Goodness-of-fit on F ²	1.018	1.044
Final R indices [I > 2σ(I)]	R1 = 0.0638, wR2 = 0.1796	R1 = 0.0404, wR2 = 0.0781
R indices (all data)	R1 = 0.0687, wR2 = 0.1909	R1 = 0.0546, wR2 = 0.0838
Largest diff. peak and hole	2.539 and -2.173 e.Å ⁻³	0.999 and -0.661 e.Å ⁻³

Table 2B.3. Crystal data and structure refinement for Compound 16a and 16b

Empirical formula	C ₁₆ H ₁₈ Cl ₁₁ N ₄ Sn, C F ₃ O ₃ S, C H ₂ Cl ₂	C ₁₆ H ₁₈ Cl ₁₁ N ₄ Sn, Cl ₃ Sn ₁
Formula weight	654.48	645.52
Temperature	100 K	100 K
Wavelength	1.54178 Å	0.71073 Å
Crystal system	Monoclinic	Triclinic
Space group	P 21/c	P -1
Unit cell dimensions	a = 12.2857 (12) Å α = 90 b = 12.3755 (13) Å β = 111.34 (4) c = 16.8821 (17) Å γ = 90	a = 8.9232 (7) Å α = 89.701 (2) b = 10.0321 (8) Å β = 85.483 (2) c = 12.4341 (10) Å γ = 72.399 (2)
Volume	2390.8 (4) Å ³	1074.48 (15) Å ³
Z	4	2
Density (calculated)	1.818 g/cm ³	1.995 g/cm ³
Absorption coefficient	12.886 mm ⁻¹	2.830 mm ⁻¹
F(000)	1296	620
Crystal size	0.08 x 0.05 x 0.03 cm ³	0.05 x 0.04 x 0.03 cm ³
Theta range for data collection	3.863 to 66.649°.	1.617 to 25.021°.
Index ranges	-14 ≤ h ≤ 14, -14 ≤ k ≤ 14, - 20 ≤ l ≤ 20	-10 ≤ h ≤ 10, -11 ≤ k ≤ 7, - 15 ≤ l ≤ 13
Reflections collected	27327	14862
Independent reflections	4007 [R(int) = 0.0251]	3475 [R(int) = 0.0151]
Completeness to theta = 28.38°	99.7 %	98.1 %
Absorption correction	Multi-scan	Multi-scan
Max. and min. transmission	0.485 and 0.679	0.868 and 0.919
Refinement method	Full-matrix least-squares on F ²	Full-matrix least-squares on F ²
Data / restraints / parameters	4222 / 0 / 301	3715 / 0 / 238
Goodness-of-fit on F ²	1.052	1.106
Final R indices [I > 2σ(I)]	R1 = 0.0251, wR2 = 0.0612	R1 = 0.0151, wR2 = 0.0348
R indices (all data)	R1 = 0.0267, wR2 = 0.0620	R1 = 0.0171, wR2 = 0.0356
Largest diff. peak and hole	0.682 and -0.657 e.Å ⁻³	0.367 and -0.300 e.Å ⁻³

Table 2B.4. Crystal data and structure refinement for Compound 17.

Empirical formula	C ₁₆ H ₁₈ Br ₃ N ₄ Sn, Br ₃ Sn
Formula weight	823.36
Temperature	100 K
Wavelength	0.7107 Å
Crystal system	Triclinic
Space group	P -1
Unit cell dimensions	a = 9.151 (2) Å α = 88.795 (5) b = 10.446 (2) Å β = 84.955 (5) c = 12.524 (3) Å γ = 71.983 (5)
Volume	1134.0 (5) Å ³
Z	2
Density (calculated)	2.411 g/cm ³
Absorption coefficient	9.258 mm ⁻¹
F(000)	764
Crystal size	0.05 x 0.05 x 0.03 cm ³
Theta range for data collection	1.632 to 27.964°.
Index ranges	-12 ≤ h ≤ 8, -13 ≤ k ≤ 13, -16 ≤ l ≤ 16
Reflections collected	18789
Independent reflections	4165 [R(int) = 0.0355]
Completeness to theta = 28.38°	99.5 %
Absorption correction	Multi-scan
Max. and min. transmission	0.636 and 0.757
Refinement method	Full-matrix least-squares on F ²
Data / restraints / parameters	5423 / 0 / 237
Goodness-of-fit on F ²	1.031
Final R indices [I > 2σ(I)]	R1 = 0.0355, wR2 = 0.0757
R indices (all data)	R1 = 0.0564, wR2 = 0.0827
Largest diff. peak and hole	1.652 and -1.569 e.Å ⁻³

2B.5 References

1. Engesser, T.A.; Lichtenthaler, M.R.; Schleep, M.; Krossing, I. *Chem. Soc. Rev.* **2016**, *45*, 789-899.
2. (a) Swamy, V.S.V.S.N.; Pal, S.; Khan, S.; Sen, S. *Dalton Trans.* **2015**, *44*, 12903; (b) Fang, H.; Wang, Z.; Fu, X. *Coord. Chem. Rev.* **2007**, *344*, 214; (c) Lee, V.Y.; Sekiguchi, A. Heavy analogs of carbenium ions: Si-, Ge-, Sn-, and Pb-centred cations, in: V.Y. Lee, A. Sekiguchi (Eds.), *Organometallic Compounds of Low-Coordinate Si, Ge, Sn and Pb*, John Wiley & Sons Ltd., Chichester, 2010, pp. 1.
3. Drago, R.S. *J. Phys. Chem.* **1958**, *62*, 353.
4. Selected examples of Ge(II) Dications. (a) Rugar, P.A.; Bandyopadhyay, R.; Cooper, B.F.T.; Stinchcombe, M.R.; Ragona, P.J.; Macdonald, C.L.B.; Baines, K.M. *Angew. Chem. Int. Ed.* **2009**, *48*, 5155; (b) Cheng, F.; Hector, A.L.; Levason, W.; Reid, G.; Webster, M.; Zhang, W. *Angew. Chem. Int. Ed.* **2009**, *48*, 5152; (c) Rugar, P.A.; Staroverov, V.N.; Baines, K.M. *Science* **2008**, *322*, 1360. Selected examples of Sn(II) Dications; (d) Schleep, M.; Hettich, C.; Kratzert, D.; Scherer, H.; Krossing, I. *Chem. Commun.* **2017**, *53*, 10914; (e) Avery, J.C.; Hanson, M.A.; Herber, R.H.; Bladec, K.J.; Rugar, P.A.; Nowik, I.; Huang, Y.; Baines, K.M. *Inorg. Chem.* **2012**, *51*, 7306; (f) Macdonald, C.L.B.; Bandyopadhyay, R.; Cooper, B.F.T.; Friedl, W.W.; Rossini, A.J.; Schurko, R.W.; Eichhorn, S.H.; Herber, R.H. *J. Am. Chem. Soc.* **2012**, *134*, 4332; (g) Schafer, F.; Winter, W.; Saak, D.; Haase, R.; Müller, T.; Pottgen, R. *Chem. Eur J.* **2011**, *17*, 10979; (h) Bandyopadhyay, A.R.; Cooper, B.F.T.; Rossini, A.J.; Schurko, R.W.; Macdonald, C.L.B.; *J. Organomet. Chem.* **2010**, *695*, 1012.
5. Probst, T.; Steigelmann, O.; Riede, J.; Schmidbaur, H. *Angew Chem. Int. Ed. Engl.* **1990**, *29*, 1397.
6. Dostalova, R.; Dostal, L.; Ruzicka, A.; Jambor, R. *Organometallics* **2011**, *30*, 2405.
7. (a) Sindlinger, C.; Aicher, F.S.W.; Wasemann, L. *Inorg. Chem.* **2017**, *56*, 548; (b) Gawron, M.; Dietz, C.; Lutter, M.; Duthie, A.; Jouikov, V.; Jurkschat, K. *Chem. Eur J.* **2015**, *21*, 16609; (c) Ochiai, T.; Franz, D.; Irran, E.; Inoue, S. *Chem. Eur J.* **2015**, *21*, 6704; (d) Bouska, M.; Dostal, L.; Lutter, M.; Glowacki, B.; Ruzikova, Z.; Beck, D.; Jambor, R.; Jurkschat, K. *Inorg. Chem.* **2015**, *54*, 6792; (e) Khan, S.; Gopakumar, G.; Thiel, W.; Alcarazo, M. *Angew. Chem. Int. Ed.* **2013**, *52*, 5644; (f) Bouska, M.; Dostal, L.; Ruzicka, A.; Jambor, R. *Organometallics* **2013**, *32*, 1995; (g) Singh, A.P.; Roesky, H.W.; Carl, E.; Stalke, D.; Demers, J.-P.; Lange, A. *J. Am. Chem. Soc.* **2012**, *134*, 4996; (h) Arii, H.; Matsuo, M.; Nakadate, F.; Mochida, K.; Kawashima, T. *Dalton Trans.* **2012**, *41*, 11195;

-
- (i) Yang, Y.; Foo, C.; Ganguly, R.; Li, Y.; So, C.W. *Organometallics* **2012**, *31*, 6538; (j) Taylor, M.J.; Saunders, A.J.; Coles, M.P.; Fulton, J.R. *Organometallics* **2011**, *30*, 1334; (k) Dias, H.V.R.; Jin, W. *J. Am. Chem. Soc.* **1996**, *118*, 9123.
8. Li, J.; Schenk, C.; Winter, F.; Scheerer, H.; Trapp, N.; Higelin, A.; Kellar, S.; Pöttgen, R.; Krossing, I.; Jones, C. *Angew. Chem. Int. Ed.* **2012**, *51*, 9557.
9. (a) Driess, M.; Yao, S.; Brym, M.; van Wüllen, C. *Angew. Chem., Int. Ed.* **2006**, *45*, 6730; (b) Jana, A.; Objartel, I.; Roesky, H. W.; Stalke, D. *Inorg. Chem.* **2009**, *48*, 7645.
10. Gaussian 09, Revision E.01, Gaussian, Inc., Wallingford CT, 2009.
11. Drew, M.G.B.; Nicholson, D.G. *J. Chem. Soc. Dalton Trans.* **1986**, 1543.
12. (a) Ehle, A.R.; Morris, M.G.; Klebon, B.D.; Yap, G.P.A.; Watson, M.P. *Synlett* **2015**, *26*, 2702; (b) Hanessian, S.; Kagotani, M.; Komaglou, K. *Heterocycles* **1989**, *28*, 1115.
13. Veith, M.; Bertsch, B.; Huch, V. *Z. Anorg. Allg. Chem.* **1988**, *559*, 73.
14. Junghans, C.H.; Schulz, A.; Villinger, A. *Chem. Commun.* **2015**, *51*, 13834.
15. Lehmann, M.; Schulz, A.; Villinger, A. *Angew. Chem. Int. Ed.* **2012**, *51*, 8087.
16. Banerjee, S.; Gangopadhyay, J.; Lu, C.-Z.; Chen, J. -T.; Ghosh, A. *Eur. J. Inorg. Chem.* **2004**, 2533.

Chapter 3

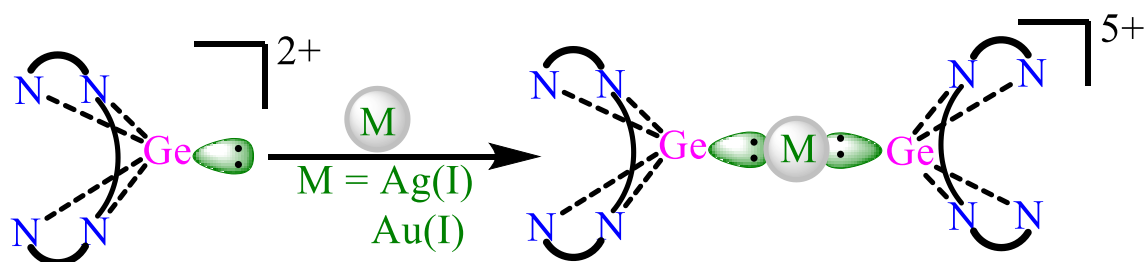
Section 3A: Direct Coordination of Germanium(II) Dicationic Center to Transition Metals

Section 3B: Bis(chlorogermyliumylidene) and its Significant Role in an Elusive Reductive Cyclization

Direct Coordination of Germanium(II) Dicationic Center to Transition Metals

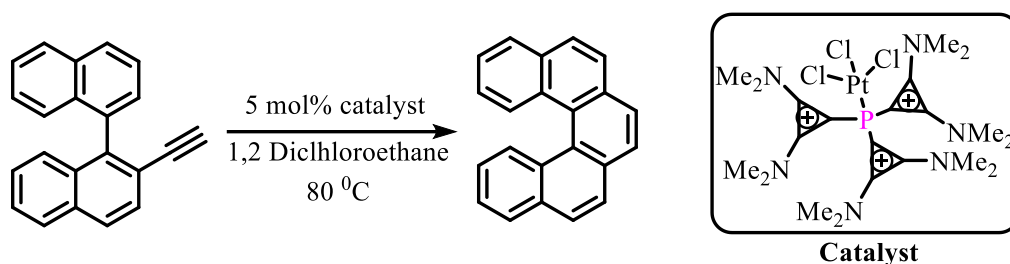
Abstract

Electron rich Germanium(II) dication Electronic stabilization of germanium(II) cations achieved in tetradentate redox active ligand either by autoionization or by removing halide. The Ge(II) dications are pyramidal in shape, with available stereochemically active lone pair on germanium for donation. The nucleophilicity of germanium (II) dication explored towards Au(I) and Ag(I) centres, overall forming the pentacationic complex. The second order perturbation interaction energy of $160 \text{ kcal mol}^{-1}$ by NBO analysis shows a strong interaction between Germanium and Au centre in **4**. The σ donation from germanium centre to transition metal and subsequent π back donation from metal to germanium depletes the electron density of metal center.



3A.1 Introduction

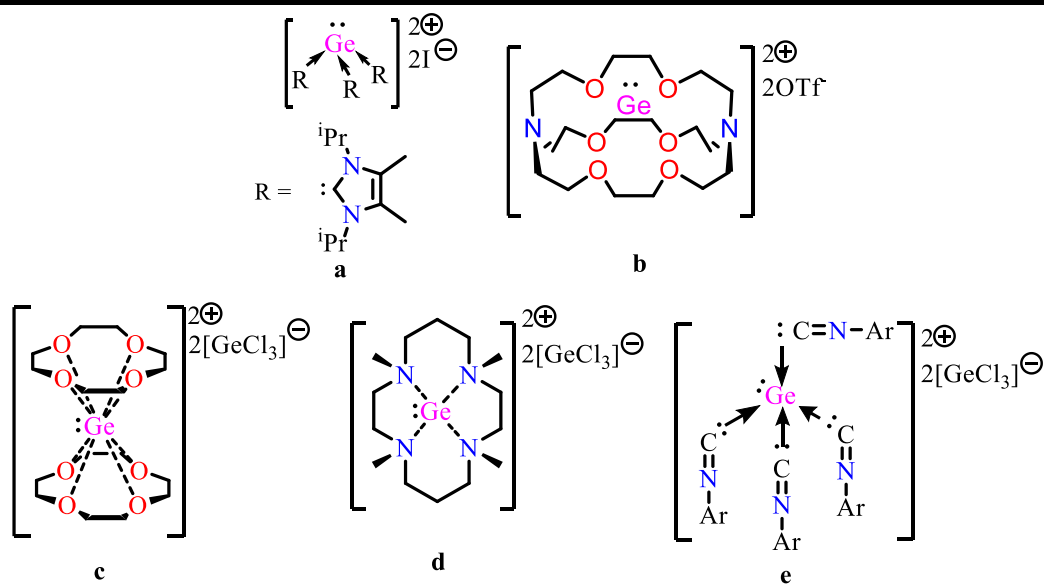
The donor properties of the ligands coordinated to transition metal centers play an essential role in determining their efficiencies as catalysts for various organic transformations. In this respect, phosphines have been used extensively as conventional ligands owing to the possible tuning of their electronic and steric environments.¹ Recently, (poly)cationic phosphines have emerged as strong π -acid ancillary ligands coordinating to transition metals.² The weaker s-donor ability of the cationic centers is partially compensated by their p-acceptance property leading to stable coordination complexes with transition metals. Such complexes efficiently catalyze organic transformations requiring high Lewis acidity at the metal center.³ In Polycationic ligands, the electron-donor site is a positively charged center, which is electronically intriguing and has a positive effect on the reaction rate of hydroarylation reaction (Scheme 3A.1).^{3b} Such highly charged cationic ligands are majorly restricted to phosphorus centers.²



Scheme 3A.1 Tricationic phosphine platinum complex as catalyst for hydroarylation reaction.

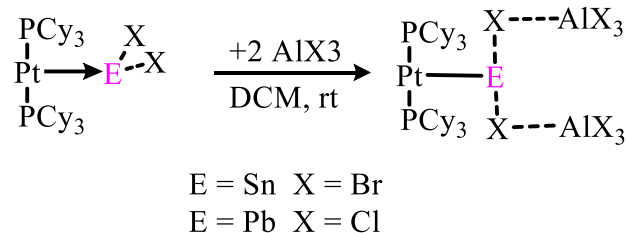
Conversely, the use of Group 14 E (II) dications [E:]²⁺ as cationic ligands have remained unexplored. Worth mentioning in contemporary research, low-valent group 14 elements are being ingeniously employed as ligands for transition metal catalysts.⁴ The isolation of germanium(II) cations is dependent on the donor ability of ligand. In the presence of stronger donor ligand, GeX₂ autoionize to cationic [LGeX]⁺ and anionic GeX₃⁻ counterparts.⁵ The handful of germanium(II) dications has been isolated to date where the highly-charged metal center is stabilized with carbenes and their analogs,⁶ cryptands,⁷ crown ethers,⁸ and azamacrocycles.⁹

In the case of **a** (Scheme 3A.1) strong donor N-heterocyclic carbene ligands ionize the GeI₂ into 2I⁻ and germanium(II) dication stabilized by three carbene centers. Baines and group for the first time used [2,2,2]-cryptand for the stabilization of Ge(II) dication **b**. Here the germanium is encapsulated within the cavity of cryptand. Later azamacrocycles **d**, crown ethers **c** also used for encapsulation of naked germanium(II) dications.



Scheme 3A.2 Reported germanium(II) dications.

Very recently, Sen and co-workers utilize electron-rich isocyanide as a σ -donor ligand in the stabilization of germanium(II) dication. The germanium centre bears the stereochemically inactive lone pair with distorted tetrahedral geometry.^{5d}



Scheme 3A.3 E(II) (E = Sn, Pb) dications complexes with platinum.

In 2015, Braunschweig and co-workers stabilized platinum complexes of in situ generated Sn(II) and Pb(II) dication (Scheme 3A.3). The computational study reveals the electron sharing bond between Pb(II) dication and Pt.¹⁰ Other than this, there are no reports where group 14 E(II) dicationic centre is coordinated to transition metal center.

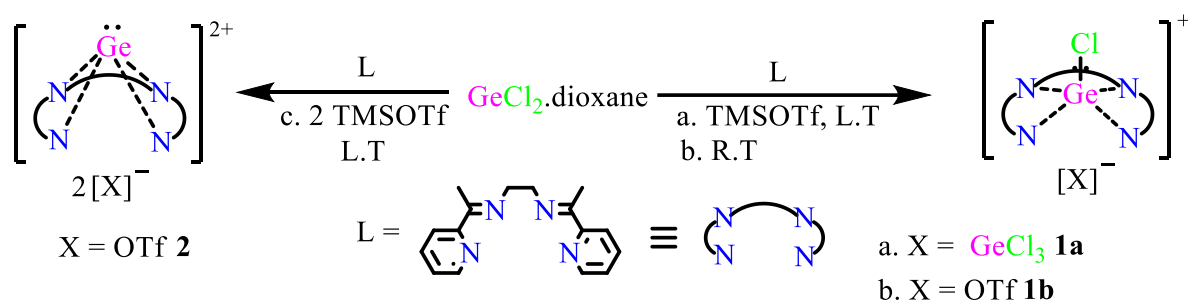
Scope of the Work

The first isolation of germanium (II) dications by Baines and co-workers using macrocyclic ligands and NHC,⁶⁻⁸ stem interest of chemist in search of new ligands for stabilization of dication. Such ambiphilic dications possess two unoccupied valence orbitals, which induce electrophilicity, simultaneously the lone pair on central atom induces nucleophilicity. The electrophilic nature of germanium dication is harvested by Macdonald and group in the reaction of crown ether stabilized germanium (II) dication with water or ammonia.¹¹ To the best of our knowledge, none of the reported Ge(II) dications exhibit nucleophilicity, due to lack of substantial lone pair directionality.

Herein we have stabilized germanium (II) dication with the flexible acyclic tetradentate ligand, where germanium holds a stereochemically active lone pair. This germanium (II) dication show coordination to the gold (I) and silver (I) centre forming barbell shape pentacationic complex. All the compounds are characterized in solid and solution states.

3A.2 Results and Discussion

3A.2.1 Chlorogermylumylidene and Germanium(II) Dication



Scheme 3A.4 Synthesis of **1a**, **1b** and **2**.

Herein, we have focused our attention on the development of a nucleophilic Ge(II) cations and coordination of the positively charged germanium center to transition metals Ag(I) and Au(I). For the purpose of inducing nucleophilicity at the Ge(II) site, we have deliberately chosen a flexible acyclic tetradentate bis(α -iminopyridine) ligand **L** instead of well-known carbenes/macrocycles,^{5–8} where the Ge(II) center was sequestered. The tetradentate ligand 2,7-bis(2-pyridyl)-3,6-diazaocta-2,6-diene (**L**) has been employed for our study. The reaction of **L** with 2 equivalent of $\text{GeCl}_2 \cdot \text{dioxane}$ in tetrahydrofuran (THF) solvent leads to a formation of **1a** in very good yield by the autoionization of GeCl_2 . The **1b** was obtained by adding one equivalent of TMSOTf (trimethylsilyl triflate) in the stoichiometric reaction of **L** and $\text{GeCl}_2 \cdot \text{dioxane}$. Here the TMSOTf was acting as chloride abstracting agent. The $[\text{LGe}]^{2+}$ compound **2** was synthesized in very high yields by the addition of two equivalents of TMSOTf (trimethylsilyl triflate) to a dichloromethane solution of $\text{GeCl}_2 \cdot \text{dioxane}$ and ligand **L** used in a 1 : 1 ratio. These germanium cations are only soluble in very polar solvents like acetonitrile, whereas sparingly soluble in less polar solvents like THF, DCM indicate the ionic nature of compounds. These all compounds are stable in solution and solid-state under an inert atmosphere for a long time. These compounds are characterized in solution state by NMR technique and in solid-state by single crystal XRD technique. In the ^1H NMR spectra of all three compounds, it shows a downfield shift in aromatic as well as an aliphatic proton with respect to their charge when compared with the free ligand. These downfield shifts in ^1H NMR revealed the coordination of ligand to the cationic germanium centre. ^{19}F NMR of compound

1b and **2** show a single peak at -79.24 and -79.60 ppm, indicate free triflate as the counter anion.

3A.2.2 Crystal Structure Analysis

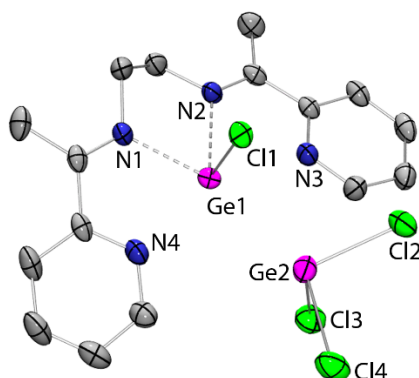


Figure 3A.1 Structure of **1a** in the solid state (thermal ellipsoids at 30%, H atoms omitted for clarity). Selected bond lengths [\AA] and angles [$^\circ$]: Ge1-Cl1 = 2.2754(9), Ge1-N1 = 2.2327(19), Ge1-N2 = 2.1764(16). N1-Ge1-N2 = 76.39 (7).

To confirm the structural features of compounds **1a**, **1b**, and **2** single crystal XRD analysis was performed. Single crystals were grown by layering the acetonitrile solution of the compound with diethyl ether at room temperature. Orange colored crystals of compound **1a** were crystallized in the triclinic crystal system with $\bar{p}1$ space group. In the crystal structure of **1a** (Ge-Cl)⁺ unit is coordinated to two imine nitrogens (N_{imine}) with distance of Ge1-N1 2.2327 (19) \AA and Ge1-N2 2.1764 (16) \AA which is comparable with the reported chlorogermylumylidenes. The four nitrogen form a slightly distorted plane (the fold angle of N1-N2-N3-N4 is approximately 12.9 $^\circ$) with chlorogermylumylidene unit fixed perpendicular in the cavity of four nitrogens. The GeCl₃⁻ counter anion is away from the coordination sphere with the closest Ge1-Cl3 distance of 4.066 \AA . Considering two nitrogens (N1, N2) and one Chlorine (Cl1) in one plane, the germanium (Ge1) occupies the fourth position forming overall geometry as trigonal pyramidal. The bond angle between two coordinating nitrogen and central germanium is N1-Ge1-N2 76.39(7) $^\circ$. The N1-Ge1-Cl1 and N2-Ge1-Cl1 bond angle is 85.86(5) and 94.85(5), respectively. Orange crystals of compound **1b** crystallize in monoclinic crystal system with P2(1)/c space group. The counter anion triflate is away from germanium cation with the closest distance between Ge1 and O of triflate is 3.906 \AA . All the S – O distances are similar in triflate (average S1-O distance 1.436 \AA) counter anion, indicate the ionic nature of triflate. The other features of **1b** are similar to **1a**.

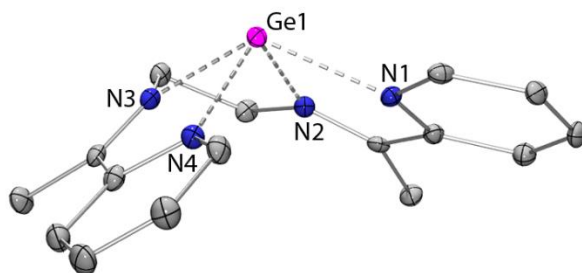


Figure 3A.2 Molecular structure of the dicationic part of **2** in the solid state (thermal ellipsoids at 30%, H atoms omitted for clarity). Selected bond lengths [\AA] and angles [$^\circ$]: Ge1–N1 = 2.224(4), Ge1–N2 = 2.088(4), Ge1–N3 = 2.102(4), Ge1–N4 = 2.163(4), N1–Ge1–N2 = 73.90(14), N2–Ge1–N3 = 72.31(14), N3–Ge1–N4 = 73.21(15).

Yellow crystals of compound **2** were grown at room temperature from an acetonitrile/diethyl ether bilayer. The structural formulation of **2** was unequivocally confirmed by single-crystal X-ray diffraction (Figure 3A.2). The four nitrogen donor sites coordinate with the Ge(II) dicationic center. The bond length of imine nitrogen and germanium [Ge1–N2 2.088(4), Ge2–N3 2.102(4)] \AA are much shorter than the bond length of pyridyl nitrogen and germanium [Ge1–N1 2.224(4), Ge1–N4 2.163(4)] \AA . Due to the torsional magnitude of the $(\text{CH}_2)_2$ – linker, the four nitrogen atoms form a slightly distorted basal coordinating plane (the fold angle N2–N3–N4–N1 is approximately 12.91), with the Ge(II) center being displaced perpendicularly by 1.03 \AA , resulting in an overall dome-shaped or pyramidal structure (sum of bond angles at the Ge center = 307.61).¹² The triflate anion is excluded from the coordination sphere of the Ge(II) center in compound **2** (the closest Ge1–O3 distance being 3.97 \AA).

3A.2.3 DFT Study

At this juncture, we turned our attention to DFT studies in pursuit of the bonding situations in the pyramidal Ge(II) dication **2**. The optimized dicationic species **2'** (triflate anion omitted in the input geometry) is in close agreement with the X-ray geometry of **2**. The HOMO of **2'** clearly shows the presence of a lone pair at the apex Ge(II) center with a significant s-character (Figure 3A.3). The s-orbital on Ge(II) is admixed with its p_z orbital, thereby enhancing the directionality of the lone pair. The empty p_x and p_y atomic orbitals of apical Ge(II) overlap with the four nitrogen based orbitals, giving rise to two sets of 5-centre-4-electron¹³ bonding situations (HOMO-8 and HOMO-9) depicted in Figure 3A.3.

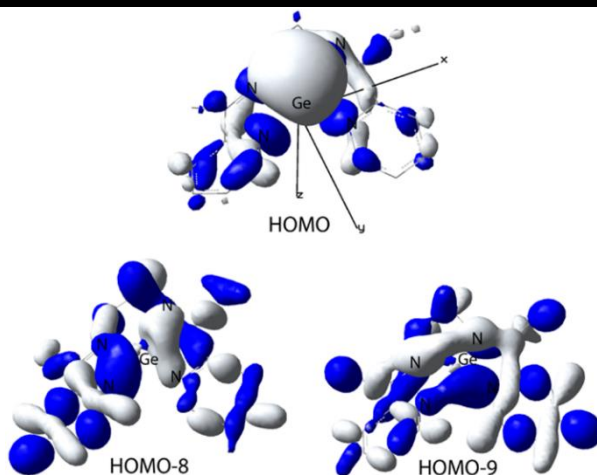


Figure 3A.3 Relevant contour plot of **2** at an isovalue of 0.3 au.

Conversely, the HOMO of **10** shows a lone pair character at the Ge(II) center with a natural orbital occupancy of 1.91e, determined by NBO analysis. Despite the positive charge on the Ge(II) center (+0.72 from Mulliken charge distribution analysis), the presence of the stereochemically active lone pair should augment its nucleophilic nature. The apically disposed Ge(II) dication is completely bare as confirmed by molecular structure and by computationally, allowing further reactivity.

3A.2.4 Electrophilic Nature

It has been inferred from the computational studies that the vacant p-orbitals on the Ge(II) center are not readily available for Lewis base coordination. In order to support the computational results, we performed NMR scale reaction of **2** with Lewis bases such as PMe_3 and *t*-BuNC. The Lewis base should show coordination with **2**, and the resulting adduct will show an upfield shift in ^1H NMR of pyridyl proton. In NMR scale reactions of **2** with *t*-BuNC with 1:1 molar ratio at room temperature did not show any reactivity with *t*-BuNC, which is confirmed by ^1H NMR study. There was no significant shift in ^1H NMR of pyridyl protons and in ^{13}C NMR of *t*-BuNC.

In NMR scale reaction of PMe_3 with **2** shows initial coordination to the Ge(II) center, as is evident from upfield and downfield shifts in ^1H and ^{31}P NMR spectra, respectively (Figure 3A.4). In ^{31}P NMR of the reaction mixture, PMe_3 shows a downfield shift from -62.04 ppm (for free PMe_3) to -12.86 ppm. Simultaneously in ^1H NMR pyridyl proton of **L** shows upfield shift due to coordination of PMe_3 . PMe_3 is a much stronger base compared to *t*-BuNC, responsible for the difference in reactivity with **2**. Notably, the $[\text{Ge}(15\text{-crown-5})][\text{OTf}]_2$ complex forms an adduct with water and ammonia, revealing its electrophilic nature.¹³

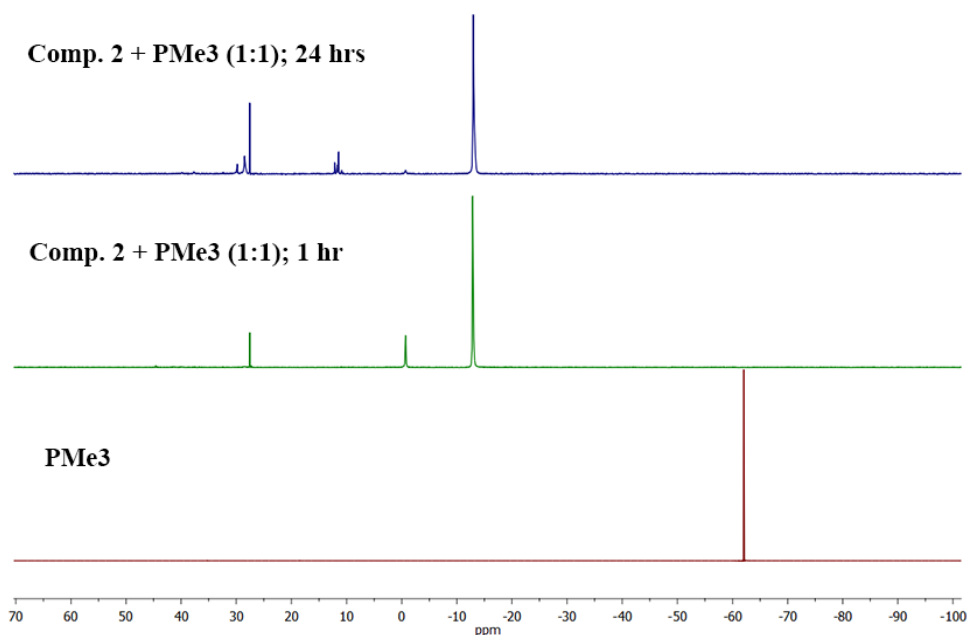
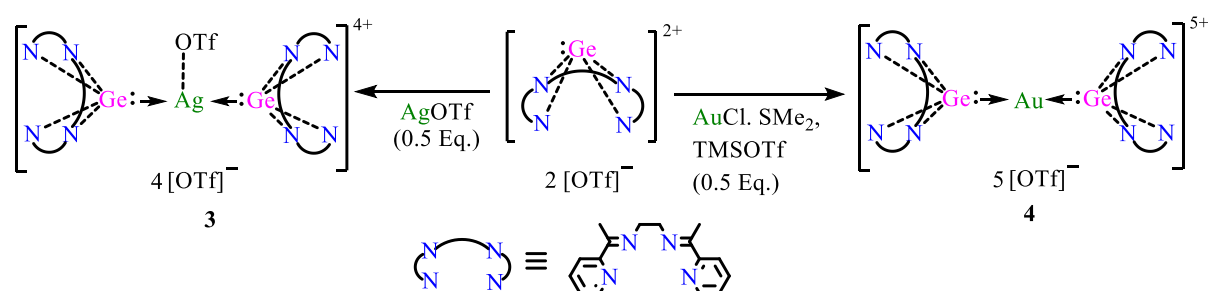


Figure 3A.4 ^{31}P NMR of **2** + PMe_3 (1:1 ratio).

3A.2.5 Nucleophilic Nature

The Ge(II) center in compound **2** is now appropriate to possess a stereochemically active lone pair of electrons and which should supplement nucleophilicity. We have explored this tailored nucleophilicity of Ge(II) dication **2** towards transition metals. Two equivalents of Ge(II) dication **2** bis-coordinated to both Ag(I) and Au(I) centers, resulting in barbell shaped structures of **2** and **3**, respectively (Scheme 3A.5), in quantitative yields.



Scheme 3A.5 Coordination of germanium(II) dication with Ag(I) and Au(I) centers.

In both cases, complexation occurred at low temperature, using AgOTf in the case of complex **3**, and an equimolar ratio of AuCl-SMe₂ and TMSOTf in the case of complex **4**. Due to the highly charged nature compound, **3** and **4** are only soluble polar solvent like acetonitrile and was insoluble in less polar solvents. Both the compounds were stable in solution and solid-state only under an inert atmosphere. Single crystals of **3** and **4** were obtained at room

temperature by diffusion of diethyl ether into the acetonitrile solution of the respective complexes. Complexes **3** and **4** were characterized by NMR techniques, and their solid state structures were elucidated using X-ray diffraction. Notably, single crystals of **3** and **4** were also obtained when the reactions were performed in a 1:1 ratio of **2** and the corresponding metal salts. In the ^1H NMR of **4** the backbone $-\text{CH}_2-\text{CH}_2-$ linker of **L** show doublet while in **3** it only shows singlet and a possible reason for this must be the different chemical environment in the solution state. All the triflate in complex **3** and **4** give a singlet in ^{19}F NMR spectroscopy, indicate the ionic nature of triflate in the solution state.

3A.2.6 Crystal Structure Analysis

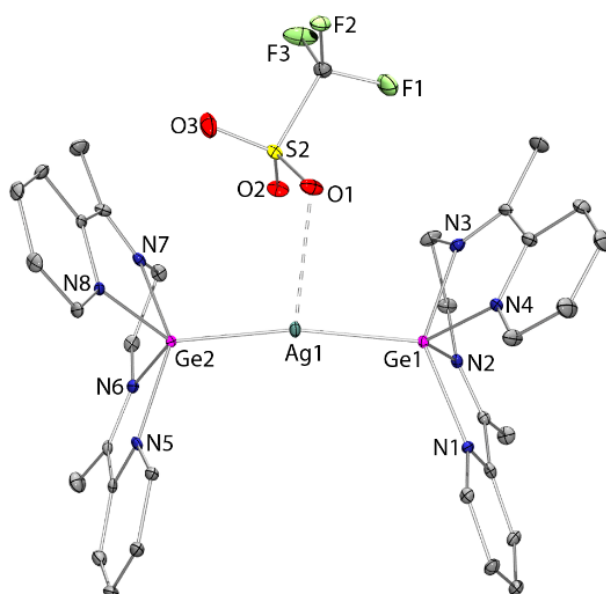


Figure 3A.5 Molecular structure of **3** in the solid state (thermal ellipsoids at 30%, H atoms, solvent molecule and four triflate counter anions omitted for clarity). Selected bond lengths [\AA] and angle [$^\circ$]: $\text{Ag1-Ge1} = 2.5362(8)$, $\text{Ag1-Ge2} = 2.5376(8)$, $\text{Ge1-N1} = 2.130(4)$, $\text{Ge1-N2} = 2.014(5)$, $\text{Ge1-N3} = 2.063(4)$, $\text{Ge1-N4} = 2.078(4)$, $\text{Ge2-N5} = 2.103(4)$, $\text{Ge2-N6} = 2.027(5)$, $\text{Ge2-N7} = 2.035(4)$, $\text{Ge2-N8} = 2.060(4)$, $\text{Ag1-O1} = 2.6349(48)$; $\text{Ge1-Ag1-Ge2} 157.67(3)$.

The complex **3** and **4** unambiguously confirmed by single crystal XRD. The yellow colour crystal of complex **3** crystallizes in triclinic system with $P\bar{1}$ space group. The asymmetric unit cell contains complex **3** with one acetonitrile solvent molecule. In solid state crystal structure, among five triflate counter anions, one triflate was found to be coordinated to the Ag center (closest Ag1-O1 atom-atom distance = $2.6349(48)$ \AA), (Figure 3A.5). The triflate coordination results in the deviation of Ge1-Ag1-Ge2 angle ($157.67(3)$) from linearity. The average Ge-Ag distance was found to be 2.54 \AA , which is greater than in the case of

amidinatogermylene–silver complexes.¹⁴ The two [LGe:]²⁺ units have mildly deviated eclipsed orientation along the Ge–Ag–Ge array.

Table 3A.1 Average Ge–N bond lengths in compound **2**, **3** and **4**

Complex	2	3		4	
average bond length (Å)		Ge1 - N	Ge2 - N	Ge1 - N	Ge2 - N
Ge – N _{imine}	2.095	2.039	2.031	1.995	1.983
Ge – N _{pyridyl}	2.192	2.104	2.081	2.049	2.054

Unlike our observations in compound **2**, complex **3** has strikingly shorter Ge–N bond distances, indicating an enhanced donation from N centers to the more electron-deficient Ge center as a consequence of metal coordination. The [LGe:]²⁺ pyramid also flattened due to the donation from the germanium centre.

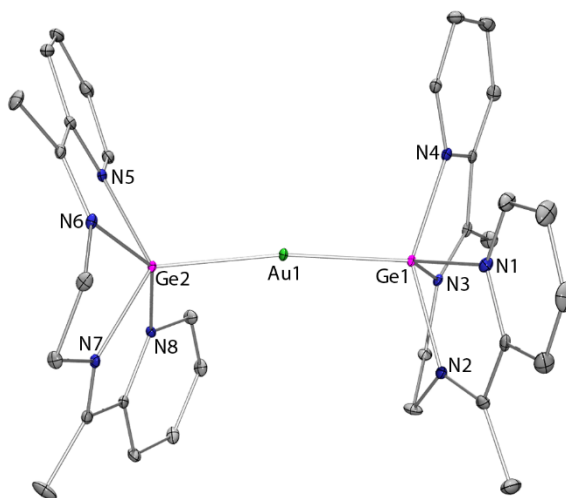


Figure 3A.6 Molecular structure of the penta-cationic part of **4** in the solid state (thermal ellipsoids at 30%, H atoms and triflate counter anions omitted for clarity). Selected bond lengths [Å] and angle [1]: Au1–Ge1 = 2.3823(6), Au1–Ge2 = 2.3857(6), Ge1–N1 = 2.034(3), Ge1–N2 = 2.002(3), Ge1–N3 = 1.989(3), Ge1–N4 = 2.063(3), Ge2–N5 = 2.027(3), Ge2–N6 = 1.994(3), Ge2–N7 = 1.972(3), Ge2–N8 = 2.072(3); Ge1–Au1–Ge2 166.538(16).

The analogous yellow crystals of pentaionic gold complex **4** crystallize in the triclinic crystal system with $\bar{p}1$ space group (Figure 3A.6). In this case, the Ge1–Au1–Ge2 angle is

closer to linearity, being 166.538(16). The two [LGe:]²⁺ units are almost in a staggered disposition, with the average Ge–Au distance being 2.38 Å. The closest approaching triflate group exhibits a Au1–O2 distance of 3.07 Å in the X-ray structure.¹⁵ Here again, the Ge–N bond distances are shorter with a relatively flattened [LGe:]²⁺ pyramid. The short Ge–N distance in **4** compared with complex **3** further complement the pentacationic nature of **3** and strong interaction between Ge and Au.

3A.2.7 DFT Study

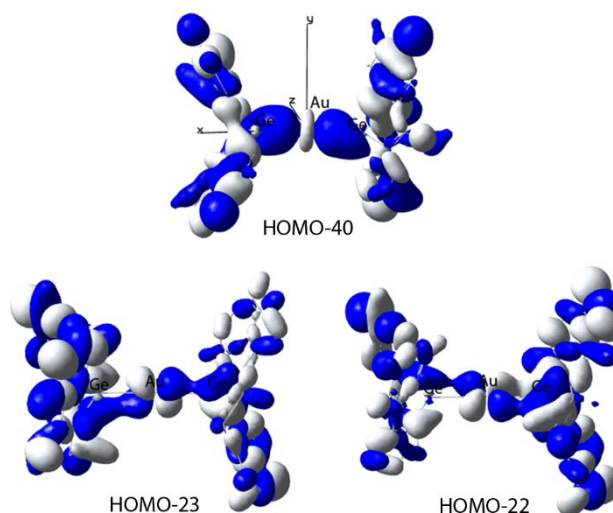


Figure 3A.7 Relevant contour plots of **4** at an isovalue 0.03 au.

We have performed DFT calculations (B3LYP/6-31G(d,p) for Ge, C, N, H and LANL2DZ for Au) with the pentacationic part of compound **3** for structural and bonding insights. Truncation of the triflate anions led to a more linear geometry (Ge–Au–Ge = 176.67 °) of the energy minimum structure **3'**, and the remaining parameters conform well to the X-ray geometry. A Wiberg bond index of 0.52 for Ge–Au and the calculated second-order perturbation interaction energy of 160 kcal mol⁻¹ from NBO analysis support a relatively strong interaction between Ge and Au orbitals,¹⁶ despite the electrostatic repulsions from the cationic ligands and metal centers. Mulliken charge analysis shows an obvious increment in positive charge on Ge centers (+0.94) upon metal coordination. The s-donation of electron pairs from the two Ge centers (predominant s-character) to vacant Au(I) sd_z² hybridized orbitals is energetically stabilized, as revealed in the very low-lying filled molecular orbital HOMO-40 (Figure 3A.7).¹⁷ Importantly, in addition to the sigma overlap between Ge and Au centers, we observed a set of clear p-interactions between the Ge p_y and p_z orbitals and filled Au d-orbitals of appropriate symmetry (HOMO-22 and HOMO-23, Figure 3A.7). The existence of such p-interactions

with the coordinating dicationic site further depletes electron density from the transition metal center, thereby enhancing Lewis acidity in the latter.

3A.3 Conclusion

We have stabilized the cationic germanium(II) centres in the redox-active tetradentate ligand. The rigid α -imino pyridine framework and flexible -CH₂-CH₂- linker in ligand allow the stabilization of Ge(II) dication with stereochemically active lone pair. The computational study suggests the mixing of p_z orbital with s orbital, which is a lone pair of germanium induces the nucleophilicity in **2**. The stereochemically active lone pair on the Ge(II) center of **2** directly binds to Ag(I) and Au(I) centers. This is the first example where an E(II) (E = group 14 element) dication has been demonstrated as a cationic ligand towards any transition metals. The presence of π -interactions in the gold complex, in addition to sigma coordination, suggests their prospects as catalysts demanding increased Lewis acidity at the transition metal center.

3A.4 Experimental Details

3A.4.1 General Remarks.

All manipulations were carried out under a protective atmosphere of argon applying standard Schlenk techniques or in a dry box. Tetrahydrofuran was refluxed over sodium/benzophenone. Dichloromethane and acetonitrile were stirred and refluxed over calcium hydride and kept over 3 Å molecular sieves. All solvents were distilled and stored under argon and degassed prior to use. Acetonitrile-*d*₃ ampoules were purchased from Sigma Aldrich and used as it is. All chemicals were used as purchased. ¹H and ¹³C{¹H} NMR spectra were referenced to external SiMe₄ using the residual signals of the deuterated solvent (¹H) or the solvent itself (¹³C). ¹⁹F and ³¹P{¹H} NMR were referenced to external C₆H₅CF₃(TFT) and 85% H₃PO₃ respectively. Solution phase UV/Vis spectra were acquired using a Thermo-Scientific Evolution 300 spectrometer using quartz cells with a path length of 1 cm. Melting points were determined under argon in closed NMR tubes and are uncorrected. Elemental analyses were performed on Elementar vario EL analyzer. Single crystal data were collected on both Bruker SMART APEX four-circle diffractometer equipped with a CMOS photon 100 detector (Bruker Systems Inc.) with a Cu K α radiation (1.5418 Å), and Bruker SMART APEX Duo diffractometer using Mo K α radiation (0.71073 Å)

3A.4.2 Synthetic Procedures

A. Compound 1a

Ligand **L** (0.70 g, 2.63 mmol) was dissolved in 10 mL of THF and was added to THF solution of GeCl₂.Dioxane (1.22g, 5.26mmol). Orange colored precipitation occurred upon overnight stirring. The precipitate was isolated via filtration and washed thrice with THF. Product was dried under vacuum yielding 1.63 g (85%) of **1a** (Decomp. 143-145 °C) as an orange solid.

Single crystal suitable for X-Ray measurement were grown by layering acetonitrile solution of the compound with diethyl ether at room temperature.

Characterization of **1a**: ¹H NMR (400 MHz, Acetonitrile-*d*₃, TMS) δ = 8.96 (ddd, *J*=4.8, 1.5, 1.0, 2H, *o*-Pyr-*H*), 8.33 – 8.09 (m, 4H, *m* and *p*-Pyr-*H*), 7.76 (ddd, *J*=7.4, 4.9, 1.3, 2H, *m*-Pyr-*H*), 4.26 (s, 2H, -CH₂-CH₂-), 2.75 (s, 3H, -CH₃) ppm. ¹³C{¹H} NMR (101 MHz, Acetonitrile-*d*₃, TMS) δ = 172.69 (C-CH₃), 149.65 (Pyr-C_o), 147.14 (Pyr-C_o), 139.35 (Pyr-C_p), 127.48 (Pyr-C_m), 125.61 (Pyr-C_m), 49.31(-CH₂-CH₂-), 17.71 (C-CH₃) ppm. UV/Vis- (acetonitrile) λ_{max} (ε) 358 nm (2376 M⁻¹cm⁻¹) Elemental Analysis: Calcd. for C₁₆H₁₈Cl₄Ge₂N₄: C, 34.73; H, 3.28; N, 10.12. Found: C, 34.58; H, 3.16; N, 10.02.

B. Compound 1b

Ligand **L** (0.4g, 1.501 mmol) was dissolved in 10 mL of THF and was added to GeCl₂.Dioxane (0.348g, 1.501 mmol) in THF, followed by addition of Trimethylsilyl trifluoromethanesulphonate (0.27 ml, 1.501 mmol). Reaction mixture was stirred overnight, orange colour compound was precipitated. Product was filtered, washed with 5 mL of THF and dried under vacuum to yielding 0.72g (91.60 %) of **1b** (decomp. 130-132 °C) as an orange solid.

Single crystal suitable for X-Ray measurement were grown by layering acetonitrile solution of the compound with diethyl ether at room temperature.

Characterization of **1b**: ¹H NMR (400 MHz, Acetonitrile-*d*₃, TMS) δ = 8.96 (ddd, *J* = 4.9, 1.6, 1.0, 2H, *o*-Pyr-*H*), 8.26 – 8.14 (m, 4H, *m* and *p* -Pyr-*H*), 7.76 (ddd, *J*=7.4, 4.9, 1.3, 2H, *m*-Pyr-*H*), 4.25 (s, 4H, -CH₂-CH₂-), 2.74 (s, 6H, -CH₃) ppm. ¹³C{¹H} NMR (101 MHz, Acetonitrile-*d*₃, TMS) δ = 172.72 (C-CH₃), 149.64 (Pyr-C_o), 147.15 (Pyr-C_o), 139.43 (Pyr-C_p), 127.52 (Pyr-C_m), 125.64 (Pyr-C_m), 122.75, 119.56 (CF₃SO₃), 49.27 (-CH₂-CH₂-), 17.62 (C-CH₃) ppm. ¹⁹F{¹H} NMR (377 MHz, CD₃CN, TFT) δ = -79.24 (TMSOTf- *F*) ppm. UV/Vis- (acetonitrile) λ_{max} (ε) 359 nm (1656 M⁻¹cm⁻¹)

Elemental Analysis: Calcd. for C₁₇H₁₉ClF₃GeN₄O₃S: C, 39.00; H, 3.47; N, 10.70. Found: C, 39.23; H, 3.56; N, 10.55.

C. Compound 2

Ligand **L** (1g, 3.75 mmol) was dissolved in dichloromethane (DCM) and was added to suspension of GeCl₂.dioxane (0.869g, 3.75 mmol) in DCM followed by addition of TMSOTf (1.40 ml, 7.70 mmol) at 0 °C. Yellow precipitate appeared and it was stirred overnight. The precipitate was filtered and wash with THF (3 * 5 mL) The product was dried under vacuum yielding 2.20g (92%) of **2** (decomp. 170-172°C) as yellow solid.

Single crystal suitable for X-Ray measurement were grown by layering acetonitrile solution of the compound with diethyl ether at room temperature.

Characterization of **2**: ¹H NMR (400 MHz, Acetonitrile-*d*₃, TMS) δ = 9.30 (d, *J*=5.4, 2H, *o*-Pyr-*H*), 8.52 (td, *J*=7.8, 1.4, 2H, *p*-Pyr-*H*), 8.45 (d, *J*=7.6, 2H, *m*-Pyr-*H*), 8.14 – 8.09 (m, 2H, *m*-Pyr-*H*), 4.52 (s, 4H, -CH₂-CH₂-), 2.75 (s, 6H, -CH₃) ppm. ¹³C{¹H} NMR: (101 MHz, Acetonitrile-*d*₃, TMS) δ = 172.34 (C-CH₃), 148.20 (Pyr- C_o), 146.95 (Pyr-C_o), 143.98 (Pyr-C_p), 129.95 (Pyr-C_m), 126.90 (Pyr-C_m), 122.51, 119.35 (CF₃SO₃), 46.95 (-CH₂-CH₂-), 16.21 (C-CH₃) ppm. ¹⁹F{¹H} NMR: (377 MHz, Acetonitrile-*d*₃) δ = -79.29 (TMSOTf- *F*) ppm. UV/VIS- (acetonitrile) λ_{max} (ε) 341 nm (2440 M⁻¹cm⁻¹) Elemental Analysis: Calcd. for C₁₈H₁₈F₆GeN₄O₆S₂: C, 33.93; H, 2.85; N, 8.79. Found: C, 33.97; H, 2.95; N, 8.85.

D. Compound 3

Compound **2** (0.20 g, 0.314 mmol) was dissolved in 10 mL of acetonitrile and added to an acetonitrile solution of Silver trifluoromethanesulphonate (0.040 mg, 0.156 mmol) at 0°C and stirred overnight at room temperature. The solvent was removed under vacuum yielding **3** (m. p. 186°C-188°C) as pale yellow solid.

Single crystal of **3** suitable for X-Ray measurement were grown by layering acetonitrile solution of the compound with diethyl ether at room temperature. Crystallization Yield = 0.140g (58.8%).

Characterization of **3**: ¹H NMR (400 MHz, Acetonitrile-*d*₃, TMS) δ = 9.30 (d, *J*=5.3, 2H, *o*-Pyr-*H*), 8.56 (t, *J*=7.8, 2H, *p*-Pyr-*H*), 8.48 (d, *J*=7.9, 2H, *m*-Pyr-*H*), 8.15 (t, *J*=6.5, 2H, *m*-Pyr-*H*), 4.52 (s, 4H, -CH₂-CH₂-), 2.78 (s, 6H, C-CH₃) ppm. ¹³C{¹H} NMR (101 MHz, Acetonitrile-*d*₃, TMS) δ = 172.47 (C-CH₃), 148.16 (Pyr-C_o), 146.31 (Pyr-C_o), 144.55 (Pyr-C_p), 130.27 (Pyr-C_m), 127.07 (Pyr-C_m), 122.54, 119.35 (CF₃SO₃), 46.57 (-CH₂-CH₂-), 16.28 (C-CH₃) ppm. ¹⁹F{¹H} NMR (377 MHz, Acetonitrile-*d*₃, TMS) δ = -79.30 (TMSOTf-*F*) ppm. UV/VIS- (acetonitrile) λ_{max} (ε) 337 nm (8640 M⁻¹cm⁻¹) Elemental Analysis: Calcd. for C₃₇H₃₆AgF₁₅Ge₂N₈O₁₅S₅: C, 29.02; H, 2.37; N, 7.32. Found: C, 29.23; H, 2.46; N, 7.39.

E. Compound 4

Trimethylsilyl trifluoromethanesulfonate (42 μ l, 0.232 mmol) was added to an acetonitrile solution of AuCl.SMe₂ (0.058g, 0.2352) at room temperature. In another Schlenk flask compound 2 (0.30 g, 0.471 mmol) was dissolved in acetonitrile (15ml) and added to above solution at 0 °C. Reaction mixture was stirred overnight at room temperature. The solvent was removed under vacuum to get 4 (m.p. 198°C-200°C) as yellow powder.

Single crystal suitable for X-Ray diffraction was grown by layering of acetonitrile solution of compound with diethyl ether at room temperature. Yield = 0.024 g (64.2%)

Characterization of 4: ¹H NMR (400 MHz, Acetonitrile-*d*₃, TMS) δ = 9.35 (d, *J*=5.4, 2H, *o*-Pyr-CH), 8.67 (t, *J*=8.5, 2H, *p*-Pyr-CH), 8.56 (d, *J*=7.5, 2H, *m*-Pyr-CH), 8.26 – 8.21 (m, 2H, *m*-Pyr-CH), 4.53 (d, *J*=50.5, 4H, -CH₂-CH₂-), 2.84 (s, 6H, C-CH₃) ppm. ¹³C{¹H} NMR (101 MHz, Acetonitrile-*d*₃, TMS) δ = 173.09 (C-CH₃), 148.74 (Pyr-C_o), 146.60 (Pyr-C_o), 144.44 (Pyr-C_p), 131.25 (Pyr-C_m), 127.61 (Pyr-C_m), 122.39, 119.21 (CF₃SO₃), 45.22 (-CH₂-CH₂-), 16.50 (C-CH₃). ppm. ¹⁹F{¹H} NMR (377 MHz, Acetonitrile-*d*₃ TFT) δ = -79.26 (TMSOTf-*F*) ppm. Elemental Analysis: Calcd. for C₃₇H₃₆AuF₁₅Ge₂N₈O₁₅S₅: C, 27.43; H, 2.24; N, 6.92. Found: C, 27.32; H, 2.16; N, 6.83.

F. Reaction of 2 with PMe₃:

In NMR tube, PMe₃ (9 μ l, 0.084 mmol) was added to compound 2 (54 mg, 0.084 mmol) dissolved in 0.6 ml of acetonitrile-*d*₃ and shaken well. The NMR spectra WAS monitored at room temperature at different time interval.

G. Reaction of 2 with ^tBuNC:

In NMR tube, ^tBuNC (8 μ l, 0.072 mmol) was added to compound 2 (45 mg, 0.072 mmol) dissolved in 0.6 ml of acetonitrile-*d*₃ and shaken well. The NMR spectra WAS monitored at room temperature at different time interval.

3A.4.3 Plots of NMR Spectra

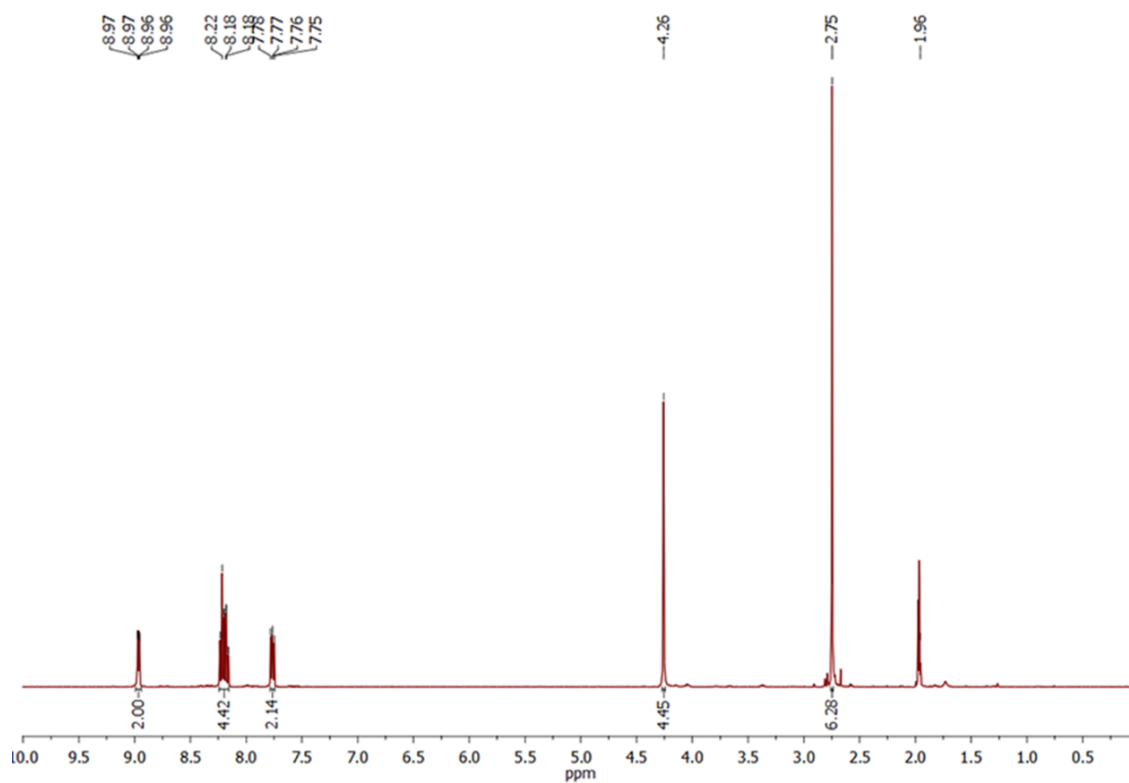


Figure 3A.8. ¹H NMR of compound 1a.

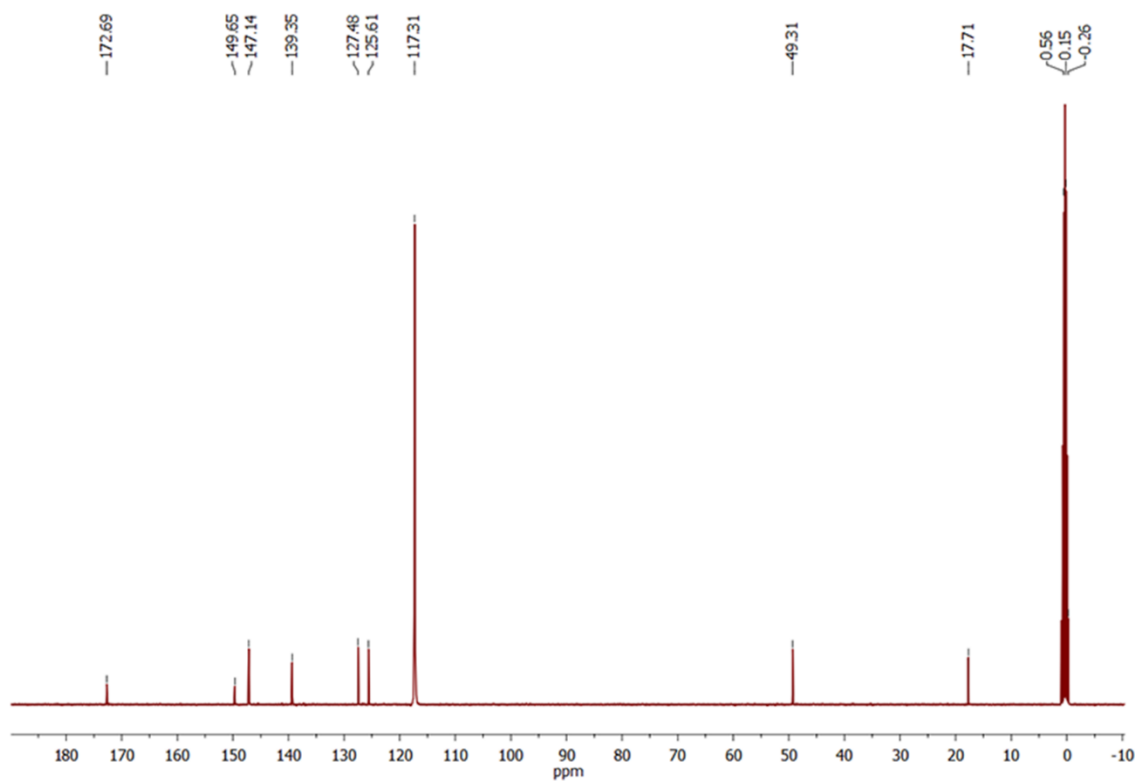


Figure 3A.9. ¹³C NMR of compound 1a.

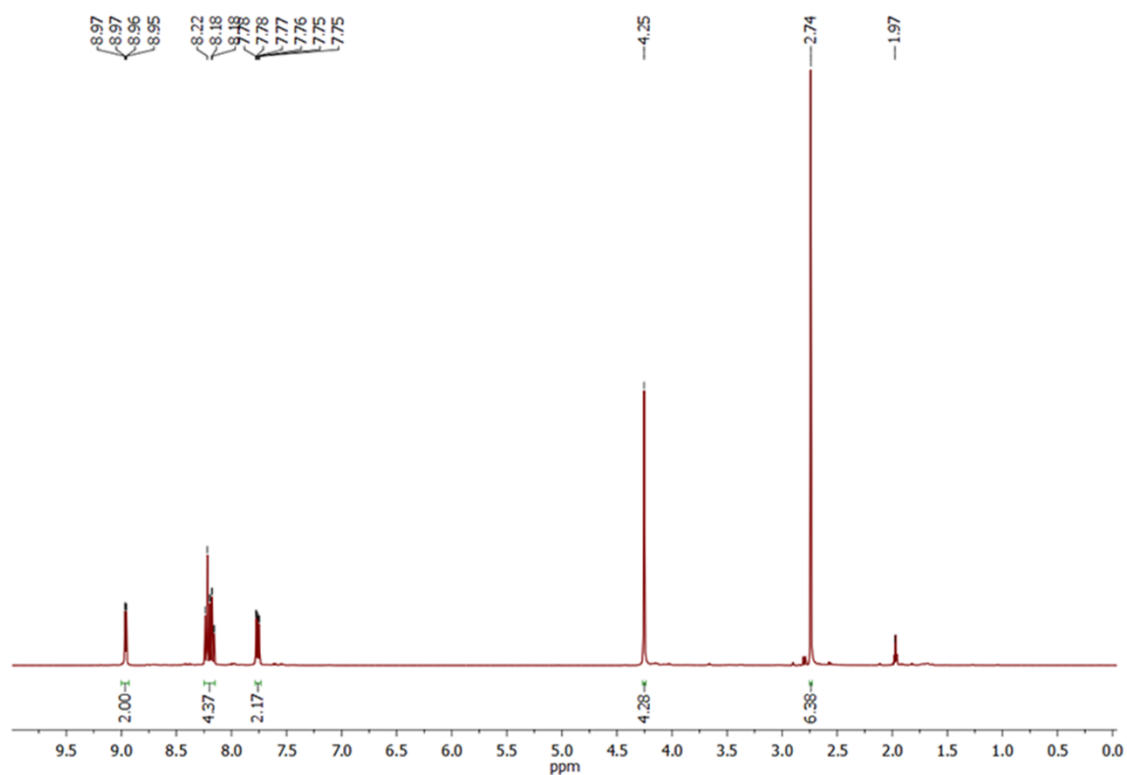


Figure 3A.10. ^1H NMR of compound **1b**.

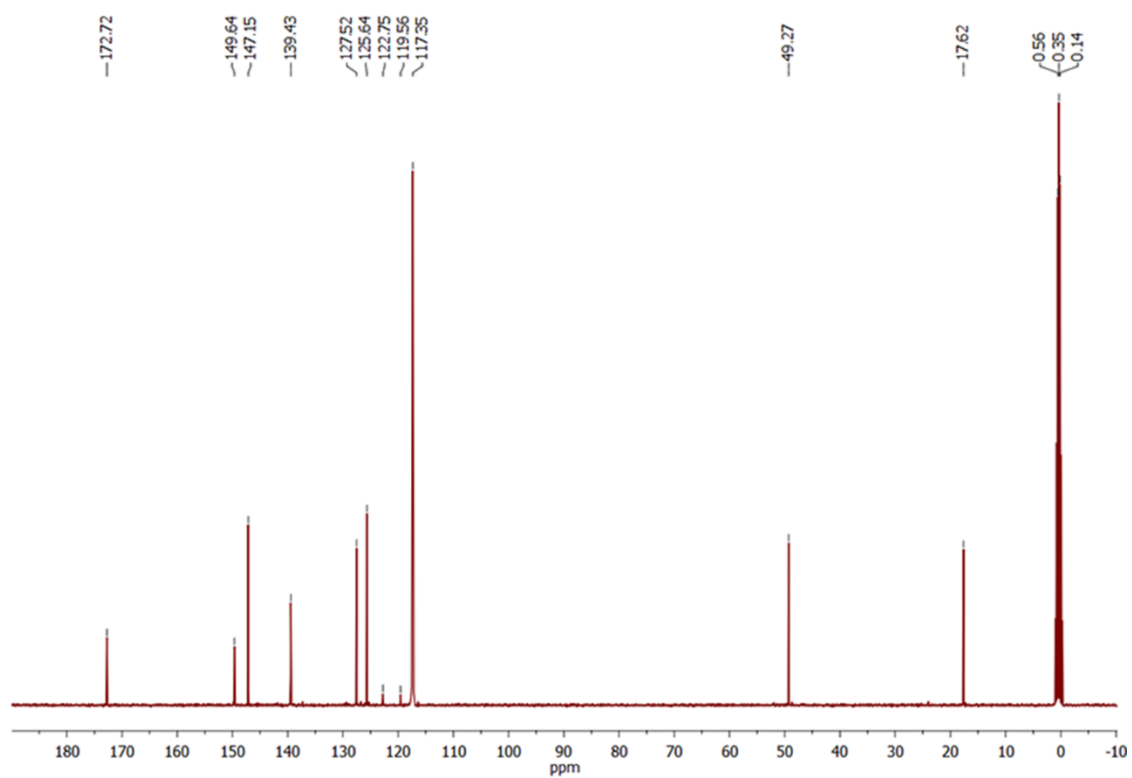


Figure 3A.11. ^{13}C NMR of compound **1b**.

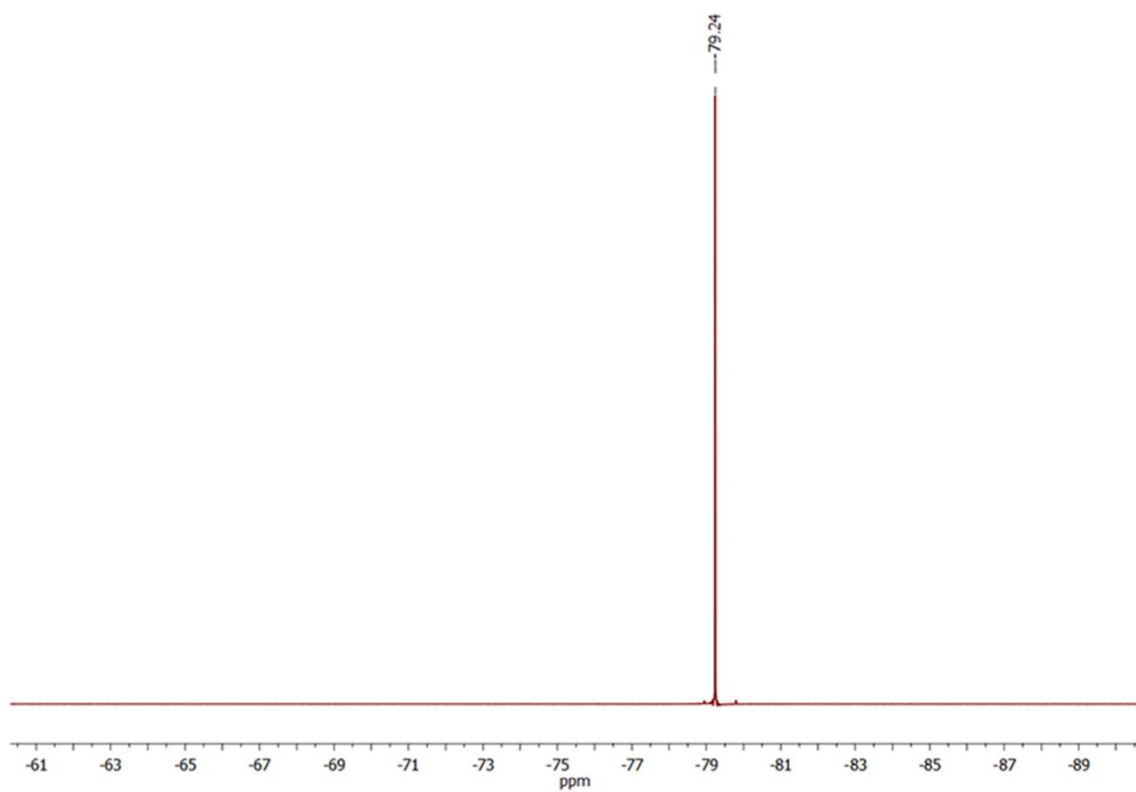


Figure 3A.12. ^{19}F NMR of compound **1b**.

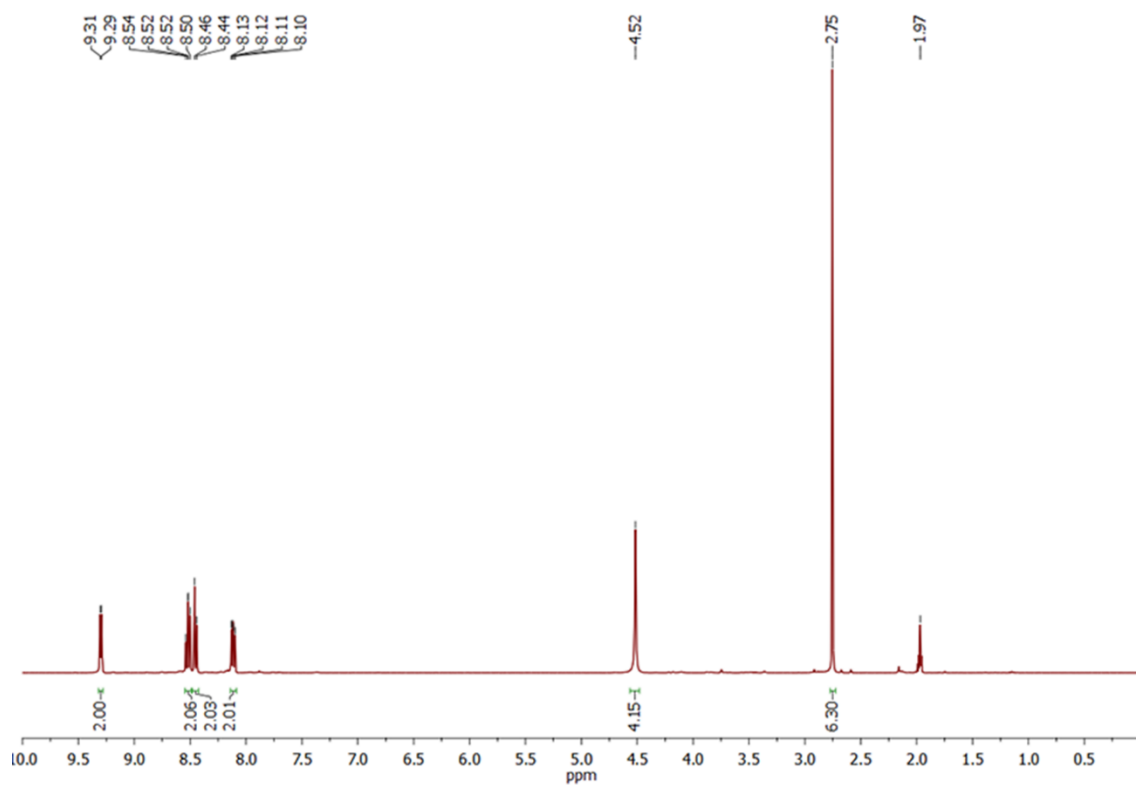


Figure 3A.13. ^1H NMR of compound **2**.

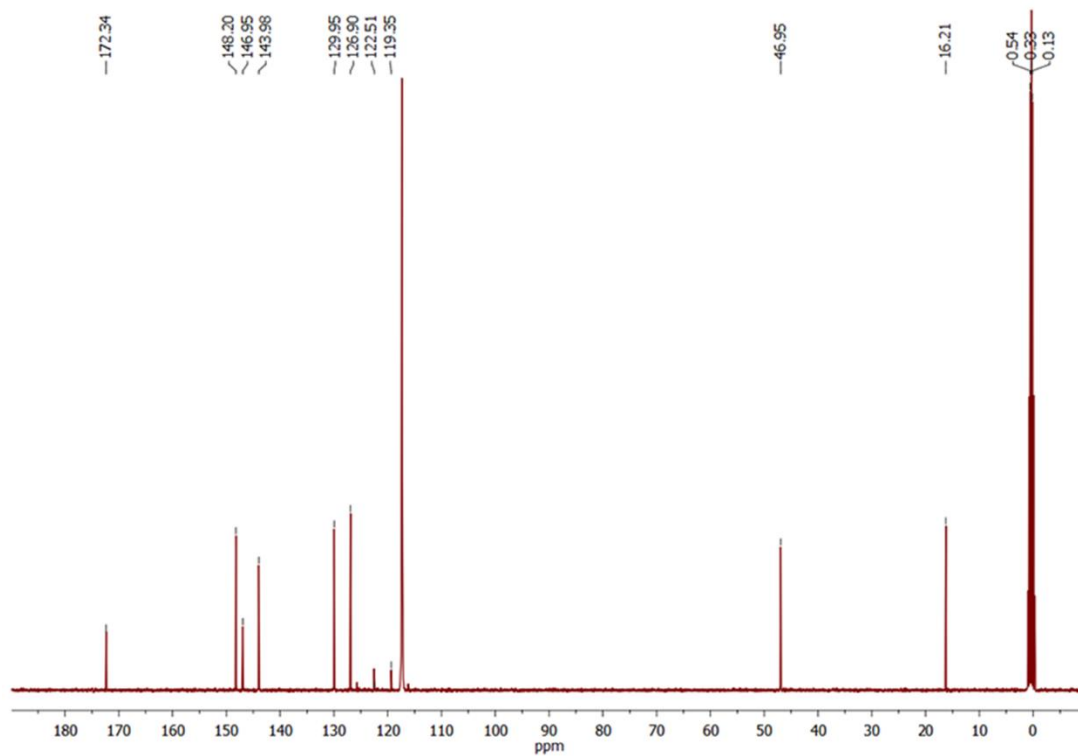


Figure 3A.14. ^{13}C NMR of compound 2.

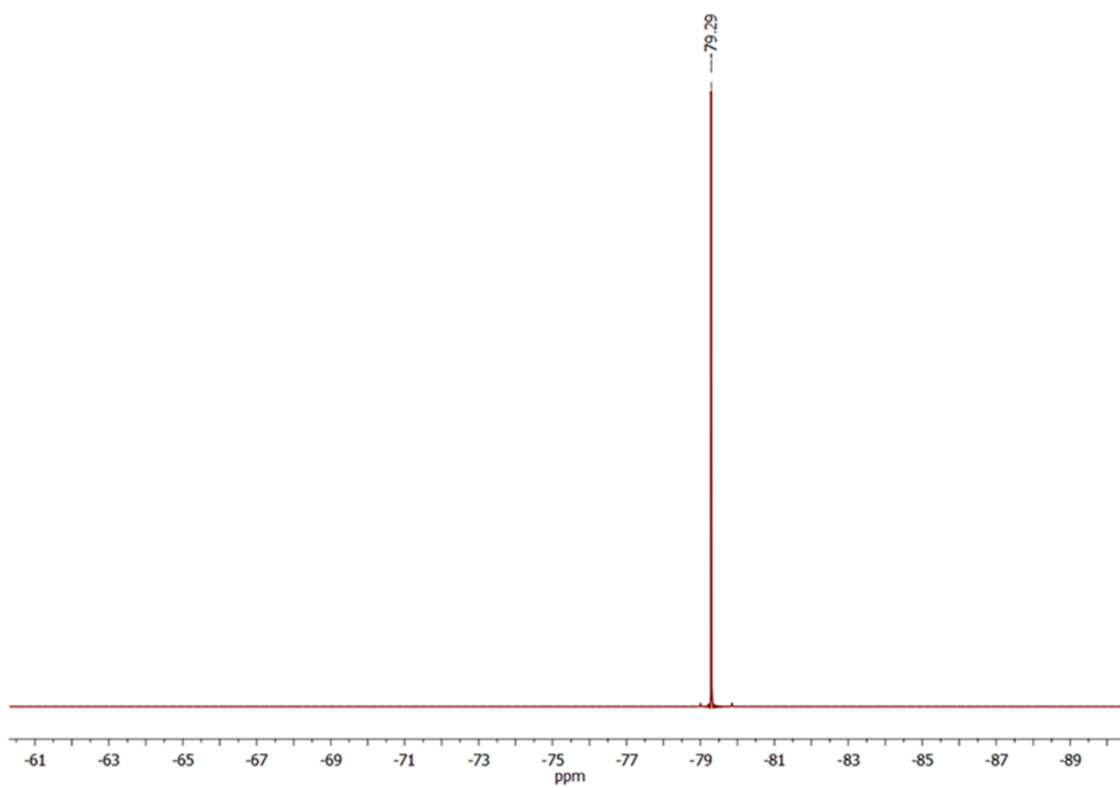


Figure 3A.15. ^{19}F NMR of compound 2.

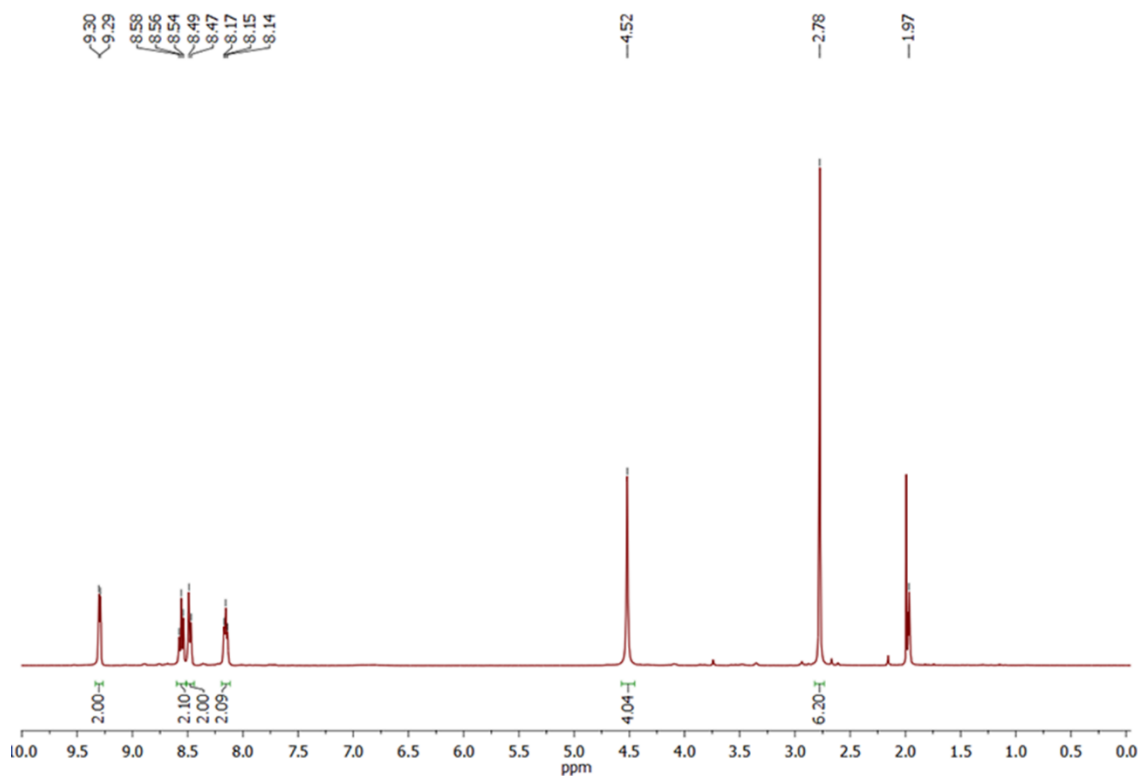


Figure 3A.16. ^1H NMR of compound 3.

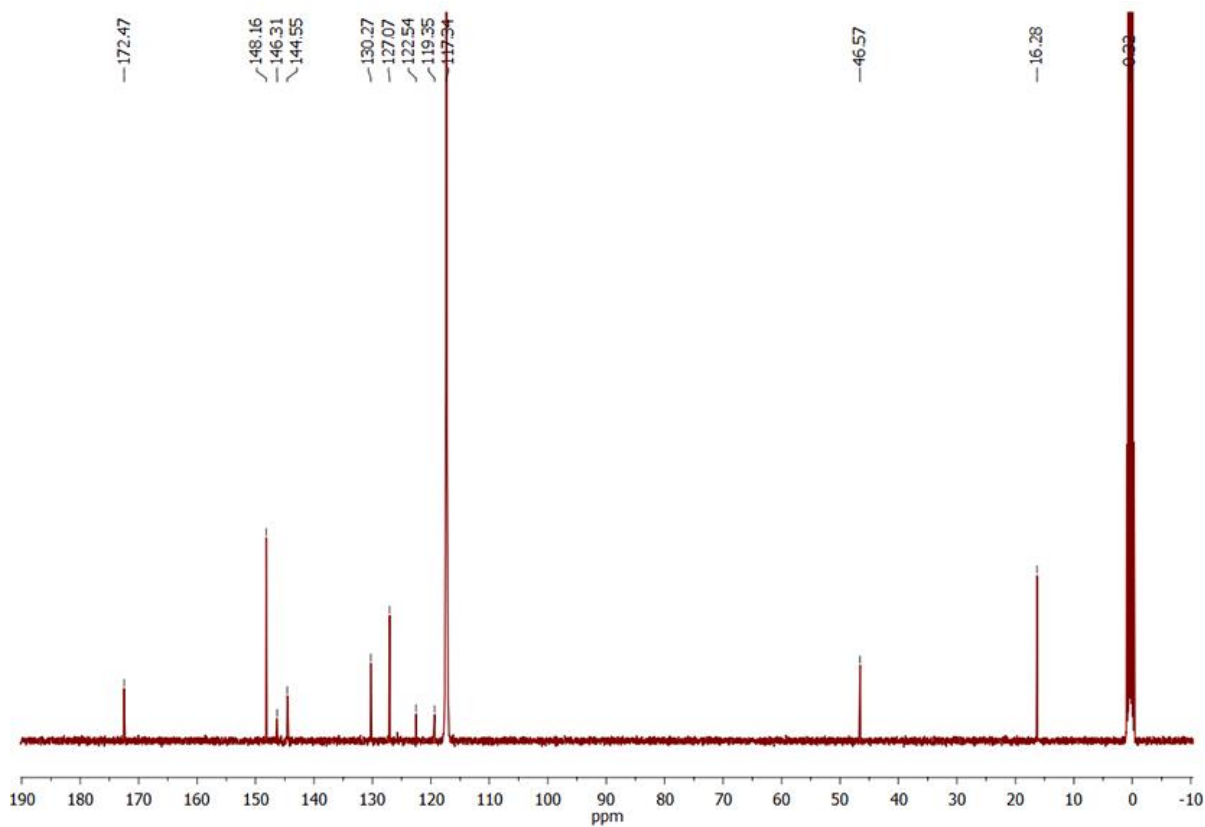


Figure 3A.17. ^{13}C NMR of compound 3.

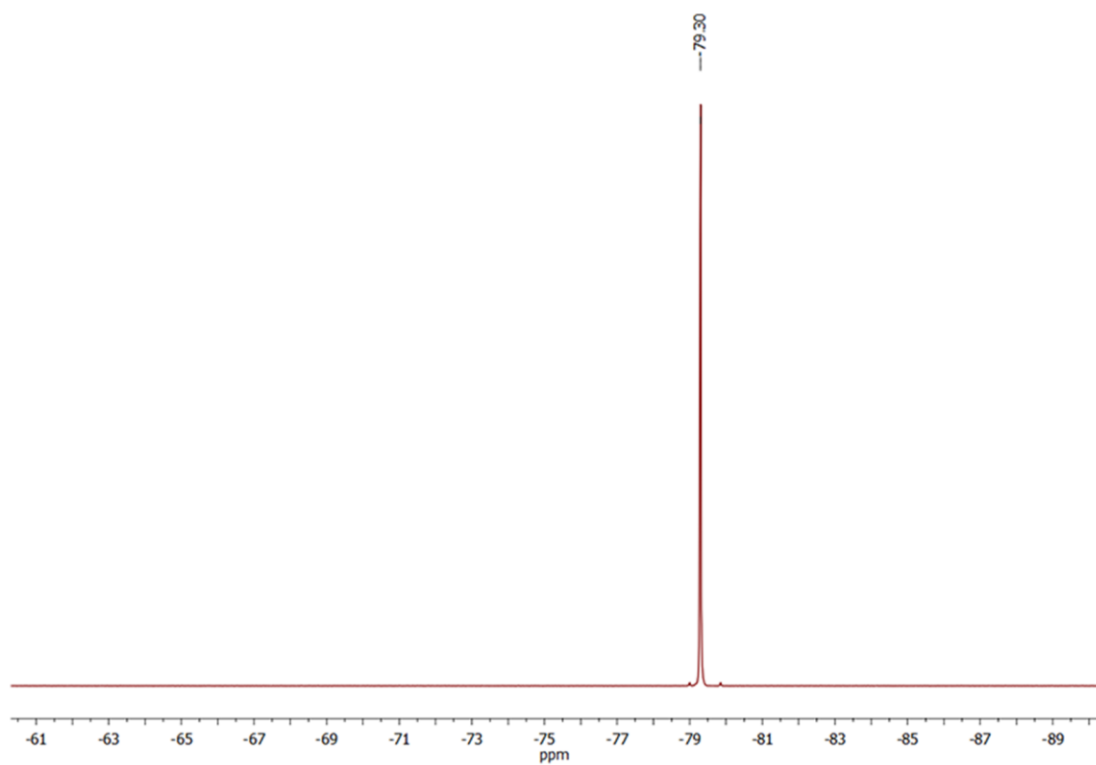


Figure 3A.18. ^{19}F NMR of compound 3.

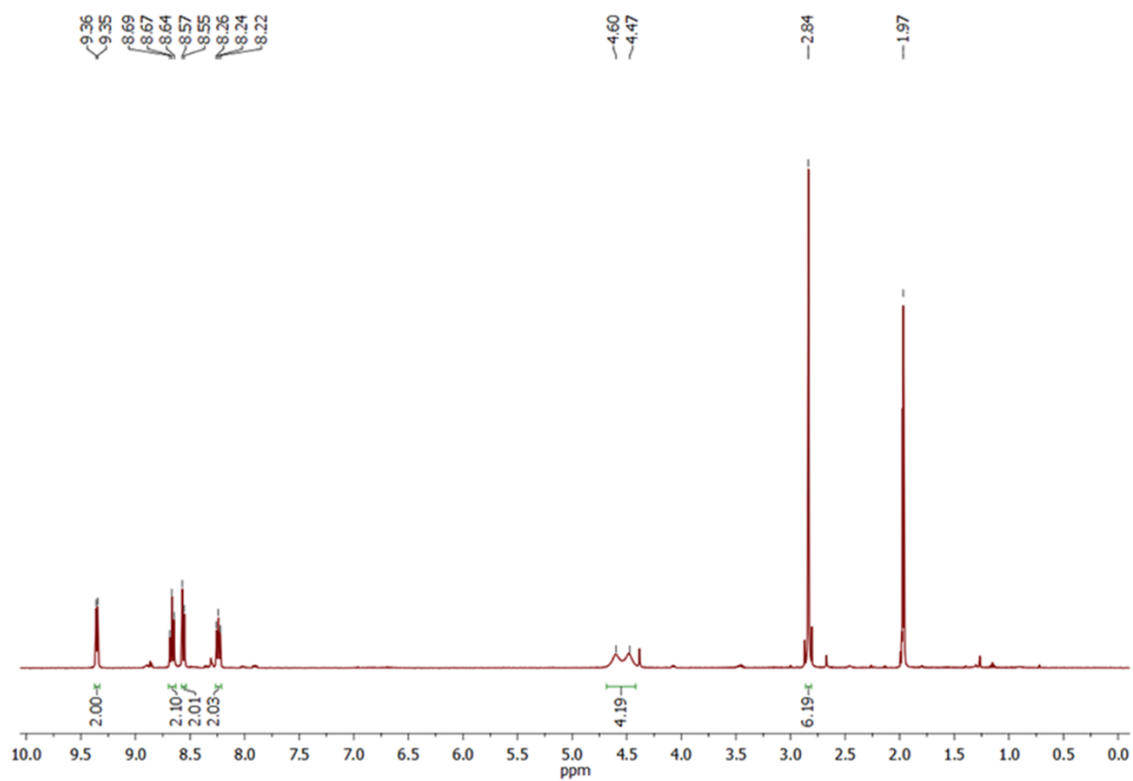


Figure 3A.19. ^1H NMR of compound 4.

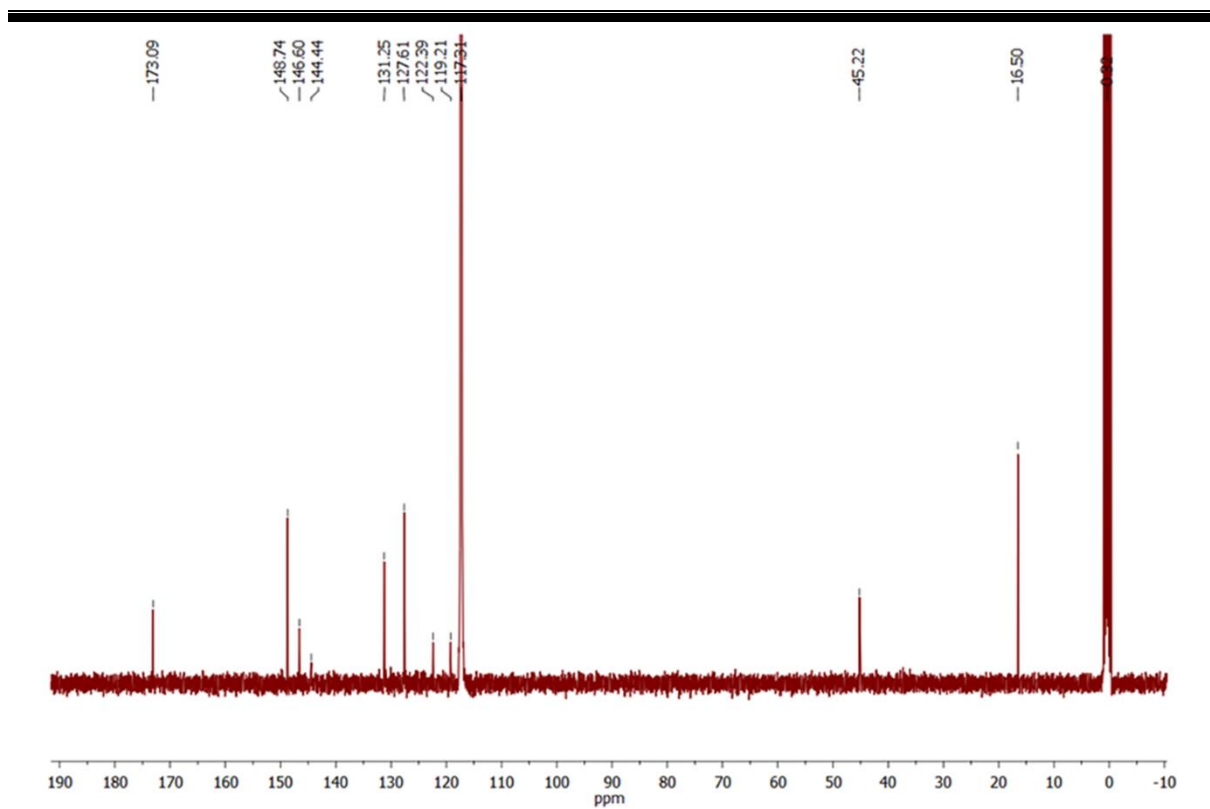


Figure 3A.20. ^{13}C NMR of compound 4.

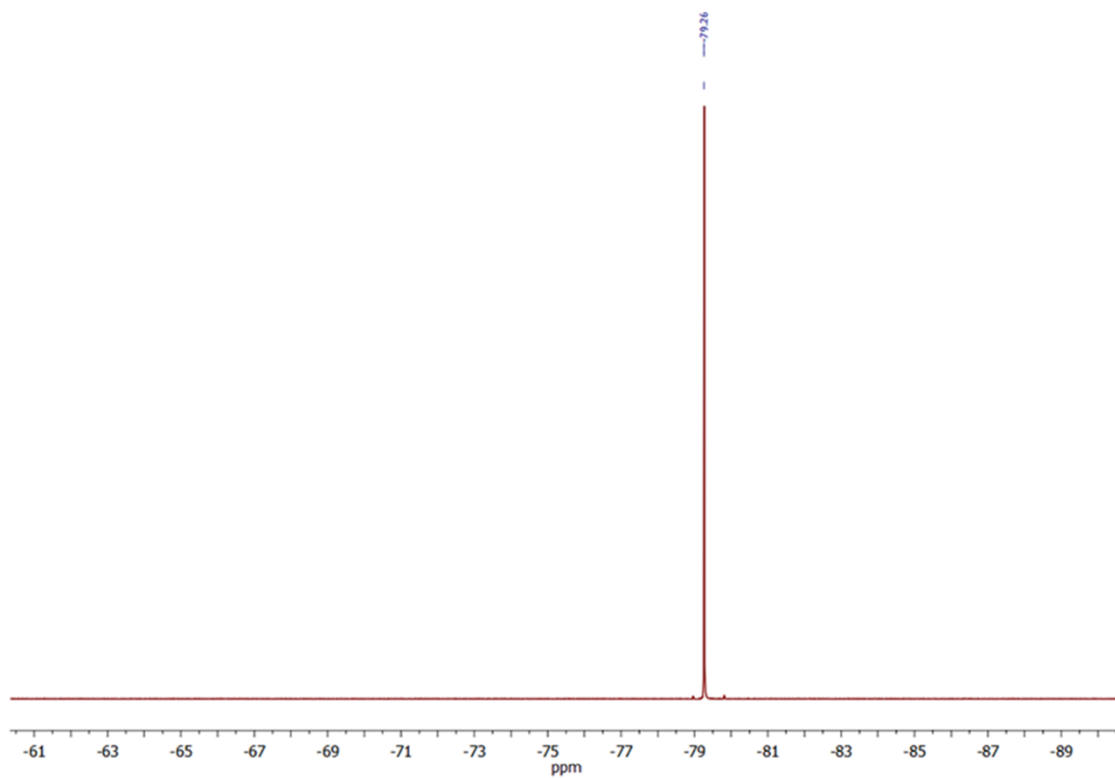


Figure 3A.21. ^{19}F NMR of compound 4.

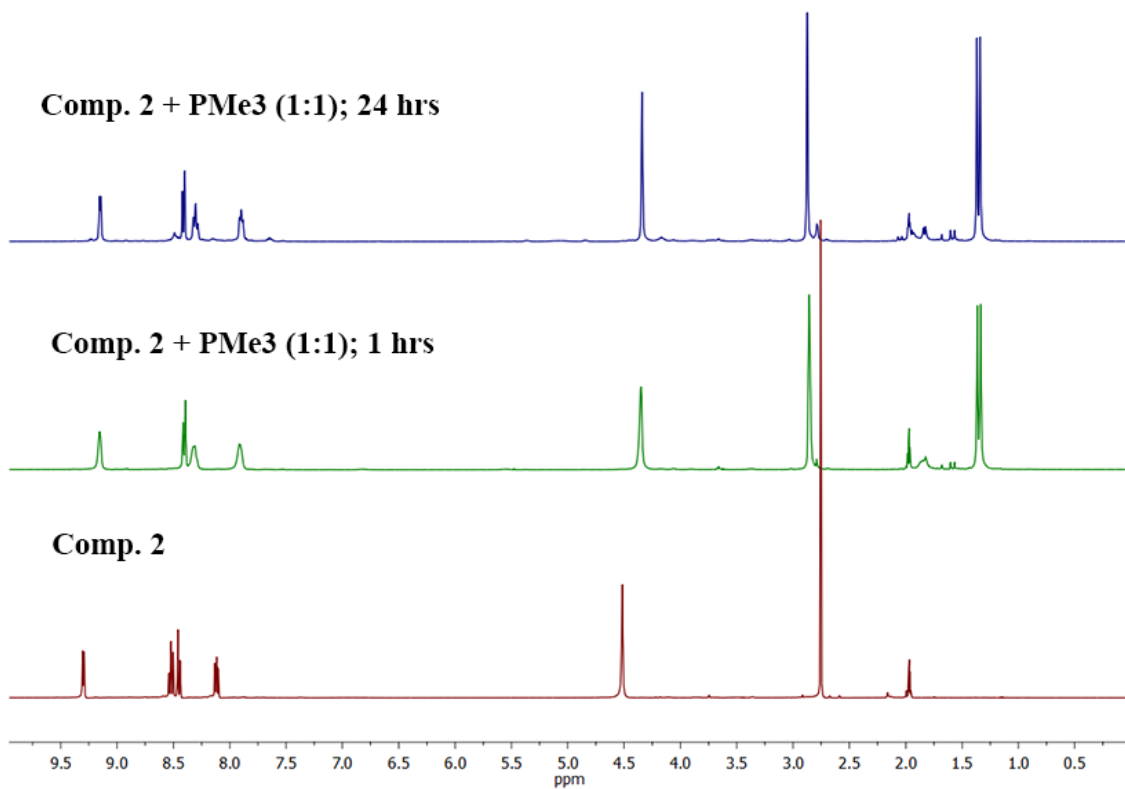


Figure 3A.22. ^1H of Comp. 2 + NMR PMe₃ (1:1).

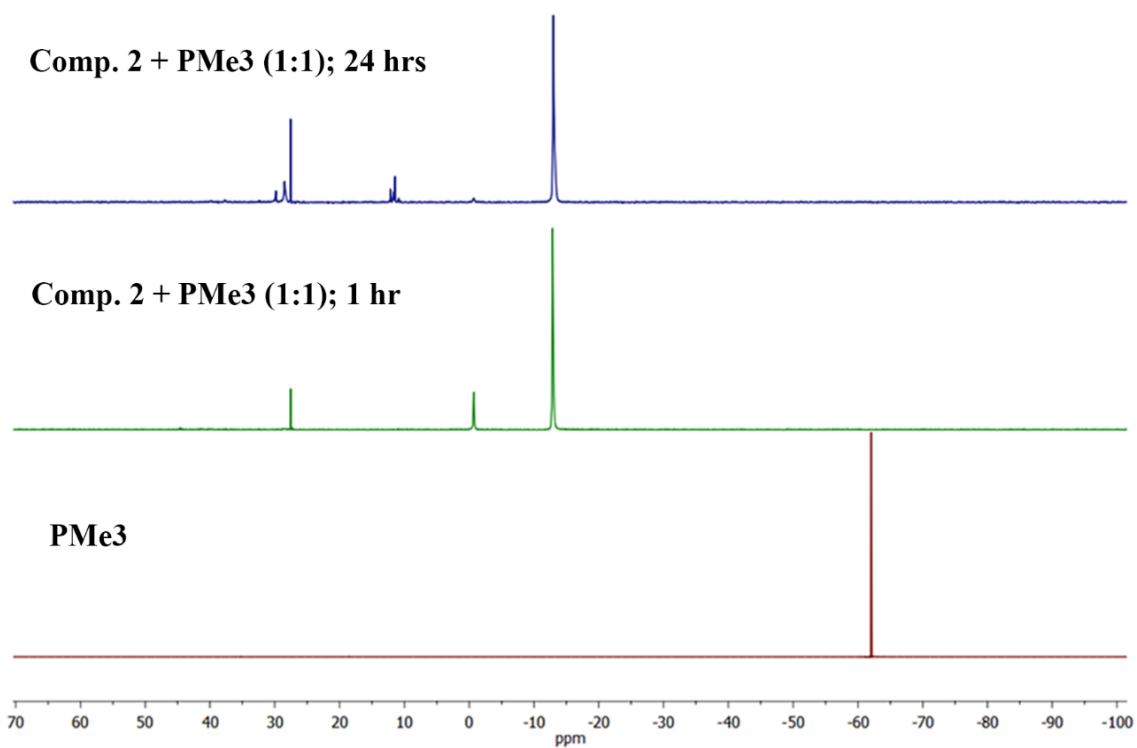


Figure 3A.23. $^{31}\text{P}\{^1\text{H}\}$ NMR of Comp. 2 + PMe₃ (1:1).

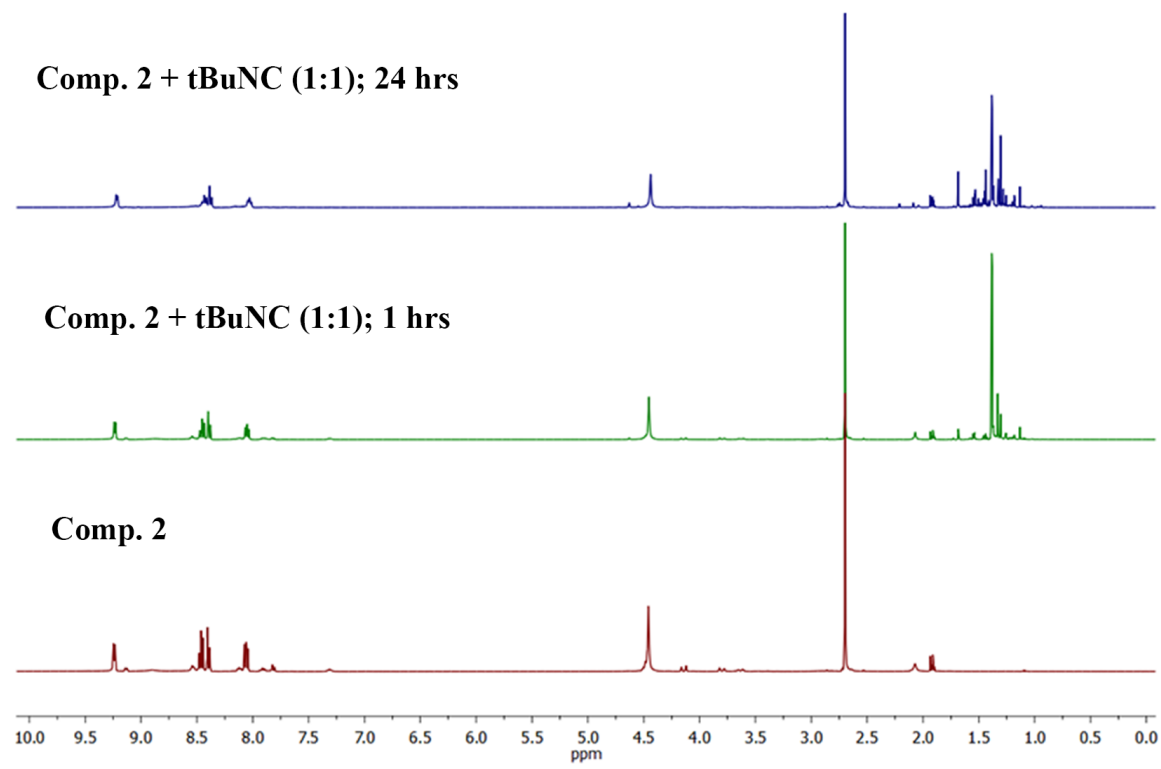


Figure 3A.24. ^1H NMR of Comp. 2 + $^t\text{BuNC}$ (1:1).

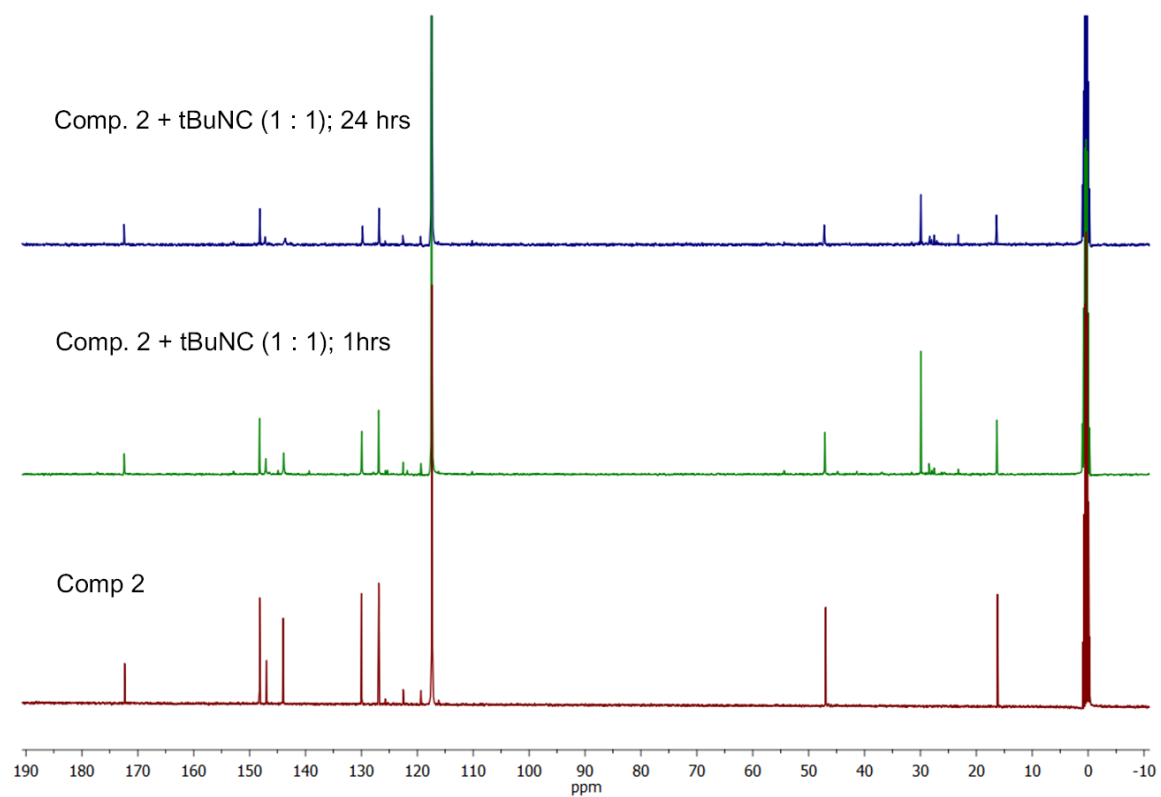


Figure 3A.25. $^{13}\text{C}\{^1\text{H}\}$ NMR of Comp. 2 + $^t\text{BuNC}$ (1:1).

3A.4.4 UV/Vis Spectra

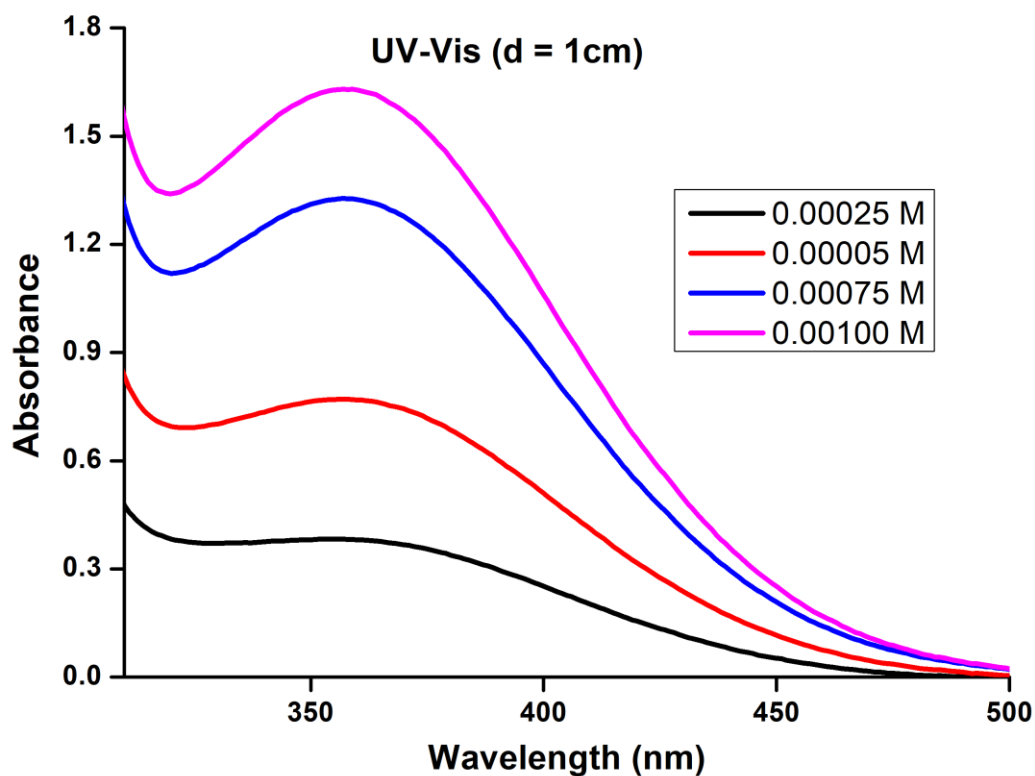


Figure 3A.26. UV-Vis spectra of 1a.

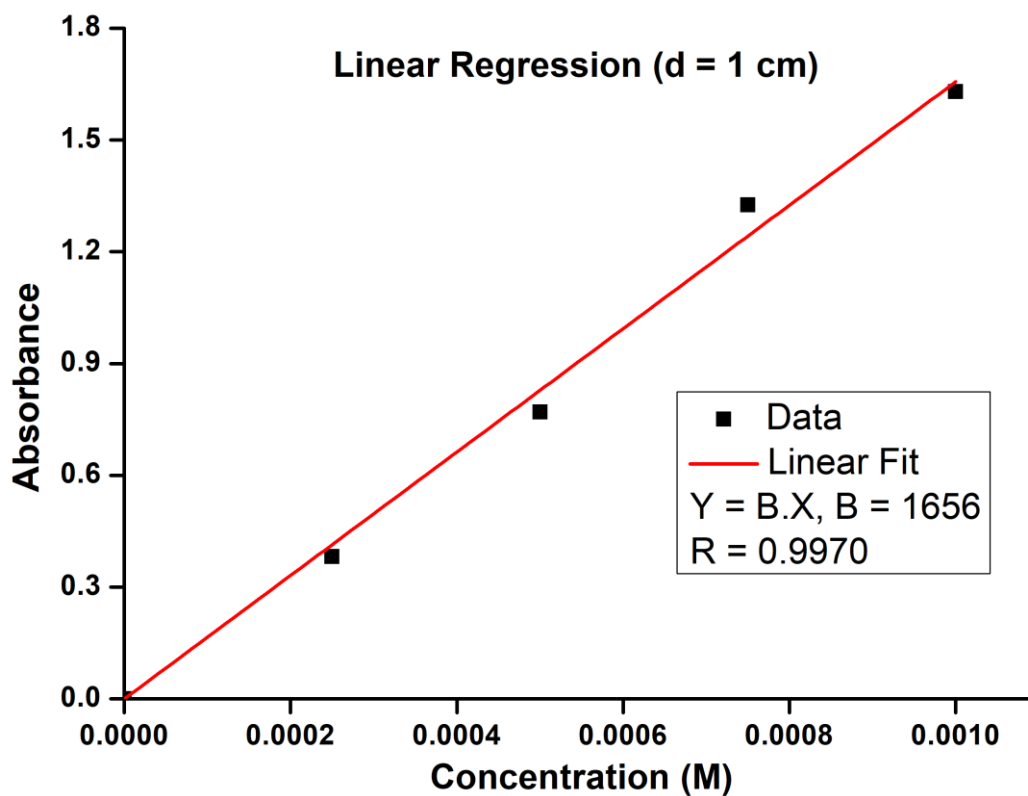


Figure 3A.28. Linear Fit for UV/Vis data of 1a.

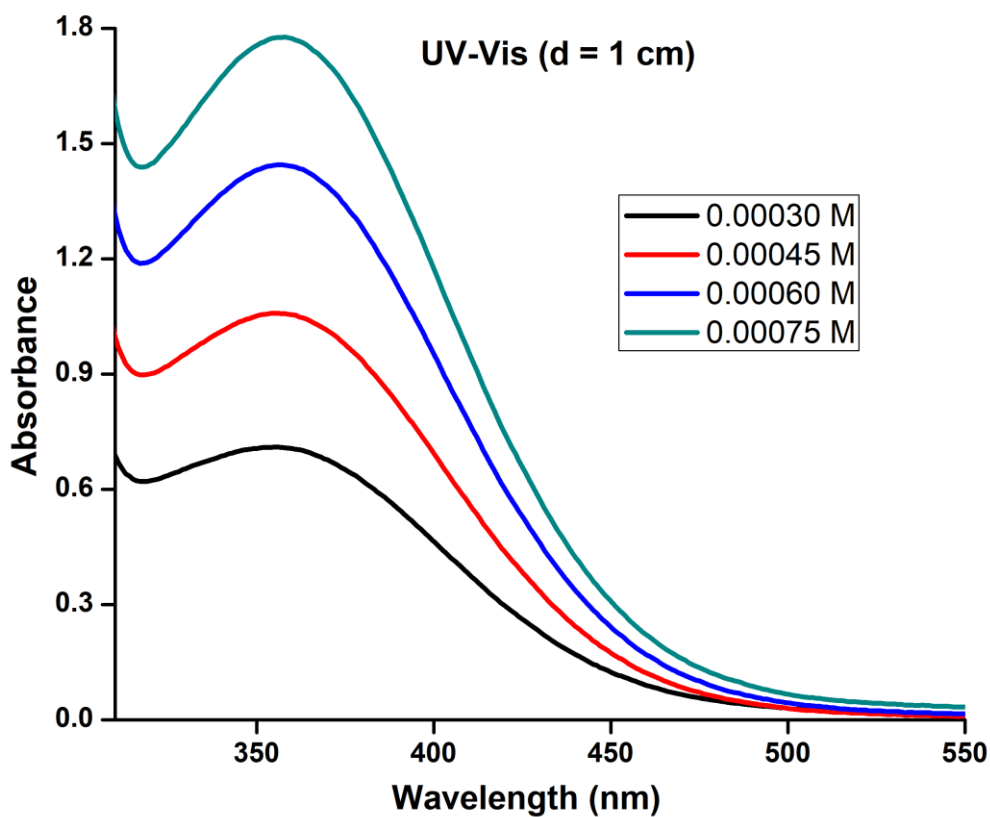


Figure 3A.29. UV-Vis spectra of 1b.

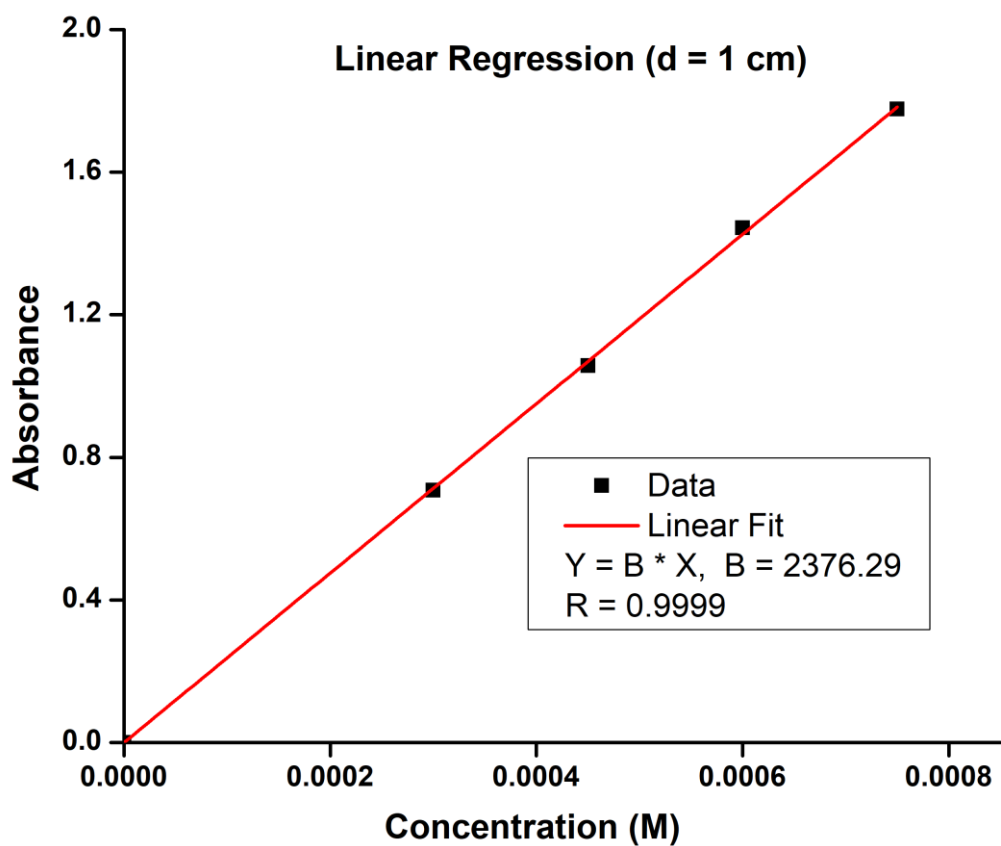


Figure 3A.30. Linear Fit for UV/Vis data of 1b.

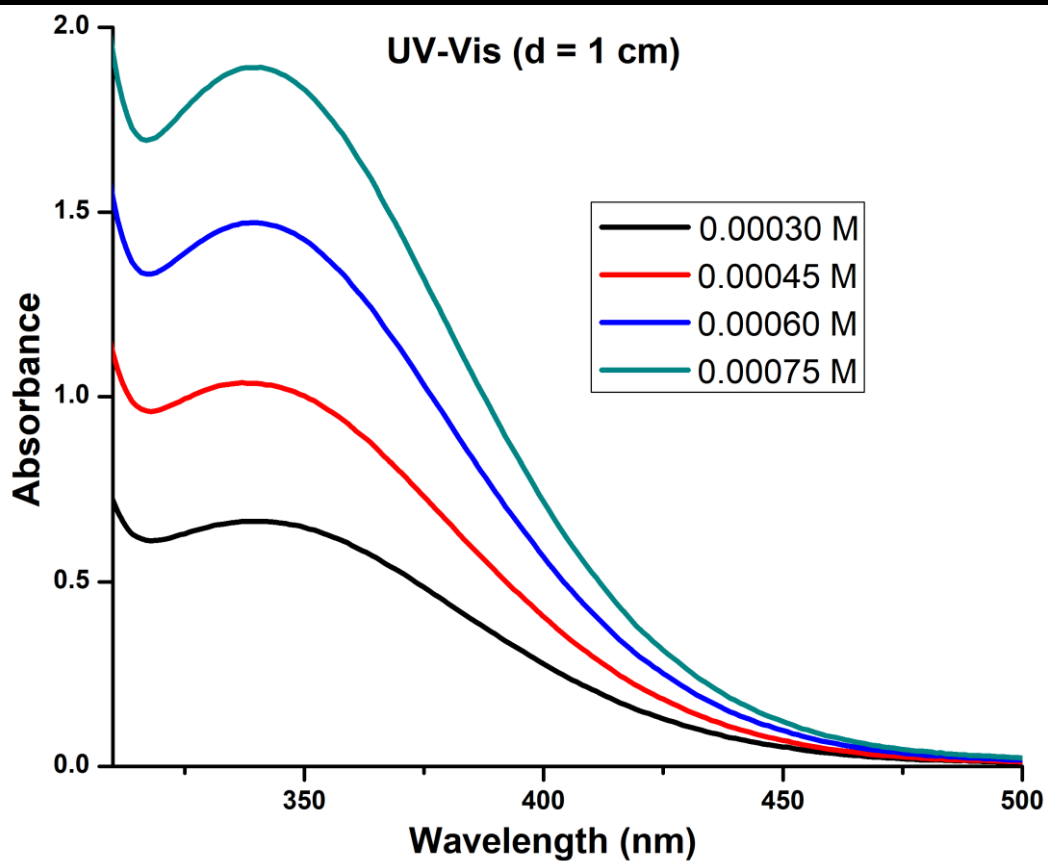


Figure 3A.31. UV-Vis spectra of 2.

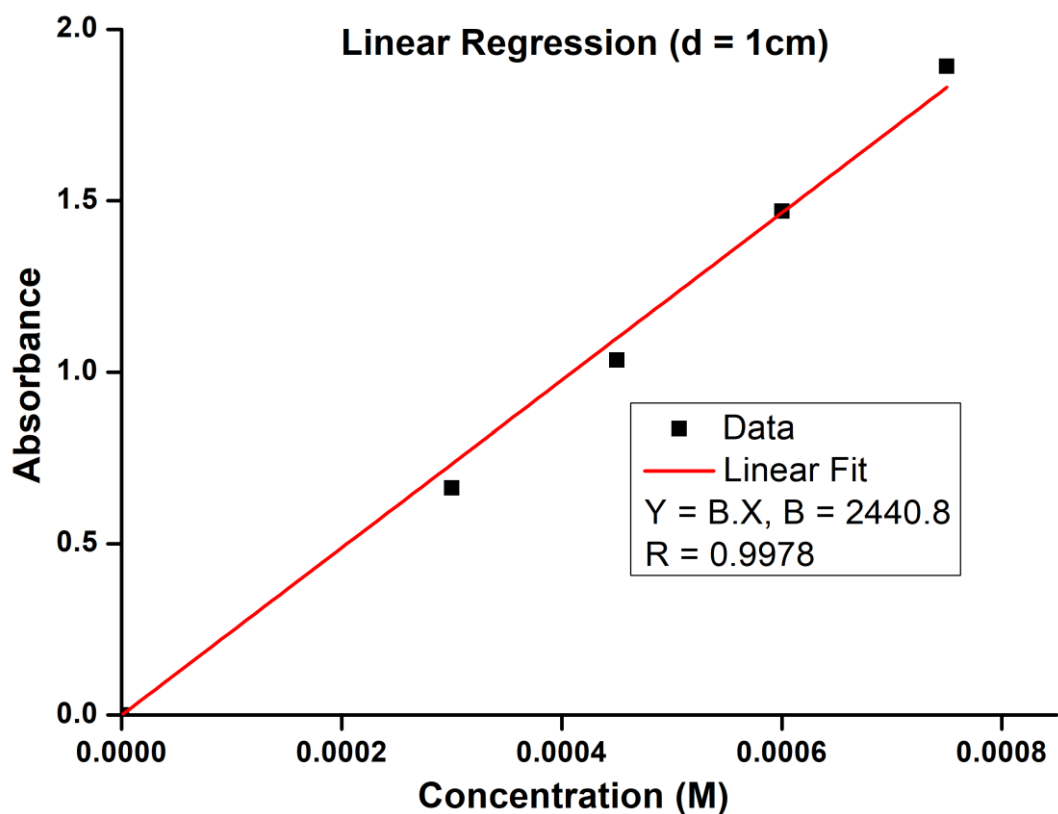


Figure 3A.32. Linear Fit for UV/Vis data of 2.

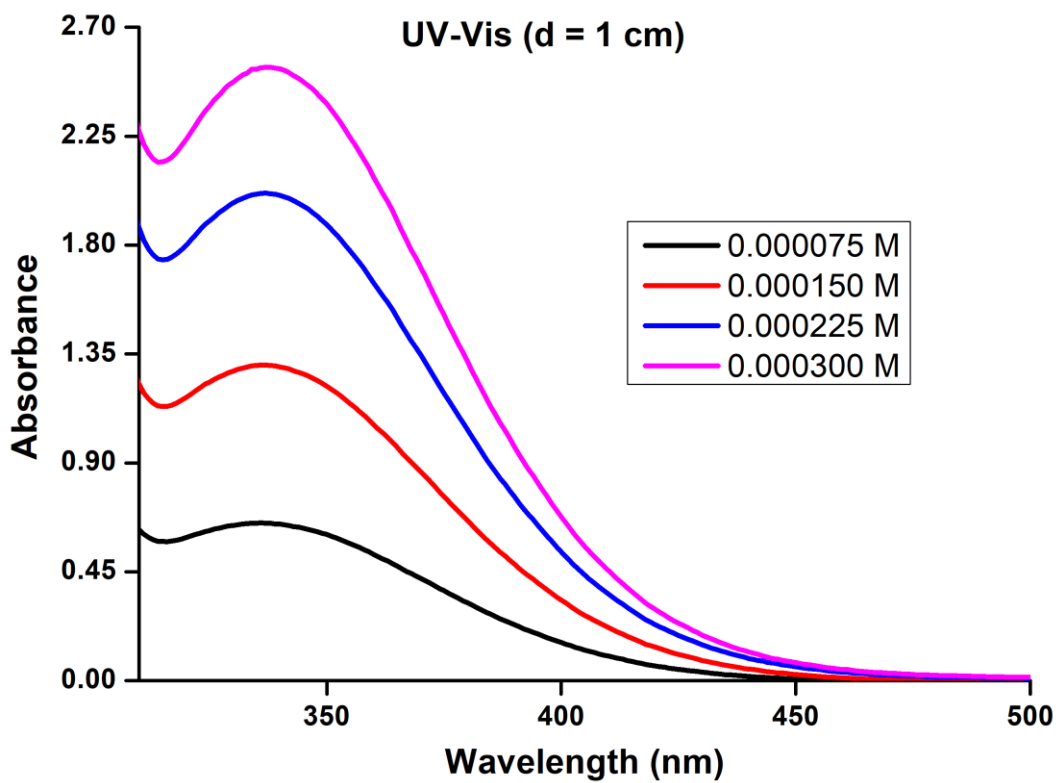


Figure 3A.33. UV-Vis spectra of 3.

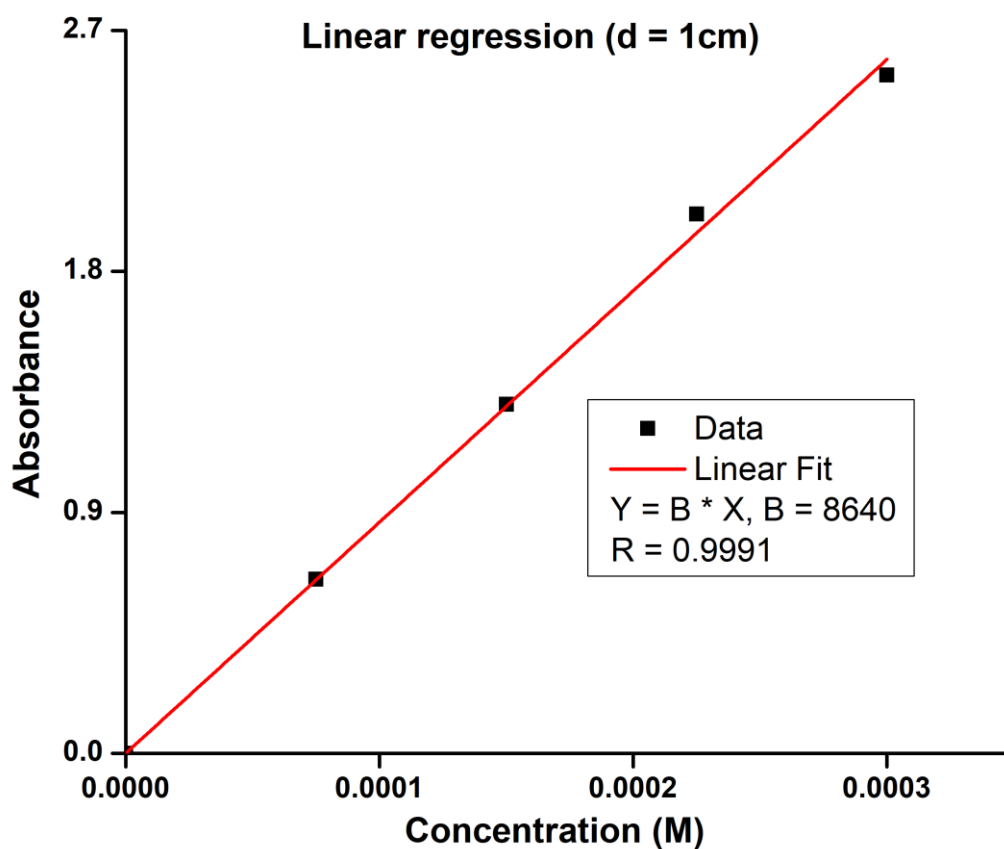


Figure 3A.34. Linear Fit for UV/Vis data of 3.

3A.4.5 X-ray Crystal Data

Table 3A.2. Crystal data and structure refinement for Comp. 1a.

Empirical formula	C ₁₆ H ₁₈ C ₁₄ Ge ₂ N ₄ , Cl ₃ Ge
Formula weight	553.32
Temperature	100 K
Wavelength	1.54178 Å
Crystal system	Triclinic
Space group	P -1
Unit cell dimensions	a = 8.872 (3) Å α = 90.296 (7) b = 10.214 (4) Å β = 93.135 (8) c = 12.585 (5) Å γ = 107.603 (7)
Volume	1085.1 (7) Å ³
Z	2
Density (calculated)	1.694 g/cm ³
Absorption coefficient	3.271 mm ⁻¹
F(000)	548
Crystal size	0.5 x 0.3 x 0.2 mm ³
Theta range for data collection	1.621 to 29.140°.
Index ranges	-12 ≤ h ≤ 11, -6 ≤ k ≤ 13, -17 ≤ l ≤ 17
Reflections collected	21205
Independent reflections	5806 [R(int) = 0.0371]
Completeness to theta = 28.38°	99.3 %
Absorption correction	Semi-empirical from equivalents
Max. and min. transmission	0.320 and 0.520
Refinement method	Full-matrix least-squares on F ²
Data / restraints / parameters	5806 / 0 / 237
Goodness-of-fit on F ²	1.097
Final R indices [I > 2σ(I)]	R1 = 0.0340, wR2 = 0.0884
R indices (all data)	R1 = 0.0476, wR2 = 0.0949
Absolute structure parameter	-0.07(9)
Largest diff. peak and hole	0.321 and -0.232 e.Å ⁻³

Table 3A.3. Crystal data and structure refinement for Comp. 1b.

Empirical formula	C ₁₇ H ₁₈ ClF ₃ GeN ₄ O ₃ S
Formula weight	523.47
Temperature	100 K
Wavelength	1.54178 Å
Crystal system	Monoclinic
Space group	P 21/c
Unit cell dimensions	a = 20.5748 (10) Å α = 90 b = 13.4785 (7) Å β = 99.802 c = 14.7382 (8) Å γ = 90
Volume	4027.5 (4) Å ³
Z	8
Density (calculated)	1.727 g/cm ³
Absorption coefficient	4.775 mm ⁻¹
F(000)	2112
Crystal size	0.9 x 0.5 x 0.3 mm ³
Theta range for data collection	4.36 to 72.44°.
Index ranges	-25 ≤ h ≤ 25, -16 ≤ k ≤ 16, -18 ≤ l ≤ 17
Reflections collected	36440
Independent reflections	7885 [R(int) = 0.0371]
Completeness to theta = 28.38°	98.2 %
Absorption correction	Semi-empirical from equivalents
Max. and min. transmission	0.9769 and 0.9499
Refinement method	Full-matrix least-squares on F ²
Data / restraints / parameters	13176 / 0 / 545
Goodness-of-fit on F ²	1.079
Final R indices [I > 2σ(I)]	R1 = 0.0520, wR2 = 0.1237
R indices (all data)	R1 = 0.0738, wR2 = 0.1359
Absolute structure parameter	-0.07(9)
Largest diff. peak and hole	0.321 and -0.232 e.Å ⁻³

Table 3A.4. Crystal data and structure refinement for Comp. 2

Empirical formula	C ₁₉ H ₂₀ C ₁₂ F ₆ GeN ₄ O ₆ S ₂
Formula weight	722.02
Temperature	100 K
Wavelength	1.54178 Å
Crystal system	Triclinic
Space group	P -1
Unit cell dimensions	a = 8.4372 (5) Å α = 69.771 (3) b = 13.0507 (8) Å β = 85.531 (3) c = 13.3070 (8) Å γ = 81.999 (3)
Volume	1360.79 (14) Å ³
Z	2
Density (calculated)	1.762 g/cm ³
Absorption coefficient	5.561 mm ⁻¹
F(000)	724.0
Crystal size	0.5 x 0.4 x 0.2 mm ³
Theta range for data collection	3.541 to 72.741°.
Index ranges	-10 ≤ h ≤ 10, -16 ≤ k ≤ 16, -16 ≤ l ≤ 16
Reflections collected	14142
Independent reflections	5317 [R(int) = 0.0371]
Completeness to theta = 28.38°	98.2 %
Absorption correction *	Semi-empirical from equivalents
Max. and min. transmission	0.9769 and 0.9499
Refinement method	Full-matrix least-squares on F ²
Data / restraints / parameters	5317 / 0 / 545
Goodness-of-fit on F ²	1.092
Final R indices [I > 2σ(I)]	R1 = 0.0613, wR2 = 0.1298
R indices (all data)	R1 = 0.0832, wR2 = 0.1417
Absolute structure parameter *	-0.07(9)
Largest diff. peak and hole *	0.321 and -0.232 e.Å ⁻³

Table 3A.5. Crystal data and structure refinement for Comp. 3

Empirical formula	C ₃₉ H ₃₉ AgF ₁₅ Ge ₂ N ₉ O ₁₅ S ₅
Formula weight	1572.14
Temperature	100 K
Wavelength	1.54178 Å
Crystal system	Triclinic
Space group	P -1
Unit cell dimensions	a = 14.699 (2) Å α = 112.989 (6) b = 15.176 (3) Å β = 103.063 (6) c = 15.433 (3) Å γ = 106.078 (6)
Volume	2819.6 (8) Å ³
Z	2
Density (calculated)	1.852 g/cm ³
Absorption coefficient	6.848 mm ⁻¹
F(000)	1564
Crystal size	0.5 x 0.4 x 0.2 mm ³
Theta range for data collection	3.36 to 73.391°.
Index ranges	-17<=h<=18, -18<=k<=18, -19<=l<=14
Reflections collected	24387
Independent reflections	10814 [R(int) = 0.0371]
Completeness to theta = 28.38°	95.4 %
Absorption correction *	Semi-empirical from equivalents
Max. and min. transmission	0.071 and 0.254
Refinement method	Full-matrix least-squares on F ²
Data / restraints / parameters	10814 / 0 / 780
Goodness-of-fit on F ²	1.031
Final R indices [I>2sigma(I)]	R1 = 0.057, wR2 = 0.1360
R indices (all data)	R1 = 0.0660, wR2 = 0.1417
Absolute structure parameter *	-0.07(9)
Largest diff. peak and hole *	0.321 and -0.232 e.Å ⁻³

Table 3A.6. Crystal data and structure refinement for Comp. 4

Empirical formula	C ₃₇ H ₃₆ AuF ₁₅ Ge ₂ N ₈ O ₁₅ S ₅
Formula weight	1620.18
Temperature	100 K
Wavelength	1.54178 Å
Crystal system	Triclinic
Space group	P -1
Unit cell dimensions	a = 12.421 (3) Å α = 85.383 (5)° b = 12.980 (3) Å β = 72.526 (5)° c = 17.648 (4) Å γ = 75.017 (5)°
Volume	2621.8 (8) Å ³
Z	2
Density (calculated)	2.052 g/cm ³
Absorption coefficient	9.527 mm ⁻¹
F(000)	1584
Crystal size	0.6 x 0.5 x 0.3 mm ³
Theta range for data collection	2.625 to 73.011°.
Index ranges	-15 ≤ h ≤ 15, -15 ≤ k ≤ 16, -19 ≤ l ≤ 21
Reflections collected	29573
Independent reflections	10213 [R(int) = 0.0371]
Completeness to theta = 28.38°	97.5 %
Absorption correction *	Semi-empirical from equivalents
Max. and min. transmission	0.008 and 0.057
Refinement method	Full-matrix least-squares on F ²
Data / restraints / parameters	10213 / 0 / 752
Goodness-of-fit on F ²	1.095
Final R indices [I > 2σ(I)]	R1 = 0.0364, wR2 = 0.0965
R indices (all data)	R1 = 0.0369, wR2 = 0.0970
Absolute structure parameter *	-0.07(9)
Largest diff. peak and hole *	0.321 and -0.232 e.Å ⁻³

3A.4.6 X-Ray Crystal Structure

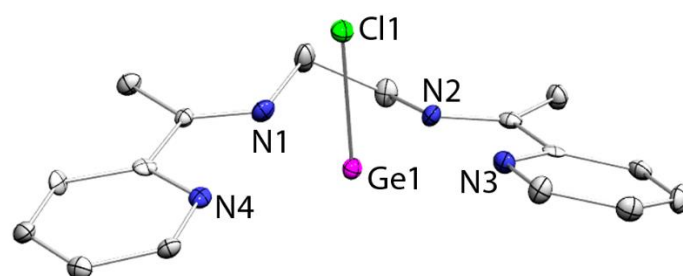


Figure 3A.35. Structure of **1b** in the solid state (thermal ellipsoids at 30%, H atoms, triflate anion omitted for clarity). Selected bond lengths [\AA]: Ge1-Cl1 = 2.2807 (18) \AA , Ge1-N1 = 2.220(5) \AA , Ge1-N2 = 2.180 (6) \AA

3A.5 References

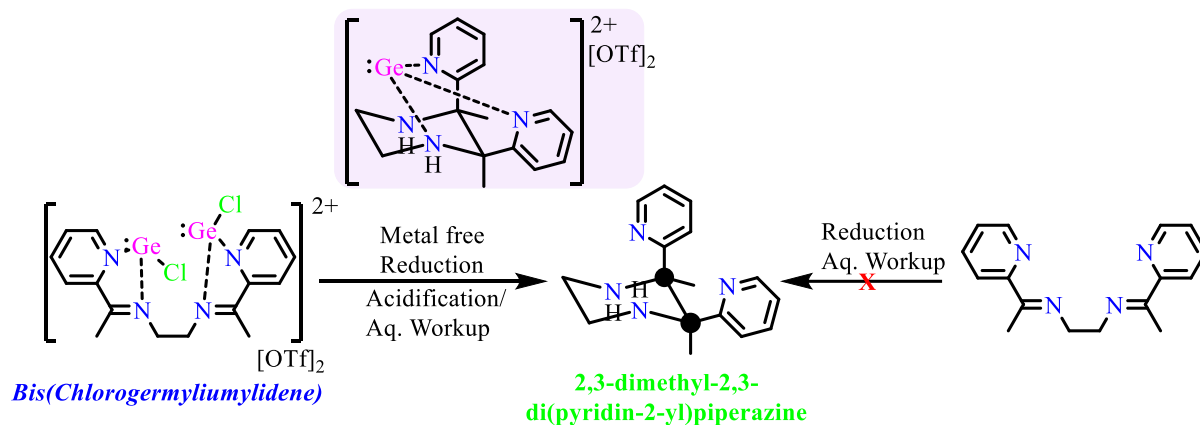
1. (a) Fernández-Pérez, H.; Etayo, P.; Pannosian, A.; Vidal-Ferran, A. *Chem. Rev.* **2011**, *111*, 2119. (b) Bayne, J. M.; Stephan, D. W. *Chem. Soc. Rev.* **2016**, *45*, 765.
2. (a) Petušková, J.; Patil, M.; Holle, S.; Lehmann, C. W.; Thiel, W.; Alcarazo, M. *J. Am. Chem. Soc.* **2011**, *133*, 20758. (b) Scheer, M.; Kuntz, C.; Stubenhofer, M.; Linseis, M.; Winter, R. F.; Sierka, M. *Angew. Chem., Int. Ed.* **2009**, *48*, 2600. (c) Dutton, J. L.; Ragogna, P. J.; *Coord. Chem. Rev.* **2011**, *255*, 1414.
3. (a) Petušková, J.; Bruns, H.; Alcarazo, M. *Angew. Chem., Int. Ed.* **2011**, *50*, 3799. (b) Carreras, J.; Patil, M.; Thiel, W.; Alcarazo, M. *J. Am. Chem. Soc.* **2012**, *134*, 16753. (b) Alcarazo, M. *Chem. – Eur. J.* **2014**, *20*, 7868. (c) M. Alcarazo, *Acc. Chem. Res.*, **2016**, *49*, 1797.
4. (a) Metsänen, T. T.; Gallego, D.; Szilvási, T.; Driess, M.; Oestreich, M. *Chem. Sci.* **2015**, *6*, 7143. (b) Ochiai, T.; Franz, D.; Wu, X.-N.; Inoue, S. *Dalton Trans.* **2015**, *44*, 10952. (b) Zhou, Y.-P.; Raoufmoghaddam, S.; Szilvási, T.; Driess, M. *Angew. Chem. Int. Ed.* **2016**, *55*, 12868.
5. Singh, A. P.; Roesky, H. W.; Carl, E.; Stalke, D.; Demers, J. –P.; Lange, A. *J. Am. Chem. Soc.* **2012**, *134*, 4998.
6. (a) Rupar, P. A.; Staroverov, V. N.; Ragogna, P. J.; Baines, K. M. *J. Am. Chem. Soc.* **2007**, *129*, 15138. (b) Xiong, Y.; Szilvási, T.; Yao, S.; Tan, G.; Driess, M. *J. Am. Chem. Soc.* **2014**, *136*, 11300. (c) Swamy, V. S. V. S. N.; Pal, S.; Khan, S. Sen, S. S. *Dalton Trans.* **2015**, *44*, 12903. (d) Swamy, V. S. V. S. N.; Yadav, S.; Pal, S.; Das, T.; Vanka, K.; Sen, S. S. *Chem. Commun.* **2016**, *52*, 7890. (e) Ochiai, T.; Szilvási, T.; Franz, D.; Irran, E.; Inoue, S. *Angew. Chem., Int. Ed.* **2016**, *55*, 11619.
7. Rupar, P. A.; Staroverov, V. N.; Baines, K. M. *Science* **2008**, *322*, 1360.
8. Rupar, P. A.; Bandyopadhyay, R.; Cooper, B. F. T.; Stinchcombe, M. R.; Ragogna, P. J.; Macdonald, C. L. B.; Baines, K. M. *Angew. Chem. Int. Ed.* **2009**, *48*, 5155.
9. Cheng, F.; Hector, A. L.; Levason, W.; Reid, G.; Webster, M.; Zhang, W.; *Angew. Chem. Int. Ed.* **2009**, *48*, 5152.
10. Braunschweig, H.; Celik, M. A.; Dewhurst, R. D.; Heid, M.; Hupp, F.; Sen, S. S. *Chem. Sci.* **2015**, *6*, 425.
11. Bandyopadhyay, R.; Nguyen, J. H.; Swidan, A.; Macdonald, C. L. B. *Angew. Chem. Int. Ed.* **2013**, *52*, 3469.
12. Fang, H.; Jing, H.; Zhang, A.; Ge, H.; Yao, Z.; Brothers, P. J.; Fu, X. *J. Am. Chem. Soc.* **2016**, *138*, 7705.

-
13. Ponec, R.; Bultinck, P.; Gupta, P.; Tantillo, D. J. *J. Phys. Chem. A*. **2006**, *110*, 3785.
 14. (a) Álvarez-Rodríguez, L.; Cabeza, J. A.; García-Álvarez, P.; Polo, D. *Organometallics* **2015**, *34*, 5479. (b) Álvarez-Rodríguez, L.; Cabeza, J.A.; García-Álvarez, P.; Polo D. *Coord. Chem. Rev.* **2015**, *300*, 1-28.
 15. (a) Preisenberger, M.; Schier, A.; Schmidbaur, H. *Dalton Trans.* **1999**, 1645. (b) Smirnova, E. S.; Echavarren, A. M. *Angew. Chem. Int. Ed.* **2013**, *52*, 9023.
 16. Wang, X.; Peng, Y.; Olmstead, M. M.; Hope, Power, P. P. *J. Am. Chem. Soc.* **2010**, *132*, 13150.
 17. Boehme, C.; Frenking, G. *Organometallics* **1998**, *17*, 5801.

Bis(chlorogermylumylidene) and its Significant Role in an Elusive Reductive Cyclization

Abstract

Germanium bringing together Bis(chlorogermylumylidene) has been strategically obtained within redox-active bis(α -iminopyridine). Metal-free reduction of **2** using organosilicon reducing agent followed by protonation led to elusive 2,3-di(pyridin-2-yl)piperazine with *meso*-stereoselectivity. Formation of persistent triplet diradical upon reduction and isolation of piperazine stabilized Ge(II) dication intermediate provide convincing evidence for the crucial role of $[\text{GeCl}]^+$ units in reductive cyclization.



3B.1 Introduction

The chemistry of germanium(II) (poly)cations with potential ambiphilicity have seen an exuberant growth in the last couple of decades.¹ Classical kinetic or electronic stabilization strategies have been used for the successful isolations of Ge(II) monocations or chlorogermylumylidenes² and Ge(II) dications.³ Although there are a handful of reports on the synthesis of chlorogermylumylidene,² there are no reports on the formation of bis(chlorogermylumylidene), where the same molecule hosts two $[\text{GeCl}]^+$ units. Whereas the neutral counterpart of it is bis(germylene) either interconnected or separated by spacer, have been established and studied well⁴ Such spacer separated bis(germylenes) are used as chelating ligand with transition metals, and shown remarkable catalytic activity in many organic transformation.⁵

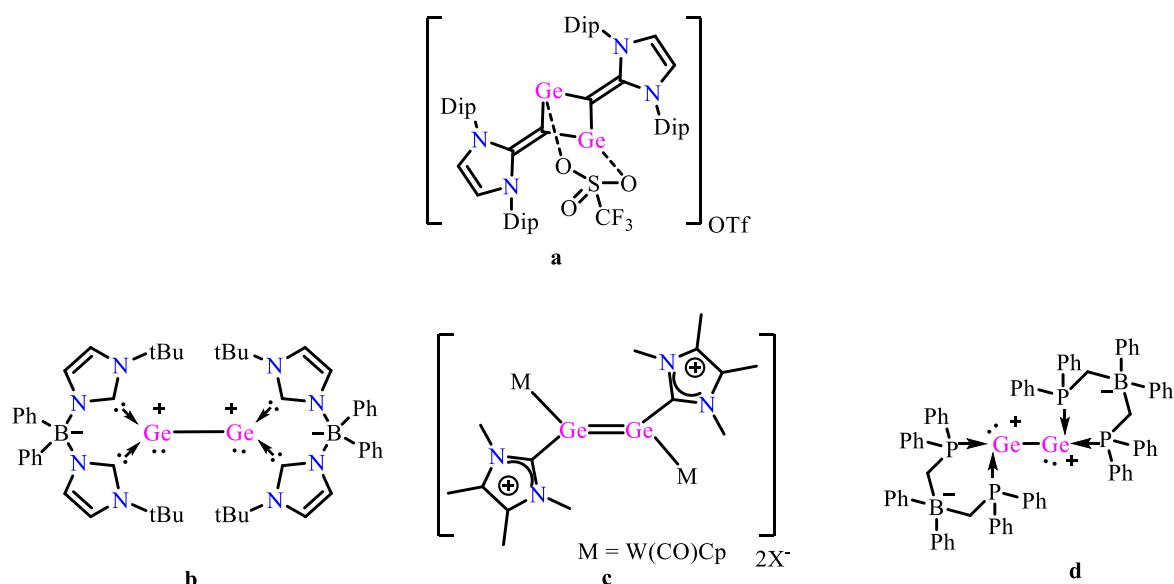
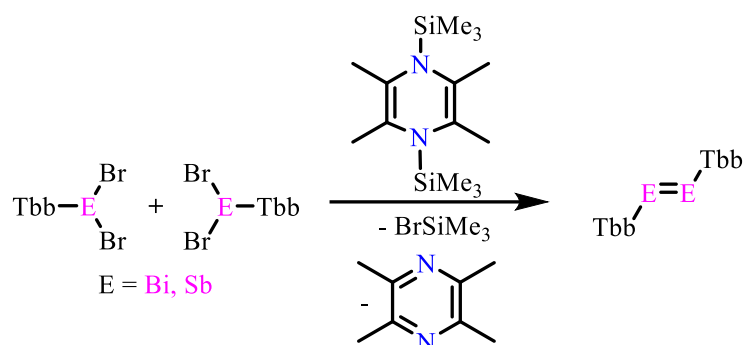


Figure 3B.1 Reported bis(germyliumylidenes).

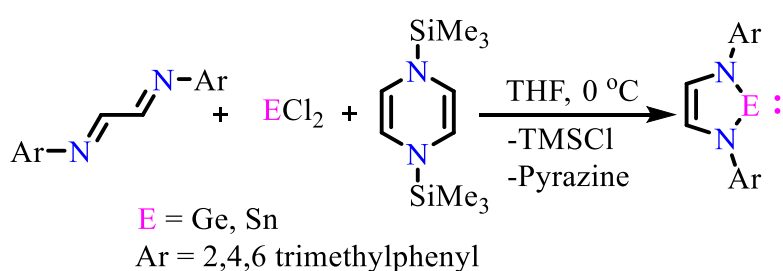
Distribution of charge into two different ligands can reduce the coulombic repulsion between two metal centre shown by the Nagase and co-workers in the dianionic disilicates.⁶ A similar strategy has been used for isolation a few of bis(germyliumylidene) (**a-d** in Figure 3B.1). Inoue et al. recently reported an *N*-Heterocyclic imine stabilized germylene-germyliumylidene **a** that has been computationally predicted to possess considerable bis(germyliumylidene) character.⁷ Other pertinent examples are zwitterionic bis(germyliumylidene)⁸ $[\text{Ge}^{\text{I}}-\text{Ge}^{\text{I}}]^{2+}$ **b**, where the positive charge is balanced by a remote anionic charge on the ligand backbone. The dimetallo digermene-1,2-diylium ion **c**⁹, possessing Ge-Ge bond between them and the dipositive charge on germanium is balanced by delocalization on imidazolium ring. Very recently, Ragogna et al.¹⁰ synthesized the $(\text{Ge}_2)^{2+}$ in

anionic phosphino borate ligand **d** by reduction of Chloro(germyliumylidene) using Mg(Nacnac).¹¹ The coulombic repulsion between two positive germanium was still barrier in stabilization and isolation of bis(chlorogermlyiumylidene).



Scheme 3B.1 Salt free synthesis of dibismuthene and distibine using organosilicon reducing agent.

The reduction of main group metal halides into their respective low valent state require specific reducing agents. Also, the by-products generated in the reaction is difficult to separate from the product and may react with a low valent metal centre. To overcome this problem, Sasamori and co-workers achieved the salt free synthesis of distibine and dibismuthene¹² using organosilicon reducing agent¹³ (Scheme 3B.1). The potential of organosilicon compounds are already used in salt free synthesis of low valent transition metals (early and late)¹⁴ and in organic synthesis.¹⁵ We have also utilize this organosilicon reducing agent in the synthesis of heavier congener of carbene in one pot (Scheme 3B.2).¹⁶



Scheme 3B.2 One pot synthesis of Germylene and Stannylene.

Scope of the present work

The accumulation of net positive charges and accompanying coulombic repulsions within one molecule provide an electrostatic impediment to bis(chlorogermlyiumylidene) isolation. However, the isolation of bis(chlorogermlyiumylidene) has remained as valuable synthetic

target both on fundamental grounds and their potential applications. Also, the potential of the main group compound in organic transformations is rarely utilized.

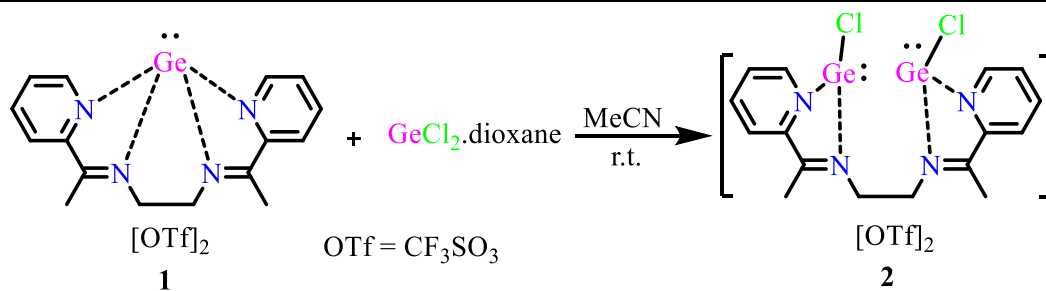
Herein we have stabilized the bis(chlorogermylumylidene) in a multidentate ligand framework, which has a flexible backbone. The complex is characterized using single crystal XRD and by NMR techniques. We have also synthesized elusive pyridyl substituted piperazine molecule, which was unrealized by transition metals and other synthetic routes with proper stereoselectivity. In this transformation, germanium plays a very crucial role of bringing together two imine units of ligand and also lowering down the reduction potentials of the ligand. The coordination of ligand with germanium in intermediate plays an essential role in giving the stereoselectivity. The intermediate was also characterized by SC-XRD and NMR techniques.

3B.2 Results and Discussion

3B.2.1 Bis(Chlorogermylumylidene)

In the last section 3A, we have reacted germanium (II) dication **1** with transition metal to check the nucleophilicity, and it did act as an electron donor. In present chapter, we have strategically manipulated the stabilization of two $[\text{GeCl}]^+$ units (compound **2**, Scheme 3B.3) within a flexible tetra-dentate 2,7-bis(2-pyridyl)-3,6-diazaocta-2,6- diene (**L**) ligand. In an effort to introduce two cationic germanium units within the tetradentate ligand **L**, we reacted Ge(II) dication $[\text{LGe}][\text{OTf}]_2$ **1** with one equivalent of GeCl_2 .dioxane in acetonitrile solvent. Overnight stirring at room temperature followed by complete removal of the solvent led to the isolation of the **L** stabilized bis(chlorogermylumylidene) **2** in a very high yield of 93% (Scheme 3B.3). Compound **2** was characterized using NMR techniques and single-crystal X-ray crystallography. UV-Vis spectroscopy in acetonitrile revealed the longest wavelength absorption at $\lambda_{\text{max}} = 337 \text{ nm}$ ($\epsilon = 4457 \text{ M}^{-1}\text{cm}^{-1}$). The ^{19}F NMR spectrum shows a single peak at -79.31 ppm revealed the triflates are free from the coordination sphere and have no interaction.

Interestingly, the formation of **2** proceeds through redistribution of chloride amongst the Ge centers in **1** and GeCl_2 .dioxane each, maintaining the overall atom economy. Notably, the straightforward reaction of GeCl_2 .dioxane with ligand **L** maintaining 2:1 stoichiometry in the presence or absence of chloride abstracting agent has always led to the isolation of



Scheme 3B.3 Reaction of **1** with one equivalent of $\text{GeCl}_2 \cdot \text{dioxane}$, yielding bis(chlorogermylumylidene) **2**.

monochlorogermylumylidene exclusively, where only one $[\text{GeCl}]^+$ unit was coordinated by the two imino N atoms. Presumably, the reaction occurs through auto-ionization due to electrostatic preference for stabilization of monocation

3B.2.2 Solid State Structure

Compound **2** crystallized in the P-1 space group as observed in the X-ray analysis (Table 1). In the molecular structure, the dicationic part comprises of the neutral ligand L hosting two distorted trigonal pyramidal Ge centers that are each coordinated by N_{imine} , N_{pyridyl} , and chlorido group (Figure 3B.2). The bonding features at both the Ge sites reproduce the benchmark reported chlorogermylumylidenes.[2] The Ge-N bond distances in **2** fall in the lower end of the usual range,[2] suggesting relatively strong $\text{N} \rightarrow \text{Ge}$ donations. The torsional degree of the $-(\text{CH}_2)_2-$ linker leads to a $\text{Cl1-Ge1}\cdots\text{Ge2-Cl2}$ dihedral angle of $99.32(4)^\circ$ with $\text{Ge1}\cdots\text{Ge2}$ separation of $5.1094(9) \text{ \AA}$.

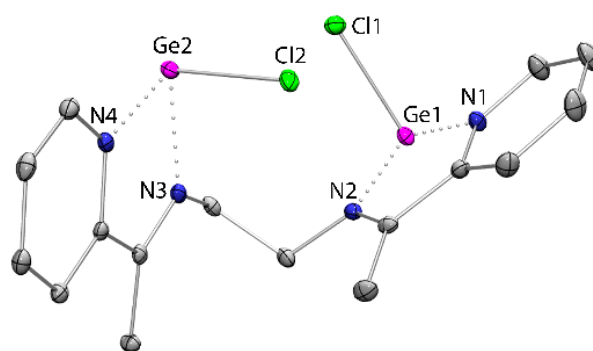


Figure 3B.2 Molecular structure of the di-cationic part of **2** in the solid state (thermal ellipsoids at 30%, H atoms and triflate counter anions omitted for clarity). Selected bond lengths [\AA] and angles [$^\circ$]: Ge1-N1 2.043(3), Ge1-N2 2.054(3), Ge1-Cl1 2.2965(9), Ge2-N3 2.074(3), Ge2-N4 2.071(3), Ge2-Cl2 2.2905(9); N1-Ge1-N2 77.85(11), N1-Ge1-Cl1 88.98(8), N2-Ge1-Cl1 91.35(8), N3-Ge2-N4 77.34(10), N3-Ge2-Cl2 93.76(8), N4-Ge2-Cl2 88.96(8).

There are no close contacts between the two triflate anions and the Ge(II) cationic centers (the closest Ge- O_{triflate} separation is 2.933(3) Å).⁴ All the S-O distance are > 1.44 Å indicate the triflate are ionic in nature and have no interaction with Ge (II) centre.

3B.2.3 Computational Details

We have performed the DFT calculations to ascertain the electronic nature of **2** at the B3LYP level, using 6-31G(d,p) as the basis set. The optimized geometry **2'** of the bis(chlorogermylumylidene) (without the two triflate anions) show congruence with the key metric parameters of the X-ray geometry. The HOMO and HOMO-1 frontier orbitals correspond to the maximum contributions from the lone pairs on two Ge centers (Figure 3B.3).

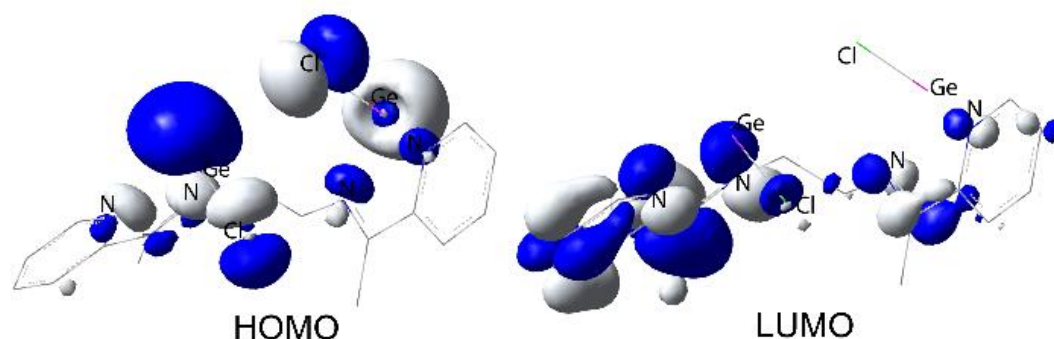


Figure 3B.3 Relevant contour plots of **2'** at isovalue 0.03 au.

The four sets of deep-seated orbitals HOMO-11 and HOMO-14 reveal 3c-4e interaction between vacant Ge p-orbital and the lone pairs on N (imino and pyridyl) atoms at both the sites (Figure 3B.4). The average Ge-N Wiberg bond indices (WBI) value is 0.37, and the Mulliken charges on Ge is 0.58. The electron density resides majorly on iminopyridyl unit of the ligand with anti-bonding character in both LUMO and LUMO+1 (Figure 3B.3).

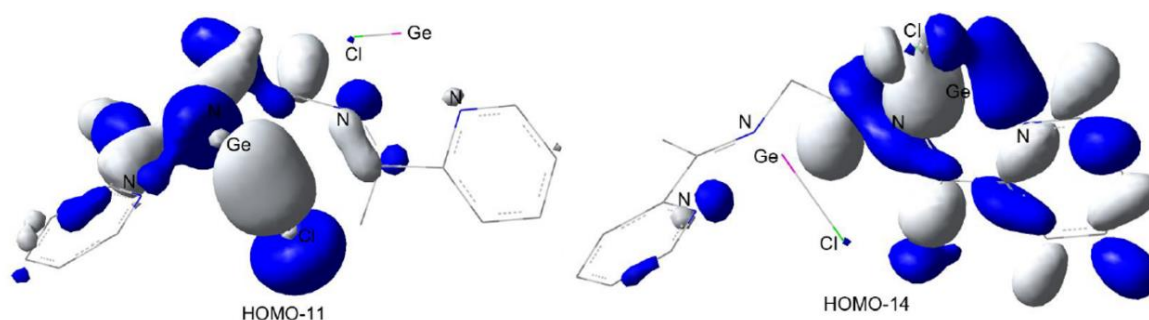
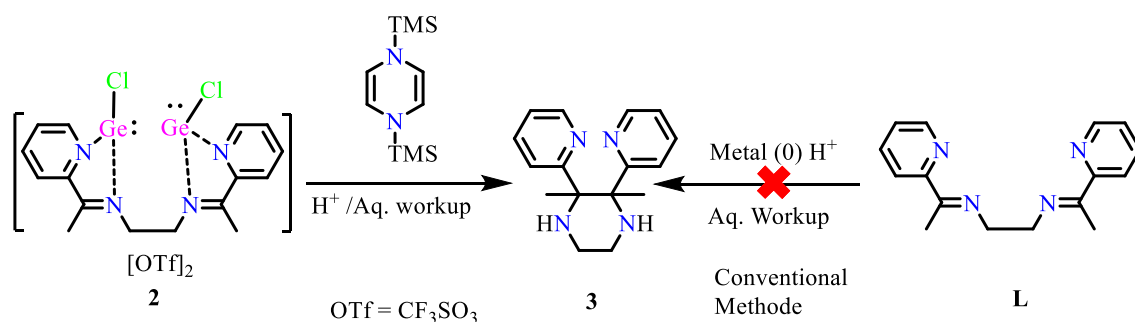


Figure 3B.4 Relevant contour plots of HOMO-11 and HOMO-14.

3B.2.4 Reduction of Bis(Chlorogermylumylidene)

The frontier electronics has inspired us to reduce **2**, envisaging the possible electron transfer to the bisimine ligand and subsequent reductive cyclization. Indeed, the reduction of **2** with one equivalent of 1,4-bis-(trimethylsilyl)-1,4-diaza-2,5-cyclohexadiene as the reductant in acetonitrile at 0°C, followed by acidification and aqueous workup effortlessly led to the formation of the unprecedented 2,3-dimethyl-2,3-di(pyridin-2-yl) piperazine **3** (Scheme 4) in an acceptable yield of 70%. Compound **3** was characterized using NMR techniques, which showed the absence of imine carbons and the formation of a new C-C bond in the ¹³C NMR spectrum. Only one diastereomer has been observed in the ¹H NMR of the crude reaction mixture.

Furthermore, a clean metal-free reduction of bis(chlorogermylumylidene) **2** under mild conditions precisely using organosilicon reductant¹⁷ has ultimately led to the quantitative formation of the hitherto unknown 2,3-di(pyridin-2-yl) substituted piperazine **3** (Scheme 3B.4) with high diastereoselectivity. Piperazine **3** provides a three-dimensional multi-dentate ligand topology which originates from unique piperazine backbone, appropriate in catalysis. Noteworthy, although piperazines are ubiquitous in biologically active compounds¹⁸ and used as a ligand in catalysis.¹⁹ There are only limited synthetic routes to 2,3-disubstituted Piperazine.²⁰ The preparation of piperazine **3** stood inept using the conventional reductive coupling methods²⁰ or from the reduction of **2** involving standard metal- based reductants. In compound **2**, the redox non-innocent nature [21] of **L** endorses the electron transfer to the ligand center upon reduction. Herein, the explicit role of the two Ge centers in **2** for the reduction and subsequent intramolecular C-C coupling of the reduced bisimine maintaining high diastereoselectivity has been addressed. Notably, the reported piperazines derived from ketimine reductive cyclizations usually suffer from lower yields.²¹



Scheme 3B.4 Preparation of **3** from **2** by reductive cyclization.

In this study, the choice of reductant plays crucial role in the synthesis of compound **3**. The high solubility of the ionic compound **2** in acetonitrile, in adjunct to its redox potential (*vide infra*), allow the clean reduction of **2** in acetonitrile using the milder organosilicon reductant.¹³ Easily removable volatiles Me₃SiCl and pyrazine are the only by-products of this reduction. Thus, metal-free reduction of **2** occurs in a homogeneous medium and is devoid of the reductant-derived metal salt and possible over-reduced impurities. Quenching the reaction led to the isolation of **3** through privileged intramolecular C-C coupling of the reduced bisimine (Scheme 3B.4). No major competing intermolecular coupling²¹ was observed in the reaction.

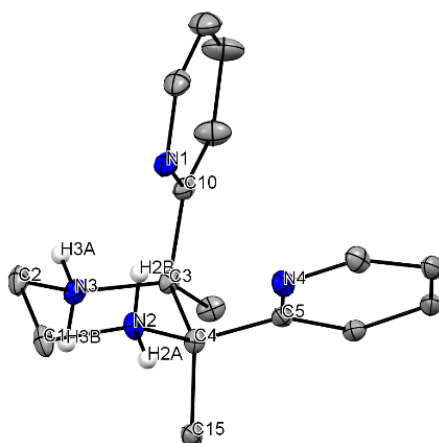
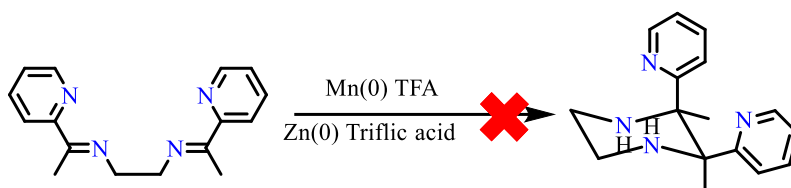


Figure 3B.5 Structure of **4** in the solid state (thermal ellipsoids at 30%, H atoms except the Namine-H, triflate anion omitted for clarity). Selected bond lengths [\AA]: C3-C4 = 1.581(3), C1-C2 = 1.506(4), C2-N3 = 1.481(4), N3-C3 = 1.531(3), C1-N2 = 1.498(3), N2-C4 = 1.511(3).

The stereochemical assignment of piperazine was confirmed to be *meso* from single crystal X-ray analysis of its doubly protonated piperazinium bis(trifluoromethanesulfonate) **4** derivative (Figure 3B.5). The piperazinium dication adopts chair configuration with the newly formed C-C bond distance being 1.581(3) \AA ,²³ which is longer than the other C-C = 1.506(4) \AA bond in the ring. More importantly, the two pyridyl groups on the adjacent stereocenters are in *cis*-disposition, on contrary to the earlier reports wherein the *trans*-2,3-diarylpiperazines were synthesized.²⁴

3B.2.5 Mechanistic investigation of Reductive Coupling



Scheme 3B.5 Unsuccessful attempts to synthesize **3**.

Attempts to reduce **2** with KC_8 ²⁵ in tetrahydrofuran medium followed by quenching led to the formation of trace amounts of piperazine (major product being the direct reduction of the C=N bonds to acyclic diamine), presumably due to inhomogeneity of the reduction medium. Piperazine **3** was inaccessible using the traditional reduction routes: reduction of **L** with $\text{Zn}(0)$ in the presence of methane sulfonic acid or $\text{Mn}(0)$ and trifluoroacetic acid led to complex mixtures with no detectable piperazine peaks. The absence of desired pyridyl substituted piperazine is due to possible coordination complexes with higher oxidation states of reducing metals.

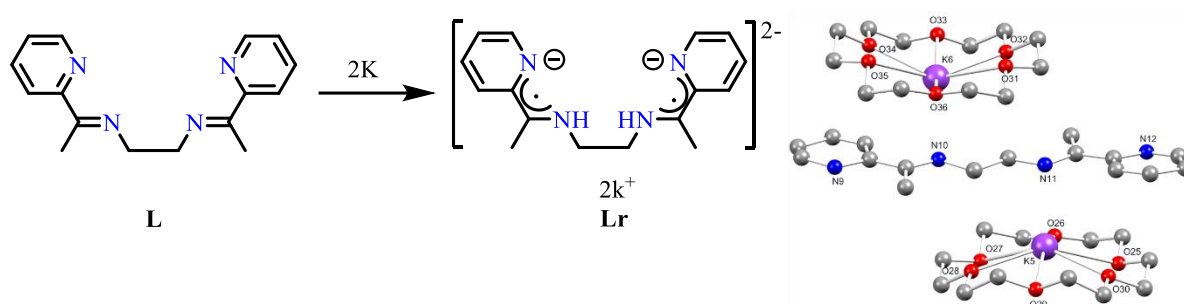


Figure 3B.6 Reduction of **L** leading to stable diradical dianion **Lr** and crystal structure of **Lr** (Ball and stick model, H atoms are omitted).

Although the reduction of **L** with potassium metal resulted in unambiguous formation of stable diradical dianion **Lr** (Figure 3B.6), no piperazine **3** was observed post acidification. As a matter of fact, 2,3-*N*-heterocycle functionalized piperazines are not known to be achieved through any of the above-mentioned routes. Rather, poly(*N*-heterocycle) functionalized piperazine has been synthesized through a visible light irradiated [3+3] coupling of azomethine ylide in the presence of Me_3Al ,¹⁷ or [3+3] dimerization of imines bearing anionic substituents.²⁴ Thus, the synthesis of **3** from the metal-free reduction of **2** gives access to both a new route and new multi-functionalized piperazine in acceptable yield.

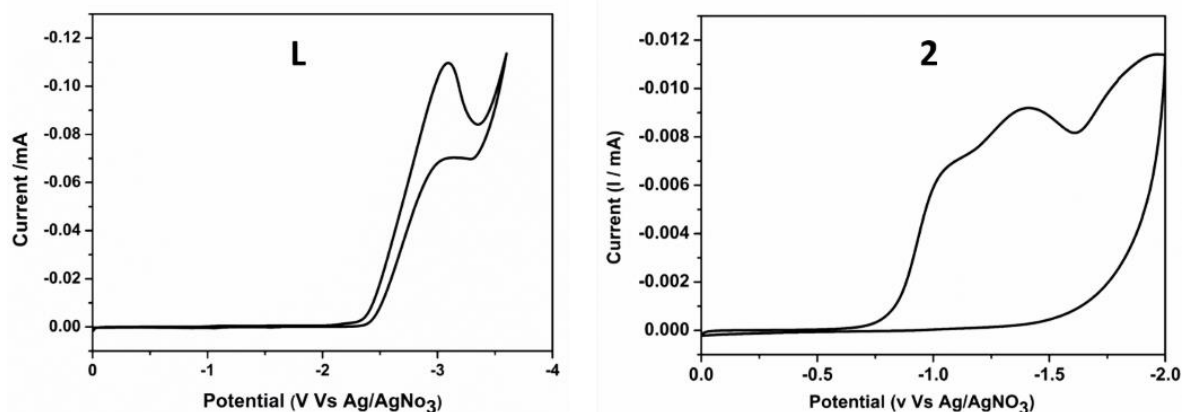


Figure 3B.7 Cyclic voltammogram of **L** and **2** (In THF containing 0.1 M tetrabutylammonium hexafluorophosphate as the supporting electrolyte recorded at a 100 mV s^{-1} scan rate).

The preparative profile of **3**, has steered our interest to study the unique role of the two $[\text{GeCl}]^+$ units in the pro-ligand compound **2**. Also, the control experiments involving the free ligand and organosilicon reductant was indicative of the key requirement of Ge cationic units for this transformation.

In order to understand the necessity of the cationic Ge unit in C-C coupling, we performed a cyclic voltammetry study. The bis(α -iminopyridine) **L** undergoes irreversible reduction at a very high potential of -3.2 V (vs. Ag/Ag^+ reference electrode) as observed in the cyclic voltammogram in THF solvent (Figure 3B.7) (no peaks found within the electrochemical window of acetonitrile); corresponding $\Delta E_{\text{HOMO-LUMO}} = 117.80 \text{ kcal/mol}$ from DFT calculations. Compound **2** shows irreversible reduction peaks in the potential range of -1.0 to -1.7 V in acetonitrile medium (Figure 3B.7). Thus, the coordination of two Lewis acidic $[\text{GeCl}]^+$ units to **L** effectively lowers the energy levels (corresponding $\Delta E_{\text{HOMO-LUMO}} = 82.15 \text{ kcal/mol}$). The reduction potential of the organosilicon reducing agent was also carried out in acetonitrile solvent show the reduction potential of -1.2 V .

Reduction of **2** using the organosilicon reductant in acetonitrile at 0°C afforded a dark green-blue solution ($\lambda_{\text{max}} = 720 \text{ nm}$) in the absorption spectra (Figure 3B.8) that was stable up to a period of 4 hours (stable up to ca. 1 hour at room temperature). The radical character of this solution²⁶ was evidenced by its EPR spectrum in acetonitrile. A 100 K X-band CW EPR spectrum of in situ generated green-blue solution and frozen subsequently features a strong signal at 3360 G ($g = 1.999$) and a weak intensity resonance at half-field 1687 G (due to forbidden transition $\Delta m_s = \pm 2$) (Figures 3B.8), corroborating the triplet state²⁷ of the persistent²⁸ diradical species **2r** (proposed structure in scheme 3B.3 and computational evidence).

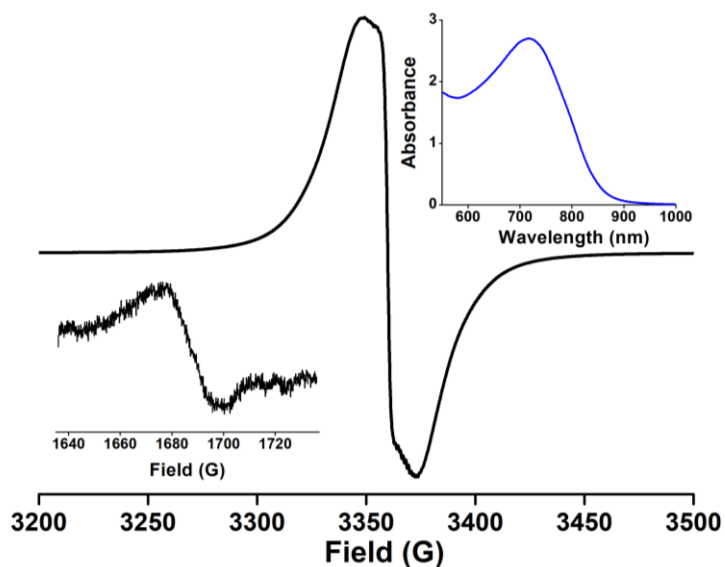


Figure 3B.8 EPR spectrum of **2r** in acetonitrile at 100 K, showing half-field resonance in the bottom left; the top right showing absorbance of **2r** ($\lambda_{\text{max}} = 720$ nm).

On the contrary, two-electron reduction of **L** gave stable isolable diradical dianion **Lr**, due to stabilization through electron delocalization²⁷ in the imino pyridyl sites. In the case of **2r**, the electron avidity of **L** gives impetus for electron transfer ensuing initial reduction. Compared to the stable nature of diradical dianion **Lr**, the persistence of **2r** might arise from the localization of electron spin on the imino carbons. Subsequent recombination through intramolecular C-C coupling provides solid proof for such a phenomenon.²⁹ It can be well perceived that the delocalized electron spin in the doubly reduced **L** provides a disincentive to ring closure.

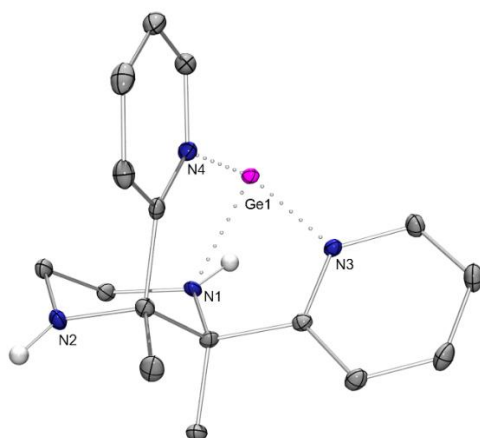
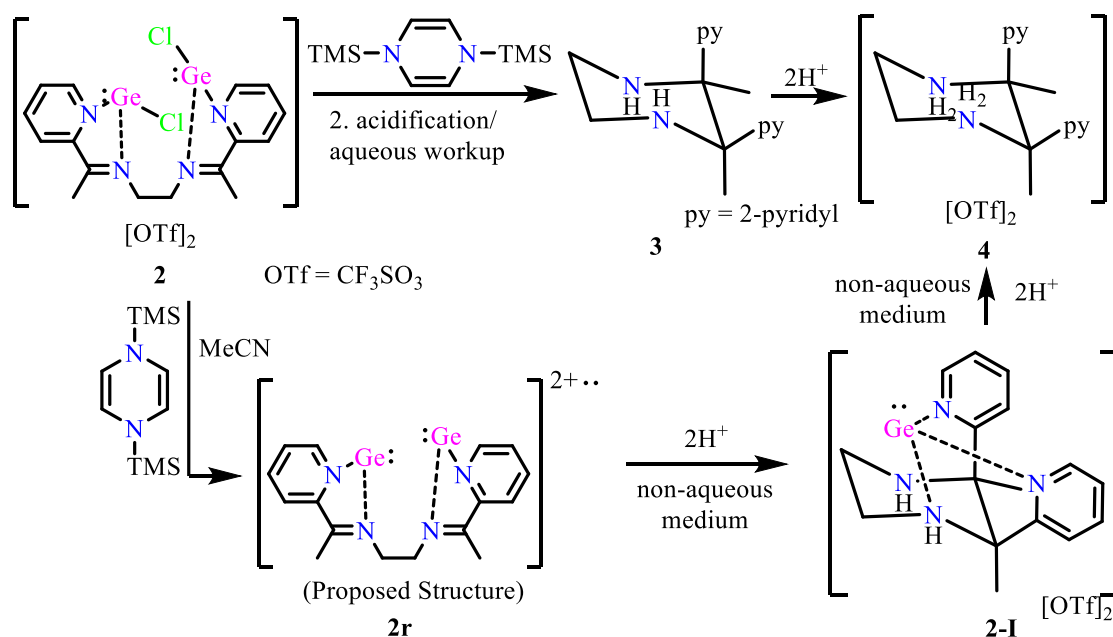


Figure 3B.9 Molecular structure of the di-cationic part of the intermediate **2-I** in the solid state (thermal ellipsoids at 30%, H atoms except N-H and triflate counter anions omitted for clarity).

Selected bond lengths [\AA] and angles [$^\circ$]: Ge1-N1 2.060(2), Ge1-N3 2.080(2), Ge1-N4 2.079(2); N1-Ge1-N3 77.69(9), N1-Ge1-N4 85.99(10), N3-Ge1-N4 84.79(9).

The anticipated formation of a Ge(II) dication as a consequence of electron migration to the ligand **L** subsequent to reduction appears conducive to preferential intramolecular C-C coupling via a template effect.³⁰ In our rigorous search for reaction intermediate, we have actually been successful in isolating the piperazine stabilized Ge(II) dication **2-I** (Scheme 3B.7). The intermediate **2-I** was formed upon protonation of the reduced mixture **2r** with two equivalents of acid in acetonitrile medium. Compound **2-I** crystallized out from the reaction medium (Figure 3B.9), which was extremely air- and moisture-sensitive. Subsequent protonation led to the piperazinium bis(trifluoromethanesulfonate) **4**. Moreover, the chelation³¹ in **2-I** controls the very high *cis*-stereoselectivity on the contrary to the usual steric preference for *dl* diastereomer.²¹

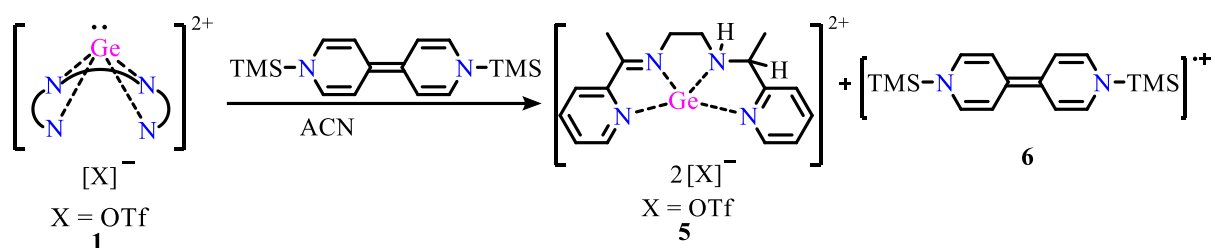


Scheme 3B.7 Proposed mechanism for synthesis of **3**.

3B.2.6 Reduction of Germanium (II) Dication and Chlorogermylumylidene

The unachieved isolation of radical cation of germanium was tried in another way, the Germanium (II) dication **1** was reacted with 4,4'-bipyridine based organosilicon reducing agent (1,1'-bis(trimethylsilyl)-1H,1'H-4,4'-bipyridinylidene) with stoichiometric ratio. The crystals of amino-imino stabilized germanium (II) dication **5** was obtained along with radical cation of 1,1'-bis(trimethylsilyl)-1H,1'H-4,4'-bipyridinylidene **6** (Scheme 3B.8). The crystals of compound **5** was characterized by SC-XRD in the solid state, but in the solution state, they

were readily decomposing. The intense blue color crystal of radical cation is very stable and also characterized by single crystal XRD.



Scheme 3B.8 Synthesis of **5** from **1**.

The organosilicon reducing agent reduces the germanium dication by one electron turning it to the radical cation of germanium (II), but the species is very reactive, which took a proton and hydrogen atom quickly from solvent turning again to dication **5**. This is a fascinating strategy to reduce one imine bond selectively out of two equivalent imine bonds.

The mono(chlorogermylumylidene) was also reacted with 0.5 Equiv. of 1,4-bis-(trimethylsilyl)-1,4-diaza-2,5-cyclohexadiene lead to formation of compound **5**. This reaction also follows a similar path as above via persistent radical cation of germanium.

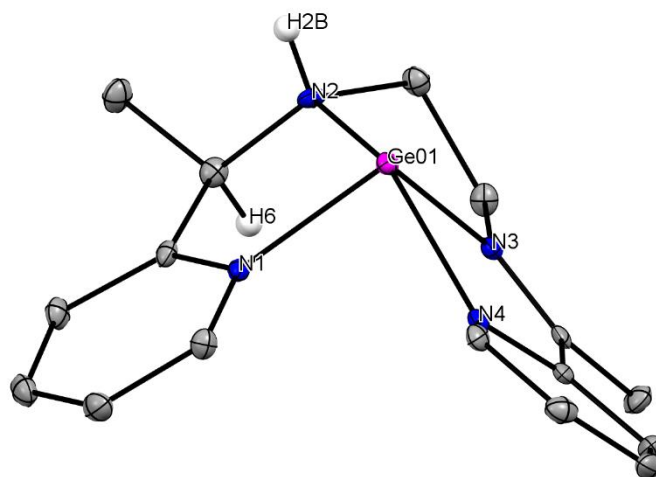


Figure 3B.10 Molecular structure of the di-cationic part of the intermediate **5** in the solid state (thermal ellipsoids at 30%, H atoms except N-H and triflate counter anions omitted for clarity). Selected bond lengths [Å] and angles [°]: Ge01-N1 2.049(2), Ge01-N3 2.052(2), Ge01 - N2 2.132(2), Ge01-N4 2.290(2); N1-Ge1-N2 77.849(9), N2 - Ge01- N3 78.62(10) N1-Ge1-N4 87.96(10), N3-Ge1-N4 73.33(9).

Compound **5** crystallized in $P\bar{1}$ space group along with a solvent molecule in the asymmetric unit cell. The torsional magnitude of $-(\text{CH}_2)_2$ - linker in ligand backbone and one amine nitrogen (N2) causes the four nitrogen atoms of ligand placed in slightly distorted basal coordinating plane (Fold angle of 32.56° between N2-N3-N4-N1) with Ge(II) center displaced perpendicular by 0.985 \AA , overall forming a domed shape structure (The sum of bond angle around Ge(II) center is 317.75°). The amino nitrogen N2-Ge01 distance is 2.132 \AA , whereas imino nitrogen N3-Ge01 distance is 2.053 \AA , revealed the stronger interaction of imino nitrogen with germanium(II) compare to amino nitrogen.

Interestingly reaction between **1** and 1,1'-bis(trimethylsilyl)-1H,1'H-4,4'-bipyridinylidene occur via single electron transfer, finally giving the product **5** and **6**. The 1,1'-bis(trimethylsilyl)-1H,1'H-4,4'-bipyridinylidene can act as electron donor-acceptor, and such activity is harvested in the next chapter for C-C and C-B bond-forming reactions.

3B.3 Conclusion

In conclusion, we have been successful in the strategic disposition of two $[\text{GeCl}]^+$ units within the bis(α -iminopyridine) leading to the first example of bis(chlorogermylumylidene) **2**. The two $[\text{GeCl}]^+$ units in **2** play dual role of both Lewis acid promoting reduction, and biasing chelation controlled intramolecular coupling with complete stereoselectivity. This meaningful chemical transformation to the unprecedented 2,3-di(pyridin-2-yl) functionalized piperazine **3** has potential relevance for considerations in catalysis. The isolation of bis(chlorogermylumylidene) has fundamental merits beyond the synthesis of piperazine.

3B.4 Experimental Details

3B.4.1 General Remarks

All manipulations were carried out under a protective atmosphere of argon, applying standard Schlenk techniques or in a dry box. Tetrahydrofuran was refluxed over sodium/benzophenone. Dichloromethane and acetonitrile were stirred and refluxed over calcium hydride and kept over molecular sieves. All solvents were distilled and stored under argon and degassed prior to use. CD_3CN ampoules were purchased from Sigma Aldrich and used as it is. All chemicals were used as purchased. Compound **1**²³ and the organosilicon reducing agent 1,4-bis(trimethylsilyl)-1,4-dihydropyrazine¹² were synthesized following the reported literature procedures. ^1H and $^{13}\text{C}\{^1\text{H}\}$ NMR spectra were referenced to external SiMe_4 using the residual signals of the deuterated solvent (^1H) or the solvent itself (^{13}C). ^{19}F NMR was referenced to external $\text{C}_6\text{H}_5\text{CF}_3$ (TFT). NMR spectra were recorded on Bruker AVANCE

III HD ASCEND 9.4 Tesla/400 MHz and Jeol 9.4 Tesla/400 MHz spectrometer. HRMS spectrum was acquired on Waters Acquity UPLC coupled with SYNAPT G2 mass spectrometer. Solution phase UV/Vis spectra were acquired using a Thermo-Scientific Evolution 300 spectrometer using quartz cells with a path length of 1 cm. Cyclic Voltammetry studies were performed with SP-300 Potentiostat/Galvanostat Biologic Science Instruments. EPR spectra were recorded on X-band Bruker EMX Plus at IIT Bombay and IISER Kolkata. Melting points were determined under argon in closed NMR tubes and are uncorrected. Elemental analyses were performed on Elementar vario EL analyzer. Single crystal data were collected on Bruker SMART APEX four-circle diffractometer equipped with a CMOS photon 100 detectors (Bruker Systems Inc.) with a Cu K α radiation (1.5418 Å).

3B.4.2 Synthetic Procedure

A. Synthesis of Bis(Chlorogermilyumylidene) 2

Compound **1** (0.5 g, 0.78 mmol) and GeCl₂.dioxane (0.18 g, 0.78 mmol) were dissolved in 30 mL of acetonitrile and stirred at room temperature for 12 hours. The solvent was removed completely under vacuum yielding 0.57 g (93%) of **2** (decomp. 153-155°C) as pale yellow solid.

Crystals suitable for X-ray measurement were grown by layering acetonitrile solution of the compound with diethyl ether at room temperature.

Characterization of **2**: ¹H NMR (400 MHz, Acetonitrile-*d*₃, TMS) δ = 9.18 (d, *J* = 4.9, 2H, *o*-Pyr-*H*); 8.60 (t, *J* = 7.5, 2H, *p*-Pyr-*H*); 8.52 (d, *J* = 8.2, 2H, *m*-Pyr-*H*); 8.16 (t, *J* = 6.2, 2H, *m*-Pyr-*H*); 4.61 (s, 4H, -CH₂-CH₂); 2.88 (s, 6H, -CH₃) ppm. ¹³C NMR (101 MHz, Acetonitrile-*d*₃, TMS) δ = 178.03 (C-CH₃); 148.95 (Pyr-Co); 146.91 (Pyr Co); 145.11 (Pyr-Cp); 130.88 (Pyr-Cm); 128.78 (Pyr-Cm); 122.45, 119.27 (CF₃SO₃); 47.71 (-CH₂-CH₂-); 17.04 (C-CH₃). ¹⁹F NMR (377 MHz, Acetonitrile-*d*₃, TFT) δ = -79.31 (TMSOTf- *F*) ppm. UV/Vis (acetonitrile) λ_{max} (ϵ) 337 nm (4457 M⁻¹cm⁻¹). Elemental Analysis: Calcd. for C₁₈H₁₈C₁₂F₆Ge₂N₄O₆S₂: C, 27.70; H, 2.32; N, 7.18. Found: C, 27.55; H, 2.71; N, 7.28.

B. Synthesis of 2-I

1,4-bis(trimethylsilyl)-1,4-dihydropyrazine (0.087 g, 0.38 mmol) was dissolved in 10 mL of acetonitrile and was added dropwise to a 20 mL acetonitrile solution of compound **2** (0.3 g, 0.38 mmol) maintaining the temperature at 0°C. The resultant intense green-blue solution was stirred for 10 minutes before adding trifluoroacetic acid (0.059 mL, 0.77 mmol). The volatile by-products were removed completely under vacuum. The solid was then redissolved in 8-10

mL of acetonitrile from which colourless single crystals of **2-I** appeared (crystallization yield = 0.036 g (15%)), (decomp. 164-166°C).

Characterization of **2-I**: ^1H NMR (400 MHz, Acetonitrile- d_3 , TMS) δ = 8.85 (d, J = 5.4, 2 H, *o*-Pyr-*H*); 8.30 (td, J = 8.2, 1.4, 2H, *p*-Pyr-*H*); 8.00(d, J = 8.3, 2H, *m*-Pyr-*H*); 7.79 (t, J = 6.3, 2H, *m*-Pyr-*H*); 5.29 (br., 2H, *NH*); 3.33 (br., 2H, - CH_2 -); 3.13(br., 2H, - CH_2 -); 1.99 (s, 6H, - CH_3) ppm. ^{13}C NMR (101 MHz, Acetonitrile- d_3 , TMS) δ = 157.19 (Pyr-Co); 146.17 (Pyr-Co); 145.44 (Pyr-Cp); 126.76 (Pyr-Cm); 126.23(Pyr-Cm); 122.28, 119.10 (CF_3SO_3); 63.77 (C- CH_3); 38.63 (- CH_2 - CH_2 -); 21.35 (C- CH_3) ppm. ^{19}F NMR (377 MHz, Acetonitrile- d_3 , TMS) δ = -79.46 (TMSOTf- *F*) ppm. Elemental Analysis: Calcd. for $\text{C}_{18}\text{H}_{20}\text{F}_6\text{GeN}_4\text{O}_6\text{S}_2$: C, 33.83; H, 3.15; N, 8.77. Found: C, 33.95; H, 3.42; N, 8.82.

C. Synthesis of Piperazine 3

1,4-bis(trimethylsilyl)-1,4-dihydropyrazine (0.058 g, 0.26 mmol) was dissolved in 10 mL of acetonitrile and was added dropwise to a 15 mL acetonitrile solution of compound **2** (0.2 g, 0.26 mmol) maintaining temperature at 0°C. The resultant intense blue-green solution was stirred for 10 minutes before quenching with trifluoroacetic acid (0.08 mL, 1.02 mmol). The volatile by-products were removed completely under vacuum. The solid residue was then washed with NaHCO_3 (10% w/v, ca. 10 mL) and the aqueous layer was extracted twice with ethyl acetate. The organic layer was dried over anhydrous Na_2SO_4 and concentrated giving yellow viscous oil. The viscous oil was dissolved in ~2 mL of dichloromethane and added dropwise to 20 mL of *n*-pentane giving a white precipitate. The white precipitate was dried under vacuum yielding 0.048 g (70%) of **3** (melting point 118 °C).

Characterization of **3**: ^1H NMR (400 MHz, Chloroform- d_3 , TMS) δ = 8.29 (ddd, J = 4.8, 1.9, 1, 2H, *o*-Pyr-*H*); 7.47 (td, J = 8.2, 2, 2H, *p*-Pyr- *H*); 7.26 (dt, J = 8.2, 1, 2H, *m*-Pyr-*H*); 6.97 (ddd, J = 7.5, 4.8, 1, 2H, *m*-Pyr-*H*); 4.50 (br., 2H, *NH*); 3.10- 3.27 (m, 4H, - CH_2 - CH_2 -); 1.87 (s, 6H, - CH_3) ppm. ^{13}C NMR (101 MHz, Chloroform- d_3 , TMS) δ = 162.62 (Pyr-Co); 146.94 (Pyr-Co); 136.53 (Pyr-Cp); 121.71 (Pyr-Cm), 121.24 (Pyr-Cm), 62.22 (C- CH_3); 40.21 (- CH_2 - CH_2 -); 23.72 (C- CH_3) ppm. Elemental Analysis: Calcd. For $\text{C}_{16}\text{H}_{20}\text{N}_4$: C, 71.61; H, 7.51; N, 20.88. Found: C, 71.79; H, 7.71; N, 20.92. HRMS (ESI-TOF) calculated for $[\text{C}_{16}\text{H}_{20}\text{N}_4 + \text{H}] +$ 269.1758; found 269.1788.

D. Synthesis of Piperazinium bis(trifluoromethanesulfonate) 4

Method I: 1,4-bis(trimethylsilyl)-1,4-dihydropyrazine (0.072 g, 0.32 mmol) was dissolved in 10 mL of acetonitrile and was added dropwise to a 20 mL acetonitrile solution of compound **2** (0.25 g, 0.32 mmol) maintaining temperature at 0°C. The resultant intense green-blue solution was stirred for 10 minutes before quenching with trifluoroacetic acid (0.1 mL, 1.28 mmol). The volatile by-products were removed completely under vacuum. The solid residue was then dissolved in 10 mL of tetrahydrofuran and filtered. The filtrate was concentrated and layered with diethyl ether to get colorless crystals of **4** (crystallization yield = 0.124 g (68%); decomp. 173-175 °C).

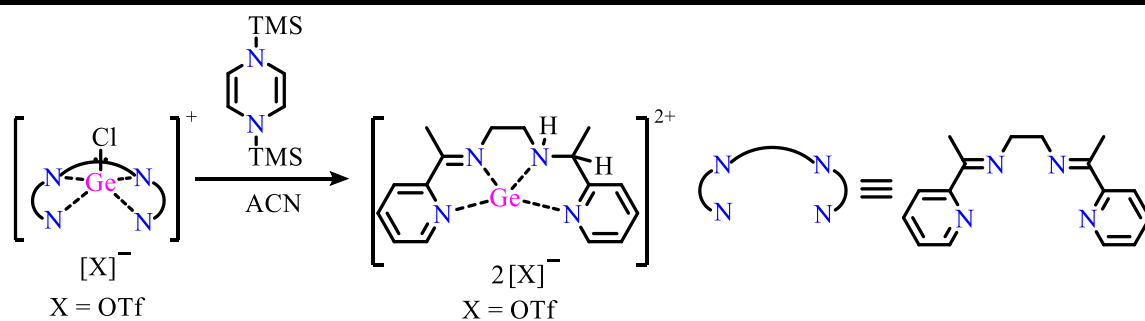
Method II: Trifluoromethanesulphonic acid (0.034 mL, 0.39 mmol) was added to 5 mL dichloromethane solution of Piperazine **3** (0.05 g, 0.19 mmol). The solution was stirred for 1 hour and then added to 20 mL of hexane resulting in white precipitate. The white precipitate was filtered, dried under vacuum yielding 0.09 g (86%) of **4** as white solid.

Characterization of **4**: ¹H NMR (400 MHz, Acetonitrile-*d*₃, TMS) δ = 9.07 (br., 4H, NH₂); 8.44 (ddd, *J* = 4.8, 1.8, 1, 2H, *o*-Pyr-*H*); 7.77 (td, *J* = 7.8, 1.4, 2H, *p*-Pyr-*H*); 7.42 (d, *J* = 8.2, 2H, *m*-Pyr-*H*); 7.34 (dd, *J* = 7.6, 4.9, 2H, *m*-Pyr-*H*); 4.11 (m, 2H, -CH₂-); 3.72 (m, 2H, -CH₂-); 2.17 (s, 6H, -CH₃) ppm. ¹³C NMR (101 MHz, Acetonitrile-*d*₃, TMS) δ = 153.12 (Pyr-Co); 147.81 (Pyr-Co); 138.52 (Pyr-Cp); 124.75 (Pyr-Cm); 122.55 (Pyr-Cm); 122.25, 119.10 (CF₃SO₃); 64.26 (C-CH₃); 36.71 (-CH₂-CH₂-); 19.28 (C-CH₃) ppm. ¹⁹F NMR (377 MHz, Acetonitrile-*d*₃, TMS) δ = -79.40 (TMSOTf-*F*) ppm. Elemental Analysis: Calcd. For C₁₈H₂₂F₆N₄O₆S₂: C, 38.03; H, 3.90; N, 9.86. Found: C, 38.15; H, 4.01; N, 10.05.

E. Synthesis of **5**

I. From **1**

The solution of 1,1'-bis(trimethylsilyl)-1H,1'H-4,4'-bipyridinylidene in 5 mL acetonitrile was dropwise added to solution of **1** in 10 mL of acetonitrile. Reaction was turned intense blue and kept for stirring at room temperature for 2 hrs. The solution was concentrated and kept for crystallization at -30 °C to get yellow crystals of **5** (30%) and blue crystals of **6** in (50%). The compound **5** was very unstable in solution state, NMR measurement was not possible in acetonitrile solvent.



Scheme 3B.9 Reduction of Chloro(germyliumylidene).

II. From Chloro(germyliumylidene) (Scheme 3B.9)

Solution of 1,4-bis(trimethylsilyl)-1,4-dihydropyridazine in 10 mL of acetonitrile solvent was added dropwise to solution of Chlorogermlyiumylidene at room temperature. Reaction mixture turned intense blue and stirred it for 2 hr at room temperature. The solvent was evaporated from reaction mixture to get blue solid, which was again dissolved in acetonitrile and kept for crystallization at $-30\text{ }^{\circ}\text{C}$. After one week crystals of **5** was appeared with the yield of 50%. The compound **5** was very unstable in solution state, NMR measurement was not possible in acetonitrile solvent

F. Synthesis of Lr

Freshly cut potassium (0.063 g, 1.61 mmol) was added to a 15 mL tetrahydrofuran solution of ligand L (0.2 g, 0.75 mmol) at room temperature. The intense red-green reaction mixture was stirred for 24 hours and then filtered. Subsequently 18-crown-6 (0.4 g, 1.50 mmol.) was added to the filtrate and stirred. The solvent was removed under vacuum. The residue was washed with hexane and dried to obtain a green solid of **Lr** (yield = 0.53 g (81%)).

Crystals suitable for X-ray measurement were grown from the saturated solution of THF at $-40\text{ }^{\circ}\text{C}$.

G. Control NMR Experiments

a. In a NMR tube, 0.6 mL of acetonitrile- d_3 was added to a mixture of ligand L (0.03 g, 0.11 mmol) and 1,4-bis(trimethylsilyl)-1,4-dihydropyridazine (0.025 g, 0.11 mmol) taken at room temperature, and shaken well. The NMR spectra was recorded after 12 hours.

b. In a NMR tube, 0.6 mL of acetonitrile- d_3 was added to a mixture of ligand L (0.035 g, 0.13 mmol) and 1,4-bis(trimethylsilyl)-1,4-dihydropyridazine (0.029 g, 0.13

mmol) taken at room temperature, and shaken well. Subsequently, HCl.Et₂O (0.26 mL, 0.52 mmol) was added to the mixture. The NMR spectra was recorded after 6 hours.

c. In a NMR tube, 0.6 mL of acetonitrile-d₃ was added to a mixture of ligand **L** (0.032 g, 0.12 mmol) and 1,4-bis(trimethylsilyl)-1,4-dihydropyrazine (0.027 g, 0.12 mmol) taken at room temperature, and shaken well. Subsequently, trifluoroacetic acid (0.037 mL, 0.48 mmol) was added to the mixture. The NMR spectra was recorded after 6 hours.

H. Trials to synthesize Piperazine **3** using conventional methods

TR1: Reduction of **2** with KC₈

To a suspension of KC₈ (0.042 g, 0.31 mmol) in 10 mL of tetrahydrofuran kept at -78 °C, was added compound **2** (0.123 g, 0.16 mmol) suspended in 10 mL of tetrahydrofuran. The suspension was slowly warmed to room temperature and the yellow solution was stirred for a period of 4 hours. Subsequently, the reaction mixture was filtered and the filtrate was quenched with trifluoroacetic acid (0.048 mL, 0.63 mmol). The colourless solution was evaporated completely. The solid residue was then washed with NaHCO₃ (10% w/v, ca. 10 mL) and the aqueous layer was extracted thrice with ethyl acetate. The organic layer was dried over anhydrous Na₂SO₄, and evaporated under vacuum to give a viscous liquid.

TR2: Reduction of **L** with Zn(0)^{20d}

To a solution of ligand **L** (0.266 g, 1.0 mmol) in 20 ml of tetrahydrofuran, were added Zinc powder (0.654 g, 10.0 mmol) and methanesulfonic acid (MsOH) (0.65 mL, 10 mmol) maintaining temperature at 0°C. The suspension was stirred for 12 hours at this temperature. Subsequently, 20 mL of saturated aqueous solution of NaHCO₃ was added, and the solution was filtered. The filtrate was extracted with dichloromethane, the organic layer was dried over MgSO₄ and evaporated to give an orange solid.

TR3: Reduction of **L** with Mn(0)^{20c}

Mn(0) (0.093 g, 1.69 mmol) was suspended in 5 mL of acetonitrile. The ligand **L** (0.3 g, 1.12 mmol) dissolved in 20 ml of toluene was added to the Mn(0) suspension at room temperature. Trifluoroacetic acid (0.26 mL, 3.38 mmol) was then added to this stirring suspension, and the mixture was stirred at room temperature for 6 hours. The organic solvent mixture was evaporated and the residue was washed with saturated aqueous solution of Na₂CO₃. The aqueous layer was extracted with chloroform, and dried over anhydrous Na₂SO₄. The volatiles were evaporated to get a viscous yellow liquid.

TR4: Reduction of L with Na

Freshly cut sodium (0.023g, 1.0 mmol) was added to 20 ml tetrahydrofuran solution of ligand L (0.115 g, 0.43mmol). The intense red-brown reaction mixture was stirred at room temperature for 24 hours and then filtered. Trifluoroacetic acid (0.13 mL, 1.72 mmol) was then added to the filtrate. The solvent was removed under vacuum and the residue was washed with saturated aqueous solution of Na₂CO₃. The aqueous layer was extracted twice with chloroform. The organic layer was dried over anhydrous Na₂SO₄ and evaporated under vacuum to get a brown solid.

3B.4.3 Plots of NMR spectra

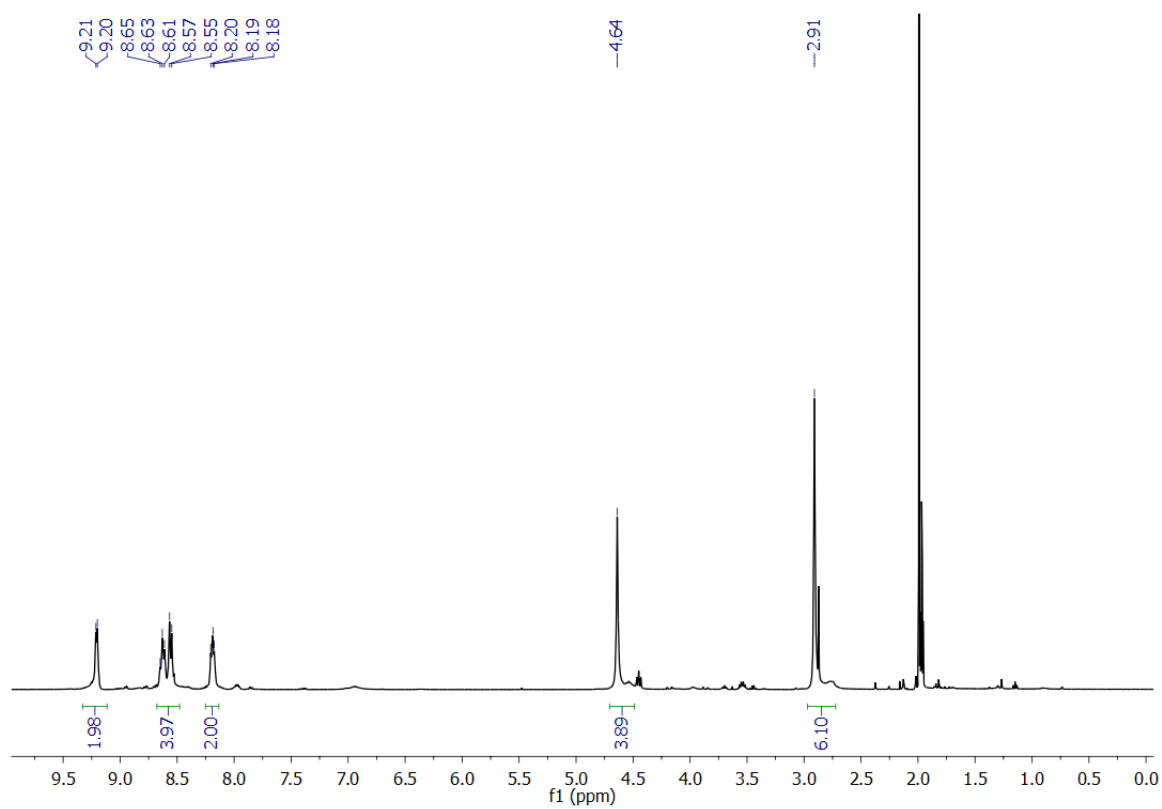


Figure 3B.11. ^1H NMR of Compound 2.

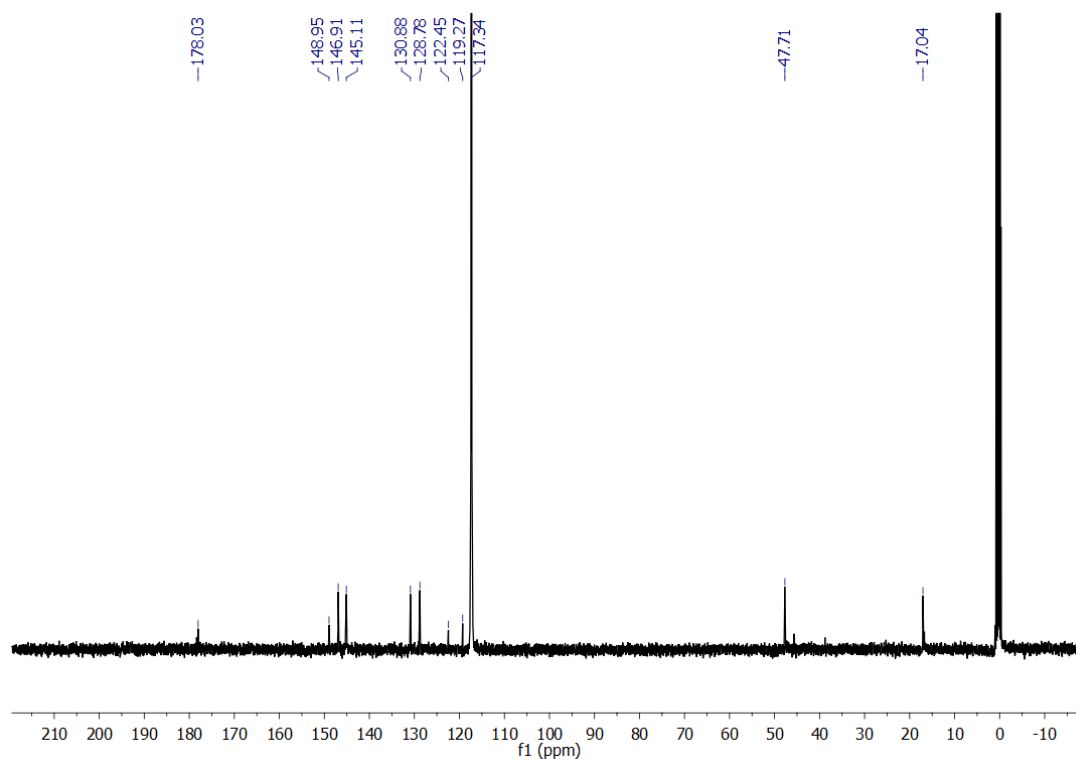


Figure 3B.12. $^{13}\text{C}\{^1\text{H}\}$ NMR of Compound 2.

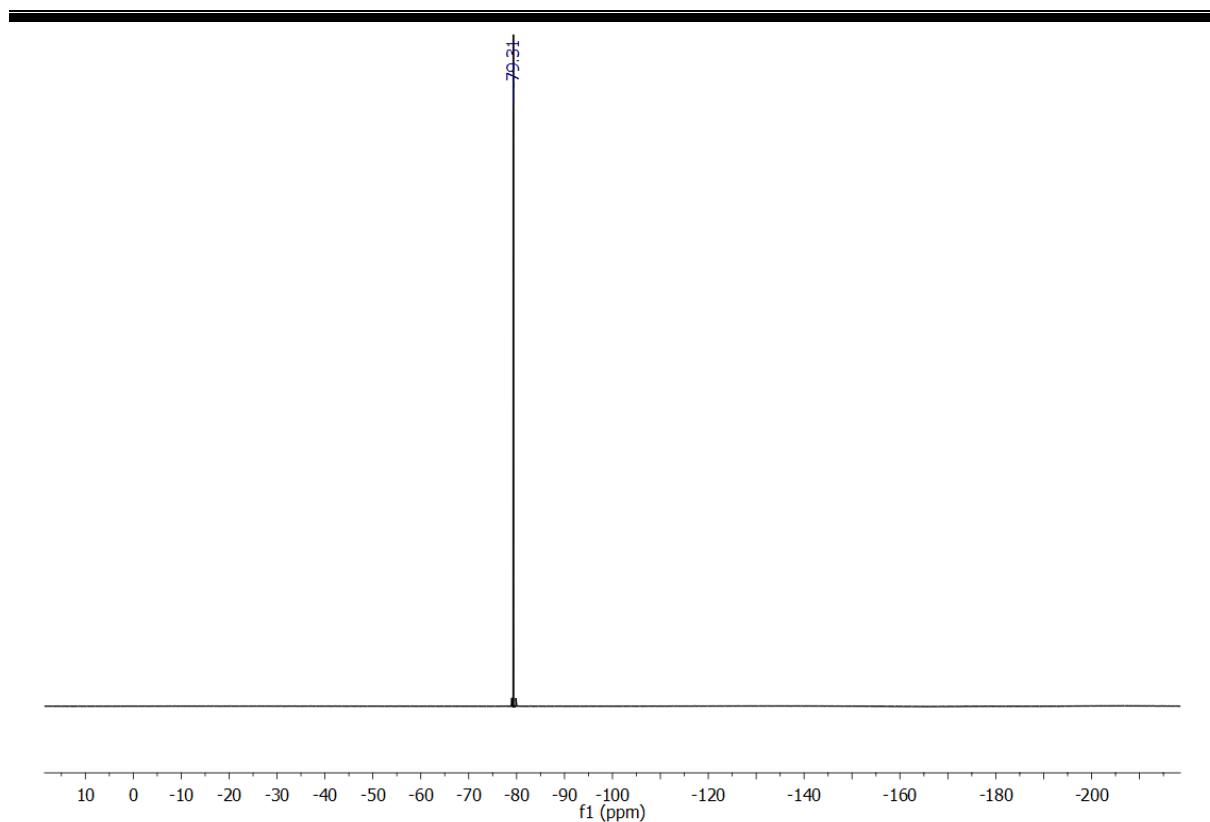


Figure 3B.13. $^{19}\text{F}\{^1\text{H}\}$ NMR of Compound 2.

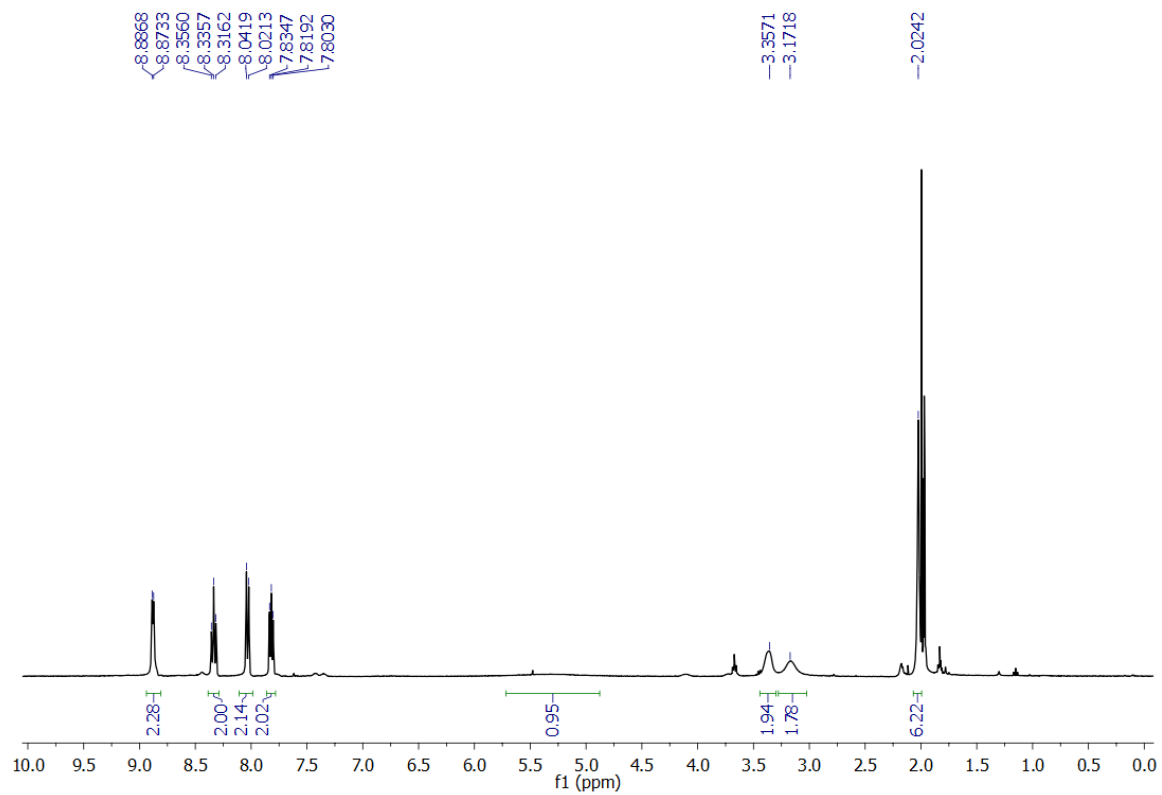


Figure 3B.14. ^1H NMR of Compound 2I.

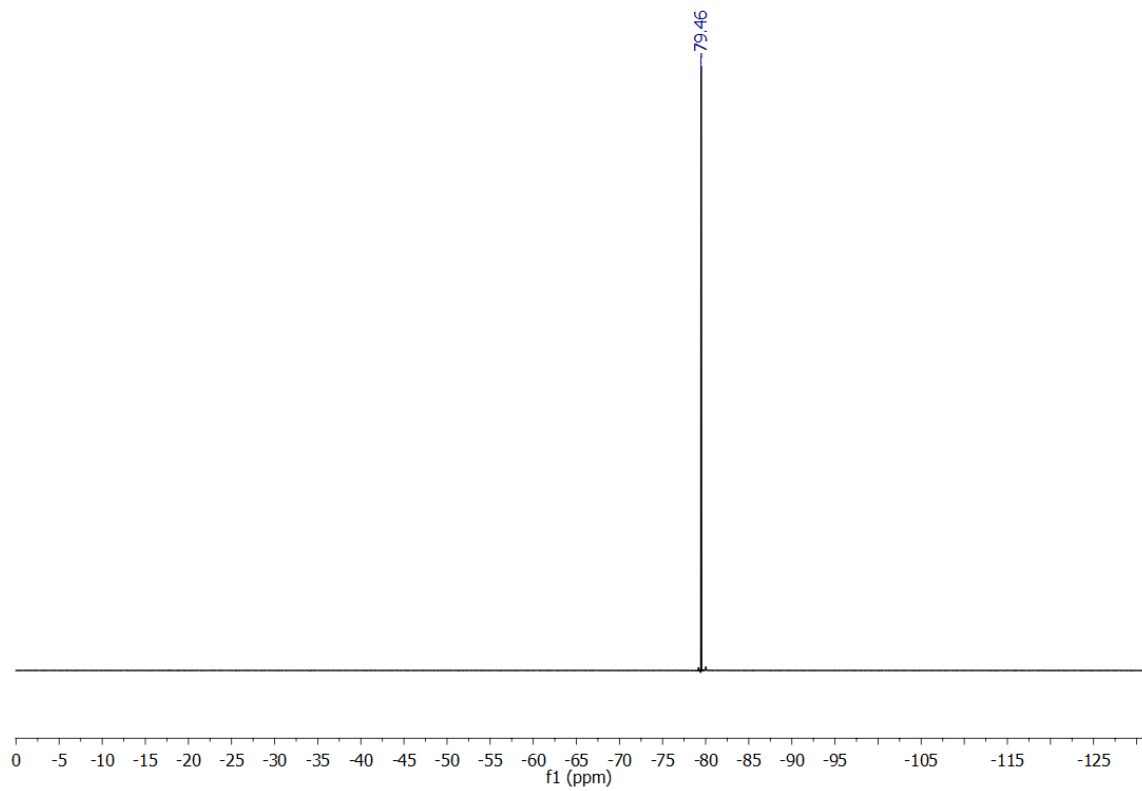


Figure 3B.15. $^{19}\text{F}\{^1\text{H}\}$ NMR of Compound **2I**.

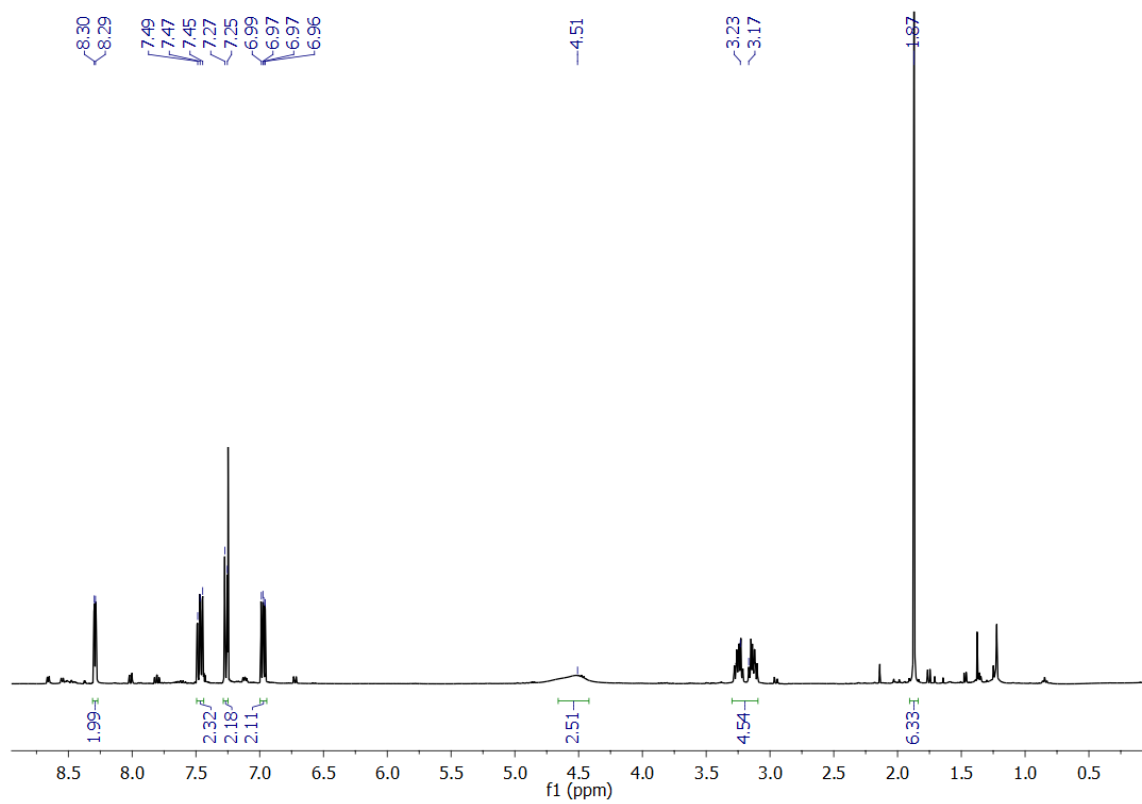


Figure 3B.16. ^1H NMR of Compound **3**.

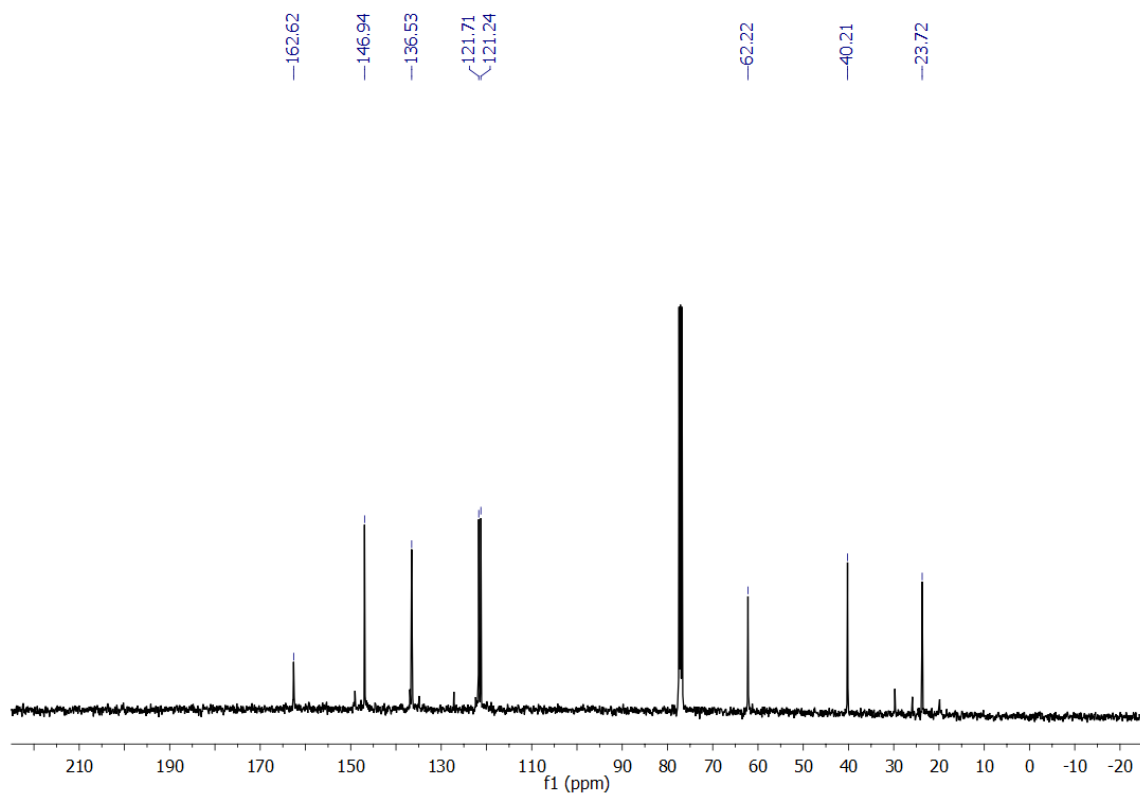


Figure 3B.17. $^{13}\text{C}\{^1\text{H}\}$ NMR of Compound **3**.

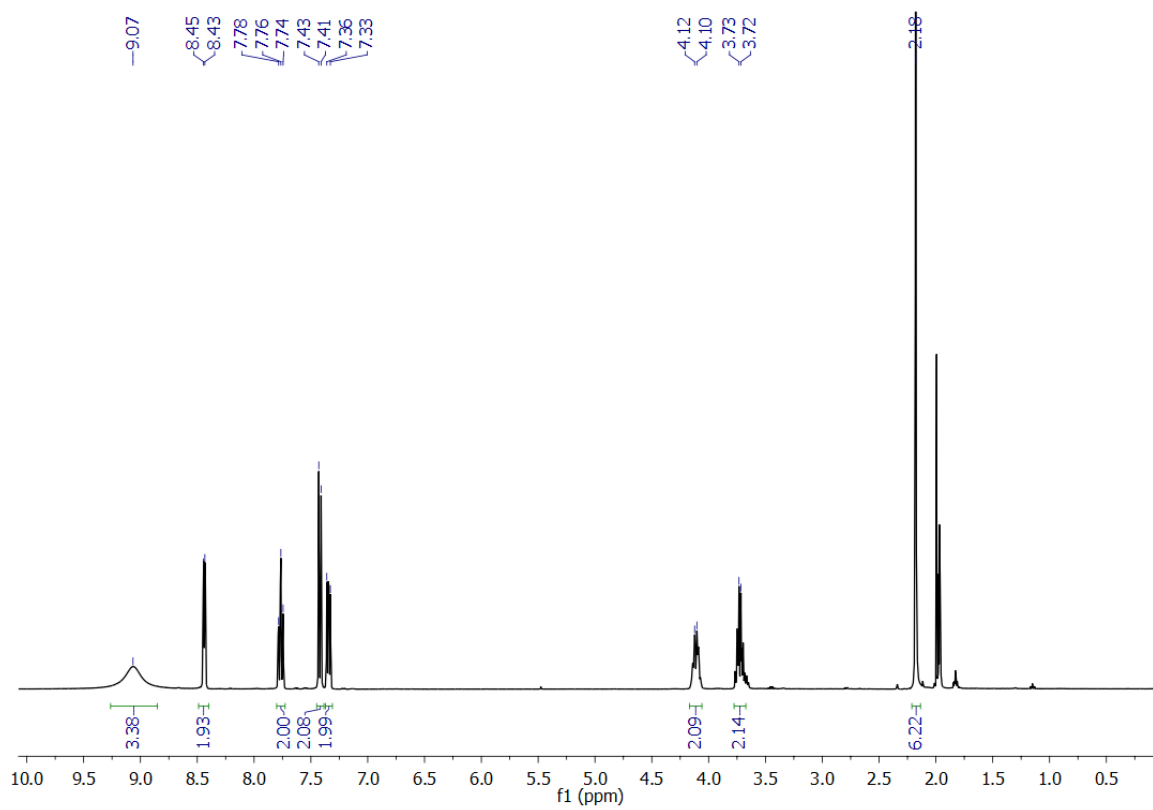


Figure 3B.18. ^1H NMR of Compound **4**.

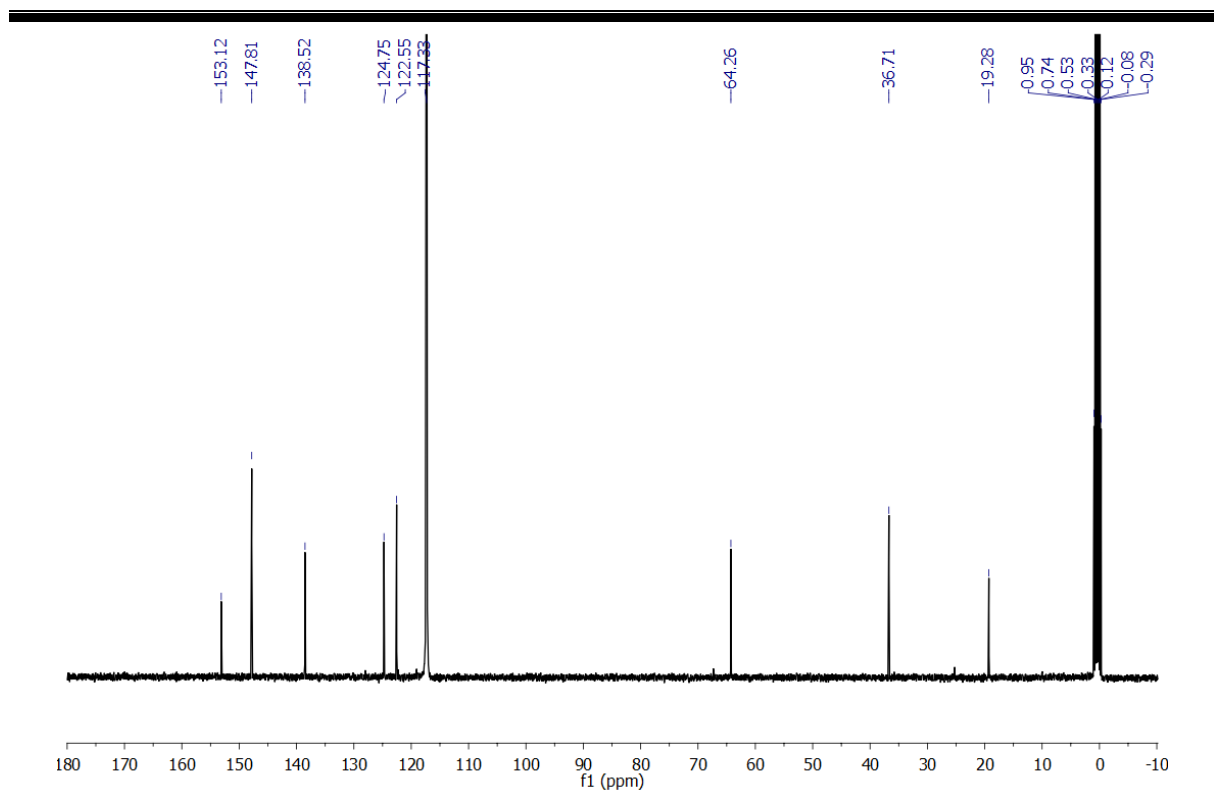


Figure 3B.19. $^{13}\text{C}\{^1\text{H}\}$ NMR of Compound 4.

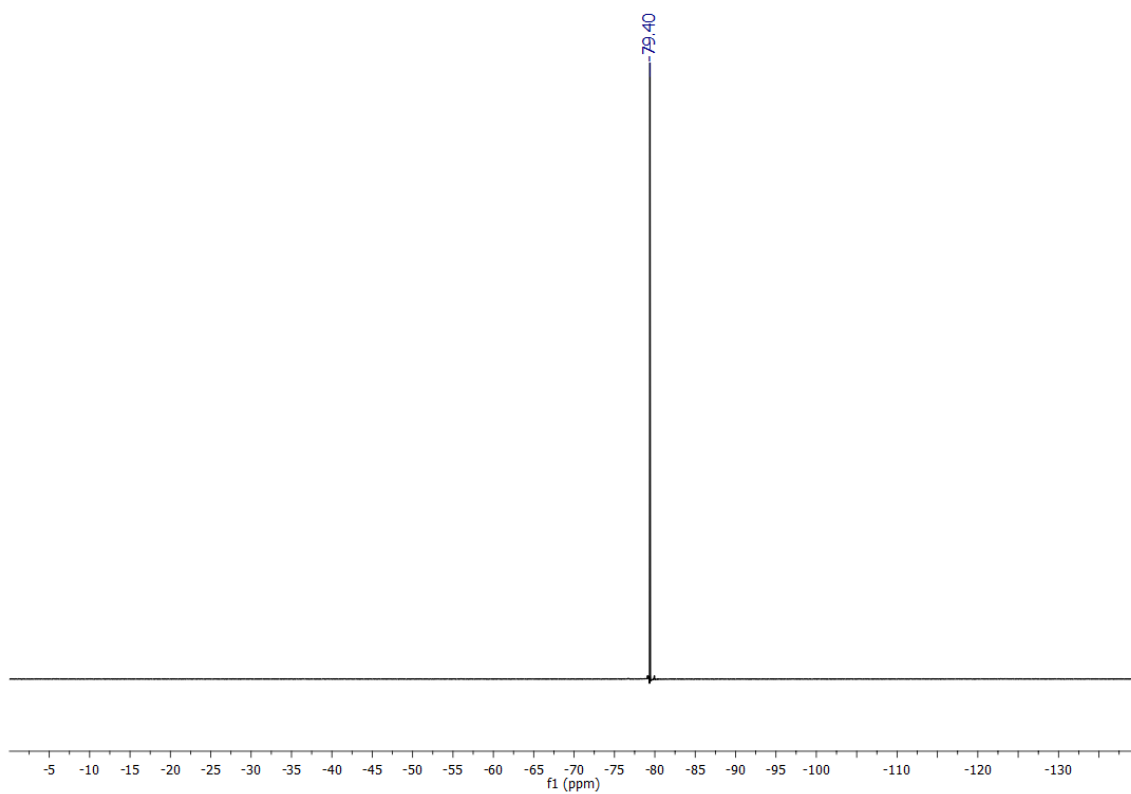


Figure 3B.20. $^{19}\text{F}\{^1\text{H}\}$ NMR of Compound 4.

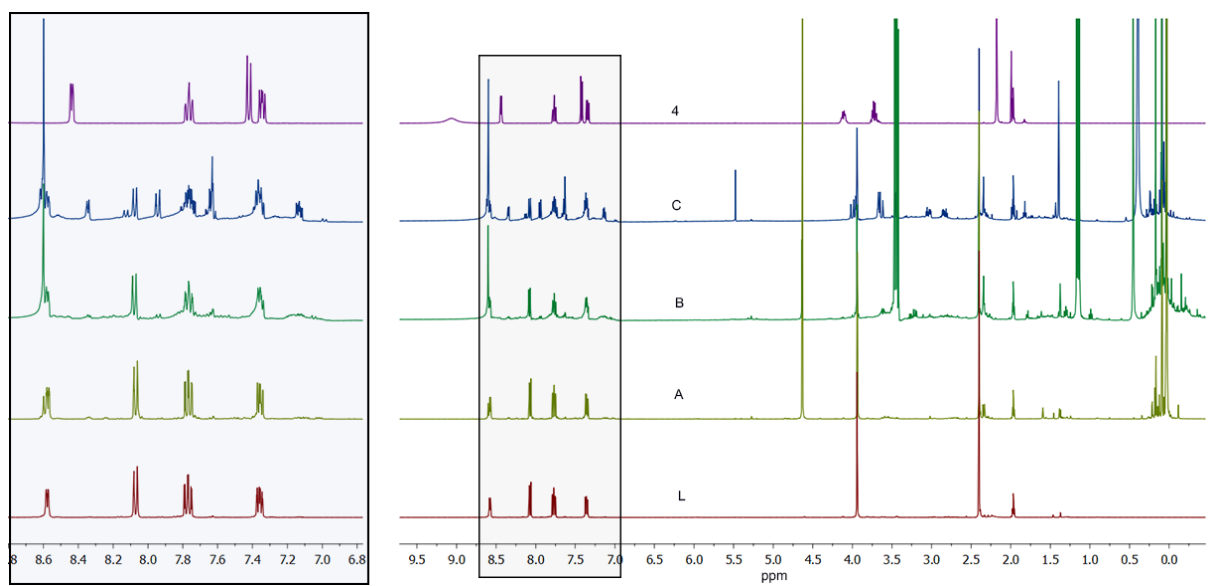


Figure 3B.21. ^1H NMR plot of Controlled Experiment.

3B.4.4 HRMS of Piperazine 3

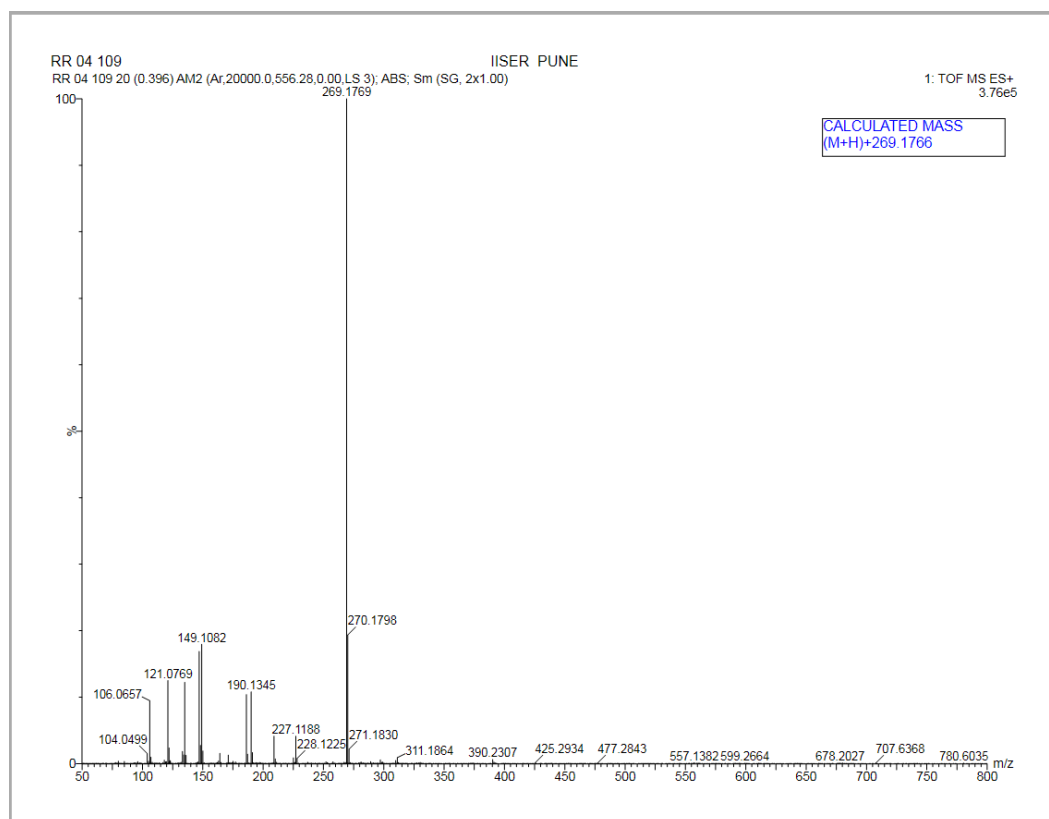


Figure 3B.22. HRMS of **3**.

3B.4.5 UV/Vis Spectra

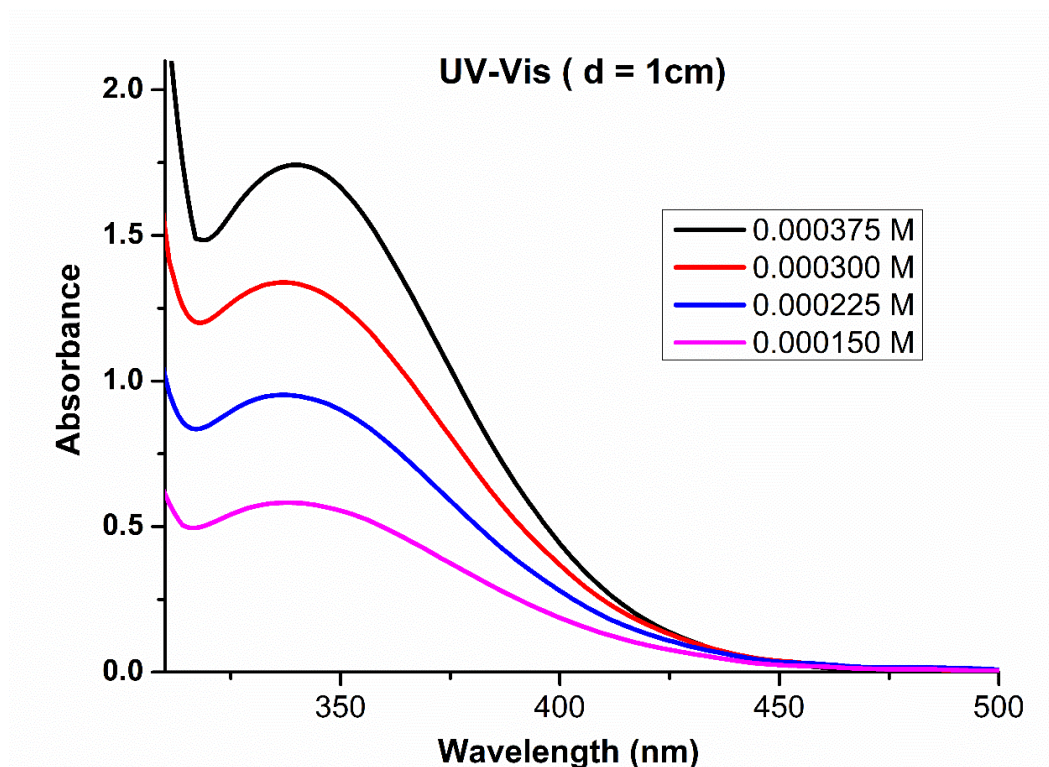


Figure 3B.23. UV-Vis spectra of compound 2 in Acetonitrile.

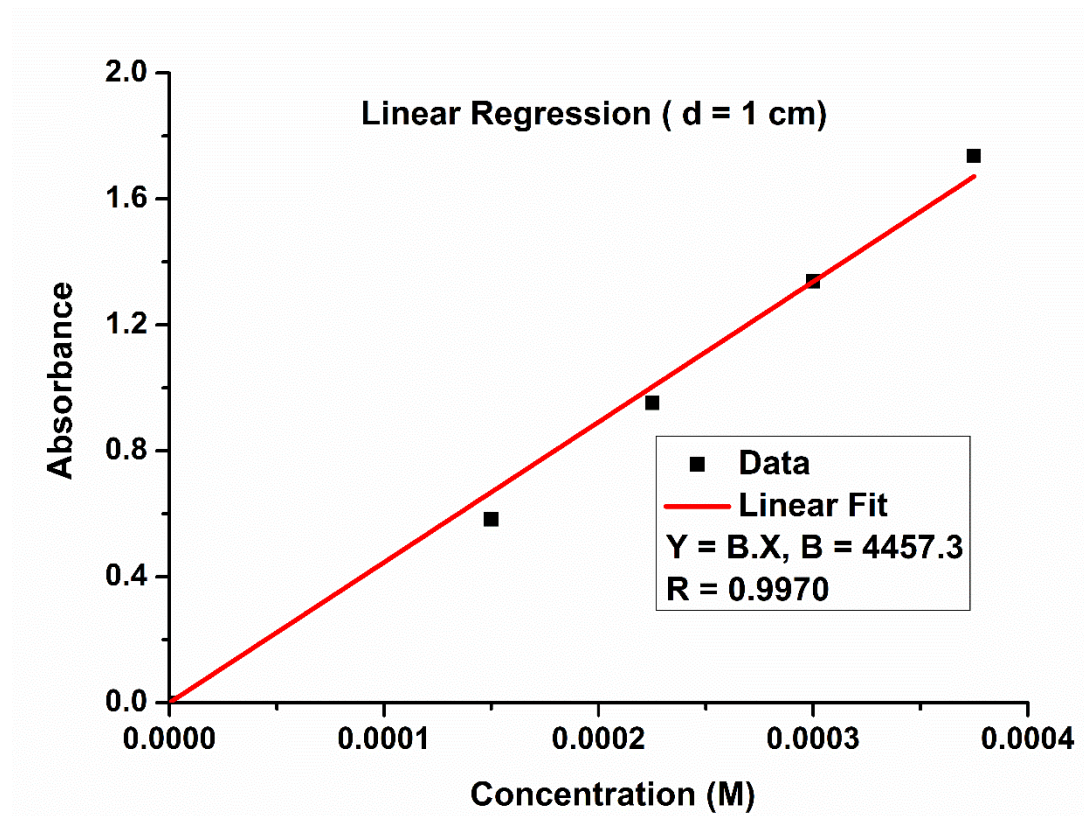


Figure 3B.24. Linear Fit for UV-Vis data of compound 2.

3B.4.6 Cyclic Voltammetry

Cyclic voltammetry (CV) measurements were carried out on a Biologic SP-300 electrochemical system using a conventional three - electrode cell in dry CH₃CN containing 0.1M tetrabutylammonium hexafluorophosphate (TBAPF₆) as the supporting electrolyte. Measurements were carried out under an Ar atmosphere. A platinum electrode (working electrode), a platinum wire (counter electrode), and Ag/AgNO₃ (reference electrode) were used. The final results were calibrated with the ferrocene/ferrocenium couple.

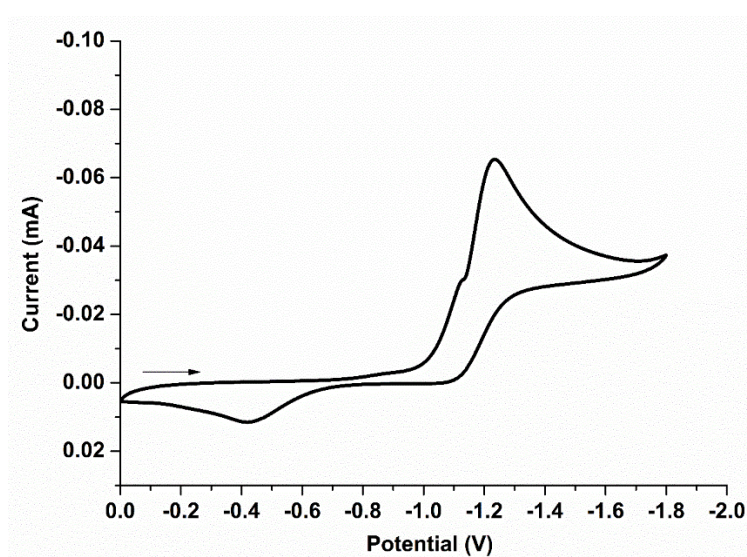


Figure 3B.25. Cyclic Voltametry of 1,4-bis(trimethylsilyl)-1,4-dihydropyrazine

(Cyclic voltammogram in acetonitrile containing 0.1 M tetrabutylammonium hexafluorophosphate as the supporting electrolyte recorded at a 100 mV s⁻¹ scan rate).

3B.4.7 EPR Spectra

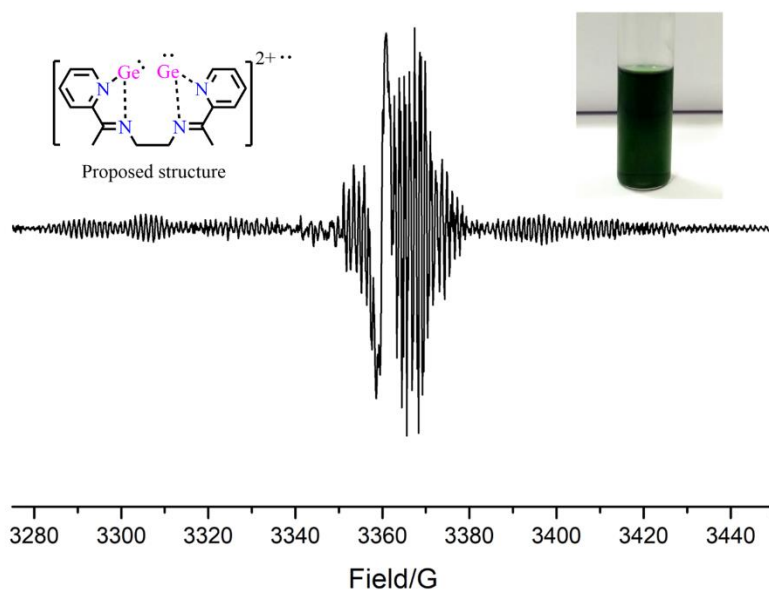


Figure 3B.26. EPR Spectrum (second derivative) of **2r** recorded in acetonitrile at 100 K. Conditions: frequency = 9.4 GHz, modulation amplitude = 1 G, microwave power = 0.3170 mW. (Inset: Green-blue solution of **2r**).

Note: For a better resolution of the half-field peak of **2r** at 1687 G (Figure 3 bottom left in maintext), EPR was recorded in acetonitrile at 100 K under the following conditions: frequency = 9.4 GHz, modulation amplitude = 11 G, microwave power = 11.5 mW.

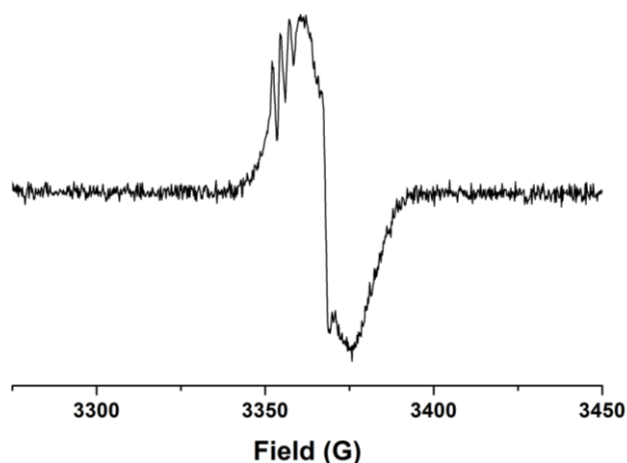


Figure 3B.27. EPR Spectrum (first derivative) of **1r** ($g_{iso} = 2.004$) recorded in toluene at 298 K. Conditions: frequency = 9.4 GHz, modulation amplitude = 2 G, microwave power = 1.12 mW.

3B.4.8 X-Ray Crystal Data

Table 3B.1 Crystal data and structure refinement of **Compound 2**

Empirical formula	C ₁₈ H ₁₈ Cl ₂ F ₆ Ge ₂ N ₄ O ₆ S ₂
Formula weight	780.56
Temperature	100 K
Wavelength	1.54178 Å
Crystal system	Triclinic
Space group	P -1
Unit cell dimensions	a = 8.3092(11) Å α = 64.284(4) b = 13.8633(19) Å β = 80.304(4) c = 13.8680(19) Å γ = 73.576(4)
Volume	1378.6(3) Å ³
Z	2
Density (calculated)	1.880 g/cm ³
Absorption coefficient	6.664 mm ⁻¹
F(000)	772
Crystal size	0.3 x 0.2 x 0.1 cm ³
Theta range for data collection	3.54 to 72.81°.
Index ranges	-10 ≤ h ≤ 10, -17 ≤ k ≤ 17, -16 ≤ l ≤ 17
Reflections collected	14028
Independent reflections	5238 [R(int) = 0.0421]
Completeness to theta = 28.38°	95.4 %
Absorption correction	Multi-scan
Max. and min. transmission	0.514 and 0.253
Refinement method	Full-matrix least-squares on F ²
Data / restraints / parameters	5238 / 0 / 363
Goodness-of-fit on F ²	1.081
Final R indices [I > 2σ(I)]	R1 = 0.0386, wR2 = 0.1080
R indices (all data)	R1 = 0.0421, wR2 = 0.1117
Largest diff. peak and hole	0.912 and -0.443 e.Å ⁻³

Table 3B.2 Crystal data and structure refinement of **Compound 2-I**

Empirical formula	C ₁₈ H ₂₀ F ₆ Ge N ₄ O ₆ S ₂
Formula weight	639.09
Temperature	100 K
Wavelength	1.54178 Å
Crystal system	Monoclinic
Space group	P 2 ₁ /c
Unit cell dimensions	a = 20.604(4) Å α = 90.00(3) b = 13.372(3) Å β = 118.50(3) c = 20.162(4) Å γ = 90.00(3)
Volume	4882(2) Å ³
Z	8
Density (calculated)	1.739 g/cm ³
Absorption coefficient	4.140 mm ⁻¹
F(000)	2576
Crystal size	0.2 x 0.12 x 0.08 cm ³
Theta range for data collection	2.44 to 66.59°.
Index ranges	-24 ≤ h ≤ 24, -15 ≤ k ≤ 15, -24 ≤ l ≤ 24
Reflections collected	9897
Independent reflections	8602 [R(int) = 0.0423]
Completeness to theta = 28.38°	99.4 %
Absorption correction	Multi-scan
Max. and min. transmission	0.718 and 0.578
Refinement method	Full-matrix least-squares on F ²
Data / restraints / parameters	8602 / 0 / 671
Goodness-of-fit on F ²	1.041
Final R indices [I > 2σ(I)]	R1 = 0.0393, wR2 = 0.0978
R indices (all data)	R1 = 0.0423, wR2 = 0.0999
Largest diff. peak and hole	1.356 and -0.828 e.Å ⁻³

Table 3B.3 Crystal data and structure refinement of Compound 4

Empirical formula	C18 H22 F6 N4 O6 S2
Formula weight	568.51
Temperature	100 K
Wavelength	1.54178 Å
Crystal system	Monoclinic
Space group	P 21/n
Unit cell dimensions	a = 11.8024(17) Å α = 90 b = 17.854(3) Å β = 113.836(5) c = 12.5096(19) Å γ = 90
Volume	2411.2(6) Å ³
Z	4
Density (calculated)	1.566 g/cm ³
Absorption coefficient	2.833 mm ⁻¹
F(000)	1168
Crystal size	0.12 x 0.09 x 0.08 cm ³
Theta range for data collection	3.86 to 66.84°.
Index ranges	-14 ≤ h ≤ 13, -19 ≤ k ≤ 21, -14 ≤ l ≤ 14
Reflections collected	19759
Independent reflections	4241 [R(int) = 0.0554]
Completeness to theta = 28.38°	99.10 %
Absorption correction	Multi-scan
Max. and min. transmission	0.797 and 0.773
Refinement method	Full-matrix least-squares on F ²
Data / restraints / parameters	4241 / 0 / 327
Goodness-of-fit on F ²	1.029
Final R indices [I > 2σ(I)]	R1 = 0.0512, wR2 = 0.1318
R indices (all data)	R1 = 0.0554, wR2 = 0.1350
Largest diff. peak and hole	0.575 and -0.484 e.Å ⁻³

Table 3B.4 Crystal data for compound **5**

Empirical formula	C ₁₉ H ₂₂ Cl ₂ F ₆ Ge N ₄ O ₆ S ₂
Formula weight	724.01
Temperature	100 K
Wavelength	1.54178 Å
Crystal system	Triclinic
Space group	P -1
Unit cell dimensions	a = 9.0423(2) Å α = 87.2210(10) b = 12.3957(3) Å β = 70.0610(10) c = 12.7280(3) Å γ = 88.3100(10)
Volume	1339.40(5) Å ³
Z	2
Density (calculated)	1.795 g/cm ³
Absorption coefficient	5.650 mm ⁻¹
F(000)	728
Crystal size	0.12 x 0.09 x 0.08 cm ³
Theta range for data collection	3.57 to 66.617°.
Index ranges	-10 ≤ h ≤ 10, -14 ≤ k ≤ 14, -15 ≤ l ≤ 15
Reflections collected	13895
Independent reflections	4703 [R(int) = 0.0431]
Completeness to theta = 28.38°	99.20 %
Absorption correction	Multi-scan
Max. and min. transmission	0.656 and 0.752
Refinement method	Full-matrix least-squares on F ²
Data / restraints / parameters	4703 / 0 / 368
Goodness-of-fit on F ²	1.052
Final R indices [I > 2σ(I)]	R1 = 0.0340, wR2 = 0.0715
R indices (all data)	R1 = 0.0431, wR2 = 0.0830
Largest diff. peak and hole	0.409 and -0.481 e.Å ⁻³

Table 3B.5 Crystal data of compound **6**

Empirical formula	C17 H26 F3 N2 O3 S Si2
Formula weight	451.64
Temperature	100 K
Wavelength	1.54178 Å
Crystal system	Orthorhombic
Space group	Iba2
Unit cell dimensions	a = 13.8129(3) Å α = 90 b = 25.7979(9) Å β = 90 c = 12.4116(3) Å γ = 90
Volume	4422.8(2) Å ³
Z	8
Density (calculated)	1.357 g/cm ³
Absorption coefficient	2.751 mm ⁻¹
F(000)	1896
Crystal size	0.12 x 0.09 x 0.08 cm ³
Theta range for data collection	3.426 to 66.747 °.
Index ranges	-16 ≤ h ≤ 16, -30 ≤ k ≤ 30, -14 ≤ l ≤ 14
Reflections collected	16645
Independent reflections	3855 [R(int) = 0.0502]
Completeness to theta = 28.38°	99.7 %
Absorption correction	Multi-scan
Max. and min. transmission	0.607 and 0.753
Refinement method	Full-matrix least-squares on F ²
Data / restraints / parameters	3855 / 1 / 259
Goodness-of-fit on F ²	0.927
Final R indices [I > 2σ(I)]	R1 = 0.0436, wR2 = 0.1106
R indices (all data)	R1 = 0.0502, wR2 = 0.1200
Largest diff. peak and hole	0.501 and -0.266 e.Å ⁻³

3B.4.9 Crystal Structure

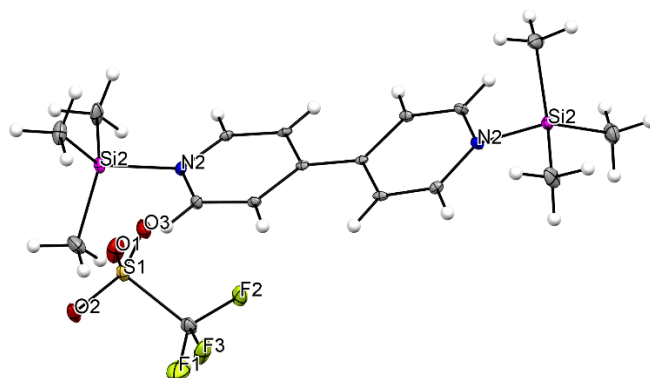


Figure 3B.28. Crystal structure of **6** in solid state (thermal ellipsoids at 30%). Selected bond lengths (Å) Si1-N1 1.823(4), Si2-N2 1.833(4).

3B.5 References

- 1 Engesser, T. A.; Lichtenthaler, M. R.; Schleep, M.; Krossing, I. *Chem. Soc. Rev.* **2016**, *45*, 755.
- 2 (a) Su, B.; Ganguly, R.; Li, Y.; Kinjo, R. *Angew. Chem. Int. Ed.* **2014**, *53*, 13106. (b) Xiong, Y.; Yao, S.; Tan, G.; Inoue, S.; Driess, M. *J. Am. Chem. Soc.* **2013**, *135*, 5004 (c) Singh, A. P.; Roesky, H. W.; Carl, E.; Stalke, D.; Demers, J. -P.; Lange, A. *J. Am. Chem. Soc.* **2012**, *134*, 4998 (d) Li, J.; Schenk, C.; Winter, F.; Scherer, H.; Trapp, N.; Higelin, A.; Keller, S.; Pöttgen, R.; Krossing, I.; Jones, C. *Angew. Chem. Int. Ed.* **2012**, *51*, 9557.
- 3 (a) Rugar, P. A.; Staroverov, V. N.; Baines, K. M. *Science* **2008**, *322*, 1360 (b) Rugar, P. A.; Staroverov, V. N.; Ragona, P. J. Baines, K. M. *J. Am. Chem. Soc.* **2007**, *129*, 15138.
- 4 (a) Green, S. P.; Jones, C.; Junk, P. C.; Lippert, K.-A.; Stasch, A. *Chem. Commun.* **2006**, 3978. (b) Nagendran, S.; Sen, S. S.; Roesky, H. W.; Koley, D.; Grub-muller, H.; Pal, A.; Herbst-Irmer, R. *Organometallics* **2008**, *27*, 5459 (c) Wang, W.; Inoue, S.; Yao, S.; Driess, M. *Chem. Commun.* **2009**, 2661; (d) Leung, W.-P.; Chiu, W.-K.; Chong, K.-H.; Mak, T. C. W. *Chem. Commun.* **2009**, 6822 (e) Jones, C.; Bonyhady, S. J.; Holzmann, N.; Frenking, G.; Stasch, A. *Inorg. Chem.* **2011**, *50*, 12315 (f) Li, J.; Schenk, C.; Goedecke, C.; Frenking, G.; Jones, C. *J. Am. Chem. Soc.* **2011**, *133*, 18622 (g) Leung, W.-P.; Chiu, W.-K.; Mak, T. C. W. *Organometallics* **2014**, *33*, 225.
- 5 (a) Zabula,; Hahn, F. E.; Pape, T. Hepp, A. *Organometallics* **2007**, *26*, 1972. (b) Hahn, F. E.; Zabula, A. V.; Pape, T.; Hepp, A. *Z. Anorg. Allg. Chem.* **2008**, *634*, 2397 (c) Brgck, A.; Gallego, D.; Wang, W.; Irran, E.; Driess, M.; Hartwig, J. F. *Angew. Chem. Int. Ed.* **2012**, *51*, 11478 *Angew. Chem.* **2012**, *124*, 11645 (d) Wang, W.; Inoue, S.; Enthaler, S.; Driess, M. *Angew. Chem. Int. Ed.* **2012**, *51*, 6167; *Angew. Chem.* **2012**, *124*, 6271 (e) Gallego, D.; Brgck, A.; Irran, E.; Meier, F.; Kaupp, M.; Driess, M.; Hartwig, J. F. *J. Am. Chem. Soc.* **2013**, *135*, 15617 (f) Gallego, D.; Inoue, S.; Blom, B.; Driess, M. *Organometallics* **2014**, *33*, 6885 (g) alvarez-Rodriguez, L.; Cabeza, J. A.; Garcia-alvarez, P.; Polo, D. *Coord. Chem. Rev.* **2015**, *300*, 1.
- 6 Kano, N.; Miyake, H.; Sasaki, K.; Kawashima, T.; Mizorogi, N.; Nagase, S. *Nat. Chem.* **2010**, *2*, 112.
- 7 Ochiai, T. ; Szilvási, T. ; Franz, D. ; Irran, E. ; Inoue, S. *Angew. Chem. Int. Ed.* **2016**, *55*, 11619.

-
- 8 Xiong, Y.; Yao, S.; Szilvási, T.; Martínez, E. B.; Grützmacher, H.; Driess, M. *Angew. Chem. Int. Ed.* **2017**, *56*, 4333.
- 9 Inomata, K.; Watanabe, T.; Tobita, H. *J. Am. Chem. Soc.*, **2014**, *136*, 14341.
- 10 Beland, V. A.; Wang, Z.; Macdonald, C. L.B.; Sham T-K.; Ragogna, P. J. *Chem. Eur. J.* **2019**, *25*, 14790-14800.
- 11 Green S. P.; Jones, C.; Stasch, A. *Science* **2007**, *318*, 1754-1758.
- 12 Mazhi, P. K.; Ikeda, H.; Sasamori, T.; Tsuragi, H.; mashima, K.; Tokitoh, N. *Organometallics* **2017**, *36*,1224-1226.(a) Saito, T.; Nishiyama, H.; Tanahashi, H.; Kawakita, K.; Tsurugi, H.; Mashima, K. *J. Am. Chem. Soc.* **2014**, *136*, (b) Yurino, T.; Ueda, Y.; Shimizu, Y.; Tanaka, S.; Nishiyama, H.; Tsurugi, H.; Mashima, K. *Angew. Chem., Int. Ed.* **2015**, *54*, 14437.
- 13 Tsuragi, H.; Mashima, K. *Acc. Chem. Res.* **2019**, *52*, 769-779.
- 14 (a) Pramanik, S.; Supriya, R.; Kando, S.; Tsuragi, H.; Mashima, K. *J. Org. Chem.* **2018**, *83*, 2409-2417. (b) Bhattacharjee, A.; Hosoya, H.; Ikeda, H.; Nishi, K.; Tsuragi, H.; Mashima, K. *Chem. Eur. J.* **2018**, *44*, 11278-11284 (c) Bhattacharjee, A.; Hosoya, H.; Yurino, T.; Nishi, K.; Tsuragi, H.; Mashima, K. *Chem. Lett.* **2019**, *48*, 888-890 (d) Hosoya, H.; Castro, L. C. M.; Sultan, I.; Nakajima, Y.; Ohmura, T.; Sato, K.; Tsuragi, H.; Suginome, M.; Mashima, K. *Org. Lett.* **2019**, *21*, 9812-9814.
- 15 Raut, R. K.; Sheikh, F. A.; Sahoo, P.; Kumar, V.; Majumdar, M. *Inorganics* **2018**, *6*, 69.
- 16 Saito, T. ; Nishiyama, H.; Tanahashi, H.; Kawakita, K.; Tsurugi, H.; Mashima, K. *J. Am. Chem. Soc.*, **2014**, *136*, 5161.
- 17 Suárez-Pantiga, S.; Colas, K.; Johansson, M. J.; Mendoza, A. *Angew. Chem. Int. Ed.*, **2015**, *54*, 14094.
- 18 (a) Borthwick, A. D. *Chem. Rev.*, 2012, **112**, 3641 (b) Horton, D. A.; Bourne, G. T.; Symthe, M. L.; *Chem. Rev.* **2003**, *103*, 893.
- 19 (a) Lino, A. M.; Gehlen, M. H. *Phys. Chem. Chem. Phys.*, **2017**, *19*, 20984 (b) Hancock, S. L.; Mahon, M. F.; Jones, M. D. *Dalton Trans.* **2011**, *40*, 2033 (c) Li, P.; Chai, Z.; Zhao, S. –Li.; Yang, Y. –Q.; Wang, H. –F.; Zheng, C. –W.; Cai, Y.-P.; Zhao, G.; Zhu, S. –Z. *Chem. Commun.* **2009**, 7369.
- 20 (a) Jung, M. E.; Rohloff, J. C. *J. Org. Chem.*, **1985**, *50*, 4909 (b) Miyake, F. Y.; Yakushijin, K.; Horne, D. A. *Org. Lett.*, **2000**, *2*, 3185 (c) Mercer, G. J.; Sigman, M. S. *Org. Lett.* **2003**, *5*, 1591 (d) Kise, N.; Oike, H.; Okazaki, E.; Yoshimoto, M.;

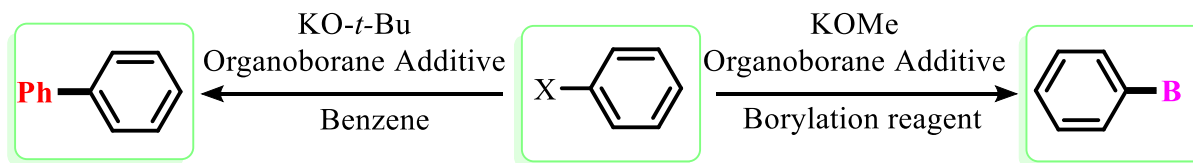
-
- Shono, T. *J. Org. Chem.* **1995**, *60*, 3980 (e) Shono, T.; Kise, N.; Shirakawa, E.; Matsumoto, H.; Okazaki, E. *J. Org. Chem.* **1991**, *56*, 3063.
- 21 (a) Dzik, W. I.; van der Vlugt, J. I.; Reek, J. N. H.; de Bruin, B. *Angew. Chem. Int. Ed.*, **2011**, *50*, 3356. (b) Nayek, H. P.; Arleth, N.; Trapp, I.; Löble, M.; Oña-Burgos, P.; Kuzdrowska, M.; Lan, Y.; Powell, A. K.; Breher, F.; Roesky, P. W. *Chem. Eur. J.* **2011**, *17*, 10814.
- 22 Raut, R. K.; Majumdar, M. *Chem. Commun.*, **2017**, *53*, 1467.
- 23 (a) Chen, Z.; Wu, J.; Chen, Y.; Li, L.; Xia, Y.; Li, Y.; Liu, W.; Lei, T.; Yang, L.; Gao, D.; Li, W. *Organometallics* **2012**, *31*, 6005 (b) Cariou, R.; Gibson, V. C.; Tomov, A. K.; White, A. J. P. *J. Organomet. Chem.* **2009**, *694*, 703.
- 24 Chu, T.; Belding, L.; van der Est, A.; Dudding, T.; Korobkov, I.; Nikonov, G. I. *Angew. Chem. Int. Ed.* **2014**, *53*, 2711.
- 25 (a) Woodul, W. D.; Carter, E.; Müller, R.; Richards, A. F.; Stasch, A.; Kaupp, M.; Murphy, D. M.; Driess, M.; Jones, C. *J. Am. Chem. Soc.* **2011**, *133*, 10074 (b) Myers, T. W.; Kazem, N.; Stoll, S.; Britt, R. D.; Shanmugam, M.; Berben, L. A. *J. Am. Chem. Soc.* **2011**, *133*, 8662 (c) Tumanskii, B.; Pine, P.; Apeloig, Y.; Hill, N. J.; West, R.; *J. Am. Chem. Soc.* **2005**, *127*, 8248.
- 26 (a) Abe, M.; *Chem. Rev.* **2013**, *113*, 7011 (b) Wentrup, C.; Regimbald-Krnel, M. J.; Müller, D.; Comba, P. *Angew. Chem. Int. Ed.* **2016**, *55*, 14600 (c) Yokoyama, Y.; Sakamaki, D.; Ito, A.; Tanaka, K.; Shiro, M. *Angew. Chem. Int. Ed.* **2012**, *51*, 9403 (d) Zhang, Q.; Khajo, A.; Sai, T.; de Albuquerque, I.; Magliozzo, R. S.; Levon, K. *J. Phys. Chem. A.* **2012**, *116*, 7629 (e) Nozawa, T.; Nagata, M.; Ichinohe, M.; Sekiguchi, A. *J. Am. Chem. Soc.* **2011**, *133*, 5773 (f) Rajca, A.; Shiraishi, K.; Vale, M.; Han, H.; Rajca, S. *J. Am. Chem. Soc.* **2005**, *127*, 9014.
- 27 Power, P. P. *Chem. Rev.*, 2003, **103**, 789.
- 28 (a) Abe, M.; Ye, J.; Mishima, M. *Chem. Soc. Rev.*, **2012**, *41*, 3808 (b) Namai, H.; Ikeda, H.; Hoshi, Y.; Mizuno, K. *Angew. Chem. Int. Ed.* **2007**, *46*, 7396 (c) Kita, F.; Adam, W.; Jordan, P.; Nau, W. M.; Wirz, J. *J. Am. Chem. Soc.* **1999**, *121*, 9265.
- 29 (a) Greene, R. N. *Tetrahedron Lett.* **1972**, *13*, 1793 (b) Taylor, L. T.; Vergez, S. C.; Busch, D. H. *J. Am. Chem. Soc.* **1966**, *88*, 3170.
- 30 (a) Zhong, Y. –W.; Izumi, K.; Xu, M. –H.; Lin, G. –Q. *Org. Lett.* **2004**, *6*, 4747. (b) Yanada, R.; Okaniwa, M.; Kieda, A.; Ibuka, T.; Takemoto, Y. *J. Org. Chem.* **2001**, *66*, 1283.

Chapter 4

Organo-main-group Compound Promoted C-C and C-B Bond Forming Reactions

Abstract

Let's become metal free. The recent breakthrough in transition-metal-free C-C and C-B bond-forming reactions using base along with additives, open the new avenues in chemistry. The ease of this reaction made it possible to achieve the multigram synthesis of many important motifs of natural products, active pharmaceutical ingredients, and organic functional materials. The reaction involves the radical species as intermediate, but the origin of radical still not elucidated with the proper mechanism. Here we report the organo-main-group additives, which can transfer electron directly, or it can form super electron donor species in situ in the reaction of a base with these organo-main-group additives. The in situ generated electron donor species are characterized by SC-XRD and EPR technique. The additives are capable of C-C coupling of unactivated arenes with haloarenes as well for C-B bond-forming reactions. The systematic competition reaction between arylation and borylation favors the C-C coupling of unactivated arenes. This present study shed light on the necessity of additive as in situ generated electron donor, which either initiate the radical reactions or catalyze the entire reaction. We have proposed two different mechanisms for C-C and C-B bond-forming reactions. The proposed mechanism is well backed by experimental proofs.



*Transition Metal Free
Coupling*

4.1 Introduction

4.1.1 Transition Metal Catalyzed Coupling Reaction

The first-ever discovery of Pd mediated C-C coupling reaction (now termed as Tsuji-Trost reaction) by J. Tsuji in 1965 paved the way for metal-catalyzed coupling reactions in the field of chemistry.¹ Then subsequent work in 1970-90s developed many important cross-coupling reactions assigned as ‘named reactions’ in textbooks. Particularly, the critical milestone was the seminal work from Heck² on the coupling of aryl halide or vinyl halide with activated alkene and Kumada³ on the coupling of the Grignard reagent with alkyl, vinyl or aryl halide. In the later stage, the catalysis using palladium complexes for the cross-coupling of organometallic compounds of Mg, Al, Zn (Negishi)⁴, Sn (Stille)⁵ and boron (Suzuki and Miyaura)⁶ was achieved. For the investigation devoted to palladium-catalyzed cross-couplings by R. F. Heck, E. Negishi, and A. Suzuki were honored with Noble Prize (Chemistry) in 2010. The extensive variation and modifications of transition metal-catalyzed coupling reaction enabled their applications in medicinal, chemical, electronics, and polymer industries. Though their severe success, they pose a risk to green chemistry owing to their following limitations.

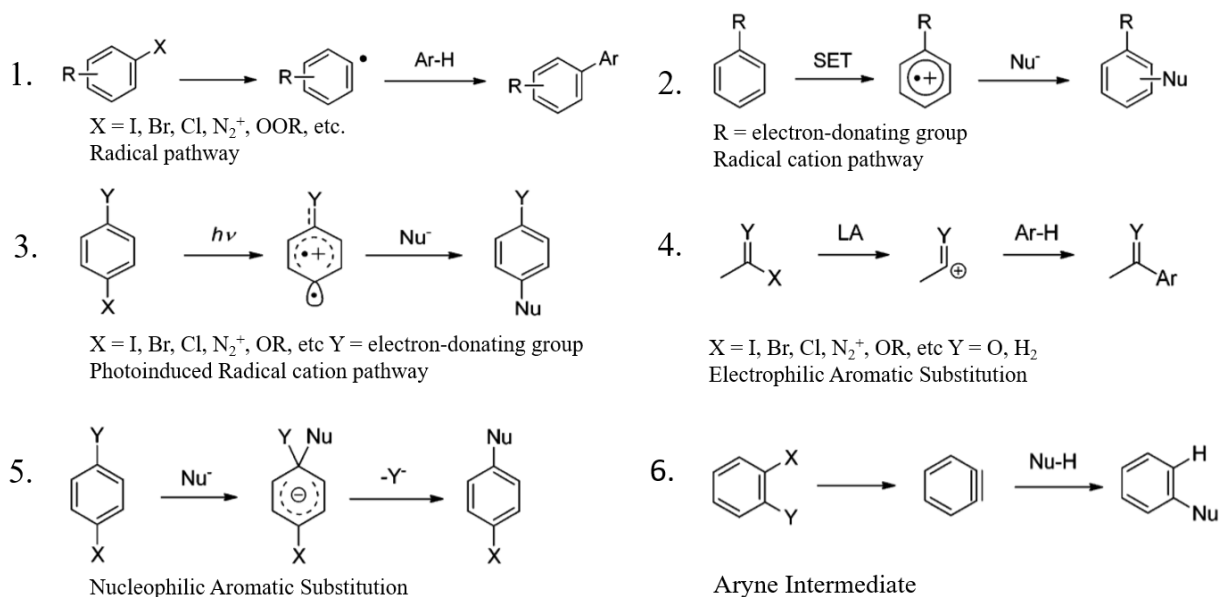
- X Transition metals are expensive.
- X Supporting ligands are expensive or difficult to prepare.
- X Transition metals are toxic; separation is tedious from the product.
- X Special additive or co-catalyst may require to increase efficiency and selectivity.

Nonetheless, the limitation of transition catalyzed cross-coupling reactions are still limited in application. This situation motivated the chemist to find alternative pathways to build the C-X bonds without the transition metals. Though it is a very challenging task, already efforts in this direction have been made to develop such chemistry.

4.1.2 Transition-metal-free Cross-coupling Reactions

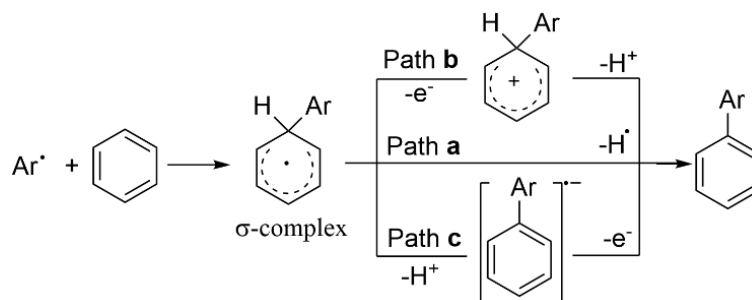
The best way to describe transition metal-free cross-coupling reaction is the reactions that mimic the transition metal cross-coupling reaction in terms of starting material and product obtained

without the use of transition metal. Depending on the reaction pathway, the transition metal-free cross-couplings are classified into **6** types, as mentioned in scheme 4.1.



Scheme 4.1 Pathways for transition-metal-free coupling reactions.

4.1.2.1 Radical pathway involves Homolytic Aromatic Substitution Reaction (HAS)



Scheme 4.2 Homolytic Aromatic Substitution (HAS) mechanism.

Homolytic Aromatic Substitution (HAS) is defined as the replacement of leaving group Y on an aromatic group by a radical attacking species.⁷ The HAS process involves the generation of radical species, which adds to the aromatic ring to form a σ - complex followed by elimination of leaving group, which is generally hydrogen radical and ends up with a cross-coupled product (**path a**, Scheme 4.2). In some cases, such as diazonium (highly electron-deficient) species, the σ - complex formed in HAS reaction can undergo through the single electron transfer (SET) process to form cationic σ - complex (cyclohexadienyl cation). The deprotonation of this cationic σ - complex leads to the formation of coupled products (**path b**, Scheme 4.2). The path c is inverse of path b, involves initial radical anion formation via loss of H^+ , followed by SET (Scheme 4.2).

The precursors used for the generation of aryl radicals are aroyl peroxide,⁸⁻⁹ arene diazonium salt. The radical species are generated by thermal decomposition from aroyl peroxide in the benzene solvent to yield the biaryl product.⁹ Whereas, in the case of arene diazonium salt, any electron source can generate aryl radical with the liberation of N₂. The electron source can be metal, photocatalyst, or organic electron donor. Aryl radicals generated from aryl halides are by electron transfer from super electron donor or by a combination of AIBN with organostannane/organosilanes,¹⁰ organoborane,¹¹ phosphites,¹² and samarium diiodide¹³ reagents. Generation of aryl radicals from arene diazonium salts and aryl halides are viable ways.

4.1.2.2 Diazonium Coupling Reaction

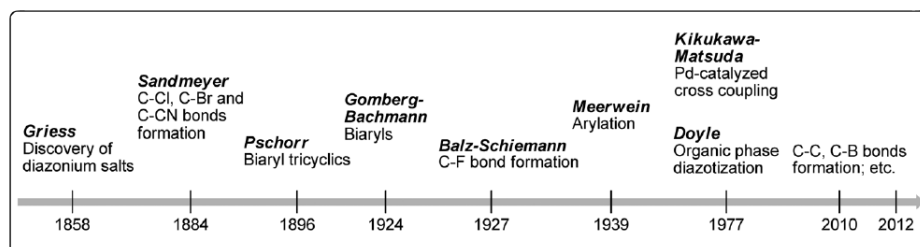


Figure 4.1 Progress of diazonium coupling reactions.

Since the discovery of arene diazonium salt in 1858,¹⁴ it proved their extensive application in synthetic chemistry. Several named reactions were evolved in the last few decades associated with arene diazonium salt shown in (Figure 4.1).¹⁵ The most striking reaction involving diazonium salt is biaryl synthesis using Cu(I) known as Pschorr reaction.¹⁶ The aryl radical is generated from arene diazonium salt, which goes for intermolecular substitution with arene. Later in 1924, Gomberg and Bachmann developed the method for radical biaryl synthesis in intermolecular fashion.¹⁷ Meerwein and co-workers in the year of 1939, got access of the stilbene by the reaction of the arene diazonium salt with α , β -unsaturated aryl compound.¹⁸

In the last two decades, there are plentiful reports on C-C and C-B bond-forming reactions which involve aryl radical intermediate generated using arene diazonium salt (Figure 4.2). Recently Sanford¹⁹ and co-worker reported the merger of photoredox catalysis with Palladium (Pd) for ligand directed arylation by C-H functionalization.

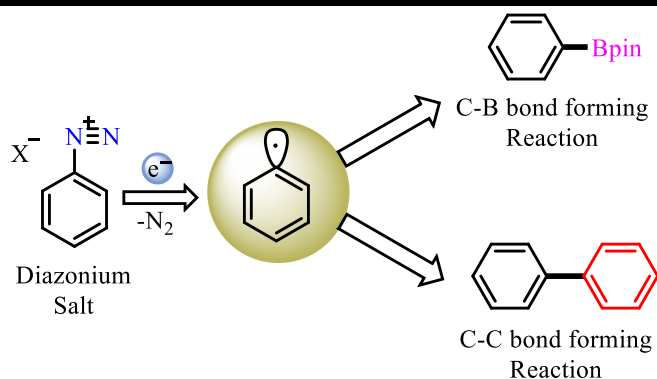
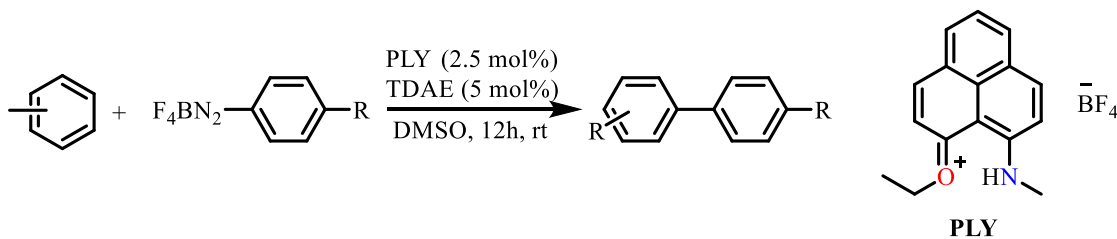


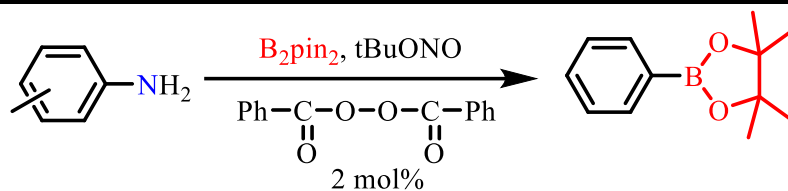
Figure 4.2 Arene diazonium salts for C-B and C-C bond formation via aryl radical.

The aryl radicals generated from diazonium salt by photoredox catalysis participate in Pd catalyzed C-H functionalization. In the following year, König and co-workers²⁰ reported the visible light-mediated direct C-H arylation of heteroarenes with arene diazonium salts without any transition metal. They also supported the radical mechanism by detecting the trapped aryl radical intermediate with 2,2,6,6-tetramethyl-1-phenoxypiperidine. Later, Corillo and co-workers also achieved room temperature, transition metal-free synthesis of biaryl using ascorbic acid as a catalyst.²¹



Scheme 4.3 Transition-metal-free phenalenyl cation catalyzed diazonium coupling.

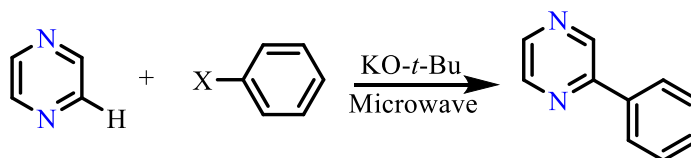
Very recently, Mondal and co-workers²² used the in situ generated phenalenyl radical (**PLY**) for C-H arylation of heteroarenes under metal-free condition without any light stimulation (Scheme 4.3). A similar catalyst also used for C-H arylation of arene.²³ They also developed the aluminum (Al) phenalenyl catalyst for the C-H arylation of arene and heteroarenes.²⁴ There are also few reports in the last decade on C-B bond-forming reaction by radical deaminative borylation route via diazonium salt.²⁵ In 2010 Wang and co-workers developed the route for conversion of arylamines to arylboronates (Scheme 4.4). In this reaction, arylamines are in situ converted to arene diazonium salt followed by borylation using benzoyl peroxide as additive.^{25a}



Scheme 4.4 Direct conversion of arylamines to pinacol boronates via diazonium salt.

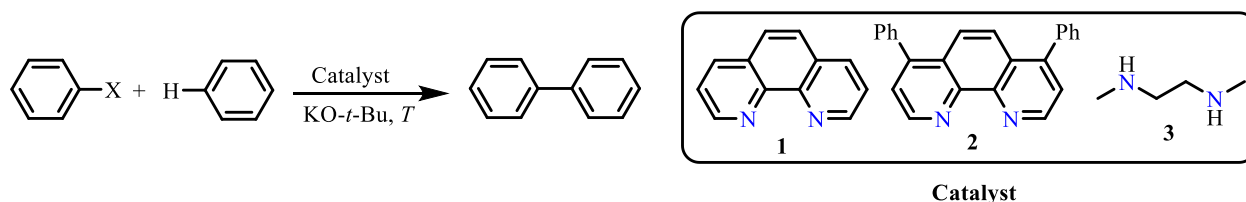
4.1.2.3 Base-Promoted Coupling of Aryl Halides with Arenes and C-B Bond Forming Reactions

The challenge of developing green and sustainable chemistry attracted chemists to develop the transition metal-free coupling reactions. The extensively studied Pd and Rh catalyzed coupling reactions are overshadowed by base-assisted homolytic aromatic substitution reaction (BHAS), when Itami and co-worker in 2008,²⁶ developed the protocol for potassium *tert*-butoxide promoted cross-coupling between nitrogen heterocycles and haloarenes (Scheme 4.5). Careful examination for trace metals in base or solvent by ICP-AES show absence of it further enhances the claim of transition metal-free coupling reactions. The mechanistic study indicated the radical pathway mechanism.



Scheme 4.5 Base promoted coupling of pyrazine with an aryl halide.

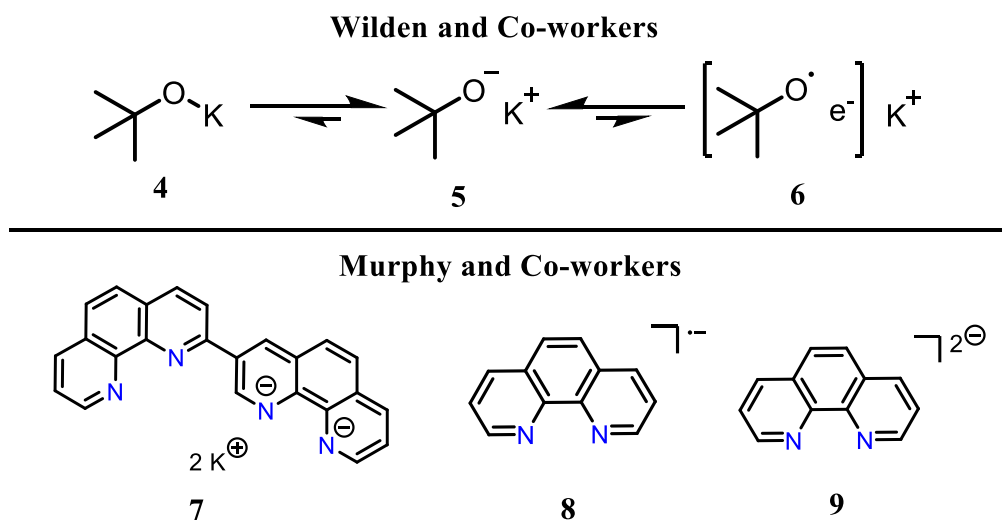
Subsequently, in 2010, three independent research group developed base promoted homolytic aromatic substitution reaction between unactivated arenes and haloarenes without a transition metal in the presence of the catalytic amount of Phenanthraline (**1** and **2**), *N,N'*-Dimethyl-ethylene diamine (DMEDA) (**3**) additives (Scheme 4.6).²⁷



Scheme 4.6 Transition-metal-free coupling of aryl halides with arene.

These reports claim the necessity of nitrogen-containing bidentate ligands in promoting the cross-coupling reactions. After that sudden burst of reports in search of new catalyst/ligand/additive for coupling reactions of haloarenes with unactivated arenes appeared.²⁸ This kind of coupling reactions are also extended to intramolecular cyclization,²⁹ Heck-type coupling,³⁰ carbonylation,³¹ hydrodehalogenation³² and borylation reaction.³³ The intramolecular cyclization by base assisted HAS given the access to fused rings, heterocycles and polycycles, which are important motifs of functional materials, natural products, and drug molecules. The aryl radicals generated from aryl halide by application of base with or without the presence of ligand are added to the double bond to yield Mizoraki-heck type coupling product. After the huge development of BHAS in the coupling reaction, the role of additive/ligand was still dubious.

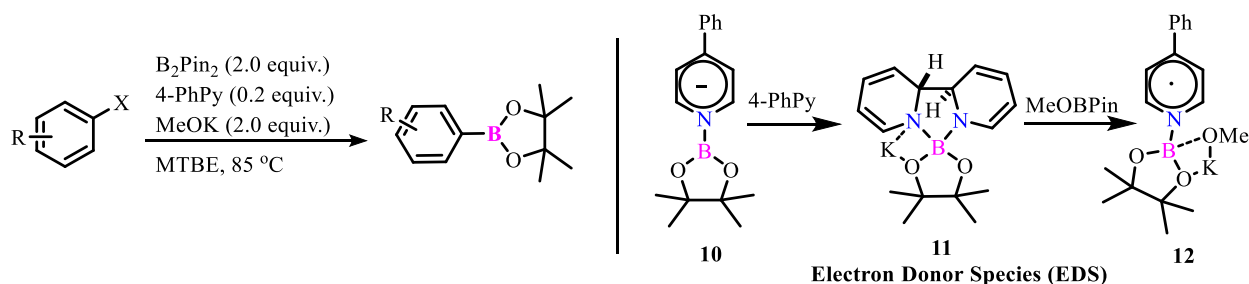
In pursuit of mechanistic understanding, Wilden and co-workers³⁴ reported their observation, only base (KO-*t*-Bu) is sufficient to reduce the aryl halide into aryl radical. He explains the concept of covalent and charge-separated species. The metal alkoxides are in equilibrium between the covalent species **4** and charge-separated species **5**. The charge-separated form again is in equilibrium with loosely bound electron species **6** and which is capable of transferring an electron (Scheme 4.7).



Scheme 4.7 Electron Donor Species from potassium *tert*-butoxide and phenanthroline.

In 2016, John Murphy and co-workers claimed KO-*t*-Bu itself is not able to transfer the electron in arene solvents to aryl halides.³⁵ Preferably the electron donor species generated from the reaction of additive/ligand with base, which transfers the electron to aryl halide. They backed

their claims with some of the electrochemical experiments and also characterized few of the electron donor species **7**, **8**, and **9** in control experiments. Some of the electron donor species generated from phenanthroline are shown (Scheme 4.7). In the same year, Jiao and co-workers also did a systematic study in understanding the mechanism of dimethyl ethylene diamine (DMEDA) promoted transition metal-free coupling. They discarded the redox type initiation pathway.³⁶ Zeng group in 2017, reported the foldamer based catalyst, where the catalyst was forming the chelating complex with KO-*t*-Bu, and the complex is acting the electron donor species, thus disproving the mechanism proposed by Murphy and Jiao.³⁷ The mechanistic study in this field is still lacking.



Scheme 4.8 Pyridine catalyzed radical borylation.

In 2017, Jiao and co-worker first time reported the efficient, scalable, easy method of pyridine catalyzed radical borylation of aryl halides (Scheme 4.7).^{33a} The idea initiated from the proposed act of generating aryl radical from aryl halide by electron donor species and simultaneous generation of pyridine stabilized boryl radical, followed by radical-radical coupling between aryl radical and pyridine stabilized boryl radical. Recently this procedure was further improved by irradiation with visible light at room temperature.³⁸

A similar strategy was used by Pinet and Pucheault for the preparation of aryl boronic esters from aryl iodide, instead, they used CsF in combination with pyridine at elevated temperature in DMSO.^{33b}

Scope of Work

The base assisted homolytic substitution reactions have crossed more than a decade after its the first appearance. Still, the mechanistic details are debatable. Base alone can transfer the electron or additive base chelate complex, or the electron donor species generated from base and additive are responsible for electron transfer. Also, KO-*t*-Bu is the only effective base except for very few reports which use a weaker base like sodium *tert*-butoxide. The aryl radicals generated by base

and additive has also used for C-B bond formation (radical borylation). But there are no reports where C-C and C-B bond formation performed using one additive. Even though having so much literature on base assisted homolytic aromatic substitution, the following questions have still retarded the development of this field.

- a) What is the role of ligand/additive?
- b) Can base alone promote the coupling reaction?
- c) Why is only KO-t-Bu useful for BHAS?
- d) Can we construct C-C and C-B bond using the same additive?

We have tried to answer all these questions in this work by hypothesizing the use of organo-main-group compound as additive. We also tried to rationalize the mechanism proposed by Murphy [34] with some experimental proofs.

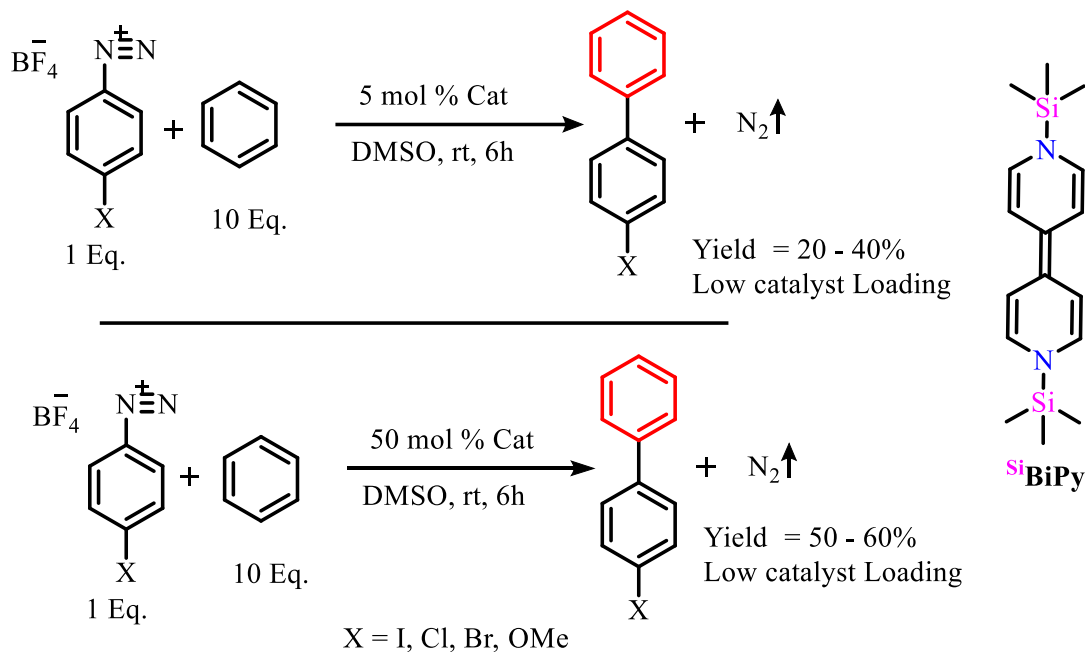
4.2 Result and Discussion

4.2.1 Organosilicon Additives Promoted C-B and C-C Bond Forming Reactions

The organosilicon compounds were synthesized as per the literature report. The additive **SiBiPy** was synthesized by reduction of 4,4'-bipyridine with sodium metal followed by the addition of trimethylsilyl chloride. The red colored product was extracted in pentane, and the pentane solution was concentrated, kept aside for crystallization to get red crystals of **SiBiPy**. Similarly, additive **SiPy** and **Si^tPy** are synthesized from pyrazine and 2,3,5,6-tetramethyl pyrazine as yellow and white color product, respectively.³⁹

The redox nature of additive **SiBiPy** was already shown in the previous chapter, here we have tested it as the catalyst for C-C and C-B coupling of arene diazonium salts. The investigation of the organosilicon catalyst was tested with direct C-H arylation of unactivated arenes, which has gained immense attention from the scientific community. Initially, the reaction was tested with diazonium salt and benzene in DMSO solvent. The yield of the expected biaryls from the reaction was quite poor, when catalyst **SiBiPy** was used in 5 mol%. Then subsequently, by increasing the catalyst loading to 50 mol %, the yield of biaryls was just raised to 55%. In the reaction vessel, the N₂ was bubbling out very intensely, generating the pressure in a reaction vessel (Scheme 4.9). Few other substituted diazonium salt also tested for C-H arylation, but the results were not much promising. Then we turned our attention from C-H arylation to borylation reaction, where bis(pinacolato)diboron as borylation source has been used in the reaction. 4-Chlorophenyl

diazonium salt was added along with ^{Si}BiPy and bis(pinacolato)diboron rce in DMSO, and the yield of corresponding borylation product was only 45%.



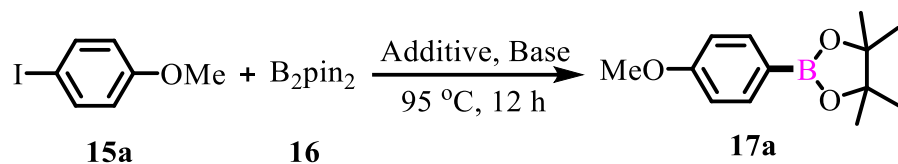
Scheme 4.9 Biaryl coupling of the aryl diazonium salt with benzene using ^{Si}BiPy catalyst.

The poor results of organosilicon compounds as a catalyst for C-H arylation and borylation of diazonium salts led us to investigate the failure. The possible reason for failure could be catalyst decomposition in the reaction progress. To understand the catalyst decomposition in the reaction mixture, the NMR scale reaction is carried out. In NMR tube, One equiv. of phenyl diazonium salt (**12**), 10 equiv. of benzene (**13**), and 1 equiv. of ^{Si}Pz was dissolved in DMSO-*d*₆ solvent and submitted for ¹H, ¹¹B, ¹⁹F, and ²⁹Si (Scheme 4.10). The ¹H NMR confirms the formation of **13** by N₂ elimination as gas bubbles along with the concomitant formation of **14** and trimethylsilyl fluoride (TMSF). The TMSF formation was confirmed by ²⁹Si NMR and ¹⁹F NMR. The Si-F coupling constant values found as $J_{\text{Si-F}} = 274.4 \text{ Hz}$ (Figure 4.47 and 4.48). Possibly the fluoride anion generated from BF₄⁻ counter anion must be attacking the electropositive silyl group of catalysts thus producing trimethylsilyl fluoride (TMSF) and **14**.

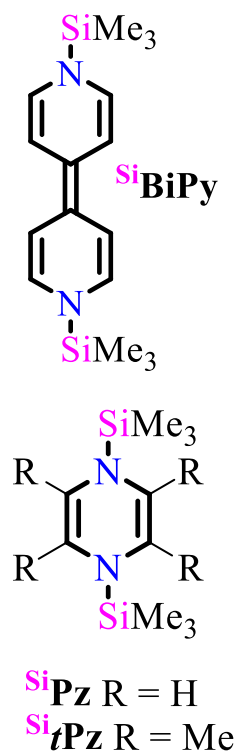
experiment conducted at a low temperatures in THF solvent, which did not show any hyperfine coupling (Figure 4.3).

The application of this radical anion as an electron donor has been attempted for radical borylation of aryl halides. A similar kind of concept is used previously by Murphy and co-workers²⁸¹ in arylation reaction. The phenanthroline based dianions **7**, anions **8** and radical anions **9** formed in the course of reaction, and are responsible for the coupling reaction.

The trial borylation reaction was performed using the 4-Iodoanisole (**15a**) as substrate and CsF as a base in DMSO solvent with B₂Pin₂ (**16**) as borylation source in the presence of ^{Si}BiPy. The reaction yielded the expected borylation product **17a** with 73% yield. This enlightening result prompted us to carry out the optimization study. Base or nucleophiles other than CsF were KF, KI, and tetrabutylammonium fluoride (TBAF) also used in optimization, but only CsF and KF were converting the aryl iodide into the product with the yield of 73% and 70% respectively. The reaction was working well at 95 °C, and DMSO found to solvent of choice over THF and MTBE. The one equivalent of 16 as borylation source was insufficient in giving a high yield of product (table 4.1).

Table 4.1 Optimization for the borylation of aryl halide.

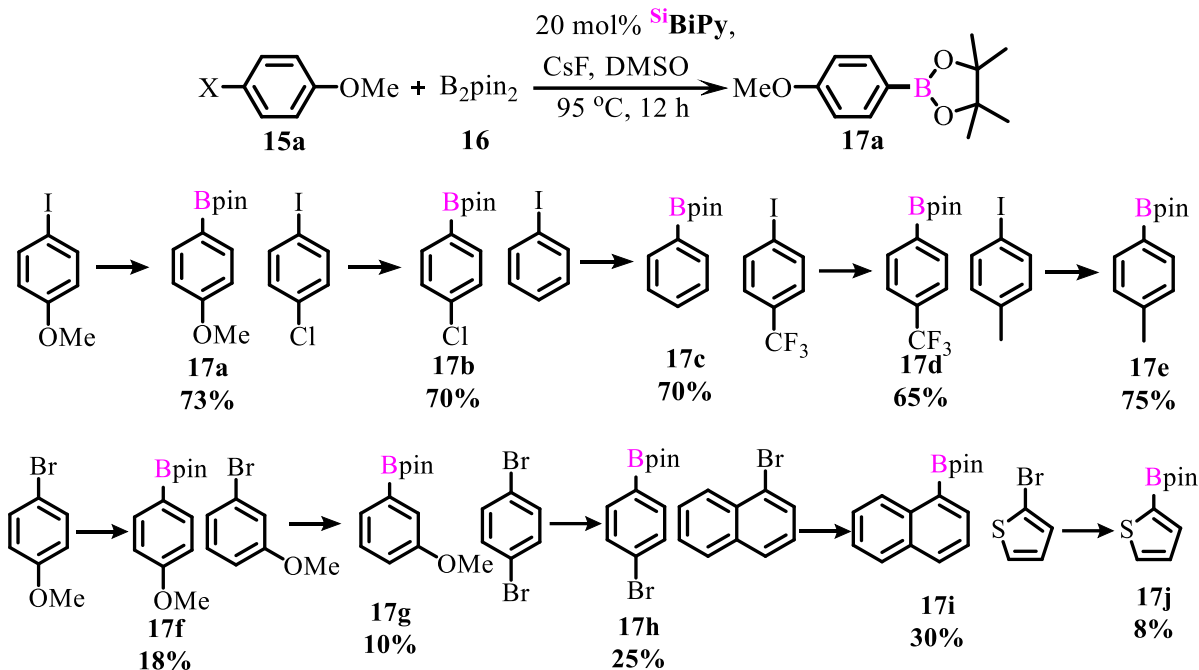
Entry	Base	Temp.	Solvent	B ₂ pin ₂	Additive	Yield (%)
1	-	95	DMSO	2 Eq.	^{Si} BiPy	-
2	CsF	95	DMSO	2 Eq.	^{Si} BiPy	73%
3	KF	95	DMSO	2 Eq.	^{Si} BiPy	70%
4	KI	95	DMSO	2 Eq.	^{Si} BiPy	-
5	TBAF	95	DMSO	2 Eq.	^{Si} BiPy	20%
6	CsF	60	DMSO	2 Eq.	^{Si} BiPy	58%
7	CsF	RT	DMSO	2 Eq.	^{Si} BiPy	23%
8	CsF	95	DMSO	2 Eq.	^{Si} Pz	-
9	CsF	95	DMSO	2 Eq.	^{Si} <i>t</i> Pz	26%
10	CsF	95	THF	2 Eq.	^{Si} BiPy	65%
11	CsF	95	MTBE	2 Eq.	^{Si} BiPy	15%
12	CsF	95	DMSO	1 Eq.	^{Si} BiPy	35%



Reaction condition: 4-Iodoanisole (0.5 mmol, 1 Equiv.), B₂pin₂ (2.4 Equiv.), Base (2 Equiv.), Additive (20 mol%), Solvent (2 mL) for 12 h in sealed tube. Isolated Yields.

With this optimized condition in hand, the generality of the reaction system was surveyed with various substrates, including Bromo- and Iodoarenes (table 4.2). The borylation of various Iodoarenes including electron donating as well as electron-withdrawing groups, carried easily with yields ranging from 65 to 75%. Particularly, the 4-Iodotoluene gave the high yield of 75% of **17e**. The electron deficient 4-Iodotrifluorotoluene yielded 65% of **17c**. Further, the bromoarenes were also attempted for borylation, notably weak yields are obtained. 4-bromothiophene just gave 8% yield of **17f**. This might be because of the weak donor ability of the electron donor species generated in the reaction, which prevents the catalytic cycle.

Table 4.2 Substrate scope for borylation of arene diazonium salt



Reaction condition: aryl halide (0.5 mmol, 1 Equiv.), B_2pin_2 (2 Equiv.), CsF (2.4 Equiv.), $^\text{Si}\text{BiPy}$ (20 mol%), Solvent (2 mL) reaction temperature $95\text{ }^\circ\text{C}$ for 12 h in sealed tube.

A similar concept has been used for C-H arylation of unactivated arenes in the base assisted homolytic aromatic substitution (BHAS) reaction. We were interested in achieving biaryl synthesis using organosilicon compound $^\text{Si}\text{BiPy}$ and CsF as a base, but unfortunately reaction did not work. The strength of the base must not be sufficient to drive the reaction forward.

We have achieved the borylation of aryl iodide using the organosilicon compound as additive and CsF as a base. Unfortunately, these additives are not efficient in borylation of aryl bromides and also not effective in the arylation of aryl halides.

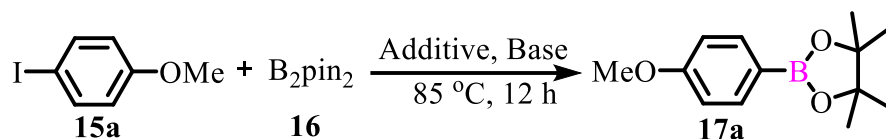
4.2.2 Organoborane Additive Promoted C-B and C-C Bond Forming Reactions

The Jiao and co-workers proved the generation of boron-based super electron donor species **10**, **11**, and **12** in pyridine catalyzed borylation. In the course of the reaction, they identified electron donor species generated by the reaction of a base with pyridine in the presence of bis(pinacolato)diboron as borylation source.⁴⁰ We commenced our journey with the concept of generation of electron donor, by the attack of the base (nucleophile) on organoborane additive.

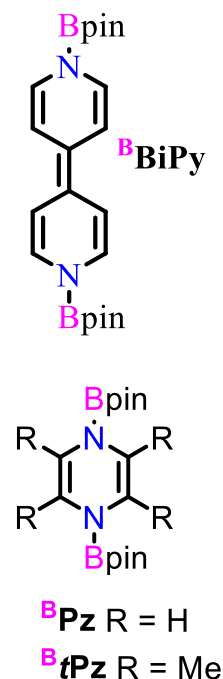
The organoborane additives ($^\text{B}\text{BiPy}$, $^\text{B}\text{Pz}$, $^\text{B}\text{tPz}$) are synthesized by following the literature reported procedures.⁴¹ 4-Iodoanisole **15a** is used as a model substrate for screening various bases

and additives. In the control experiment, the reaction was performed without the additive leading to complete recovery of starting material. The reaction was also done without base, but as above, we recovered only starting material.

Table 4.3 Optimization of reaction condition for borylation



Entry	Base	Solvent	Additive	Yield (%)
1	-	MTBE	^B BiPy	<5%
2	KO- <i>t</i> -Bu	MTBE	^B BiPy	45%
3	NaO- <i>t</i> -Bu	MTBE	^B BiPy	65%
4	LiO- <i>t</i> -Bu	MTBE	^B BiPy	71%
5	KOMe	MTBE	^B BiPy	78%
6	NaOMe	MTBE	^B BiPy	72%
7	LiOMe	MTBE	^B BiPy	68%
8	KOMe	MTBE	^B Pz	35%
9	KOMe	MTBE	^B <i>t</i> Pz	<5%
10	KOMe	THF	^B BiPy	50%
11	KOMe	DMSO	^B BiPy	38%
12	KOMe	MTBE	-	5%

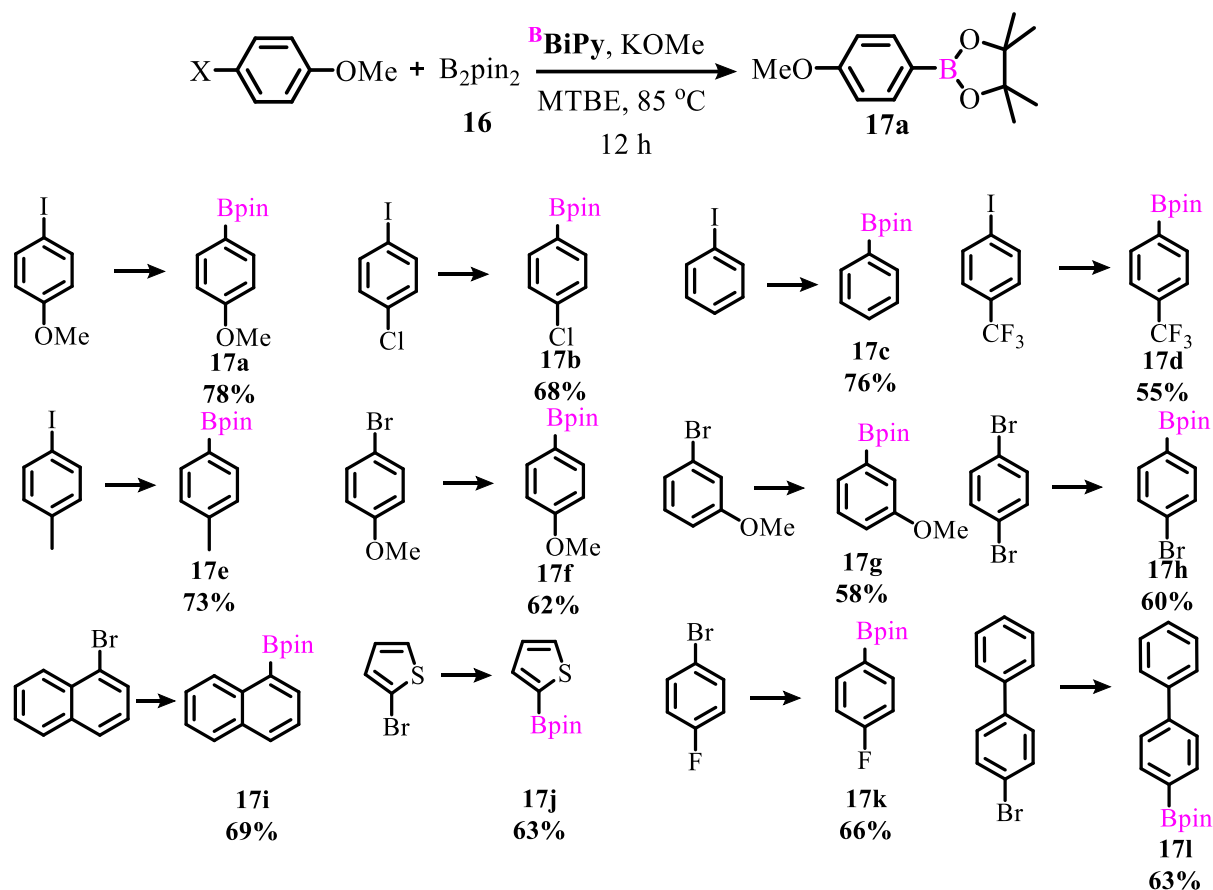


Reaction condition: 4-Iodoanisole (0.5 mmol, 1 Equiv.), B₂pin₂ (2 Equiv.), Base (2.4 Equiv.), Additive (20 mol%), Solvent (2 mL) reaction temperature 85 °C for 12 h in sealed tube. Isolated yields.

Then we screened several bases, in which potassium methoxide served the best by giving 78% yield **17a**. Potassium *tert*-butoxide gave only a 45% yield, but we did not recover starting material. The other side product could be the hydrodehalogenation product such as anisol. The THF, methyl *tert*-butyl ether (MTBE), and DMSO solvents were also screened, out of which MTBE worked well. The other solvents are a possible sources of hydrogen, which lead to

dehydrohalogenation products. The additive **B**BiPy was the best, whereas **B**Pz and **B**tPz were not much effective for borylation. This could be because of the donor ability and stability of electron donor species generated during the reaction. In the case of **B**tPz, the tetra-methyl groups on the pyrazine must be causing the steric hindrance to attack in the generation of electron donor species and also high instability of dianion due to inductive effect (table 4.3).

Table 4.4 Substrate scope for borylation reaction

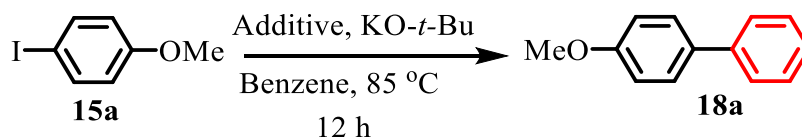


Reaction condition: aryl halide (0.5 mmol, 1 Equiv.), B_2pin_2 (2 Equiv.), KOMe (2.4 Equiv.), 1 (20 mol%), Solvent (2 mL) reaction temperature 85 °C for 12 h in sealed tube. Isolated Yields.

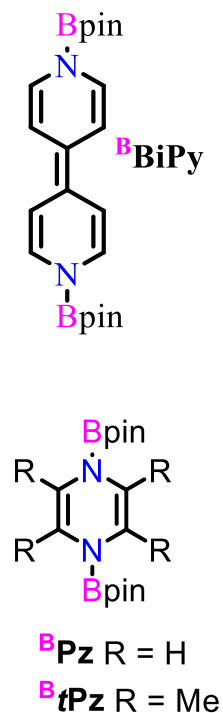
Having the optimized condition in hand, we tried borylation for Iodo-, Bromo- and chloroarenes (table 4.4). The Iodo- and Bromoarenes gave a good yield of respective borylation products, whereas in the case of chloroarenes additive were not effective. Reaction worked well for the electron-withdrawing substituent as well as electron-donating substituted arenes. The electron-donating methoxy group in 4-Iodoanisole gave the yield of 78% of **17a**, whereas the

electron-withdrawing trifluoro-methyl group in 4-Iodotrifluorotoluene gave the corresponding borylation product **17d** with the yield of 55%. The bromoarenes turned into corresponding products with yields ranging from 59% to 69%. 1-Bromonaphthelene and 4-bromobiphenyl converted into respective borylation products in a good yield of 69% of **17i** and 63% of **17l**, respectively. The 5-membered thiophene ring in 1-Bromothiophene did not have any adverse effect on borylation and gave 63% yield of **17j**. In the case of 1,4-dibromo benzene, by maintaining the ratio of base and borylation agent, we got mono borylation bromoarene as major product with 60% yield of **17h**.

As the electron donor species were effective in borylation, we were interested for arylation by C-H functionalization of unactivated arenes. The reaction of **15a** with potassium *tert*-butoxide as base in benzene solvent was tried for arylation with ^BBiPy as additive. Interestingly it gave respective biphenyl product **18a** in a good yield of 73%.

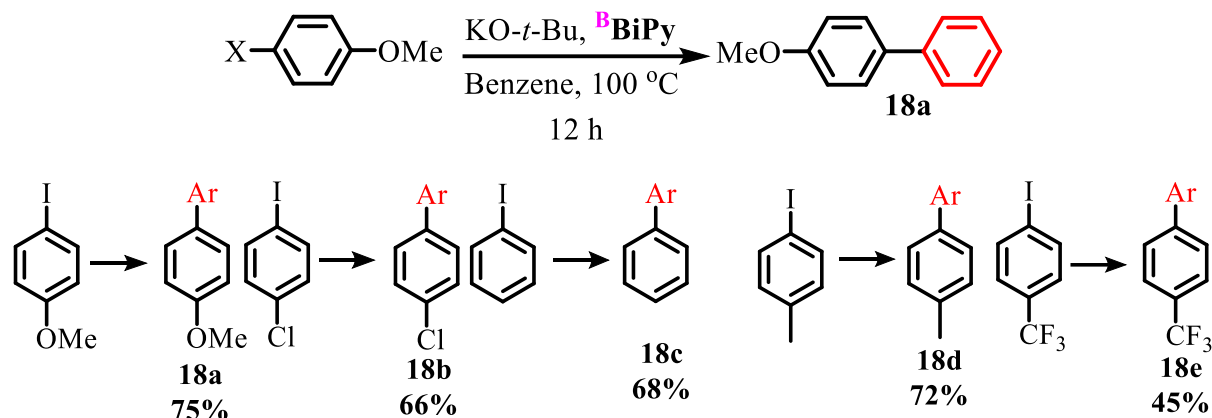
Table 4.5 Optimization of reaction condition for C-H arylation

Entry	Base (Eq.)	Additive (Eq.)	Yield (%)
1	-	^B BiPy (0.2)	-
2	KO- <i>t</i> -Bu (3)	^B BiPy (0.2)	75%
3	NaO- <i>t</i> -Bu (3)	^B BiPy (0.2)	-
4	LiO- <i>t</i> -Bu (3)	^B BiPy (0.2)	-
5	KOMe (3)	^B BiPy (0.2)	-
6	NaOMe (3)	^B BiPy (0.2)	-
7	LiOMe (3)	^B BiPy (0.2)	-
8	KO- <i>t</i> -Bu (3)	^B BiPy (0.1)	70 %
9	KO- <i>t</i> -Bu (3)	^B Pz (0.2)	60 %
10	KO- <i>t</i> -Bu (3)	^B <i>t</i> Pz (0.2)	28 %
11	KO- <i>t</i> -Bu (2)	1	45 %



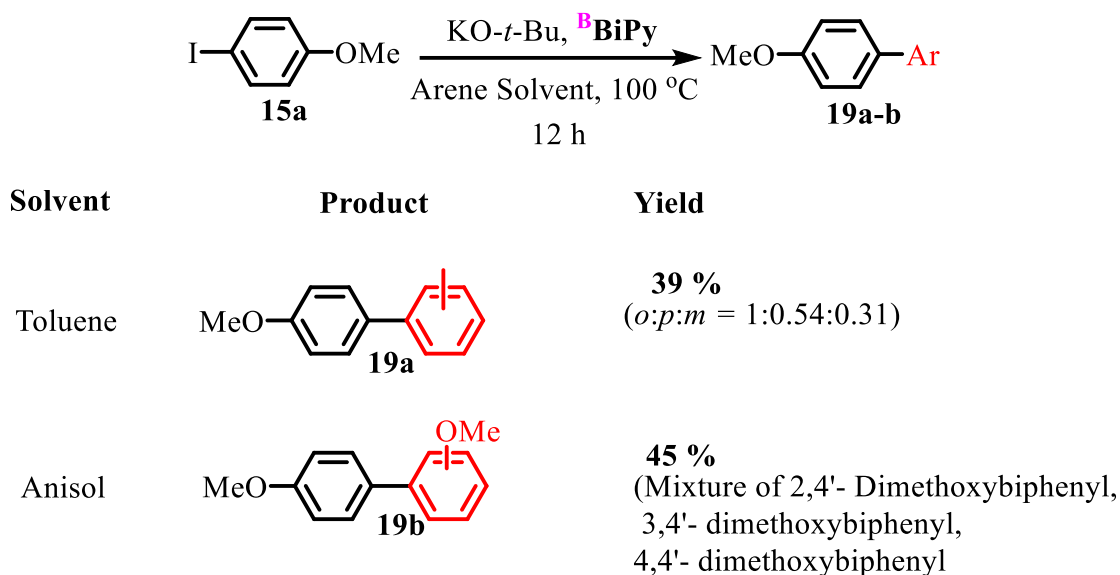
Reaction condition: 4-Iodoanisole (0.5 mmol, 1 Equiv.), Additive, Base (2.4 Equiv), Benzene (2 mL) reaction temperature 85 °C for 12 h in sealed tube. Isolated Yields.

The reaction condition is optimized for the C-H functionalization of arenes (Table 4.5). All the bases suitable for borylation were not suitable for the arylation of unactivated arene except potassium *tert*-butoxide. Additive ^BBiPy was giving better yields compare to ^BPz and ^B*t*Pz. 3 equiv. of potassium *tert*-butoxide and 20 mol% of ^BBiPy gave the highest yields and considered as an optimized condition.

Table 4.6 Substrate scope for C-H arylation of benzene

Reaction condition: Haloarene (0.5 mmol, 1 Equiv.), Additive **1** (0.2), ^tBuOK (2), Benzene (2 mL) reaction temperature 100 °C for 12 h in sealed tube. Isolated Yields.

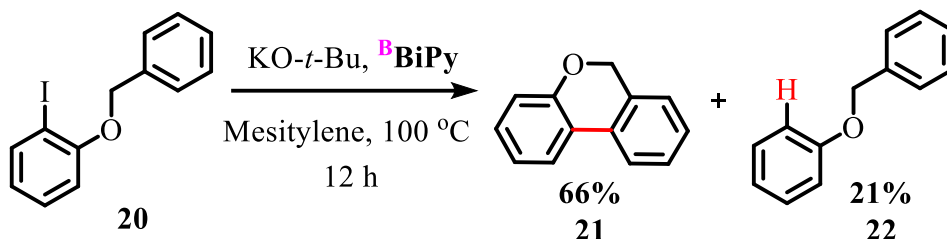
Further, to confirm the generality of the reaction, different Iodoarene were coupled with benzene (Table 4.6). The electron-deficient 4-(trifluoromethyl)Iodobenzene turned into respective biphenyl **18e** with a yield of 45% while electron-donating 4-Iodoanisole gave 75% yield of **18a**.

Table 4.7 C-H arylation with Toluene and Anisole

Reaction condition: Haloarene (0.5 mmol, 1 Equiv.), Additive **1** (0.2), KO-*t*-Bu (2), arene (2 mL) reaction temperature 100 °C for 12 h in sealed tube.

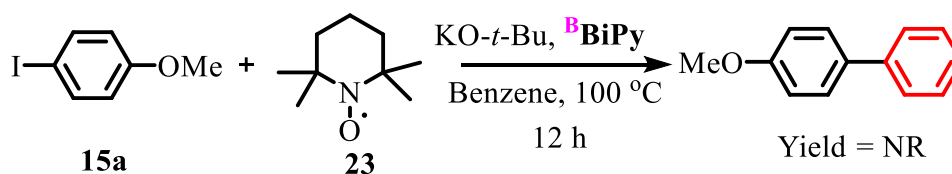
Further, instead of benzene as a coupling partner toluene, and anisole were used under a similar condition (Table 4.7). Toluene gave a moderate yield of 39% of **19a** with *ortho*-

substitution is most favored followed by *meta*- and *para*- substitution. In the case of anisol as a coupling partner, it gave a mixture of products of **19b** with *ortho*- as majorly dominated over *meta*- and *para*-. This lack in regioselectivity of the product is the outcome of the involvement of radical species. The generated aryl radical is highly reactive and gives such uncontrolled distribution in the product.



Scheme 4.11 Intramolecular arylation by radical trap.

The intramolecular cyclization in mesitylene solvent at 100 °C with potassium *tert*-butoxide as a base was achieved from 1-(benzyloxy)-2-Iodobenzene **20** as substrate (Scheme 4.11). It gave the cyclized product 6*H*-benzo[*c*]chromene **21** with a yield of 66% and hydrodehalogenated (benzyloxy)benzene **22** product in 21% yield. The hydrodehalogenated product must be observed due to the impurities in the mesitylene solvent. The cyclized product formation revealed the radical is generated, which gets added to the benzyl group of the same molecule. Then, to confirm the radical involvement in the coupling reaction, a radical trap experiment was conducted. The reaction was performed using (2,2,6,6-Tetramethylpiperidin-1-yl)oxyl (TEMPO) as a radical trap, in this case no biaryl product was observed. The aryl radicals generated in the reaction, which gets coupled with TEMPO radical and prevents the further reaction (Scheme 4.12).



Scheme 4.12 Radical quenching by TEMPO.

The diverse effect of the base in C-B and C-C bond forming reaction raised our interest in the mechanism of these reactions. Initially, additive ^BBiPy was reacted with potassium methoxide and sodium methoxide along with sequestering agent (crown ethers), gave the purple crystals of radical anion of bipyridine in separate experiments (Scheme 4.12). The radical anion of bipyridine

was confirmed by SC-XRD unambiguously. The molecule **24** was crystallized in the orthorhombic crystal system with Pna 21 space group. Two pyridine rings of the 4,4-bipyridine molecule are almost planar with a torsional angle of 2.47°. The counter cation potassium (K) is tethered to one of the nitrogen (N1) at a distance of 2.571(5) Å and also hold by 18-C-6 molecules. The structural features of the radical anion with sodium counter cation **25** are almost similar. The sodium (Na) is 2.466 (8) Å and 2.517 (8) Å away from nitrogen of the two separate bipyridine molecule (Figure 4.5).

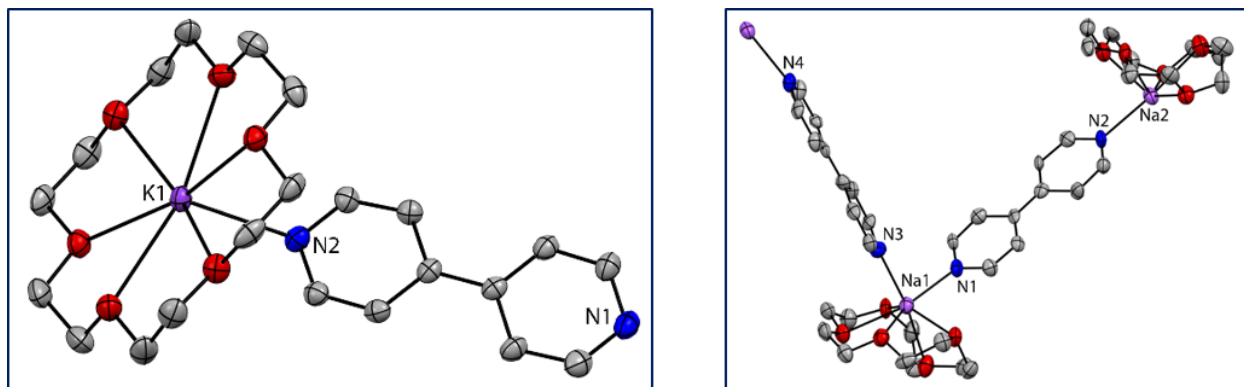
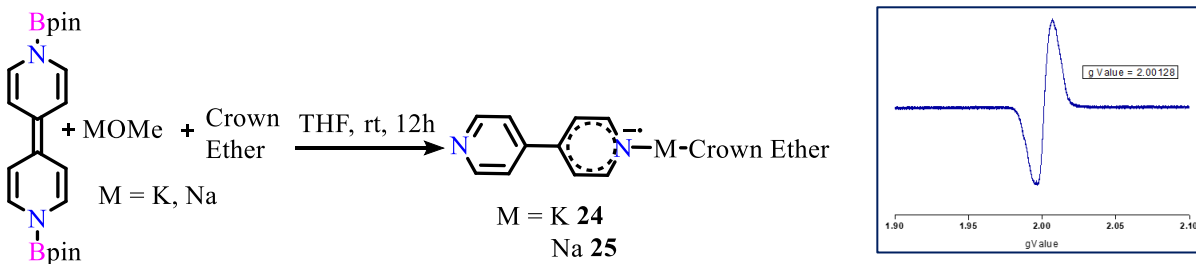


Figure 4.5 Molecular Structure of **24** and **25**.



Scheme 4.13 Radical anion (**24** and **25**) synthesis and EPR of **24**.

These bipyridine radical anions were further confirmed by EPR measurement, which gave a sharp single peak at *g* value 2.0022 matching with free organic radical species (*g* value for organic radical ranges from 1.99 – 2.01). In the EPR experiment, we did not find any hyperfine coupling. Based on the above experiment, the KOMe and NaOMe were also able to generate electron donor species, still, it was unable to perform an arylation reaction. Then by considering the reported mechanism, we thought that, deprotonation of cyclohexadienyl radical into the cyclohexadienyl radical anion requires a strong base, and other bases are not strong enough to do it.

In NaOMe, the group 1 metal methoxides are essentially a covalent species and has weak basicity. The basicity can be increased by making it a charge-separated ionic species. The 15-C-5 can shift the equilibrium to charge-separated species from covalent species, thus increasing the basicity. To confirm it, we added 15-C-5 in the reaction of arylation along with sodium methoxide as a base, and to our surprise, we found the C-C coupled product with a yield of 53%. This is the first result of sodium methoxide promoted C-H arylation by a homolytic aromatic substitution reaction.

Borylation of bromoarenes was very facile, whereas arylation of bromoarenes was occurring with very low yields. The difference between the two reactions is solvent (MTBE for borylation and Benzene for arylation reaction) and the extra borylating source bis(pinacolato)diboron in borylation reaction. Leaving aside solvent, we focused on the use of bis(pinacolato)diboron in arylation reaction. Before that, we performed a competition experiment between borylation and arylation of iodoarenes, with benzene as a solvent. Two equivalent of **16** was added in the reaction of 4-Iodoanisole, found only arylated (biaryl) product **18a** over competitive **17a** borylation product. The concentration of benzene is 40 times higher than the **16**, and this could be the possible reason for favor. Then arylation of bromoarene was performed in the presence of 1 Equiv. of **16** in benzene solvent, and gratifyingly it gave 53% yield of biaryl **18a**. It means bis(pinacolato)diboron is not just the boron source, what is more it helps in the reduction of bromoarenes into aryl radical. This information leads us to conclude that additive **^BBiPy** is acting catalytically, and its dianionic form is effective in reducing the bromoarenes into aryl radical. The 4,4'-bipyridine generated in the reaction mixture, again turned into additive **^BBiPy**, by insertion into bis(pinacolato)diboron. This way organoborane **^BBiPy** act catalytically.

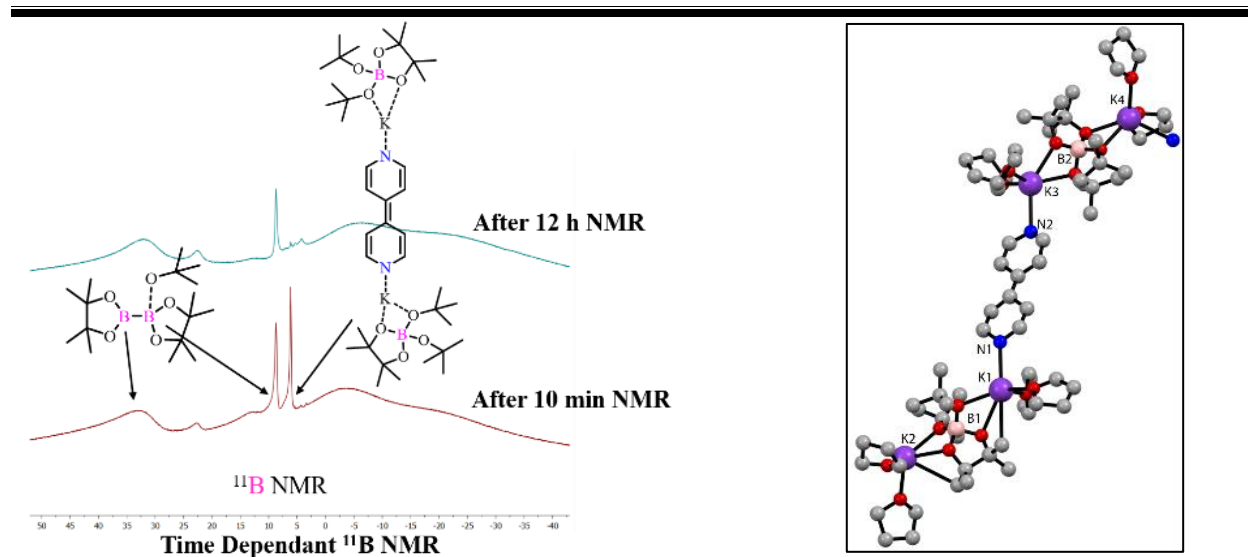


Figure 4.6 Time-dependent ^{11}B NMR plots of reaction mixture and crystal structure of **A1.K1**.

The electron donor species could be dianion with or without the pinacolboron group, which is confirmed separately in another experiment. The ^{11}B NMR measurement of the reaction mixture was performed after 5 minutes and after 12 hours of reaction, the NMR spectra showed disappearance of peak at 4 ppm after 12 hours, led us to assume that the peak for radical donor species involves the boron compound (Figure 4.6). In the control experiment, $^{\text{B}}\text{BiPy}$ and $\text{KO-}t\text{-Bu}$ in THF solvent at room temperature, we could able to isolate few crystals of **26**, which perhaps responsible for the same peak. The compound **26** is di-anionic in nature and crystallized in P2_1 space group. Two borate anions are still coordinated with potassium and bipyridine in the molecular structure.

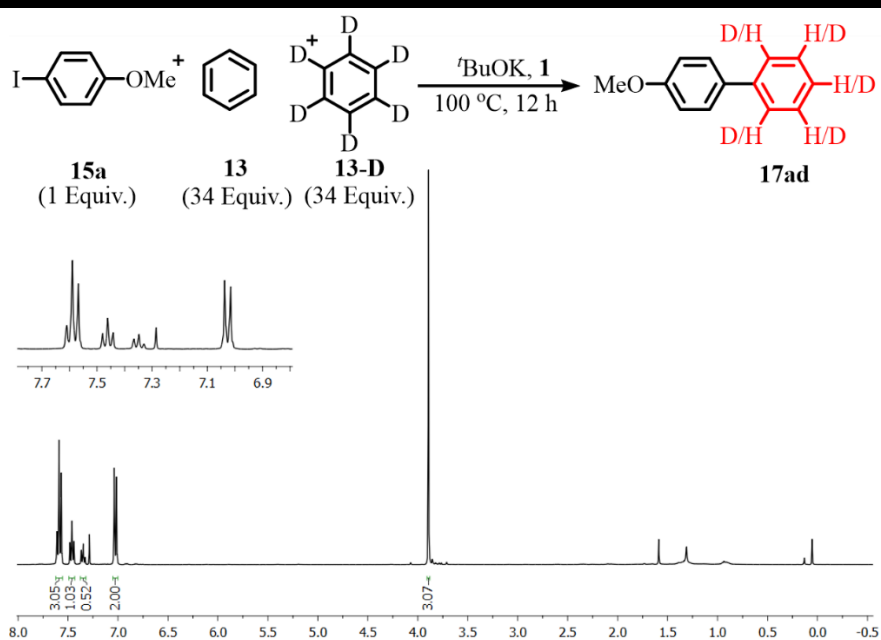


Figure 4.7 KIE experiment and ^1H NMR plot.

In order to understand the C-H bond breaking is not the rate-determining step, the Kinetic isotope effect (KIE) was determined from an intermolecular competition reaction. KIE is the change in the rate of reaction when it's isotope replaces one of the atom in the reactant. Basically, it is a ratio of rate constant for a chemical reaction involving the lighter (k_L) and heavier (k_H) isotopically substituted reactant.

$$KIE = k_L/k_H$$

KIE can be calculated from the ^1H NMR integrals by considering the relative amount of product formed in the C-H and C-D functionalization. In KIE, the product formed is directly proportional to rate constants in intermolecular competition reaction between two different isotopically labelled reactant. A kinetic isotope experiment of 4-Iodoanisole with the mixture of equal moles of benzene and deuterated benzene gave $k_{H/D}$ value 1.08, which suggest the absence of KIE (Figure 4.7). According to Simmons and Hartwig⁴² the absence of KIE is an indicative of C-H bond cleavage is not occurring in the rate-determining step.

Having all these observations and information along with literature reports by others³³⁻³⁵, a radical-mediated mechanism is proposed, as represented in figure 4.8. The catalytic cycle begins with the attack of the base on additive generating electron donor species, which transfers one electron to the aryl halide reducing it to the radical anion of aryl halide, parallelly it forms

bipyridine. The generated radical anion of aryl halide loses halide anion leaving aryl radical, which adds to B_2pin_2 , giving the aryl boronic ester as a product. The generated bipyridine again reacts with the B_2pin_2 generating back $^B BiPy$, and the catalysis continues to the next catalytic cycle of borylation (Figure 4.8).

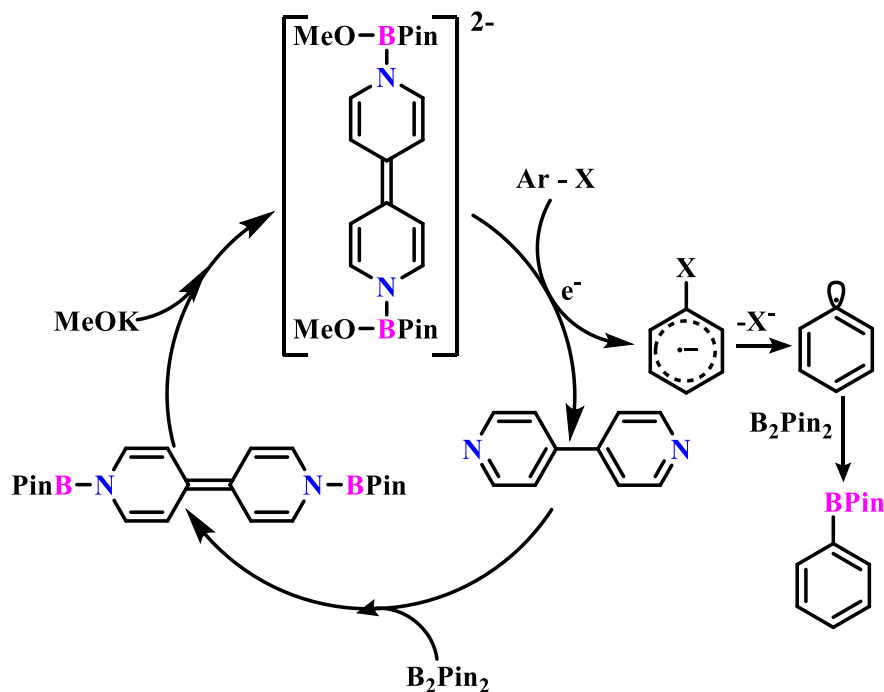


Figure 4.8 Proposed mechanism for borylation of aryl halides.

Whereas, in the case of arylation of aryl Iodides, the electron donor species generated from the reaction of base and $^B BiPy$, reduces the aryl halide to aryl radicals by removal of iodide. The aryl radical adds to benzene generating cyclohexadienyl radical as the intermediate, which then deprotonation by base form the biaryl radical anion. Subsequently, the biaryl radical anion transfer the electron to the aryl iodide by thus generating the product and aryl radical enables the catalytic cycle (Scheme 4.9).

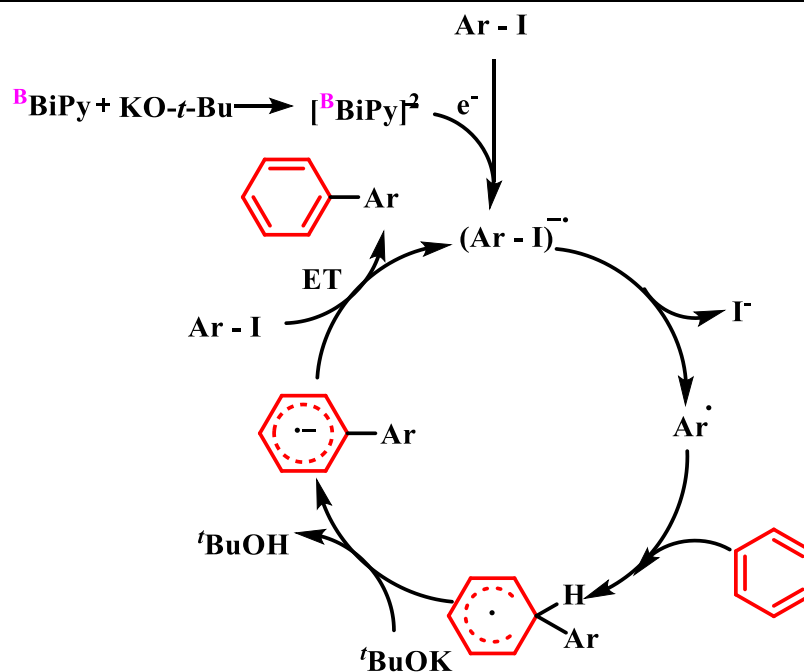


Figure 4.9 Proposed Mechanism for arylation of aryl iodides.

4.3 Conclusion

In conclusion, we have developed the organo-main-group additives for C-H functionalization of unactivated arenes and C-B bond forming reactions. The redox reversibility of these additives diminished in diazonium coupling reaction due to the decomposition, but this led to the formation of electron donor species from the additives, that are capable of transferring an electron to aryl halides. The aryl radical generated this way was used for C-C and C-B bond formation reaction. The organoborane additives are more potent for borylation as well as arylation of aryl halides over organosilicon additives. The C-C bond formation is more favored over C-B bond formation, revealed by the competition experiment. We have arrested the possible electron donor and characterized them by single-crystal XRD techniques. The result from the KIE experiment suggests the C-H bond cleavage is not the rate-determining step. The organoborane additives are working catalytically in C-B the bond-forming reaction, while they are initiators for arylation reaction.

4.4 Experimental Details

4.4.1 General Remarks

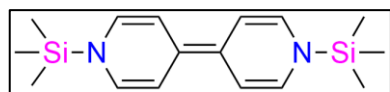
Unless otherwise mentioned, all reactions were performed using standard schlenk techniques or in MBraun glovebox under an atmosphere of argon. Anhydrous MTBE (98%) solvent was purchased from Sigma Aldrich. THF, Benzene were dried over sodium/benzophenone. Dry DMSO was obtained by refluxing over calcium hydride and storing over 3 Å molecular sieves. All other solvents were used as received. All chemicals are purchased from Sigma Aldrich, Alfa Aesar, Avra and used as received. ^1H , ^{13}C , ^{11}B , ^{19}F , and ^{29}Si NMR spectra were recorded on Bruker (400.44 MHz) spectrometers. ^1H NMR and ^{13}C NMR data were reported as follows: chemical shift in ppm downfield from tetramethylsilane, ^{11}B NMR data were reported in ppm downfield from $\text{BF}_3\cdot\text{OEt}_2$. ^{19}F NMR data were reported in ppm downfield from $\text{C}_6\text{H}_5\text{CF}_3$. ^{29}Si NMR was recorded in ppm downfield from tetramethylsilane. High-resolution mass spectra were recorded on a JEOL JMS-SX102A (EI) spectrometer. Single crystal data were collected on both Bruker SMART APEX four-circle diffractometer equipped with a CMOS photon 100 detector (Bruker Systems Inc.) with a Cu $\text{K}\alpha$ radiation (1.5418 Å), and Bruker SMART APEX Duo diffractometer using Mo $\text{K}\alpha$ radiation (0.71073 Å).

4.4.2 EPR Measurement

The sample of radical anion of **1.Cs**, **1.K** dissolved in 0.3 mL of tetrahydrofuran solvent, transfer it to quartz EPR tube and sealed under argon atmosphere. The EPR is conducted on JES – FA200 JEOL ESR spectrometer with X band. The modulation frequency = 100 kHz, Modulation Width = 0.05 mT and sweep time = 2.0 min. The frequency of instruments was 9100.512 kHz.

4.4.3 Synthetic Procedures

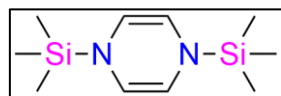
A. Synthesis of 1,1'-bis(trimethylsilyl)-1H,1'H-4,4'-bipyridinylidene ($^{\text{Si}}\text{BiPy}$)^{39a}



In an oven-dried 50 mL round-bottom flask, freshly cut sodium pieces (0.523 g, 0.023 mol, 3.0 equiv.) was suspended in THF (10 mL) under Ar atmosphere. Chlorotrimethylsilane (2.9 mL, 0.023 mol, 3.0 equiv.) was added slowly to the THF suspension. Subsequently, 4,4'-Bipyridine (1.19 g, 0.008 mol, 1.0 equiv.) dissolved in THF (30 mL), and added slowly to the THF suspension containing sodium pieces using dropping funnel at room temperature. After stirring for 24 h at room temperature, the solvent was removed under vacuum. The product was washed three times with toluene under argon

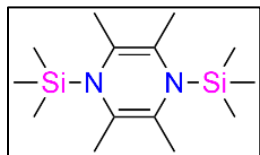
atmosphere. All the washings are collected, concentrated, and kept for crystallization at low temperatures. The target compound was collected as a red-colored crystalline solid in 75% yield. ^1H NMR (400 MHz, Benzene- d_6) δ -0.09 (s, 18H, NSiMe $_3$), 5.75 (d, J = 8.3 Hz, 4H, NCH=CH), 5.83 (d, J = 7.7 Hz, 4H, NCH=CH) ppm. ^{13}C NMR (101 MHz, Benzene- d_6) δ 128.71, 111.73, 111.19, 0.21 ppm.

B. Synthesis of 1,4-bis(trimethylsilyl)-1,4-dihydropyrazine ($^{\text{Si}}\text{Pz}$)^{39b} This is a



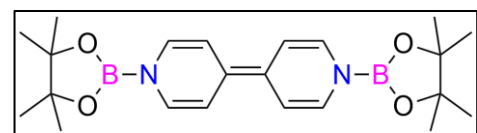
literature modified experimental procedure. In a flame dried schlenk flask lithium (0.8 g, 0.115 moles, 1 Equiv.) was suspended in 30 mL of THF solvent under an argon atmosphere. Pyrazine (3.0 g, 0.037 moles, 3 Equiv.) was taken in another schlenk flask in 10 mL of THF solvent slowly transferred to a flask containing suspended lithium. The reaction cools down to 10 °C, then trimethylsilyl chloride (12 mL, 0.094 moles) was added dropwise using pressure equalizer funnel. The reaction mixture was stirred for 6 hours at low temperature. The Solvent was removed in vacuo, the product was extracted in pentane. Pentane was removed in vacuo to get the target compound as yellow-colored crystalline solid with the yield of 85% as highly air and moisture sensitive compound. ^1H NMR (400 MHz, Benzene- d_6) δ 4.71 (s, 1H), 0.00 (s, 5H) ppm. ^{13}C NMR (101 MHz, Benzene- d_6) δ 117.40, 0.21 ppm. ^{29}Si NMR (80 MHz, Benzene- d_6) δ 4.67 ppm.

C. Synthesis of 2,3,5,6-tetramethyl-1,4-bis(trimethylsilyl)-1,4-dihydropyrazine ($^{\text{Si}}\text{tPz}$)^{39c}



In a 100 mL Schlenk-flask 2,3,5,6-tetramethylpyrazine (0.8 g, 5.9 mmol, 1.0 equiv.) and chlorotrimethylsilane (2.4 mL, 18.9 mmol, 3.2 equiv.) were dissolved in THF (300 mL) in an argon atmosphere and freshly cut potassium slices (0.8 g, 20.5 mmol, 3.5 equiv.) were added. The reaction mixture was stirred for 7 days at room temperature and filtered. The solvent was removed in vacuo, and the product was extracted in pentane. The pentane solution was concentrated and cooled to -30 °C to get the title compound as colorless crystals with the yield of 65% as highly moisture and air-sensitive crystals. Storage and handling in a glove-box is recommended ^1H -NMR (300.1 MHz, Chloroform- d_3): δ = 0.15 (s, 18H), 1.69 (s, 12H) ppm.

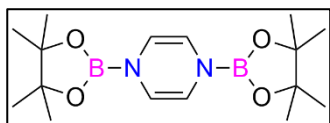
D. 1,1'-bis(4,4,5,5-tetramethyl-1,3,2-dioxaborolan-2-yl)-1H,1'H-4,4'-bipyridinylidene



($^{\text{B}}\text{BiPy}$)^{41a} In a glove box, a high pressure tube made of quartz having PTFE stopcock, equipped with a magnetic stirring bar, was charged with 4,4'-bipyridine (2.0 g, 12.80

mmol), bis(pinacolato)diboron (3.57 g, 14.08 mmol), and benzene (10 mL). The reaction mixture turned dark orange brown colored homogeneous solution. The tube was sealed by the stopcock and was taken out from the glove box. The mixture was stirred at 110 °C for 16 hours. A colored precipitate (bright orange or yellow) was formed on the inside wall of the tube. The yellow-colored solid was washed with benzene and pentane to remove unreacted bipyridine, followed by drying in vacuo. The N,N'-diboryl-4,4'-bipyridinylidene (**^BBiPy**) was obtained as a yellow solid with high purity as highly air and moisture sensitive compound. The storage and handling of compound is recommended in the glovebox. ¹H NMR (400 MHz, Chloroform-*d*₃) δ 6.23 (s, 4H), 5.64 (s, 4H), 1.25 (s, 24H). ¹¹B NMR (128 MHz, Chloroform-*d*₃) δ 23.34 ppm.

E. 1,4-bis(4,4,5,5-tetramethyl-1,3,2-dioxaborolan-2-yl)-1,4-dihydropyrazine (^BPz**)^{41b}**



In a glove box, a high pressure tube with a screw cap PTFE stopcock charged with pyrazine (0.35 g, 4.4 mmol), bis(pinacolato)diboron (1.06 g, 4.2 mmol) and 5 mL of THF solvent. The tube was sealed under argon atmosphere, and the solution was stirred at room temperature for 2 hours. The solvent was removed in vacuo to get high purity white colored solid. ¹H NMR (400 MHz, Chloroform-*d*₃) δ 5.13 (s, 4H), 1.19 (s, 24H). ¹³C NMR (101 MHz, Chloroform-*d*₃) δ 113.21, 82.99, 24.51. ¹¹B NMR (128 MHz, Chloroform-*d*₃) δ 21.74 ppm.

F. 2,3,5,6-tetramethyl-1,4-bis(4,4,5,5-tetramethyl-1,3,2-dioxaborolan-2-yl)-1,4-



dihydropyrazine (^BtPz**)^{41b}** In a glove box, a high pressure tube with a screw cap PTFE stopcock charged with 2,3,5,6-tetramethylpyrazine (0.5 g, 3.69 mmol), bis(pinacolato)diboron (0.93 g, 3.32 mmol) and 5 mL of THF solvent. The tube was sealed under argon atmosphere and the solution was stirred at room temperature for 2 hours. The solvent was removed in vacuo to get high purity white colored solid ¹H NMR (400 MHz, Chloroform-*d*₃) δ 2.30 (s, 12H), 1.09 (s, 24H). ¹³C NMR (101 MHz, Chloroform-*d*₃) δ 147.96, 82.74, 24.86, 20.95 ppm.

G. Experimental procedure for arylation from arene diazonium salt

I. 5 mol% catalyst In a sealed tube, arene diazonium salt (1.04 mmol, 1 Equiv.), ^{Si}BiPy (5 mol %), benzene (10 equiv.) was added in 2 mL of DMSO solvent. The sealed tube packed under argon atmosphere and kept for stirring at room temperature for 12 hours. The product was extracted in the DCM solvent and evaporated to get the crude product, further purified by column chromatography.

II. 50 mol% of catalyst In a sealed tube, arene diazonium salt (1.04 mmol, 1 Equiv.), ^{Si}BiPy (50 mol %), benzene (10 equiv.) was added in 2 mL of DMSO solvent. The sealed tube packed under argon atmosphere and kept for stirring at room temperature for 12 hours. The product was extracted in the DCM solvent and evaporated to get the crude product, further purified by column chromatography.

H. Experimental procedure for borylation from arene diazonium salt

I. 10 mol% of catalyst In a sealed tube arene diazonium salt (1.04 mmol, 1 Equiv.), additive (10 mol %), bis(pincolato)diboron (2 equiv.) was added in 2 mL of ACN solvent. The sealed tube packed under argon atmosphere and kept for stirring at room temperature for 12 hours. The product was extracted in the DCM solvent and evaporated to get the crude product. The crude product was eluted through column chromatography (2:98 ethyl acetate : hexane).

J. ^{Si}Pz Catalyst decomposition/NMR scale experiment- In an NMR tube, Phenyl diazonium salt and ^{Si}Pz added in 0.6 mL of DMSO-*d*₆. The NMR tube shakes for 5 minutes, then submitted for ¹H, ¹¹B, ²⁹Si, and ¹⁹F NMR measurement. All the NMR spectra are given below.

K. Synthesis of Radical Anion

I. 14⁻Cs (From ^{Si}BiPy) CsF (0.101 g, 0.66 mmol) was added to ^{Si}BiPy (0.100 g, 0.33 mmol) in 10 mL of THF solvent followed by 18-C-6 (0.175 g, 0.66 mmol). The reaction mixture initially was red, later turned to dark blue.

II. 24 (From ^BBiPy) KOMe (0.034g, 0.487 mmol) was added to ^BBiPy (0.100 g, 0.243 mmol) in 10 mL of THF solvent followed by 18-C-6 (0.128 g, 0.487 mmol). The reaction mixture instantly turned into a blue color solution. The reaction mixture was filtered through a pad of Celite, concentrated to 5 mL. The filtrate was kept in -30 °C freezer to get purple crystals of **24**.

III. 25 (From ^BBiPy) NaOMe (0.026 g, 0.487 mmol) was added to ^BBiPy (0.100 g, 0.243 mmol) in 10 mL of THF solvent followed by 15-C-5 (0.107 g, 0.487 mmol). The reaction mixture instantly turned into a blue color solution. The reaction mixture was filtered through a pad of Celite, concentrated to 5 mL. The filtrate was kept in -30 °C freezer to get purple crystals of **25**.

IV. 26 (From ^BBiPy) KO-t-Bu (0.055 g, 0.487 mmol) was added to ^BBiPy (0.100 g, 0.243 mmol) in 10 mL of THF solvent The reaction mixture instantly turned red color solution. The reaction mixture was instantly kept for crystallization at -30 °C to get very few red colored crystals of **26**.

L. Experimental procedure for borylation of aryl halides (^{Si}BiPy catalyst)

Aryl halide (0.34 mmol), ^{Si}BiPy (0.068 mmol), CsF (0.156 g, 1.02 mmol) and bis(pincolato)diboron (0.68 mmol) was added in sealed tube followed by DMSO solvent (2ml) under argon atmosphere and set for stirring at 95 °C for 12 h. After cooling down to room temperature, the reaction was quenched with 5 ml water, and the product was extracted in diethyl ether (10 mL X 3). The combined organic layer was dried over anhydrous sodium sulfate, concentrated under vacuum. The crude product was purified by column chromatography

M. Experimental procedure for arylation of aryl halides (^{Si}BiPy catalyst)

Aryl halide (0.34 mmol), ^{Si}BiPy (0.068 mmol), CsF (0.156 g, 1.02 mmol) was added in a sealed tube followed by benzene solvent (2ml) under argon atmosphere and set for stirring at 100 °C for 12 h. After cooling down to room temperature, the reaction was quenched with 5 ml water, and the product was extracted in diethyl ether (10 mL X 3). The combined organic layer was dried over anhydrous sodium sulfate, concentrated under vacuum. The crude product was purified by column chromatography

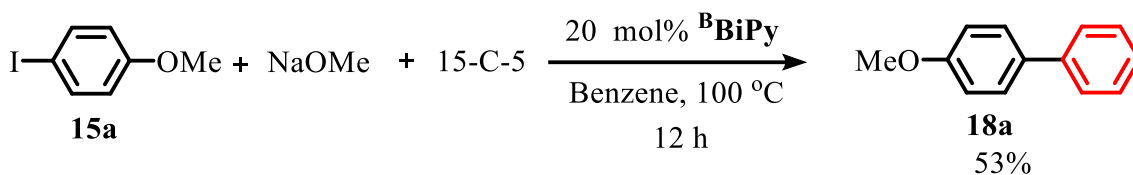
N. Experimental procedure for borylation of aryl halides (^BBiPy catalyst)

Aryl halide (0.427 mmol), ^BBiPy (0.085 mmol), KOMe (0.06 g, 0.854 mmol) was added in a sealed tube followed by MTBE solvent (2ml) under argon atmosphere and set for stirring at 85 °C for 12 h. After cooling down to room temperature, the reaction was quenched with 5 ml water, and the product was extracted in diethyl ether (10 mL X 3). The combined organic layer was dried over anhydrous sodium sulfate, concentrated under vacuum. The crude product was purified by column chromatography.

O. Experimental procedure for arylation of aryl Iodide (^BBiPy catalyst)

Aryl halide (0.427 mmol), ^BBiPy (0.085 mmol), KO-*t*-Bu (0.095g, 0.854 mmol) was added in a sealed tube followed by benzene solvent (2ml) under argon atmosphere and set for stirring at 100 °C for 12 h. After cooling down to room temperature, the reaction was quenched with 5 ml water, and the product was extracted in diethyl ether (10 mL X 3). The combined organic layer was dried over anhydrous sodium sulfate, concentrated under vacuum. The crude product was purified by column chromatography.

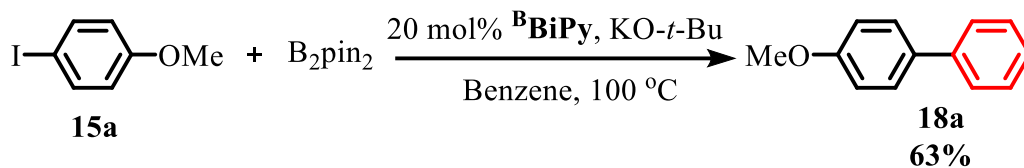
P. Role of base strength in arylation (Using NaOMe and 15-C-5)



Scheme 4.14 Reaction with NaOMe and Crown ether.

4-Iodoanisole (0.05 g, 0.213 mmol), ^BBiPy (0.018 g, 0.042 mmol), NaOMe (0.023 g, 0.427 mmol) and 15-C-5 (0.094 g, 0.427 mmol), was added in sealed tube followed by benzene solvent (1 mL) under argon atmosphere and set for stirring at 100 °C for 12 h. After cooling down to room temperature, the reaction was quenched with 5 ml water, and the product was extracted in diethyl ether (10 mL X 3). The combined organic layer was dried over anhydrous sodium sulfate, concentrated under vacuum. The crude product was purified by column chromatography.

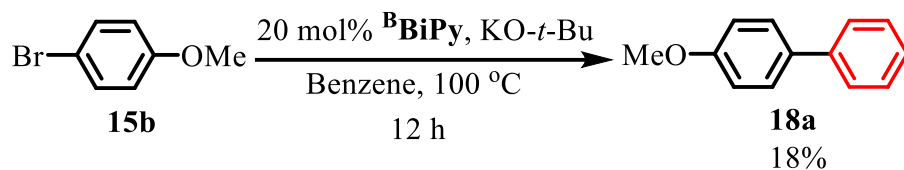
Q. Competition experiment (Borylation Vs. Arylation)



Scheme 4.15 Competition reaction between borylation and arylation.

4-Iodoanisole (0.05 g, 0.213 mmol), ^BBiPy (0.018 g, 0.042 mmol), KO-*t*-Bu (0.042 g, 0.427 mmol) and bis(pinacolato)diboron (0.108 g, 0.427 mmol), was added in sealed tube followed by benzene solvent (1 mL) under argon atmosphere and set for stirring at 100 °C for 12 h. After cooling down to room temperature, the reaction was quenched with 5 ml water, and the product was extracted in diethyl ether (10 mL X 3). The combined organic layer was dried over anhydrous sodium sulfate, concentrated under vacuum. The crude product was purified by column chromatography.

R. Experimental procedure for arylation of 4-Bromoanisole (Using bis(pinacolato)diboron)



Scheme 4.16 Competition reaction between borylation and arylation.

4-Bromoanisole (0.079 g, 0.424 mmol), $^B\text{BiPy}$ (0.034 g, 0.084 mmol), $\text{KO-}t\text{-Bu}$ (0.143 g, 1.27 mmol) and bis(pincolato)diboron (0.107 g, 0.424 mmol), was added in sealed tube followed by benzene solvent (2 mL) under argon atmosphere and set for stirring at 100 °C for 12 h. After cooling down to room temperature, the reaction was quenched with 5 ml water, and the product was extracted in diethyl ether (10 mL X 3). The combined organic layer was dried over anhydrous sodium sulfate, concentrated under vacuum. The crude product was purified by column chromatography.

S. Intramolecular arylation by radical trapping

1-(benzyloxy)-2-Iodobenzene **20** (0.132 g, 0.427 mmol), $^B\text{BiPy}$ (0.035 g, 0.0854 mmol), $\text{KO-}t\text{-Bu}$ (0.095 g, 0.854 mmol) was added in sealed tube followed by mesitylene solvent (2 mL) under argon atmosphere and set for stirring at 100 °C for 12 h. After cooling down to room temperature, the reaction was quenched with 5 ml water, and the product was extracted in diethyl ether (10 mL X 3). The combined organic layer was dried over anhydrous sodium sulfate, concentrated under vacuum. The crude product was purified by column chromatography (10:90 ethyl acetate: hexane) eluted as a mixture of **20**, 6*H*-benzo[*c*]chromene (66%) **21** and (benzyloxy)benzene (21%) **23** confirmed by ^1H NMR (Figure.4.49).

T. Radical Trapping by TEMPO

4-Iodoanisole (0.05 g, 0.213 mmol), $^B\text{BiPy}$ (0.017 g, 0.042 mmol), $\text{KO-}t\text{-Bu}$ (0.047 g, 0.042 mmol) and (2,2,4,4-tetramethylpiperidine-1-yl)oxyl (TEMPO) (0.033 g, 0.213 mmol), was added in sealed tube followed by benzene solvent (1 mL) under argon atmosphere and set for stirring at 100 °C for 12 h. After cooling down to room temperature, the reaction was quenched with 5 ml water, and the product was extracted in diethyl ether (10 mL X 3). The combined organic layer was dried over anhydrous sodium sulfate, concentrated under vacuum. The crude product was purified by column chromatography.

U. Time-dependent ^{11}B NMR measurement in borylation reaction

4-Iodoanisole (0.05 g, 0.213 mmol), ^BBiPy (0.018 g, 0.042 mmol), KOMe (0.030 g, 0.427mmol) was added in sealed tube followed by MTBE solvent (2ml) under argon atmosphere and set for stirring at 85 °C.

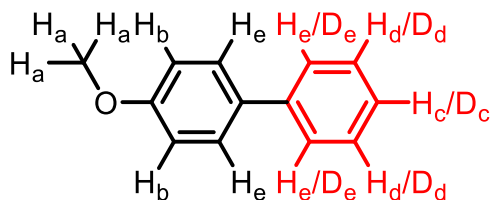
The experiment was performed separately and submitted for NMR after a certain time

After 5 Min – solvent was removed in vacuo, sample submitted for NMR in DMSO-*d*₆

After 12 hours – solvent was removed in vacuo, sample submitted for NMR in DMSO-*d*₆

V. Kinetic Isotope Effect

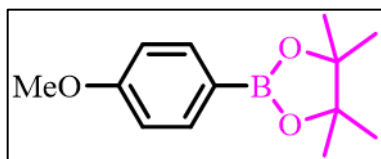
4-Iodoanisole (0.1 g, 0.427 mmol), ^BBiPy (0.035 g, 0.085 mmol) and KO-*t*-Bu (0.095 g, 0.85 mmol) was added in sealed tube followed by benzene (1 mL) and Benzene -*d*₆ (1 mL) under argon atmosphere and set for stirring at 100 °C for 12 h. After cooling down to room temperature, the reaction was quenched with 5 ml water, and the product was extracted in diethyl ether (10 mL X 3). The combined organic layer was dried over sodium sulfate, concentrated under vacuum. The crude product was purified by column chromatography eluted with hexane.



The KIE is calculated by taking the ratio of NMR integral of a proton {H_c} to {1 - H_c}.

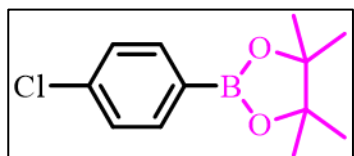
4.4.4 Spectroscopic Data

I. 2-(4-methoxyphenyl)-4,4,5,5-tetramethyl-1,3,2-dioxaborolane (17a) ¹H NMR (400



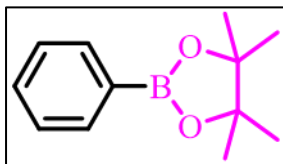
MHz, Chloroform-*d*₃) δ 7.76 – 7.78 (m, 2H), 6.90 – 6.93 (m, 2H), 3.85 (s, 3H), 1.35 (s, 12H) ppm. ¹³C NMR (101 MHz, Chloroform-*d*₃) δ 162.14, 136.50, 113.30, 83.56, 55.09, 24.86 ppm.

II. 2-(4-chlorophenyl)-4,4,5,5-tetramethyl-1,3,2-dioxaborolane (17b) ¹H NMR (400

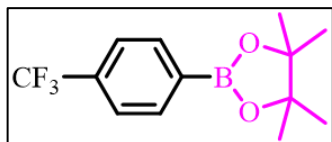


MHz, Chloroform-*d*₃) δ 7.76 – 7.74 (m, 2H), 7.37 – 7.35 (m, 2H), 1.36 (s, 12H) ppm. ¹³C NMR (101 MHz, Chloroform-*d*₃) δ 137.52, 136.11, 128.00, 84.01, 24.86 ppm.

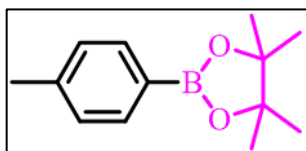
III. **4,4,5,5-tetramethyl-2-phenyl-1,3,2-dioxaborolane (17c)** ^1H NMR (400 MHz, Chloroform- d_3) δ 7.85 (d, $J = 8.0$ Hz, 1H), 7.49 (t, $J = 7.4$ Hz, 1H), 7.40 (t, $J = 7.2$ Hz, 1H), 1.38 (s, 6H) ppm. ^{13}C NMR (101 MHz, Chloroform- d_3) δ 134.73, 131.25, 127.71, 83.78, 24.88 ppm.



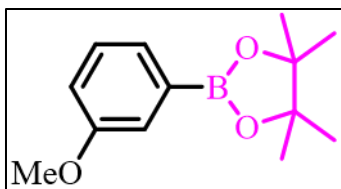
IV. **4,4,5,5-tetramethyl-2-(4-(trifluoromethyl)phenyl)-1,3,2-dioxaborolane (17d)** ^1H NMR (400 MHz, Chloroform- d_3) δ 7.80 – 7.76 (m, 2H), 6.94 – 6.90 (m, 2H), 3.85 (s, 3H), 1.36 (s, 12H) ppm. ^{13}C NMR (101 MHz, Chloroform- d_3) δ 162.14, 136.51, 113.31, 83.55, 55.09, 24.86 ppm.



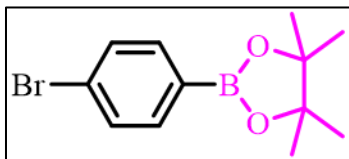
V. **4,4,5,5-tetramethyl-2-(p-tolyl)-1,3,2-dioxaborolane (17e)** ^1H NMR (400 MHz, Chloroform- d_3) δ 7.73 (d, $J = 7.9$ Hz, 1H), 7.24 – 7.20 (m, 1H), 2.39 (s, 2H), 1.37 (s, 6H) ppm. ^{13}C NMR (101 MHz, Chloroform- d_3) δ 141.40, 134.81, 128.52, 83.62, 24.87, 21.74 ppm.



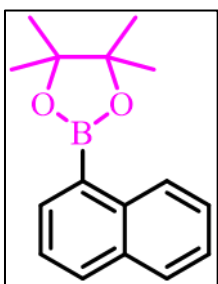
VI. **2-(3-methoxyphenyl)-4,4,5,5-tetramethyl-1,3,2-dioxaborolane (17g)** ^1H NMR (400 MHz, Chloroform- d_3) δ 7.43 (d, $J = 7.2$ Hz, 1H), 7.37 – 7.30 (m, 2H), 7.04 (ddd, $J = 8.2, 2.8, 1.1$ Hz, 1H), 3.86 (s, 4H), 1.37 (s, 14H) ppm. ^{13}C NMR (101 MHz, Chloroform- d_3) δ 159.03, 128.94, 127.19, 118.69, 117.92, 83.83, 55.25, 24.87 ppm.



VII. **2-(4-bromophenyl)-4,4,5,5-tetramethyl-1,3,2-dioxaborolane (17h)** ^1H NMR (400 MHz, Chloroform- d_3) δ 7.68 (d, $J = 8.3$ Hz, 1H), 7.53 (d, $J = 8.4$ Hz, 1H), 1.36 (s, 6H) ppm. ^{13}C NMR (101 MHz, Chloroform- d_3) δ 136.30, 134.73, 131.25, 130.95, 127.70, 126.23, 84.04, 24.86 ppm.

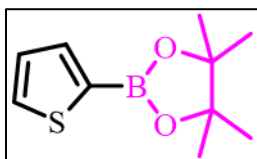


VIII. **4,4,5,5-tetramethyl-2-(naphthalen-1-yl)-1,3,2-dioxaborolane (17i)** ^1H NMR (400



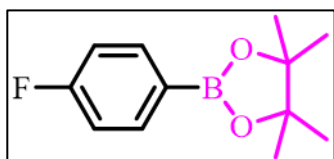
MHz, Chloroform- d_3) δ 8.80 (d, $J = 8.4$ Hz, 1H), 8.11 (dd, $J = 6.8, 1.3$ Hz, 1H), 7.96 (d, $J = 8.2$ Hz, 1H), 7.86 (d, $J = 8.0$ Hz, 1H), 7.60 – 7.47 (m, 3H), 1.46 (s, 12H) ppm. ^{13}C NMR (101 MHz, Chloroform- d_3) δ 136.92, 135.64, 133.21, 131.61, 128.41, 128.34, 126.33, 125.48, 124.97, 83.74, 24.98 ppm.

IX. **4,4,5,5-tetramethyl-2-(thiophen-2-yl)-1,3,2-dioxaborolane (17j)** ^1H NMR (400 MHz,



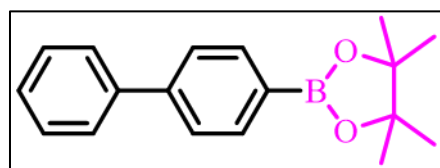
Chloroform- d_3) δ 7.67 (ddd, $J = 5.6, 4.1, 0.9$ Hz, 1H), 7.22 (dd, $J = 4.7, 3.5$ Hz, 1H), 1.37 (s, 6H) ppm. ^{13}C NMR (101 MHz, Chloroform- d_3) δ 137.16, 132.37, 128.22, 84.09, 77.35, 77.03, 76.72, 24.77 ppm.

X. **2-(4-fluorophenyl)-4,4,5,5-tetramethyl-1,3,2-dioxaborolane (17k)** ^1H NMR (400



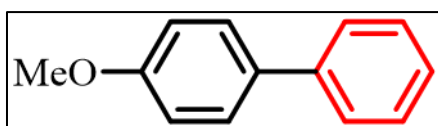
MHz, Chloroform- d_3) δ 7.82 (dd, $J = 8.6, 6.2$ Hz, 2H), 7.10 – 7.04 (m, 2H), 1.36 (s, 6H) ppm. ^{13}C NMR (101 MHz, Chloroform- d_3) δ 166.34, 163.85, 137.01, 136.93, 114.94, 114.74, 83.91, 24.86 ppm.

XI. **2-([1,1'-biphenyl]-4-yl)-4,4,5,5-tetramethyl-1,3,2-dioxaborolane (17l)** ^1H NMR (400



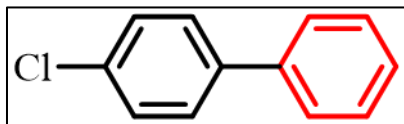
MHz, Chloroform- d_3) δ 7.92 (d, $J = 8.0$ Hz, 2H), 7.66 – 7.62 (m, 4H), 7.47 (t, $J = 7.5$ Hz, 2H), 7.38 (t, $J = 7.3$ Hz, 3H), 1.39 (s, 6H) ppm. ^{13}C NMR (101 MHz, Chloroform- d_3) δ 143.89, 141.03, 135.25, 128.77, 127.55, 127.24, 126.47, 83.83, 24.89 ppm.

XII. **4-methoxy-1,1'-biphenyl (18a)** ^1H NMR (400 MHz, Chloroform- d_3) δ 7.54 (t, $J = 8.3$ Hz,



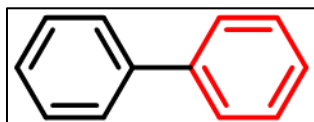
4H), 7.41 (t, $J = 7.7$ Hz, 2H), 7.30 (t, $J = 7.4$ Hz, 1H), 6.98 (d, $J = 8.7$ Hz, 2H), 3.85 (s, 3H) ppm. ^{13}C NMR (101 MHz, Chloroform- d_3) δ 159.16, 140.85, 133.80, 128.73, 128.17, 126.75, 126.67, 55.38 ppm.

XIII. **4-chloro-1,1'-biphenyl (18b)** ^1H NMR (400 MHz, Chloroform- d_3) δ 7.56-7.48 (m 4H),



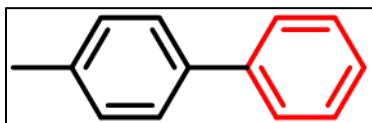
7.46-7.34 (m, 5H) ppm. ^{13}C NMR (101 MHz, Chloroform- d_3) δ 159.16, 140.85, 133.80, 128.73, 128.17, 126.75, 126.67, 55.38 ppm.

XIV. **1,1'-biphenyl (18c)** ^1H NMR (400 MHz, Chloroform- d_3) δ 7.65 (d, $J = 7.1$ Hz, 4H), 7.49



(t, $J = 7.6$ Hz, 4H), 7.40 (t, $J = 7.3$ Hz, 2H) ppm. ^{13}C NMR (101 MHz, Chloroform- d_3) δ 141.27, 128.78, 127.28, 127.20 ppm.

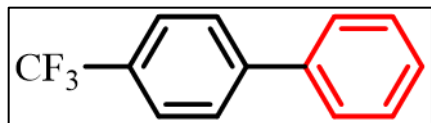
XV. **4-methyl-1,1'-biphenyl (18d)** ^1H NMR (400 MHz, Chloroform- d_3) δ 7.66 (d, $J = 7.2$ Hz,



2H), 7.57 (d, $J = 8.1$ Hz, 2H), 7.50 (t, $J = 7.6$ Hz, 2H), 7.39 (t, $J = 7.4$ Hz, 1H), 7.32 (d, $J = 8.1$ Hz, 2H), 2.47 (s, 3H) ppm. ^{13}C NMR (101 MHz, Chloroform- d_3) δ 141.21,

138.41, 137.06, 129.53, 128.76, 127.05, 127.02, 21.16 ppm.

XVI. **4-(trifluoromethyl)-1,1'-biphenyl (18e)** ^1H NMR (400 MHz, Chloroform- d_3) δ 7.66 (d,



$J = 7.2$ Hz, 1H), 7.57 (d, $J = 8.1$ Hz, 1H), 7.50 (t, $J = 7.6$ Hz, 4H), 7.39 (t, $J = 7.4$ Hz, 2H), 7.32 (d, $J = 8.1$ Hz, 1H), 2.47 (s, 2H) ppm. ^{13}C NMR (101 MHz,

Chloroform- d_3) δ 141.21, 138.41, 137.06, 129.53, 128.76, 127.05, 127.02, 21.16 ppm.

4.4.5 Plots of NMR Spectra

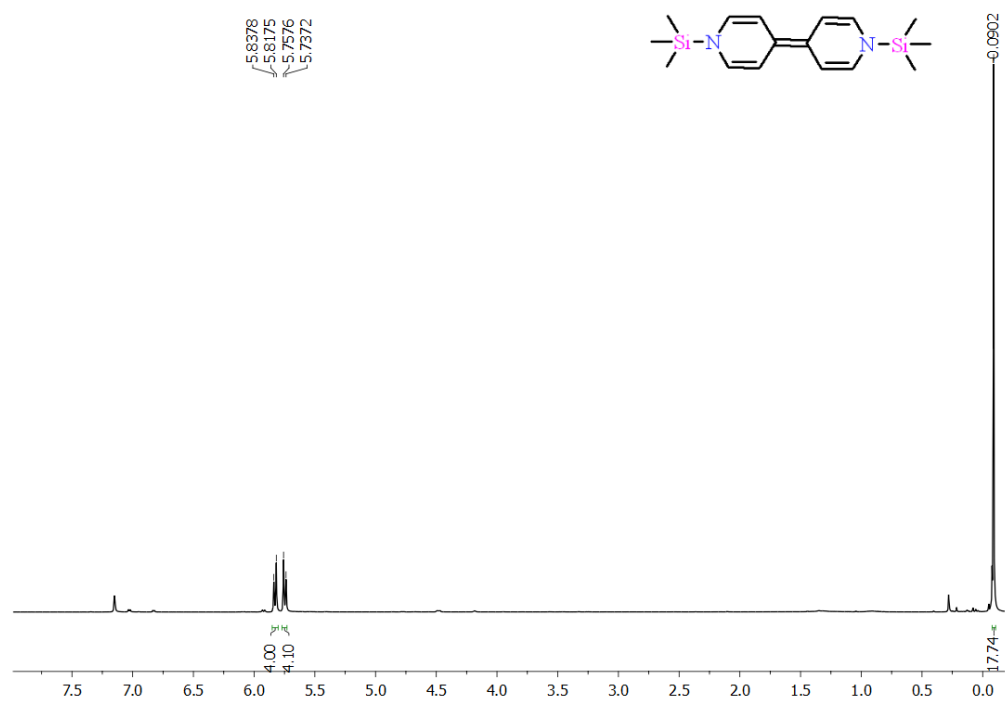


Figure 4.10 ^1H NMR of compound SiBiPy .

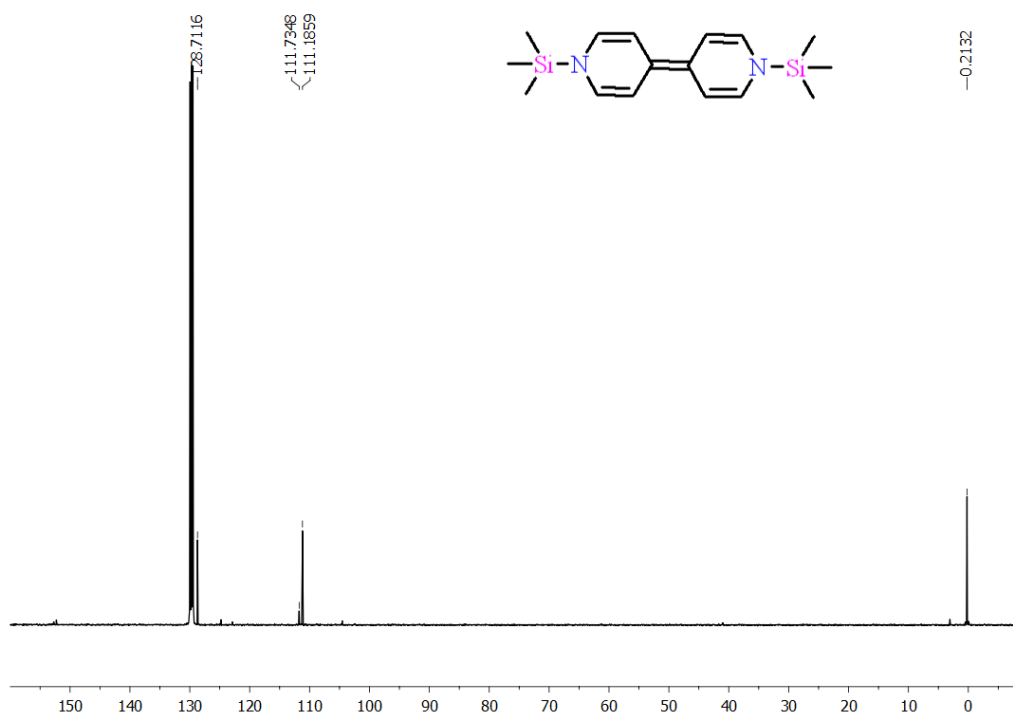


Figure 4.11 ^{13}C NMR of compound SiBiPy .

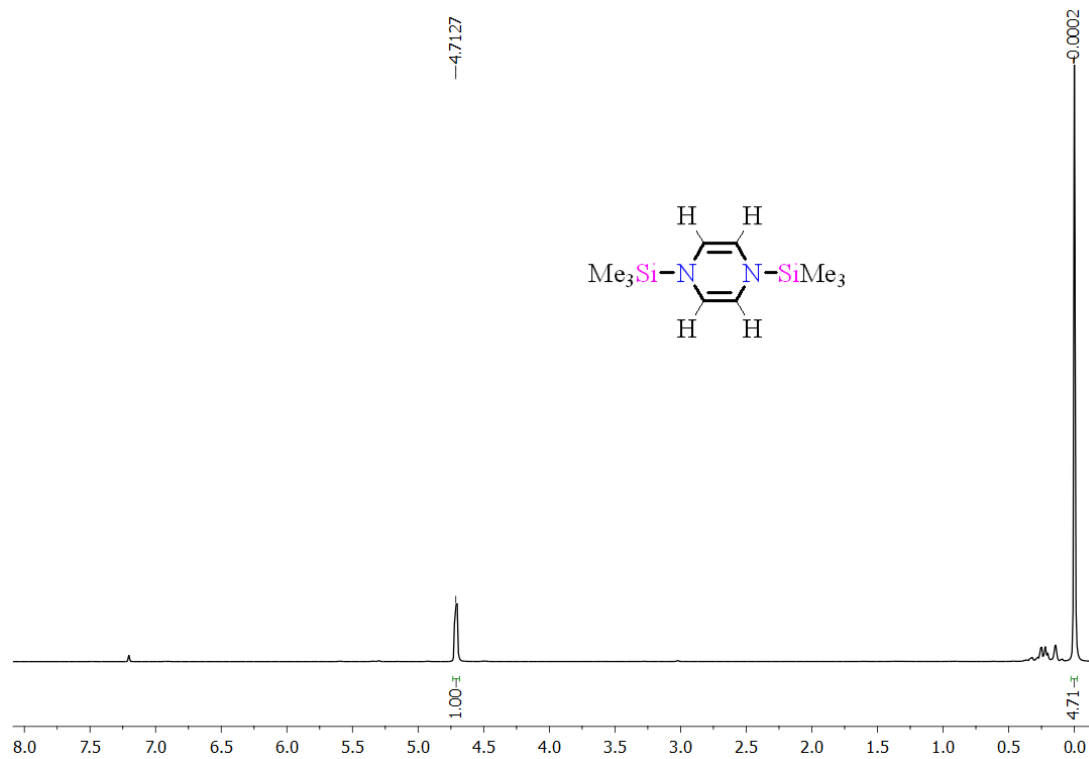


Figure 4.12 ^1H NMR of compound SiPz .

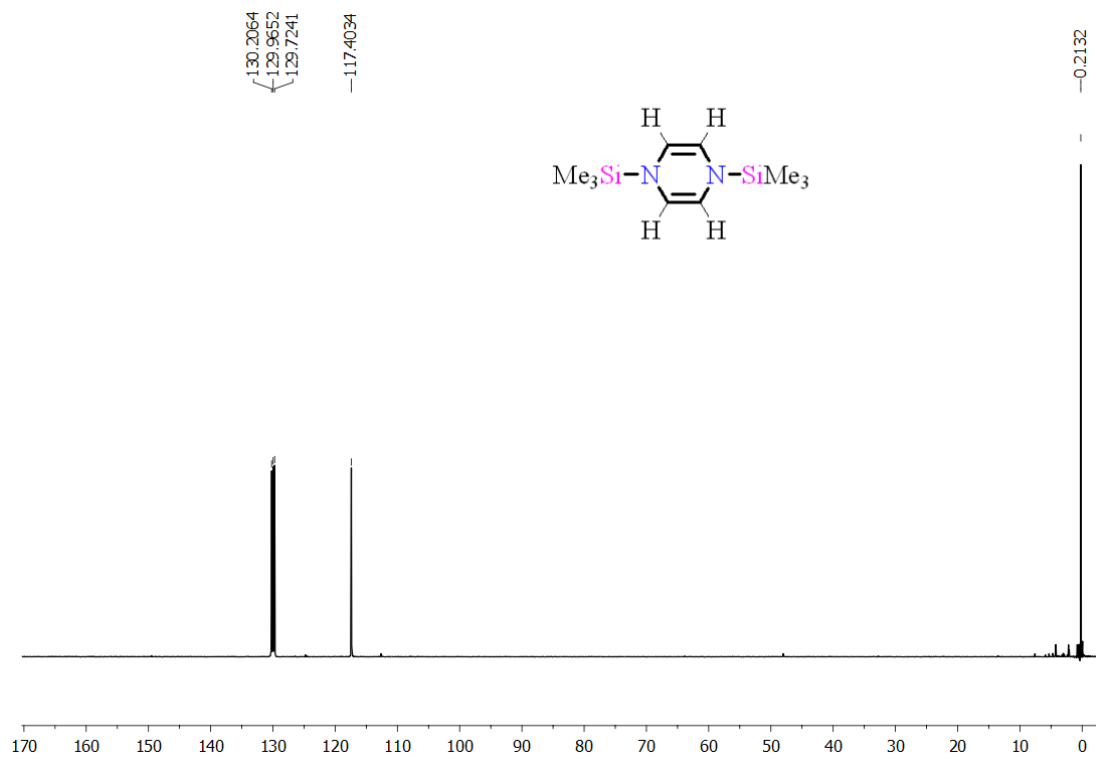


Figure 4.13 ^{13}C NMR of compound SiPz .

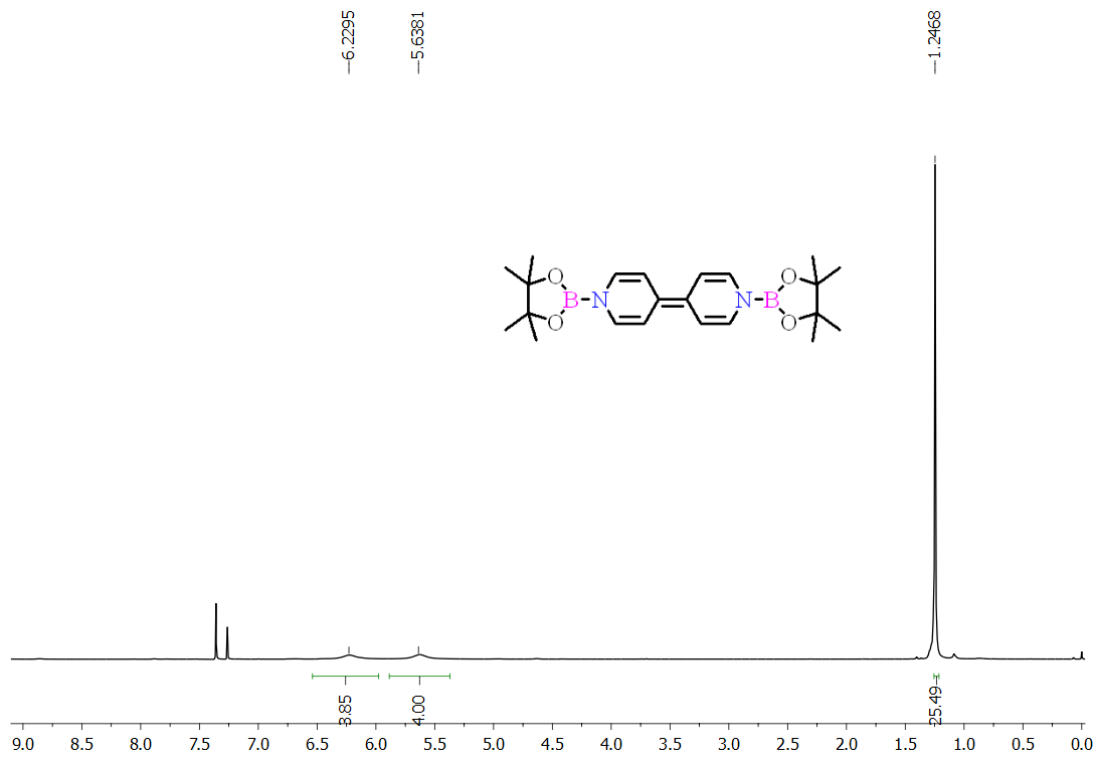


Figure 4.14 ^1H NMR of compound B^{BiPy} .

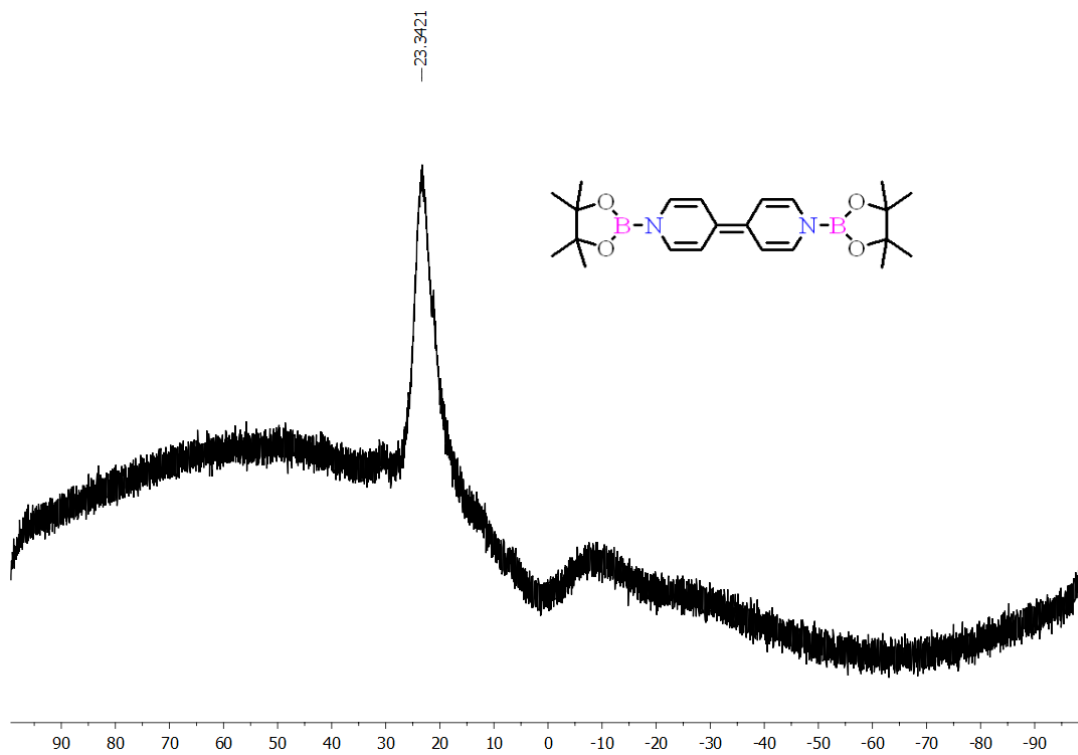


Figure 4.15 ^{11}B NMR of compound B^{BiPy} .

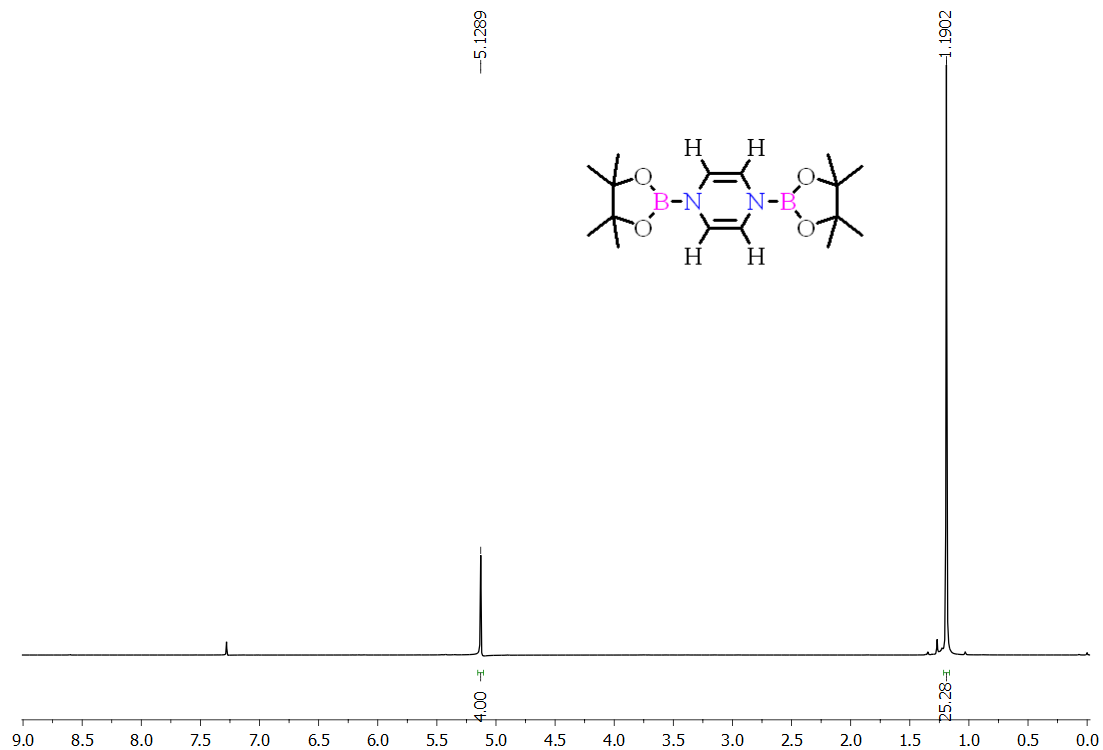


Figure 4.16 ^1H NMR of compound **BPz**.

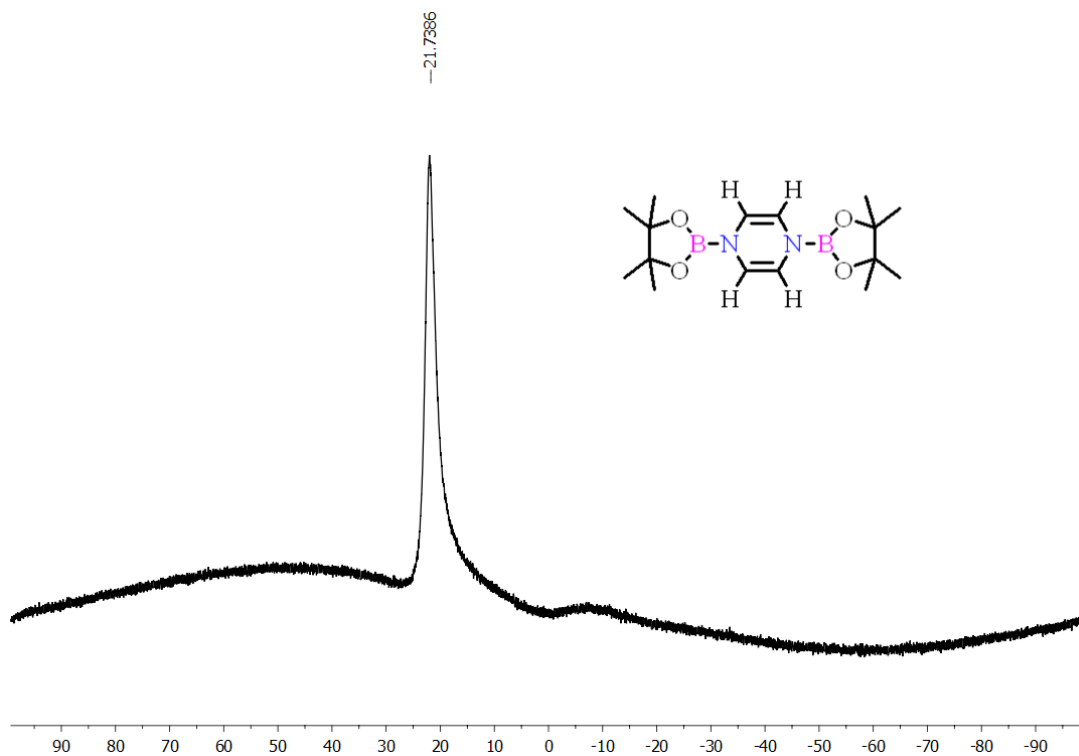


Figure 4.17 ^{11}B NMR of compound **BPz**.

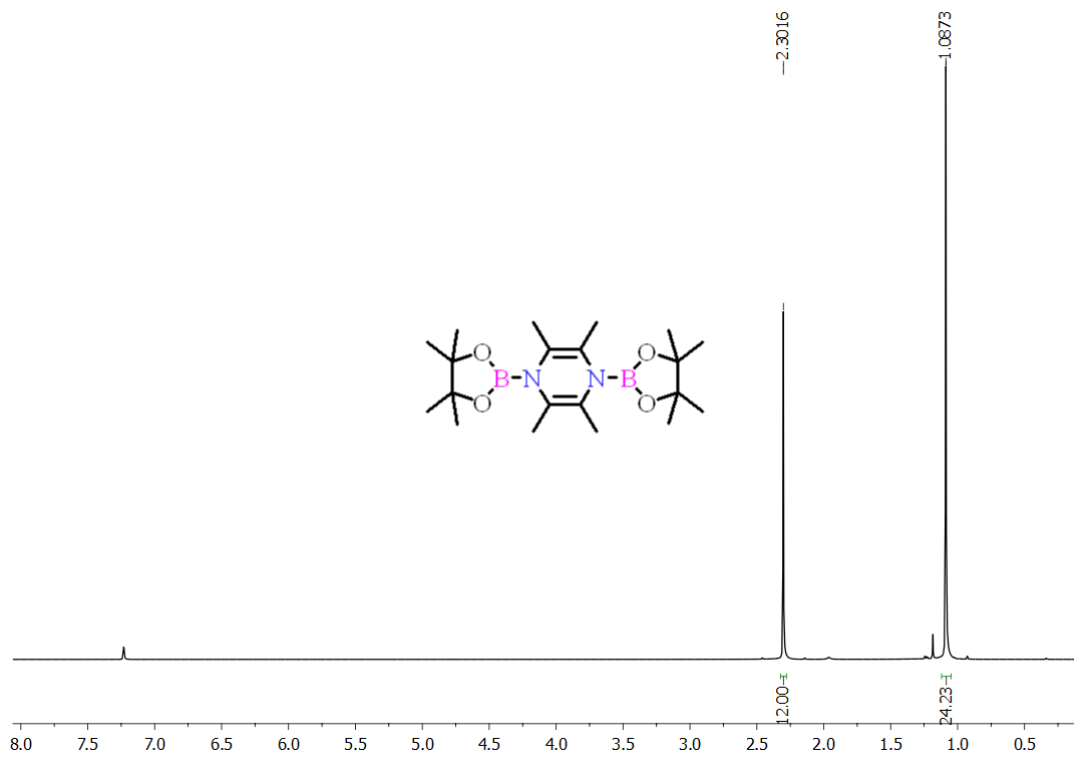


Figure 4.18 ^1H NMR of compound B_tPz .

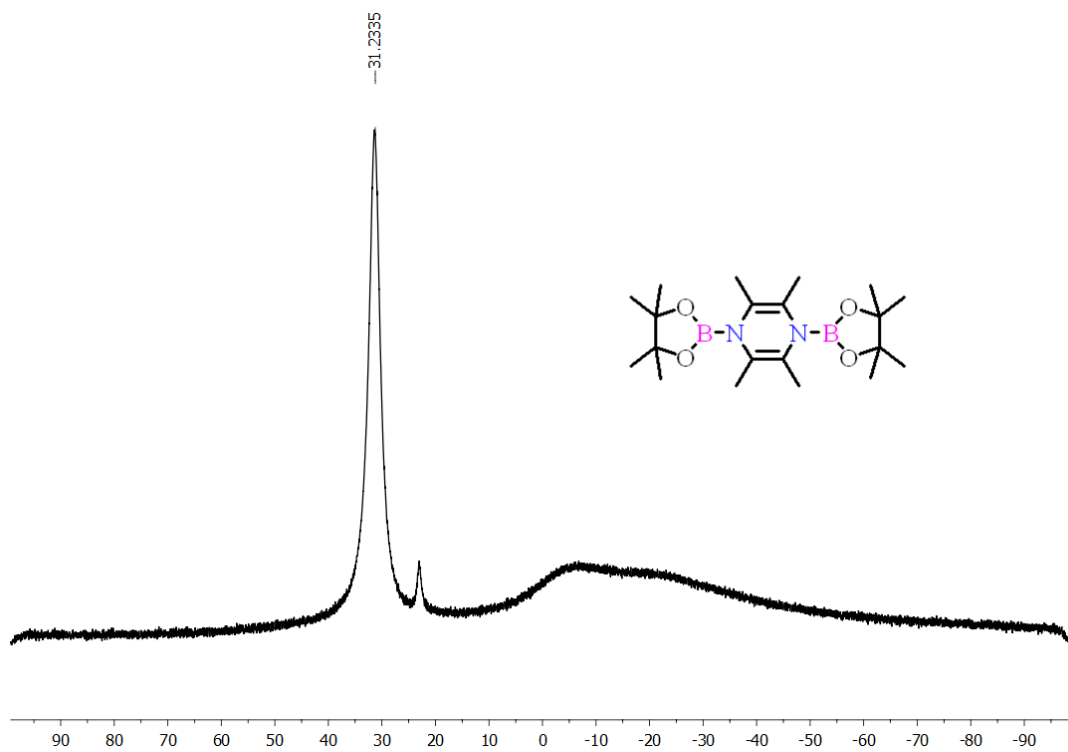


Figure 4.19 ^{11}B NMR of compound B_tPz .

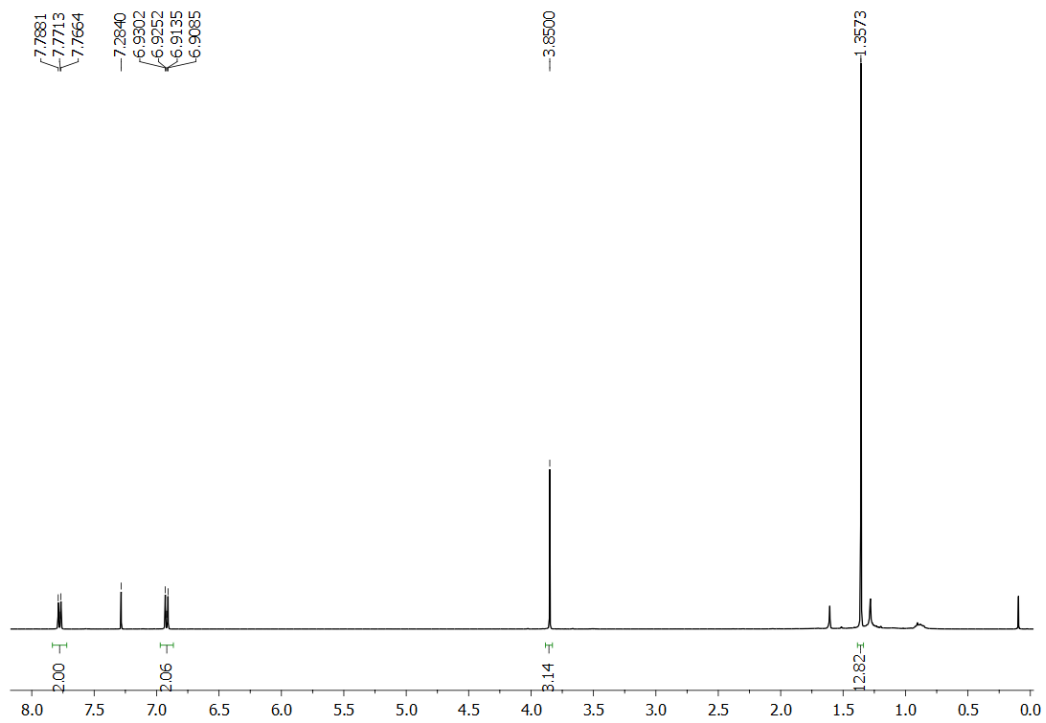


Figure 4.20 ^1H NMR of compound 17a.

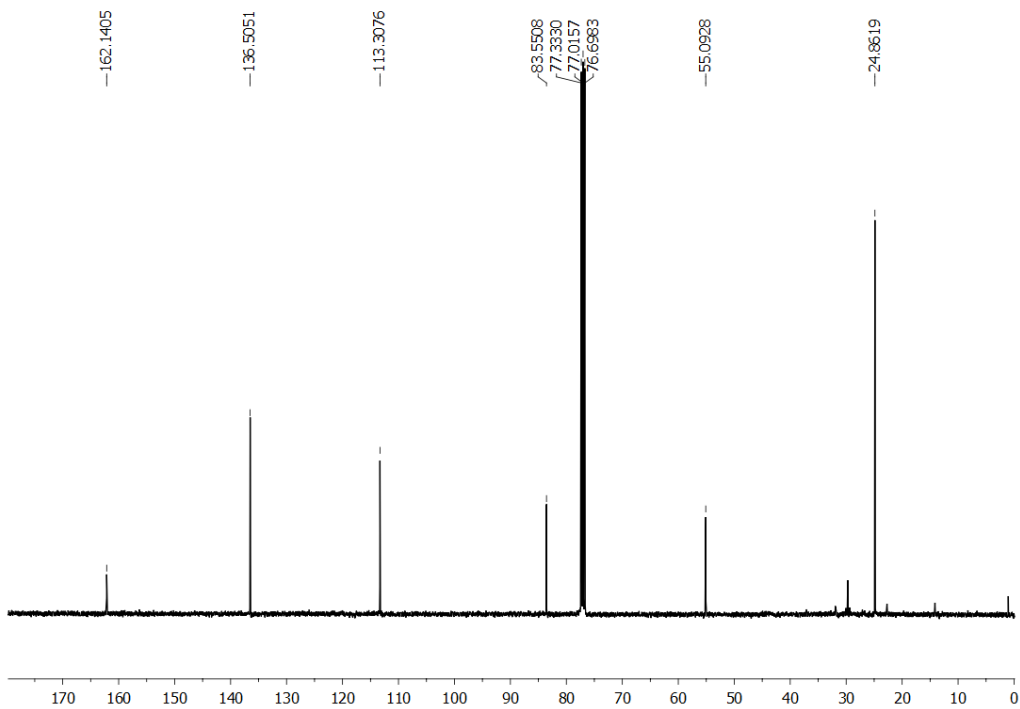


Figure 4.21 ^{13}C NMR of compound 17a.

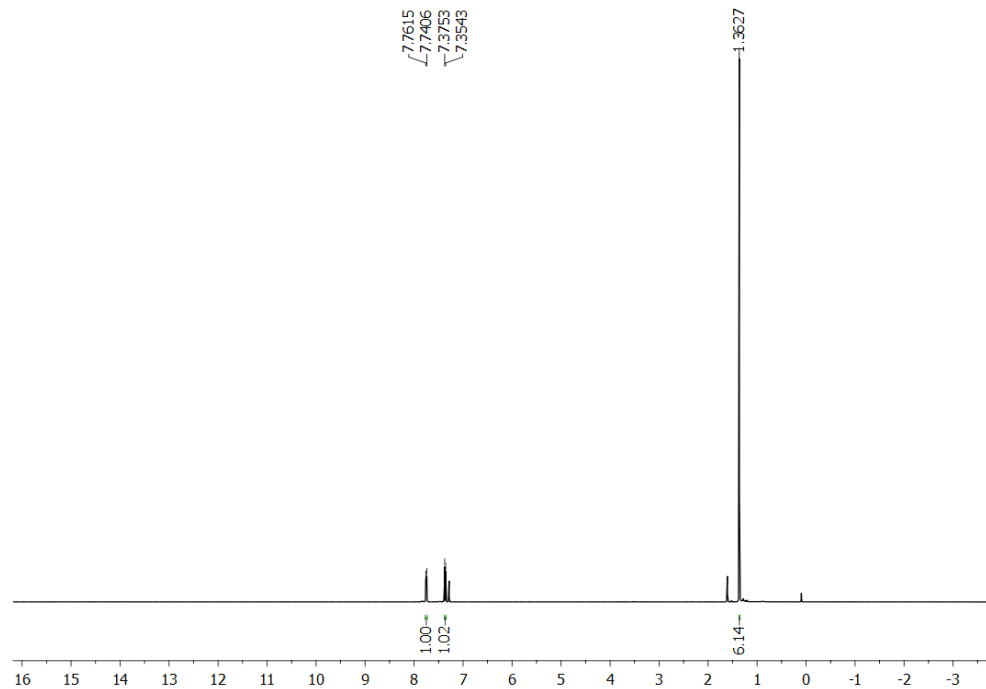


Figure 4.21 ¹H NMR of compound 17b.

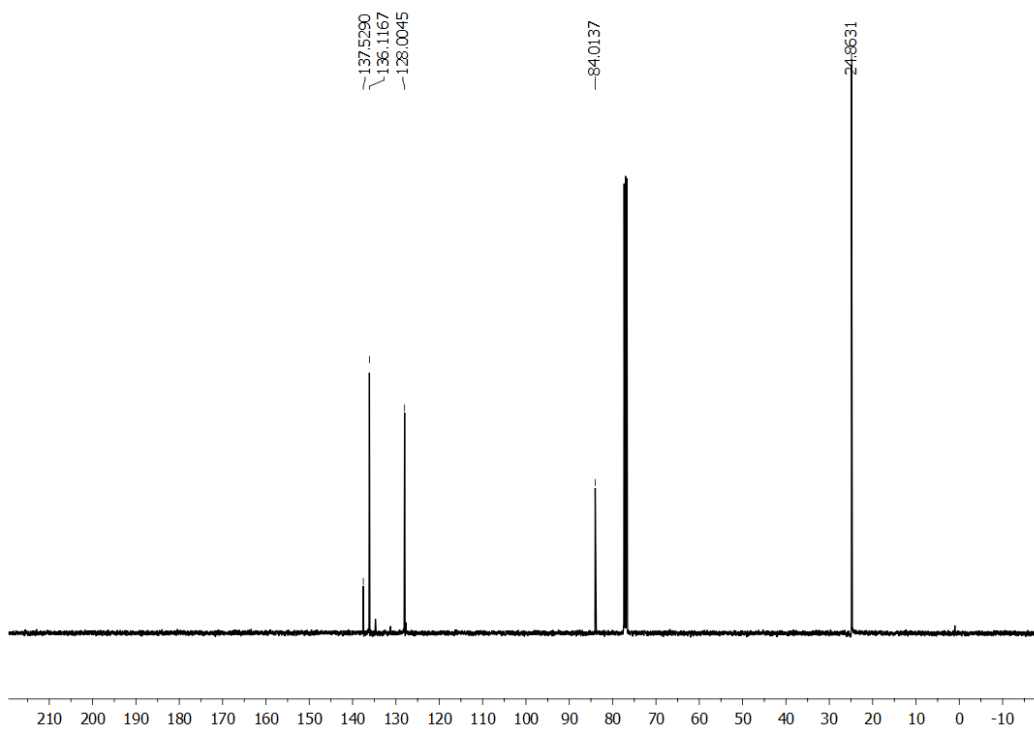


Figure 4.21 ¹³C NMR of compound 17b.

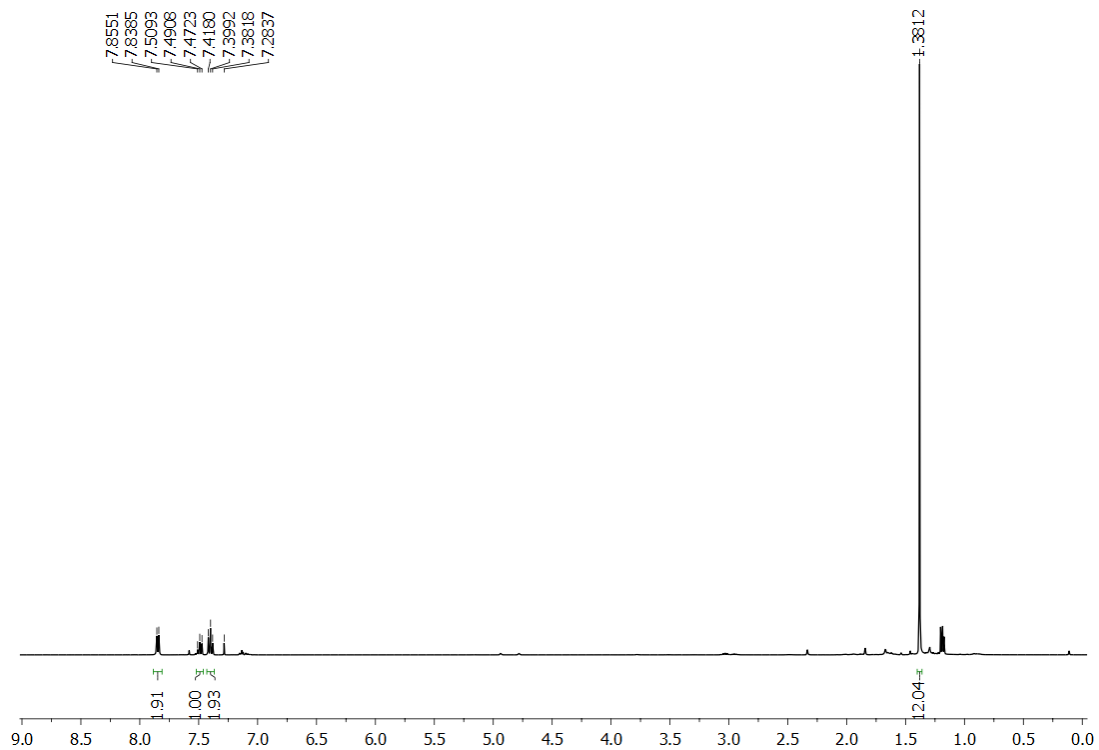


Figure 4.22 ¹H NMR of compound 17c.

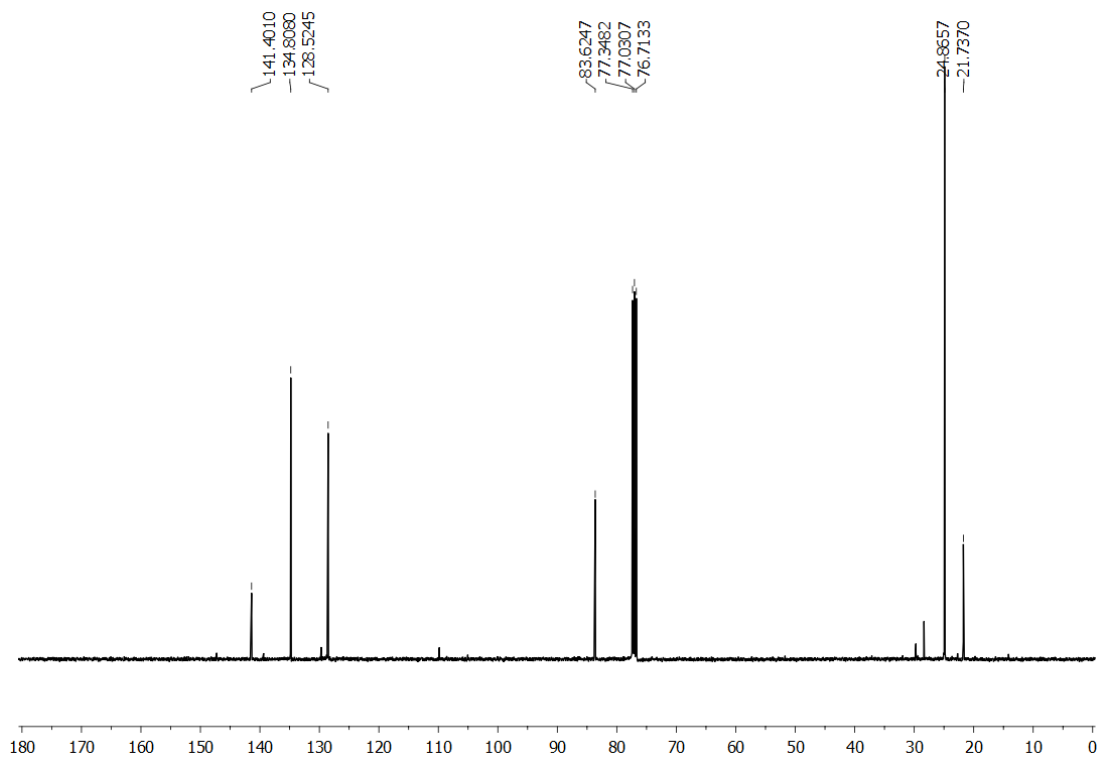


Figure 4.23 ¹³C NMR of compound 17c.

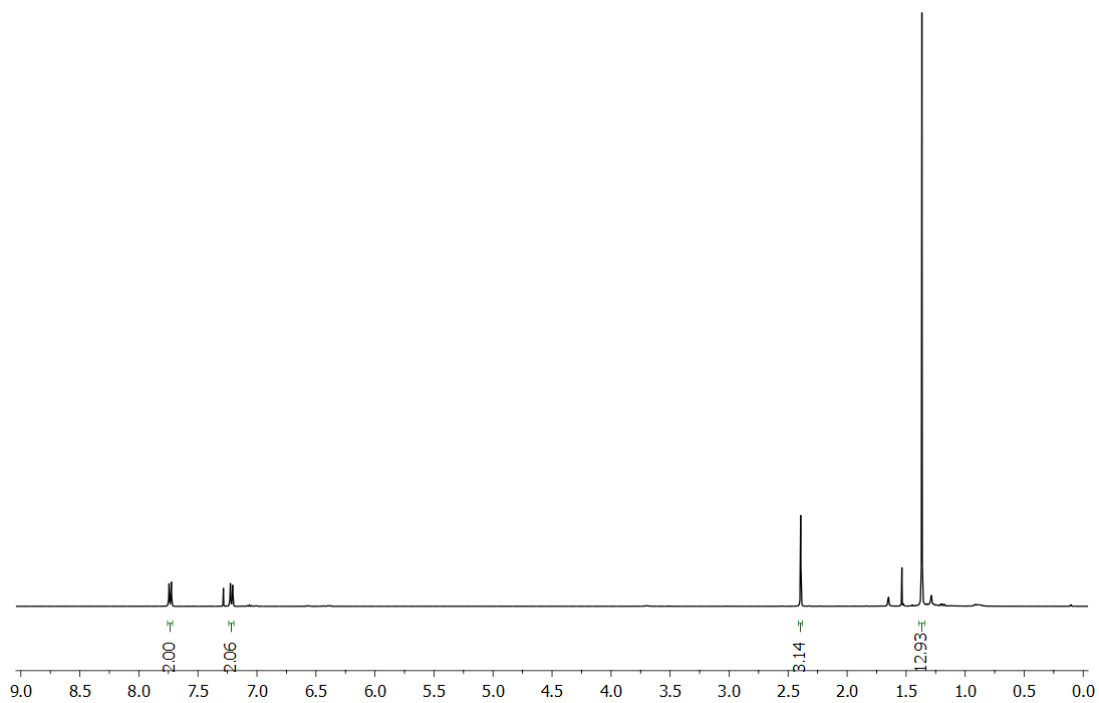


Figure 4.24 ^1H NMR of compound **17e**.

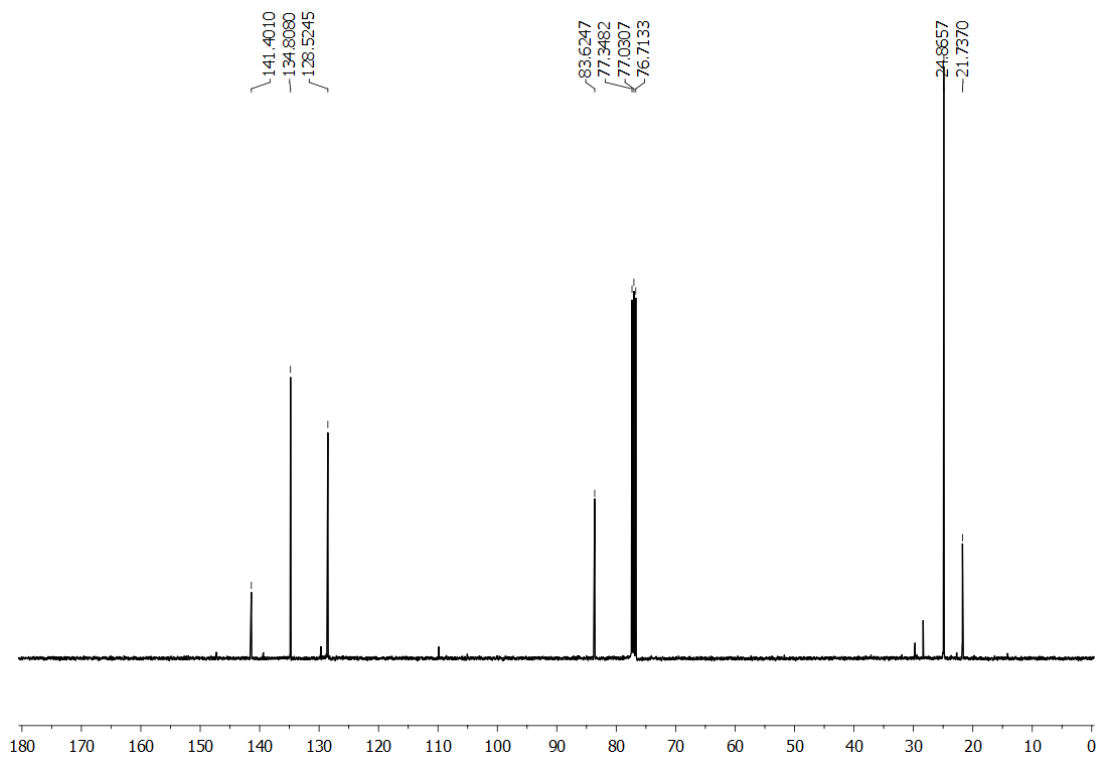


Figure 4.25 ^{13}C NMR of compound **17e**.

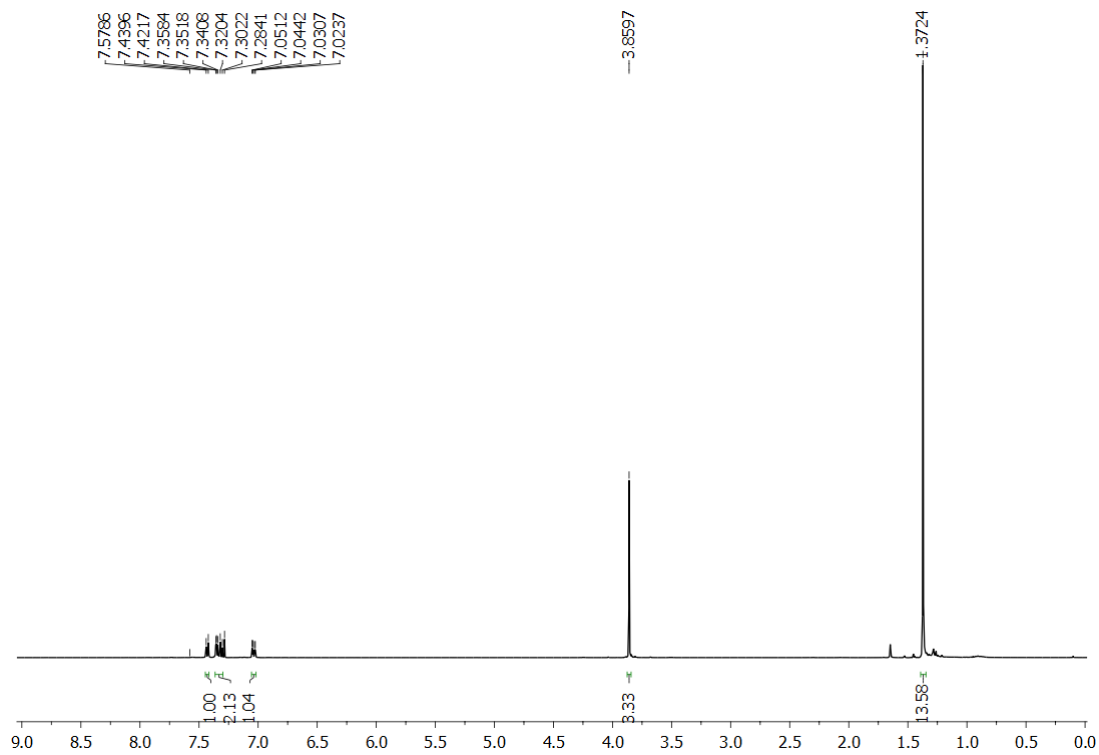


Figure 4.26 ^1H NMR of compound **17g**.

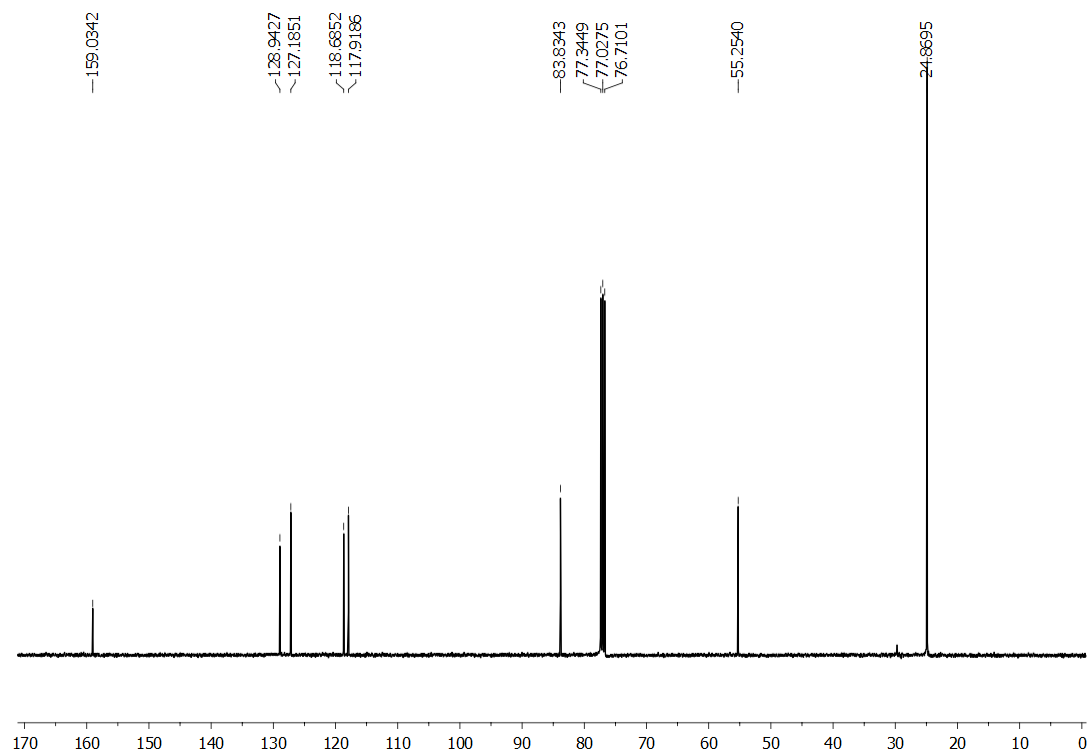


Figure 4.27 ^{13}C NMR of compound **17g**.

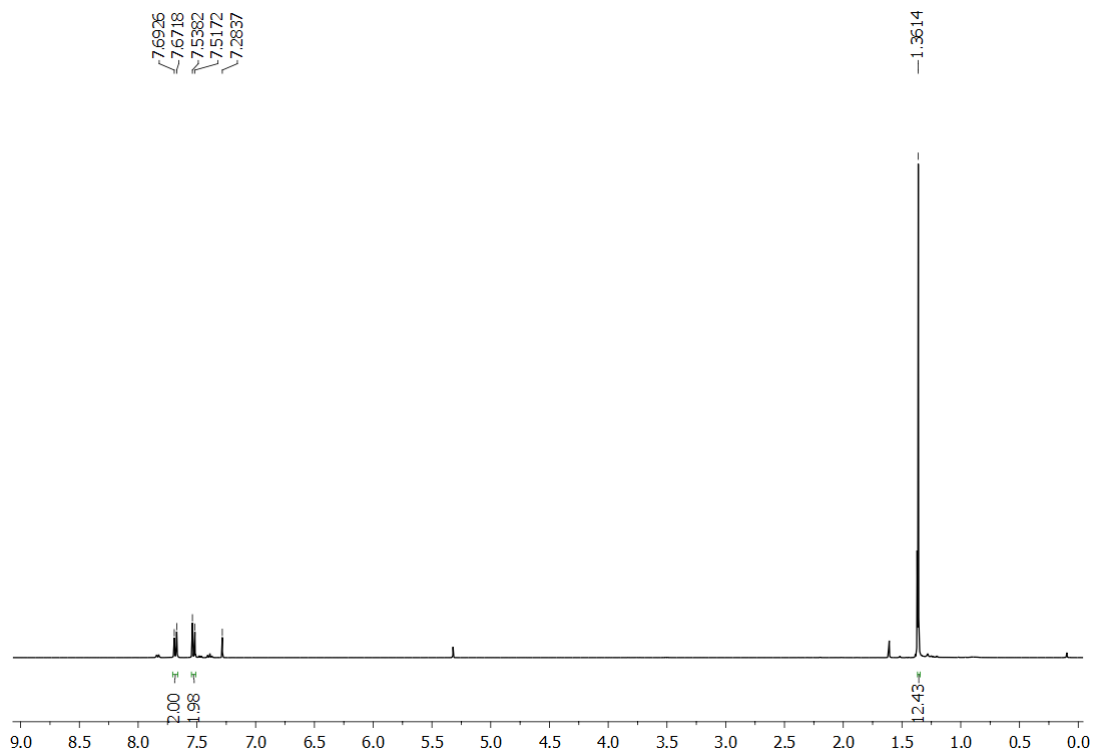


Figure 4.28 ¹H NMR of compound 17h.

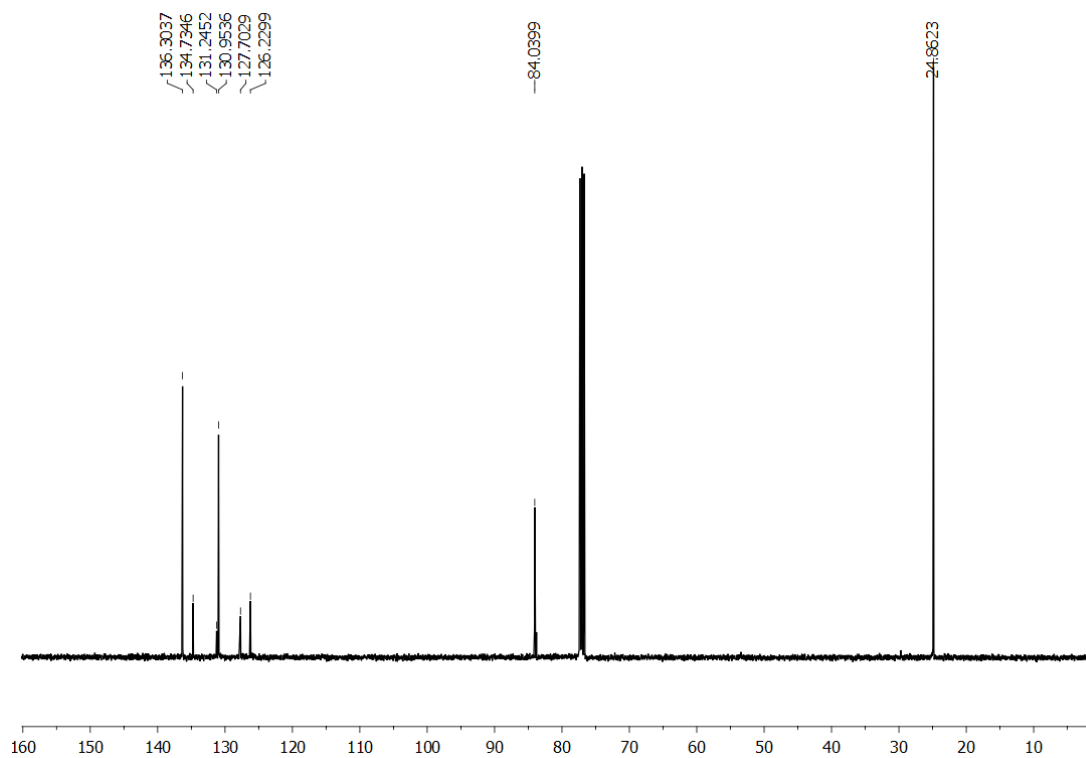


Figure 4.29 ¹³C NMR of compound 17h.

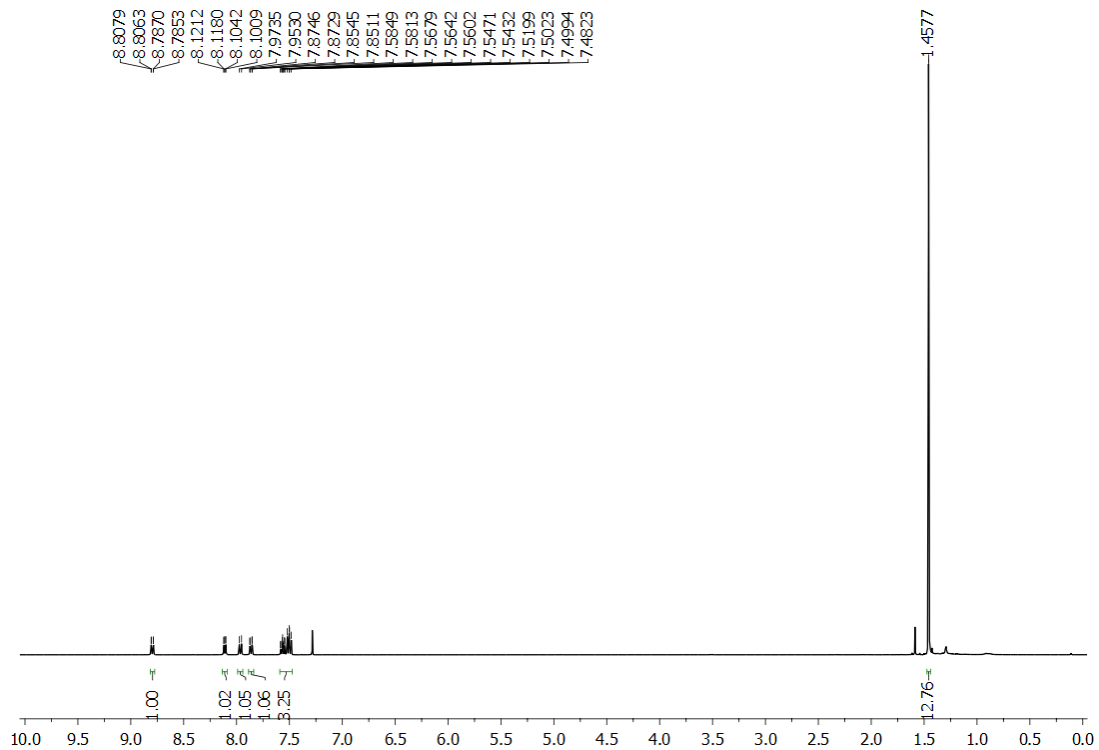


Figure 4.30 ^1H NMR of compound **17i**.

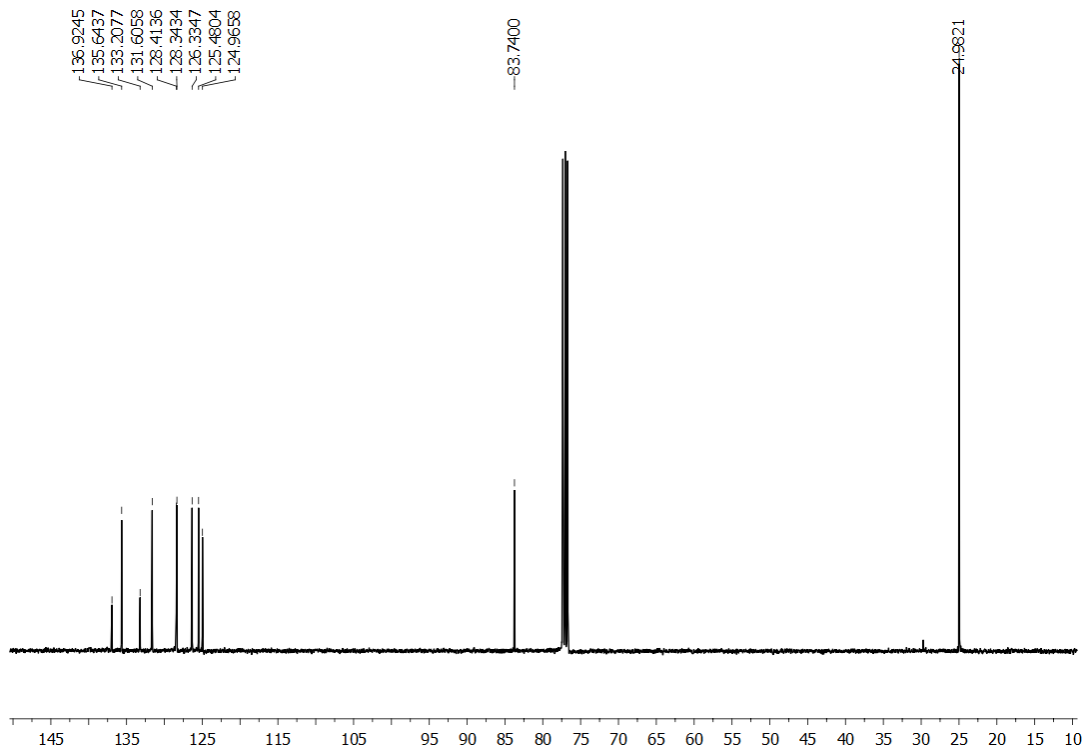


Figure 4.31 ^{13}C NMR of compound **17i**.

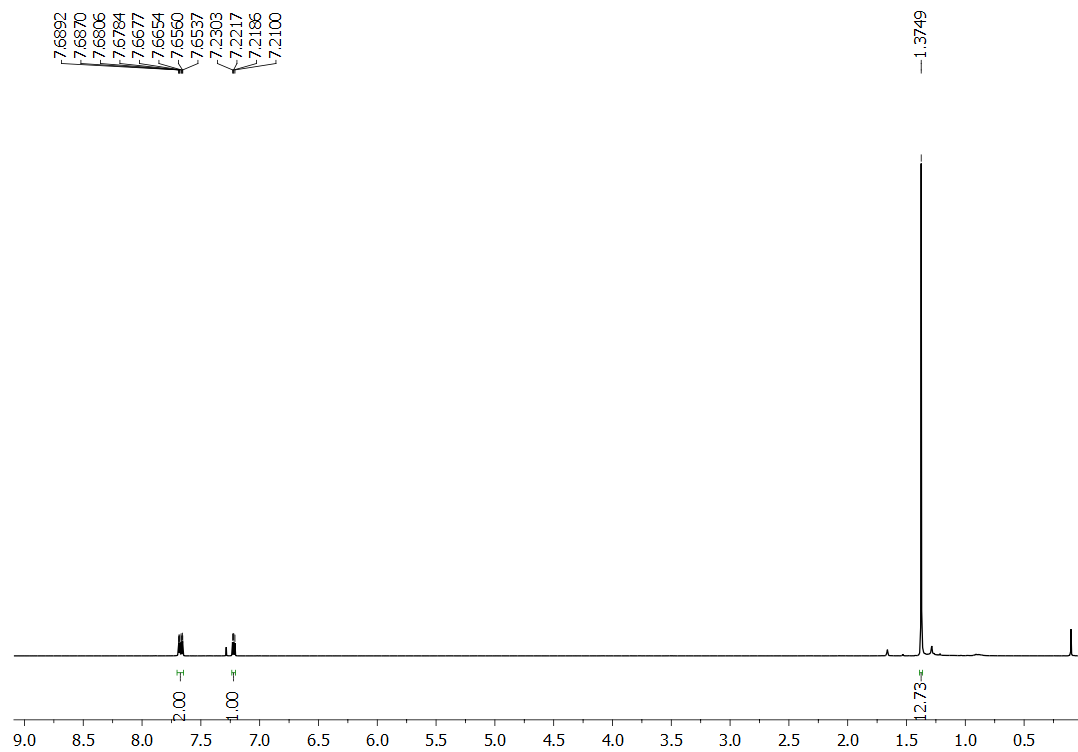


Figure 4.32 ^1H NMR of compound **17j**.

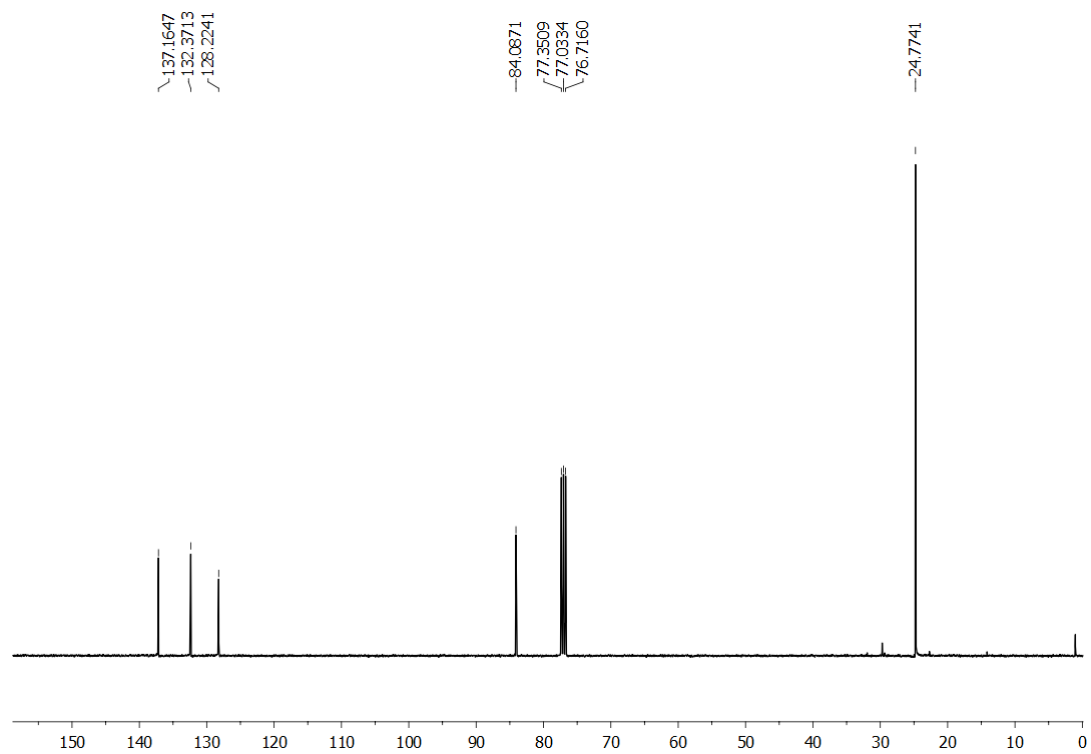


Figure 4.33 ^{13}C NMR of compound **17j**.

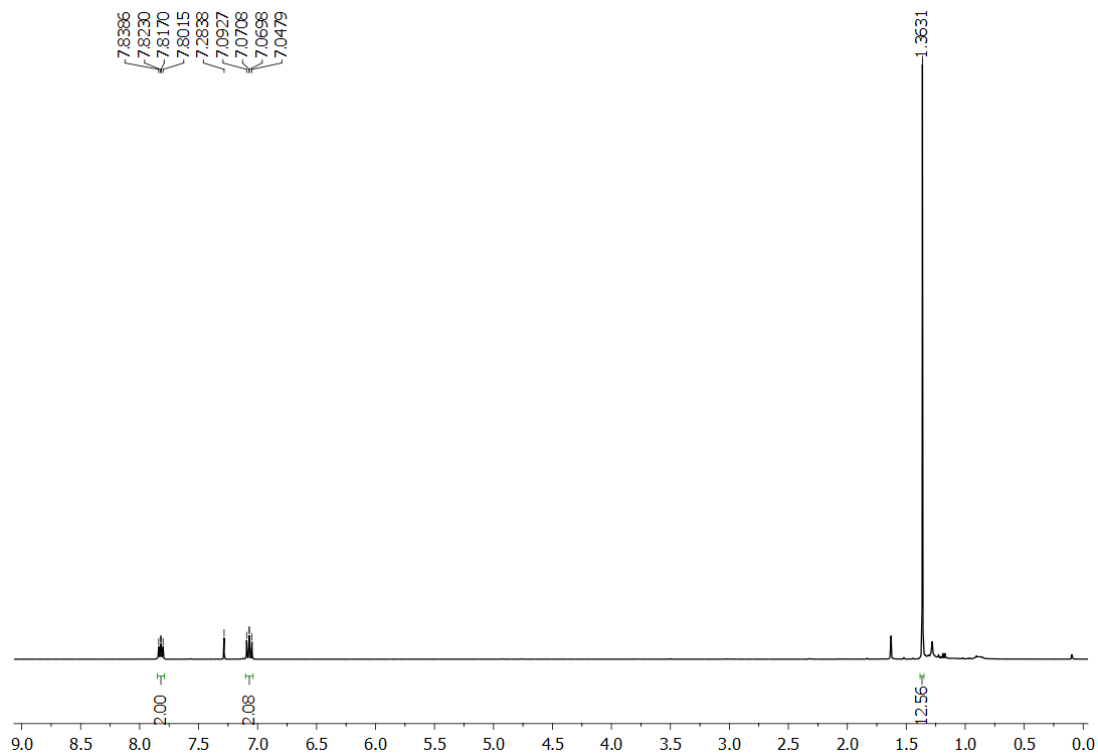


Figure 4.34 ^{13}C NMR of compound **17k**.

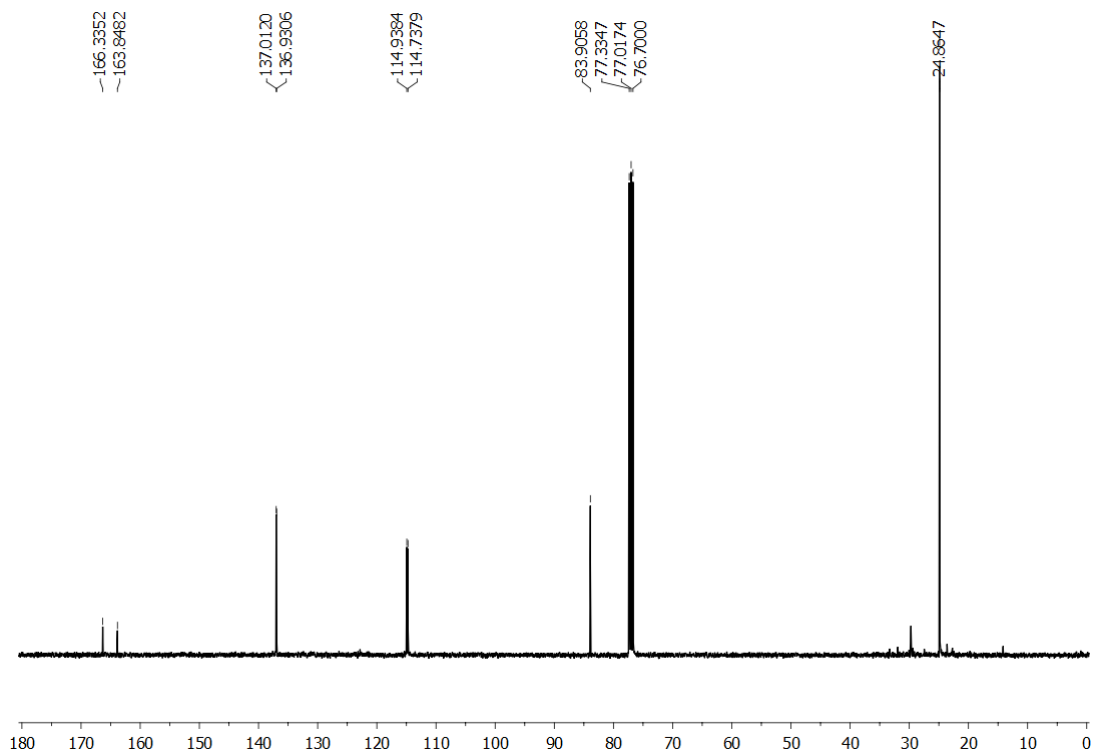


Figure 4.35 ^{13}C NMR of compound **17k**.

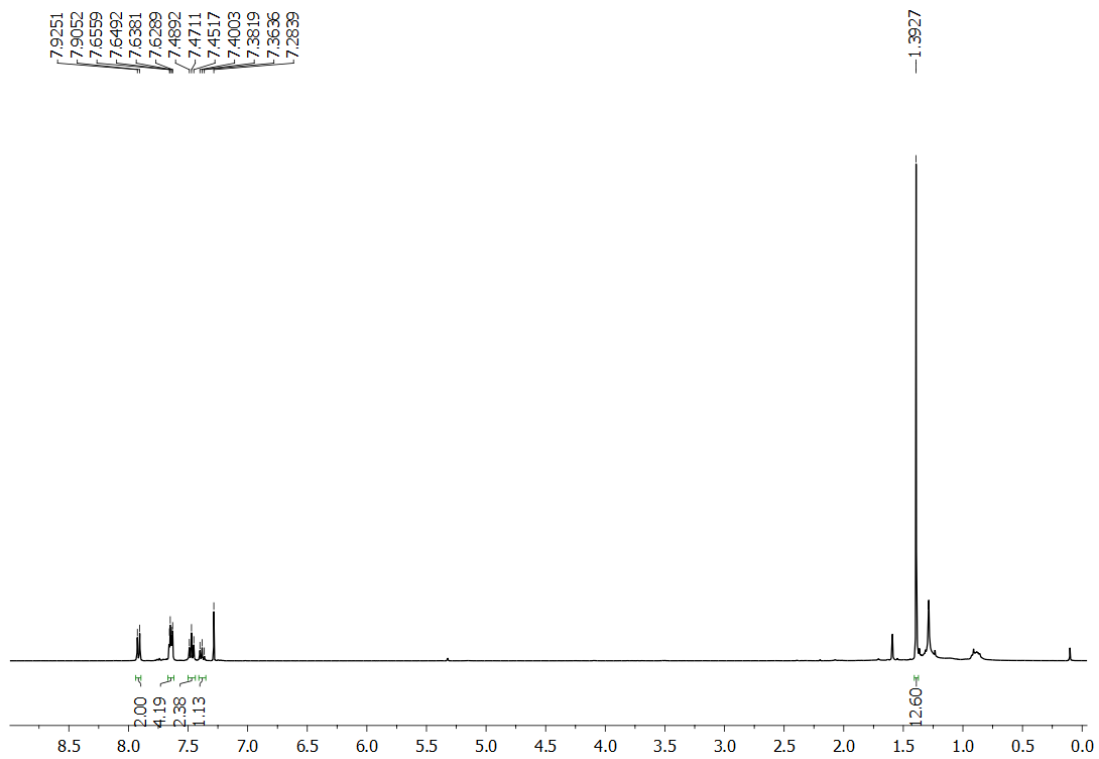


Figure 4.36 ¹H NMR of compound 17l.

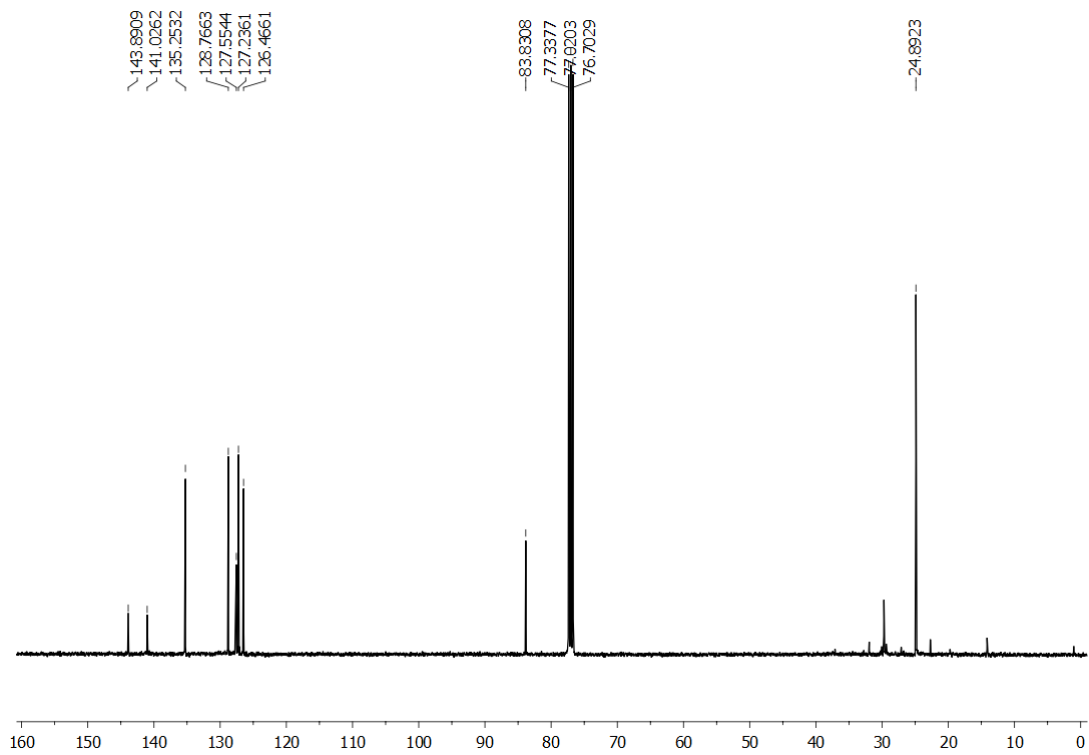


Figure 4.37 ¹³C NMR of compound 17l.

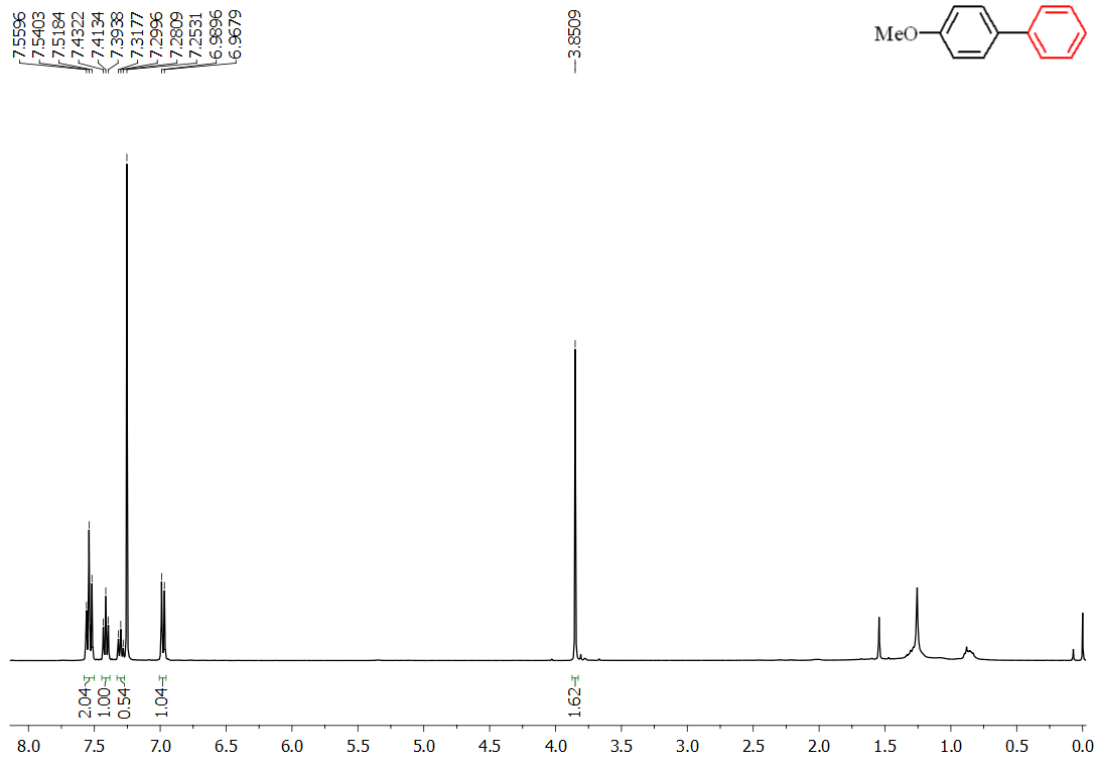


Figure 4.38 ^1H NMR of compound 18a.

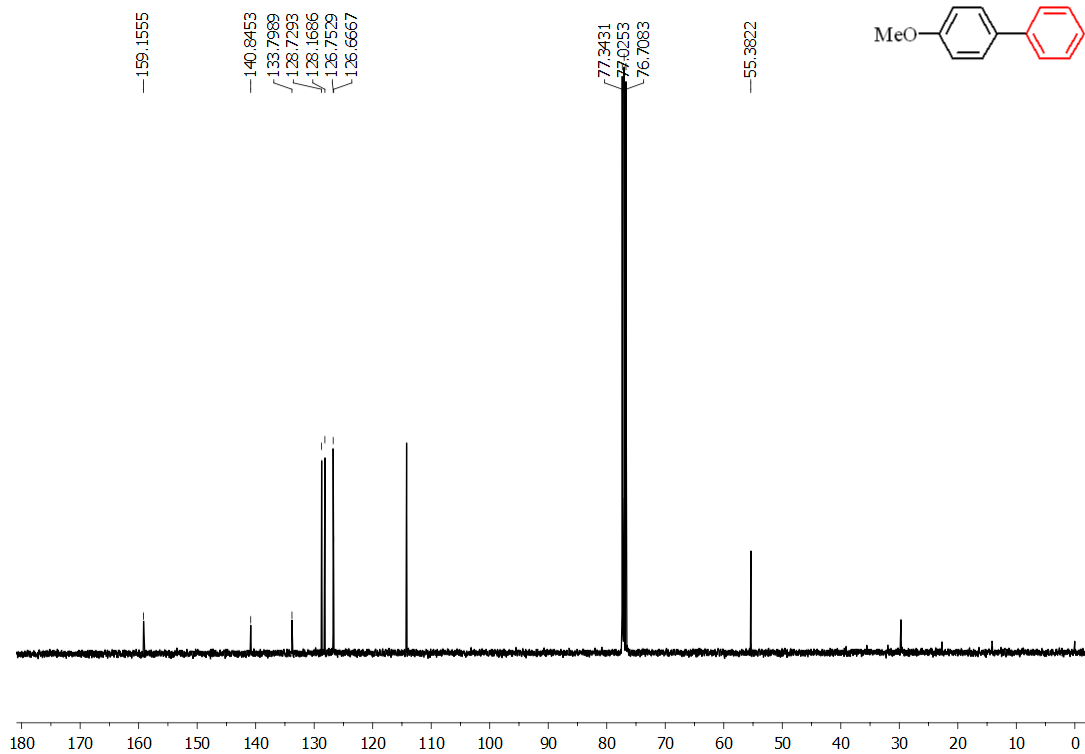


Figure 4.39 ^{13}C NMR of compound 18a.

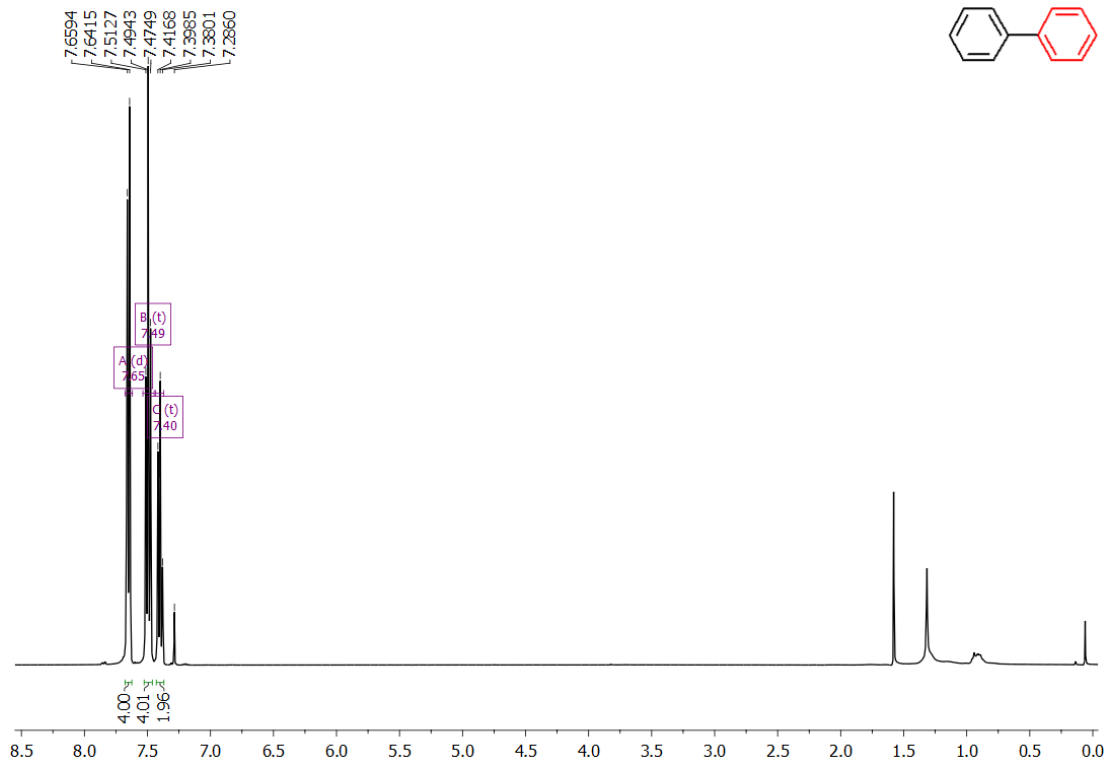


Figure 4.40 ^1H NMR of compound **18c**.

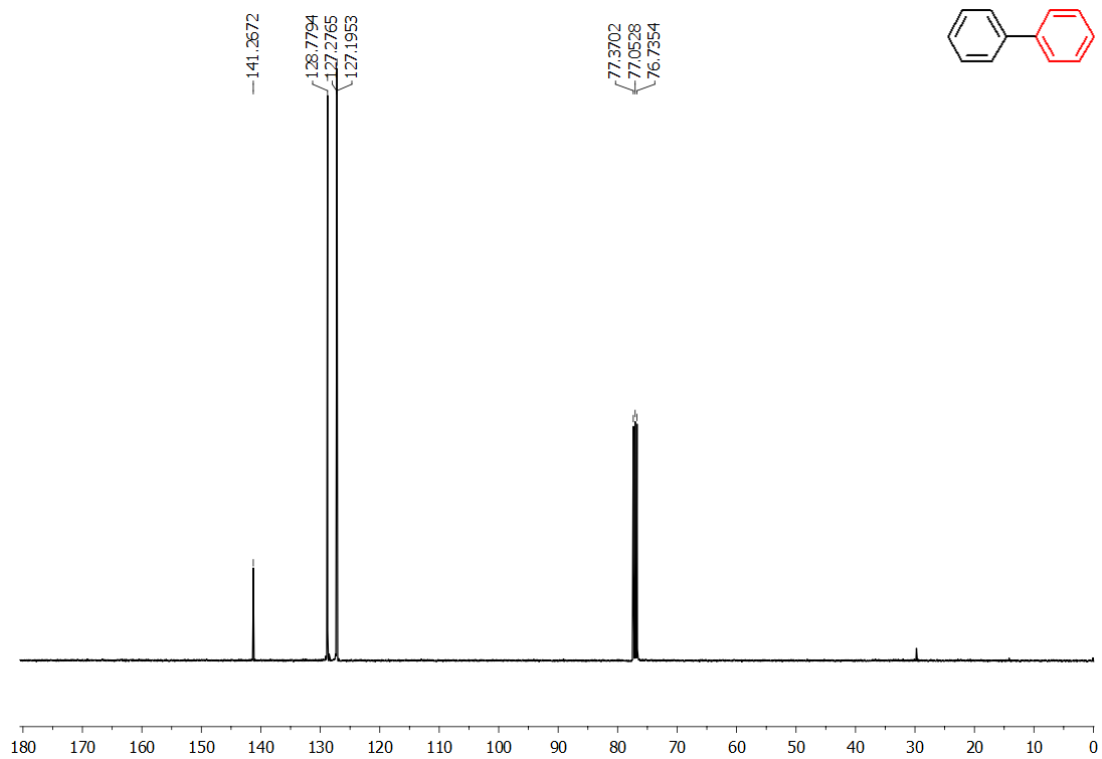


Figure 4.41 ^{13}C NMR of compound **18c**.

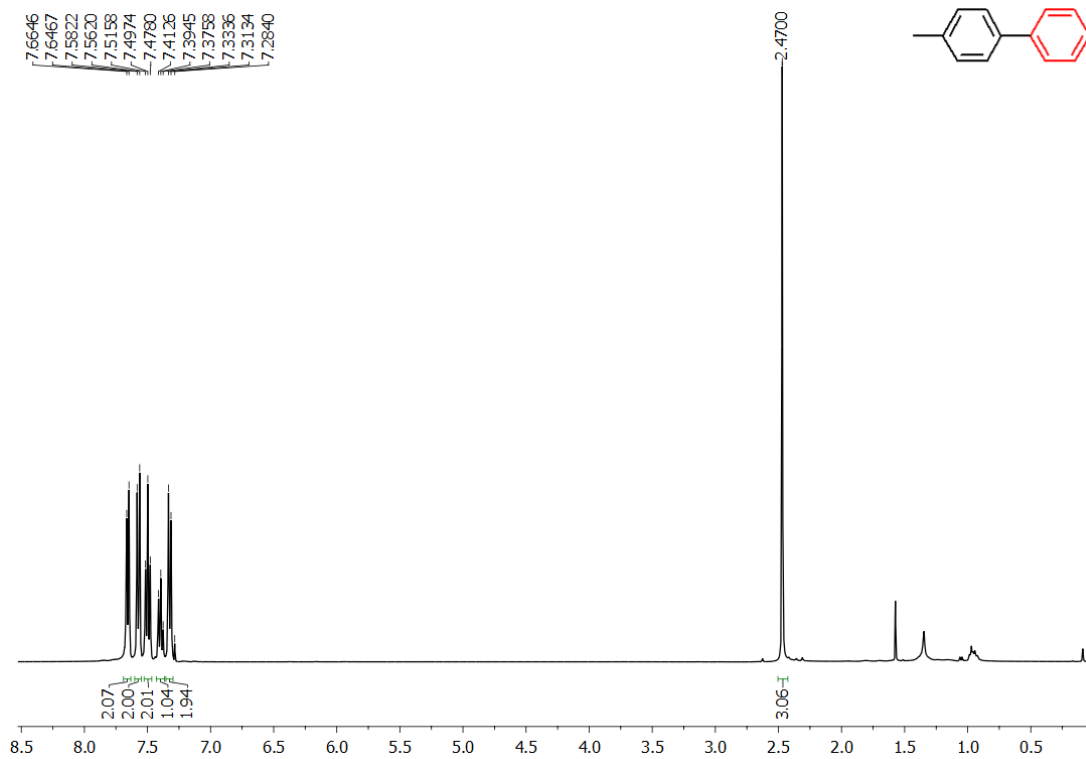


Figure 4.42 ^1H NMR of compound 18d.

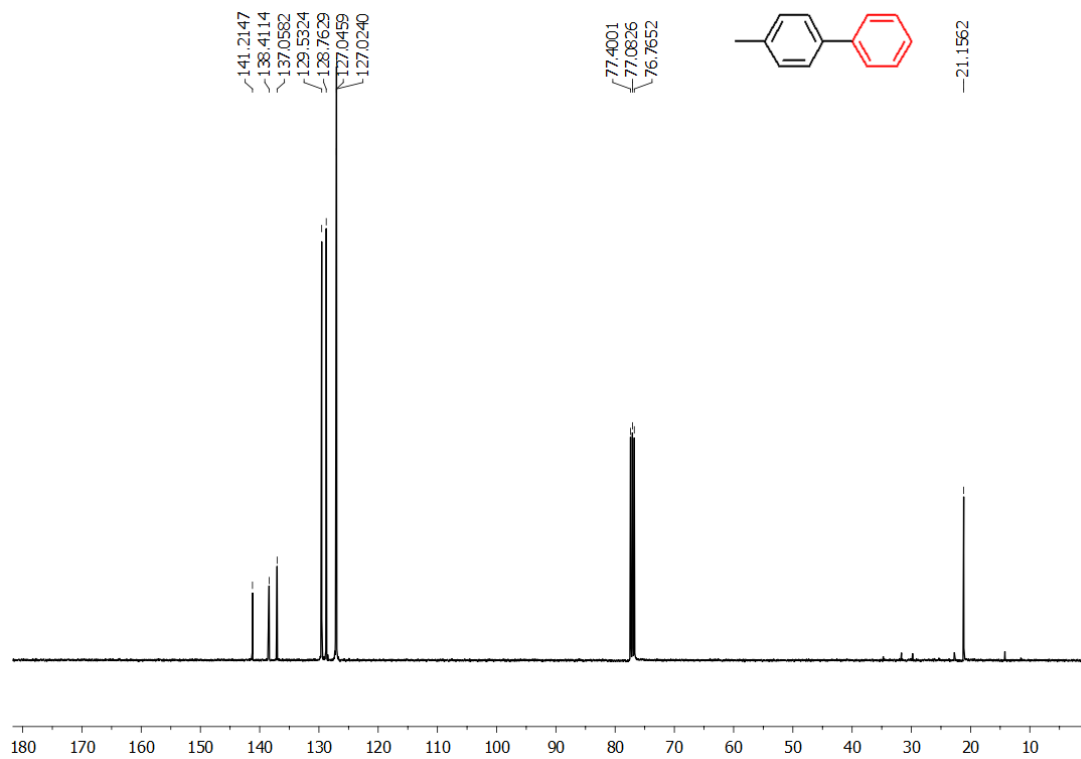


Figure 4.43 ^{13}C NMR of compound 18d.

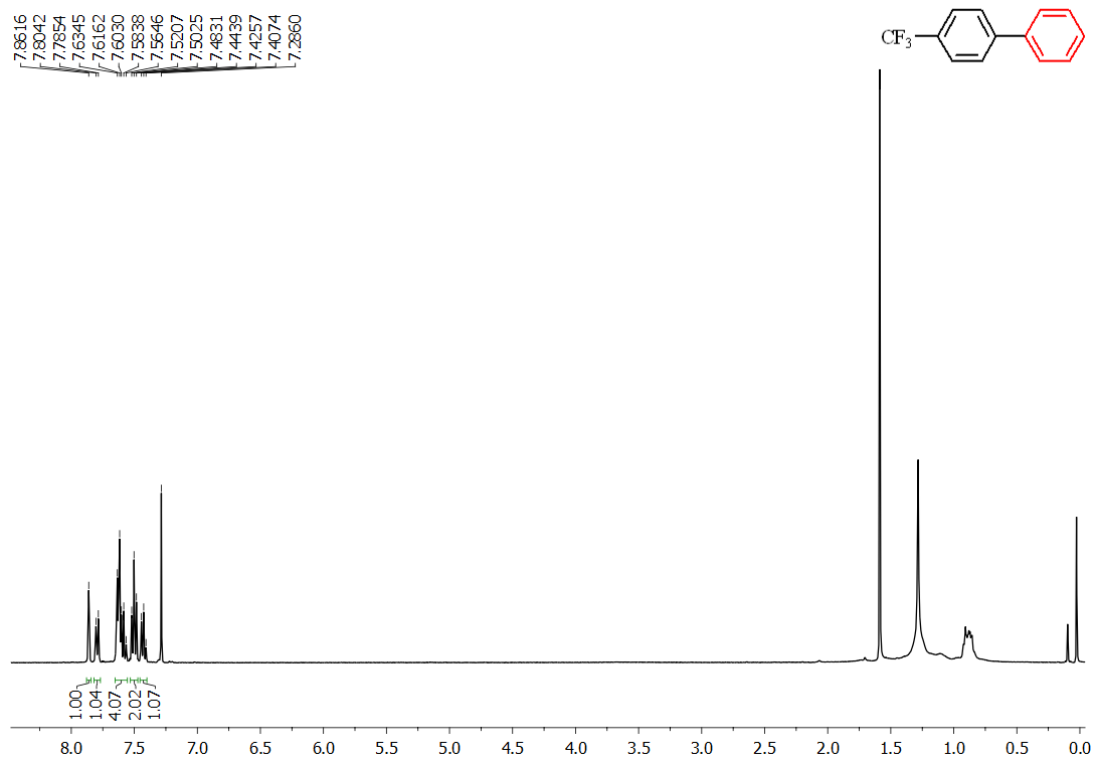


Figure 4.44 ¹H NMR of compound 18e.

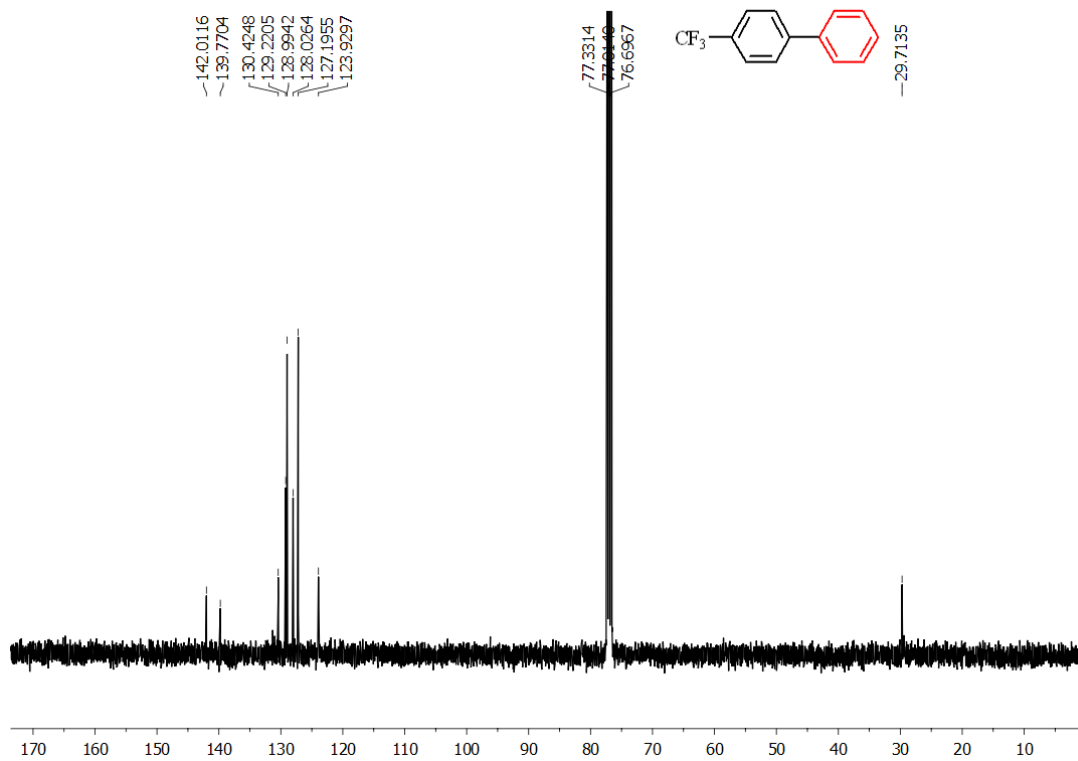


Figure 4.45 ¹³C NMR of compound 18e

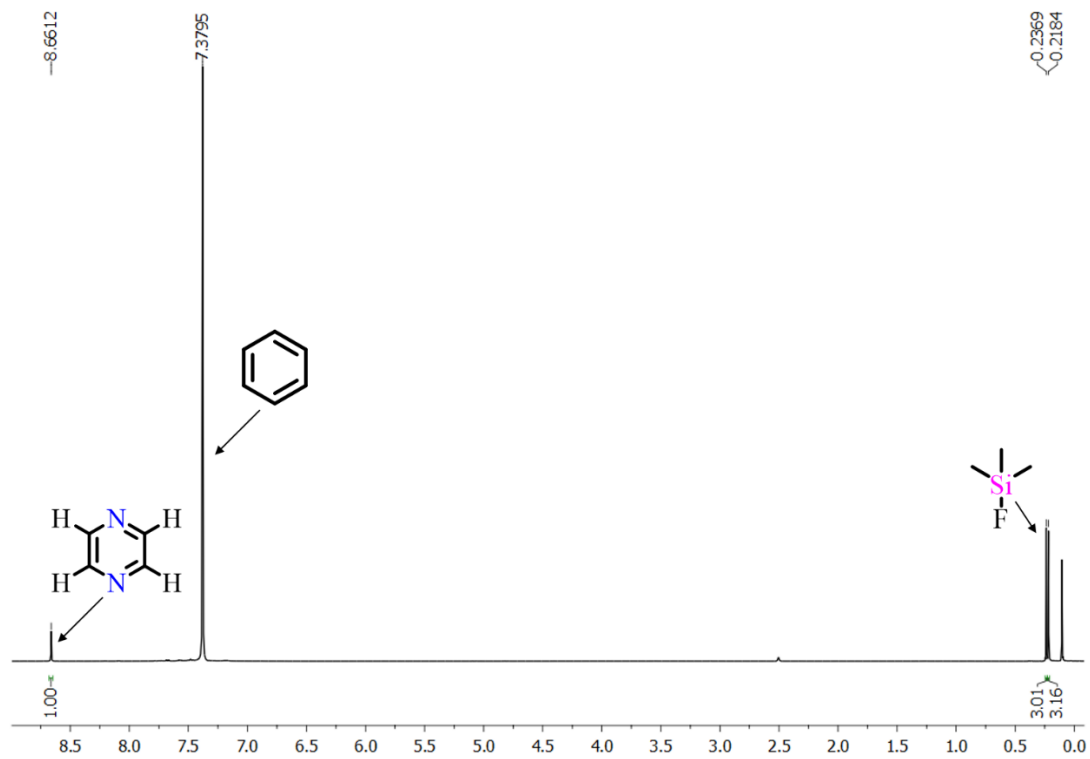


Figure 4.46 ^1H NMR of reaction mixture of $^{\text{Si}}\text{Pz}$ + Phenyldiazonium salt + Benzene.

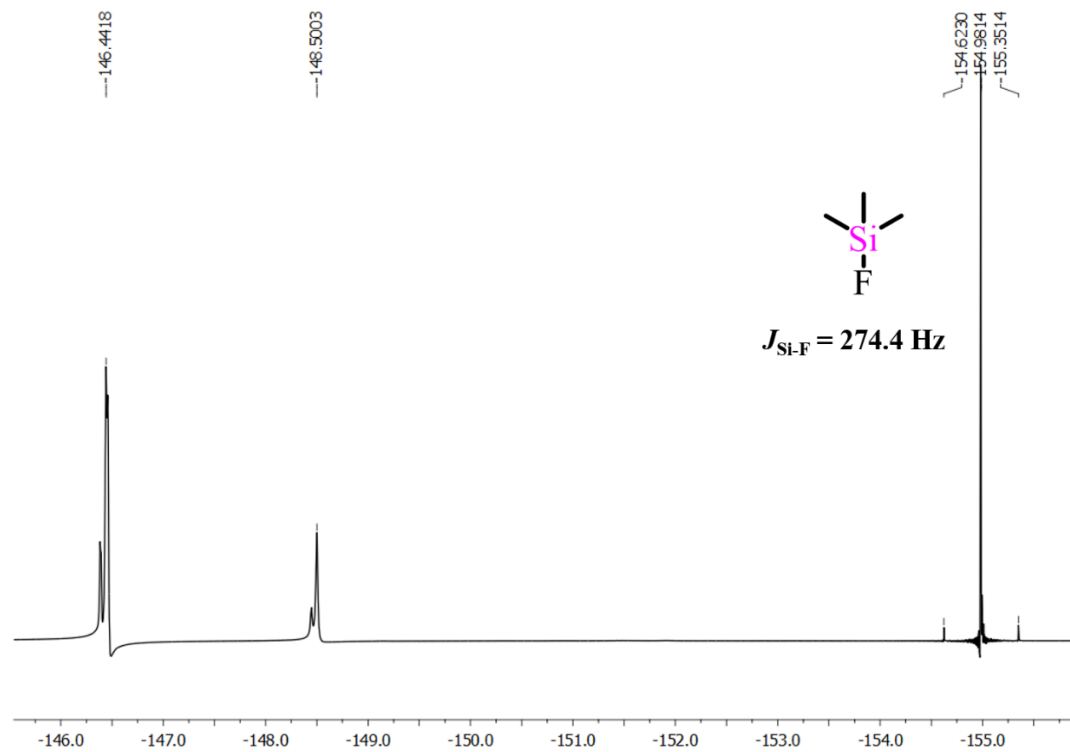


Figure 4.47 ^{19}F NMR of reaction mixture of $^{\text{Si}}\text{Pz}$ + Phenyldiazonium salt + Benzene.

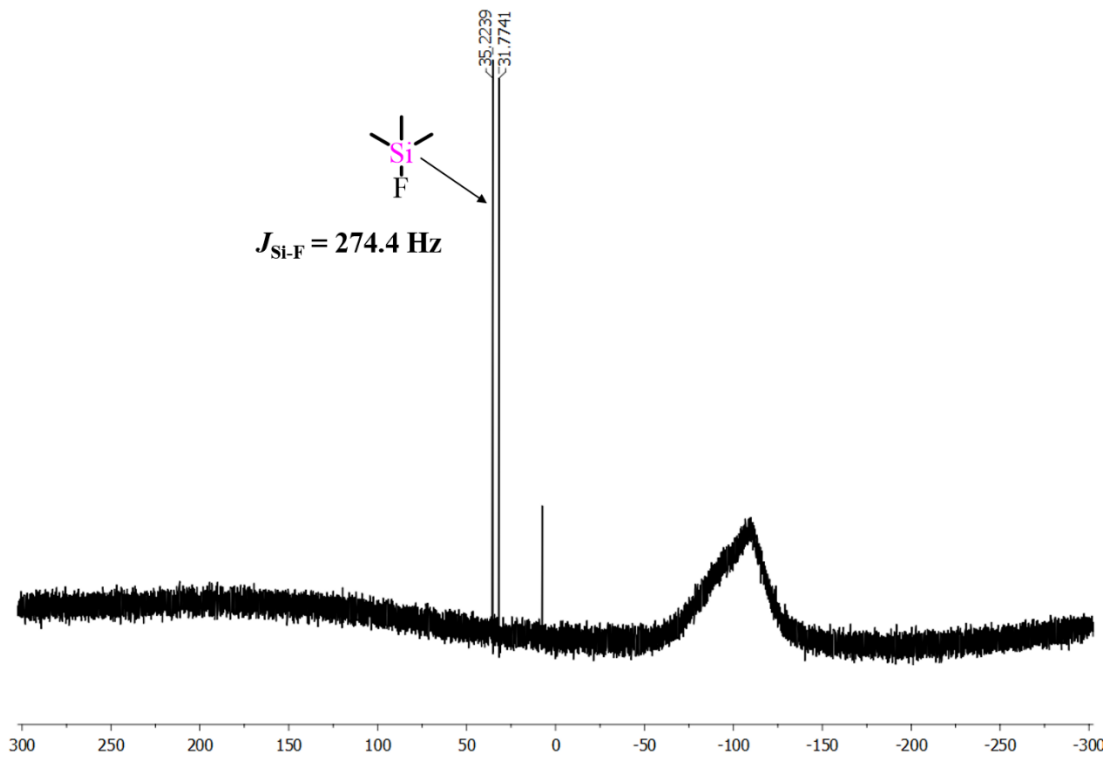


Figure 4.48 ^{29}Si NMR of reaction mixture of $^{\text{Si}}\text{Pz}$ + Phenyldiazonium salt + Benzene.

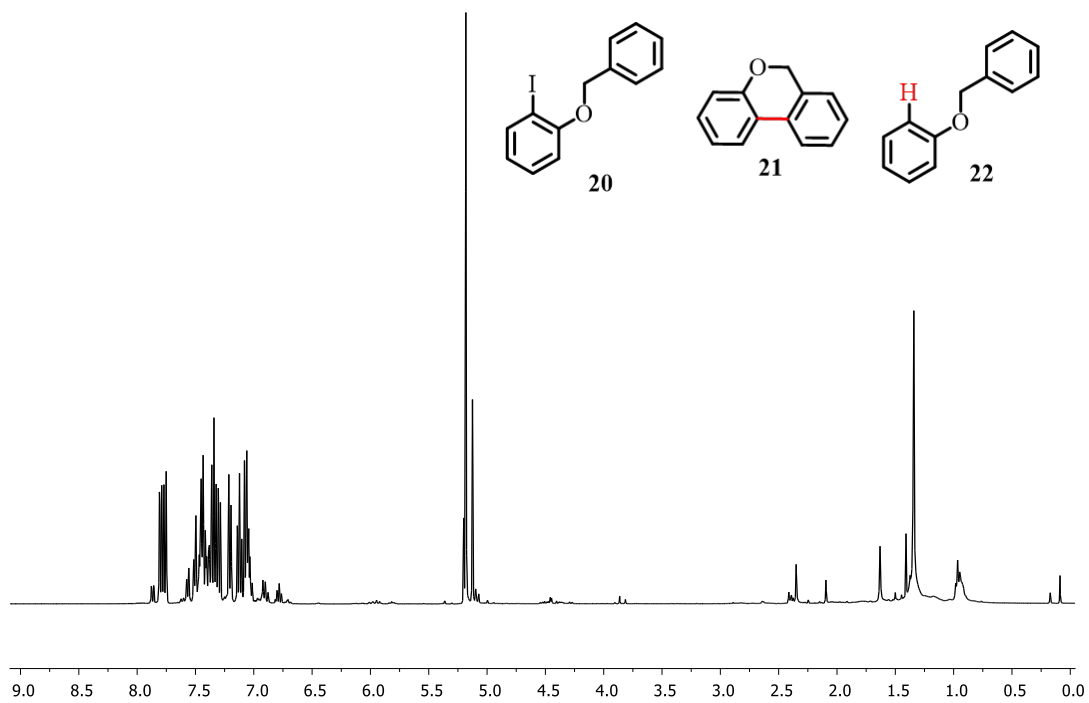


Figure 4.48 ^1H NMR of **20** + **21** + **22**.

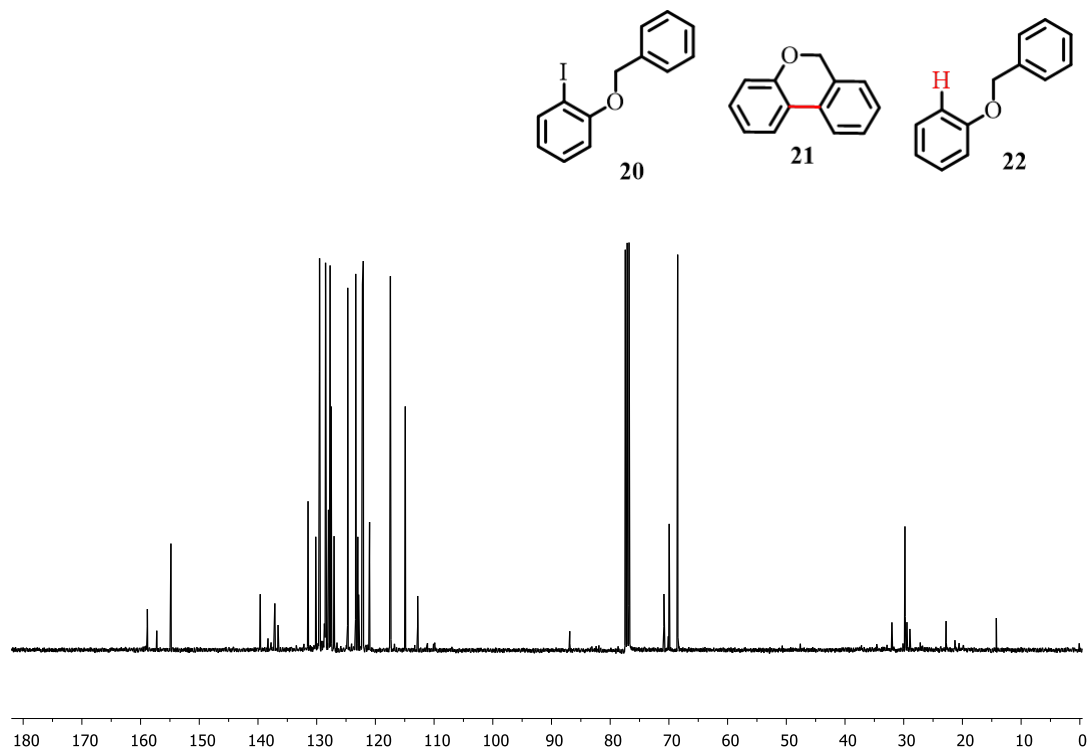


Figure 4.48 ^{13}C NMR of **20** + **21** + **22**.

4.4.6 X-Ray Crystallographic data

Table 4.8 Crystal data and structure refinement of **Compound 24**

Empirical formula	C ₂₂ H ₃₁ K N ₂ O ₆
Formula weight	458.59
Temperature	100 K
Wavelength	0.71073 Å
Crystal system	Orthorhombic
Space group	Pna21
Unit cell dimensions	a = 8.825(5) Å α = 90.00 b = 24.995(15) Å β = 90.00 c = 10.643(6) Å γ = 90.00
Volume	2348(2) Å ³
Z	4
Density (calculated)	1.297 g/cm ³
Absorption coefficient	0.265 mm ⁻¹
F(000)	976
Crystal size	0.391 x 0.291 x 0.253 cm ³
Theta range for data collection	1.629 to 28.537°.
Index ranges	-11 ≤ h ≤ 11, -33 ≤ k ≤ 33, -14 ≤ l ≤ 14
Reflections collected	33097
Independent reflections	5870 [R(int) = 0.1402]
Completeness to theta = 28.38°	99.0 %
Absorption correction	Multi-scan
Max. and min. transmission	0.936 and 0.903
Refinement method	Full-matrix least-squares on F ²
Data / restraints / parameters	5870 / 0 / 6280
Goodness-of-fit on F ²	0.898
Final R indices [I > 2σ(I)]	R1 = 0.0654, wR2 = 0.1484
R indices (all data)	R1 = 0.1402, wR2 = 0.1917
Largest diff. peak and hole	0.330 and -0.483 e.Å ⁻³

Table 4.9 Crystal data and structure refinement of **Compound 25**

Empirical formula	C ₂₀ H ₂₈ N ₂ Na O ₅
Formula weight	399.43
Temperature	100 K
Wavelength	0.71073 Å
Crystal system	Triclinic
Space group	P -1
Unit cell dimensions	a = 14.937(13) Å α = 90.00 b = 16.377(14) Å β = 91.15(2) c = 16.549(14) Å γ = 90.00
Volume	4048(6) Å ³
Z	8
Density (calculated)	1.311 g/cm ³
Absorption coefficient	0.112 mm ⁻¹
F(000)	1704
Crystal size	0.32 x 0.20 x 0.15 cm ³
Theta range for data collection	1.231 to 28.606°.
Index ranges	-19 ≤ h ≤ 19, -21 ≤ k ≤ 22, -22 ≤ l ≤ 22
Reflections collected	64772
Independent reflections	20216 [R(int) = 0.3531]
Completeness to theta = 28.38°	99.0 %
Absorption correction	Multi-scan
Max. and min. transmission	0.965 and 0.983
Refinement method	Full-matrix least-squares on F ²
Data / restraints / parameters	20216 / 0 / 1009
Goodness-of-fit on F ²	1.172
Final R indices [I > 2σ(I)]	R1 = 0.1546, wR2 = 0.3449
R indices (all data)	R1 = 0.3531, wR2 = 0.4104
Largest diff. peak and hole	0.677 and -0.534 e.Å ⁻³

4.5 References

1. Tsuji, J.; Takahashi, H.; Morikawa, M. *Tetrahedron Lett.* **1965**, *49*, 4387-4388.
2. Heck, R. F.; Nolley, J.P.; *J. Org. Chem.* **1972**, *37*, 14, 2320-2322
3. Tamao, K.; Sumitani, K.; Kumada, M. *J. Am. Chem. Soc.* **1972**, *94*, 4374-4376
4. (a) King, A. O.; Okukado, N.; Negishi, E. *J. Chem. Soc., Chem. Commun.* **1977**, 683-684; (b) Baba, S.; Negishi, E. *J. Am. Chem. Soc.* **1976**, *98*, 6729-673.
5. Milstein, D.; Stille, J. K. *J. Am. Chem. Soc.* **1978**, *100*, 3636-3638.
6. Miyaura, N.; Yamada K.; Suzuki, A. *Tetrahedron Letters.* **1979**, *20*, 3437-3440.
7. (a) Williams, G. H. Homolytic Aromatic Substitution; Pergamon: Oxford, 1960. (b) Tiecco, M.; Testafari, L. In *Reactive Intermediates*; Abramovitch, R. A., Ed.; Plenum Press: New York, 1982; Vol. 3, pp 61-111. (c) Perkins, M. J. In *Free Radicals*; Kochi, J. K., Ed.; Wiley: London, 1973; Vol. 2, pp 231-271. (d) Walters, W. A. *The Chemistry of Free Radicals*; Wiley: Boca Raton, FL, 1967
8. (a) Augood, D. R.; Williams, G. H. *Chem. Rev.* **1957**, *57*, 123-190. (b) Gill, G. B.; Williams, G. H. *J. Chem. Soc.* **1966**, *8*, 880.
9. Chalfont, G. R.; Hey, D. H.; Liang, K. S. Y.; Perkins, M. J. *J. Chem. Soc. B* **1971**, 233-245.
10. (a) Chatgililoglu, C. *Chem. Eur. J.* **2008**, *14*, 2310-2320. (b) Chatgililoglu, C. *Chem. Rev.* **1995**, *95*, 1229-1251. (c) Curran, D. P.; Keller, A. I. *J. Am. Chem. Soc.* **2006**, *128*, 13706-13707. (d) McLoughlin, P. T. F.; Clyne, M. A.; Aldabbagh, F. *Tetrahedron* **2004**, *60*, 8065-8071. (e) Baguley, P. A.; Walton, J. C. *Angew. Chem., Int. Ed.* **1998**, *37*, 3072-3082.
11. (a) Ryokawa, A.; Togo, H. *Tetrahedron* **2001**, *57*, 5915-5921 (b) Harrowven, D. C.; Sutton, B. J.; Coulton, S. *Org. Biomol. Chem.* **2003**, *1*, 4047-4057. (c) Majumdar, K. C.; Basu, P. K.; Mukhopadhyay, P. P.; Sarkar, S.; Ghosh, S. K.; Biswas, P. *Tetrahedron* **2003**, *59*, 2151-2157. (d) Curran, D. P.; Keller, A. I. *J. Am. Chem. Soc.* **2006**, *128*, 13706-13707. (e) Bowman, W. R.; Elsegood, M. R. J.; Stein, T.; Weaver, G. W. *Org. Biomol. Chem.* **2007**, *5*, 103-113 (f) Pedersen, J. M.; Bowman, W. R.; Elsegood, M. R. J.; Fletcher, A. J.; Lovell, P. J. *J. Org. Chem.* **2005**, *70*, 10615-10618.
12. Murphy, J. A.; Tripoli, R.; Khan, T. A.; Mali, U. W. *Org. Lett.* **2003**, *7*, 3287-3289. (b) Khan, T. A.; Tripoli, R.; Crawford, J. J.; Martin, C.; Murphy, J. A. *Org. Lett.* **2003**, *5*, 2971-2974.
13. (a) Molander, G. A.; Haring, L. S. *J. Org. Chem.* **1990**, *55*, 6171-6176. (b) Curran, D. P.; Fevig, T. L.; Totleben, M. J. *Synlett* **1990**, 773. (c) Inanaga, J.; Ujikawa, O.; Yamaguchi, M.

-
- Tetrahedron Lett.* **1991**, 32, 1737-1740. (d) Curran, D. P.; Tottleben, M. J. *J. Am. Chem. Soc.* **1992**, 114, 6050-6058.
14. Griess, J. P. *Ann. Chem. Justus Liebigs*, **1858**, 106, 123.
 15. Mo, F.; Dong, G.; Zgang, Y.; Wang, J. *Org. Biomol. Chem.* **2013**, 11, 1582-1593.
 16. Pschorr, R. *Ber. Dtsch. Chem. Ges.* **1896**, 29, 496
 17. (a) Gomberg, M.; Bachmann, W. E. *J. Am. Chem. Soc.*, **1924**, 46, 2339-2343. (b) Wetzel, A.; Pratsch, G.; Kolb, R.; Heinrich, M. R. *Chem.–Eur. J.*, **2010**, 16, 2547-2556.
 18. Meerwein, H.; Buchner, E.; Emsterk K. *Prakt. Chem.* **1939**, 152, 237.
 19. Kalyani, D.; McMurtrey, K. B.; Neufeldt, S. R.; Sanford, M. S. *J. Am. Chem. Soc.*, **2011**, 133, 18566-18569.
 20. Hari, D. P.; Schroll, P.; König, B. *J. Am. Chem. Soc.*, **2012**, 134, 2958-2961.
 21. Crisstomo, F. P.; Martin, T.; Carrillo, R. *Angew. Chem., Int. Ed.*, **2014**, 53, 2181-2185.
 22. Ahmed, J.; P, S.; Vijaykumar, G.; Jose, A.; Raj, M.; Mandal, S. K. *Chem. Sci.* **2017**, 8, 7798–7806.
 23. Ahmed, J.; Chakraborty, S.; Jose, A.; P, S.; Mandal, S. K. *J. Am. Chem. Soc.* **2018**, 140, 8330–8339.
 24. Vardhanapu P. K.; Ahmed, J.; Jose, A.; Shaw, B. K.; Sen, T. K.; Matthews, A.K., Mandal, S. K. *J. Org. Chem.* **2019**, 84, 1, 289-299.
 25. (a) Mo, F.; Jiang, Y.; Qiu, D.; Zhang, Y.; Wang, J. *Angew. Chem., Int. Ed.*, **2010**, 49, 1846-1849. (b) Yu, J.; Zhang, L.; Yan, G. *Adv. Synth. Catal.*, **2012**, 354, 2625-2628; (c) Ahammed, S.; Nandi, S.; D. Kundu, D.; Ranu, B. C. *Tetrahedron Lett.*, **2016**, 57, 1551-1554. (d) Hernández, J. G. *Beilstein J. Org. Chem.* **2017**, 13, 1463 —1469; (e) Chandrashekar, H. B.; Maji, A.; Halder, G.; Banerjee, S.; Bhattacharyya, S.; Maiti, D. *Chem. Commun.*, **2019**, 55, 6201-6204.
 26. Yanagisawa, S.; Uyeda, K.; Taniguchi, T.; Itami K. *Org. Lett.* **2008**, 10, 4673-4676.
 27. (a) Sun, C-L.; Li, H.; Yu D-G.; Yu, M.; Zhou, X.; Lu, X-Y.; Huang, K.; Zheng, S-H.; Shi, Z-J. *Nat. Chem.* **2010**, 2, 1044-1049. (b) Liu, W.; Cao, H.; Chang, H.; Ching, K. H.; He, C.; Kwong, F. Y.; Lei, A. *J. Am. Chem. Soc.* **2010**, 132, 16737-16740. (c) Shirakawa, W.; Itoh, K.; Hagashino, T.; Hayashi, T. *J. Am. Chem. Soc.* **2010**, 132, 15537-15539.
 28. (a) Qiu, Y. T.; Liu, Y. H.; Yang, K.; Hong, W.; Li, Z.; Wang, Z.; Yao, Z.; Jiang, S. *Org. Lett.* **2011**, 13, 3556-3359. (b) Yong, G-P.; She, W-L.; Zhang, Y-M.; Li, Y-Z. *Chem. Commun.* **2011**, 47, 11766-11768. (c) Liu, H.; Yin, B.; Gao, Z.; Li, Y.; Jiang, H. *Chem. Commun.* **2012**,
-

-
- 48, 2033-2035. (d) Chen, W-C.; Hsu, Y-C.; Shih, W-C.; Lee, C-Y.; Chuang, W-H.; Tsai, Y-F.; Chen, P. P-Y.; Ong, T-G. *Chem. Commun.* **2012**, *48*, 6702-6704. (e) Tanimoro, K.; Ueno, M.; Takeda, K.; Kirihata, M.; Tanimori, S. *J. Org. Chem.* **2012**, *77*, 7844-7849. (f) Zhao, H.; Shen, J.; Guo, J.; Ye, R.; Zeng, H. *Chem. Commun.* **2013**, *49*, 2323-2325. (g) Liu, W.; Tian, F.; Wang, X.; Yu, H.; Bi, Y. *Chem. Commun.* **2013**, *49*, 2983-2985. (h) Dewanji, A.; Murarka, S.; Curran, D. P.; Studer, A. *Org. Lett.* **2013**, *15*, 6102-6105. (i) Li, B.; Qin, X.; You, J.; Cong, X.; Lan, J. *Org. Biomol. Chem.* **2013**, *11*, 1290-1293. (j) Sharma, S.; Kumar, M.; Kumar, V.; Kumar, N. *Tetrahedron Lett.* **2013**, *54*, 4868-4871. (k) A, S.; Liu, S.; Li, H.; He, C.; Mu, Y. *Asian J. Org. Chem.* **2013**, *2*, 857-861. (l) Zhou, S.; Anderson, G. M.; Mondal, B.; Doni, E.; Ironmonger, V.; Kranz, M.; Tuttle, T.; Murphy, J. A. *Chem. Sci.* **2014**, *5*, 476-482. (m) Ghosh, D.; Lee, J-Y.; Liu, C-Y.; Chiang, Y-H.; Lee, H. M. *Adv. Syn. Cat.* **2014**, *356*, 406-410. (n) Zhu, Y-W.; Yi, W-B.; Qian, J-L.; Cai, C. *ChemCatChem.* **2014**, *6*, 733-735. (o) Bhakuni, B. S.; Yadav, A.; Kumar, S.; Kumar, S. *New. J. Chem.* **2014**, *38*, 827-836. (p) Wu, Y.; Choy, P. Y.; Kwong, F. Y. *Org. Biomol. Chem.* **2014**, *12*, 6820-6823. (q) Liu, W.; Xu, L.; Bi, Y. *RSC Adv.* **2014**, *4*, 44943-44947. (r) Song, Q.; Zhang, D.; Zhu, Q.; Xu, Y. *Org. Lett.* **2014**, *16*, 5272-5274. (s) Zhou, S.; Doni, E.; Anderson, G. M.; Kane, R. G.; MacDougall, S. W.; Ironmonger, V. M.; Tuttle, T.; Murphy, J. A. *J. Am. Chem. Soc.* **2014**, *136*, 17818-17826.
29. (a) Roman, D. S.; Takahashi, Y.; Charette, A. B. *Org. Lett.* **2011**, *13*, 3242-3245. (b) Sun, C. L.; Gu, Y. F.; Huang, W. P.; Shi, Z. J. *Chem. Commun.* **2011**, *47*, 9813-9815. (c) Rueping, M.; Leiendecker, M.; Das, A.; Poisson, T.; Bui, L. *Chem. Commun.* **2011**, *47*, 10629-10631. (d) Bhakuni, B. S.; Kumar, A.; Balkrishna, S. J.; Sheikh, J. A.; Konar, S.; Kumar, S. *Org. Lett.* **2012**, *14*, 2838-2841. (e) De, S.; Ghosh, S.; Bhunia, S.; Sheikh, J. A.; Bisai, A. *Org. Lett.* **2012**, *14*, 4466-4469. (f) Wu, Y.; Wong, S. M.; Mao, F.; Chan, T. L.; Kwong, F. Y. *Org. Lett.* **2012**, *14*, 5306-5309. (g) Masters, K-S.; Brase, S. *Angew. Chem. Int. Ed.* **2013**, *52*, 866-869. (h) Wertjes, W. C.; Wolfe, L. C.; Waller, P. J.; Kalyani, D. *Org. Lett.* **2013**, *15*, 5986-5989. (i) Bhakuni, B. S.; Yadav, A.; Kumar, S.; Patel, S.; Sharma, S.; Kumar, S. *J. Org. Chem.* **2014**, *79*, 2944-2954.
30. (a) Shirakawa, E.; Zhang, X.; Hayashi, T. *Angew. Chem. Int. Ed.* **2011**, *50*, 4671-4674. (b) Sun, C. L.; Gu, Y. F.; Wang, B.; Shi, Z. J. *Chem. Eur. J.* **2011**, *17*, 10844-10847. (c) Guastavino, J. F.; Buden, M. E.; Rossi, R. A. *J. Org. Chem.* **2014**, *79*, 9104-9111.
-

-
-
31. Zhang, H.; Shi, R.; Ding, A.; Lu, L.; Chen, B.; Lei, A. *Angew. Chem. Int. Ed.* **2012**, *51*, 12542-12545.
 32. (a) Leu, W.; Fanyi, H. *Tetrahedron* **2017**, *73*, 931-937. (b) Dewanji, A.; Muck-Lichtienfeld,; Studer, A. *Angew. Chem. Int. Ed.* **2016**, *55*, 6749-6752. (c) Jouha, J.; Khouili, M.; Hiebel, M-A.; Guillaumet, G.; Suzenet, F. *Tetrahedron Lett.* **2018**, *59*, 3108-3111.
 33. (a) Zhang, L.; Jiao, L. *J. Am. Chem. Soc.* **2017**, *139*, 607-610. (b) Pinet, S.; Liautard, M.; Debiais, M.; Pucheault, M. *Synthesis*, **2017**, *49*, 4759-4768.
 34. Cuthbertson, J.; Gray, V. J.; Wilden, J. D. *Chem. Comm.* **2014**, *79*, 2944-2954.
 35. Barham, J. P.; Coulthard, G.; Emery, K. J.; Doni, E.; Cumine, F.; Nocera, G.; John, M. P.; Berlouis, L. E. A.; McGuire, T.; Tuttle, T.; Murphy, J. A. *J. Am. Chem. Soc.* **2016**, *138*, 7402-7410.
 36. Zhang, L.; Yang, H.; Jiao, L.; *J. Am. Chem. Soc.* **2016**, *138*, 7151-7160.
 37. Zhao, H.; Shen, J.; Ren, C.; Zeng, W.; Zeng, H. *Org. Lett.* **2017**, *19*, 2190-2193.
 38. Zhang, L.; Jiao, L. *J. Am. Chem. Soc.*, **2019**, *141*, 9124-9128.
 39. (a) *Chem.Eur.J.* **2018**, *24*, 11278-11282 (b) *Science of Synthesis*, 2002, 4, 451-472. (c) *Chem.Eur.J.* **2015**, *21*, 5693-5696.
 40. Zhang, L.; Jiao, L. *Chem. Sci.* **2018**, *9*, 2711-2722.
 41. (a) Ohmura, T.; Morimasa, Y.; Suginome, H. *J. Am. Chem. Soc.* 2015, *137*, 2852-2855. (b) Oshima, K.; Ohmura, T.; Suginome, H. *Chem. Commun.* **2012**, *48*, 8571-8573.
 42. Simmons, E. M.; Hartwig, J. F. *Angew. Chem. Int. Ed.* **2012**, *51*, 3066 - 3072